A LATE QUATERNARY HISTORY OF AGULHAS-BENGUELA INTERACTIONS FROM TWO SEDIMENT CORES ON THE WESTERN CONTINENTAL SLOPE OF SOUTH AFRICA

AMANDA JANE RAU

B.Sc. (Hons) (University of Cape Town)

M.Sc. (Applied Geology) (University of Natal, Durban)

Thesis Presented for the Degree of

DOCTOR OF PHILOSOPHY

in the Department of Geological Sciences

Faculty of Science

University of Cape Town

August 2002

DECLARATION

I hereby declare that the work presented in this thesis is my own, except where otherwise stated. This thesis reports the results of original work that I have undertaken from October 1997 to August 2002 in the Departments of Geological Sciences and Archaeology (Stable Isotope Laboratory) at the University of Cape Town. I performed all sample processing and analyses, except for the stable oxygen and carbon isotope determination on calcitic foraminifera, which were undertaken at various overseas laboratories, whose assistance is fully acknowledged.

Amanda Jane Rau

signature removed

12 August 2002

ABSTRACT

Changes in circulation and productivity in the southeastern South Atlantic Ocean over the last 850 kyr are investigated through the multiproxy study of two giant piston cores, MD962080 and MD962084, retrieved from the Agulhas Bank and Olifants River continental slopes of South Africa. The stable oxygen isotope record of the benthic foraminifer, *Cibicidoides wuellerstorfi,* and the planktonic taxon, *Globorotalia inflata,* provide the stratigraphic framework from which the age models were created.

The results indicate that biotic responses to surface hydrological changes in the study area are complex and involve both high- and low-frequency variations. Palaeoproductivity proxies (organic carbon, $\delta^{13}C_{org}$, $\delta^{15}N$ and $\delta^{13}C_{inflata}$) indicate low glacial productivity over both core sites. Although productivity in the Southern Benguela Region was considerably higher than over the Agulhas Bank Slope, upwelling did not sustain the elevated levels of productivity associated with better known the Northern Benguela Region. Higher $\delta^{13}C_{org}$ values on the Olifants River Slope than on the Agulhas Bank Slope reflect differences in dominant plankton species in the two regions. Nitrogen isotope ratios indicate that, whilst there is a general excess of nutrients in glacial waters in the Southern Benguela, nutrient deficiency on the Agulhas Bank Slope leads to recycled production and nitrogen fixation.

The planktonic foraminiferal populations bear a clear Transitional to Subantarctic character with *Globorotalia inflata* and *Neogloboquadrina pachyderma* (dextral) being the dominant taxa. Influx of Subantarctic waters into the Agulhas Bank region is indicated by the increased occurrence of the Subantarctic Assemblage during glacial periods. The varying contribution to the bottom-water masses, from predominantly North Atlantic Deep Water to a greater contribution of Upper Circumpolar Deep Water in glacial periods, is inferred from enhanced carbonate preservation during cold stages.

Changes from offshore oligotrophic to mixed intermediate-old upwelled surface-water masses over the Olifants River Slope are indicated by the inverse relationship between the Transitional and Mixed-Intermediate foraminiferal assemblages. During Stage 9 unusually strong upwelling is indicated by the maximum concentration of the Subantarctic foraminifer, *Neogloboquadrina pachyderma* (sinistral). Variable input of Agulhas Current waters into the southeast Atlantic is indicated by the presence of Tropical and Subtropical planktonic foraminiferal species. In addition to precessional and eccentricity cycles, the foraminiferal assemblages exhibit high-frequency variations at 10 to 15 kyr, suggesting that the influx of Subantarctic waters into the Southern Benguela Region is related to equatorward migration of

the Antarctic sea-ice fields. The positive correlation between coarse fraction and carbonate contents suggests that textural variability may at times be affected by winnowing.

The foraminiferal records show a deviation from high-frequency variability between stages 11 and 7 to the development of a glacial-interglacial cyclicity and a transition to overall warmer conditions after 250 kyr B.P. A concurrent change in mean $\delta^{15}N$ indicates a change in nitrate source, and a change from dominantly calcareous (foraminifera and nannoplankton) to siliceous (diatoms) primary producers suggests a relative decrease in the strength of trade-wind-driven upwelling at this time.

The near-continuous presence of the tropical species *Globorotalia menardii* in both cores implies that the exchange of water from the South Indian Ocean to the South Atlantic Ocean, a crucial factor in global thermohaline circulation, was never entirely obstructed by equatorward migrations of the Subtropical Convergence during glacial periods, over the last 850 kyr. This finding contradicts the argument for a more easterly retroflection of the Agulhas Current and the closing of the "Cape Valve" during glacial periods.

PREFACE

This thesis came about as a result of the IMAGES II-NAUSICAA programme, led by Dr Philippe Bertrand of the Département Géologie et Océanographie, Université Bordeaux I, France. Through the participation of Dr John Rogers of the Department of Geological Sciences on the NAUSICAA cruise (September-October, 1996), material was made available for research at the University of Cape Town. As the other participants in NAUSICAA were mostly interested in studying the high-resolution records obtained from the Namibian continental shelf and slope, the opportunity fell to us to study the palaeoceanography of the waters around the southern tip of Africa, including the history of the southern Benguela Region, changes in which impact directly on the economy and climate of South Africa. Two cores were chosen, core MD962080 retrieved from the Agulhas Bank Slope and core MD962084, from the Olifants River Slope.

The first 3½ years of this research was funded by grants form the National Research Foundation, South Africa and from the Franco-South African Science and Technology Programme.

Through a joint project funded by the Franco-South African Science and Technology Programme, I enjoyed close co-operation with Dr Jacques Giraudeau from the Université Bordeaux I, France, who also participated in the NAUSICAA cruise. I first visited Bordeaux in October 1997 with Dr Rogers in order to sample the cores and to attend the post-cruise meeting in nearby Archachon, which Assoc. Prof. Julia Lee-Thorp also attended. I subsequently spent a month in Bordeaux (October, 1998), being trained by Dr Giraudeau in the identification of planktonic foraminifera. At this time, Dr Giraudeau also picked specimens of the benthic foraminifer, *Cibicidoides wuellerstorfi*, from the top 14m of core MD962080, that I took to Gif-sur-Yvette for analysis. During my visit to the laboratory in Gif-sur-Yvette I learned the preparation and analytical procedures for oxygen isotope analysis of benthic foraminifera, with the view of undertaking further analyses myself at the University of Cape Town. On a later visit to Cape Town, Dr Giraudeau instructed me in the use of a factor-analysis programme, which I used to determine the foraminiferal assemblages. I would like to thank Dr Giraudeau for his time and patience, his friendly support and prompt responses to queries. Dr Giaudeau's advice and assistance in writing the final draft of a paper published in *Marine Geology* (of which he is a co-author) were invaluable.

Various people assisted me with the determination of oxygen isotope ratios of foraminifera that provided the stratigraphic framework for the age models I subsequently created for the cores.

Carbon and oxygen isotopic measurements of specimens of the benthic foraminifer, *Cibicidoides wuellerstorfi*, for the top 14 m of Core MD962080, were performed at the Laboratoire des Sciences du Climat et de l'Environnement, Gif-sur-Yvette, France, under the supervision of Dr Claire Waelbroeck. Stable isotope analyses of the planktonic foraminiferal species, *Globorotalia inflata* for core MD962080 was undertaken at the Centre for Ocean Research, National Taiwan University, Keelung, Taiwan under the supervision of Dr Min-Te Chen. Specimens of *Globorotalia inflata* from core MD962084 were analysed at the Fachbereich Geowissenschaften, Universität Bremen, Germany, under the supervision of Dr Monica Segl, Dr Ralph Schneider and Assoc. Prof. Lee-Thorp. Both Drs Chen and Schneider were members of the shipboard scientific team during the NAUSICAA cruise. I picked the planktonic specimens, initially in Bordeaux (the top 10 m of core MD962080) under the guidance of Dr Giraudeau and then in Cape Town.

Some control samples for total organic carbon content were analysed on a LECO CHNS analyser by Ms Heather Sessions, under the supervision of Dr Geoff Bailey, at the Department of Marine and Coastal Management (formerly Sea Fisheries Research Institute), Cape Town, South Africa, for comparison purposes. All these analyses were done free-of-charge in the interest of scientific collaboration, for which I and my supervisors are grateful.

Dr Jean-Luc Mélice, a visiting scientist to the Department of Oceanography, University of Cape Town, enlightened me in the usefulness of wavelet analysis when applied to climatic data and instructed me in the use of the programme he had written. I would like to thank him for accepting my limited understanding and attending to my queries in the rushed last days of his stay in Cape Town. This is an emerging technique in palaeoclimatic studies. My experience in this field is nascent. As a result interpretations given in the thesis are made with caution.

Except where stated above, I performed all the laboratory work and data manipulation presented in this thesis. I undertook all sample preparation, processing and analysis, picking and counting of foraminifera. I performed the statistical and continuous wavelet analysis.

Some of the material in this thesis has been published. The publication, listed below, has a number of co-authors, whose contribution to the article varied substantially.

Rau, A.J., Rogers, J., Lutjeharms, J.R.E., Giraudeau, J., Lee-Thorp, J.A., Chen, M.-T. and Waelbroeck, C., 2002. A 450-kyr record of hydrological conditions on the western Agulhas Bank Slope, south of Africa. *Marine Geology* 180: 183-201.

In this paper, all foraminiferal data and interpretation of assemblages was my own work and I collated and wrote the paper. The idea to study the relationship between sediment texture and bottom water chemistry came from Dr Jacques Giraudeau. The discussion on the sources of the terrigenous sand fraction was the work of Dr John Rogers. Prof. Johann Lutjeharms contributed to the section dealing with the hydrographic setting and Drs Min-Te Chen and Claire Waelbroeck provided the isotope data for the stratigraphic age model.

I would like to thank my supervisors for obtaining funding to support my research and providing the opportunity to attend two international conferences (6^{th} International Conference on Palaeoceanography, Lisbon, Portugal, August 1998; XV International Congress of the International Union for Quaternary Research, Durban, South Africa, August 1999) and one local conference (South African Society for Quaternary Research Biennial Meeting, Saldanha Bay) at which I presented preliminary results. I also participated in two international workshops (Quaternary evolution of the Benguela coastal upwelling system, Carcans, France, April 2000; Linking continental environmental Quaternary history of Southern Africa with ocean currents and Antarctica, Cape Town, May 2002). The opportunity to discuss my work with contemporaries and experts in relevant fields, as well as being made aware of current research was being conducted, contributed greatly to my knowledge and understanding of palaeoceanography in general and to my own particular research. The palaeoceanographic community is very open with help and ideas and focuses on the development of young scientists.

I would like to thank Dr Geoff Bailey (Department of Marine and Coastal Management, Cape Town) and Assoc. Prof. Frank Shillington (Department of Oceanography, University of Cape Town) for proof reading Chapters 6 and 7, respectively. Their advice regarding technical approach and handling of the data was most helpful. Assoc. Prof. Shillington was very obliging in his time, always willing to discuss the current physical oceanography of the study areas and offering advice. I thank him for his open door. I would also like to thank Messrs John Lanham and Ian Newton (Archaeometry Laboratory, University of Cape Town) for their assistance in dealing with the pernickety mass-spectrometer during the measurements of nitrogen and organic carbon isotope ratios.

I would like to express my appreciation to both my supervisors, Assoc. Prof. Julia Lee-Thorp and Dr John Rogers, for their support and encouragement throughout this thesis and in particular, their patience and understanding with regards to the time-demands of my family.

Lastly, but most importantly, I would like to thank my family; my husband Grant and my daughter Nastasha Amy for their love, endless patience and the ability to survive the rushed and disorganised lifestyle of these last 2½ years. To my mother, without whose support, both practical and emotional, I would not have completed this thesis, I express my sincere gratitude.

CONTENTS

APPENDICES

LIST OF FIGURES

LIST OF TABLES

CHAPTER 1: INTRODUCTION

This thesis investigates the history of water column dynamics recorded in marine sediment cores from two sites on the western continental slope of South Africa. These particular site locations were chosen because they potentially record the history of inter-ocean exchange of thermocline waters, a crucial component of global circulation that impacts on global climate. The palaeoceanography of the area is researched by means of a number of proxies: planktonic foraminifera, calcium carbonate, sediment texture, organic carbon, stable isotope ratios of organic carbon and nitrogen, as well as oxygen and carbon isotope ratios of foraminifera. Each of these proxies sheds light on a different aspect of the hydrological conditions in the areas under investigation. These data are used compare the two sites and to study variations through time. Wavelet analysis allows the frequency of variations to be determined.

1.1 BACKGROUND

The debate about climate warming has stimulated interest in climate fluctuations and led to intense interest and research in long-term climatic cycles. The southern hemisphere, being more oceanic in character than the northern hemisphere, plays the dominant role in the redistribution of solar radiation energy (Meadows, 2001). It has been proposed that the amount of warm, salty water that escapes westward from the southern Indian Ocean into the southeast Atlantic Ocean has a direct effect on the overturning of the whole Atlantic Ocean by the eventual increase in intensity of North Atlantic Deep Water (NADW) formation (Weijer *et al.*, 1999). This thermohaline circulation, or conveyor belt (Broecker, 1991), plays an important role in global climate through the transfer of warm water to high northern latitudes (Broecker, 1987). The transfer of heat to the North Atlantic, generation of NADW and the ultimate return of NADW to the southern oceans by the conveyor belt (Fig.1.1) impacts on global energy distribution (Broecker *et al.*, 1985). Changes in the thermohaline circulation are considered to be a primary cause of sub-Milankovitch scale global climate changes (Broecker and Denton, 1990). Variations in heat transport to the northern hemisphere have been invoked as a possible cause for abrupt climatic change (Broecker *et al.*, 1985), with major changes in the global circulation system occurring during transitions from glacial to interglacial periods (Boyle and Keigwin, 1982; Shackleton *et al.*, 1983).

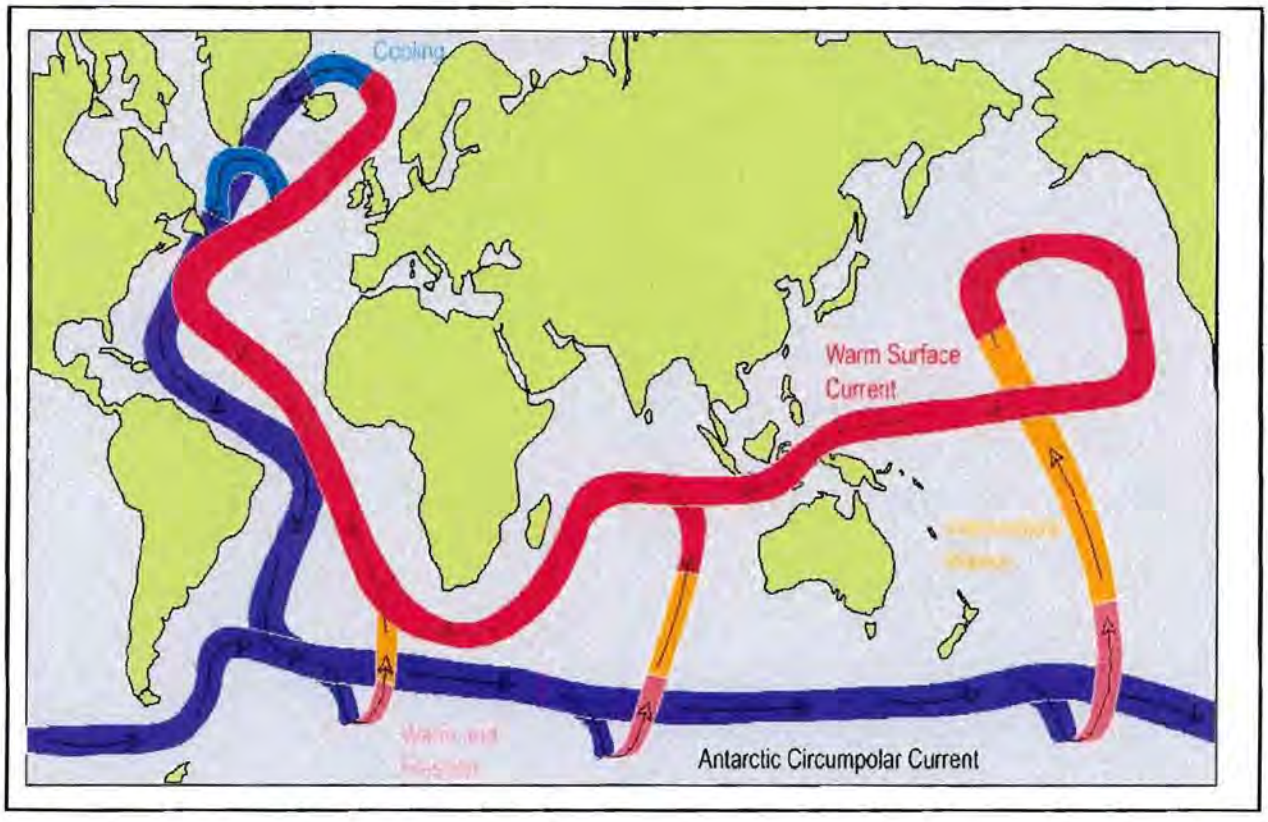

Figure 1.1: The thermohaline conveyor belt. (From Döös *et al.*, 2002).

Shedding of warm Agulhas rings from the Agulhas Current, an Indian Ocean western boundary current, into the southeastern Atlantic Ocean, forms the means by which heat and salt are transmitted between the two oceans (Fig.1.2). It has been suggested (e.g. Berger and Wefer, 1996) that the influx of warm saline Indian Ocean water into the South Atlantic around the tip of Africa (referred to as the "Cape Valve") was shut off during glacial periods. Conceivably, this inter-ocean exchange via the Agulhas Current could be shut off by a substantial equatorward migration of the Subtropical Convergence (STC) and/or changes in the inertia of the Agulhas Current (De Ruijter, 1982; Matano *et al.*, 1998). It is presumed that the West Wind Drift, south of Africa, was greatly strengthened during glacial periods (Wefer *et al.*, 1996) and that the Subantarctic and Polar Fronts moved equatorward as a result of sea-ice expansion (Burckle *et al.*, 1988). This is thought to have resulted in a concurrent equatorward migration of the STC (McIntyre *et al.*, 1989). The Agulhas Current probably flowed more strongly in glacial periods and conceivably retroflected further eastwards than at present (De Ruijter *et al.*, 1999; Lutjeharms and van Ballegooyen, 1988a,b). It is also possible that under extreme conditions ring shedding is reduced, although which climatic changes would result in reduced ring shedding is still largely a matter of speculation (Lutjeharms and de Ruijter, 1996). These factors could hinder transfer of Agulhas waters into the south Atlantic and possibly even cause a total shut down of the "Cape Valve", allowing the intrusion of cold subantarctic waters into the Southern

Benguela Region.

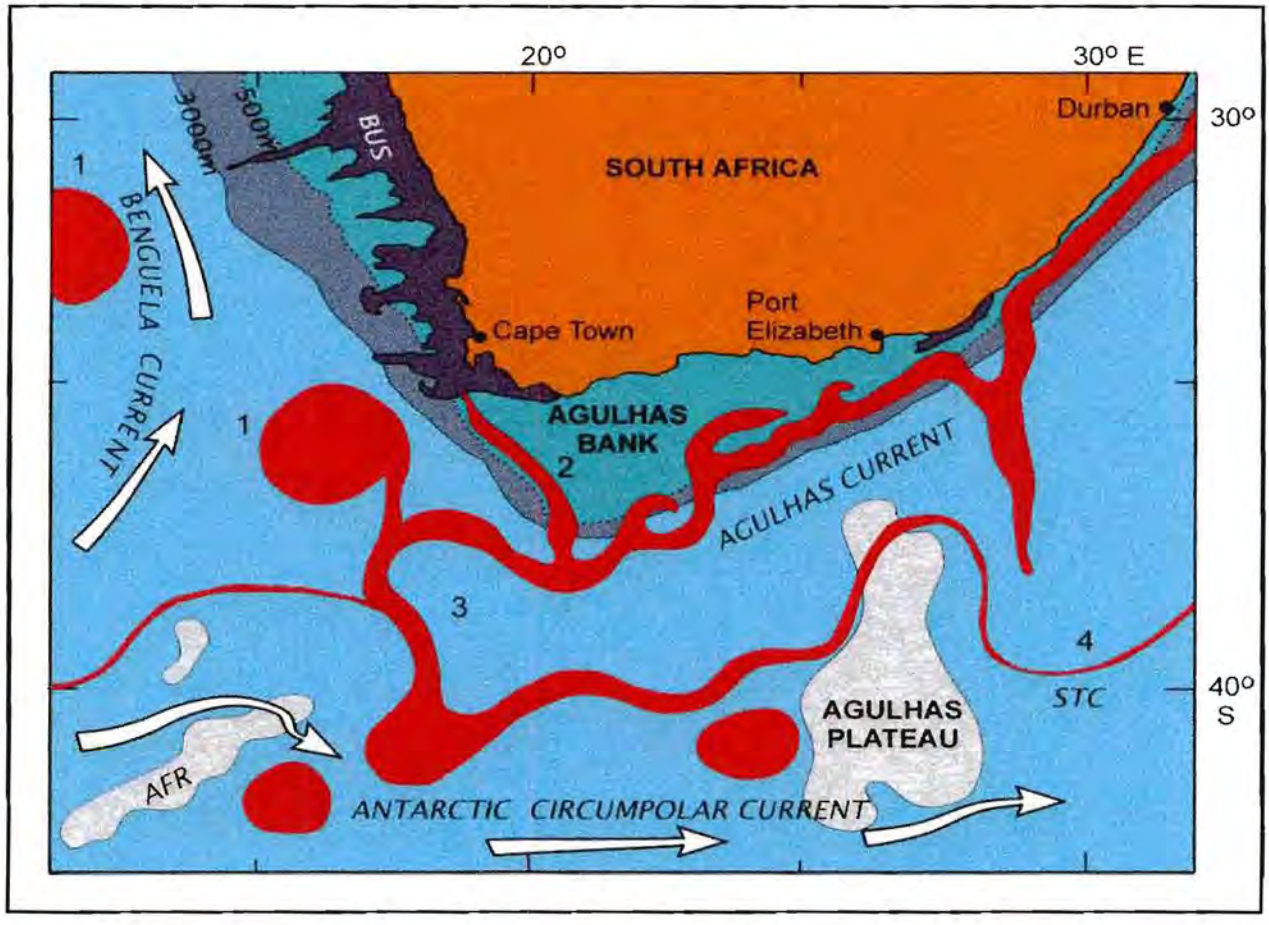

Figure 1.2: Schematic of the Agulhas Current and Southern Benguela Region. Agulhas rings (1) and filaments (2) are shed at the Agulhas Retroflection and are carried equatorward by the Benguela Current. The rest of the water of the Agulhas Current flows eastward along the Subtropical Convergence (STC) (4). Cool waters of the Benguela coastal upwelling system (BUS) are shown along the west coast of South Africa. AFR= Agulhas Fracture Ridge (After Rau *et al.*, 2002).

The Benguela Current is the eastern boundary current of the South Atlantic (Fig.1.2). It is one of the most productive upwelling systems in the world and, as such, influences the global carbon budget (Christensen and Giraudeau, 2002). The Benguela Upwelling System supports large- and small-scale fisheries of regional and national importance. Some researchers (e.g. Wefer *et al.*, 1999), among others, have suggested that upwelling intensity increased dramatically during glacial periods. The history of the contribution of warm water from the shedding of Agulhas rings into the Benguela System and variations in upwelling intensity are of central importance to the understanding of the history of oceanic productivity off southwestern Africa. By tracing the influx of warm Indian Ocean water or cold Subantarctic water into the Southern Benguela Region, patterns of heat transfer and variability in productivity can be determined.

Marine sediments deposited on the continental margins off southern Africa encode the history of water-column conditions and dynamics and hold the key to understanding regional responses and global climatic shifts. With the advent of modern analytical techniques that allow for the quick processing of large quantities of samples, there has been a move towards medium- to long-term, high-resolution studies. The high sedimentation rates off the west coast of southern Africa provide an ideal environment for the gathering of such high-resolution data.

The purpose of long-term climatic reconstruction is clear: if we do not understand (or have a clear knowledge of) climate change and its variability in the past we cannot place, for example, the recent rise in atmospheric CO_2, the depletion of the ozone layer or global warming into perspective. The multi-proxy approach of the research presented in this thesis aims to present a clearer picture of Late Quaternary changes in circulation patterns and productivity from the oceans at the southern tip of Africa.

1.2 STUDY MOTIVATION

The recognition of the importance of Indian-Atlantic transfer of thermohaline waters around the southern tip of Africa (Gordon, 1985) to the thermohaline conveyor, has aroused interest in the oceanographic processes occurring around southern Africa, with the result that there has been a spate of research cruises to this part of the world in recent decades.

A number of studies (e.g. Bé and Duplessy, 1976; Hayes *et al.*, 1976; Prell *et al.*, 1979; Morely and Hays, 1979; Prell *et al.*, 1980; Howard and Prell, 1992; Niebler,1995; Hodell *et al.*, 2000) have focussed on the southern oceans in order to provide insight into NADW formation and glacial-interglacial (G-IG) cycles. The majority of studies have interpreted the palaeoceanographic history of the southern Indian and Atlantic Oceans predominantly in terms of latitudinal movements of the Subtropical Convergence (STC) and the Antarctic Polar Front (APF).

The Late Quaternary history of the Agulhas Current has been mainly been interpreted from a single core in the Mozambique Basin, southwest Indian Ocean (Hutson, 1980; Prell *et al.*, 1980), two short cores (spanning the last 150 000 years) from the Agulhas Passage off the south coast of South Africa (Winter and Martin, 1990) and a piston core recovered from the continental slope south of Cape

Town (Flores *et al.*, 1999) . The two most recent studies, by Flores *et al.* (1999) and Winter and Martin (1990), argue that there has been no lateral shift in the position of the Agulhas Retroflection for the periods under investigation.

Prior to the IMAGES II-NAUSICAA cruise of 1996 and Ocean Drilling Program, Leg 175 (1997), the history of the Benguela Upwelling System has been interpreted from studies centred in the Northern Benguela Region, focussing mainly on cores collected from the Walvis Ridge. Thus, the history of the Northern Benguela Upwelling System is relatively well understood (e.g. Berger and Wefer, 1996; Diester-Haas, 1985; Diester-Haas *et al.*, 1990; Esper *et al.*, 2000; Kirst *et al.*, 1999; Lange *et al.*, 1999; Little *et al.*, 1997a, b; Wefer *et al.*, 1996), but relatively little is known of the history of the more southerly part of the Benguela System. It is expected that the Southern Benguela System had a more complex history, due to greater variability of inputs into the system, such as latitudinal shifts in the South Atlantic Anticyclone, as well as heat and salt transfer from the Indian Ocean. Changes in circulation patterns of this system would affect upwelling and climate on the subcontinent and would mirror wider changes in global atmospheric and ocean circulation.

The research presented in this thesis forms part of the multi-national IMAGES-II or NAUSICAA (**N**amibia **A**ngola **U**pwelling **S**ystem and **I**ndian **C**onnection to the **A**ustral **A**tlantic) programme. The IMAGES (**I**nternational **M**arine **P**ast **G**lobal Changes **S**tudy) programme was initiated in January 1995 to facilitate a large and rapid increase in the understanding of Quaternary palaeoceanography through the study of long marine sediment cores. The main aim of NAUSICAA is to explore the history of the Indian Ocean-Atlantic Ocean connection and the Southeastern Atlantic upwelling system during the Late Quaternary (Bertrand *et al.*, 1997, Chen *et al.*, 1998, Rogers, 1999). Figure 1.3 illustrates the coring locations of the IMAGES II-NAUSICAA cruise of the *Marion Dufresne*, in October-November 1996.

This research comprises the study of two undisturbed giant CALYPSO cores MD962080 and MD962084 (Fig.1.3). The site for the 22 m-long core MD962080, retrieved from the Agulhas Bank Slope in 2488m water depth, lying poleward of the direct influence of coastal upwelling, is ideally located to record the history of water mass exchange between the Indian and South Atlantic Oceans and productivity variations at the southern tip of Africa. The Olifants River Slope, the site of the 35 m-long MD962084 (1408m water depth), would record signals from the Namaqua upwelling cell

Town (Flores *et al.*, 1999) . The two most recent studies, by Flores *et al.* (1999) and Winter and Martin (1990), argue that there has been no lateral shift in the position of the Agulhas Retroflection for the periods under investigation.

Prior to the IMAGES II-NAUSICAA cruise of 1996 and Ocean Drilling Program, Leg 175 (1997), the history of the Benguela Upwelling System has been interpreted from studies centred in the Northern Benguela Region, focussing mainly on cores collected from the Walvis Ridge. Thus, the history of the Northern Benguela Upwelling System is relatively well understood (e.g. Berger and Wefer, 1996; Diester-Haas, 1985; Diester-Haas *et al.*, 1990; Esper *et al.*, 2000; Kirst *et al.*, 1999; Lange *et al.*, 1999; Little *et al.*, 1997a, b; Wefer *et al.*, 1996), but relatively little is known of the history of the more southerly part of the Benguela System. It is expected that the Southern Benguela System had a more complex history, due to greater variability of inputs into the system, such as latitudinal shifts in the South Atlantic Anticyclone, as well as heat and salt transfer from the Indian Ocean. Changes in circulation patterns of this system would affect upwelling and climate on the subcontinent and would mirror wider changes in global atmospheric and ocean circulation.

The research presented in this thesis forms part of the multi-national IMAGES-II or NAUSICAA (**N**amibia **A**ngola **U**pwelling **S**ystem and **I**ndian **C**onnection to the **A**ustral **A**tlantic) programme. The IMAGES (**I**nternational **M**arine **P**ast **G**lobal Changes **S**tudy) programme was initiated in January 1995 to facilitate a large and rapid increase in the understanding of Quaternary palaeoceanography through the study of long marine sediment cores. The main aim of NAUSICAA is to explore the history of the Indian Ocean-Atlantic Ocean connection and the Southeastern Atlantic upwelling system during the Late Quaternary (Bertrand *et al.*, 1997, Chen *et al.*, 1998, Rogers, 1999). Figure 1.3 illustrates the coring locations of the IMAGES II-NAUSICAA cruise of the *Marion Dufresne*, in October-November 1996.

This research comprises the study of two undisturbed giant CALYPSO cores MD962080 and MD962084 (Fig.1.3). The site for the 22 m-long core MD962080, retrieved from the Agulhas Bank Slope in 2488m water depth, lying poleward of the direct influence of coastal upwelling, is ideally located to record the history of water mass exchange between the Indian and South Atlantic Oceans and productivity variations at the southern tip of Africa. The Olifants River Slope, the site of the 35 m-long MD962084 (1408m water depth), would record signals from the Namaqua upwelling cell

(Shannon, 1985), reflecting changes in circulation patterns in the Southern Benguela Upwelling System and indirectly, record changes in the surface-water advections via the "Cape Valve".

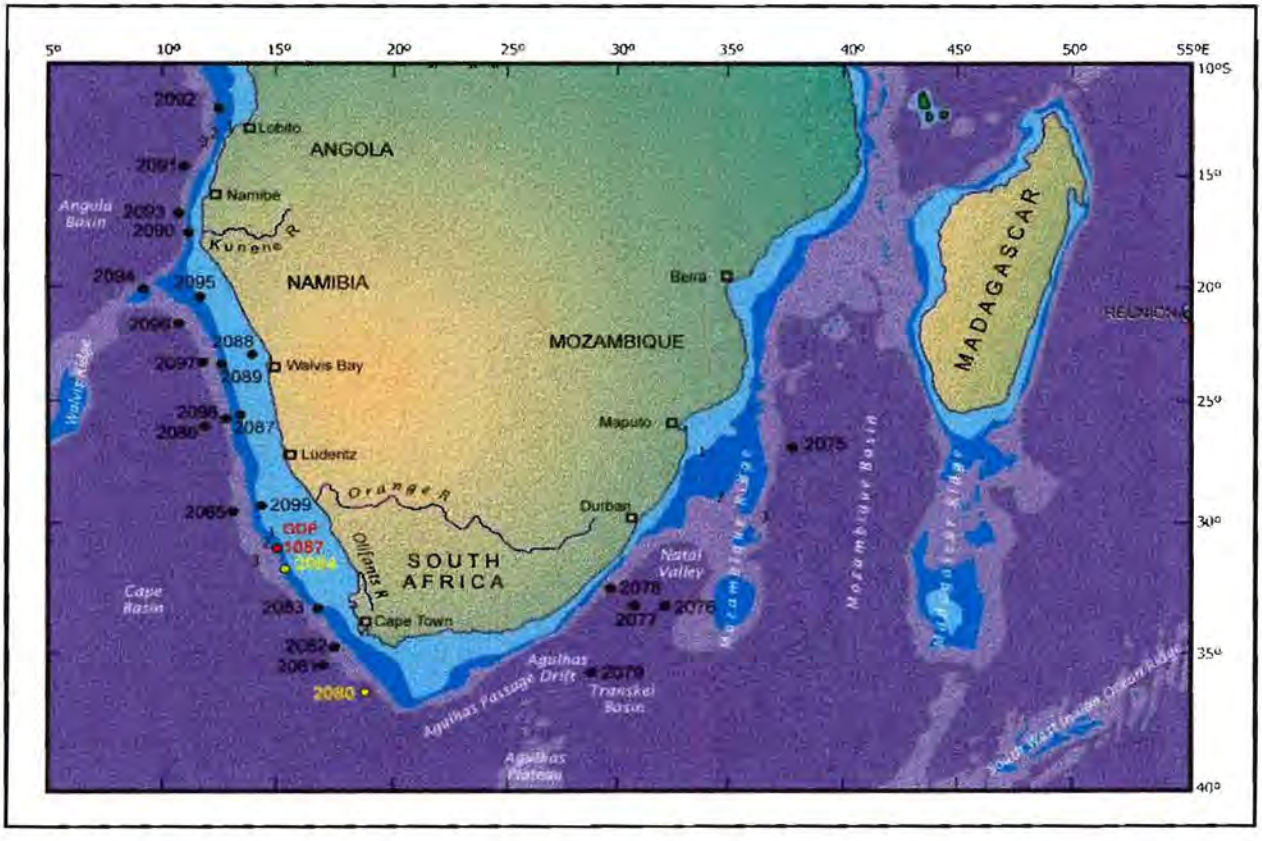

Figure 1.3: Core locations of the IMAGES II_NAUSICAA programme, *Marion Dufresne* cruise of October-November 1996. Locations of the cores studied in this thesis are shown in yellow. ODP Site 1087 is indicated in red. Isobaths (1,2,3) in kilometres. (After Bertrand *et al.*, 1997).

1.3 MAIN OBJECTIVES OF THIS RESEARCH

The main aims of this research are broadly centred around global climatic variations on glacial-interglacial (G/IG) timescales in the Late Quaternary, spanning the last 850 000 years. By studying sediments from two cores located in different oceanic regimes, the general objectives are

1) to establish a history of hydrographic conditions and productivity variations through the Late Quaternary in each region;
2) to identify any major climatic shifts on local, regional and/or global scales during the time period under investigation;
3) to assess whether the transfer of Indian Ocean water into the South Atlantic was interrupted during glacial periods as a result of equatorward migration of the Subtropical Convergence and

4) to investigate the timing of changes observed in the records.

These issues are investigated using various proxies in order to provide a range of information that, together, can be used to increase our knowledge of the palaeoceanographic conditions that prevailed around the southern tip of Africa in the Late Quaternary:

- foraminiferal oxygen isotope records are used to develop an age-model for each core;
- planktonic foraminiferal assemblages are used to indicate changes in surface-water conditions over the core sites;
- variations in productivity and nutrient availability and utilisation are investigated using stable isotope ratios of organic carbon, nitrogen and carbon from planktonic foraminiferal tests as well as total organic carbon content;
- information relating to bottom-water dynamics and chemistry is provided by sediment texture, calcium carbonate content and carbonate preservation.

These proxy data are used to investigate both local and regional changes throughout the last 850 kyr (kiloyears) on varying timescales. The timing of these changes are investigated using a relatively new technique, continuous wavelet transform, in order to identify any periodicity and, where possible, to relate these changes to Milankovitch-type cycles of precession, obliquity and eccentricity (Milankovitch, 1930). This is done in order to ascertain the forcing and feedback mechanisms driving the fluctuations and to determine regional and global relations.

1.4 ORGANISATION OF THESIS

This thesis consists of 8 chapters. Chapter 2 provides the regional setting of the areas in which the cores were taken. Hydrographic and atmospheric conditions are reviewed, focussing on major circulation patterns affecting areas of the core sites. A brief description of surficial sediments is presented.

Chapter 3 describes the sediment cores and the sampling methods. An age-model is created for each core from the stable oxygen isotope records of the benthic foraminifer , *Cibicidoides wuellerstorfi* and the planktonic foraminifer *Globorotalia inflata* (in the case of core MD962080) and the planktonic foraminifer *Globorotalia inflata* in the case of core MD962084. Differences in

sedimentation rates at the two sites are highlighted. Surface-water temperature variations, as indicated by the oxygen isotope ratios are discussed.

Chapter 4 documents the interpretation of planktonic foraminiferal census counts and the grouping of foraminiferal assemblages. Planktonic foraminifera are widely used for palaeoceanographic reconstruction because of their potential to "freeze" geochemical information in their shells. Planktonic foraminifera are niche-specific, thriving in certain temperature and salinity conditions. Recent studies (Giraudeau, 1993; Niebler and Gersonde, 1998) document the usefulness of planktonic foraminifera as tracers of present surface-water masses in the South Atlantic. The high abundance and good preservation of these calcareous microfossils in the sediment from both cores facilitates reconstruction of the surface circulation around the southern tip of Africa. Variations in planktonic foraminiferal assemblages reflect the varying dominance of different water masses over the core locations. The individual records of *Globorotalia menardii* are used to interpret fluctuations in inter-ocean thermohaline water transfer during the Late Quaternary.

Physico-chemical characteristics of the sediment record are presented in Chapter 5. Variations in calcium carbonate, sand and coarse-fraction content, as well as a foraminiferal preservation index, are used to infer changes in circulation due to bottom-current intensity and water-mass chemistry, as well as changes in surface productivity.

The reconstruction of the productivity history of the regions, using four different proxies, is presented in Chapter 6. The combination of organic-matter content and composition and ^{13}C content is a potentially powerful approach for addressing the nature and pace of ecological and environmental change in both the modern and ancient ocean (Freeman, 2001). The preservation of the isotopic signal of organic carbon and nitrogen in the sediments allows for the hindcasting of variations in productivity and nutrient availability. Carbon and nitrogen isotopes record changes in nutrient dynamics in the water column. Results of stable isotope analysis of the sediment are also discussed in Chapter 6. In addition, atomic carbon to nitrogen (C/N) ratios are used to infer the origin of the sedimentary organic matter.

Because these physico-chemical parameters are mainly governed by meteorological and hydrological conditions, the timing of changes can point to possible forcing and feedback mechanisms driving the variations. Chapter 7 shows how wavelet analysis reveals the dominant frequencies of the observed

variations in the proxy records. In addition to the well-known Milankovitch orbital cycles, super- and sub-Milankovitch cycles are observed. Within-core and between-core comparisons are made using cross-wavelet analysis.

Chapter 8 is an overview of all the results, drawing together the main findings of each of the previous chapters. A comparison of the two cores is made and inferences are drawn about the activity of Agulhas-water exchange and the functioning of the "Cape Valve". A discussion of the main conclusions derived from this research is presented.

All appendices to this thesis are found on the CD inserted into the back sleeve. Scanning electron micrographs and environmental characteristics of the planktonic foraminifera counted in this study are also shown in Appendix 3 at the end of this thesis.

1.5 DEFINITIONS

The following terms are used throughout the thesis:

- The words "summer" or "winter" refer to the austral summer/winter, unless otherwise stated.
- The boundary between the Northern Benguela Region (NBR) and the Southern Benguela Region (SBR) lies south of the main Lüderitz upwelling zone, around 27°S (Giraudeau and Rogers, 1994).
- The abbreviations kyr (kilo years or 1000 years) and kyr B.P. (kilo years before present) are used throughout.

CHAPTER 2: REGIONAL SETTING

This chapter provides the setting for the study area. The chapter consists of a review of the hydrological and atmospheric conditions impacting on the research area; including bathymetry, meteorological and regional and local ocean circulation. A brief description of the surficial sediments is given in the last section of this chapter. A broad regional review of the characteristics of the South Atlantic seafloor and the meteorology of southern Africa is presented first. This is followed by a brief description of general circulation in the South Atlantic and a more detailed description of the oceanographic features that directly impact on the core sites. The systems are described from east to west, following the general oceanographic circulation.

2.1 BATHYMETRY AND TOPOGRAPHY

Three main basins comprise the abyssal plain of the Southeast Atlantic Ocean. The Agulhas Basin lies to the south of the African continent and is bounded to the northwest by the Agulhas Ridge (Fig. 2.1). North of the Agulhas Ridge, the Cape and Angola Basins are separated by the Walvis Ridge, which runs in a southwesterly direction from its abutment with the Namibian coast, at approximately 20°S, towards the Mid-Atlantic Ridge. The Walvis Ridge forms a barrier to the northward and southward flow of waters below a depth of 3000 m (Shannon and van Rijswijck, 1969; Nelson and Hutchings, 1983) and in so doing exerts a major influence on the circulation in the Southeast Atlantic. Two marginal sedimentary basins, the Orange and Walvis Basins are found under the passive continental margin off the west coasts of South Africa and Namibia.

The bathymetry of the continental margin off the west and south coasts of southern Africa is variable (Fig. 2.1). The margin is divided into four distinct morphological zones; the nearshore rocky platform, the continental shelf, continental slope and the continental rise. South of 33°S there is a single deep (500 m) shelf break, but further north double shelf breaks are common, e.g. off Cape Columbine (between 32°S and 33°S) (Dingle, 1973a). Near Walvis Bay (23°S) there are inner (200-380m and 140 m) and outer shelf breaks (500 m and 400 m) (Bremner, 1981a). The Cape Canyon (Simpson and Forder, 1968), running oblique to the margin, is the only major submarine canyon to intersect both the slope and the shelf and was probably initiated during the

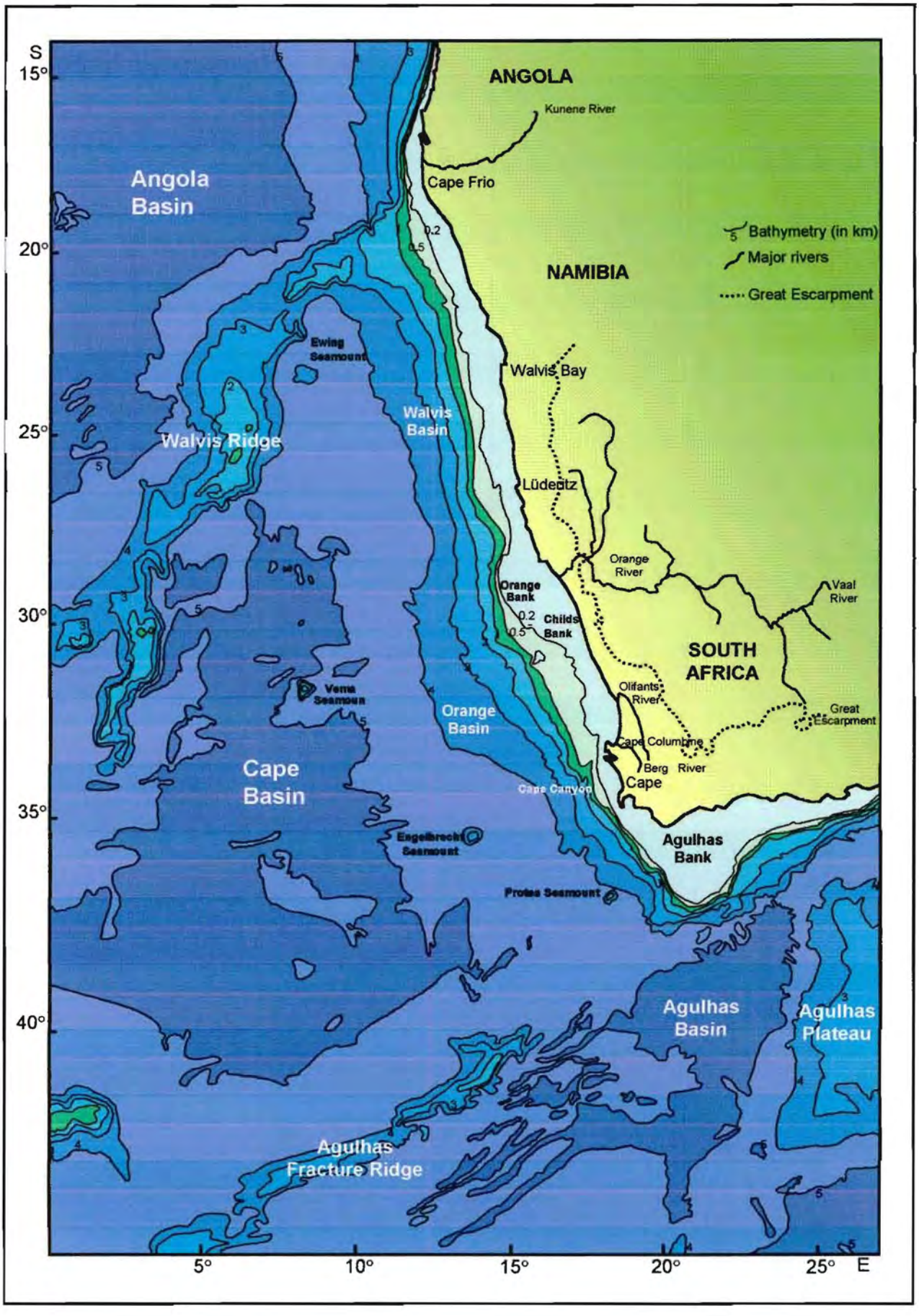

Figure 2.1: Bathymetry and major seafloor features of the Southeast Atlantic and Southwest Indian Oceans. (After Dingle and Hendey, 1984; Dingle *et al.*, 1983; Gilchrist and Summerfield, 1990; Partridge and Maud, 1987; Shannon, 1985; Shannon and Nelson, 1996; Smith and Sandwell, 1996; Wefer *et al.*, 1998.)

major Oligocene regression by a proto-Olifants River (Dingle and Hendey, 1984). The Agulhas Bank, a relatively wide (230 km), shallow feature (<200 m), forms the southern-most margin of the continental shelf (Dingle, 1973b; Shannon and Nelson, 1996). The shelf narrows northwards, with narrowest sections off the Cape Peninsula (40 km), south of Lüderitz (75 km) and off southern Angola (20 km) (Bremner *et al.*, 1986; Birch *et al.*, 1986). The nearshore rocky platform is narrow off Cape Columbine (9 km), but widens to 37 km off St Helena Bay (Birch and Rogers, 1973; Birch *et al.*, 1986). High sedimentation rates off the Orange River in the Mesozoic led to the outbuilding of the Orange Shelf (180 km). Cappings of Neogene limestones form both Childs Bank and Orange Banks, (Dingle, 1973a; Rogers and Bremner, 1991).

The oceanic conditions of the region affect the adjacent landmass. The west coast of southern Africa comprises a relatively narrow coastal plain, which rises to the main escarpment 50 - 200 km inland (Shannon and Nelson, 1996) (Fig. 2.1). The coastline is characterised by its regular nature and general lack of embayments, except for Lüderitz and Walvis Bay. However, several prominent headlands occur south of 32°S. Granite outcrops at Cape Columbine and Cape Town form the southern boundaries of bays, leaving bays to the north (St Helena Bay and Table Bay) and protected bays to the south (Saldanha Bay and False Bay). A large peninsula (the Cape Peninsula) lies south of Cape Town, the topography of which plays an important role in wind forcing over the adjacent shelf sea (Shannon and Nelson, 1996).

2.2 METEOROLOGY

The climate of southern Africa is inherently variable on a wide range of timescales, through annual, decadal to millennial and beyond (Meadows, 2001). Significant variations in the patterns of precipitation and temperature, are a key component of southern African climate. Some of the climatic variations have been shown to be in-phase with global climate forcings, such as solar radiation changes due to orbital eccentricities (Partridge, 1997).

The general atmospheric circulation in the low and temperate latitudes of the South Atlantic is dominated by trade winds and westerly winds (Preston-Whyte and Tyson, 1988). In the austral winter, the subtropical high-pressure cell is more strongly developed and situated farther northwest resulting in intensified SE-trade winds (Fig. 2.2). In opposite seasons and hemispheres, trade winds alternate in strength and directions, so strong SE-trades co-occur with weak NE-trades and *vice versa*. The Inter-Tropical Convergence Zone (ITCZ), a zone of moist,

warm, rising air, separates the two trade wind systems. The importation of warm, moist air masses from south of the equator is an important mechanism related to the northward cross-equatorial heat transport in the surface waters of the South Atlantic. The position of the ITCZ changes seasonally in response to the changing strengths of the trade winds. The strong westerly zonal winds south of Africa (Fig. 2.2) blow year-round, reaching maximum intensity in winter (Shannon and Nelson, 1996).

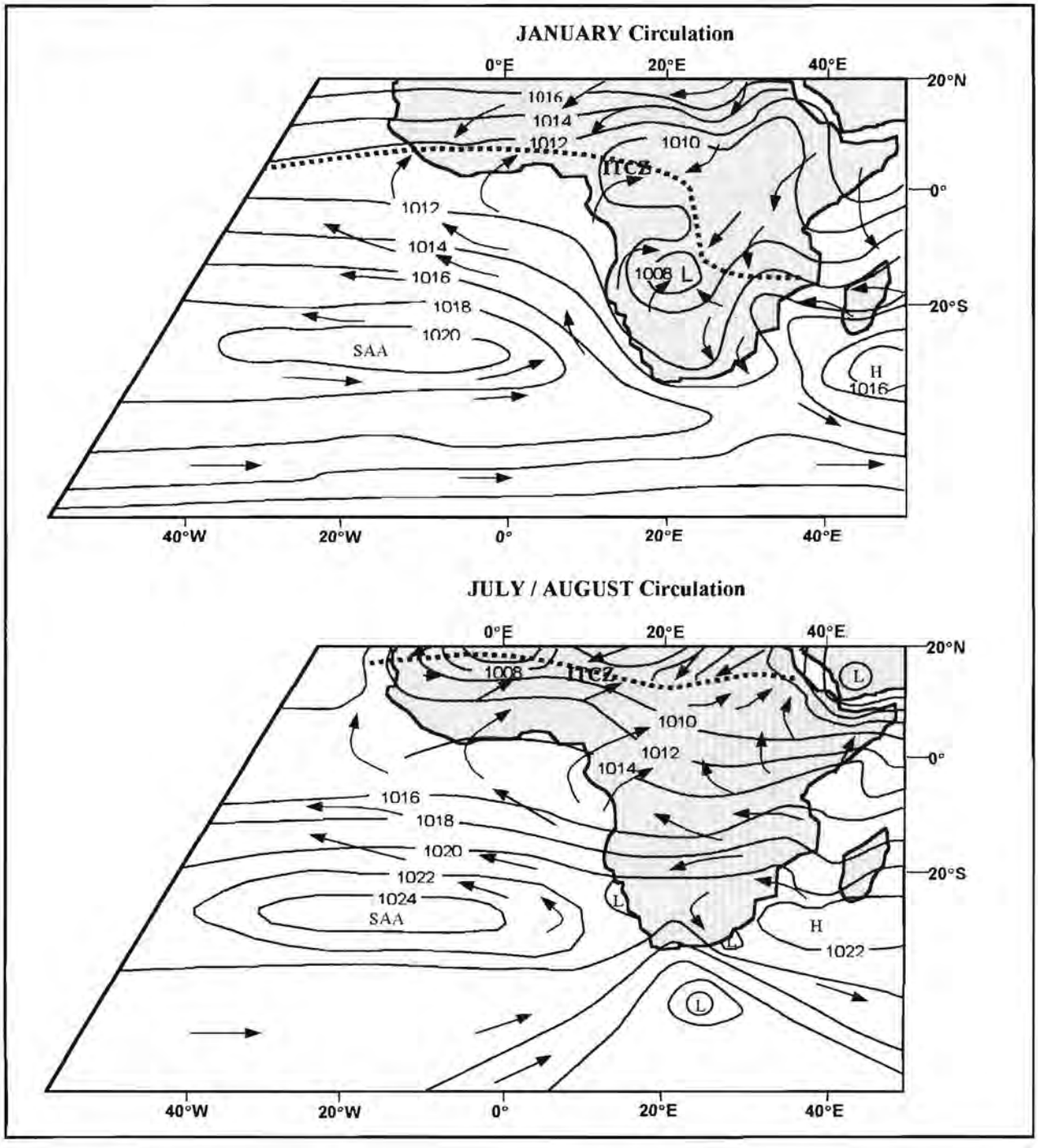

Figure 2.2: Schematic illustration of the general features of atmospheric surface circulation, showing winds and pressure fields, over Africa. The Inter-Tropical Convergence Zone (ITCZ) is indicated by a dashed line. SAA = South Atlantic Anticyclone, L = low pressure cell, H = high pressure cell. (After Gasse, 2000 and Preston-Whyte and Tyson, 1988.)

Over the Agulhas Bank, zonal winds increase polewards, particularly over the Agulhas Current where atmospheric turbulence is extreme (Jury, 1992). Easterly longshore winds, dominating during spring and summer, exhibit sharp offshore velocity gradients. These winds move surface water southwards with resultant offshore Eckman transport and coastal upwelling (Schumann, 1989). Conversely, westerly wind dominance characterises winters in the area south of the Agulhas Bank. However, there is not a simple seasonal dichotomy in this area. The weather systems crossing the Agulhas Bank can bring alternately easterly, then westerly, winds within a few days (Schumann, 1989).

The prevailing winds over the Benguela region are controlled by the anticyclonic South Atlantic high-pressure system, the pressure field over the adjacent subcontinent and by cyclones moving eastwards across the southern part of the continent, produced by perturbations in the subtropical jet stream (Nelson and Hutchings, 1983). The South Atlantic Anticyclone (SAA) is maintained throughout the year (Fig. 2.2), but undergoes seasonal changes in pressure intensity (3-4 mb; Shannon, 1985) and position, moving over 6 degrees of latitude and up to 13 degrees of longitude (Preston-Whyte and Tyson, 1988). In winter, the SAA moves northwards and westwards in response to strengthening of the southern westerly wind belt. Pressures over the continent change radically from well-developed lows in summer to a weak high in winter as the continental low and ITCZ move northwards (Fig. 2.2), with resultant seasonality in the pressure gradients (Shannon and Nelson, 1996). The curved anticyclonic flow, associated with the SAA, is steered along the coast by the interior thermal barrier set up by desert-like conditions of the coastal plain and the orography of the continental escarpment (Nelson and Hutchings, 1983). As a result, the winds along the western coast of southern Africa are predominantly southerly and upwelling-favourable. Coast-parallel, upwelling-favourable winds extend as far as southern Angola. North of about 15°S, winds are generally weaker and directed more offshore (Shannon, 1985).

As in other eastern boundary current systems, the offshore areas are influenced by anticyclonic wind stress curl. The area of strongest longshore winds in all seasons lies just south of 25°S (Central Namibia), the latitude of the coastal wedge-shaped area of strongest cyclonic wind-stress curl. The wedge, being approximately 200 km wide, is most limited in poleward extent during winter (June and July), while from late spring to early autumn (October-April), it extends past Cape Columbine and around the Cape Peninsula (Shannon and Nelson, 1996). Other areas of cyclonic wind-stress curl are located north of Cape Frio at approximately 15°S during April

and May and from October to January, and along the south coast of South Africa near 25°S year-round.

The Benguela coastal region is characterised by hot, dry adiabatic "berg" winds blowing seaward off the western escarpment when high pressure cells form over the subcontinent in winter (Shannon and Anderson, 1982). These winds are locally intensified by topographic features such as river valleys. Satellite imagery reveals that they transport significant quantities of terrigenous material out to sea. The warm air flows over the cold marine boundary layer after passing the coast (Shannon and Nelson, 1996). Land-sea breezes occur along the west coast where an interior coastal plain exists, resulting in a strong diurnal rotary wind component (Jury *et al.*, 1985).

There are distinct inter-annual variations in the synoptic wind field of the greater Benguela region, the most significant of which is related to the *El Niño* - Southern Oscillation (ENSO). ENSO events represent the maximum reversals of the Walker Circulation (Preston-Whyte and Tyson, 1988). The Walker Circulation, a significant feature of the Southern Hemisphere atmospheric circulation, is a linked series of zonal atmospheric circulation cells that are directly responsive to sea-surface temperatures over the eastern and western Pacific Ocean. As temperatures change, a major atmospheric pressure oscillation, the Southern Oscillation (SO), is set up between the south-east Pacific subtropical high and the Indonesian equatorial low (Preston-Whyte and Tyson, 1988). The SO exerts a modulating effect on the rainfall of southern Africa. During the low phase of the SO, the convergence zone (and subsequent high rainfall) moves offshore (Preston-Whyte and Tyson, 1988) and longshore (upwelling-inducing) winds in the extreme southern Benguela weaken (*El Niño* phase). Conversely, during the high phase (*La Niña*), longshore winds strengthen, particularly along the south coast of South Africa (Shannon and Nelson, 1996).

2.3 HYDROGRAPHIC SETTING

2.3.1 Water Masses and Large-scale Circulation

There are a number of water masses present off the west and south coast of southern Africa, including tropical and subtropical surface waters, thermocline waters (comprising South Atlantic Central Water, South Indian Central Water, tropical Atlantic Central Water), Antarctic Intermediate Water (AAIW), North Atlantic Deep Water (NADW) and Antarctic Bottom Water

(AABW).

The Southeast Atlantic is unique in that meridional heat transport in the upper ocean is equatorward, whereas all other oceans exhibit poleward surface heat transport. The near-surface currents of the SE Atlantic are part of a global circulation system, whereby warm surface waters are transported across the equator to the northern North Atlantic. Upon cooling, these highly saline waters (salinity increased by evaporation across the equator during transport from the South Atlantic) sink and mix with deep waters in the Nordic seas forming NADW. In turn, NADW in turn flows southward in the deep ocean crossing the equator in the deep western basin of the Atlantic, eventually mixing with Antarctic waters (Wefer *et al.*, 1996). The mixture is transported to the other oceans by the Circumpolar Current giving rise to the global thermohaline circulation system (Gordon, 1986). Major changes in the global circulation system occur during transitions from glacial to interglacial conditions. It is assumed that the Atlantic circulation cell is reduced or interrupted during glacial times, leading to a reduction in NADW formation (Charles and Fairbanks, 1990) as a result of increased sea-ice coverage in the NADW source areas, which is enhanced by reduced heat transport from the South Atlantic. It has been suggested that most of the NADW leaving the Atlantic Ocean is balanced by a warm upper layer return flow from the Indian Ocean (Gordon, 1986) and that this warm source turns on and off in tune with glacial-interglacial cycles (Berger *et al.*, 1987; Berger and Wefer, 1996).

The South Atlantic surface-water current system is dominated by the subtropical South Atlantic anticyclonic gyre (SAA), which is the result of the general atmospheric circulation dominated by trade winds and west winds, as described above. Strong southerly trade winds tend to move heat equatorward, whilst strong NE-trades hinder heat transport northwards across the equator (Wefer *et al.*, 1996). High surface-water temperatures in the Atlantic are found around the ITCZ. Northward cross-equator heat transport is most pronounced during the boreal summer, with the ITCZ in its northernmost position (15°N). The heat transfer weakens during February and March when the ITCZ reaches its southernmost position at 3°N above west Africa (Servain and Legler, 1986).

The thermocline water mass is upwelled along the coast and constitutes, in a modified form, the shelf waters of the Benguela System (Shannon and Nelson, 1996). Thermocline waters overlie AAIW, the core of which is at 700 – 800 m in the Southeast Atlantic (Fig. 2.3) and deeper at 1100 m in the South Indian Ocean and Agulhas Retroflection area (Valentine *et al.*, 1993).

AAIW of Indian Ocean origin (transported by the Agulhas Current) is more saline and less well oxygenated than AAIW originating from the South Atlantic Current (Shannon and Nelson, 1996). Gordon *et al.* (1992) highlight the significance of the transfer of AAIW and lower thermocline water from the Indian to the Atlantic Ocean and estimate that up to 50% of AAIW in the Benguela region is of Indian Ocean origin. AAIW circulation follows that of the overlying thermocline waters flowing with the Agulhas Current, the Agulhas Retroflection, the South Atlantic Current, the Benguela Oceanic Current and flows poleward west of the shelf break as far as 30°S. AAIW is carried northwards and westwards by the Benguela Oceanic Current and South Atlantic gyre, crossing the Greenwich meridian south of 24°S (Shannon and Nelson, 1996). The present circulation of the deep South Atlantic is dominated by interactions between south-flowing NADW and northward-flowing Circumpolar Deep Water (CDW) (Reid, 1989). The density characteristics of these water masses are such that the CDW is divided into an upper and lower branch by a thick layer of relatively warm, saline and well-oxygenated NADW lying between 1500 m and 3500 m (Reid, 1996). The Cape Basin is dominated by Lower Circumpolar Deep Water (LCDW) at depths below 3500 m (Reid, 1989). The Walvis Ridge acts as a barrier to the equatorward flow of AABW that lies at depths in excess of 4000 m (Fig. 2.3), although some leakage of AABW across the Ridge is reported (Shannon and O'Toole, 1998). In the Cape Basin circulation of AABW is cyclonic, and along the continental margin beneath the Benguela, the flow is poleward (Reid, 1996).

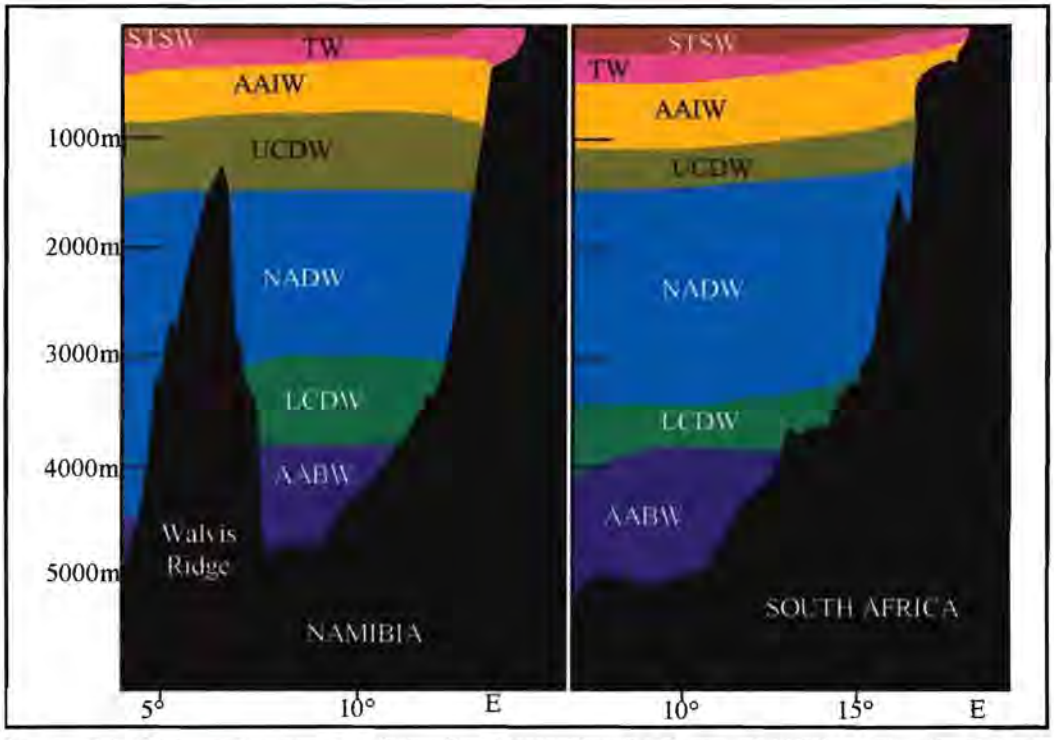

Figure 2.3: Main water masses of the Southeast Atlantic Ocean. AABW= Antarctic Bottom Water, LCDW = Lower Circumpolar Deep Water, NADW = North Atlantic Deep Water, UCDW = Upper Circumpolar Deep Water, AAIW = Antarctic Intermediate Water, TW = Thermocline Water, STSW = Subtropical Surface Water. (After Shannon and O'Toole, 1998).

2.3.2 The Agulhas System

The Agulhas Current (Fig. 2.4) carries South Indian Subtropical Surface Water, Antarctic Intermediate Water and some remnants of Red Sea Water and Tropical Indian Surface Water into the Agulhas Retroflection region (Valentine *et al.*, 1993). At the Retroflection, the Agulhas Current turns back on itself (Lutjeharms and van Ballegooyen, 1988a) and most of its waters subsequently flow eastward as the Agulhas Return Current. During this process, the Retroflection loop can occlude to pinch off an Agulhas ring that will subsequently drift off into the South Atlantic Ocean, carrying with it its load of South Indian water masses (Fig. 2.4). This is believed to be the major mechanism for inter-ocean exchange south of Africa. However, the conditions governing the area of retroflection are poorly understood. The precise location of the Retroflection is variable and may, under extreme conditions, lie far upstream (Lutjeharms and van Ballegooyen, 1988b), thus preventing Indian Ocean water from even reaching the region south of Africa and contributing to inter-ocean exchange. The southern boundary of the Benguela Upwelling System can be considered as the Agulhas Retroflection area (Shannon and Nelson, 1996).

To the south, the large-scale circulation of the region is constrained by the Subtropical Convergence. This front lies at about 42°S (Lutjeharms, 1985) with a central temperature at the sea surface of 14°C. It forms the generic border to the Southern Ocean and its Antarctic Circumpolar Current (Fig. 2.4). It is characterised by extensive meridional meanders and a range of eddies (Lutjeharms and Valentine, 1988a), making it a most complex feature.

Based on investigations spanning a period of 10 years, it was shown that Agulhas rings may be present over the Agulhas Bank Slope about 12% of the time (Lutjeharms and Valentine, 1988b). Agulhas filaments, tendrils of warm surface water from the Agulhas Current (Lutjeharms and Cooper, 1996), also move across this location, since their preferred trajectories lie at the shelf edge (Fig. 2.3). Recent results have shown that such northward movement at this shelf edge may be interspersed by southward movement due to the presence of cyclonic (clockwise) eddies (Penven *et al.*, 2001). These eddies (Fig. 2.4) are thought to be lee eddies, driven by the Agulhas Current moving past the eastern side of the Agulhas Bank. Agulhas rings, Agulhas filaments and lee eddies are not the only complicating factors hindering the understanding of water mass movements in the region.

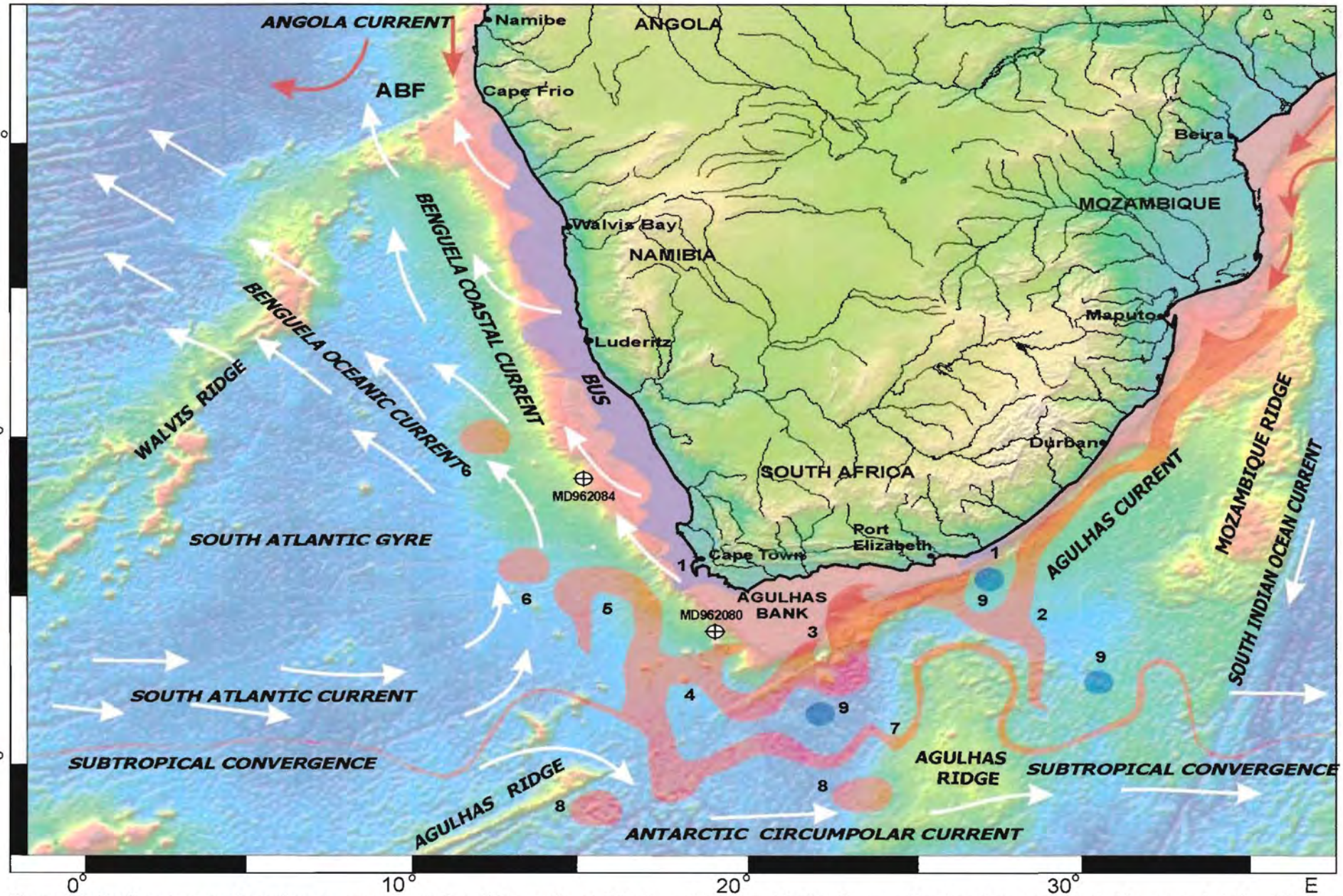

Figure 2.4: Seafloor topography and upper ocean circulation of the southeast Atlantic and southwest Indian Oceans. Core locations are indicated by crossed circles. The area is dominated by the Benguela and Agulhas Current systems. ABF = Angola Benguela Front; BUS = Benguela Upwelling System; 1 = coastal upwelling; 2= Natal Pulse; 3 = Agulhas filaments; 4 = Agulhas retroflection; 5 = ring formation; 6 = Agulhas ring; 7 = Agulhas Return Current; 8 = warm eddy; 9 = cold eddy. Refer to text for details. (After Smith and Sandwell, 1996; Lutjeharms, 1996; Shannon and Nelson, 1996; Wefer *et al.*, 1996).

During the formation of an Agulhas ring, northward penetration of Subantarctic Surface Water from south of the Subtropical Convergence has been observed between the Agulhas Retroflection and the newly formed ring (Lutjeharms and van Ballegooyen, 1988b). These intrusions (Fig. 2.4) may carry this cold water over the Agulhas Bank Slope (Shannon *et al.*, 1989), particularly if a cyclonic lee eddy is present. With a reduced frequency of ring formation, the incidence of penetrations of Subantarctic water into the region could also be decreased (Lutjeharms and Meyer, submitted). Which climatic changes could bring about reduced ring shedding is still largely a matter of speculation (Lutjeharms and de Ruijter, 1996).

There is great variability in spatial flow in the Agulhas Retroflection area. Seasonal, decadal and interannual changes in flux and themohaline characteristics determine the frequency, dimensions and the heat and salt content of Agulhas rings shed into the Southeast Atlantic Ocean (Valentine *et al.*, 1993). Local winds steer these intrusions by a complicated adjustment of the ocean pressure field, which is dependent on seasonal, annual and interannual variability in the westerly wind system south of Africa (van Ballegooyen *et al.*, 1994). Unpredictable episodic variability in the inner Benguela system occurs when rings move in the direction of the slope and shelf break along the eastern boundary.

Water on the Agulhas Bank is strongly stratified in summer, but less so in winter. Oxygen-depleted water occasionally occurs inshore on the Agulhas Bank (Shannon and Nelson, 1996). Seasonal changes in stratification on the Agulhas Bank are controlled by advection and insolation (Swart and Largier, 1987). The effect of periodicity in the longshore wind is critical. The modal structure of shelf waves depends on the frequency of wind acceleration and relaxation and shelf waves interact with upwelling. They are possibly also involved with the production of filaments (van Ballegooyen *et al.*, 1994). The seasonal behaviour of cross-coast winds is important from a biological aspect and depends on various factors including the albedo of the adjacent landmass, cloud cover and the longshore wind pattern, all of which vary interannually (Bailey and Chapman, 1991).

2.3.3 The Benguela System

Shannon and Nelson (1996) consider the Benguela region to be that part of the Southeast Atlantic lying between 14°S (southern Angola) and 37°S (tip of the Agulhas Bank) with the western boundary at the 0° meridian, thereby encompassing the coastal upwelling system, frontal jet and the eastern part of the South Atlantic Gyre. The Benguela Current is regarded as the eastern boundary current of the South Atlantic Gyre. The southern boundary of the Benguela system can be considered as the Agulhas Retroflection area (Shannon and Nelson, 1996). This definition is preferred to a definition based on coastal upwelling, as Schumann *et al.* (1982), amongst others, have shown that upwelling extends along much of the south coast of South Africa, as far as 25°S. East of 20°E the shelf break of the Agulhas Bank coincides with the edge of the Agulhas Current (Fig. 2.4), resulting in topographic steering of the current. In addition, there are marked changes in the wind field south of 37°S, with westerly winds predominating year-round. Thus, the southern boundary of the Benguela system is controlled by a combination of oceanographic, topographic, meteorological and biological factors (Shannon and Nelson, 1996). The Angola-Benguela Front (ABF) marks the northern boundary of the Benguela region. This surface frontal zone is most intense within 250 km of the coast and can be traced westward as far as 0°. The ABF is most marked in the upper 50 m of the water column, but can be identified to at least 200 m. This zone is a permanent feature, migrating seasonally between 14°S and 17°S. The ABF is maintained through a combination of factors including coastal orientation, bathymetry, stratification, wind stress and the opposing flow directions of the Benguela and Angola Currents (Jansen *et al.*, 1996).

The Benguela Current system comprises two different oceanographic regimes (Stramma and Petersen, 1989; Petersen and Stramma, 1991): the Benguela Coastal Current (BCC) that transports cold water from the wind-dominated coastal area equatorward and the Benguela Oceanic Current (BOC). The BOC is the most important element of meridional equatorward heat transport in the South Atlantic, transporting warmer waters northwards and westward by geostrophic flow (Fig. 2.4). The Benguela Current System comprises waters from a number of different sources: Occasional intrusions of Subantarctic surface waters from across the Subtropical Convergence northeast of the Agulhas Ridge (Shannon *et al.*, 1989); temperate surface waters derived from the South Atlantic Current near 40°S (Petersen and Stramma, 1991) and warm subtropical Indian Ocean surface waters via the Agulhas Current (Gordon *et al.*, 1992).

The general net poleward subsurface flow on the Benguela shelf is well established (De Decker, 1970; Nelson, 1989). The poleward undercurrent flows with varying strength and varying degrees of seasonal dependence. It is further identified by its low oxygen content. This, together with the poleward flow of NADW and AABW, as well as AAIW at least to 30°S, implies that the net flow of the bulk of the water column at the eastern boundary is polewards (Shannon and Nelson, 1996), with the exception of the surface water under the influence of wind and the shelf-edge jet. Only much further west, in the BOC, is the flow of the top 1500 m northward. The contribution of upwelled water to this northward flow is relatively small and decreases with depth. It may be that the 10-fold broadening of the shelf from the Cape Peninsula to the Agulhas Bank diffuses the poleward undercurrent, making it difficult to identify. There is also evidence that the current moves offshore into the Cape Point Valley (Shannon *et al.*, 1981).

2.3.3.1 The Upwelling Zones

The upwelling area of the BCC is fed from the thermocline by South Atlantic Central Water (SACW), which originates at the Subtropical-Subantarctic Front by the mixing and sinking of subtropical and Subantarctic surface waters (Lutjeharms and Valentine, 1987). Filaments of the cold, nutrient-rich upwelled water extend up to 600 km offshore (Lutjeharms and Stockton, 1987), where they mix with low-productivity oligotrophic waters forming a zone of intermediate productivity. Some of this intermediate water sinks below the mixed layer along the BCC-BOC convergence (Wefer *et al.*, 1996).

The location and characteristics of the main upwelling cells (Fig. 2.5) have been documented by numerous authors including Nelson and Hutchings (1983), Shannon (1985), Lutjeharms and Meeuwis (1987). Seven cells have been identified along the west coast (Fig. 2.5). The principal Lüderitz cell is semi-permanent, whilst the Columbine and Cape Peninsula cells are more seasonal than those within the central and northern Benguela (Shannon and Nelson, 1996). The upwelling cells are normally located near regions of cyclonic wind-stress curl and, in most cases, where there is a change in orientation of the coastline (Lutjeharms and Meeuwis, 1987). The typical westward extent of the upwelling, excluding major filaments, is between 150 and 250 km, this last figure being associated with the Lüderitz cell (Shannon and Nelson, 1996).

The Benguela upwelling system can be divided into two distinct regimes; the Southern Benguela Region (SBR) and the Northern Benguela Region. The boundary between the two regions lies south of the main Lüderitz upwelling zone, around 27°S (Giraudeau and Rogers, 1994). The differing effect of seasonal migration of the pressure systems is clearly evident in the northern and southern Benguela systems.

Figure 2.5: Main upwelling cells in the Benguela Upwelling System and along the south coast of South Africa. The southern Benguela cells are more seasonal than the northern Benguela cells. The south coast cells tend to be seasonal and ephemeral. (After Shannon and Nelson, 1996.)

The equatorward shift in the pressure systems in winter has a more pronounced effect in the SBR, where the frequency of westerly component winds (i.e. upwelling-unfavourable) is significant. The result is that wind-induced upwelling in the southern Benguela is highly seasonal, reaching a maximum in the spring-summer. North of 31°S (Hondeklip Bay), the macroscale wind field exhibits less seasonal variation, resulting in perennial upwelling.

However, there is still a spring-summer maximum and autumn minimum as far north as 25°S (Meob Bay). Although the winds off central and northern Namibia show relatively little seasonal variation, there are nonetheless slight maxima in upwelling-favourable conditions during April-May and October. An important modulation of upwelling in the southern Benguela is provided by wind relaxation or reversals, associated with the passage of cyclones south of the continent during the upwelling season (Nelson and Hutchings, 1983). Cells of low pressure, which form near Lüderitz and travel round the coast as trapped waves, are associated with the approach of cyclonic systems. The cyclonic rotation of air around these systems suppresses upwelling locally as the wave travels along the coast (Shannon and Nelson, 1996). Along the south coast of South Africa upwelling is more episodic and associated with capes such as Cape Agulhas (Schumann *et al.*, 1982, Lutjeharms and Meeuwis, 1987).

2.4 SURFICIAL SEDIMENTS

Ocean currents, offshore winds, river run-off and topography all influence the distribution of sediments on the continental slope. Rogers and Bremner (1991) identified three main classes of unconsolidated surficial sediments on the shelf and upper slope from the eastern Agulhas Bank to the Kunene River: terrigenous, biogenic and authigenic. Sources of terrigenous sediments are wind-blown dust particles and river outflow into the ocean. Biogenic sediments form from the flux of organisms (or their remains) from the surface waters to the seafloor, whilst remineralisation of certain components at the seafloor accounts for the authigenic deposits.

2.4.1 Regional Distribution of Dominant Components

The western continental margin is dominated by biogenic sedimentation, related to the high productivity of the upwelling system (Fig. 2.6a). The shelf deposits between the Olifants and the Orange Rivers comprise mainly terrigenous river-borne sediments and can be up to 40 km wide and 15 m thick (Birch *et al.*, 1976). The northern belt, which lies over the middle shelf between Conception Bay and Cape Frio, comprises organic-rich (>5% organic carbon) diatomaceous oozes. Foraminifera are the dominant biogenic component along the continental margin of southwestern Africa and planktonic foraminifera predominate seaward of the middle shelf (Rogers and Bremner, 1991).

Although authigenic sediments (comprising mostly glauconite and phosphorite) do occur on the eastern Agulhas Bank, they are more prominent under the Benguela Upwelling System (Fig. 2.6a). In general these sediments are found along the middle and outer shelves in the zones where foraminiferal oozes lie below the shelf break (Rogers and Bremner, 1991).

Terrigenous sediment is restricted to the inner and middle shelves on the western margin (Fig. 2.6a) and is mainly related to river input (Rogers and Bremner, 1991). The high input of terrigenous sediment onto the wave-dominated submarine Orange Delta is redistributed parallel to the coastline. Littoral drift, resulting from southwesterly swells (De Decker, 1988) transports gravel and sand northwards, while south of the Orange River the mud fraction is transported in suspension over the mud belt by the poleward undercurrent (De Decker, 1970; Nelson, 1985). Aeolian transport of terrigenous dust offshore is most dominant off the arid Namibian coast. Numerous plumes are visible on satellite imagery (Shannon and Anderson, 1982; Rogers and Bremner, 1991).

The Agulhas Bank is dominated by biogenic sediments (Fig. 2.6a) However, there is a clear distinction between shelly sediments on the eastern Agulhas Bank and foraminiferal oozes on the western Agulhas Bank (Fig. 2.6a), marking the southern sedimentological boundary of the Benguela ecosystem (Rogers and Bremner, 1991). The northern sedimentological boundary is marked by the biogenic foraminiferal ooze on the Walvis shelf and terrigenous quartzose sediment on the Kunne shelf (Fig.2.5a). These sedimentological boundaries coincide with the physical oceanographic boundaries, defined by Shannon (1985) and Shannon and Nelson (1996) as the Agulhas Bank Divide and the Angola Benguela Front, respectively. On the Agulhas Bank, a terrigenous mud belt along the inner-middle shelf is diverted southwards (Fig. 2.6a) by the westward-widening pre-Mesozoic inner-shelf outcrop flanking the western Agulhas Bank (Rogers and Bremner, 1991). The inner-shelf wedge of Holocene terrigenous sediment thins rapidly seawards to a thin (<2 m) veneer on the middle shelf. Palaeovalleys are found at the mouths of the Breede and Gouritz Rivers, testifying to periods of downcutting when the sea level was lowered by up to 130 m at the last glacial maximum (Rogers and Bremner, 1991). For most of the Quaternary, however, sea-level never dropped low (below –50 m) enough to expose large portions of the Agulhas Bank (van Andel, 1989).

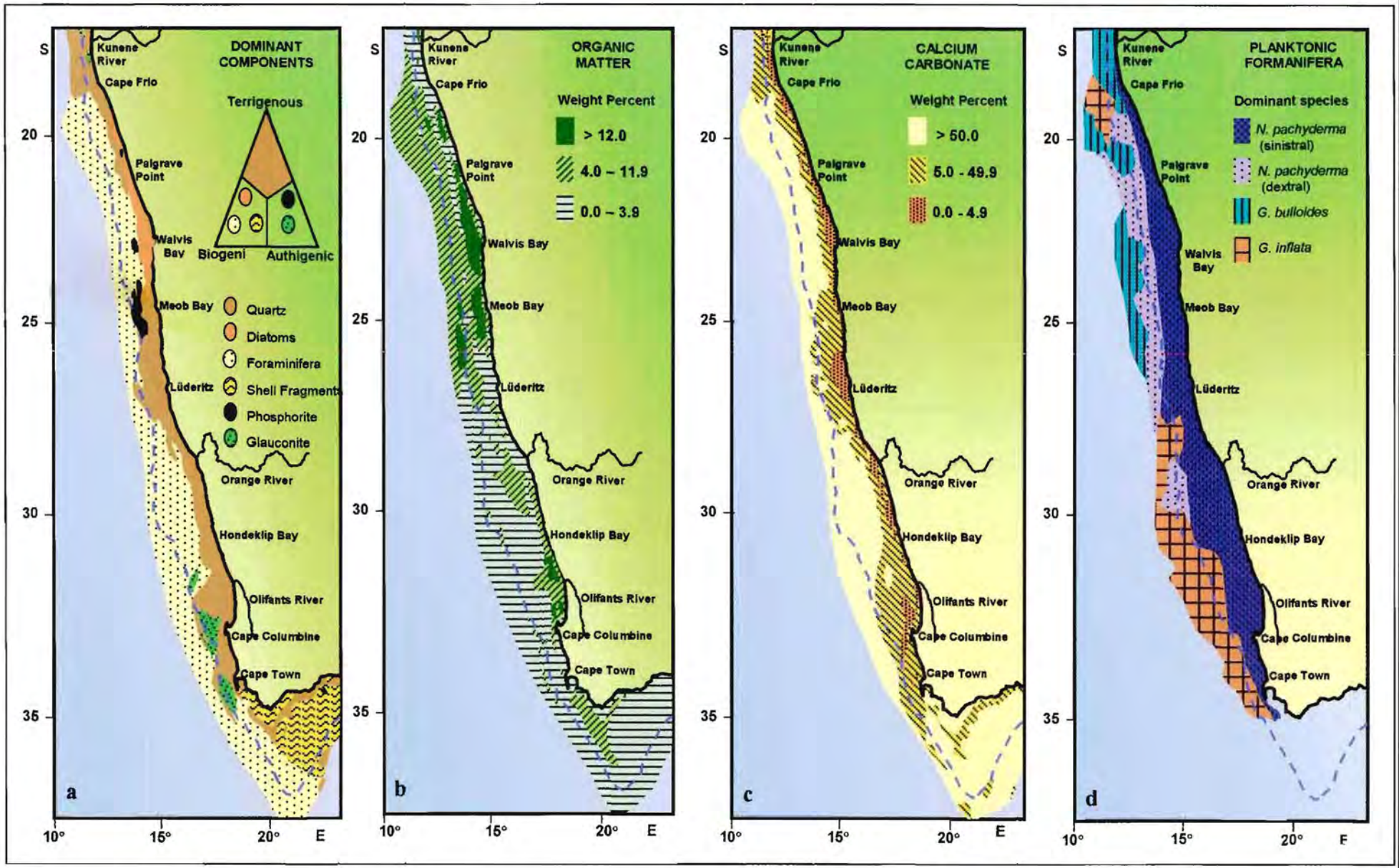

Figure 2.5: Regional distribution of surficial sediment components. (a) Dominant Components, (b) Organic Matter, (c) Calcium Carbonate and (d) Planktonic foraminifera. A dashed blue line represents the 500 m isobath. After Rogers and Bremner (1991), (a.b.c) and (d) after Giraudeau (1993). Little *et al.* (1997) and Ufkes *et al.* (2000).

2.4.2 Organic Matter

The Agulhas Bank Divide is marked by low concentrations of organic matter (<1%) on the eastern Agulhas Bank and moderate concentrations on the western Agulhas Bank (Birch and Rogers, 1973; Birch *et al.*, 1986; Rogers and Bremner, 1991). Sediments on the Agulhas Bank Slope are characterised by low organic matter content (Fig. 2.6b). The inner and middle shelves from the western Agulhas Bank to Lüderitz are characterised by coast-parallel belts of organic-rich sediments (Fig. 2.6b). However, the organic-rich belt between Cape Columbine and the Orange River coincides with the terrigenous mud belt (Rogers and Bremner, 1991). High concentrations of organic matter, beneath a relatively stagnant gyre, lead to two zones of oxygen-deficient bottom waters in the southern Benguela; north of St Helena Bay and off the Orange River. The sediments off the Orange River are, however, strongly diluted by terrigenous material delivered by summer floods. The poleward increase in organic matter south of the Orange River is parallelled by an increase in benthic faecal pellets, which is intimately associated with the distribution of both mud and organic matter (Rogers and Bremner, 1991). There is a similar increase seawards off the Orange River. Both increasing trends are partly ascribed to less dilution by terrigenous material with increasing distance from the Orange River mouth. The relative lack of organic matter and benthic faecal pellets in the central Benguela (the perennial Lüderitz upwelling area) is attributed to vigorous upwelling over the narrow shelf (Rogers and Bremner, 1991).

The sediments beneath the northern Benguela ecosystem are considered to be some of the most organic-rich sediments in the Atlantic Ocean with concentrations reaching up to 28.9% (Rogers and Bremner, 1991). High concentrations of organic matter are found across most of the shelf and along the slope between Lüderitz and the Kunene River (Fig. 2.6b). A 50-km-wide elongated deposit of unconsolidated diatomaceous ooze lies on the inner shelf off Walvis Bay and stretches coast-parallel for 500 km from Palgrave Point to Meob Bay (Bremner, 1981b). Benthic faecal pellets are rare and often absent in the highly organic-rich diatomaceaous ooze off Walvis Bay, probably because the dysaerobic conditions discourage the presence of burrowing infauna. The abrupt southern termination of organic-rich sediment containing faecal pellets coincides with the poleward extent of oxygen-deficient waters described by Chapman and Shannon (1985) stretching from the oxygen minimum north of the Walvis Ridge to Lüderitz (Rogers and Bremner, 1991).

2.4.3 Calcareous Components

Calcareous biogenic sedimentation has occurred on the outer shelf and the slope beneath the Benguela Ecosystem since the Late Tertiary (Siesser, 1972). The Agulhas Bank Divide is not identified by this component, because the characteristic compoents on either side of the Divide, molluscan fragments on the eastern Agulhas Bank and planktonic foraminifera on the western Agulhas Bank, are both calcareous. A belt of low-carbonate sediments crosses the inshore section of the Agulhas Bank (Fig. 2.6c). Rogers (1971) attributes the diminished values to dilution by terrigenous sediments from Holocene and Pleistocene rivers.

The Cape Peninsula and Cape Columbine upwelling cells bring cold water to the surface landward of an oceanic front associated with a shelf-edge jet (Shannon, 1985). These conditions push stenothermal planktonic foraminifera beyond the shelf break and over the slope, resulting in low-carbonate sedimentation on the inner shelf south of Hondeklip Bay (Rogers and Bremner, 1991).

Neither terrigenous input from the Orange River, nor the seasonal Namaqua upwelling cell seem to have any dilution effect on the foraminiferal ooze on the Orange Shelf (Fig. 2.6c).

The Lüderitz upwelling cell in the central Benguela has the most dramatic effect on the distribution of the foraminiferal ooze. This is the largest area of very low carbonate values (<5%). As there is no terrigenous input at this location, adjacent to the arid Namib Desert, only the vigorous upwelling can account for the marked seaward shift in the landward boundary of the foraminiferal ooze (Rogers and Bremner, 1991).

The northern boundary of the Benguela System at the ABF is clearly identifiable (Fig. 2.6c) as the foraminiferal ooze dominating the Benguela sediments is replaced equatorwards by terrigenous sediment on the Kunene shelf, derived from the Kunene River (Rogers and Bremner, 1991).

CHAPTER 3: THE CORES:- SAMPLING, DESCRIPTION and OXYGEN ISOTOPE STRATIGRAPHY

This chapter deals with the material and methods used in this research. Sampling methods and brief visual descriptions of the cores are presented. Before data can be interpreted to any degree, age-determination of the sediments is required. Oxygen isotope ratios provide the stratigraphic framework from which age-models are created. Varying sedimentation rates at each of the core sites are discussed.

3.1 INTRODUCTION

The IMAGES programme was initiated to increase understanding of Quaternary palaeoceanography and climate through the study of long marine sediment cores. Central to any palaeoclimatic study is the determination of an age model. The use oxygen of isotope ratios of foraminiferal tests to determine stratigraphy in sediment cores is a standard technique widely employed in the field of palaeoceanography. Alternate methods include ^{14}C and $^{230}Th/^{234}Th$ for younger records, biostratigraphy for low-resolution studies and magnetostratigraphy in older records. Each of these techniques has its own associated constraints. I have adopted the isotope stratigraphy approach as it is best suited to the nature of the material used in this research and because it allows comparison with related studies.

3.2 THE CORES

3.2.1 Core Descriptions

3.2.1.1 Core MD962080 (Agulhas Bank Slope)

This 22 m-long core, taken in a depth of 2488 m on the western slope of the Agulhas Bank is the most southerly of the NAUSICAA cores (Figure 1.3, pg. 1-6). Figure 3.1 is a schematic representation of Core MD962080. The core is slightly disturbed at the top and from 5 - 5.5 m. The lithology comprises interbedded watery, light yellowish brown foram ooze to light grey foram-bearing ooze to grey nanno ooze, which alternate in decimetre-thick sequences (10 - 70 cm). The contacts are mostly sharp, but still gradational contacts. Some bioturbation is seen in the finer-grained nanno-oozes between 1340 and 1380 cm. The more massive foram oozes are

characteried by a low mud fraction, giving rise to a watery consistency, which increases with increasing foram content. Siliceous sponge spicules and radiolaria are present. Other biosilica skeletons are rare in both lithologies. Minor amounts of sand-size detrital grains of quartz, mica and pelletal glauconite are present (Bertrand *et al.*, 1997; Rogers, 1999; Rau *et al.*, 2002). Core loss occurred from 748 to 765 cm and 946 to 955 cm, so no samples were taken at 750-751 cm, 760-761 cm and 950-951 cm. No sub-bottom profile was available for this core site. Thus, as there is no direct evidence available from visual observation, the core logs and descriptions (Bertrand et al., 1997; Rogers, 1999) and oxygen isotope profiles, it is assumed that there was no downslope transport of material from higher up on the slope.

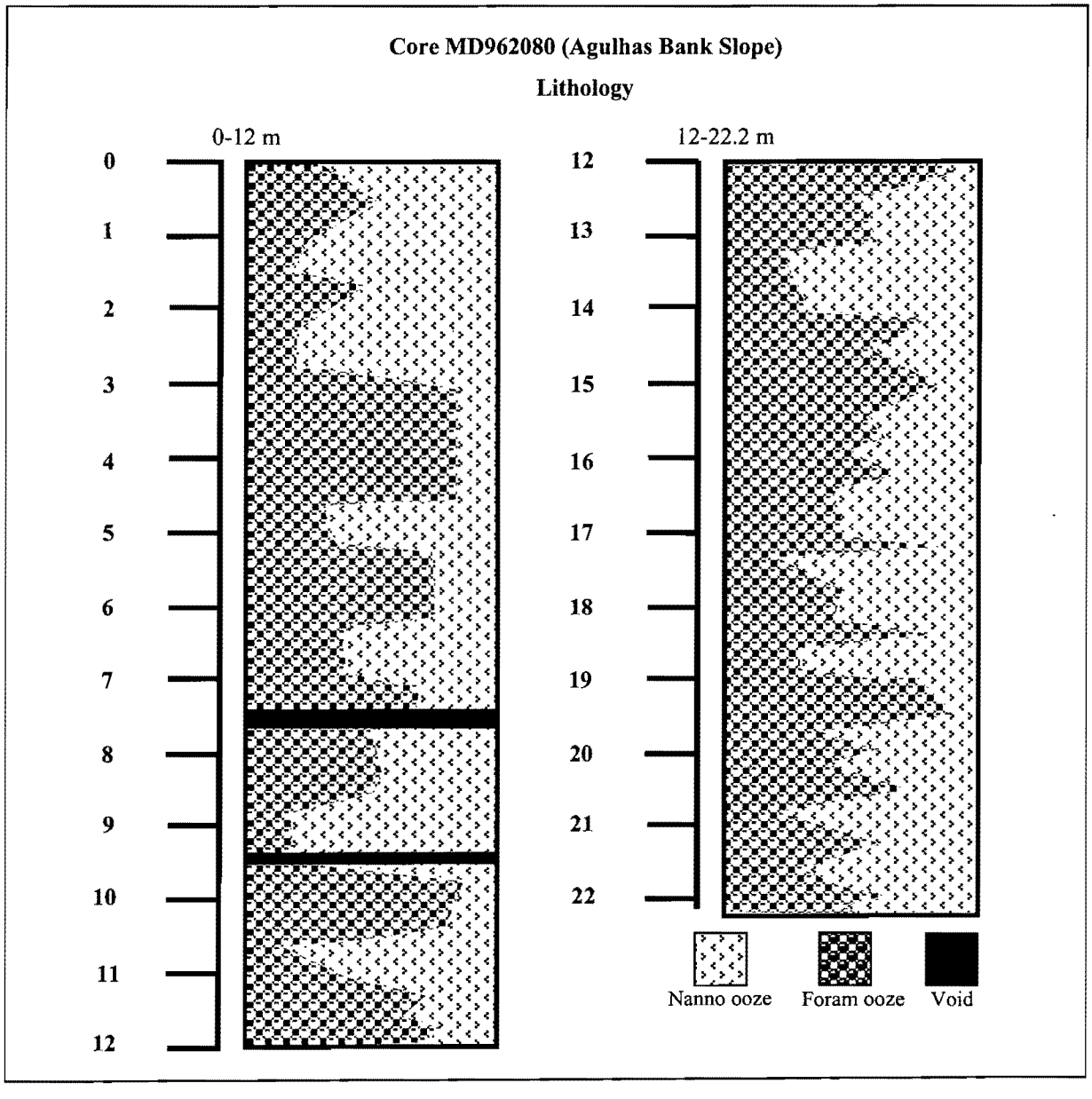

Figure 3.1: Semi-quantiative schematic representation of the main lithologies of core MD962080, based on on-board smear-slide examinations. (After Bertrand *et al.*, 1997).

3.2.1.2 Core MD962084 (Oliphants River Slope)

This 35 m-long core, taken in a depth of 1408 m on the Olifants River Slope, comprises interbedded light grey to dark olive grey watery foram nanno oozes and finer-grained nanno foram oozes (Fig. 3.2). The contacts are mostly gradational. Detrital quartz silt and sand are present only in trace amounts amounts. A foram nanno ooze mud-flow occurs between 220 and 250 cm (Bertrand *et al.*, 1997; Rogers, 1999). The lower section (28 - 35 m) of the core is a finer-grained, silty nanno ooze, with a distinctly firmer, more cohesive texture, than in the upper parts of the core. The lower 4 m of the core are disturbed and the core split length-wise from 31.5m to the bottom. Samples were analysed down to 30 m. Core loss between 569 and 585 cm prevented samples being taken at 570-571 and 580-581 cm (Fig. 3.2).

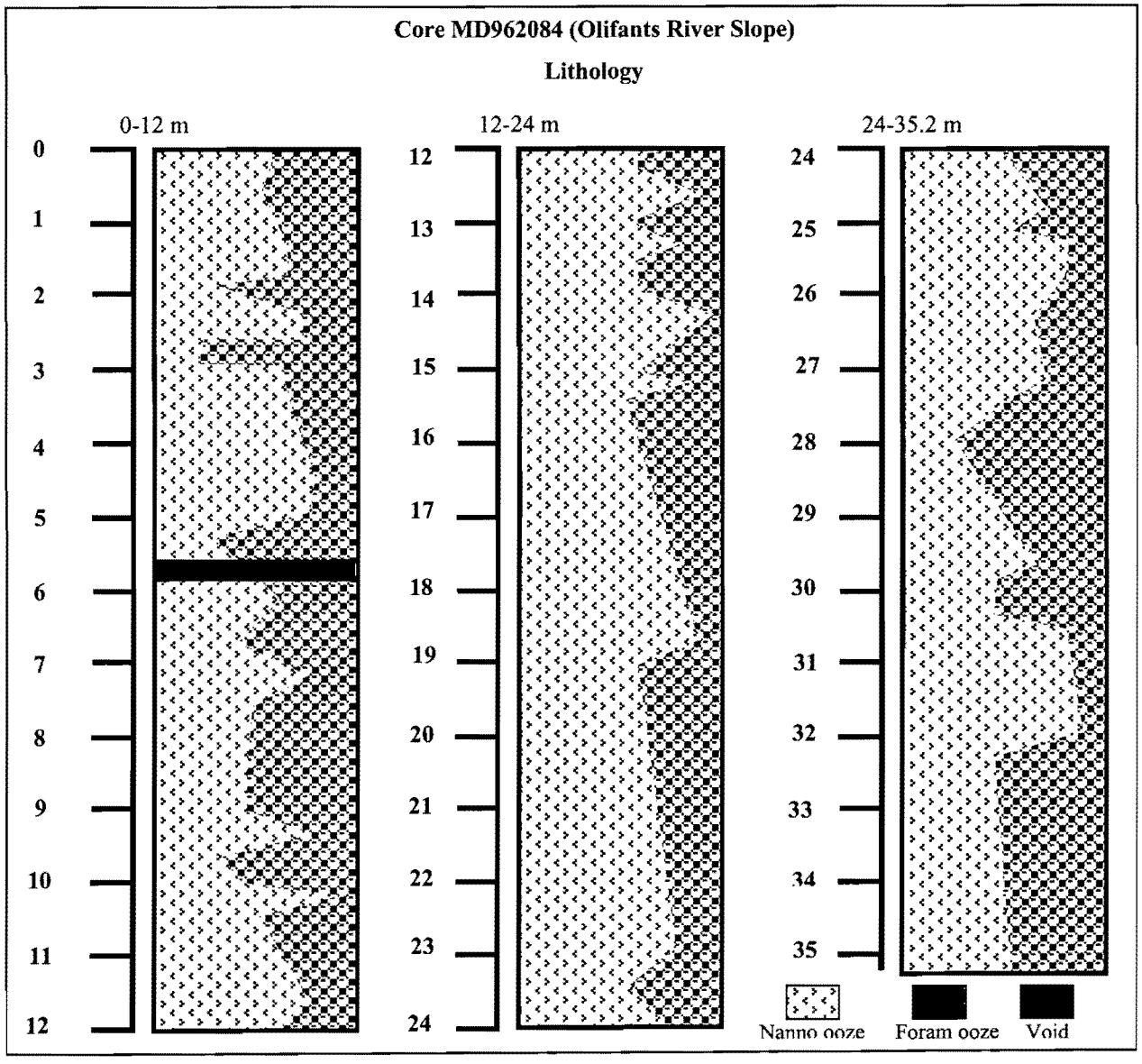

Figure 3.2: Semi-quantiative schematic representation of the main lithologies of core MD962084, based on on-board smear-slide examinations. (After Bertrand *et al.*, 1997).

Examination of the sub-bottom profile for this site and the undisturbed nature of this core (ascertained from visual observation, core logs and descriptions (Bertrand et al., 1997; Rogers, 1999) and oxygen isotope profiles, led to the assumption that there was no downslope transport of material from higher up on the slope.

3.2.3 Core Retrieval and Shipboard Analysis

Cores MD962080 and MD962084 were retrieved from the western Agulhas Bank Slope (36°19'S, 19°28'E, 2488m) and the Olifants River Slope (31°44.5'S, 15°31'E, 1408m) repsectively (Fig. 1.3, p 1-6), using a giant *Calypso* piston corer. The cores were collected during the IMAGES II-NAUSICAA cruise of the *Marion Dufresne* in October-November 1996. The cores were cut into 1.5 m lengths, capped and sealed, before non-destructive, whole core multi-sensor track (MST) measurements of P-wave velocity, density (via gamma-ray attenuation) and magnetic susceptibility were made at 2 cm intervals (Bertrand *et al.*, 1997; Rogers, 1999). Each section was then split lengthwise into an archive and a working half. Spectral reflectance, using 16 different wavelengths between 400 and 700 nm was recorded at 5 cm intervals. Density data collected onboard are used to calculate bulk mass accumulation rates (section 3.3). Spectral reflectance is compared to carbonate content and discussed in Chapter 5. Representative subsamples were taken for smear-slide analysis under a binocular microscope and nannofossils in samples from the end of each 1.5 m section were examined. An age estimate was made for the base of each core. All data were then used to compile a log for each core (Bertrand *et al.*, 1997).

3.2.4 Sampling Methods

Both the working and archive halves of the split cores are stored at 4°C in the refrigerated store room in the basement of the Département de Géologie et Océanographie, Université de Bordeaux I, France. The working halves of cores MD962080 and MD962084 were sampled at 10 cm intervals in Bordeaux, in October 1997 by myself and Dr J. Rogers. Each 1 cm-thick slice was cut with an aluminium sample tool shaped and sized to fit the split core and was then placed in a plastic minigrip bag and sealed. The samples were shipped to South Africa and arrived in Cape Town in December 1997. They were freeze-dried, then subdivided into 3 subsamples for (1) sedimentological analysis; (2) stable light isotope determination (bulk nitrogen and organic carbon) and (3) planktonic foraminiferal census counts and oxygen and carbon isotope

determinations on benthic and planktonic foraminifera. Each separate, freeze-dried subsample was weighed to obtain the total mass before any analysis was undertaken.

3.3 STABLE OXYGEN ISOTOPE STRATIGRAPHY

3.3.1 Overview

Oxygen isotope ratios of foraminiferal tests from deep-sea sediment cores have been used as indicators of past climate change since the pioneering work of Emiliani (1955). Oxygen isotopes of foraminiferal tests primarily reflect changes in ocean temperature, whilst the $\delta^{18}O$ of the ocean reflects salinity, which varies in relation to the amount of locked in the ice caps (Wefer et al., 1999). The study of Pleistocene oxygen isotope ratios has been used to estimate changes in Northern Hemisphere glaciation (Shackleton, 1967). $H_2{}^{16}O$ is preferentially locked into continental ice sheets, resulting in ^{18}O enrichment of sea water during glacial periods. The oxygen isotope ratio in foraminifera varies with the $\delta^{18}O$ of the water in which their tests are deposited and differs from the water by an amount dependent on the temperature of calcification (Chappell and Shackleton, 1986). In addition to ice volume effects, numerous factors can influence the depth variation of $\delta^{18}O$ of foraminifera in sediment cores, including local temperature, evaporation, bioturbation, variations in sedimentation rate and vital effects (Bolton *et al.*, 1995). These factors and differing water compositions (which vary both spatially and temporally) contribute to $\delta^{18}O$ differences between cores. The use of deep-water benthic foraminifera for isotope stratigraphy is generally preferred since their isotopic signal primarily reflects global ice-volume change as temperatures of deep water masses are thought to have changed very little throughout the Quaternary (Chappell and Shackelton, 1986). In planktonic foraminifera $\delta^{18}O$ in is more likely to be affected by local changes (surface salinity, temperature, seasonal depth habitat). The glacial to post-glacial change in $\delta^{18}O$ of the benthic foraminifera is on average slightly greater than 1‰. Approximately two thirds of the $\delta^{18}O$ signal in $CaCO_3$ is related to ice volume and about one third reflects temperature change (Wefer *et al.*, 1999).

Pisias *et al.*, (1984) correlated and stacked seven globally representative benthic-foraminiferal oxygen isotope records to construct a "standard" stratigraphy for deep-sea sediments spanning the last 300,000 years. The more commonly used SPECMAP stack (Imbrie et al., 1984) was constructed from the isotope measurements of shallow-dwelling planktonic foraminifera in five deep-sea cores at widely distributed open-ocean sites in low and mid-latitudes. The $\delta^{18}O$ data

were used to develop a timescale for the past 780 kyr. Bassinot *et al.* (1994b) refined this model particularly for ages below MIS 16 and this curve is now accepted as a more accurate measure for older records.

The correlation of individual $\delta^{18}O$ records to a globally representative record is obviously not a trivial procedure. There is a certain amount of subjectivity in this approach and consequently in determining the final age model, which is prone to errors.

3.3.2 Methods

Specimens of the benthic foraminifer *Cibicidoides* (previously called *Planulina* or *Cibicides,*recently referred to as *Fontbotia) wuellerstorfi* were picked from the whole >125 μm fraction by Dr Jacques Giraudeau for the top 14m of core MD962080. Following the standard procedures of Laboratoire des Sciences du Climat et de l'Environnement, Gif-sur-Yvette, all specimens in each sample were picked (usually 3-4 specimens, but in some samples only 1 specimen was found). The specimens were cleaned in methanol and ultrasonicated for 3 - 5 seconds to remove adhering silt-size coccoliths and other small particles. The cleaned specimens were then roasted under vacuum in a small oven at 400° C to burn off any organic matter. The isotopic composition of the foraminifera is measured from the CO_2 released when the calcareous foraminiferal test is treated with dehydrated phosphoric acid at a constant temperature of 90°C. This procedure was undertaken using a Kiel automated carbonate device coupled to a Finnigan MAT251 mass-spectrometer. The mean reproducibility of the benthic measurements is 0.05‰.

Sixty specimens of the planktonic foraminifera *Globorotalia inflata* were picked from the 250-350μm size fraction for all samples in both cores in Cape Town. Samples from core MD962080 were sent to the Centre for Ocean Research, National Taiwan University for analysis, whilst samples from core MD962084 were analysed at the Fachbereich Geowissenschaften, Universität Bremen. The standard laboratory procedures were followed at each institution. In Taiwan, the picked specimens were cleaned twice by ultrasonic vibration for 10-15 seconds to remove adhering fine particles. Samples were then treated with NaClO at room temperature for 24 hours to remove organic matter. The isotopic ratios were determined using a Finnegan Delta Plus mass spectrometer with a Kiel automated carbonate device. Average values from the screened duplicate or triplicate results were calculated and reported. According to standard practice in the Universität Bremen laboratory samples do not undergo any pre-treatment. The standard gasses

used in the determination of oxygen isotope ratios are calibrated against the National Bureau of Standards carbonate standard NBS19 (Hut, 1987; Coplen, 1988). A precision of 0.08‰ for $\delta^{18}O$ measurements of the calcite standards was achieved. As per convention, isotope ratios are reported relative to the international standard, Vienna Pee Dee Belemnite (VPDB), using the δ notation:

$$\delta^{18}O = [(^{18}O/^{16}O)_{sample}/(^{18}O/^{16}O)_{standard} - 1] \text{ per mil;}$$

3.3.3 Age Models

3.3.3.1 Core MD962080 (Agulhas Bank Slope)

Stratigraphy for core MD962080 is based on the oxygen isotope record of the benthic foraminifer *Cibicides wuellerstorfi* (Fig. 3.3). The isotope curve was compared to the SPECMAP stack (Imbrie *et al.*, 1984) and the curve derived by Bassinot *et al.* (1994b) for periods beyond MIS 15. Thirty significant peaks were correlated and provided the age-control points for the top 14 m of the core. Minima and maxima in $\delta^{18}O$ were chosen rather than isotopic stage boundaries. Oxygen isotope ratios of the planktonic foraminifer *Globorotalia inflata* were compared to the benthic data and provide a second stratigraphic control. Sedimentation rates were calculated between the age-control points and ages were then linearly interpolated to achieve a final age model.

The oxygen isotope records show typical glacial-interglacial (G-IG) fluctuations. The lowest $\delta^{18}O$ values were measured during marine isotope events 5.5, 9.3 and 11.3. These are the warmest periods in the Late Pleistocene. The highest value of +4.38‰ defines Marine Isotope Stage (MIS) 16 as the period of greatest ice volume and probably the coldest period in the record. MIS 6, 10 and 18 record the next highest $\delta^{18}O$ values. There is a strong degree of agreement between the two records, although the surface-water (planktonic) record registers increased $\delta^{18}O$ values in MIS 12 with no co-incident increase in the benthic record. It is generally assumed that the oxygen isotope signature of benthic foraminifera records the global ocean signature, primarily that of ice volume changes, whilst planktonic foraminifera are more influenced by local and regional changes, including temperature (Wefer *et al.*, 1999).

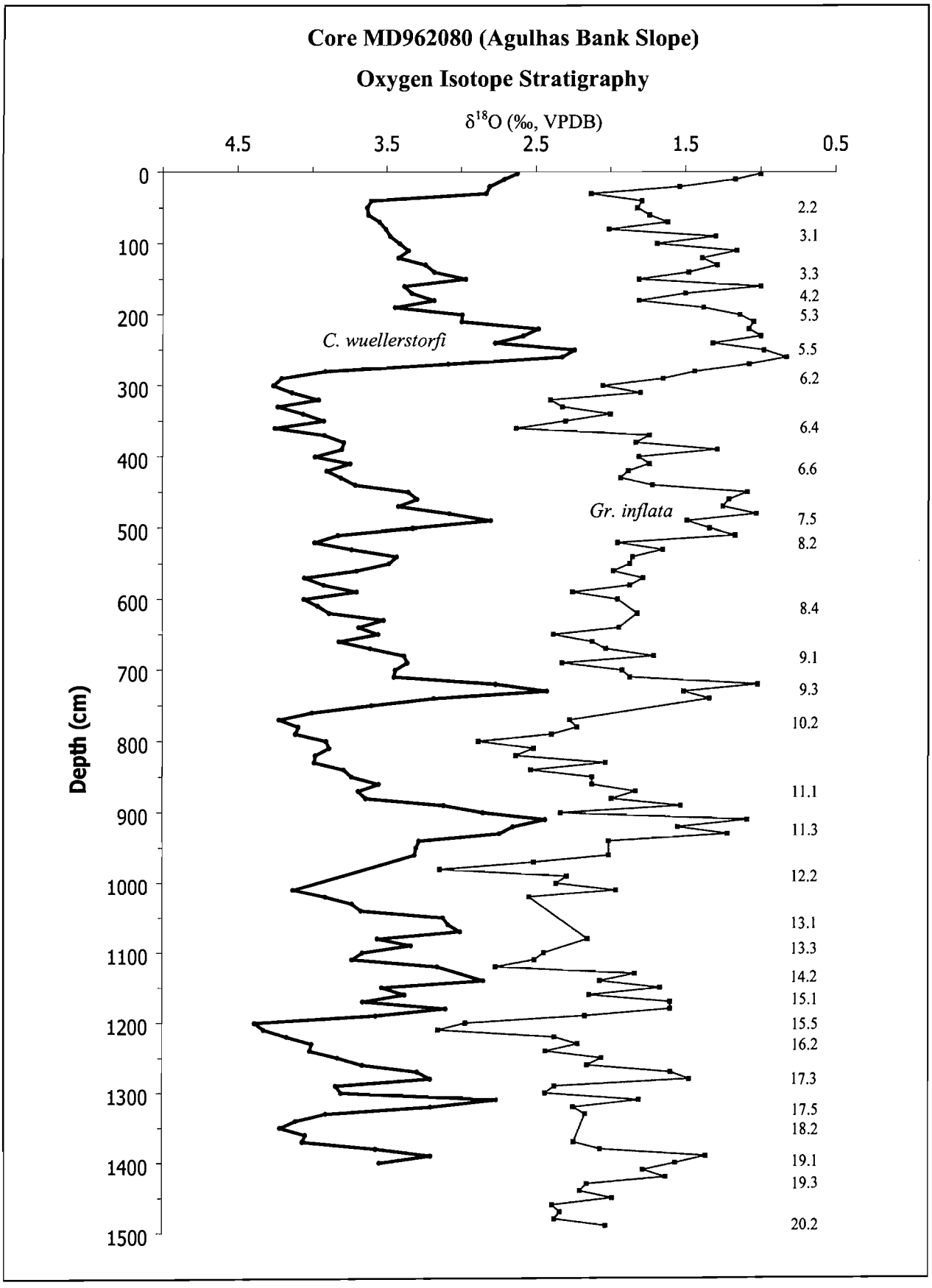

Figure 3.3: Oxygen isotope ($\delta^{18}O$) depth profile for the benthic foraminifer *Cibicidoides wuellerstorfi* (left) and the planktonic foraminifer *Globorotalia inflata* (right) for core MD962080. Age control points (marine isotope events) are shown to right of profiles.

In core MD962080 the planktonic record leads the benthic record at most glacial terminations. This is consistent with research (e.g. Blunier *et al.*, 1998) which suggests that G-IG changes in the Northern Hemisphere lagged changes in the Southern Hemisphere, as the benthic record generally reflects the global signal and the planktonic record is more influenced by local changes. By comparing Antarctic and Greenland ice-core records, Blunier *et al.* (1998) showed that on average Antarctic climate change leads that of Greenland by 1–2.5 kyr for the period 47-23 kyr B.P.

3.3.3.2 Core MD962084 (Oliphants River Slope)

As a result of the very low occurrence of the benthic foraminiferal species *Cibicidoides wuellerstorfi*, a lack of training in identifying the correct species and due to time constraints, I did not attempt to pick this species for isotope stratigraphy. Instead, at the suggestion of Dr Giraudeau, the oxygen isotope record of the planktonic foraminifer *Globorotalia inflata* from core MD962084 (Fig. 3.4b) was compared with that from nearby ODP site 1087, hole 1087A, (Fig. 1.3, pg. 1-6) for which there was an established age model (Pierre *et al.*, 2001) based on the $\delta^{18}O$ record of the benthic foraminifer *C. wuellerstorfi* (Fig.3.4a). The ODP site lies at a depth of 1371m, 16 minutes of latitude north and 12 minutes of longitude west of the MD962084 site and was considered to be close enough to provide a compatible age model. Twenty isotope events were identified in the *C. wuellerstorfi* record and provided the age-control points for the time framework (Pierre *et al*, 2001). Thirty-three significant peaks in the *Gr. inflata* record of core MD962084 were correlated to the ODP Site 1087 record, the SPECMAP stack and the curve of Bassinot *et al.* (1994b). Sedimentation rates were calculated between those time-points and ages were then linearly interpolated to achieve a final age model. Once age models had been determined it was decided to undertake further analysis to a common age. Thus, the top 15 m of core MD962080, and the top 30 m of core MD962084 were studied.

Periods of least ice volume are indicated by low $\delta^{18}O$ values in MIS 11, 9 and 5. Decreased planktonic $\delta^{18}O$ values reflect ice sheet reduction as well as warming in the Holocene. The highest value of +4.27‰ shown in the benthic record of ODP Site 1087 occurs in MIS 12, whilst stages 20, 16 and 12 are indicated as periods of increased ice volume and associated lower temperatures by the planktonic record of core MD962084. Figure 3.5 shows the "goodness of fit" between the age-corrected isotope records and the standard curves.

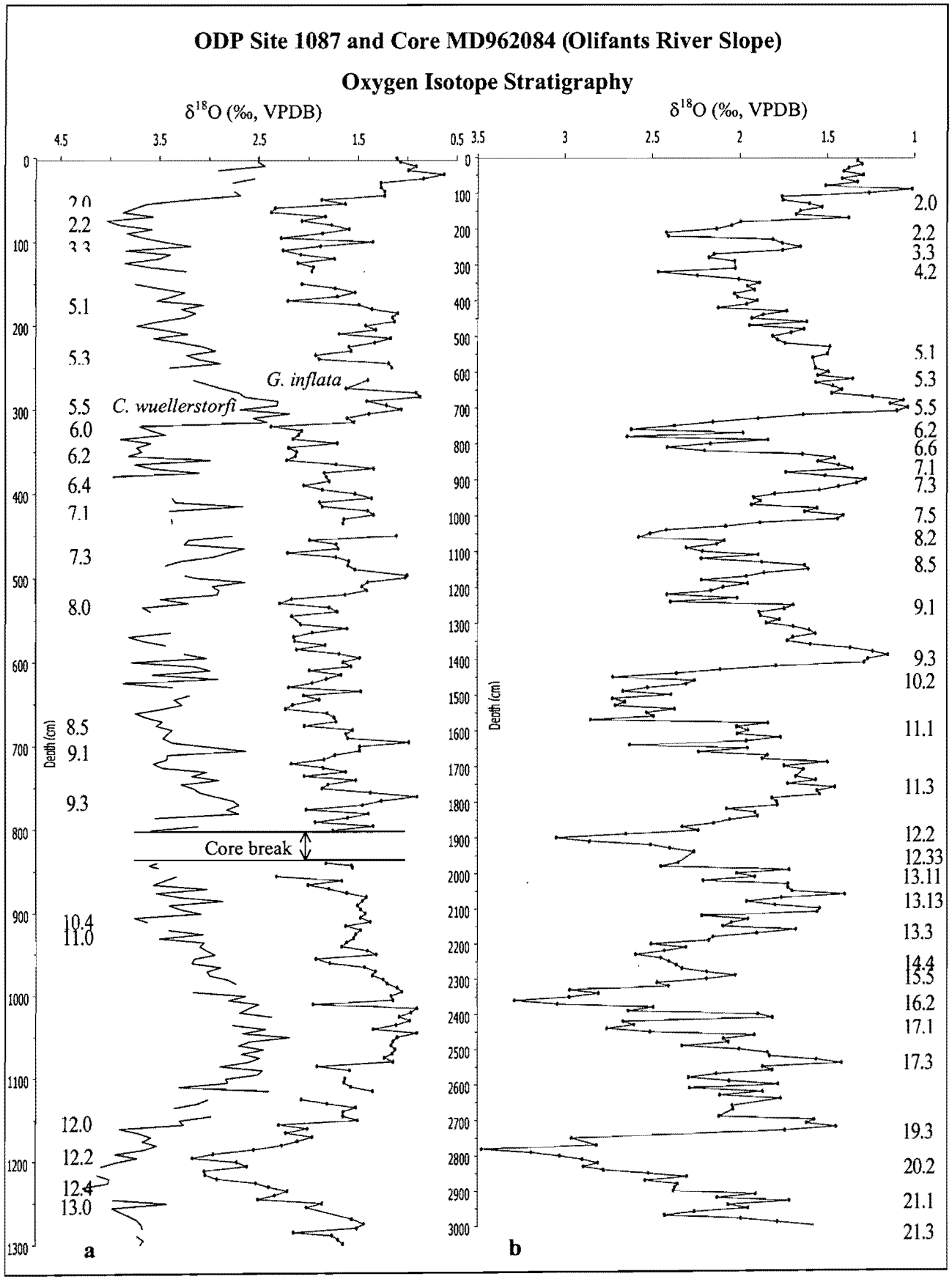

Figure 3.4: Oxygen isotope ($\delta^{18}O$) depth profiles for (a) the benthic foraminifer *Cibicidoides wuellerstorfi* (left) and the planktonic foraminifer *Globorotalia inflata* (right) for ODP Site 1087 Hole A (Pierre *et al*, 2001) and (b) the planktonic foraminifer *Globorotalia inflata* for core MD962084. Age control points (marine isotope events) for ODP Site 1087 and core MD962084 are shown to left and right of profiles, respectively.

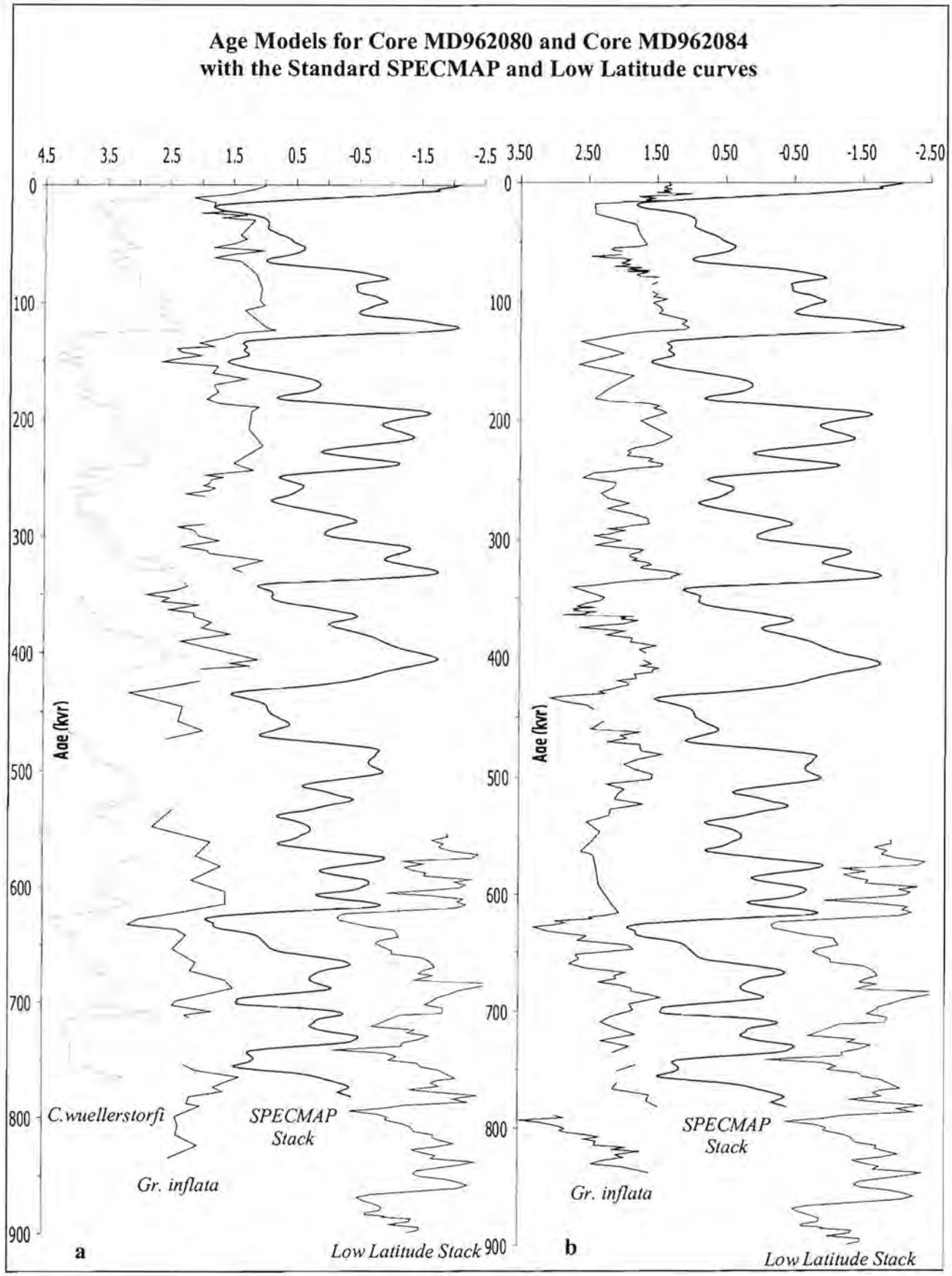

Figure 3.5: Oxygen isotope ($\delta^{18}O$) age models for (a) core MD962080 and (b) core MD962084.plotted together with the standard SPECMAP Stack (Imbrie *et al.*, 1984) and Low Latitude Stack (Bassinot *et al.*, 1994) to the right of the $\delta^{18}O$ profiles.

3.3.4 Sedimention and Bulk Mass Accumulation Rates

3.3.4.1 Core MD962080 (Agulhas Bank Slope)

The bulk mass accumulation rate (BMAR) was calculated using the sedimentation rate according to the formula:

$$BMAR = SR*DBD$$

Where SR (cm/kyr) = sedimentation rate

DBD (g/cm^3) = dry bulk density = 2.65* (GRAPE-1)/(2.65-1)

GRAPE (g/cm^3) = gamma ray attenuation

Sedimentation rates for core MD962080 range between 0.56 and 5.5 cm/kyr with an average of 2.35 cm/kyr for the last 835 kyr (Fig 3.6a). During the Pleistocene, sedimentation rates on the Agulhas Bank Slope fell within or below the average marine range of 2-3 cm/kyr (Gorgas and Wilkens, 2002), with a few exceptions around 730, 250 and 150 kyr B.P, where higher rates are recorded.

3.3.4.2 Core MD962084 (Olifants River Slope)

Sedimentation rates for core MD962084 range between 0.8 and 15.4 cm/kyr with an average of 5.4 cm/kyr for the last 835 kyr (Fig. 3.6b). Sedimentation rates on the Olifants River Slope (mean = 5.4 cm/kyr) are considerably higher than on the Agulhas Bank Slope (mean = 2.35 cm/kyr) for the period under investigation. Nonetheless, they are much lower than sedimentation rates in the Northern Benguela Region (Lüderitz cell mean = 15cm/kyr) and in the Angola Basin, where rates of up to 60 cm/kyr have been measured (Berger *et al.*, 2001). In general, sedimentation rates at the site of core MD962084 are greater than average marine sedimentation rates (~2-3 cm/kyr) (Gorgas and Wilkens, 2002), except for a few periods of very low sedimentation at around 550-600, 150, and 20-50 kyr B.P. (Fig 3.6b). Periods of distinctly high sedimentation rates (>10 cm/kyr) occurred around 350, 90 and 20 kyr B.P. The sedimentation rates were used to extrapolate the bulk mass accumulation rate (BMAR).

The BMAR records for both cores (Figs 3.7a & b) show that, in general, sediment accumulated at much higher rates during glacial intervals than during interglacial periods.

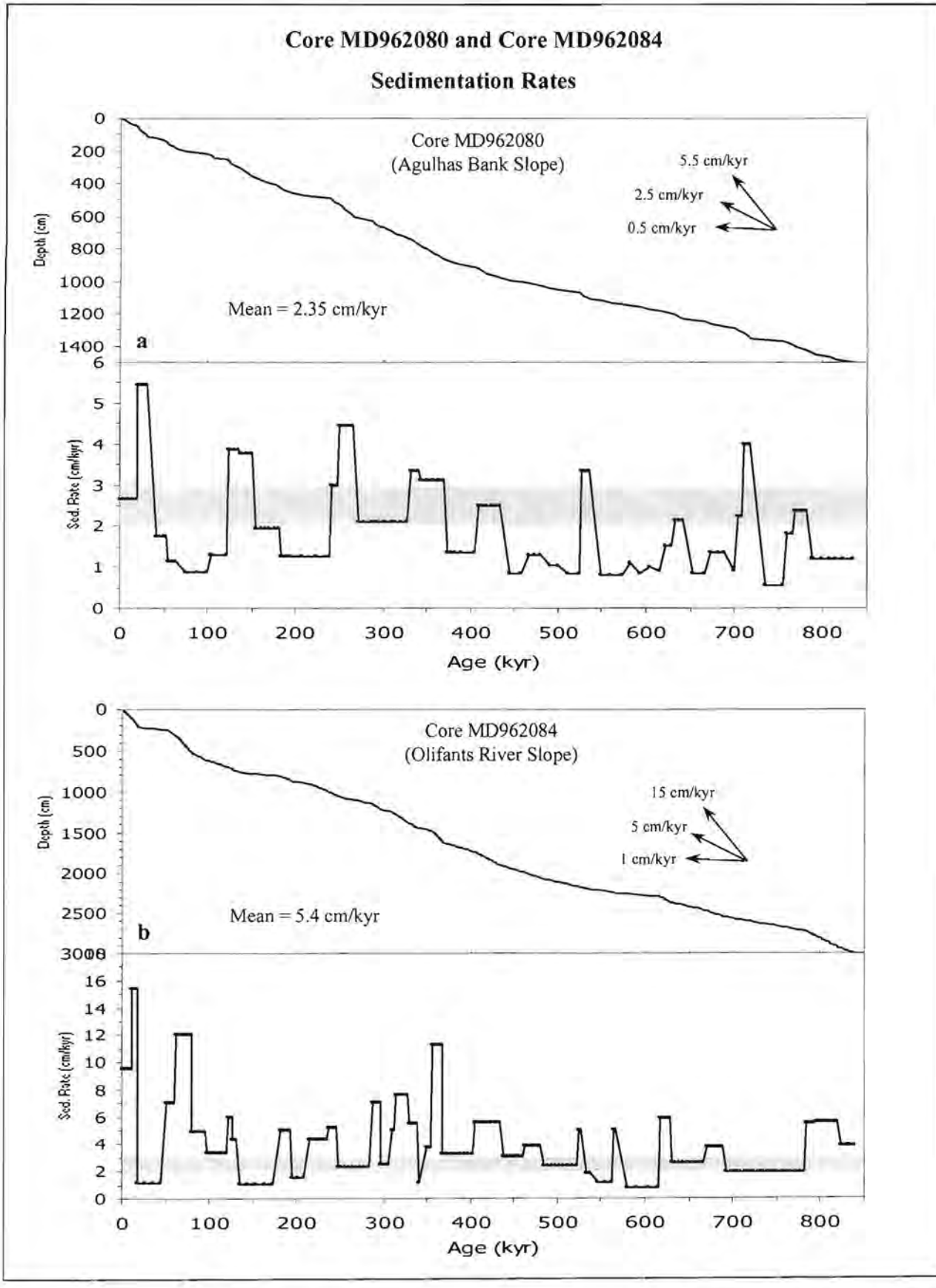

Figure 3.6: Sedimentation rates showing depth versus calculated age for core (a) MD962080 and (b) MD962084. Average marine sedimentation rates are indicated by shading.

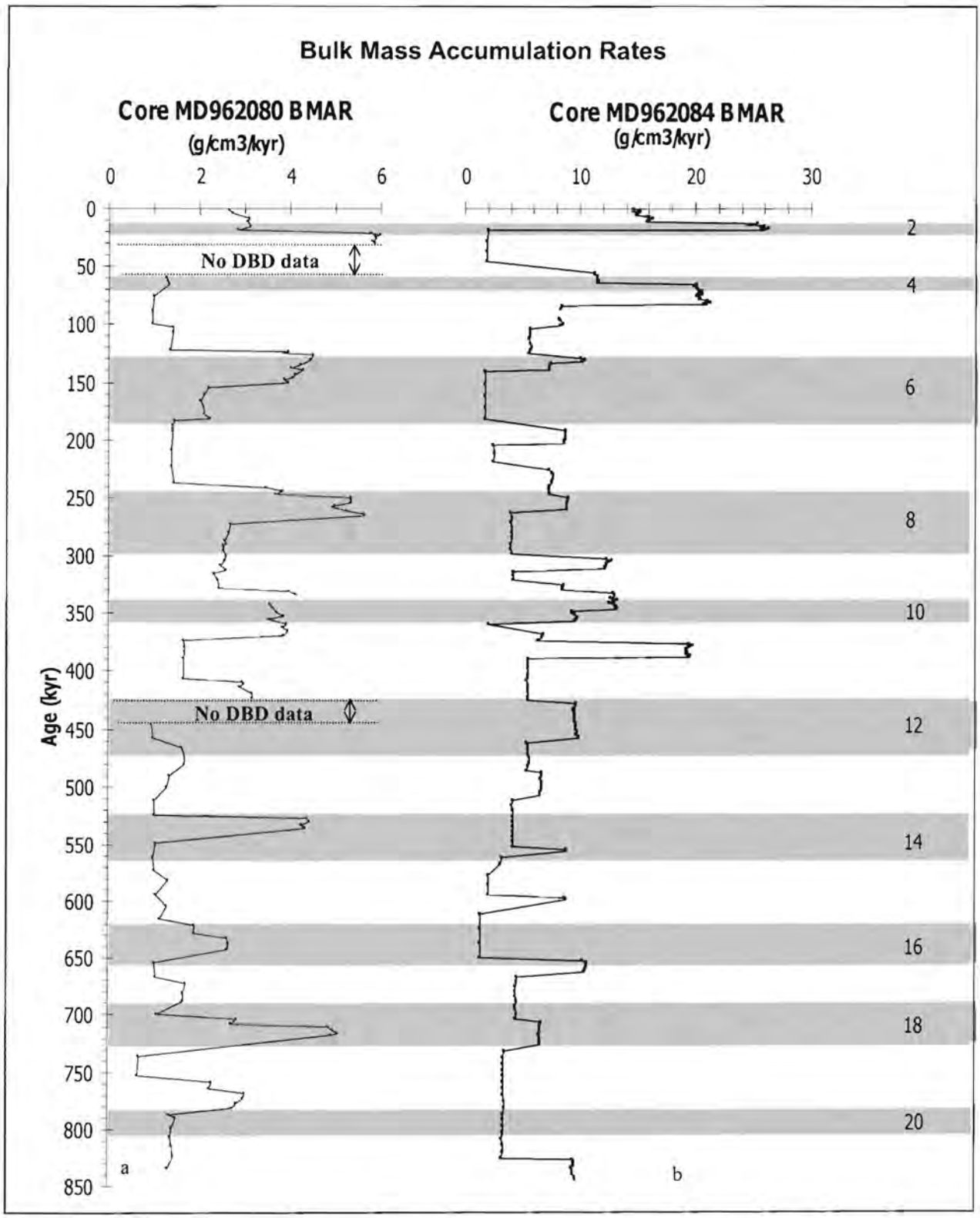

Figure 3.7: Bulk mass accumulation rates (BMAR) for cores MD962080 (a) and MD962084 (b). Grey-shaded bars represent inferred glacial marine isotope stages (MIS).

CHAPTER 4: PALAEOCIRCULATION:- PLANKTONIC FORAMINIFERA CENSUS COUNTS AND ASSEMBLAGES

This chapter introduces the reader to the various planktonic foraminiferal species that were counted in the cores. The chapter contains a review of previous micropalaeontological studies relating to the palaeoceanographic history of the Subtropical Convergence, the Agulhas Current region and the Benguela Current System. The results of individual species counts and subsequent factor analysis, from which assemblages were determined, are presented and discussed. The tropical species *Globorotalia menardii* is considered to reflect the transfer of Indian Ocean surface-water into the South Atlantic Ocean (Berger and Vincent, 1986; Berger and Wefer, 1996). Therefore, results of a separate count of *Gr. menardii* are presented and discussed in terms of glacial-interglacial variations in the Agulhas Current and Retroflection.

4.1 INTRODUCTION

Planktonic foraminifera are niche specific, thriving in certain temperature and salinity conditions. Recent studies (Giraudeau, 1993; Niebler and Gersonde, 1998) document the reliability of planktonic foraminifera as tracers of present surface water masses in the South Atlantic. Hodell (1993) and Howard and Prell (1992) used planktonic foraminiferal data from the Subantarctic region and the Southern Indian Ocean, respectively, to interpret latitudinal fluctuations in the Antarctic Polar Front Zone (APF) and the Subtropical Convergence (STC) during the Late Pleistocene. The generally high abundance and good preservation of these calcareous microfossils in the cores allows reconstruction of the varying dominance of different water masses over the Agulhas Bank and Olifants River slopes through time. Individual species that are counted provide insight into the environmental characteristics of the surface water masses overlying the core sites. Counts of one species, *N. pachyderma* (sinistral), document a period of intense upwelling in the Southern Benguela Region (SBR). Statistical techniques are used to determine foraminiferal assemblages from which changes in surface-water masses are infered. Thus, foraminiferal assemblages provide a history of the hydrological conditions over the core sites for last 850 kyr. Results point to local changes as well as suggesting latitudinal changes in the positions of the STC and the Agulhas Retroflection and longitudinal changes in the frontal zones of the Benguela Upwelling System (BUS).

4.2 PREVIOUS WORK

Although there are numerous micropalaeontological studies of sediments from both the North and South Atlantic, the Indian and the Southern Oceans, few of these studies fall within the region of the cores used in this research. Numerous studies have focused on the upwelling history of the Northern Benguela Region as well as past latitudinal migrations of the Subtropical Convergence and Antarctic Polar Front. The following sections provide a review of micropalaeontological studies, focussing on planktonic foraminifera, in areas related to the two core sites.

4.2.1 The Subtropical Convergence and southern hydrological fronts

Meridional shifts of the Subtropical Convergence (STC) and the Antarctic Polar Front (APF) in the southern Indian Ocean have been documented by, amongst others Bé and Duplessy (1976), Hayes *et al.* (1976), Prell *et al.* (1979), Morely and Hays (1979), Prell *et al.* (1980), Niebler (1995). In the southern Indian Ocean the relative abundance of species of living planktonic foraminifera is related to the position of the STC (Prell *et al.*, 1979). Faunal indicators have been used to trace the location of the STC and the adjacent water masses in the past. Depending on the faunal criteria, previous reseachers have suggested a range of variability in the past position of the STC from no change to a northward displacement of as much as 10° during the Late Quaternary. Variations in the shell size of *Orbulina universa* were used to suggest that the STC migrated north of 31°S eight times over the last 540 kyrs (Bé and Duplessy, 1976). As a result of his study of planktonic foraminiferal assemblages in cores from the southeastern Indian Ocean, Williams (1976) suggested five episodes of northward displacement of the STC over the last 500 kyr. The distribution of diatoms led Burckle and Clarke (1976) to conclude that there was little or no movement of the STC during the Last Glacial Maximum (LGM). However, they suggested that in many areas the Antarctic Convergence had moved northward, resulting in a constricted Subantarctic zone. Conversely, a significant cooling south of 20°S during the LGM, identified by Prell *et al.* (1976) suggested that the STC may have been north of its present position at this time. Prell *et al.* (1979) used faunal assemblages derived from the analysis of planktonic foraminifera in core-top samples in the southern Indian Ocean, to infer a northward migration of the STC of <5° during any glacial stage in the last 500 kyr. Their data also suggested that the STC was located south of its present position during interglacial stages 13,11, 9 and 7, but not during MIS 5, when the STC was deemed to lie close to 35°S. Howard and Prell

(1992) used a transect of piston cores between 42° and 48°S in the southwest Indian Ocean to reconstruct the latitudinal distribution of planktonic foraminifera and used the variations in the fauna to imply changes in the positions of the STC and APF over the past 500 kyr. Their data indicate that the STC lay north of its present position at ~40°S for most of this time period, with four brief poleward excursions during the interglacial of the Early Holocene and in MIS 5e, 9 and 11.

4.2.2 The Agulhas Current Region

The Agulhas Current has played a significant role in the circulation of the southern Indian Ocean since the Middle Tertiary (Martin *et al.*, 1982). Hutson (1980) used planktonic foraminifera from a core in the southwest Indian Ocean to suggest pronounced seasonal variations in the circulation of the Agulhas Current during the Last Glacial Maximum. He suggests that the Agulhas Current decreased in intensity during glacial periods. Prell *et al.* (1980) using the same core, support this view, reporting a cooler, shallower Agulhas Current, showing great seasonality during the Last Glacial Maximum (LGM) (Martin *et al.*, 1982). Martin and Flemming (1988) argued that, due to its characteristic proximity to the continental slope and the fact that the continental slope of southeastern Africa is very steep and straight, the Agulhas Current would not have deviated greatly from its present path during glacial periods. The temperature and mean position of the current flow have been stable for the last 150 000 years at least (Winter and Martin, 1990). Changes in palaeoproductivity over this time period are due to changing nutrient supply as a result of eddy formation, lowering of sea level and varying coastal upwelling intensity (Winter and Martin, 1990). Winter and Martin (1990) argue that there has been no lateral shift in the position of the Agulhas Retroflection over the last 150 000 years and that any interruption in the leakage of Indian Ocean water into the Southeast Atlantic is unlikely. This interpretation is extended back in time by Flores *et al.* (1999) who used the abundance of coccolithophores and some planktonic foraminifera in a piston core recovered from south of Cape Town, to infer that that the Agulhas Basin was under the influence of the Agulhas Current Retroflection for the last million years. However, they interpret a strong glacial-interglacial (G-IG) cyclicity for the Retroflection region. They identify the "Mid-Brunhes climatic event" occurring at ~400-300 kyr B.P. (Jansen *et al.*, 1986) by the maximum abundance of the coccolithophore *Gephyrocapsa caribbeanica.* They interpret intense cold periods (such as MIS 12) to be linked to an equatorward displacement of the STC and an easterly position of the Agulhas Retroflection.

4.2.3 The Benguela Region

The most significant monitor of oceanographic changes off southwest Africa is the upwelling intensiy of the Benguela Coastal Current. Oberhänsli (1991) distinguished the coastal and geostrophic branches of the Benguela Current and the Angola Current over the northeastern Walvis Ridge by analysis of plankonic foaminiferal assemblages from DSDP site 532. Intensified upwelling and westward (seaward) expansion of the coastal upwelling cells occurred during glacial stages 12, sporadically through MIS 10-8, 6 and 4-2. Increased abundance of *Neogloboquadrina dutertrei* signify incursions of the warm Angola Current during MIS 11, sporadically in MIS 8-6 and early in MIS 5 (Oberhänsli, 1991). Oberhänsli *et al.* (1992) examined the standing stock of planktonic foraminifera in surface and subsurface waters of the southeast Atlantic during the austral summer of 1988. During this time the standing stock appeared to be influenced by hydrographic regimes (e.g. oxygen concentration, phytoplankton abundance, reproductive cycles), rather than being linked only to temperature and salinity, which define the water masses. Standing stocks were highest when productivity was intermediate and crops were drastically reduced when primary productivity was very high.

Planktonic foraminiferal assemblages in surface sediments from the Benguela Current System region of the southwest African continental margin were determined by Giraudeau (1993). Three dominant foraminiferal assemblages were identified representing the upwelling zones (*Neogloboquadrina pachyderma* (s)) in the Northern Benguela Region, the productive intermediate mixed zone (*Globigera bulloides* and *Neogloboquadrina pachyderma* (d)) and the offshore oligotrophic environment (*Globorotalia inflata*) in he Southern Benguela Region. The distribution of individual foraminiferal species are closely related to the surface hydrology of the Benguela Upwelling System (Giraudeau and Rogers, 1994), primarily related to sea surface temperature (SST), whilst nannofossils are correlated to chlorophyll-a concentrations and nutrient supply.

Using mollusc shells from surficial sediments, Pether (1994) suggested warmer conditions in the Benguela system off Namaqualand during the deglacial transgression than at present. He implied enhanced advection of Agulhas Current water close to the shelf and concomitant supression of upwelling associated with the southward migration of the zonal wind profile south of the continent and reduced trade winds over the southwest Indian Ocean. These data are supported by 'spikes' of tropical species in cores off Namiba (Charles and Morely, 1988).

Correlations between relative abundance patterns of *N. pachyderma* (s) from the equatorial Guinea Basin, the Angola Basin and the northern Cape Basin (McIntyre *et al.*, 1989) suggest that the inshore oceanography of the entire eastern margin of the South Atlantic is dominated by variations in the intensity and zonality of the trade wind system and that upwelling intensity is the primary control on faunal distribution and SST patterns (Little *et al.*, 1997a). The intensity and position of the upwelling centres in the Northern Benguela Region off Namibia over the last 160 kyr respond to changes in the strength and zonality of the trade wind system (Little *et al.* (1997b). Using rapid fluctuations of *N. pachyderma* (s) in a core from the Northern Benguela Region (NBR) to indicate changes in upwelling intensity over the last 140 kyr, Little *et al.* (1997a) interpret periods of high abundance to indicate increased intensity and zonality of the South Atlantic trade winds. There is a good correlation between periods of high *N. pachyderma* (s) abundance and the Dansgaard-Oeschger cycles from the GISP2 ice core, which suggests large-scale global climatic connections. However, in isotope stages 4-2, their data indicate that the South Atlantic leads the North Atlantic in response to changes in the trade wind system.

4.3 METHODS

Planktonic foraminifera were concentrated by deflocculating the foraminiferal subsamples in a 3M solution of sodium hexametaphosphate, prior to washing through a 125-micron sieve. This size-fraction was chosen to facilitate comparison with previously published planktonic foraminiferal assemblage data from the Southeast Atlantic (Giraudeau, 1993; Little *et al.*, 1997a,b; Niebler and Gersonde, 1998). The >125 μm fractions were oven-dried overnight at 105°C, weighed and then examined under a binocular microscope placed next to a desktop personal computer. A simple *Lotus123* programme was written to serve as a counter for the species census counts. On average, 280 specimens per sample were identified to species level following the classical taxonomy of Bé (1969) and Parker (1962). This number allows for statistically significant analyses of relative abundances greater than about 1 %. All lower relative abundance counts are subject to statistical uncertainty. The raw counts for all species were converted into relative abundances and are reported as percentages of the total number of specimens counted. The raw data are given in Appendix 4. The results of the census counts are discussed before the next section, Factor Analysis, is presented.

Individual species-abundance variations exhibit high-frequency erratic signals. Q-mode Factor Analysis (Imbrie and Kipp, 1971) was performed in order to extract major groupings and trends not

obvious from the individual species records. Factor analysis indicates the major faunal components that account for the majority of the total variance in the census data. The factor scores, which give the species composition of each assemblage, are shown in Appendix 5. The varimax factor components, which give the composition of each sample in terms of the resultant assemblage, are plotted in the results section. Each factor can be characterised by a dominant taxon and one or two subordinate taxa.

Seventeen species were chosen for identification, based on previous work in the Benguela region and on the presence of the species in the cores. Only these seventeen species were identified in the census counts. All other specimens (whether identifiable or not) were counted in an "other" category. Table 4.1 provides the main environmental characteristic of each of the species. A more detailed description of the ecological niches preferred by each species, along with scanned electron micrographs to illustrate each species, is given in Appendix 3. The species are described from coldest to warmest environments. Bé and Tolderlund (1971) and Bé and Hutson (1977) combined *Globigerina falconensis* and *Globigerina bulloides* counts in their study of the biogeographic patterns of foraminifera because the two species show morphological intergradation. However, later work (Giraudeau, 1993; Niebler and Gersonde, 1998) indicated that *Gg. falconensis* occurs more frequently in sediments underlying subtropical waters. Therefore, the occurrence of each species is cited individually in this study. Forms exhibiting a small last chamber with an apertural lip and a small aperture were classified as *Gg. falconensis* (as defined by Malmgren and Kennett, 1977). This species, so identified, is also smaller overall than *Gg. bulloides*. The scarcity of *Globorotalia truncatulinoides* in the sediments off southern Africa necessitated a combined presentation of counts in this study. The sinistral variety is more common than the dextral variety in both cores. Some researchers (e.g. Chang *et al.*, 1999) combine *Neogloboquadrina dutertrei* with the subpolar species *Neogloboquadrina pachyderma* (d), citing morphological intergradation. However, in this research the species are counted separately based on their environmental preferences. Specimens which showed a wide and deep umbilicus and five or more chambers with a charcteristic rosette pattern were classified as *N. dutertrei,* as defined by Kennett and Srinivasan (1983). All intergrades (transitional forms with four to five chambers and compact tests without umbilical teeth) were combined with *N. pachyderma* (d). *Globorotalia menardii menardii ss* and *Globorotalia menardii tumida* were combined into a single category *Globorotalia menardii*.

Table 4.1: Summary of main environmental characteristics of the planktonic foraminiferal species counted. See Appendix 3 for more detailed descriptions.

SPECIES	CHARACTERISTIC	WATER MASS
Neogloboquadrina pachyderma (s) (Ehrenberg, 1861)	Dominant south of STC	Polar
Neogloboquadrina pachyderma (d) (Ehrenberg, 1861)	Cool, mesotrophic, high nutrient levels of upwelled filaments.	Subpolar
Turborotalia quinqueloba (Natland, 1938)	Intermediate-deep waters, limited water stratification.	Subpolar
Globigerina bulloides (d'Orbigny, 1826)	Mixed subpolar-subtropical waters, productive environments offshore of upwelling cells.	Subpolar- cool subtropical
Globigerinita glutinata (Egger, 1893)	Widespread, cosmopolitan, abundant under cool (10°C) and warm (28°C) conditions with deep-mixed surface layer adjacent to upwelling zones.	Transitional/ Warm
Globorotalia inflata (d'Orbigny, 1839)	Dominant in southern transitional zone north of STC, deep dweller (~200m), low nutrient content, reduced primary productivity.	Transitional, warm - cool temperate.
Globorotalia truncatulinoides (d'Orbigny, 1839)	Oligotrophic, high salinity waters, deep-dweller.	Transitional, deep-waters
Globorotalia scitula (Brady, 1882)	Sparse, but widespread, cool deep waters (>100m), high occurrence in plankton near Agulhas Current.	Cool-temperate, deep-waters
Globorotalia hirsuta (d'Orbigny, 1839)	Southern transitional zone, minimal stratification, rare.	Warm-temperate
Globorotalia crassaformis (Galloway and Wissler, 1927)	Temperate, high salinity waters, below thermocline.	Warm-temperate, below thermocline
Globigerina falconensis (Blow, 1959)	Warmer variation of *Gg. bulloides,* underlies subtropical waters.	Warm-temperate
Globigerinella calida (Parker, 1962)	More common in mid-low latitudes, mixed-layer species with warm water at depth.	Warm subtropical, mixed-layer.
Neogloboquadrina dutertrei (d'Orbigny, 1839)	Common in tropical productive environments, associated with western boundary currents, warm waters at depth & chlorophyll maximum.	Warm-temperate, Boundary currents
Globigerinoides ruber (alba) (d'Orbigny, 1839)	Most abundant species in equatorial, subtropical, oligotrophic Indian Ocean waters, 14-30°C, low salinity range,~35.5 potential salinity units (psu).	Subtropical
Globigerinoides trilobus (Reuss, 1850)	Temperate to tropical waters, favours cooler waters than ecological variant *Gs. sacculifer.*	Subtropical-Tropical
Globigerinoides sacculifer (Brady, 1877)	Most abundant species in tropical waters, 24°-30°C, tolerance for broad range of salinity	Tropical
Globorotalia menardii (Parker, Jones and Brady, 1865)	Peaks in tropical, equatorial surface waters, 22°C, 35 psu	Tropical

The scarcity, but relative importance of the tropical species *Gr. menardii* as a tracer of warm tropical/subtropical Indian Ocean waters (e.g. Berger and Wefer, 1996), prompted a separate count on the total >125μm fraction. *Globorotalia menardii* ss and *Globorotalia tumida* were combined into a single category *Globorotalia menardii.* The *Gr. menardii* counts are expressed as absolute abundance (number of specimens per gram of sediment in the >125μm fraction). These values were subsequently converted to accumulation rate (number of specimens/cm^2/kyr), calculated by multiplying concentration (number of specimens per gram bulk sample) by the bulk mass accumulation rate (acquired from onboard measurements), and are expressed as such in section 4.6.

4.4 PLANKTONIC FORAMINIFERAL CENSUS COUNTS

The results of planktonic foraminiferal species census counts counts presented here are discussed before the factor analysis and resultant foraminiferal assemblages are presented and discussed.

4.4.1 Results

4.4.1.1 Core MD962080 (Agulhas Bank Slope)

Seventeen taxa were identified in the >125um sediment fraction of core MD962080, from the Agulhas Bank Slope. Raw data are presented in Appendix 4 and summary statistics of relative abundances are given in Table 4.2. The foraminiferal population is dominated by two species: *Globorotalia inflata* and *Neogloboquadrina pachyderma* (dextrally coiled), accounting for, on average, 43.6% of the total assemblege . The subordinate taxa (mean > 1%), in order of decreasing average abundance are: *Globigerinita glutinata, Globigerina bulloides, Globigerina falconensis, Neogloboquadrina dutertrei, Globigerinoides trilobus, Globorotalia scitula, Globigerinoides sacculifer, Globigerinoides ruber* (alba*), Turborotalia quinqueloba, Neogloboquadrina pachyderma* (sinistrally coiled) and *Globorotalia truncatulinoides.*

Table 4.2: Summary statistics of relative abundance for planktonic foraminiferal census counts for core MD962080, Agulhas Bank Slope, in order of relative abundance.

SUMMARY STATISTICS % Core MD962080 (Agulhas core)				
Species	**Minimum**	**Maximum**	**Mean**	**Std Dev.**
Globorotalia inflata	7.38	40.74	24.64	5.54
Neogloboquadrina pachyderma (d)	8.54	36.24	19.48	4.57
Globigerinita glutinata	3.53	18.18	9.82	2.83
Globigerina bulloides	2.60	17.02	7.79	3.38
Globigerina falconensis	1.56	13.51	5.75	2.23
Globigerinoides trilobus	0.75	11.75	4.52	2.41
Neogloboquadrina dutertrei	0.00	9.09	3.35	1.90
Globorotalia scitula	0.00	8.98	3.27	1.59
Globigerinoides sacculifer	0.00	6.77	3.12	1.42
Globigerinella calida	0.00	6.80	2.40	1.19
Globigerinoides ruber (alba)	0.00	6.38	2.14	1.39
Turborotalia quinqueloba	0.00	6.80	2.02	1.25
Neogloboquadrina pachyderma (s)	0.00	7.38	1.58	1.59
Globorotalia truncatulinoides	0.00	5.33	1.49	1.09
Globorotalia crassaformis	0.00	5.03	0.76	0.72
Globorotalia hirsuta	0.00	2.67	0.65	0.72
Globorotalia menardii	0.00	1.48	0.21	0.32

Gr. inflata comprises, on average, over 24 % of the foraminiferal population and has the maximum recorded abundance of 40.7% (Table 4.1). The fluctuations in abundances (Fig. 4.1a) are not influenced by global glacial-interglacial (G-GI) cycles, but rather vary on shorter time-scales in response to regional and local conditions. Peak abundances occur in warm MIS 11, as well as towards the end of glacial MIS 8, whilst minimum abundances are recorded in glacial MIS 14 and at the start of MIS 20. The most erratic fluctuations in *Gr. inflata* abundances occur in glacial MIS 6. On average, the period MIS 11 – 6 shows higher relative abundances, with relatively lower abundances in both the older (MIS 21 – 12) and younger (MIS 5 – 1, with the exception of MIS 3) sections of the core.

N. pachyderma (d) is the second most abundant species in the foraminiferal assemblage (mean 19.3%, max. 36.2%). The *N. pachyderma* (d) record corresponds roughly to G-IG cycles, increasing in abundance during glacial stages, with peak abundances in MIS 14, at the onset of glaciation in MIS 8 (Fig. 4.1b) and in MIS 2. Minimum occurrences are seen in MIS 11 and 6/5e at Termination

II. Lower relative abundances are seen in the older section (MIS 21 – 14), with above-average abundances in stages MIS 10 – 6 and MIS 4 - 2.

As expected from the cosmopolitan nature of this species, the record for *Ga. glutinata* does not readily reflect distinct variations in water masses and global climate (Fig. 4.1c). Minimum and maximum abundances occur in both glacial and interglacial periods. Relatively high abundances occur at glacial terminations in stages MIS 20, 18, 16, 10 and 6, whilst relatively low abundances occur at the onset of glaciation and the end of stages MIS 19 and 7. Peak abundances occur in stages MIS 15 and 4, whilst minima occur also in MIS 15, as well as MIS 14, 7 and 5. Lower than average abundances are seen in stages MIS 12 – 7, with above average abundances in stages MIS 21 – 13 and MIS 6 – 4.

The *Gg. bulloides* record (Fig. 4.1d) shows peaks in abundances in glacial stages MIS 10, 6, and 2 and at the termination of MIS 4, as well as in warm stage MIS 9. Variations in the rest of the record are less clearly linked to G-IG cycles. There is a general trend of increasing abundances upcore to MIS 10 with relatively small fluctuations, after which a long-term cyclicity (~200 kyr) is recorded from MIS 10 – 5. Minimum abundances occur in warm MIS 13, 11, 9 and 3.

The records for *Gg. bulloides* and *Gg. falconensis* (Figs. 4.1d and e) are broadly similar for the last 130 kyr with increased abundances at Termination II and in glacial MIS 2 and decreases during MIS 3 and 1. The rest of the records do not show much similarity, except for the smaller range in fluctuations from MIS 21 - 11. This supports the reasoning behind separate counts for the two species, suggesting the two forms are recording different water conditions.

Fluctuations in the abundances of the subtropical species *Gs. trilobus* occur on time-scales less than global G-IG scales (Fig. 4.1f). The record shows below average abundances for the interval MIS 11 – 6, with increased abundances before (MIS 21 – 12) and after (MIS 5 – 1). Peaks in abundances occur in MIS 17, on either end of MIS 13 and in MIS 5e. Minimum abundances are recorded regularly through the MIS 11 – 6 interval, as well as in MIS 14, 12 and 2.

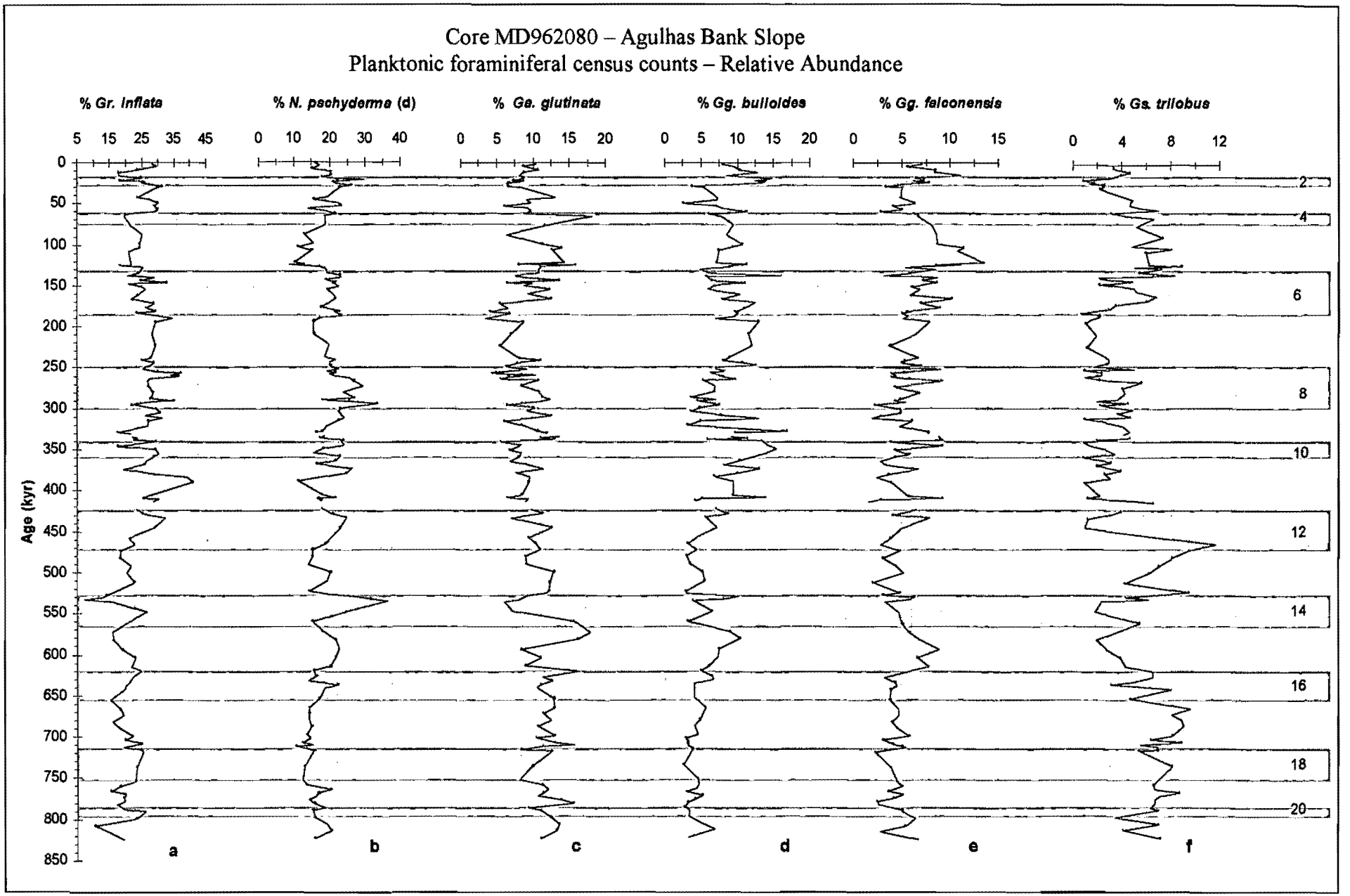

Figure 4.1: Foraminiferal relative abundances for core MD962080. Grey-shaded bars represent inferred glacial marine isotope stages (MIS).

As a common western boundary current species, *N. dutertrei,* contributes less than expected to the overall foraminiferal population (mean 3.4 %, max. 9%). This may be due to the low nutrient content of the Agulhas Current, as this species prefers high-productivity waters (Thunell and Reynolds, 1984). There is no clear G-IG cyclicity, although the upper portion of the record (MIS 8 – 1) shows a tendency toward lower abundances in glacial periods (Fig. 4.1g). The range of variability is also more constrained than in the rest of the record. Higher relative abundances are seen in the older section of the core (MIS 21 – 11), with lower than average abundances in the younger portion.

The species *Gr. scitula* accounts for 3.3% (mean, max. <9%) of the foraminiferal population. The upcore record is complicated with no clear global climatic (G-IG) modulation on abundances (Fig. 4.1h). Minimum and maximum abundances occur in both glacial and interglacial periods. The record is more erratic, with a greater range of variability in the last 400 kyr.

The record for *Gs. sacculifer* exhibits a general G-IG cyclicity, with relatively lower abundances in glacial periods and increased abundances in warmer intervals (Fig. 4.1i). This cyclicity is more obvious from stage MIS 10 – 1. There is a sharp increase in abundances at most glacial terminations (e.g. MIS 18, 14, 10, 8 and 6) as well as at the onset of glaciation at MIS 2. Warm interglacial stage MIS 11 shows anomalously low abundances compared to other interglacial periods. There is a change from, on average, higher abundances in the older portion of the core (MIS 21 – 12) to relatively lower abundances for the last 420 kyr.

The top 250 kyr of the record for *Ge. calida* (Fig. 4.1j) shows a general G-IG cyclicity with increased abundances during glacial stages (MIS 6, 4 and 2) and lower relative abundances in the warm stages (MIS 7, 5, 3 and 1). This trend is absent from the bottom section of the core except for relatively low abundances in MIS 11 and minima in MIS 19 and 17. Peaks in abundances occur just after glacial terminations, in early MIS 17, 15 and 9.

The occurrence of the warm water species *Gs. ruber* (alba) is low, making up < 7% (max.) of the total foraminiferal population. The record exhibits relatively large, erratic fluctuations (Fig. 4.1k). Peak abundances occur at G-IG boundaries MIS 18/17 and MIS 15/14 as well as within warm stages MIS 11, 5 and 1. There is a trend toward relatively lower abundances during glacial periods in the older portion of the core (MIS 21 – 12).

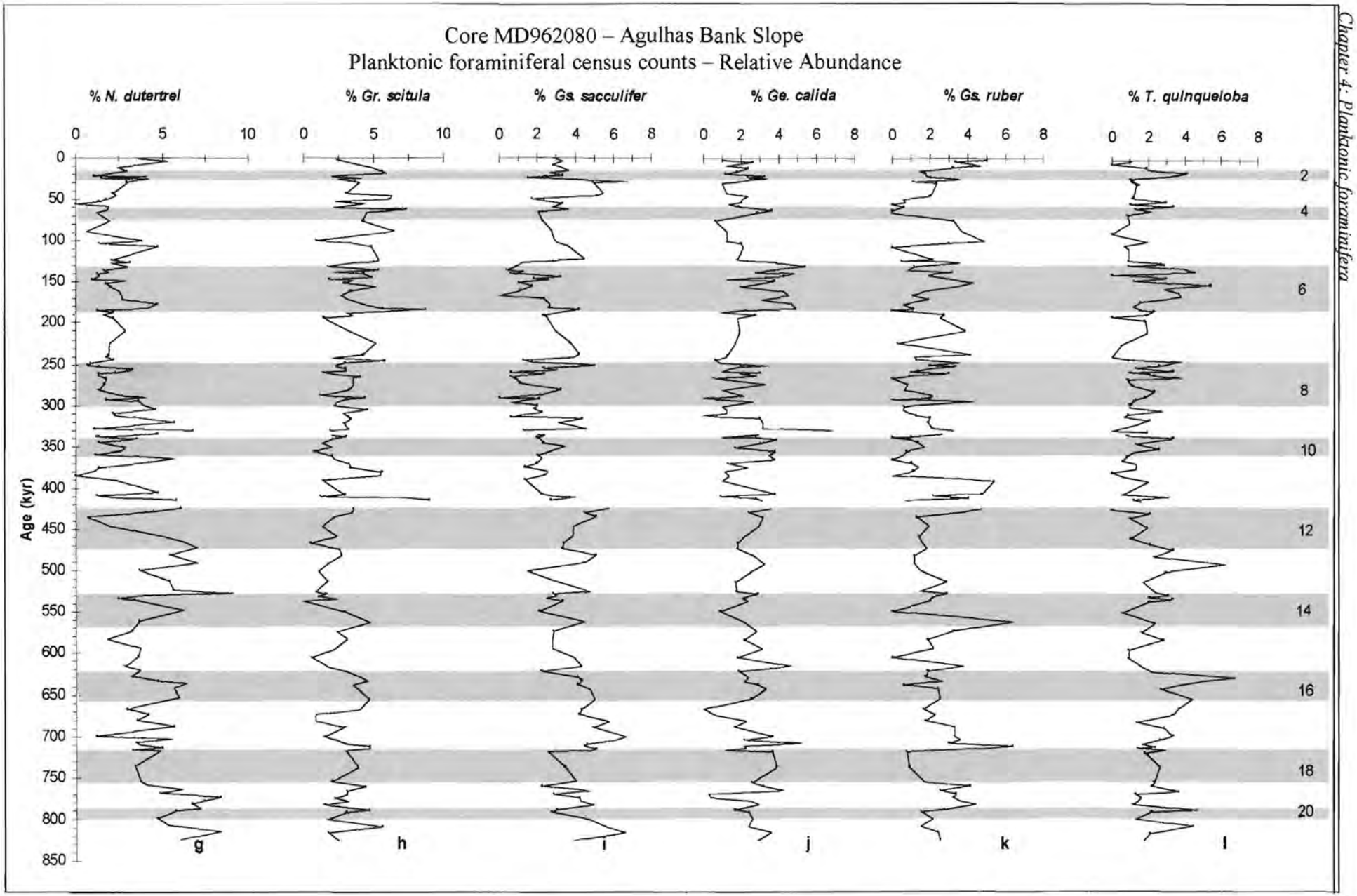

Figure 4.1cont.: Foraminiferal relative abundances for core MD962080. Grey-shaded bars represent inferred glacial marine isotope stages (MIS).

The record for *T. quinqueloba* (Fig. 4.1l) reveals, in general, above-average abundances for the the period MIS 21 – 12, together with a larger range of variation in abundances. The younger portion of the record shows a trend towards G-IG cyclicity with peaks in abundances late in glacial stages MIS 10, 8. 6, 4 and 2 and relatively lower abundances in warm stages MIS 7, 5 and 1. Maximum abundances occur in glacial stages MIS 16 and 6 and, anomalously, in interglacial MIS 13.

N. pachyderma (s), whilst low in average abundances (mean 1.7%, max. 7.4 %), is the cold water end-member of the faunal assemblage. Peak abundances occur in glacial periods (MIS 18,14, 8, 6), and the record shows a general trend towards increased abundances in glacial periods and decreased abundances in warm periods (Fig. 4.1m). The record shows a relatively higher abundances, and greater range of variability, of this species in the bottom half of the core (MIS 21 –12), with, on average, relatively lower abundances in the younger portion of the core, with the exception of cold stage MIS 8.

The combined sinistral and dextral forms of *Gr. truncatulinoides* account for < 1.5% (mean, max. 5.3%) of the total foraminiferal population in this core. Seasonal fluctuations and a relatively low rate of reproduction may explain the sparseness of this species in the sediments (Bé and Tolderlund, 1971), as well as an intolerance for vertical temperature and salinity gradients. The record shows rapid fluctuations in abundances within glacial and interglacial periods (Fig. 4.1n). Peak abundances occur at the onset of warmer conditions (early MIS 17, 13 and 9) as well as within warm stages MIS 17, 13 and 5 and, anomalously, in cold MIS 8. As with the *N. Pachyderma* (s) record, the lower portion of the record (MIS 21 – 12) shows a larger range of variability, with the upper half showing rapid fluctuations and, on average, lower relative abundances.

The low contribution of *Gr. crassaformis* to the overal foraminiferal population (mean < 1%, max. 5%), makes interpretation of the upcore record difficult. The record from MIS 21 – 12 shows a greater range of variability and, on average, higher relative abundances, than the younger section of the record (Fig. 4.1o). There is a trend towards G-IG cyclicity in the top section of the core (MIS 8 – 4) with, on average, higher abundances in warm stages (MIS 7, 5) and relatively lower abundances in glacial stages MIS 8 and 6. However, peak abundances occur in both warm and cold stages (e.g. MIS 17, 14, 13, 8, 7, early stage 3 and MIS 2).

The low occurrence of *Gr. hirsuta* in the foraminiferal assemblage results in an erratic record (Fig. 4.1p) with no clear trends or cyclicity. Peaks in abundances occur in both glacial (MIS 18, 14, 10)

and interglacial (MIS 19, 17, 15, 13, 7, 5 and 3) intervals. The scarcity of this species in the foraminiferal assemblage may be related to *Gr. hirsuta*'s low tolerance of elevated surface salinity (see Appendix 3).

The rarity (mean 0.21%) of the tropical species *Gr. menardii* in the foraminiferal assemblage is indicated by the erratic relative abundance record (Fig. 4.1q). The importance of this species as an indicator of inter-ocean exchange, however, prompted a separate study of this species, which is discussed in Section 4.6 (pg.4-37).

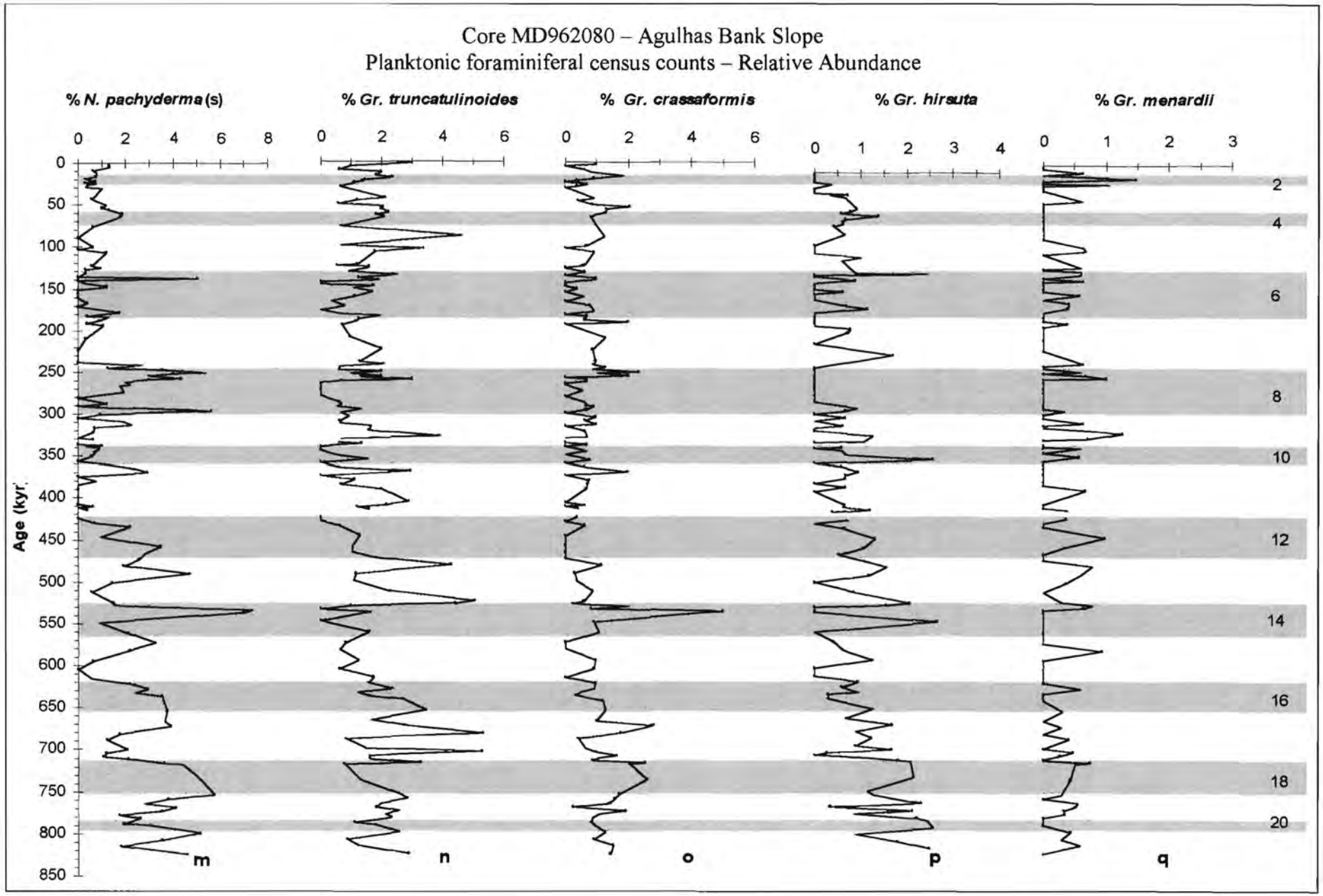

Figure 4.1 cont.: Foraminiferal relative abundances for core MD962084. Grey-shaded bars represent inferred glacial marine isotope stages (MIS).

4.4.1.2 Core MD962084 (Olifants River Slope)

The same seventeen taxa were also identified in the >125um sediment fraction of Core MD962084 from the Olifants River Slope. Raw data are presented in Appendix 4 and summary statistics are given in Table 4.3. As with the Agulhas Bank Slope core (MD962080), the foraminiferal population is dominated by two species: *Globorotalia inflata* and *Neogloboquadrina pachyderma* (dextrally coiled), accounting for, on average, 38.5% of the total assemblage, as compared to 43.6% in Core MD962080. The subordinate taxa (mean > 1%), in order of decreasing average abundance are: *Globigerinita glutinata, Globigerina bulloides, Globigerinoides trilobus, Globigerina falconensis, Neogloboquadrina dutertrei, Globorotalia scitula, Globigerinoides sacculifer, Globigerinella calida, Globorotalia truncatulinoides, Turborotalia quinqueloba, Neogloboquadrina pachyderma* (sinistrally coiled), *Globigerinoides ruber* (alba) and *Globorotalia hirsuta.*

Table 4.3: Summary statistics for planktonic foraminiferal abundance counts for core MD962084, Olifants River Slope, in order of relative abundance.

SUMMARY STATISTICS % Core MD962084 (Benguela core)				
Species	**Minimum**	**Maximum**	**Mean**	**Std Dev.**
Globorotalia inflata	11.66	34.12	20.43	3.53
Neogloboquadrina pachyderma (d)	7.07	28.57	18.07	3.66
Globigerinita glutinata	2.25	14.62	7.60	2.05
Globigerina bulloides	0.00	14.96	5.28	3.48
Neogloboquadrina dutertrei	1.08	14.80	5.43	2.12
Globigerinoides trilobus	0.00	11.75	5.07	2.43
Globigerina falconensis	0.32	13.03	3.66	2.03
Globorotalia scitula	0.00	11.11	3.19	2.10
Globigerinoides sacculifer	0.40	6.48	3.16	1.16
Globigerinella calida	0.43	6.73	2.92	1.08
Globorotalia truncatulinoides	0.00	10.69	2.89	1.85
Turborotalia quinqueloba	0.00	9.64	2.55	1.46
Neogloboquadrina pachyderma (s)	0.39	10.55	2.42	1.27
Globigerinoides ruber (alba)	0.00	10.00	2.30	1.53
Globorotalia hirsuta	0.00	4.58	1.28	0.94
Globorotalia crassaformis	0.00	2.90	0.66	0.58
Globorotalia menardii	0.00	1.33	0.17	0.27

Gr. inflata comprises, on average, over 20 % of the foraminiferal population and records the maximum abundance of 34.12% (Table 4.3). The fluctuations in abundances (Fig. 4.2a) are not influenced by global G-GI cycles, but rather vary on shorter time-scales in response to regional and local conditions. Peak abundances occur in warm MIS 13 and 11, whilst minimum abundances are recorded in glacial MIS 12, 8 and in warm stage 17. There is a long-term cyclicity in the lower section of the record, with relatively low abundances in the intervals MIS 19 – 17, MIS 12 and MIS 10 – 9 and increased relative abundances from MIS 16 – MIS 13, MIS 11 and MIS 8.

The second most abundant species is *N. pachyderma* (d) peaking at 28.5% (mean 18%). As with *Gr. inflata*, abundances changes do not follow a G-IG pattern (Fig. 4.2b). In the interval MIS 12 – 8, both maximum and minimum abundances are centered on isotope stage boundaries (e.g. MIS 13/12, late stage 11, MIS 10/9 and MIS 8/7). This section of the record exhibits the most rapid fluctuations in abundances. There is a general increasing trend over the last 125 kyr, with a sharp decrease in glacial MIS 2.

The record for *Ga. glutinata* shows three phases of abundance variations: the interval MIS 21 – 12 has increased relative abundances, MIS 11 – 8 shows decreased abundances and MIS 7 – 2 shows relatively higher abundances with a sharp decrease in stage 1(Fig. 4.2c).

Although no G-IG cyclicity is seen in the record for *Gg. bulloides*, marked changes are apparent on longer and shorter timescales (Fig. 4.2d). The interval MIS 21 – 13, displays, on average, higher relative abundances than the period MIS 12 – 7. As with the dominant cold-end member, *N.pachyderma* (d), this record exhibits a general increasing trend over the last 125 kyr, with a sharp decline in MIS 1. A marked decrease is noted in glacial MIS 6.

Fluctuations in relative abundances of *N. dutertrei* display a trend towards G-IG cyclicity with, in general, decreased abundances in glacial intervals (Fig. 4.2e). Peak abundances occur at stage bondaries (MIS 16/15, 12/11, 8/7), as well as within warm stages 15, 11 and 7. On average, the lowest relative abundances occur in the youngest portion of the record, MIS 5 – 1.

Gs. trilobus has above average relative abundances in the lower 2/3 of the record (MIS 21 – 8). The last 250 kyr of the record show, not only lower relative abundances, but also minimal fluctuations (Fig. 4.2f). Fluctuations for the entire period studied occur on timescales shorter than G-IG timescales, reflecting the dominating effect of regional and local changes over global climatic cycles.

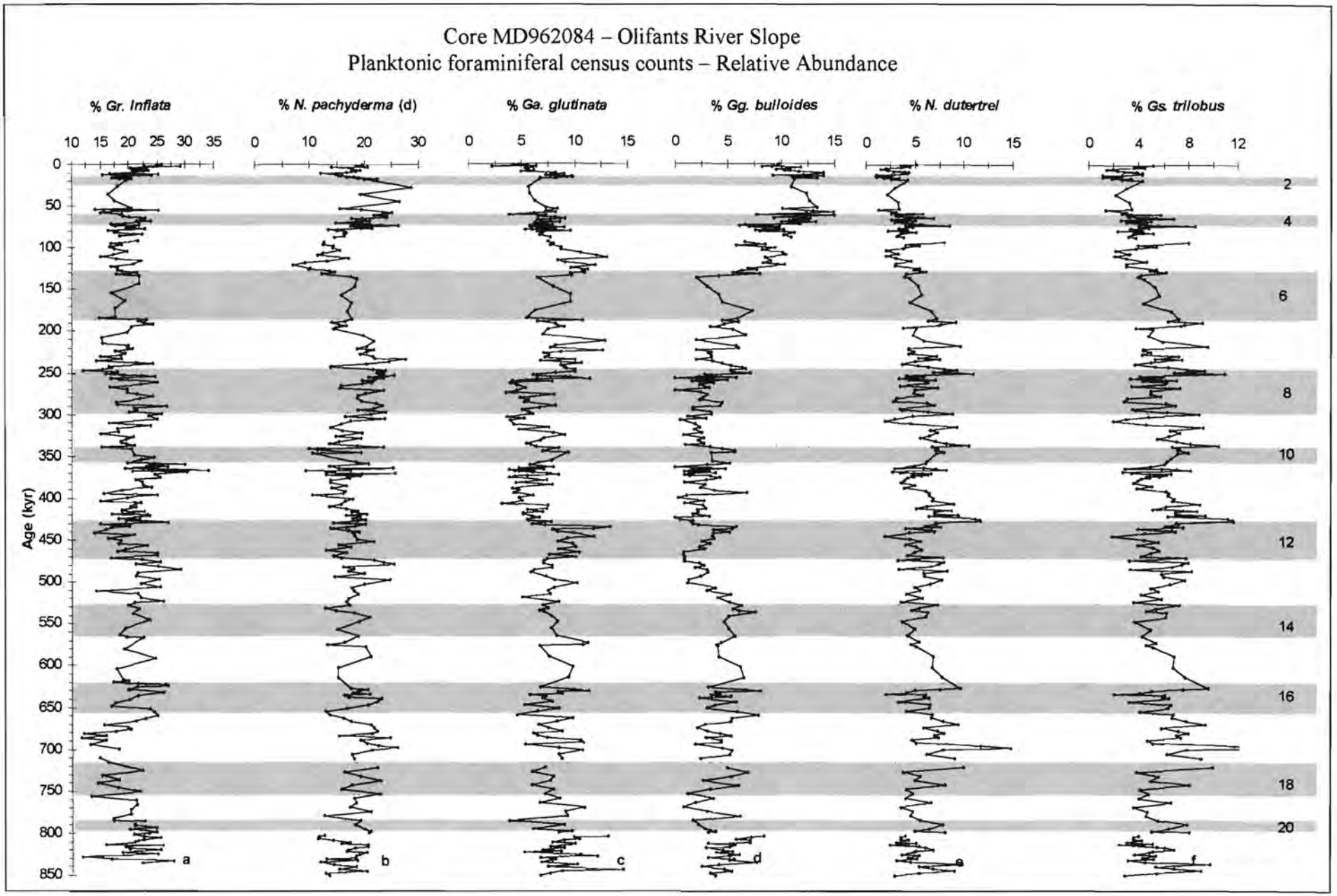

Figure 4.2: Foraminiferal relative abundances for core MD962084. Grey-shaded bars represent inferred glacial marine isotope stages (MIS).

In an opposing trend to the species discussed above, abundance counts for *Gg. falconensis* are below average for the lower 2/3 of the core (MIS 21 – 8), with an overall increase in relative abundances and in range of variability in the last 250 kyr (Fig. 4.2g). Peak abundances occur in both glacial (MIS 16, 12, 4) and interglacial stages late stage 11, 7 and 5). This record is broadly similar to the *Gg. bulloides* record above to MIS 10.

A high range of variability is seen in the relative abundances of the species *Gr. scitula* (Fig. 4.2h). Sharp increases in abundances are seen at the onset of glaciation in MIS 18 and 16. The interval MIS 12 – 7 shows a relatively limited range of variability with high-frequency fluctuations occurring on less than G-IG timescales.

The relative abundances of the warm-water species *Gs. sacculifer* show little or no cyclicity for the lower 400 kyr of the record (i.e MIS 21 – 12). Despite the high-frequency variability in the top half of the record, a long-term (~100 kyr) cyclicity is evident (Fig. 4.2i). Peak abundances occur in the late stages of warm interglacial periods (MIS 15, 13, 5) as well as in MIS 7 and, surprisingly, in glacial stages 16, 12 and 2. Minimum abundances tend to be within glacial periods (MIS 18, 10, 8, 6), with the exception of a sharp decrease in MIS 11. There is a general decreasing trend over the last 125 kyr, culminating in a minimum abundance count in MIS 1.

With an average contribution of ~3% (max. 6.7 %), *Ge. calida* does not appear to be under the dominant influence of global G-IG cycles. No obvious trends are evident in the oldest portion of the record (MIS 21 – 14). From MIS 14 – 7, a ~50kyr cyclicity develops (Fig. 4.2j). High-frequency fluctuations are seen in the last 80 kyr of the record.

Although both sinistral and dextral forms of *Gr. truncatulinoides* account for < 3% (mean, max.10.7%) of the total foraminiferal population, some interesting trends are apparently from the relative abundance record (Fig. 4.2k). A substantial increase is seen in MIS 11 and also to a lesser extent in MIS 8. There is a general tendancy towards increased abundances during warm stages and and lower relative abundances in glacial periods (with the exception of MIS 8 and a peak in MIS 18). The youngest portion of the record (MIS 4 – 2) has, on average, the lowest abundances as well as a restricted range of variability.

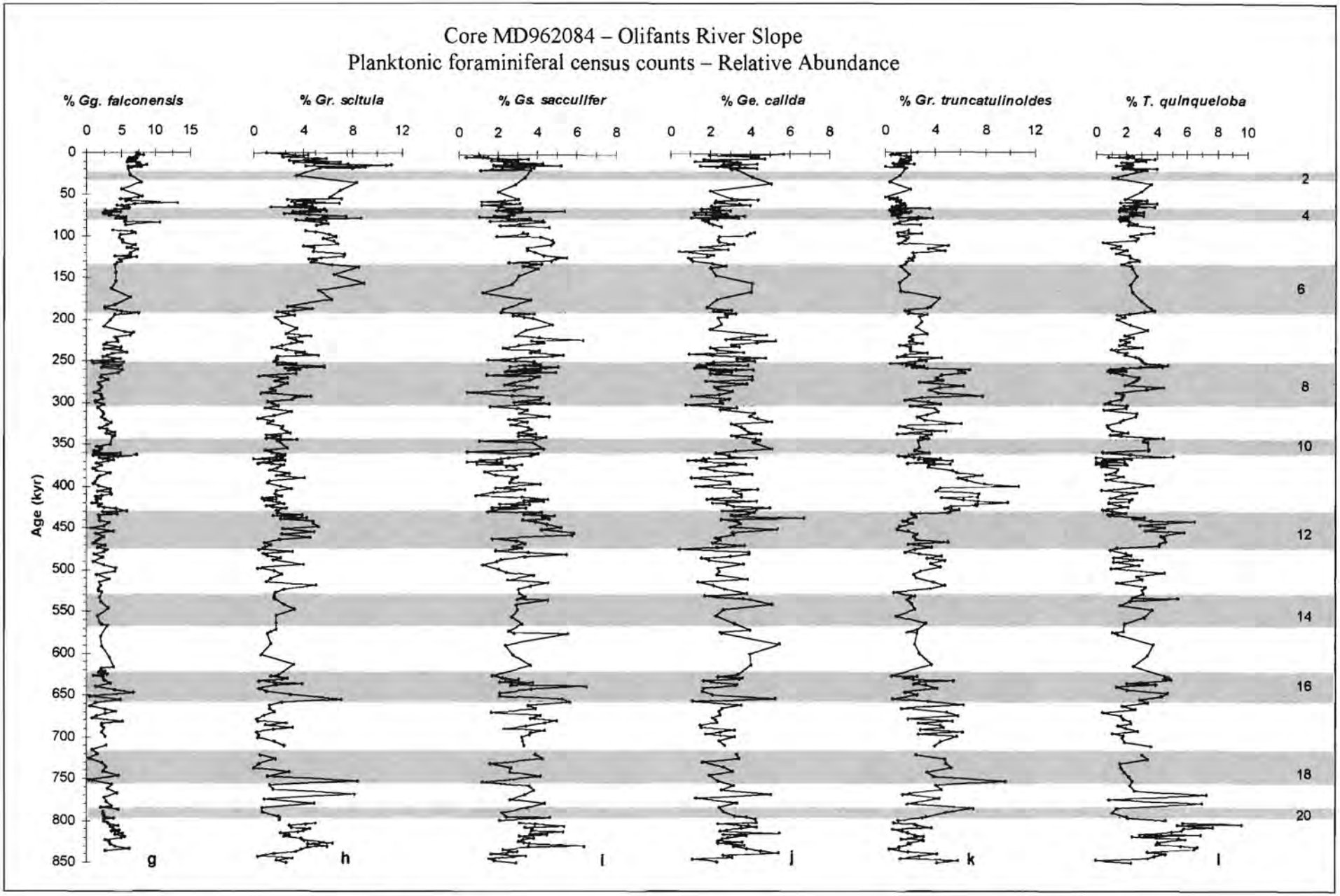

Figure 4.2 cont.: Foraminiferal relative abundances for core MD962084. Grey-shaded bars represent inferred glacial marine isotope stages (MIS).

The record for *T. quinqueloba* shows, on average, relatively higher abundances during glacial periods and lower abundances in interglacials, except over the last two cycles recorded (MIS 21-18), where the trend is reversed (Fig. 4.2l). Maximum abundances occur in glacial stages MIS 20, 14, 12, either end of MIS 10 and 8, and anomalously in MIS 19. The warm interval MIS 11 exhibits a sustained decrease in relative abundances and there is also a noticeable decrease in late MIS 5.

The cold end-member of the faunal assemblage, *N. pachyderma* (s), contributes only 2.4% (mean) to the total foraminiferal population. The most noteworthy aspect of this record is the peak in abundances (reaching >10%) during MIS 9 (Fig. 4.2m). This unique event is recorded in two other cores from the southeast Atlantic; core MD962085 recovered to the north of this site on the Orange River Slope (Chang *et al.*, 1999) and ODP site 1087 to the northeast in the southern Cape Basin (Giraudeau *et al.*, 2001). Anomalously high abundances of *N. pachyderma* (s) are aslo reported in a core recovered from the Walvis Ridge (Ufkes *et al.*, 2000)

Gs. ruber is the warm end-member of the Benguela fauna, rarely exceeding 2 % in surface sediments of the southern Beguela region (Giraudeau, 1993). Peak occurrences are recorded in warm stages 21, 19, 11, 9 and 7 (Fig. 4.2n). There are noticeable increases at glacial-interglacial transitions 20/19, 8/7, 6/5 and 2/1, but the maximum abundance of 10% occurs at the end of warm interglacial stage 11. There are a number of general shifts in relative abundances throughout this record. Below-average abundances are seen in intervals MIS 18 – 12 and MIS 6 – 1, whilst the intervals MIS 20 – 19 and MIS 11 – 7 record higher than average relative abundances.

Although the contribution of *Gr. hirsuta* to the overall foraminiferal population is low (mean 1.3%, max.4.6%), certain trends are apparent in the abundance record (Fig. 4.2o). The bottom 2/3 of the record (MIS 21 – 8) have, on average, lower abundances, but a greater range in variability than the younger portion (MIS 7 – 4). The lowest average abundances occur in the most recent part of the record (MIS 4 – 1). Peaks in abundances occur in both glacial (MIS 20, 18, 16, 12) and interglacial (MIS 13, 11, 9, 7, 5e and 3) intervals.

The low occurrence of *Gr. crassaformis* in the foraminiferal assemblage (mean < 1%, max. 3%), results in an erratic record (Fig. 4.2p). There is a higher contribution to the abundance record from stage 21 – 12. This is also the period of greatest range in variability. Peak abundances occur within glacial (MIS 16) and interglacial (MIS 13) stages, in the latter stages of warm periods (MIS 11 and 9), at the onset of glaciation (MIS 6) and early stage 1.

The very low relative abundances (mean 0.17%) of the tropical species *Gr. menardii* in the foraminiferal assemblage testifies to the rarity of the species in these sediments, resulting in an erratic relative abundance record (Fig. 4.2q). This species is futher discussed in Section 4.6.

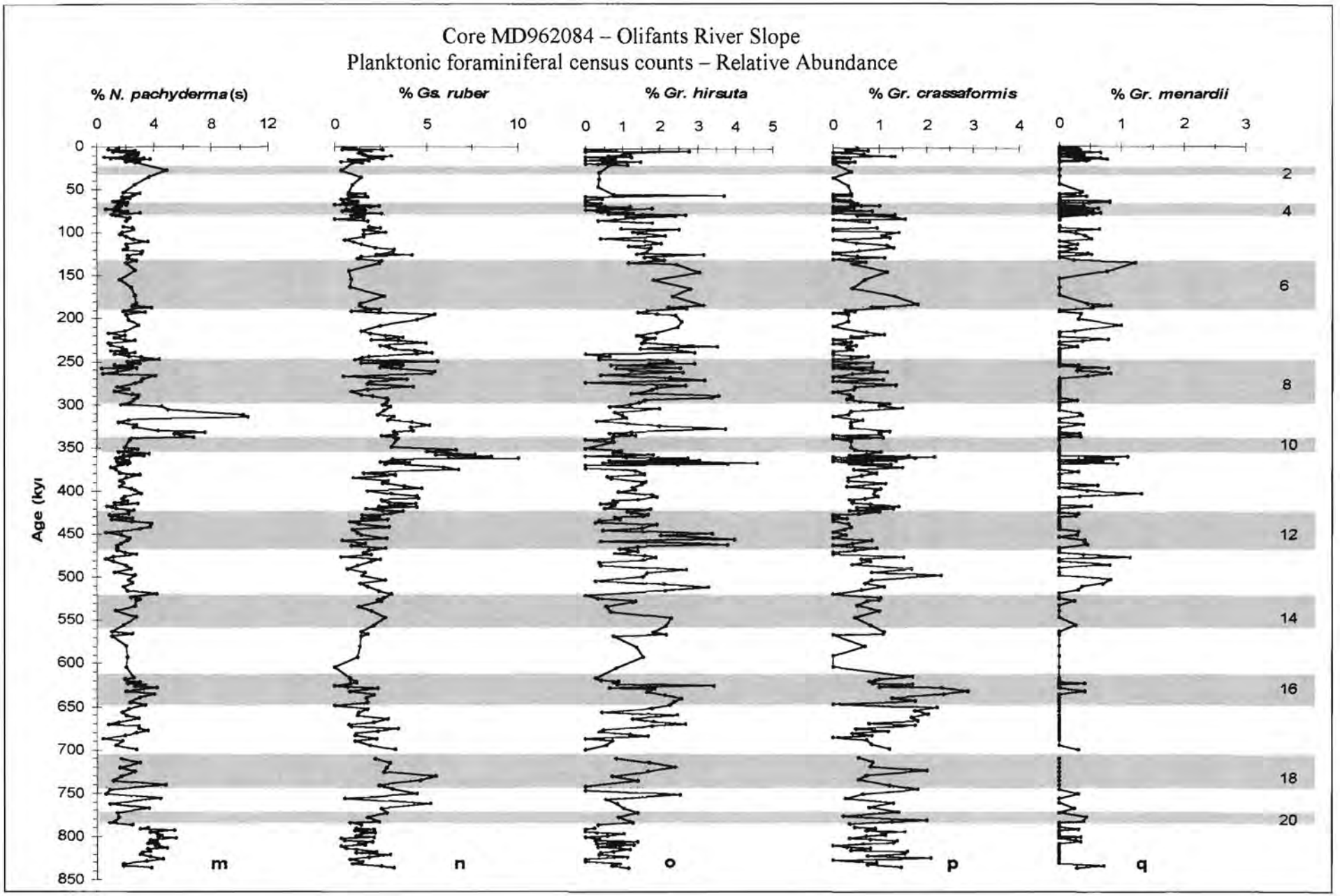

Figure 4.2 cont.: Foraminiferal relative abundances for core MD962084. Grey-shaded bars represent inferred glacial marine isotope stages (MIS).

4.4.2 Discussion

4.4.2.1 Core MD962080 (Agulhas Bank Slope)

Core MD962080 does not display the typical Agulhas Current foraminiferal composition – dominated by tropical to subtropical species *N. dutertrei*, *Gs. sacculifer* and *Gs. ruber* nor an Agulhas Bank assemblage defined by *Gs. ruber*, *N. dutertrei* and *N. pachyderma* (d) (Lowry, 1987). Although all of these species are present in the foraminiferal population, with the exception of *N. pachyderma* (d) and *N. dutertrei*, they do not occur in the significant quantities one might expect. This is no doubt due to the complex nature of the mixture of water masses that pass over the core site under varying circumstances. What is noticeable, however, is that the 'warm' species are generally more abundant during interglacial periods, whilst *N. pachyderma* (d) displays a G-IG pattern with increased abundances during glacial stages. The most definitive species is the warm-water western boundary current species *N. dutertrei*. This species peaks in the steep thermocline area associated with the chlorophyll maximum (Thunell and Reynolds, 1984) and its preferred environment (50 m depth, 14 - 18°C, 33 - 35 psu) corresponds to the water-column characteristics of the western Agulhas Bank Region (Fig. 4.3a). The G-IG cyclicity displayed by this species, with peak abundances at glacial terminations, suggests an increased influence of Agulhas Current waters over the core site during these periods. With the exception of *N. pachyderma* (d), the upcore distributional trends of the dominant planktonic foraminiferal species show little or no correlation to global G-IG cycles, but rather fluctuate on time-scales in response to local or regional hydrographic changes.

4.4.2.2 Core MD962084 (Olifants River Slope)

Lowry (1987) defined the Benguela Ecosystem planktonic foraminiferal assemblage to be dominated by the polar species *Neogloboquadrina pachyderma* sinistrally coiled (s) and the transitional species *Globorotalia inflata*. Giraudeau (1993) identified three foraminiferal assemblages with (1) the polar taxa *Neogloboquadrina pachyderma* (s) and *Globigerina quinqueloba* in the upwelling areas; (2) transitional species *Globorotalia inflata* and *Globorotalia truncatulinoides* in the offshore environment and (3) *Neogloboquadrina pachyderma* (d) and *Globigerina bulloides* preferentially distributed in the highly productive intermediate zones of the Benguela System, where upwelled and oligotrophic waters mix. The salinity and temperature characteristics of the surface waters for the SBR are shown in Fig. 4.3b. The dominant species of the planktonic foraminiferal population in core

MD962084 suggest an admixture of offshore and intermediate/old-upwelled waters. The foraminiferal record shows a poorly defined G-IG cyclicity for the period MIS 12 – 8. There is an inverse relationship between *Gg. bulloides* and *Gr. inflata*, suggesting a change in dominance from offshore to intermediate waters over the core site. The faunal population indicates that MIS 11 was the warmest stage in the period under investigation and points to reduced upwelling and the presence of warm stratified surface waters during warm periods MIS 13, 11 and 7. An unique episode of peak abundance of *N. pachyderma* (s) is recorded in MIS 9. This taxon is closely associated with strong coastal upwelling in the SBR (Giraudeau, 1993; Giraudeau and Rogers, 1994) and is the dominant taxon south of the Antarctic Polar Front (Niebler and Gersonde, 1998). However, an incursion of polar water to this latitude, during one of the warmest climatic stages, seems an unlikely possibility. It is possible that this signal reflects an unusually strong upwelling pulse, the causes of which are debateable. Increases in abundances of *Gs. ruber* at G-IG transitions are unlikely to be due to incursions of warm tropical waters from the Angola Current down to this southerly position, but are more likely to be a result of increased thermocline and intermediate water transfer of Indian Ocean waters via the Agulhas Current. This corresponds to the increases in the warm-water, western boundary current species *N. dutertrei* in the Agulhas Bank core MD962080 described above.

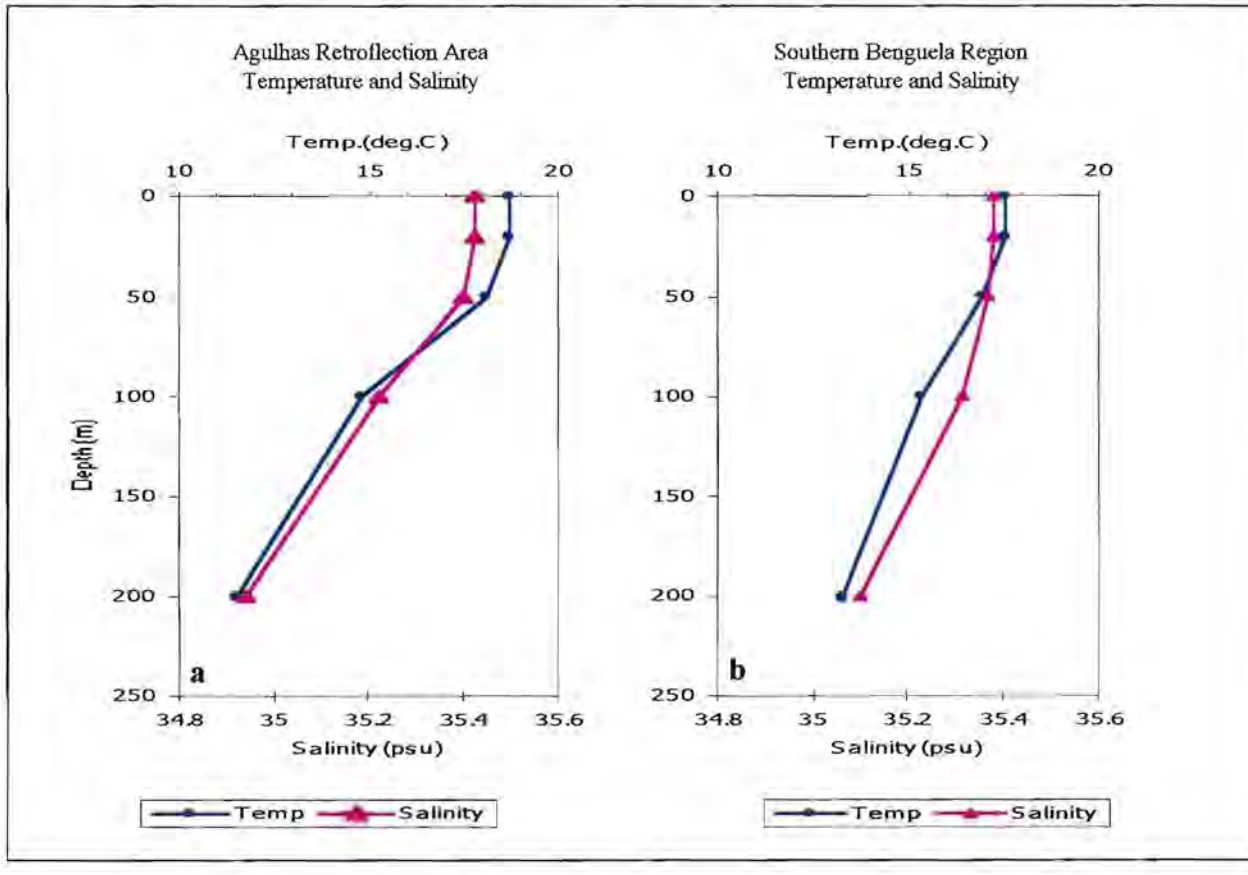

Figure 4.3: Average temperature and salinity data from 1921- 1998 for the areas 35-37°S, 18-20°E (a) and (b) 31-33°S, 14-16°E. Data supplied by Dr M. Grundling from the South African Data Centre for Oceanography (SADCO).

4.5 PLANKTONIC FORAMINIFERAL ASSEMBLAGES

Individual species abundance variations exhibit high-frequency erratic signals, probably reflecting the complexity of the surface hydrological conditions over the Agulhas Bank Slope and in the SBR. Q-mode Factor Analysis (Imbrie and Kipp, 1971) was therefore performed in order to extract major groupings and trends not obvious from the individual species records.

4.5.1 Results

4.5.1.1 Core MD962080 (Agulhas Bank Slope)

Factor analysis indicates that four faunal components account for more than 98% of the total variance in the census data. The factor scores which give the species composition of each assemblage are shown in Table 4.4. Each factor can be characterised by a dominant taxon and one or two subordinate taxa.The varimax factor components, which give the composition of each sample in terms of the resultant assemblage, are plotted in Figure 4.4 and are listed in Appendix 5.

Factor 1 (38% of the total variance) is defined by *Gr. inflata,* the most abundant species of the transitional zone between Subantarctic and subtropical waters. The present-day foraminiferal assemblage dominated by *Gr. inflata* occurs north of the Subtropical Convergence (STC). The Transitional Assemblage (Factor 1) fluctuates independently of global G-IG cycles (Fig. 4.4a). Variations in abundances occur on shorter timescales in response to local hydrographic changes. There is a change in mean contribution of this factor to the total foraminiferal population from relatively lower values prior to ca 450kyr to relatively higher values in the middle part of the core studied (MIS 11 – 60), to lower values in the younger portion of the core.

Factor 2 (30 % of the total variance) bears a cosmopolitan signature, characterised by *Ga. glutinata*, with lesser contributions by *Gs. trilobus, Gs. sacculifer* and *N. dutertrei*. *Ga. glutinata* is one of the most widespread species, occurring over a wide range of temperatures and salinity. *Gs. trilobus* and *Gs. sacculifer* are abundant in subtropical and tropical waters. *N. dutertrei* is associated with western boundary currrents and exhibits a wide biogeographic range of tropical and subtropical environments. This assemblage shows the opposite trend to the Transitional Assemblage with higher relative contribution prior to 450 kyr, lower relative contributions in the middle period (MIS 11 – 6) and higher relative contributions thereafter (Fig. 4.4b). A glacial-interglacial cyclicity develops from

MIS 9 upcore, with higher values during warm periods.

Table 4.4: Varimax factor score matrix for core MD962080, Agulhas Bank Slope.

FACTOR SCORES Core MD962080 (Agulhas Bank Slope)				
Variable	**Factor 1**	**Factor 2**	**Factor 3**	**Factor 4**
N. pachyderma (s)	-0.057	0.156	0.123	-0.165
N. pachyderma (d)	0.137	0.097	**0.959**	-0.166
Gg. bulloides	0.139	-0.208	0.207	**0.675**
Gr. scitula	0.038	0.086	-0.023	0.134
Ga. glutinata	-0.236	**0.605**	0.024	0.327
Gr. inflata	**0.928**	0.262	-0.166	-0.001
Gg. falconensis	-0.037	0.043	0.057	**0.569**
Gr. hirsuta	-0.017	0.086	-0.017	-0.039
Gr. truncatulinoides	-0.027	0.144	-0.034	-0.006
Gs. ruber	-0.020	0.125	-0.029	0.078
Gs. trilobus	-0.160	**0.480**	-0.074	0.002
Gs. sacculifer	-0.048	**0.326**	0.003	-0.019
N. dutertrei	-0.087	**0.341**	0.033	-0.170
Gr. menardii	-0.004	0.013	0.002	0.004
Gr. crassaformis	-0.001	0.050	0.013	-0.045
Ge. calida	-0.017	0.077	0.050	0.056
T. quinqueloba	-0.047	0.126	0.036	0.005

Factor 3 is a monospecific assemblage, exclusively defined by *N. pachyderma* (d) and accounting for 23% of the total variance. *N. pachyderma* is the cold-end member of the foraminiferal population and reflects cold Subantarctic waters. This Subantarctic assemblage bears an unique signal. Firstly, there is no clear change in overall contribution from 450 - 200 kyr B.P. as seen in the previous factors. Secondly, a G-IG cyclicity is expressed throughout the top two thirds of the core, with higher values characterising cold periods (Fig. 4.4c). This relationship is not apparent prior to MIS 14.

Factor 4 is characterised by *Gg. bulloides* and *Gg. falconensis*. This cool-water assemblage contributes the least to the overall variance (only 7%), but has an interesting signal, differing somewhat from the previous three factors. Although *Gg. bulloides* is common in off-shelf waters of the SBR, the location of the core makes it unlikely that the occurrence of these two species is a result of coastal upwelling. Distributions of *Gg. falconensis*, considered a psuedomorph of *Gg.*

bulloides, are skewed towards warmer, more saline water masses. The combination of the two species probably reflects waters within the Agulhas Retroflection region, a mixed water mass with contributions from cool northern Subantarctic waters from north of the STC and warm, saline waters of the Agulhas Current, filaments and rings. This cool-temperate assemblage has relatively high contributions in the bottom portion of the record, ending with a sharp decrease in MIS 14 (Fig. 4.4d). There is an increasing trend over the next 200 kyr (530 – 330 kyr B.P.) with another sharp decrease in MIS 9. A second increasing trend ends in a sharp increase in relative contribution at the MIS 6/5 stage boundary. From there, the relative contribution decreases upcore until MIS 2. The period MIS 10 – 4 is characterised by relatively lower values during glacial stages with increased values in warm periods.

Although minor in the overall foraminiferal population in the core (thus not identified in the factor analysis), the subtropical and tropical species *Gs. ruber* (alba), *Gs. trilobus, Gs. sacculifer, Gr. menardii* and *N. dutertrei* need to be considered as potential indicators of warm surface waters over the core site. Their relative abundances were therefore summed to define a Tropical /Subtropical Assemblage. *N. dutertrei* is associated with western boundary currents, with highest percentages occurring in the sediments of equatorial regions and along continental margins (Bé and Tolderlund, 1971). *Gs. ruber* (alba), *Gs. trilobus* and *Gs. sacculifer* are widespread species, dominating in subtropical and tropical waters. The dominance of *Gs. ruber* (alba) appears to increase in the oligotrophic Indian and Atlantic Central Waters. Although only a trace component of the foraminiferal population, *Gr. menardii* is an important indicator species of tropical Indian Ocean waters. This Tropical/Subtropical assemblage exhibits a clear G-IG cyclicity after 350 kyr B.P. (Fig. 4.4e) with minimum abundances occurring during glacial periods MIS 10, 8, 6, 4 and 2 and peak abundances in warm periods. No such cyclicity is present in the older portion of the core. The bottom half of the record (MIS 21 – 12) displays, on average, higher abundances and lower fequecy fluctuations than the middle interval (MIS 11 – 6). There is an average increase in relative abundances in the last 200kyr.

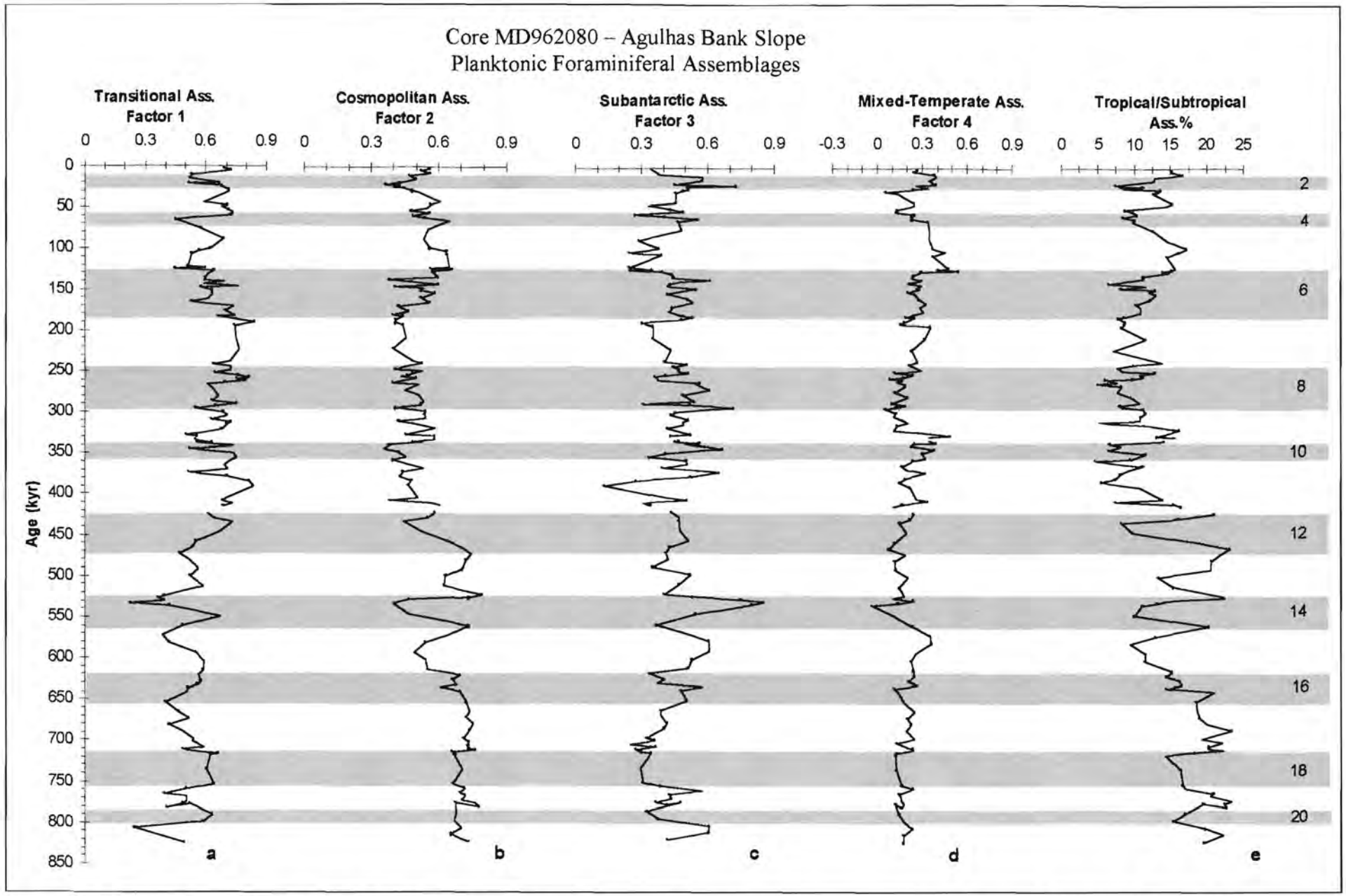

Figure 4.4: Foraminiferal assemblages (a-d) as defined by factor analysis and (e) summed percentages of the warm water species for core MD962080. Grey-shaded bars represent inferred glacial marine isotope stages (MIS).

4.5.1.2 Core MD962084 (Olifants River Slope)

As is the case for core MD 962080, factor analysis indicates that four faunal components account for 98% of the total variance in the census data. The factor scores are shown in Table 5.5. Although the same dominant species appear as in the Agulhas Bank Slope core, the assemblages are somewhat different in this Benguela core. The varimax factor components are plotted in Figure 4.5 and are listed in Appendix 5. Communalities are generally higher in the solution for core MD962080 than for this core, but both matrices displayed values averaging > 0.98.

Table 4.5: Varimax factor score matrix for core MD962084, Olifants River Slope.

FACTOR SCORES Core MD962084 (Olifants River Slope)				
Variable	**Factor 1**	**Factor 2**	**Factor 3**	**Factor 4**
N. pachyderma (s)	0.028	0.028	0.033	0.172
N. pachyderma (d)	**0.859**	0.313	-0.081	-0.297
Gg. bulloides	-0.149	**0.671**	-0.207	-0.051
Gr. scitula	-0.071	**0.311**	-0.124	0.227
Ga. glutinata	0.128	0.157	-0.053	**0.722**
Gr. inflata	-0.082	**0.341**	**0.910**	-0.037
Gg. falconensis	-0.080	**0.347**	-0.061	0.013
Gr. hirsuta	0.024	-0.007	0.045	0.052
Gr. truncatulinoides	0.151	-0.121	0.165	-0.026
Gs. ruber	0.020	-0.049	0.172	-0.026
Gs. trilobus	0.283	-0.237	0.180	**0.321**
Gs. sacculifer	0.057	0.049	0.008	**0.317**
N. dutertrei	0.304	-0.106	0.079	0.152
Gr. menardii	-0.005	0.006	0.009	0.000
Gr. crassaformis	0.006	-0.010	0.044	-0.004
Ge. calida	0.071	0.044	0.016	0.122
T. quinqueloba	0.022	0.053	-0.020	0.183

Factor 1 is exclusively defined by *N. pachyderma* (d) and accounts for 31% of the total variance. This cold end-member of the faunal population is dominant in waters in the vicinity of the STC and also in mesotrophic, nutrient-rich upwelled filaments of the Benguela Upwelling System (BUS). The assemblage shows high-frequency fluctuations with no G-IG cyclicity (Fig. 4.5a). There is an increasing trend from the bottom of the record to MIS 17. There is a change in mean contribution

of this factor to the total foraminiferal population from relatively lower values in the period MIS 16 – 11 to slightly higher values in the middle part of the core studied (MIS 10 – 7) to lower values after 200 kyr B.P.

Factor 2 is dominated by *Gg. bulloides*, with minor contributions from *Gr. inflata, Gg. falconensis* and *Gr. scitula.* This factor accounts for 33% of the total variance. *G. bulloides* is a common component of outer-shelf sediments on the seaward side of upwelling cells in the SBR, prefering the relatively lower nutrient levels away from upwelling filaments. Giraudeau and Rogers (1994) reported *Gg. bulloides* as the "intermediate" factor between upwelling and offshore regions. *Gr. inflata* defines the transitional zone between warm and cool temperate regions, with lower nutrient content and reduced primary productivity. *Gr. inflata* inhabits offshore regions in the southern Benguela. *Gg. falconensis* is the warmer-water variation of *Gg. bulloides*, occurring more frequently in sediments underlying subtropical waters. *Gr. scitula* is associated with cool, deeper waters, with a preference for areas with low seasonal salinity variation, low vertical temperature and density gradients. This factor is an indicator of intermediate conditions between warm oligotrophic waters and cool upwelled waters. Offshore waters with decreased productivity and nutrient content are indicated by this assemblage. The record shows a change in contribution from relatively higher values prior to MIS 12 to relatively lower values for the period MIS 12 – MIS 8, after which there is a general increase in contribution of this factor to the foraminiferal population (Fig. 4.5b).

The Transitional Assemblage, (Factor 3) defined by *Gr. inflata* acccounts for as much as 30 % of the total variance. This mono-specific assemblage reflects surface waters with temperatures in excess of 17°C with a relatively low phytoplankton biomass. This assemblage is characteristic of outer-shelf and slope sediments of the SBR region. This assemblage shows low-frequency fluctuations of the order of ~200 kyr (Fig. 4.5c). This record shows relatively lower contributions prior to 650 kyr B.P., followed by a period of consistently average contributions from MIS 16 – 12, then an increase in relative contribution from MIS 11 – MIS 8 and relatively lower values for the last 250 kyr. There is an overall negative correlation between this factor and the previous factor with high abundances of the Intermediate Assemblage associated with low abundances of this Transitional Assemblage and *vice versa.*

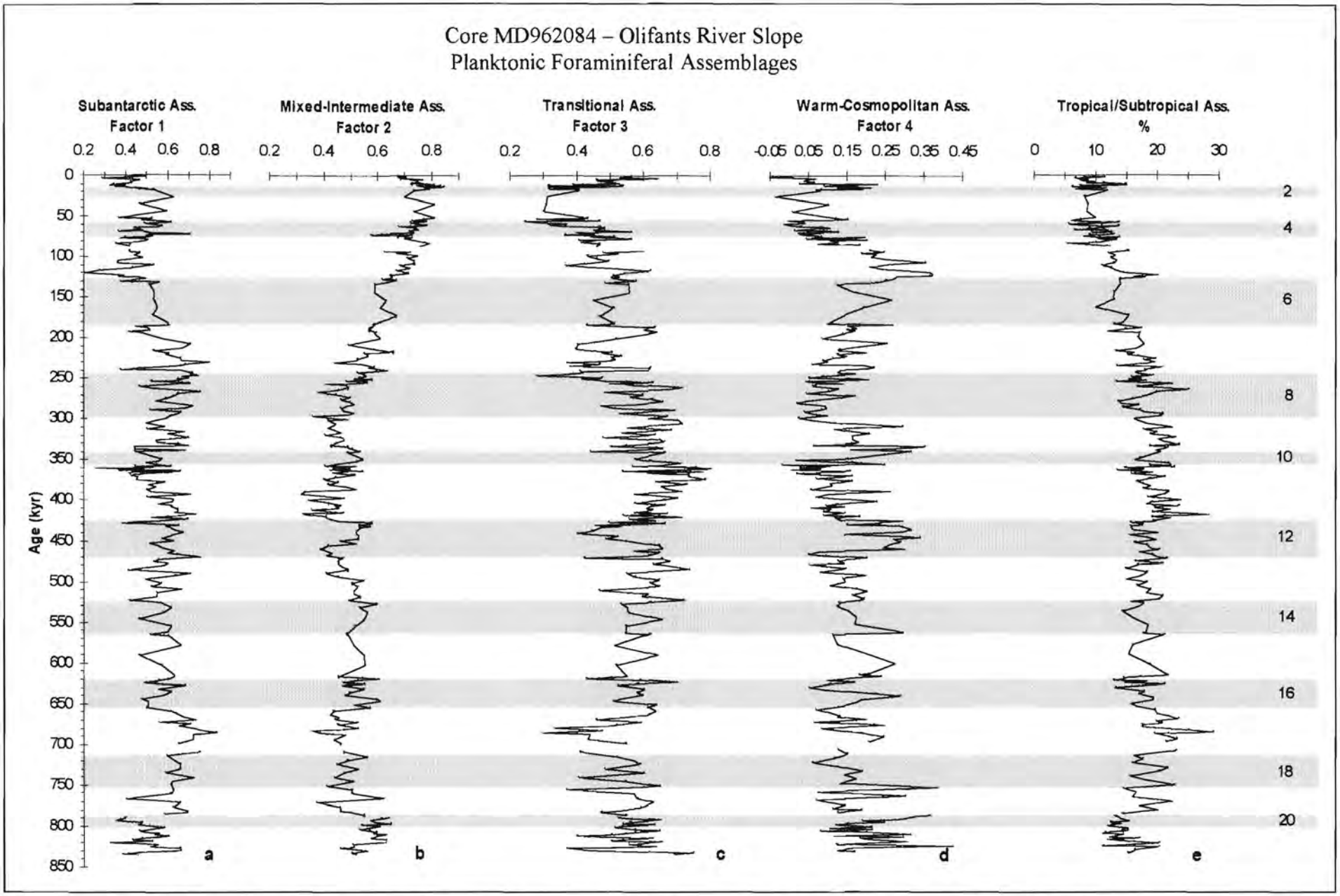

Figure 4.5: Foraminiferal assemblages (a-d) as defined by factor analysis and (e) summed percentages of the warm water species for core MD962084. Grey-shaded bars represent inferred glacial marine isotope stages (MIS).

Factor 4 is only a small contributor to the overall assemblage group (3% of total variance). It is characterised by the cosmopolitan species *Ga. glutinata* with lesser contributions of the subtropical and tropical species *Gs. trilobus* and *Gs. sacculifer*. This assemblage is indicative of warm waters, possibly related to the passage of Agulhas rings and filaments. The record (Fig. 4.5d) shows high-frequency fluctuations with no cyclicity for the last ~400 kyr (MIS 21 – 12). The period MIS 12 – 8 shows fluctuations in the order of ~50 kyr. There is a general decreasing trend till MIS 6 after which there is a sharp change to an increasing trend for the youngest part of the record, ending with a minimum contribution of this factor to the overall foraminiferal population. A rapid increase in abundance is seen at glacial terminations (MIS 10/9, 8/8, 6/5 and 2/1).

The summed abundances of the subtropical and tropical species *Gs. ruber* (alba), *Gs. trilobus, Gs. sacculifer, Gr. menardii* and *N. dutertrei* define the Tropical/Subtropical Assemblage. This assemblage is not defined in the factor analysis, but considered to be important as a possible indicator of warm water transfer from the Indian to the Atlantic Ocean. The oldest portion of the record (MIS 21 – 17) shows an increasing trend which ceases at MIS 16 (Fig. 4.5e). There is a change in mean contribution of this factor from relatively lower values from MIS 15 – 12 to relatively higher values for the period MIS 11 – 7, after which there is a general decreasing trend for the last 200 kyr of the record. The last 450 kyr of the record (MIS 12 – 1) show a tendency to G-IG cyclicity with slightly lower values in glacial stages and slightly increased values in warm periods.

4.5.2 Discussion

4.5.2.1 Core MD962080 (Agulhas Bank Slope)

This core, taken at 36°16'S, lies in a zone influenced by waters from the Agulhas Current and the Agulhas Retroflection, as well as waters from south of the southeast Atlantic Ocean (refer Fig 2.4, pg.2-10). The dominance of Transitional and Subantarctic planktonic foraminifera suggest that the core site has been under the influence of cool-temperate mixed water masses, with impacts from the warm waters of the Agulhas Current, as indicated by the strong presence of a warm-cosmopolitan assemblage. The planktonic foraminiferal record shows a number of changes in hydrographic conditions over the last 850 kyr.

In general, prior to 500 kyr B.P., the data record long-term, low-frequency changes in surface water conditions. The foraminiferal assemblage data indicate rapid changes to intensely cold conditions in

glacial stages MIS 14 and 12. The faunal record suggests that MIS 14 was one of the coldest periods of the Pleistocene. Such cold periods are linked to increased advection of Subantarctic waters over the core site, possibly associated with equatorward displacements of the STC.

The interval MIS 11 – 7 records a change in surface-water dynamics. Variations in abundances exhibit high-frequency fluctuations, as well as a shift in the mean contribution of each factor. Previous researchers (e.g. Prell *et al.*, 1979; Howard and Prell, 1992; Flores *et al.*, 1999) have established that the STC lay south of 42°S for this period, but also suggest an equatorward migration together with an easterly shift in the Agulhas Retroflection during glacial stages. The increased abundances of cold-water planktonic foraminifera tend to support this theory. However, the decline in warm-water species is not large or rapid enough to indicate a collapse of the AgulhasRetroflection or a total lack of influence of Agulhas waters over the core site at this time.

There is a change in surface-water conditions at 200-250 kyr B.P. Planktonic foraminiferal assemblages indicate that this shift represents a transition at the core location, from the presence of a mixed northern Subantarctic and Transitional surface-water mass, with limited variability on G-IG time-scales during the MIS 11 - 7 interval, to overall warmer conditions as well as the development of a G-IG cyclicity for the period MIS 7 – 1 (Fig. 4.4). Data from numerous locations in the Southern Hemisphere show a transition to more "interglacial" conditions at about this time or earlier, in a change referred to as the "Mid-Brunhes climatic event" (Jansen *et al.*, 1986). Flores *et al.* (1999) identify a warm episode (MIS 11 – 7) in the nannofossil assemblages of a core retrieved to the northwest of core MD962080, which they interpret to reflect the "Mid-Brunhes climatic event".

Surface-water changes, following glacial-interglacial cyclicity, are mostly expressed at the site location by advection of cold subpolar waters during glacial intervals, as indicated by the *N. pachyderma* (d)-rich foraminiferal assemblage (Fig. 4.4c). This probably reflects equatorward shifts of the Antarctic Polar Front (APF) and associated subpolar waters during periods of Antarctic ice sheet growth. Despite being less abundant, the presence of tropical and subtropical planktonic foraminifera (Fig. 4.4e) throughout the length of the core studied, suggests that these advections of subpolar waters to the core location did not induce a drastic equatorward shift in the position of the STC or at least indicate that any substantial equatorward displacement of the STC was limited to south of the core location (36°S). This is particularly significant since it implies that the exchange of water from the South Indian Ocean to the South Atlantic Ocean was never entirely obstructed by the STC during any of these periods. It is conceivable that a more equatorward location of this front

could nonetheless force the Agulhas Current Retroflection eastward and limit the throughflow of warmer subtropical water, either as Agulhas rings or as Agulhas filaments.

4.5.2.2 Core MD962084 (Olifants River Slope)

This core is situated in the SBR seaward of the seasonal Namaqua upwelling cell in an area influenced by nutrient-rich upwelled waters, the filamentous region of mesotrophic old upwelled waters, the oligotrophic waters of the South Atlantic gyre, as well as the sporadic incursions of warm saline Indian Ocean waters carried by Agulhas rings. The dominance of Transitional and Subantarctic planktonic foraminifera suggests that the core site has been under the influence of cool-temperate, mesotrophic mixed water masses.

There is a general G-IG correlation of eutrophic species (*N. pachyderma, N. dutertrei*, and *T. quinqueloba*), with increased abundances in glacial periods. This implies a generally higher nutrient and productivity level in the glacial SBR. The negative correlation between the Intermediate and the Transitional Assemblages (Fig. 4.5 b&c), may indicate changes in dominant water masses over the core site from offshore oligotrophic to intermediate conditions, associated with east-west movements in frontal zones of the BUS and also possibly movements in the Southern Ocean hydrological belts.

The maximum concentration in the cold-end member of the faunal population *N. pachyderma* (s) during MIS 9 is co-incident with a shift to an increase in mean contribution of the Subantarctic Assemblage. This event is interpreted as an unusually strong upwelling event, possibly caused by extreme southerly movement of the South Atlantic Anticyclone and associated southeasterly wind regimes (Giraudeau *et al.*, 2001), as it is unlikely that polar/subpolar waters "leaked" through the STC during this interval, which together with MIS 11, has been identified as one of the warmest stages in the last 500 kyr with extreme poleward shifts in the STC and polar front zones (Howard and Prell, 1992; Niebler, 1995).

Rapid increases in abundances of the Warm Cosmopolitan Assemblage at glacial terminations, together with increased abundances of the Tropical/Subtropical Assemblage in warm periods over the last 450 kyr, suggest higher transfer of thermocline and intermediate waters from the Indian Ocean via the Agulhas Current during this period.

The last 200 kyr show a definite trend of either increasing or decreasing contributions in all of the

assemblages (Fig. 4.5a–e). There is a rough G-IG cyclicity within the dominant fauna during this period. Giraudeau *et al.* (2001) report a change in planktonic foraminiferal distribution trend at 250 kyr B.P. in the ODP Site 1087 core retrieved from the continental slope northwest of core MD962084. Variations in abundances of the dominant species change from an ill-defined G-IG relationship prior to MIS 7 to a clear G-IG cyclicity thereafter. These shifts in distributional trends may, in part, be viewed as a local response to the global oscillation of the "Mid-Brunhes climatic event".

4.6 *GLOBOROTALIA MENARDII*

4.6.1 Introduction

Some researchers (e.g. Berger and Vincent, 1986; Charles and Morley, 1988; Berger and Wefer, 1996) have suggested that *Globorotalia menardii* is a reliable indicator of inter-ocean exchange around the southern tip of Africa. They propose that the disappearance of this species in the tropical Atlantic (Ericson and Wollin, 1968) may be related to closing of the "Cape Valve" and consequent cessation of surface-water transfer from the southwest Indian Ocean to the southeast Atlantic Ocean during glacial periods. The opening of the "Cape Valve" and leakage of Indian Ocean surface water into the Southeast Atlantic Ocean via the Agulhas Current is cited as a plausible mechanism for reseeding of this taxon in the tropical Atlantic during warm periods.

4.6.2 Methods

Gr. menardii is a rare species within the foraminiferal population of both cores (< 2% mean relative abundance). Thus, a separate count was undertaken on the whole >125μm fraction. The counts, expressed as absolute abundance (number/g sediment >125μm) are found in Appendix 6. These values were subsequently converted to an accumulation rate (number of specimens/cm^2/kyr).

4.6.3 Results

4.6.3.1 Core MD962080 (Agulhas Bank Slope)

Although the relative contribution of *Gr. menardii* to the overall foraminiferal population of core MD962080 is negligible (max <2 %), the separate count of absolute abundance reveals that this species is present throughout the length of core studied (Fig. 4.6a). The abundance record exhibits high-frequency fluctuations. There is a general pattern of slightly increased abundance values in warm stages, particularly in the early stage of MIS 15 and the late stages of MIS 13 and 5. Although warm stage MIS 11 does record some increase in *Gr. menardii* abundance, it is not the noticeable maximum that one might expect. The upcore pattern of accumulation rate of *Gr. menardii* (Fig. 4.6b) differs dramatically from the record of summed tropical/subtropical species (Fig. 4.4e, pg.4-30). Accumulation peaks of *Gr. menardii* are centred on the final phase of glacial intervals in stages 16, 12, 10, 8 and 6. The inconsistent pattern at the top of the record, where the peak accumulation is at the MIS 3/2 boundary, might be a result of the poorly constrained stratigraphy toward the top of the core. There is a fairly consistent average accumulation rate below MIS 6. Little correlation with the *Gr. menardii* biozones defined for the tropical Atlantic (Ericson and Wollin, 1968) are observed. The biozones are shown on the extreme right of the abundance and accumulation records (Figure 4.6).

4.6.3.2 Core MD962084 (Olifants River Slope)

Gr. menardii does not contribute more than 2% to the overall foraminiferal population of core MD962084. However, the absolute abundance record indicates a near-continuous presence for the time period younger than 450 kyr B.P. (Fig. 4.7a). There are some samples in the older portion of the core, where no *Gr. menardii* were found. On average, *Gr. menardii* is one seventh as abundant in this core as compared to the Agulhas Bank Slope core, MD962080 (mean 7.5 vs 54.5). The period from late stage 13 to early stage 9 is characterised by consistently high abundance. There is an increasing trend over the last 50 kyr. As with core MD962080, the accumulation rate pattern for core MD962084 (Fig. 4.7b) differs markedly from the record of summed tropical/subtropical species (Fig. 4.5e, pg.4-33). Peak accumulation rates of *Gr. menardii* occur at G-IG boundaries (MIS 12/11, 10/9, 6/5 and 2/1), as well as within MIS 8 and at the onset of glaciation at MIS 20. With the exception of the high values at the MIS 10/9 boundary, these peak occurrences are co-incident with

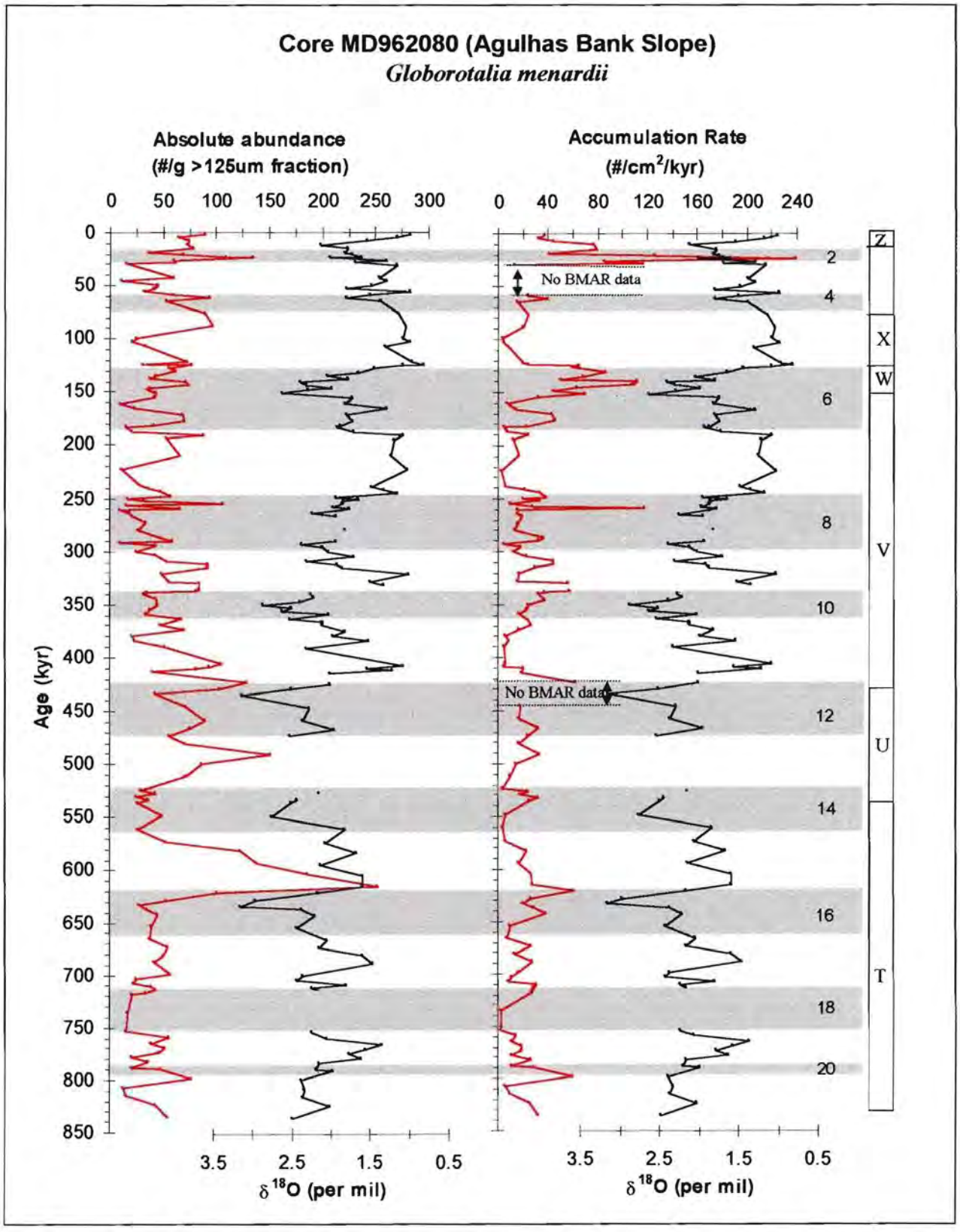

Figure 4.6: *Globorotalia menardii* (red) absolute abundance (a) and accumulation rate (b) for core MD962080. Planktonic oxygen isotopes (black) are plotted on the right. Approximate boundaries of the *Gr. menardii* zones for the tropical Atlantic (after Ericson and Wollin, 1968) are shown on the far right. Grey-shaded bars represent inferred glacial marine isotope stages (MIS). Note the different scales on Figs 4.6 and 4.7.

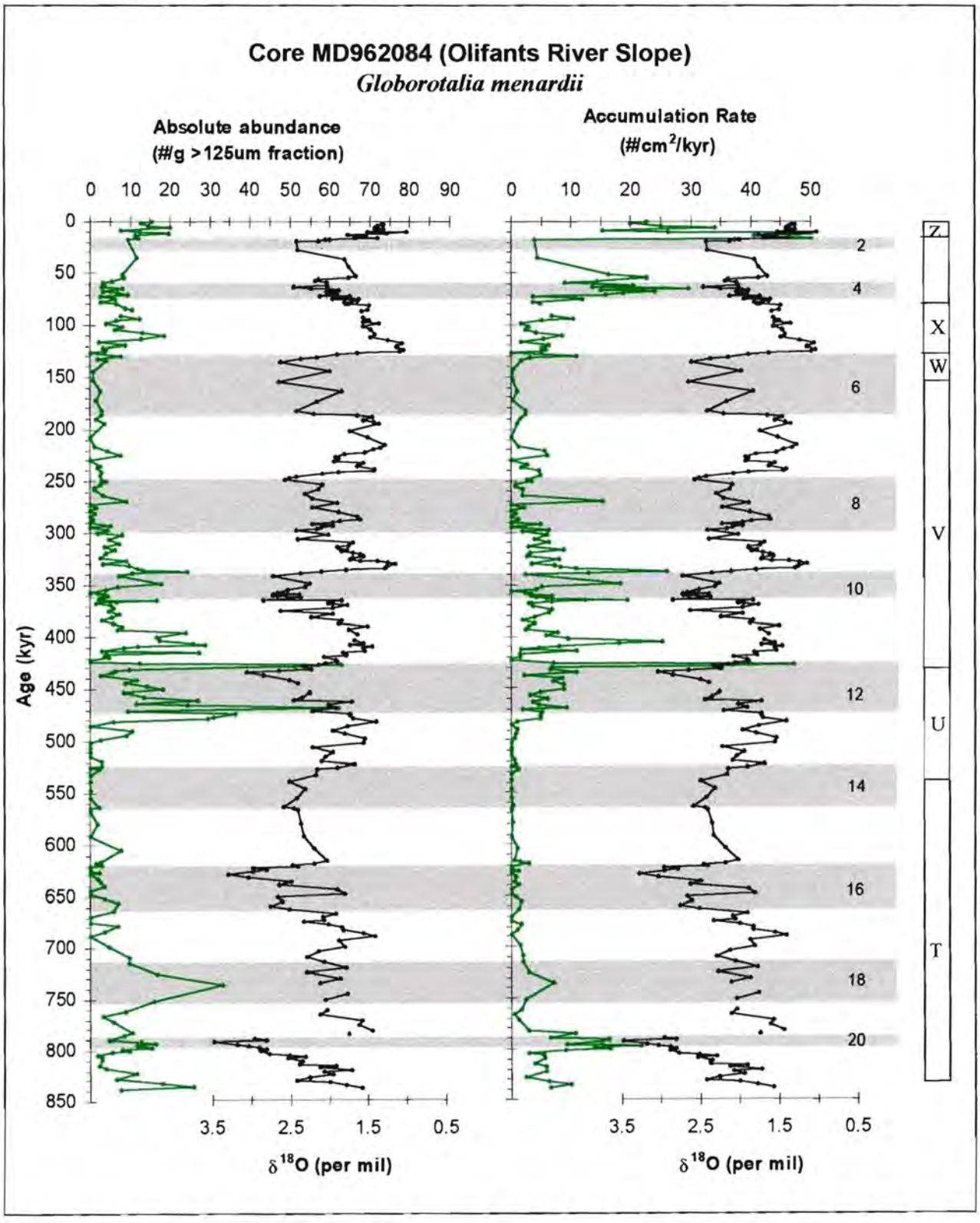

Figure 4.7: *Globorotalia menardii* (green) absolute abundance (a) and accumulation rate (b) for core MD962084. Planktonic oxygen isotopes (black) are plotted on the right. Approximate boundaries of the *Gr. menardii* zones for the tropical Atlantic (after Ericson and Wollin, 1968) are shown on the far right. Grey-shaded bars represent inferred glacial marine isotope stages (MIS). Note the different scales on Figs 4.6 and 4.7.

the *Gr. menardii* biozone boundaries U-V, W-X and Y-Z in the tropical Atlantic (Ericson and Wollin, 1968). There is also a certain degree of consistency between the accumulation data and the biozones as defined by Ericson and Wollin (1968). The *Gr. menardii* complex in the T-zone accounts, on average, for a smaller proportion of the foraminiferal assemblage, especially in the South Atlantic (Ericson and Wollin, 1968), which corresponds with the consistently low values in the lower half of core MD962084. *Gr. menardii* accumulation rates are high in zones V, Y and Z, which were identified as zones of abundant *Gr. menardii* occurrence in the tropical Atlantic Ocean (Ericson and Wollin, 1968). Pether (1994) identified two periods (at ~ 10 kyr B.P. and 12.5-13.5 kyr B.P.) of enhanced advection of Agulhas waters into the SBR by the discovery of bivalves that presently inhabit the warm-temperate Algoa biogeographic province of the eastern Agulhas Bank region. The deglacial timing of these molluscan "Algoa events" is coincident with the period of maximum *Gr. menardii* accumulation rate in core MD962084.

4.6.4 Discussion

4.6.4.1 Core MD962080 (Agulhas Bank Slope)

The upcore pattern of accumulation rate of *Gr. menardii* in core MD962080 bears a unique signature of maximum Indian Ocean water leakage at glacial terminations. A comparison with the distributional trend of dominant planktonic foraminiferal assemblages (Fig. 4.4, pg. 4-30) suggests that this specific dynamic of Indian Ocean water inflow acted independently of changes in the nature of surface water masses in the vicinity of the western Agulhas Bank Slope.

The occurrence of *Gr. menardii* throughout the length of core studied implies that Indian Ocean water passed over the Agulhas Bank (and very likely into the South Atlantic Ocean) throughout the last 850 kyr. The core site lies under the area of present Agulhas ring shedding (Fig. 4.8). Some authors (e.g. Berger and Vincent, 1986) have suggested the possibility of a cessation of inter-ocean exchange due to the obstruction of the Agulhas Retroflection by substantial equatorward migration of the STC during glacial periods. Shannon *et al.* (1990), among others, suggest that the present zonal position of the Agulhas Retroflection regime may be controlled by the volume transport/inertia of the Agulhas Current. Even if the Agulhas Retroflection had been constrained to remain far to the east during glacial periods, Agulhas rings and filaments may still have passed through the gap remaining between the southern tip of the Africa (which shifted poleward during glacial lowstands) and the STC (which shifted equatorward during glacial periods). Even in the unlikely event of this

gap being closed, water derived from the Agulhas Current could nonetheless have passed over the Agulhas Bank. This leakage would, however, have been of a different nature, consisting of surface water only and not deep-reaching Agulhas rings. The consistently higher values in this core, compared to those in core MD962084, reflect the greater influence of tropical waters over this core site for the period investigated.

4.6.4.2 Core MD962084 (Olifants River Slope)

Despite the relatively small contribution of *Gr. menardii* to the overall foraminiferal population in core MD962084, the almost continuous presence of this species, as shown in the absolute abundance record (Fig. 4.7a), implies that, while the volume and intensity may have varied, transfer of tropical Indian Ocean waters into the SBR has continued almost uninterrupted, for at least the last 850 kyr. This supports the inference expressed above that, for this period, the input of Indian Ocean water to the South Atlantic was not directly controlled by the dynamics of Southern Ocean waters and their associated belt of hydrological fronts. These transfers appear to have been strongest at glacial terminations. If, as indicated by the coherence of molluscan and foraminiferal data, one assumes that the occurrence of *Gr. menardii* in the SBR is related to the functioning of the "Cape Valve", then the maximum accumulation rate of this species reflects maximum transfer of Agulhas waters around the tip of Africa. Thus, the Agulhas Current flowed most strongly in the late stages of glacial periods. If, as suggested by this data, Agulhas water leakage continued in glacial times, then the Holocene resurgence of the Agulhas Current would not necessarily be solely responsible for the reseeding of *Gr. menardii* into the Atlantic Ocean, as suggested by Berger and Vincent (1986).

Tropical species such as *Gr. menardii*, *Sphaerodinella dehiscens* and *Globorotalia conglobatus* are found in the living and fossil planktonic foraminiferal assemblages of the Northern Benguela Region (NBR) (Giraudeau, 1993; Ufkes *et al.*, 1998) and the South Atlantic and South Indian subtropical gyres (Bé and Tolderlund, 1971; Bé and Hutson, 1977). The scarcity or absence of these species in the Olifants River Slope core, MD962084, implies that extended periods of extreme surface warming, associated with extensive transfer of warm Agulhas waters into the southeast Atlantic and complete cessation of coastal upwelling did not occur in the SBR over the last ~850 kyr. However, remote sensing and drogue studies have shown that the most common present path for Agulhas Rings shed into the Benguela System has a northwest trajectory, offshore of the Olifants River Slope core site (Fig. 4.8), so the passage of rings may not be consistently recorded in this core. This is not to say that periods of warm surface water and relaxed upwelling do not and have not occurred in the region

of the core site.

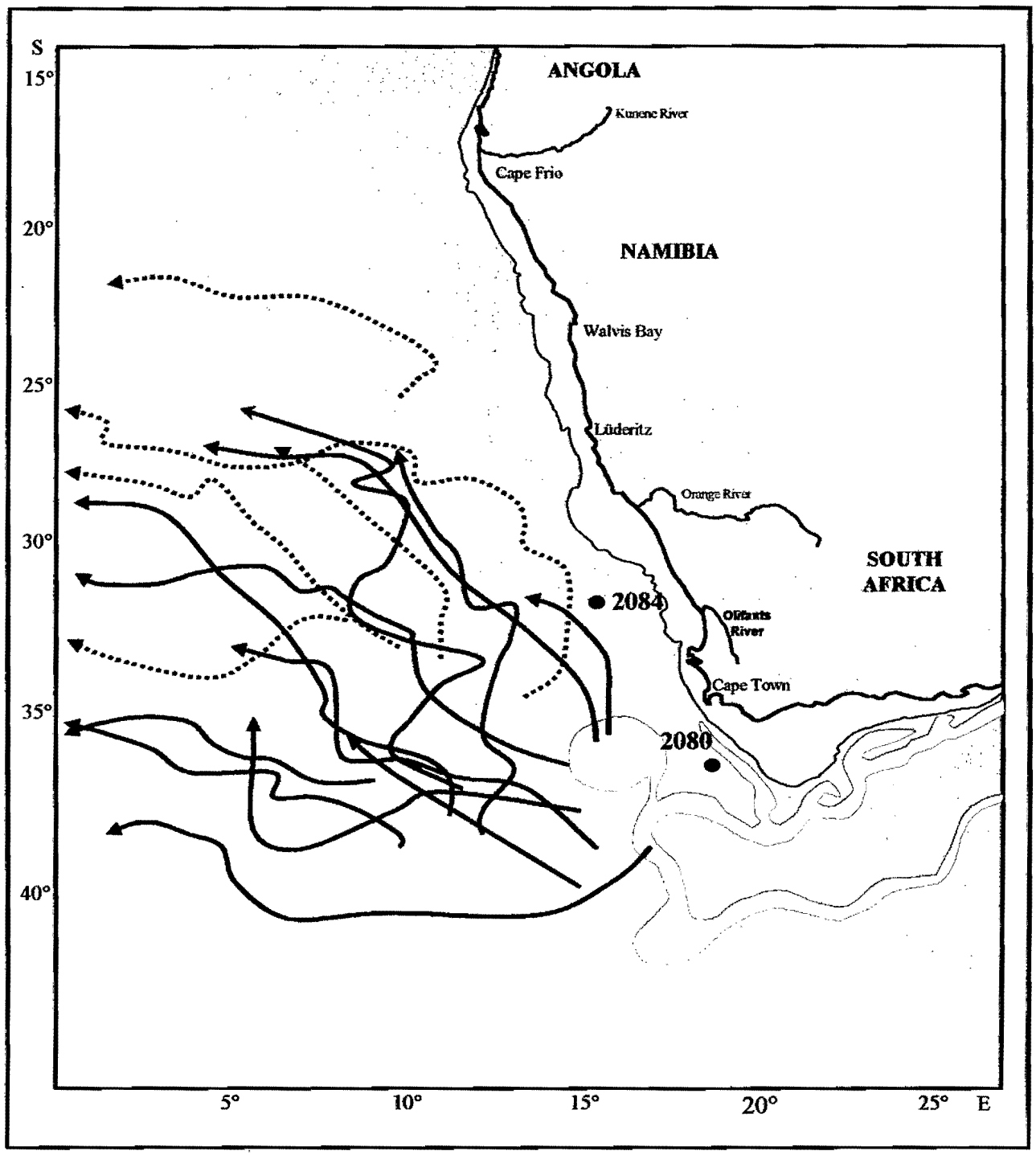

Figure 4.8: Paths of observed Agulhas Rings for the years 1986-87, 1993, 1994, and 1995. Paths of rings that split off from rings shed at the Agulhas Retroflection are shown as dashed lines. Core locations are indicated by black dots with core numbers. (After Gordon and Haxby, 1990 and Schouten, 2001).

Although it is unlikely, as this is a fairly robust species, that variations in *Gr. menardii* abundance and accumulation are influenced by calcite preservation/dissolution cycles, this possibility is explored in the following chapter in section 5.4.

CHAPTER 5: PHYSICO-CHEMICAL CHARACTERISTICS:- CALCIUM CARBONATE, SEDIMENT TEXTURE and PRESERVATION

This chapter deals with the physico-chemical characteristics of the core sediments. The use of calcium carbonate as a tool for identifying glacial-interglacial cycles is discussed. The sediment textural record and a foraminiferal preservation index are presented before the results discussed in conjunction with the carbonate content.

5.1 INTRODUCTION

The use of weight percent calcium carbonate (% $CaCO_3$) as a carbonate-preservation indicator is well documented (e.g. Berger, 1973; Volat *et al.*, 1980). The intensity of carbonate dissolution varies greatly from area to area and also on glacial-interglacial (G-IG) timescales. As opposed to organic carbon, carbonate content is generally high in sediments below low-productivity areas (Wefer *et al.*, 1999) and can be low in highly productive areas as a result of dissolution and/or dilution. In oligotrophic areas, carbonate accumulation may serve as a primary productivity indicator in sediments lying above the lysocline.

However, variations in % $CaCO_3$ in a single core cannot simply be interpreted as an index of preservation, because the relative abundance of carbonate is controlled by the balance of productivity over dissolution and also by dilution due to the influx of non-carbonate material, such as terrigenous sediments (fluvial or aeolian). The conversion of % $CaCO_3$ to $CaCO_3$ mass accumulation rate (MAR) accounts for the dilution effect (Howard and Prell, 1994). High carbonate accumulation rates are usually associated with periods of high biogenic productivity (Bassinot *et al.*, 1994a).

Foraminiferal tests tend to break down into smaller fragments as carbonate dissolution increases (Thunell, 1976). The coarse fraction (>125μm) or sand fraction (>63μm) of the sediment reflects the preservation of foraminiferal tests, with low sand contents indicating enhanced dissolution. Foraminiferal fragmentation is one of the most reliable indices of carbonate dissolution (e.g. Berger, 1967; Crowley, 1983; Peterson and Prell 1985; Le and Shackleton, 1992). Weight percent coarse fraction and foraminiferal number (number of planktonic foraminifera per gram sediment) are systematically related (Howard and Prell, 1994) and changes in these indices are attributed to

(1) sedimentological factors such as foraminiferal-test dissolution (Peterson and Prell, 1985; Howard and Prell, 1994), winnowing by bottom currents (Wu and Berger, 1991) and/or dilution by fine-grained non-biogenic particles (Bassinot *et al.*, 1994a) and
(2) ecological factors such as lower foraminiferal production and/or a change in dominance between nannofossils and foraminifera (Howard and Prell, 1994; Bassinot *et al.*, 1994a).

Spectral reflectance, carried out on board the coring cruise, is used as a first-pass indicator of $CaCO_3$ content. However, a comparison of the carbonate content with the spectral reflectance data (IMAGES Homepage) shows a number of discrepancies in the major trends of the data sets and highlights that the use of spectral reflectance as an indication of carbonate content is not entirely representative.

5.2 PREVIOUS WORK

Since the early work of Arrhenius (1952) it has been established that carbonate contents of equatorial pelagic sediments show cyclic variations associated with Pleistocene G/IG changes (e.g. Berger, 1973; Moore *et al.*, 1982; Crowley, 1985; Farrell and Prell, 1989; Le and Shackleton, 1992). Indo-Pacific carbonate fluctuations show increased dissolution during interglacial periods and enhanced preservation during glacials (e.g. Berger, 1973; Farrell and Prell, 1989). In contrast, in the Atlantic and Southern Oceans, dissolution generally increased during glacial periods (e.g. Crowley, 1983; Howard and Prell, 1994).

Most studies dealing with carbonate dissolution have focused on deep-sea sediments below the lysocline where high-amplitude fluctuations in carbonate content or calcareous microfossil preservation are recorded (e.g. Berger, 1973; Peterson and Prell, 1985; Farrell and Prell, 1989). As a result there are fewer data on dissolution cycles above the lysocline (e.g. Droxler *et al.*, 1983). It has been shown that foraminiferal fragmentation is one of the most reliable indices of carbonate dissolution (Thunell, 1976; Le and Shackleton, 1992). In their study of sediments on Ninetyeast Ridge in the eastern equatorial Indian Ocean, Peterson and Prell (1985) showed that 60% of the whole sand-sized planktonic foraminifera had already broken up at the level of the lysocline, whereas only 20 –30% of the total carbonate was estimated to be lost to dissolution. It has been shown that decrease in coarse fraction content is a much more sensitive indicator of dissolution than carbonate content (Berger *et al.*, 1982; Peterson and Prell, 1985).

In a study of carbonate preservation in the Southern Ocean, Howard and Prell (1994) used cores from the Southeast Indian Ridge and the deep southern Cape Basin to show that, during glacial periods, carbonate dissolution was enhanced in areas that are today bathed in Circumpolar Deep Water. They estimate that glacial $CaCO_3$ production was lower than at present and deduce that lysoclines shoaled during glacial stages over the past 500 kyr. Significant reductions in carbonate mass accumulation rate occurred between 2000 and 4000 m during glacial stages. There is a strong correlation between $CaCO_3$ preservation in the Southern Ocean and Northern Hemisphere ice volume (Howard and Prell, 1994), with enhanced dissolution during glacial cycles coincident with reduced supply of nutrient-depleted NADW to the Southern Ocean, implying a greater influence of more corrosive bottom waters. Coarse-fraction records from the tropical Indian Ocean display high-amplitude oscillations on the order of 500 kyr for the last 1500 kyr (Bassinot *et al.*, 1994a). The data indicate that changes in grain size are mainly the result of carbonate dissolution through the breakdown of sand-size foraminifera, resulting in an increase in the fine-fraction. The "Mid-Brunhes dissolution cycle", a period of high carbonate dissolution between ~700-200 kyr B.P.(Bassinot *et al.*, 1994a), is obvious within the irregular long-term dissolution oscillation. The dominance of 100-kyr and 41-kyr periodiciteis and the lack of a clear 21-kyr cycle over the last 1500 kyr implies that changes are driven by deep-water circulation. In the Late Pleistocene coarse-fraction variations are associated with G/IG cycles (Bassinot *et al.*, 1994a).

Diester-Haass (1985) used both opal distribution and carbonate dissolution cycles to trace the coastal upwelling signal of the Benguela Current as far back as the Late Miocene. She concluded that upwelling activity intensified at the eastern Walvis Ridge during interglacial periods. In the Walvis Ridge area carbonate accumulation was lowest in MIS 2 and 4, largely in response to dissolution induced by CO_2-rich bottom waters (Summerhayes *et al.*, 1995). Terrigenous sedimentation off Namibia (mainly aeolian) was highest during these periods as easterly "Berg" winds became more dominant (Summerhayes *et al.*, 1995).

Bickert and Wefer (1996) used sand contents (as a representation of carbonate dissolution) and benthic $\delta^{13}C$ records to reconstruct the history of deep water circulation in the South Atlantic for the last 360,000 years. Cores taken at ~ 4000 m water depth in the equatorial Atlantic showed a strong 100-kyr cyclicity with low sand contents (equating to strong dissolution) in glacial periods. Cores from the southeast Atlantic exhibit coarse-fraction fluctuations with decreases in sand contents during transitions from interglacial to glacial periods and overall higher sand contents during interglacial

periods. The data also exhibit a general increasing trend over the last 400 kyr, superimposed on short-term variability. Contrary to the deductions of Howard and Prell (1994), Bickert and Wefer (1996) conclude that, throughout the Late Pleistocene, the lysocline did not rise above 3800m in the southeast Atlantic. Instead, variations in the sand contents are related to productivity cycles, with low sand contents corresponding to high organic carbon accumulation rates. Records from the Angola and Cape Basins exhibit fluctuations similar to dissolution variability in the Pacific Ocean, implying globally driven changes in the carbon reservoir (Bickert and Wefer, 1996). Peak carbonate production at high southern latitudes occurred during MIS 11, resulting in the deposition of light-coloured, carbonate-rich sediments above the lysocline throughout the Southern Ocean (Hodell *et al.*, 2000). The analysis of five gravity cores from the eastern South Atlantic Ocean show significantly high accumulation of calcareous dynoflagellate cycsts during Termination 1 and 2 (Esper *et al.*, 2000). The assumed increase in carbonate preservation, coinciding with high cyst production and low organic matter productivity-related dissolution, is interpreted to reflect low-productivity conditions during the transitions from glacial to interglacial conditions (Esper *et al.*, 2000).

5.3 METHODS

Percent calcium carbonate was calculated by measuring the mass difference after the sub-samples for organic carbon stable light isotopes were treated with 1M HCl, left to stand overnight, agitated in an ultrasonic bath for 2 minutes and left to settle for 30 minutes. The samples were then centrifuged, the supernatant drained off and the samples rinsed with distilled water and re-centrifuged. This process was repeated three times. The rinsed samples were freeze-dried overnight and then weighed.

5.4 RESULTS

Following the methods of Howard and Prell (1994), Bassinot *et al.* (1994a) and Bickert and Wefer (1996) the dataset for this study comprises (a) $\%CaCO_3$, (b) % sand (= dry weight of >63 μm fraction / dry weight of total sample), (c) % coarse fraction (= dry weight of >125 μm fraction / dry weight of total sample), (d) preservation index (= % whole foraminifera / whole foraminifera + fragments) and (e) carbonate mass accumulation rate ($CaCO_3$ MAR = weight fraction $CaCO_3$ x dry bulk density x linear sedimentation rate). Raw data are presented in Appendix 7 and plots of these proxies versus age are shown in Figures 5.1 and 5.2.

5.4.1 Core MD962080 (Agulhas Bank Slope)

Carbonate content varies between 61 and 85 % (mean 74%). There is no clear overall G-IG cycle, with fluctuations in abundance occurring on shorter timescales (Fig. 5.1a). The highest continuous carbonate contribution is recorded in MIS 11. This period of high carbonate production corresponds with observations by Hodell *et al.* (2000), who report distinctive light-coloured, carbonate-rich sediments above the lysocline occuring throughout the Southern Ocean during MIS 11. High $\%CaCO_3$ values are also found in MIS 9, with brief episodes of high occurrence in MIS 17 and 16. The minimum values recorded in MIS 7 contrast with this trend towards increased carbonate content during interglacials in the middle section of the core. There is a general decreasing trend in $\%CaCO_3$ from the bottom of the core to MIS 14, after which the trend is towards increased carbonate content. This increasing trend ceases in MIS 8, when there is a change to, on average, lower carbonate values.

The sand fraction (>63 μm) is dominated by calcareous planktonic foraminifera. The core can be divided into three sections based on the abundance of sand (Fig. 5.1b). The bottom portion from MIS 21 – 16 and the top third (MIS 10 – 1) are significantly coarser (more sand content) than the section from MIS 15 – 11, where the lowest sand contents are recorded in interglacial stages MIS 13 and 11. There is a general G-IG cyclicity with higher sand contents during glacial periods. Coarser textures are best developed in glacial stages 16 and 6, with high sand contents also occurring in MIS 20, 10 and 8.

The coarse fraction (>125 μm) consists almost exclusively of planktonic foraminifera. The coarse fraction abundance (Fig. 5.1c) mirrors the sand contents (Fig. 5.1b). As with $\%CaCO_3$ there is a general decreasing trend in both sand content and the coarse fraction from the bottom of the core to MIS 14.

The record of whole tests versus fragments (or preservation index) shows, as does that of the textural data, enhanced preservation during glacial periods (Fig. 5.1d). Enhanced preservation occurs in the late stages of glacial periods MIS 16 and 8, but also in early MIS 14 and at the beginning of interglacial stage 11. Glacial preservation-events are not equal in amplitude; MIS 6 records the strongest consistent preservation-event. Several incidents of dissolution are seen within interglacial intervals MIS 19, 11 and 9. A low-frequency variability is evident in this record.

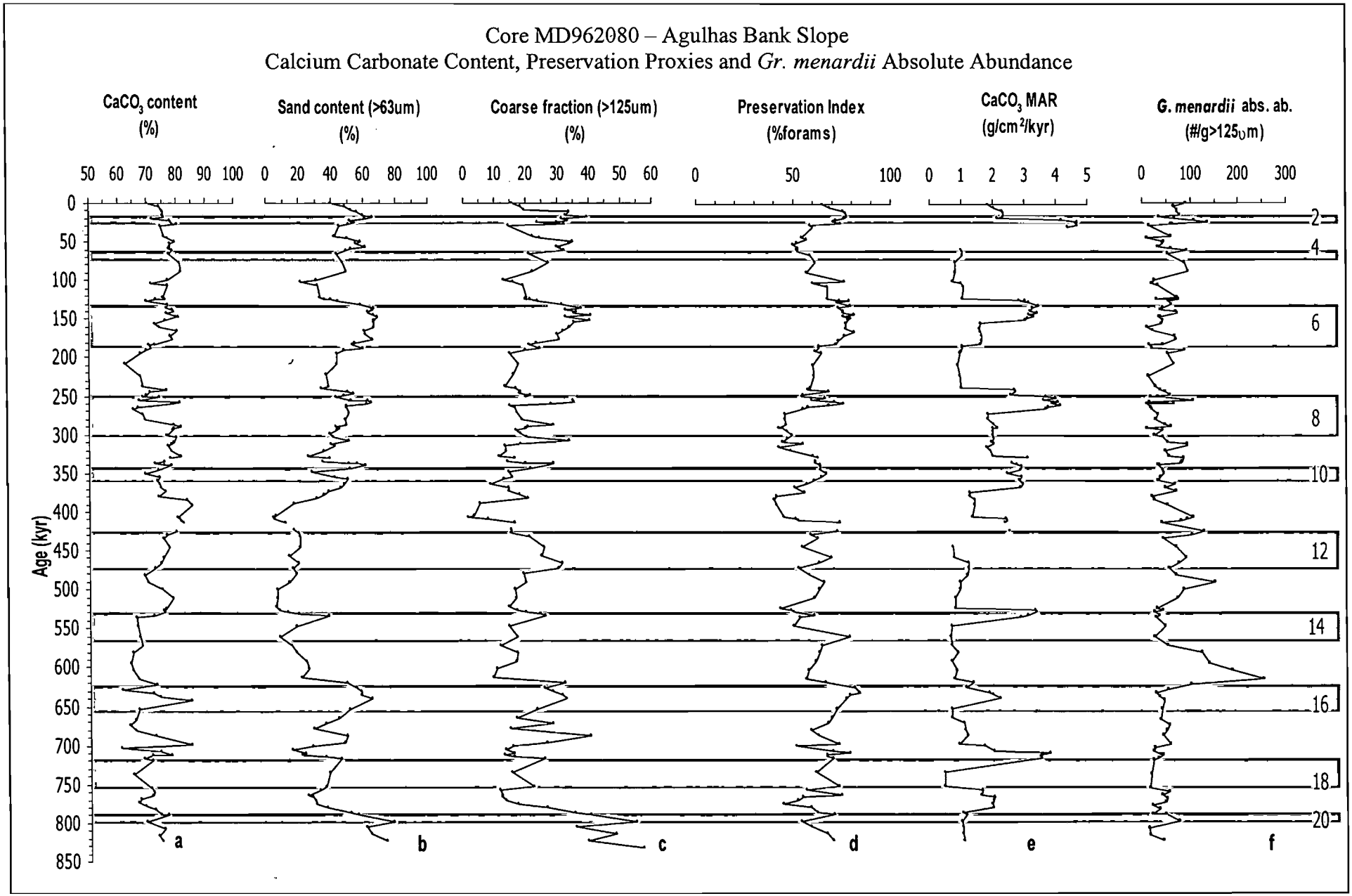

Figure 5.1: (a) Calcium carbonate contents, (b) sand contents (>63μm), (c) coarse fraction contents (>125μm), (d) Preservation Index (e) carbonate mass accumulation rate and (f) *Gr. menardii* absolute abundance for core MD962080. Grey-shaded bars represent inferred glacial marine isotope stages (MIS).

The $CaCO_3$ MAR, which corrects for the processes of dilution and winnowing, shows a temporal pattern generally similar to the other proxies, with increased carbonate accumulation in glacial periods and lower accumulation rates during warm stages (Fig. 5.1.e). Peak accumulation rates are centred on the final stages of glacial cycles or at G-IG transitions (e.g. MIS 18/17 and late stages14, 8, 6 and 2.), with minimum values often occurring at the onset of glaciation (e.g. MIS19/18, 17/16, early MIS 14 and 12. Interglacial stages 15, 13, 7 and 5 are periods of consistently low accumulation rates.

In addition, while there is a consistent increase in all records in MIS 2, peaks in absolute abundance of *Gr. menardii* are not directly linked to the carbonate preservation indices (Fig.5.1f). Variations in *Gr. menardii* accumulation rate follow changes in $CaCO_3$ MAR indicating that sediment accumulation is the dominating factor in these records. These data suggest that variations in *Gr. menardii* abundance and accumulation rate are not driven by carbonate preservation/dissolution cycles.

5.4.2 Core MD962084 (Olifants River Slope)

Core MD962084 is more carbonate-rich than core MD962080 with carbonate content varying between 75 and 95 % (mean 86% compared to 74% for core MD962080). There is a change upcore from below-average to increased carbonate content at the end of MIS 16. The last 450 kyr of the record (Fig. 5.2a) shows a tendency towards G-IG cyclicity, with increased carbonate content during glacial periods and lower amounts in interglacial intervals. Prior to 450 kyr BP there is no clear G-IG cyclicity. As with core MD962080, minimum values are recorded in MIS 7. Low carbonate contents are also seen in interglacial intervals MIS 17 and 5. Carbonate contents peak in the final stages of glaciation or at transitions from glacial to interglacial conditions during MIS 18/17, 14/13 and 12/11. The glacial interval MIS 6 has constantly high carbonate values. This contrasts with records from the NBR which document significant carbonate dissolution early in MIS 6 (Volbers and Henrich, 2002).

This core is much muddier (i.e. lower sand contents) than the Agulhas Bank Slope core, with an average sand content of 12% (compared to 42% for core MD962080). The lower half of the core (up to MIS 11) has, on average, < 10 % sand contents, with the exception of the very bottom, where the texture is relatively coarse (Fig. 5.2b). There is high frequency (shorter than G-IG timescales) variability within this section of the core. A G-IG cyclicity develops in the last 400 kyr of the record,

with coarser textures (increased sand contents) in glacial periods. The data also exhibit a general coarsening-upward trend over the last 400 kyr, superimposed on short-term variability.

The coarse fraction (>125 μm) consists almost exclusively of planktonic foraminifera. The coarse fraction contents (Fig. 5.2c) broadly mirror the sand contents, with a general trend towards coarser sediment during glacial periods, although the frequency and amplitude of the fluctuations are greater for the interval MIS 11-6.

The Preservation Index has a slightly different pattern from the other proxies. Firstly, the G-IG cyclicity over the last 450 kyr is not as pronounced. Although there are strong preservation episodes in glacial periods (e.g. MIS 12, 6 and 4), the record also shows preservation events at the beginnings of interglacials such as MIS 15, 9, 7 and 3. Secondly, there are two distinct phases to the record. There is a general trend towards increased dissolution (thus lower preservation) from the bottom of the core to MIS 12. Thereafter, the trend changes to enhanced preservation upcore.

Unlike the $CaCO_3$ MAR record of core MD962080, this record shows low accumulation rate during MIS 6. This is a period of increased values in all other proxies. The $CaCO_3$ MAR record shows a general pattern of high carbonate accumulation rates at G-IG transitions (Fig. 5.2e). Accumulation rates peak at glacial terminations (e.g. MIS 20/19, 16/15, 14/13, and in late MIS 12 and 2). Conversely, high accumulation rates are also recorded at the onset of glaciation at MIS 14, 10 and 4. High carbonate accumulation is seen in both glacial stage 8 and interglacial MIS 9.

There is no apparent association between the calcium carbonate preservation indices and records of absolute abundance for the foraminifera *Gr. menardii* (Fig. 5.2f). These results indicate that the occurrence of *Gr. menardii* reflects incursions of Agulhas waters into the Southeast Atlantic and that the presence of this foraminifer in the sediment record is not substantially affected by calcite dissolution and preservation.

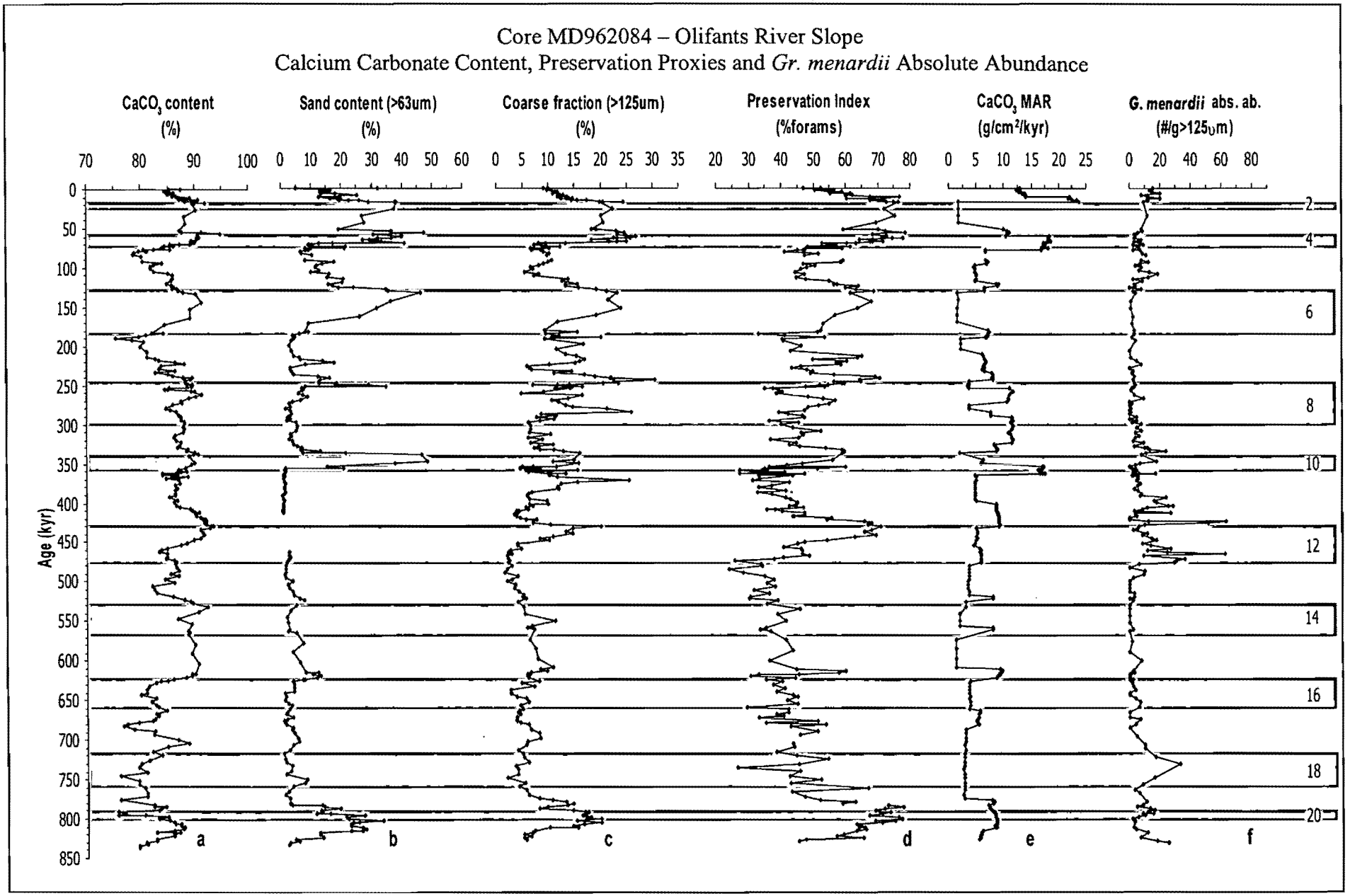

Figure 5.2: (a) Carbonate contents, (b) sand contents (>63μm), (c) coarse fraction contents (125μm), (d) Preservation Index (e) carbonate mass accumulation rate and (f) *Gr. menardii* absolute abundance for core MD962084. Grey-shaded bars represent inferred glacial marine isotope stages (MIS).

5.5 DISCUSSION

5.5.1 Core MD962080 (Agulhas Bank Slope)

The data point to MIS 11 as being the period of highest carbonate production over the last 850 kyr. Carbonate contents do not show any G-IG cyclicity, but while $\%CaCO_3$ is often used as a proxy for carbonate dissolution, it is not necessarily a true reflection in all areas. Variations in $\%CaCO_3$ are a combination of carbonate production, preservation and dilution by non-carbonate sediments. Dilution by terrigenous sediments is unlikely because, under interglacial conditions (as at present), the core site lies far from the coastline. However, during Pleistocene lowstands, the southern tip of Africa would lie southeast of its present position, close to the core latitude at 36°S, but farther east at 21°E (core longitude 19°28'E).

Coarse fraction variations are associated with G/IG cycles with coarser textures defining glacial stages. The positive correlation between coarse fraction content and preservation index argues for dissolution as a controlling mechanism, such that changes in grain size are mainly the result of carbonate dissolution through the breakdown of sand-size foraminifera resulting in an increase in the fine-fraction. The long-term evolutionary trend of coarsening-upward sediment from MIS 11 is consistent with earlier studies in the Atlantic, Pacific and Indian Oceans (Bickert and Wefer, 1996), referred to as the "Mid-Brunhes dissolution cycle" (Bassinot *et al.*, 1994a).

Winnowing of fine particles by bottom currents, which is important down to depths of at least 2500m (Wu and Berger, 1991), must be considered as a driving mechanism for the textural variability. This core lies at a depth of 2488 m. However, variability in carbonate MAR indicates that the carbonate cycles of the western Agulhas Bank are not simply the result of dilution by terrigenous sediments and /or winnowing of fine sediments, but that they must be driven by changes in carbonate productivity and/or preservation. The BMAR record (Fig. 3.6a, pg. 3-13) shows that sediments over the core site accumulated at much higher rates during glacial periods than interglacials. Thus, the combination of coarse sediment and high BMAR, and the fact that the sediments consist predominantly of nanno- and foraminiferal oozes, suggests that enhanced productivity and subsequent increased deposition and preservation of sand-size planktonic foraminifera during glacial periods are the controlling factors in the textural variability.

The results from these proxies generally contrast with carbonate data for the Southern Ocean, where carbonate contents vary on G-IG time-scales with increased dissolution / lower carbonate production during glacial periods (e.g. Howard and Prell, 1994; Hodell *et al.*, 2000). Howard and Prell (1994) suggest that, during glacial periods, carbonate dissolution was enhanced in areas that are today bathed in Circumpolar Deep Water (CDW) and that significant reductions in carbonate mass accumulation rate occurred between 2000 and 4000 m during glacial stages. Although it falls within the low-accumulation depth range, the core site presently lies at a depth of 2488m, under the influence of the less corrosive NADW (Reid, 1989) (Figure 2.3, pg. 2-8). However, the increase of coarse fraction contents during glacial periods and the decrease during interglacial periods are in agreement with the dissolution-preservation history of deep-sea records from the Indo-Pacific (Berger, 1973; Farrell and Prell, 1989) and the tropical Indian Ocean (Bassinot *et al.*, 1994a). Also, Flores (pers. comm. 2001) found a similar record of increased foraminiferal preservation in a core taken southwest of Cape Town (northwest of this core).

5.5.2 Core MD962084 (Olifants River Slope)

Variations in four of the proxies; $\%CaCO_3$, % sand, coarse fraction and preservation index show a G-IG cyclicity for the last ~500 kyr, with a trend towards higher values during glacial periods. The lack of a G-IG cyclicity in the BMAR and carbonate MAR data, together with the positive correlation between carbonate contents and coarse fraction contents, suggests that winnowing by bottom currents must be considered as a driving force for the observed textural variability, for at least parts of the record. In particular, the low accumulation rate during MIS 6 and increased values in all other proxies indicates that winnowing may be responsible for the coarse textures, high preservation index and high carbonate content during this period. The "Mid-Brunhes dissolution cycle" is obvious within the long-term textural oscillation from MIS 11 - 6.

The change to an, on average, higher carbonate content at the end of MIS 16 is coincident with a period of minimal sand contents, which lasts until the onset of glaciation at MIS 10. This period is also characterized by low coarse fraction values. This change in textural composition cannot be attributed to winnowing (data show low sand contents therefore higher mud contents) or dissolution (data show higher carbonate contents), but rather suggests a change in the dominant carbonate contributor from larger sand-size foraminifera to silt- and clay-size calcareous nannoplankton. As with core MD962080, there is a change upcore from an overall high carbonate content to slightly

lower values at around 250 kyr B.P. Schneider *et al.* (1996) provide evidence for a change in sediment deposits along the Namibian shelf from a carbonate-rich sediments between MIS 15 and 8, to carbonate-poor sediments in younger intervals. This sedimentological pattern is probably indicative of a change in dominant primary producers (calcareous nannofossils and planktonic foraminifera versus siliceous diatoms) and might be interpreted as a response to a change in the nutrient content of upwelled water over the continental margin of southwest Africa (Berger and Wefer, 1996). In addition Stuut *et al.* (2002) show an overall decrease in the size of aeolian dust off the Namibian coast from ca. 250 kyr B.P. to younger periods, reflecting a relative decrease in trade-wind strengths. Enhanced Benguela circulation, prior to 250 kyr B.P., would have reduced the flow of the poleward Angolan undercurrent along the southwest African margin, which presently constitutes the main silicate source for upwelled waters in the Benguela region (Bailey, pers comm, 2002). Upwelling of silicate-poor subsurface waters off southwest Africa would consequently result in massive production and subsequent sedimentation of carbonate producers.

Bickert and Wefer (1996) argue for a global carbonate control over the last 450 kyr, based on the congruency of the sand contents record for a core taken on the slope of the Walvis Ridge in the northern Cape Basin to the Pacific record. Their data show high sand contents at the beginning of interglacial periods. However, peaks in coarse fraction content for core MD962084 are located towards the late stages of glacial periods. The discrepancy between the data sets may be a reflection of bottom-water chemistry. The present circulation of the deep South Atlantic is dominated by interactions between south-flowing NADW and northward-flowing Circumpolar Deep Water (CDW). The density characteristics of these water masses are such that the CDW is divided into an upper (above 1500m) and lower (below 4000m) branch by NADW (Reid, 1989). The Cape Basin is dominated by Lower Circumpolar Deep Water (LCDW) at depths below 4000m. Whereas the Cape Basin and the Pacific data come from deep-sea sediments (below 4000m), core MD962084 lies at the intermediate depth of 1400m. The site currently lies close to the boundary between NADW and the overlying Upper Circumpolar Deep Water (UCDW) (Figure 2.3, pg. 2-8). CDW is undersaturated with respect to carbonate concentration, whereas NADW is slightly superaturated (Bickert and Wefer, 1996), linking the calcite lysocline of the Cape Basin to the mixing zone of northern and southern water masses. An increased contribution of CDW over the core site during glacial periods may contribute to the preservation/dissolution signal. Preservation peaks are often centred on periods of rapid deglaciation rather than at glacial maxima (e.g. around 250, 330, and 620 kyr BP). Berger and Vincent (1986) and Bassinot *et al.* (1994a) reported preservation spikes coinciding with

deglaciation in the equatorial Pacific and Indian Oceans, respectively. The preservation spike corresponding to the last deglaciation, also seen in the Agulhas Bank Slope core, is thought to be a global phenomenon (Berger, 1977; Bassinot *et al,* 1994a).

CHAPTER 6: PALAEOPRODUCTIVITY and NUTRIENT SUPPLY:- ORGANIC CARBON, CARBON ISOTOPES and NITROGEN ISOTOPES

This chapter deals with the chemical palaeoproductivity proxies of the core sediments. Organic matter preserved in the sediments is quantified and the stable isotopes of organic carbon, nitrogen and inorganic carbon are determined and interpreted. Sampling and analytical methods pertaining to all the proxies presented in this chapter are reported. Information about the admixture of terrestrial carbon in the sediments is provided by the C/N ratios. Studies involving organic carbon and nitrogen isotopes are limited in the study areas, so a broader review of the use these proxies in marine sediments is undertaken.

6.1 INTRODUCTION

Palaeoproductivity cycles in the ocean are of great interest because of the close links to CO_2 draw-down, wind regimes, ocean circulation, nutrient distribution and biogeography. Upwelling is closely linked to the trade wind system, which causes Ekman transport of warm surface-waters away from the coast and subsequent upwelling of deeper, cooler, nutrient-enriched waters. "Primary productivity" is the rate of generation of organic material, so organic carbon can be considered the most direct index of palaeoproductivity. The $\delta^{13}C$ of organic matter in sediments reflects the degree of phytoplankton production. A relatively new proxy for ocean productivity is the application of nitrogen isotope ratios in the sediments. "Recycled production" is distinguished from "new production", depending on whether the nitrogen used in producing organic matter is derived from nitrate (new) or ammonia and urea (recycled) (Eppley and Peterson, 1979). In addition, carbon to nitrogen (C/N) ratios can be used to infer the source of the organic matter in the sediment and point to factors potentially affecting preservation. The classical marker for sea-surface fertility is the $^{13}C/^{12}C$ ratio of carbon-secreting organisms (Wefer *et al.*, 1999). Planktonic foraminifera are the primary tools for the reconstruction of the palaeo-carbon isotopic composition of surface waters (Mulitza *et al.*, 1999).

6.2 OVERVIEW

6.2.1 Total Organic Carbon

Generally, there is a strong relationship between productivity in surface waters and organic carbon accumulation in the underlying sediments (Sarnthein *et al.*, 1988). Organic carbon content of sediments below the central gyres is extremely low, whilst in upwelling areas organic carbon content of the sediments is high. Thus, changes in organic carbon content reflect changes in productivity. However, the relationship between organic matter accumulation and productivity is non-linear (Berger and Wefer, 1990) because, in any one place, the variations in sedimentation rates are commonly much smaller than the changes in organic matter content. Furthermore, bacteria in the sediment are continuously decomposing organic carbon. This results in a general trend towards lower productivity estimates with increasing age of the sediment (Wefer *et al.*, 1999). Organic carbon, the most common proxy for palaeoproductivity in low-latitude coastal-upwelling sediments (Schneider *et al.*, 1994), may be more dependent on changes in burial rates than on productivity changes *per se*.

Fluctuations in total organic carbon (TOC) content give an indication of Late Quaternary variations in productivity and thus, allow reconstruction of upwelling intensity in the Cape Basin on a qualitative basis. It has been shown (Müller *et al.*, 1997) that fluctuations in TOC content in sediments from the Benguela System are similar to the variability of the marine biomarker contents, indicating that TOC contents primarily reflect marine export production. Enhanced upwelling injects cold, nutrient-rich water into the surface mixed layer, which results in high export productivity of organic carbon. Thus, periods of high organic carbon burial and low SST are indicative of intense upwelling (Kirst *et al.*, 1999).

6.2.2 Stable Organic Carbon Isotopes

Marine phytoplankton assimilates inorganic carbon, mainly via Rubisco activity in the Calvin-Benson cycle that discriminates against the presence of the heavy isotope ^{13}C in particulate matter (Descolas-Gros and Fontugne, 1990). This leads to low $^{13}C/^{12}C$ ratios in the plankton (Fontugne and Duplessy, 1978). In the marine environment, the range of values of carbon isotopic fractionation between particulate tissue of phytoplankton and CO_2 or HCO^-_3 dissolved in seawater can be more than 20‰ (Descolas-Gros and Fontugne, 1985). Measurements of $\delta^{13}C_{org}$ of phytoplankton particulate carbon

in various parts of the global ocean yield values of –14 to -35‰ (Descolas-Gros and Fontugne, 1990). These values depend on the fractionation between various fractions of dissolved inorganic carbon and the phytoplankton. The variation in carbon isotopic composition of marine phytoplankton has been primarily related to SST variation (Sackett *et al.*, 1965) with an inverse relationship between carbon isotopic fractionation and SST. However, the magnitude of fractionation is also related to species and growth rates (Fontugne and Duplessy, 1981). Marine phytoplankton in tropical and temperate environments have $\delta^{13}C_{org}$ values of about -20‰ to –22‰, whereas values for Antarctic phytoplankton are about -27‰. Deep-water particulate organic carbon (POC) is about 2 to 3 per mil more negative than surface water POC (Fontugne and Duplessy, 1981). The average range for deep-sea sediments is reported to be –18‰ to -22‰ (Goericke, 1994).

The isotopic composition of organic carbon is a useful parameter for quantifying the depositional history of marine sediments (Sackett, 1964). The $\delta^{13}C_{org}$ content of total organic carbon does not change significantly after deposition, thus the same variations observed in modern organic matter should also be observed in sediments (Sackett, 1964). Rau *et al.* (1989) proposed that $\delta^{13}C_{org}$ of sedimentary organic matter may be used as a proxy for ambient molecular CO_2 in the ocean surface water and that high p_{CO2} was responsible for the low $\delta^{13}C_{org}$ values found in the marine sedimentary record. This allows for an independent approach to estimating palaeo-flux of matter to evaluate the strength of the biological pump. However, in areas of high productivity, such as upwelling systems, the variations in $CO_{2\,(aq)}$ cannot account for the measured $\delta^{13}C_{org}$ values (Bentaleb *et al.*, 1996). Phytoplankton carbon metabolism is a major factor governing variations in the stable isotopic composition of organic matter in the euphotic layer (Bentaleb *et al.*, 1996). In subtropical and tropical areas, phytoplankton diversity leads to large differences in carbon metabolism and consequently to different levels of carbon isotopic fractionation (Bentaleb *et al.*, 1996). The interpretation that changes in sedimentary records of photosynthetic fractionation reflect past CO_2 and/or nutrient changes assumes that, in the past, phytoplankton responded to their environment in a similar way to that which is observed today in the modern ocean. At least three factors influence the isotopic composition of marine organic matter: (1) the $\delta^{13}C$ of the inorganic carbon used as the substrate for photosynthesis, (2) the $[CO_{2\,(aq)}]$ and (3) photosynthetic carbon demand, which is directly related to primary productivity (Shemesh *et al.*, 1993). So, an increase in productivity or decrease in $[CO_{2\,(aq)}]$ should enrich the organic matter in ^{13}C.

The bulk $\delta^{13}C_{org}$ values may reflect the $\delta^{13}C$ of multiple organic carbon sources (from diatoms, coccolithophorids, secondary producers etc.) and may further be influenced by an unknown contribution of terrigenous carbon. The admixture of terrestrial carbon can be accounted for, to an extent, by C/N ratios, where values >15 indicate a terrestrial origin and values of 4 – 10 are considered to be marine, (Meyers, 1994; Wefer *et al.*, 1999) and also by $\delta^{13}C_{org}$ in the organic matter using the mean values of ~-21‰ for marine material and -27 to - 28‰ for most terrestrial plants (Müller *et al.*, 1994). However, in South Africa , C_4 grasses are more abundant over most of the country, including on the south coast (where terrestrial run-off could affect sediments on the Agulhas Bank), but in the winter rainfall region of the western Cape Province C_3 grasses dominate (Vogel and Fuls, 1978). The $\delta^{13}C$ values for C_3 species range between –20 and –34 ‰, whilst C_4 species have much lower values, ranging from –16 to ~-9‰ (Vogel and Fuls, 1978).

6.2.3 Stable Nitrogen Isotopes

Primary production in the modern ocean is thought to be nitrogen-limited, although in some areas production may be constrained by micronutrients such as iron. Nitrogen has a much shorter residence time (of the order of $10^3 – 10^4$ kyr) than phosphorous (~10^5 kyr) and its abundance in the ocean is more likely to fluctuate on glacial–interglacial timescales (Ganeshram *et al.*, 1995). Nitrogen is believed to be the limiting nutrient for phytoplankton growth in the Benguela region (Chapman and Shannon, 1985). Nitrate upwelled from deep oxygenated waters has an isotopic signature of 5-6‰ (Wada *et al.*, 1975; Liu and Kaplan, 1989). When nitrate is abundant in the euphotic zone, phytoplankton discriminate against ^{15}N during nitrate uptake, with the result that the residual nitrate becomes progressively enriched in ^{15}N. Phytoplankton production increases $\delta^{15}N$ as the residual nitrate is consumed and as nitrate becomes more depleted in the surface waters (Altabet *et al.*, 1991; Natakusa *et al.*, 1992).

Analysis of core tops (Francois *et al.*, 1992) revealed that the $\delta^{15}N$ of total nitrogen in marine sediments reflects the signal produced in the surface waters. The surface-water relationship of increasing $\delta^{15}N$ with increasing NO_3^- depletion by phytoplankton is generally transmitted directly to the sediments. Early diagenesis appears to increase $\delta^{15}N$ at the sediment-water interface in some areas (e.g. south of the Antarctic Polar Front) by 5 – 7‰, but the diagenetic overprinting does not obliterate the surface signal; rather it is offset by a more-or-less constant value (Altabet and Francois,

1994). Thus, $\delta^{15}N$ of sediments can be used as an indicator of past changes in the degree of nitrate utilisation in the overlying water column with higher utilisation resulting in sediments enriched in 15N (Francois *et al.*, 1992). However, the interpretation of $\delta^{15}N$ signatures in organic matter in the water column and sediment is complicated because the isotopic ratios are subject to modification through kinetic fractionation effects. Modifications to nitrate pools include ammonification, nitrification and denitrification. Also, the transfer of nitrogen through the trophic levels is characterised by a systematic increase in $\delta^{15}N$ (Minagawa and Wada, 1984; Fry, 1988; Hansson *et al.*, 1997).

In the absence or near absence of oxygen, such as in areas of very high productivity and high sedimentation rates, nitrate is used as an electron acceptor in the bacterially mediated degradation of particulate organic matter (POM), resulting in denitrification. Denitrification renders the isotopic source nitrate enriched in ^{15}N and as denitrification proceeds, the residual nitrate in the oxygen-depleted subsurface waters becomes progressively isotopically enriched (Ganeshram *et al.*, 1995). Today, water-column denitrification occurs primarily in three areas: the eastern tropical North Pacific, the eastern tropical South Pacific and the Arabian Sea (Ganeshram *et al.*, 2000). It has been suggested that denitrification, by changing the marine nitrogen inventory and affecting the draw-down of atmospheric CO_2, may be an internal forcing mechanism for climatic change during major glacial-interglacial (G-IG) transitions (Altabet *et al.*, 1999). Sediment denitrification leads to a net loss of fixed nitrogen from the ocean (Ganeshram *et al.*, 2000), which is an important limiting factor for marine productivity, and can act as a sink for atmospheric CO_2 (Altabet *et al.*, 1999).

In contrast to denitrification, nitrogen fixation is the process by which marine organisms, mainly cyanobacteria, use atmospheric N_2 as a nitrogen source, producing photosynthate that is isotopically similar to atmospheric nitrogen. Altabet (1988) showed that in oligotrophic areas, where there is complete utilisation of the available nitrate, the mean $\delta^{15}N$ of particles sinking out of the upper ocean is equal to the mean $\delta^{15}N$ of the nitrate utilised by the phytoplankton. The average $\delta^{15}N$ value for marine nitrate is +4.6‰ and the range for nitrogen fixers is –6 to +6‰. In eutrophic systems, such as the Benguela Upwelling System, where surface water nitrate concentrations are high, food chains are relatively short (i.e. fewer trophic steps), thus the increase in $\delta^{15}N$ of POM is smaller than in other types of systems (Biggs *et al.*, 1989; Wu *et al.*, 1997).

Nitrogen is more rapidly lost than carbon during degradation of POM, thus there is a much greater variation in $\delta^{15}N$ values than in $\delta^{13}C_{org}$ values (Altabet and McCarthy, 1985).

6.2.4 Stable Carbon Isotopes of Planktonic Foraminifera

In the modern ocean, the distribution of ^{13}C and ^{12}C is controlled by a combination of biological and thermodynamic processes. Biological uptake of CO_2 and subsequent conversion into organic matter selectively removes carbon depleted in ^{13}C, resulting in isotopic enrichment of the residual inorganic carbon (Freeman, 2001). The carbon isotope ratio of carbonate-secreting organisms is set by competing processes of CO_2 exchange with air, removal of carbon in solids by export production and re-supply of dissolved carbon from subsurface waters. The $\delta^{13}C$ composition of planktonic foraminifera is affected by the $\delta^{13}C_{\Sigma CO2}$ of the surrounding water, but also by vital effects, the depth of calcification and postdepositional dissolution (Mulitza *et al.*, 1999). A foraminiferal shell calcified in equilibrium should be 1‰ more positive than the dissolved CO_2 of the surrounding seawater (Romanek *et al.*, 1992). There are three major fractionation processes (vital effects) additional to the original equilibrium fractionation for the formation of CO_3 from dissolved CO_2, which affect the $\delta^{13}C$ of the foraminiferal shell (Ravelo and Fairbanks, 1995): (1) incorporation of light metabolic carbon, (2) photosynthetic utilisation of light carbon by symbionts that increases the available ^{13}C for calcification and (3) kinetic fractionation effects related to biological processes.

The "biological pump" creates an isotopic gradient with ^{13}C-enriched surface waters and isotopically depleted and CO_2-rich waters at depth. Thus, the ^{13}C values of planktonic foraminifera in sediments below productive surface waters will be enriched in residual ^{13}C, whereas the contemporaneous benthic foraminifera will be relatively depleted in ^{13}C because of dilution by ^{12}C from settling organic carbon that is oxidised at depth.

Surface waters are generally enriched in ^{13}C relative to deep waters because photosythesis preferentially uses ^{12}C to form organic matter. However, upwelling of deep, nutrient-rich waters introduces ^{13}C-depleted CO_2 into the surface waters, consequently ^{13}C depletion in inorganic carbon is observed when deep, nutrient-rich waters are upwelled to the surface (Freeman, 2001). Fractionation of carbon isotopes between air and water is temperature-sensitive, with lower temperatures leading to greater fractionation. Hence, cold surface waters have a tendency toward high $\delta^{13}C$ ratios, all other factors being equal (Wefer *et al.*, 1999). The $\delta^{13}C$ signal recorded in a particular species of planktonic foraminifera reflects past fluctuations in surface-water productivity or upwelling (Mortlock *et al.*, 1991; Schneider *et al.*, 1994)

6.3 PREVIOUS WORK

Fontugne and Duplessy (1986) used the $^{12}C/^{13}C$ ratios and organic carbon content of deep-sea sediment cores recovered from the North Indian Ocean to interpret variations in the monsoon regime over the last 180 kyr. Their data indicate that organic carbon content of the sediment, which is related to local productivity, was greater during glacial periods in areas where production is dependent on the strength of the NE monsoon. They showed $\delta^{13}C_{org}$ depletion of Holocene sediments compared to glacial sediments, except in the upwelling environment along the Arabian coast, where Holocene sediments showed $\delta^{13}C_{org}$ enrichment relative to the glacial sediments.

Using a sediment record from ODP Site 925 in the tropical Atlantic, Ohkouchi and Wada (1997) show a 3‰ increase in $\delta^{13}C_{org}$ values from the Oligocene to the Middle Quaternary. The $\delta^{13}C_{org}$ values in the Quaternary were -21‰, which is similar to modern sedimentary $\delta^{13}C_{org}$ values (Dean *et al.*, 1986).

Mueller and Voss (1999) measured the organic carbon and nitrogen isotopic ratios and C/N ratios in six sediment cores from six coastal lagoons in order to reconstruct the local palaeoenvironments of the southern Baltic Sea region during the Holocene. The C/N values and $\delta^{13}C_{org}$ and $\delta^{15}N$ ratios of major organic matter sources were used to determine the origin of sedimentary organic matter. Results yielded clearly identifiable stages in the development of the water bodies that are related to regional sea-level fluctuations.

A million-year record of $\delta^{15}N$ for ODP site 722B on the Owen Ridge in the Arabian Sea was reported by Altabet *et al.* (1999). Downcore $\delta^{15}N$ data record clear climatically linked oscillations in denitrification at the major orbital periods. Denitrification was greatest during interglacial periods and was less significant during most glacial periods. The authors argue that since $\delta^{15}N$ leads ice volume by 6 kyr at the 100-kyr period, increased denitrification may have had an important role in bringing about glacial terminations by changing the marine nitrogen inventory, thus affecting productivity and increasing the draw-down of atmospheric CO_2. Nitrogen isotope measurements on sediment cores from the eastern tropical North Pacific, the eastern tropical South Pacific and the Arabian Sea were used by Ganeshram *et al.* (2000) to infer a substantial decrease in denitrification during glacial periods and, consequently, that the oceanic nitrogen content may have been modulated on G-IG timescales by changing rates of denitrification. The decreases in $\delta^{15}N$ corresponded to

decreased accumulation of biogenic sedimentary components, suggesting that reduced denitrification may have been forced by reduced upwelling, decreased export productivity and consequently lower oxidant demand.

6.3.1 The Subtropical Convergence and southern hydrological fronts

One of the first attempts at deriving a palaeoceanographic record from the $\delta^{13}C$ composition of foraminiferal calcite was undertaken by Shackleton (1977). The records showed lower $\delta^{13}C$ ratios at the Last Glacial Maximum (LGM) than during the Holocene, which was interpreted as an injection of light terrestrial carbon into the ocean. However, records of $\delta^{13}C_{org}$ and $\delta^{15}N$ in diatoms and $\delta^{13}C$ from the polar planktonic foraminifera *N. pachyderma* (sinistral) from a core in the Southern Ocean (Shemesh *et al.*, 1993) show that low foraminiferal $\delta^{13}C$ values in the LGM are indicative of reduced glacial primary productivity compared to the Holocene.

A number of authors (e.g. Fischer, 1991; Francois *et al.*, 1993a) have observed strong variations in $\delta^{13}C_{org}$ and $\delta^{15}N$ of surface water particulate organic matter across the southern hydrological fronts in the South Atlantic, Indian and Southern Oceans. Francois *et al.* (1993a) showed that the $\delta^{15}N$ of suspended POM decreases markedly across the Subtropical Convergence (STC) from ~-2‰ in the cold, nutrient-rich polar and subpolar waters to +7‰ in the oligotrophic waters north of the STC. Coincidentally, sediment $\delta^{15}N$ increased from ~+5‰ to a maximum of +11‰ from the polar region to just north of the STC. Francois *et al.* (1993b) measured sediment $\delta^{15}N$ to evaluate changes in nitrate utilisation in the overlying surface waters associated with palaeoflux variations in southwest Indian Subantarctic waters. They found sediment $\delta^{15}N$ to be 1.5‰ higher during glacial MIS 2 and deglaciation than during relatively warm MIS 3 and the Holocene. The results point to nitrate depletion of the surface waters at this time due to the presence of a meltwater lid causing increased stratification and reduced supply of nitrate to the surface waters during the LGM and early deglaciation. Using $\delta^{13}C_{org}$, $\delta^{15}N$ and other geochemical proxies in the sediment record from a core in the Southern Ocean, Francois *et al.* (1997) showed that surface water stratification south of the Antarctic Polar Front contributed substantially to the reduction in atmospheric CO_2 during the last glacial. Francois *et al.*, (1992) suggest that during the LGM, Subantarctic waters in the SE Indian Ocean and, possibly, waters just south of the glacial Antarctic Polar Front, became more nutrient deficient whilst moving equatorward. This increased nutrient depletion may have contributed to the

decrease in nutrient concentration often observed in glacial intermediate waters.

Popp *et al.* (1999) showed that variations in carbon dioxide concentrations, phytoplankton taxonomy and nutrient variations influence the isotopic composition of organic matter in the Antarctic Polar Front region. Bentaleb *et al.* (1996) showed that phytoplankton populations on either side of the STC have different carbon metabolisms. North of the STC, communities are predominately mixo/heterotrophic and $\delta^{13}C_{org}$ values of sea-surface particulate organic matter does not directly reflect the $[CO_{2(aq)}]$, whereas south of the STC autotrophic phytoplankton dominate and there is a good relationship between $\delta^{13}C_{(POC)}$ and $[CO_{2\ (aq)}]$. Their results also suggest lower glacial productivity in the Southern Ocean.

Comparisons of planktonic foraminiferal oxygen isotopic records for peak interglacial conditions over the past 450 kyr reveals that, in the high southern latitudes, MIS 11 was not substantially warmer than other interglacial periods, although this warm period did last longer (Hodell *et al.*, 2000). High benthic carbon isotope values during MIS 11 in cores bathed in Circumpolar Deep Water (CPDW) suggest a strong input of NADW into the Southern Ocean at that time. The highest planktonic $\delta^{13}C$ values were also recorded in MIS 11, possibly reflecting upwelled CPDW with a greater contribution from NADW as well as lower whole ocean nutrient inventories (Hodell *et al.*, 2000). Increased NADW production reflects intensification of overturning in the North Atlantic and strengthened heat transfer from the southern to the northern hemisphere.

6.3.2 The Agulhas Current Region

A study on pelagic fish from the west and south coast of South Africa showed that $\delta^{13}C_{org}$ is significantly higher in hake bone from the west coast than in hake bone from the south coast (Parkins, 1993). Pelagic fish and plankton, sampled from the west coast, were more enriched in ^{13}C than samples from the Agulhas Bank, indicating that fish on the Agulhas Bank are consuming plankton one size-class lower than fish on the more productive west coast (Sholto-Douglas. 1992). The difference in the type of plankton consumed (omnivorous euphausiids on the west coast versus herbivorous zooplankton on the south coast and Agulhas Bank) was cited as a cause for the depleted $\delta^{13}C_{org}$ values on the south coast. Additionally the $\delta^{15}N$ of both hake muscle and bone was significantly higher on the west coast than on the south coast. Moreover, there was a marked

decrease in $\delta^{15}N$ towards the southwestern sector of the south coast areas examined. Besides the dietary influence, which was recorded in the $\delta^{13}C_{org}$, Parkins (1993) suggested that the difference in $\delta^{15}N$ values might be linked to a difference in the available source of inorganic nitrogen (nitrate versus ammonium). Mullin *et al.*, (1984) found lower $\delta^{15}N$ in zooplankton where the principal nutrient source was ammonium rather than nitrate. The most important nitrogen source in the Southern Benguela Region (SBR) is nitrate (Probyn, 1985), whilst plankton production in oceanic waters and on the eastern Agulhas Bank is supported mainly by regenerated nitrogen (Probyn, 1985; Probyn *et al.*, 1995). The importance of recycled nitrogen to primary production on the eastern Agulhas Bank was demonstrated by Probyn *et al.*, (1995). Measurements of primary productivity and nitrogen uptake using ^{15}N-labelled NO_3, NH_4 and urea showed that primary productivity was exceptionally large at stations characterised by shallow mixing depths. The results showed that primary productivity was largely regeneration-based and ammonium uptake and regeneration were in approximate balance over the photic zone.

6.3.3 The Benguela Region

During the Middle and Late Miocene, sedimentary organic matter concentrations on the Walvis Ridge in the Cape Basin (DSDP sites 362 and 532), were highest in periods of maximum ice volume (Diester-Haass *et al.*, 1990). This observation and the inconsistent relationship of organic carbon with opal concentrations, lead to the conclusions that organic matter in the cores was derived from near-bottom downslope transport from the upper slope and shelf areas during periods of lowered sea-level. Summerhayes *et al.* (1995) studied a 6.5 m-long piston core on the continental slope close to Walvis Bay to see if the intensity and location of upwelling in the Benguela Current Upwelling System off Namibia had changed significantly in the last 70,000 years. They used the accumulation of organic matter to interpret temporal changes in upwelling intensity. The data showed high-frequency fluctuations and not the pattern of increased upwelling and higher productivity in glacial periods and lower productivity due to less upwelling in interglacial stages as envisaged by, among others, Wefer *et al.*, 1999. In the last 70,000 years, maximum accumulation of organic matter occurred during interstadial stage 3, coincident with cold SST, strengthened upwelling-favourable winds and minimal solar insolation. Summerhayes *et al.* (1995) favour changes in productivity rather than preservation/remineralization as the processes responsible for Late Quaternary variations in sedimentary organic carbon in the Benguela System.

In contrast, there is a two-to four-fold increase in TOC in glacial sediments compared to interglacial sediments in cores from the Walvis Ridge and off Angola (Schneider *et al.*, 1996). In core GeoB 1028 from the Walvis Ridge, a trend towards higher productivity over the last 150 kyrs is seen in the increasing TOC content and the greater amplitudes of TOC between glacial and interglacial sediments. This, together with an increased abundance of *N. pachyderma* (s) (Little *et al.*, 1997a,b) in this and other cores recovered from the Walvis Ridge (GeoB 1220, 1032, 1031) indicates that offshore transport of coastal upwelling filaments increased over the last 150 000 years (Wefer *et al.*, 1996). TOC records from the northern Benguela regions (~23°S) for the last 150 000 years suggest generally enhanced palaeoproductivity and intensified upwelling during MIS 2-4, with maximum upwelling occurring between 50 and 35 kyrs B.P. (Kirst *et al.*, 1999). This is supported by the strong inverse correlation between alkenone-derived SST and TOC. However, the data also point to intrusive warm-water events, possibly similar to modern Benguela Niños, resulting in elevated surface-water temperatures during glacial stages 2 and 6 (Kirst *et al.*, 1999).

Holmes (1996) measured stable nitrogen isotopes in bulk sediments and sinking particles to evaluate changes in relative nutrient utilisation in surface waters of the subtropical southeast Atlantic Ocean. The data showed that low $\delta^{15}N$ values coincided with low SST and high organic matter content, indicating higher surface nitrate availability because the reduced depletion of the surface nitrate pool was associated with increased productivity. In addition, the surface nitrate pool was less depleted during glacial periods as indicated by the lower $\delta^{15}N$ values of glacial sediments compared to interglacial sediments. Comparisons of bulk $\delta^{15}N$ with $\delta^{13}C_{org}$ and C/N ratios showed that neither diagenesis nor terrestrial input affected the isotopic signals in the sediments of the Angola Basin (Holmes *et al.*, 1996). $^{15}N/^{14}N$ in the region are primarily controlled by the extent of nitrate utilisation, with productivity in nearshore waters less nitrate-limited relative to offshore waters. In contrast, $\delta^{13}C_{org}$ values did not exhibit the same trends relating to nutrient uptake or productivity. Sedimentary $^{15}N/^{14}N$ ratios ranging from 5‰ to 9.5‰ were measured by Holmes *et al.* (1997) in two gravity cores recovered from the Angola Basin. The $\delta^{15}N$ values were negatively correlated to SST and organic carbon content.

Holmes *et al.* (1998) used samples from a sediment trap moored at 2196 m water depth over the Walvis Ridge to show that the $\delta^{15}N$ signal of particles sinking out of the euphotic zone is controlled by changes in surface nitrate concentration and can be correlated to variations in productivity. There was a significant correlation between $\delta^{15}N$ and SST, with low SSTs associated with relatively low

$\delta^{15}N$ values, indicating recently upwelled water with high nitrate concentrations. High SSTs characterised water that had been at the surface for some time and was therefore depleted in nutrients, leading to enrichment in the phytoplankton $\delta^{15}N$ signal.

Schneider *et al.* (1994) used the differences between the $\delta^{13}C$ records of two different planktonic foraminiferal species to reconstruct changes in upwelling intensity and productivity off the Congo River for the last 190 kyr. They showed that the $\delta^{13}C$ value of *Gg. bulloides* increased in upwelling regions relative to the open ocean. This is attributed to the late seasonal occurrence of *Gg. bulloides,* when primary production has already decreased the nutrient concentrations and subsequently increased the $\delta^{13}C$ of the surface waters. The $\Delta\delta^{13}C$ ($\delta^{13}C$ *Gg. bulloides* - $\delta^{13}C$ *Ga. ruber*) record corroborates the organic carbon signal, indicating that upwelling and productivity increased off the Congo in times of enhanced zonal intensity of the southeast trade winds.

A comparison of high-resolution inorganic carbon isotope records from the Southern Ocean, the northern Benguela Upwelling Region (NBR) and the equatorial Atlantic by Mulitza *et al.* (1999) revealed that the low $\delta^{13}C$ signal recorded in the Southern Ocean during the last deglaciation was transferred to the low-latitude sites. In the NBR, increased seasonal production off Namibia elevated surface water $\delta^{13}C$, obscuring the deglaciation signal, but the signal was seen strongly in the nutrient-deficient tropical Atlantic, where the $\delta^{13}C$ variability is lower than in the mid- and high-latitudes. The authors argue that the deglacial minimum is due to a change in the preformed isotopic signal of the source waters south of the Polar Front and that the thermodynamic imprint is transferred from the Southern Ocean by AAIW.

Pierre *et al.* (2001) used the oxygen and carbon isotope records of three planktonic foraminiferal species and one benthic foraminifer from ODP Site 1087 on the continental slope north of Cape Columbine, to provide new information on the climatic and hydrological changes over the last 500 kyr. They find that the coldest and warmest intervals for this time period are MIS 12, and MIS 11 and 5 respectively. Planktonic and benthic $\delta^{13}C$ records show large oscillations related to major changes in the productivity regime, rather than following climatic (G-IG) cycles.

A number of proxies for productivity, including organic carbon concentration and C/ N ratios were used by Christensen *et al.* (2002) to investigate the impact of the intensification of Northern Hemisphere glaciation on the Southern Benguela Current System for the period 4 – 2 Ma. Peaks in

biogenic components (opal and organic carbon) are linked to increased productivity as well as enhanced preservation. Christensen *et al.* (2002) conclude that sedimentary history of ODP Site 1085, offshore of the Orange River, was controlled by low-latitude processes linked to precession, rather than high-latitude processes.

6.4 METHODS

6.4.1 Total Organic Carbon

The percentage total organic carbon was calculated using the percentage composition of organic carbon derived from the organic carbon isotope analysis. The percentage elemental composition in each sample was obtained using the following formulae:

$$\alpha = (\%_{std} \text{ x weight}_{std})/(\text{Area}_{std})$$

and

$$\%_{sample} = (\alpha \text{ x Area}_{sample})/(\text{weight}_{sample})$$

Alpha is derived for each element (at least once for each run) from the known percentage composition and weight of the reference sample. Some control samples were analysed on a LECO CHNS analyser at the Department of Marine and Coastal Management (formerly Sea Fisheries Research Institute), Cape Town, South Africa, for comparison purposes.

6.4.2 Stable Organic Carbon Isotopes

The low nitrogen content and high carbonate content of the sediments necessitated that separate samples were prepared and analysed individually for nitrogen and organic carbon. Measurements of $\delta^{13}C_{(org)}$ were made on 30 mg bulk samples for core MD962080 and on 50 mg bulk samples from core MD962084, due to the higher carbonate content of this core. The samples were decalcified by treatment with excess 1M HCl. They were left to stand overnight, then agitated in an ultrasonic bath for 2 minutes, left to settle for 30 minutes and then centrifuged. The supernatant was drained off and the samples were rinsed with distilled water and centrifuged again. This procedure was repeated 3 times. The rinsed samples were freeze-dried overnight. The isotopic ratios were determined from 5 mg decalcified samples using a Carlo Erba elemental analyser directly coupled to a Finnigan MAT 252 mass spectrometer at the Archaeometry Laboratory, University of Cape Town, South Africa.

Valine, Merck gel, ANU sucrose and a plant (locally grown nasturtium) were used as internal standards. The $\delta^{13}C$ values of these standards have previously been determined against international standards. The isotopic compositions are reported relative to Vienna Pee Dee Belemnite (VPDB) in the standard notation:

$$\delta^{13}C_{org} = [(^{13}C/^{12}C)_{sample}/(^{13}C/^{12}C)_{standard} - 1] \text{ per mil}$$

The analytical reproducibility of the standards is 0.2‰. The reproducibility of samples was worse (up to 0.5‰), presumably because of the variable composition within each sample.

6.4.3 Stable Nitrogen Isotopes

The stable nitrogen isotope measurements were made using 30 mg ground bulk sediment. The isotope ratios were determined using the elemental analyser and mass spectrometer as described for the organic carbon isotopes. The high carbonate content and large sample mass necessitated the insertion of a "scrubber" of *Ascarite* (a compound comprising NaOH on asbestos) immediately after the combustion column to absorb the CO_2 and to prevent the mass spectrometer from being flooded with CO_2. The isotope ratios are reported relative to the standard, atmospheric nitrogen, using the δ notation:

$$\delta^{15}N = [(^{15}N/^{14}N)_{sample}/(^{15}N/^{14}N)_{standard} - 1] \text{ per mil.}$$

The internal standards used were Atropine, Merck gel and a locally grown plant (nasturtium); chosen because its $\delta^{15}N$ is close to that of marine sediments. The internal laboratory standards have previously been standardised against international standards (N1, N2). The analytical precision of the isotope measurements for the standards is 0.3‰, with less precision in reproducibility of the samples owing to the variable elemental composition in each sample.

Organic carbon/nitrogen (C/N) ratios were calculated using TOC and nitrogen concentrations.

6.4.4 Stable Carbon Isotopes of Planktonic Foraminifera

Sixty specimens of the planktonic foraminifer *Globorotalia inflata* were picked from the 250-350 μm size fraction for all samples in both cores. Samples from core MD962080 were sent to the Centre for Ocean Research, National Taiwan University, Keelung, Taiwan for analysis. According to standard laboratory procedure, the picked specimens were cleaned twice by ultrasonic vibration for

10-15 seconds to remove adhering fine particles. Samples were then treated with NaClO at room temperature for 24 hours to remove organic matter. The $^{13}C/^{12}C$ ratios were determined using a Finnegan Delta Plus mass spectrometer with a Kiel automated carbonate device. Average values from the duplicate or triplicate analyses were calculated and reported. Samples from core MD962084 were analysed at the Fachbereich Geowissenschaften, Universität Bremen, Germany. According to standard practices in the Bremen laboratory the samples did not undergo any treatment prior to isotopic analysis. The precision for the carbonate standards is 0.08‰. Carbon isotopic data are calibrated with respect to National Bureau of Standards NBS19 (Hut, 1987; Coplen, 1988). As per convention, isotope ratios are reported relative to the international VPDB standard, using the δ notation:

$$\delta^{13}C = [(^{13}C/^{12}C)_{sample} / (^{13}C/^{12}C)_{standard} - 1] \text{ per mil.}$$

6.5 RESULTS

Following the methods of Kirst *et al.* (1999) TOC concentration, rather than calculated accumulation rate (TOC AR), is presented and discussed. This allows for comparison with work undertaken in the northern Cape Basin (e.g. Kirst *et al.*, 1999; Little *et al.*, 1987a,b; Schneider *et al.*, 1996). Following the reasoning of Bentaleb *et al.* (1996), it is assumed that the $\delta^{13}C_{org}$ values of the sedimentary organic carbon are not sufficiently altered by early diagenesis and are representative of the isotopic composition of the phytoplankton. Denitrification has been discounted as having affected the $\delta^{15}N$ signal of core MD962080, due to the low TOC content and the fact that the core is not located below highly productive surface waters. Moreover, subsurface hypoxia is unlikely to occur at the depth and location of this core, as the influence of intermediate water masses keeps the water column oxygenated (Bailey, pers. comm., 2002). Plots of these proxies versus age are shown in Figures 6.1 and 6.2. Raw data are presented in Appendix 8.

6.5.1 Core MD962080 (Agulhas Bank Slope)

Total organic carbon (TOC) content in core MD962080 is relatively low, ranging between 0.5 and 2.7% (mean 1.41%). There is an increasing trend upcore (Fig. 6.1a). Variations in concentration are typically < 1%. In general, there is a tendency towards increased carbon content during interglacial periods. Peak values (>2%) occur in warm stages 11, 7, 5 and in the Holocene. Periods

of increased organic carbon content are coincident with periods of low sand contents (Fig. 5.1b, pg. 5-6). TOC concentrations are relatively low during glacial periods MIS 20, 18, 14, 12 and 8 compared to the adjacent interglacial stages.

When % organic carbon is recalculated as MAR (Fig. 6.1b), increased C_{org} MAR is shown to occur at G-IG boundaries (MIS18/17, 14/13), late stages 8 and 6 and in MIS 2. The period MIS 11 – 6 records generally high biogenic MAR, as also shown in high $CaCO_3$ (Fig 5.1e) reflecting the high productivity of the "Mid-Brunhes climatic event". (Jansen *et al.*, 1986).

Organic $\delta^{13}C$ values range between –19‰ and -24‰ (Fig. 6.1c), which is within the typical range for modern marine plankton (-17‰ to -25‰) and marine sediments (-18‰ to –22‰) (Dean *et al*, 1986; Goericke, 1994). The dashed line at -23‰ marks the boundary between typical values for tropical/temperate marine organic matter (-20‰) and terrestrial plants (-27‰ to -28‰) (Müller *et al.*, 1994; Meyers, 1994). A mean C/N ratio of 7 (equal to the Redfield ratio) and an average $\delta^{13}C_{org}$ value of -21‰ confirm the marine origin of the organic matter for the majority of the record (Redfield, 1934). This is to be expected, given the core locality at the southern tip of the African margin, as it is unlikely that, even at sea-level lowstands, terrigenous material would have been deposited at the core site. The strongly depleted $\delta^{13}C_{org}$ signal in MIS 7 is consistent with increased organic carbon content and low C/N ratio (Fig. 6.1d). In contrast, the low $\delta^{13}C_{org}$ values at the beginning of MIS 14 coincides with an increase in organic carbon content and a relatively high C/N ratio.

Bulk nitrogen isotope values are generally low compared to values in sediments from the Arabian Sea, the eastern equatorial Pacific and the subtropical southeast Atlantic (Altabet *et al.*, 1999; Ganeshram *et al.* 2000; Holmes *et al.*, 1997). $\delta^{15}N$ values range from 0.8‰ to 8‰ (Fig. 6.1e). Glacial $\delta^{15}N$ values tend to be lighter than the $\delta^{15}N$ values of interglacial sediments. A change in mean $\delta^{15}N$ occurs in the record around 250 kyr B.P. Firstly, the range of variability in the younger portion of the record is significantly more constrained than in the older portion of the record and secondly, an upcore trend towards heavier values develops (Fig. 6.1e).

The planktonic foraminiferal $\delta^{13}C$ record for *Gr. inflata* ranges from 0.013‰ to 1.46‰ (Fig. 6.1f). The record can be broadly divided into three sections. The section from the bottom to MIS 13 shows an increasing trend, after which there is a change in the mean and a decreasing trend to more

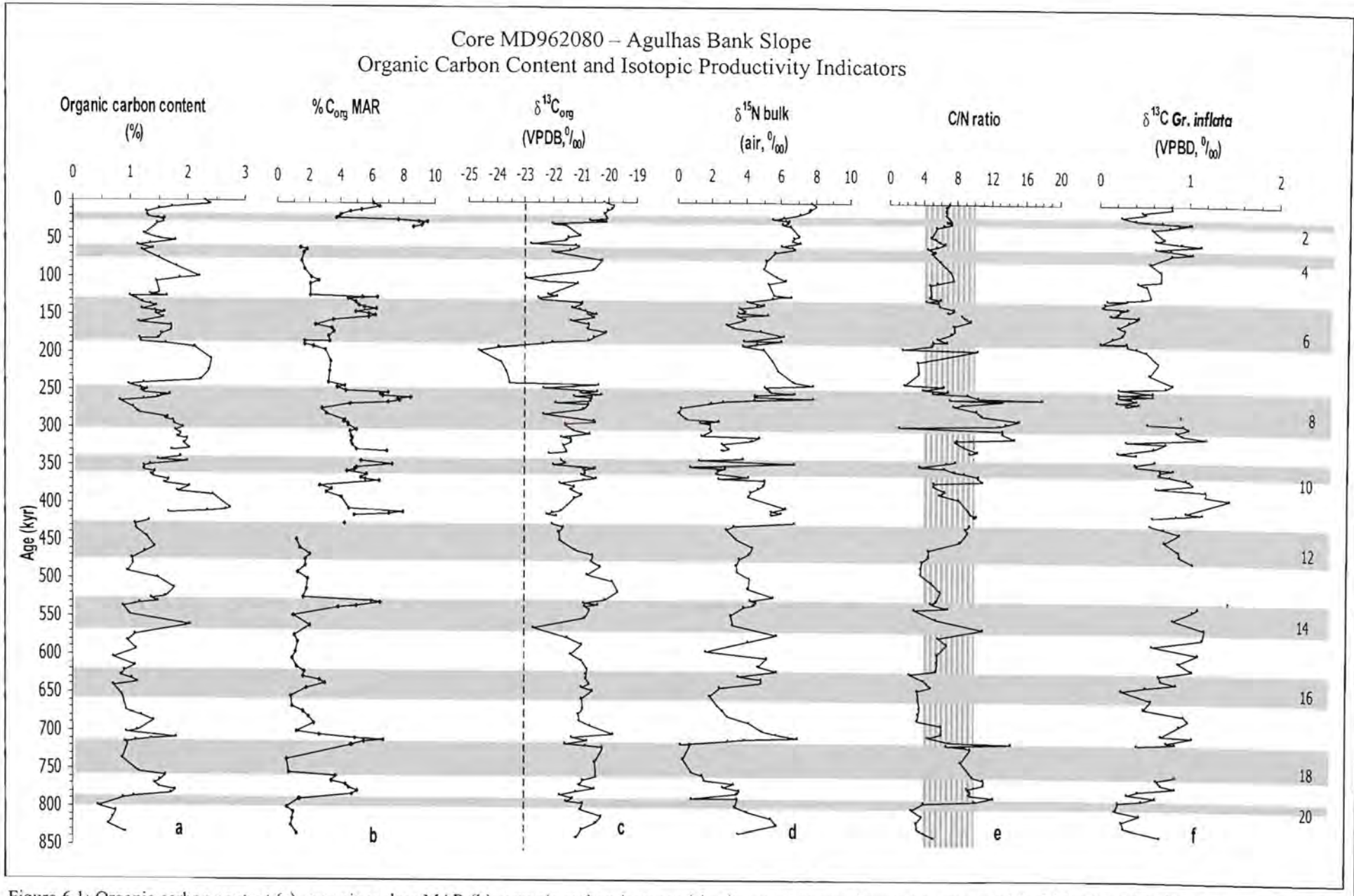

Figure 6.1: Organic carbon content (a), organic carbon MAR (b), organic carbon isotopes (c), nitrogen isotopes from bulk sediment (d), C/N ratios with shaded area representing the normal marine range (Meyers, 1994) (e) and carbon isotopes for the planktonic foraminifera *Globorotalia inflata* (f) for core MD962080. Grey-shaded bars represent inferred glacial marine isotope stages (MIS).

depleted values. The youngest portion of the core (MIS 5-top) shows above average $\delta^{13}C$ values. Although there is no clear G-IG cyclicity, $\delta^{13}C$ values are generally lower during glacial periods. Low values are not confined to glacial periods in the lower portion of the core (MIS 21-9), although low values are recorded in glacial stages 20 and 16 (Fig. 6.1f). The lowest $\delta^{13}C$ values are recorded in MIS 6, reflecting the general decrease in seawater $\delta^{13}C_{\Sigma CO2}$ at this time (Mackensen and Bickert, 1999). Similar decreases have been reported for planktonic records from various parts of the Atlantic Ocean (e.g. Curry and Crowley, 1987; Schneider *et al.*, 1994). The last 200 kyr of the record is similar in character to the $\delta^{13}C$ signal from the nutrient-depleted western Equatorial Atlantic (Curry and Crowley, 1987), showing sharp increases at stage boundaries at Termination III and II, as well as a trend from low to high values from the last deglaciation to the Holocene. The "Mid-Brunhes climatic event", at 400-300 kyr B.P. (Jansen *et al.*, 1986), known to be a period of high pelagic carbonate production, is weakly registered by the slightly elevated $\delta^{13}C$ values for the period ~270 – 400 kyr B.P.

6.5.2 Core MD962084 (Olifants River Slope)

There is approximately a three-fold increase in the organic carbon content of core MD962084 (Fig. 6.2a) compared to that of core MD962080. The range (3-10%) and mean value of 6% is considerably higher than for most deep-sea sediments from the South Atlantic (mean ~0.5%) (Keswani *et al.*, 1984). There is no apparent increasing trend upcore as seen in the Agulhas Bank Slope core. Peak TOC values occur in warm stages, with glacial intervals generally recording a lower carbon content, although glacial stage MIS 14 is characterised by a relatively high carbon content (Fig. 6.2a).

Organic $\delta^{13}C$ values range between –15‰ and -23‰ (Fig. 6.2c). These values are typical for marine organic matter (Dean *et al.*, 1986). The mean $\delta^{13}C_{org}$ record for core MD962084 (-20.06‰) is enriched relative to that of core MD962080 (-21.14‰), and is close to $\delta^{13}C$ values of -20 to -21‰ for Holocene sediments on the Namibian shelf (Dean *et al.*, 1986). The $\delta^{13}C_{org}$ values for bulk organic carbon in core MD962084 are more constrained than those for core MD962080. There is a general increasing trend upcore throughout the record (Fig. 6.2c). The record does not show a true G-IG cyclicity, but the heaviest $\delta^{13}C_{org}$ values are recorded during warm stages (e.g. MIS 21, 7, 5), particularly during warm MIS 11. Depleted values are seen in glacial stages in the upper half of the record (Fig. 6.2c).

When $\%C_{org}$ is converted to C_{org} MAR two periods of very high organic carbon MAR are noted (Fig. 6.2b); at the MIS 11/10 transition and again at the MIS 2/1 boundary. Both these episodes are co-incident with periods of elevated $CaCO_3$ Mar (Fig. 5.2e) reflecting high biogenic MAR at those times.

The predominantly marine source for the organic carbon is supported by the C/N ratios. C/N ratios vary from 1.12 to 21.10 with a mean of 9.45 (Fig. 6.2d), which is slightly higher than the Redfield ratio (Redfield, 1934). Most of the C/N ratios are intermediate between unaltered marine algal organic matter (5-8), shore vegetation (15 -16) and fresh terrestrial material (10-35) (Meyers, 1994; Mueller and Voss, 1999). High C/N ratios (>12) are associated with depleted $\delta^{15}N$ values, which implies a change in the nitrogen source, rather than a change in the organic matter source.

Bulk sediment nitrogen isotope values range between 0.2 and 7.12‰ (Fig. 6.2e). The range of values is highly constrained prior to 500 kyr B.P, after which a long-term cyclicity develops with a larger variability. There is a general pattern of higher $\delta^{15}N$ values during interglacial periods and low values in glacial periods for the last 350 kyr (i.e. from MIS 10 to the Holocene). The high $\delta^{15}N$ values are generally coincident with high TOC and high $\delta^{13}C_{org}$ values. In contrast, stages 11 and 12 show the opposite trend, with very low $\delta^{15}N$ values corresponding to a period of organic carbon enrichment in MIS 11 and *vice versa* for MIS 12. As in core MD962080, there is a strong upcore trend towards higher $\delta^{15}N$ values over the last ~200 kyr (Fig. 6.2e).

The measured $\delta^{13}C$ of *Gr. inflata* ranges from 0.32‰ to 1.76‰ (Fig. 6.2f). Three long-term phases are observed. The bottom half of the core (MIS 21 to MIS 12) exhibits an increasing upcore trend. This trend changes to record relatively depleted values upcore from MIS 12 to the stage 6/5 boundary. The last ~130 kyr of the record are characterised by high-frequency, limited-range fluctuations and relatively elevated average $\delta^{13}C$ values (Fig. 6.2f). The same trend from low to high values from the last deglaciation to the Holocene, seen in core MD962080, is again observed in this core. There is also a shift, between MIS 6 and 5, with an increasing trend lasting to early MIS 4 (about 70 kyr). A period of slightly higher values between ~420 and 260 kyr B.P. is coincident with the "Mid-Brunhes climatic event" (Jansen *et al.*, 1986). More striking is the extended period of ^{13}C enrichment from MIS 15 – 12 (Fig. 6.2f).

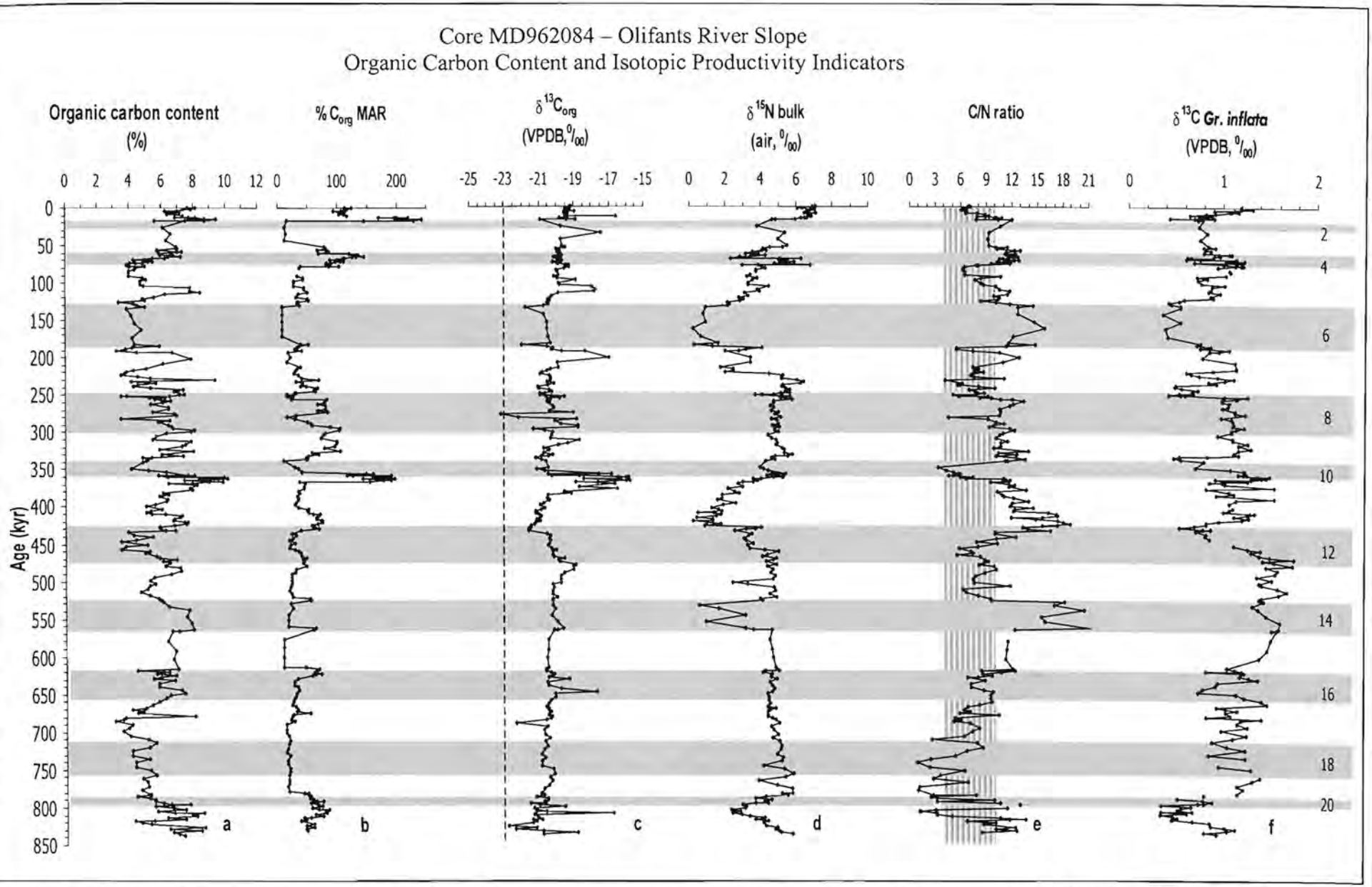

Figure 6.2: Organic carbon content (a), organic carbon MAR (b), organic carbon isotopes (c), nitrogen isotopes from bulk sediment (d), C/N ratios with shaded area representing the normal marine range (Meyers, 1994) (e) and carbon isotopes for the planktonic foraminifera *Globorotalia inflata* (f) for core MD962084. Grey-shaded bars represent inferred glacial marine isotope stages (MIS).

6.6 DISCUSSION

6.6.1 Core MD962080 (Agulhas Bank Slope)

Periods of high organic carbon content are coincident with low sand content, suggesting that variations in the sand content (Chapter 5) are probably related to productivity cycles, being noticeably higher in warm stages MIS 11 and 5. The observation that organic carbon content increases during the Holocene (and other warm periods) suggests relatively low glacial productivity over the core site. High $\delta^{13}C$ values for *Gr. inflata* in warm stages are indicative of increased surface productivity, whilst low surface productivity is indicated by depleted $\delta^{13}C$ values, during MIS 8, 6 and 2. The indications that productivity was lower during the LGM than in the Holocene are in accord with other studies where data reflect low glacial productivity in the southern Atlantic (Mortlock *et al.*, 1991, Shemesh *et al.*, 1993, Bentaleb *et al*, 1996).

The period of very low $\delta^{13}C_{org}$ values in MIS 7 is consistent with increased organic carbon content and probably reflects enhanced phytoplankton production. Regional changes in phytoplankton populations can lead to changes in sedimentary bulk organic $\delta^{13}C$ values, which, on their own, may not necessarily reflect widespread oceanographic or climatic change (Pancost *et al.*, 1999). The average $\delta^{13}C_{org}$ signal is more depleted than typical tropical marine organic matter, possibly reflecting the influence of cooler waters over the core site. The greater depletion of $\delta^{13}C_{org}$ in this core, compared to core MD962084, likely reflects the difference in dominant species in the two areas; the SBR has a higher standing stock of omnivorous euphausiids, whilst herbivorous copepods dominate the plankton on the south coast of South Africa at present (Hutchings *et al.*, 1991). Furthermore, dinoflagellates are presently prolific in the SBR, but quite scarce in the Agulhas Bank region (Hutchings *et al.*, 1991).

Glacial $\delta^{15}N$ values are generally lighter than the $\delta^{15}N$ of interglacial sediments and could indicate less intense depletion of the surface nitrate pool during glacial periods. Such an increase would imply an increase in nutrient concentration advected northward from the Southern Ocean. However, Francois *et al.* (1992) argue for a progressive nutrient deficiency with increasing equatorward migration by Subantarctic waters in glacial periods. In addition, incomplete nitrate utilisation is a phenomenon that largely affects $\delta^{15}N$ in deep-sea settings, where Fe-limitation inhibits rapid uptake of nitrate (Ganeshram *et al.*, 2000). Thomalla (2001) suggests that Fe is the limiting nutrient south of the STC. Very depleted $\delta^{15}N$ values can reflect fixation of nitrogen from the atmosphere by

cyanobacteria in periods of low nutrient availability. However, nitrogen fixation is normally only significant when nitrate concentrations in surface waters are very low or during periods of enhanced denitrification (Ganeshram *et al.*, 2000). The input of terrigenous material could also affect the $\delta^{15}N$ signal. Yet, the C/N ratios indicate that the organic matter has a marine source. During glacial lowstands, the newly emergent coastal plain of the Agulhas Bank would have experienced terrestrial run-off (Dingle and Rogers, 1972), although this terrestrial run-off was predominantly to the East Coast of South Africa rather than towards the west (Dingle *et al.*, 1987). Furthermore, C/N ratios are low at the LGM lowstand.

The presence of ammonium at the sediment-water interface would best account for depleted $\delta^{15}N$ values. In areas of low or less intense upwelling, the principal nitrogen source for phytoplankton is regenerated nitrogen (ammonium). This has been shown to be the case on the Agulhas Bank at present (Parkins, 1993; Probyn, 1985; Probyn *et al.*, 1995) and would account for the depleted $\delta^{15}N$ signal. This, coupled with nutrient-deficient glacial waters, would also facilitate nitrogen fixation by cyanobacteria, accounting for the $\delta^{15}N$ values approaching zero during glacial stages 20, 18 and 8.

The elevated C/N ratios in MIS 8 (a time of high C_{org} MAR, but low %N), reinforce this interpretation of low nitrogen availability.

The high $\delta^{15}N$ values (up to 8‰) seen in core MD962080 at the terminations of stages 18 and 8 and in the Holocene, are unlikely to be a result of denitrification. The relatively low organic matter content of the sediments and low burial rates and the relative scarcity of dinoflagellates (a species thriving in oxygen-depleted waters) in the Agulhas Bank region (Hutchings *et al.*, 1991) suggest that the possibility of regular or long-term anoxia in the water column in unlikely. Alternatively, as the core site lies offshore of a very sporadic and seasonal upwelling area, the possible effects of bacterial remineralisation or diagenesis on the $\delta^{15}N$ signal must be considered. Enriched $\delta^{15}N$ values may be a consequence of oxidation during periods of somewhat increased productivity or due to nitrification of NO_3^- and NH_4 as a result of mineralisation.

There are a number of suggestions to explain the general upcore enrichment in $\delta^{15}N$ which is particularly prevalent over the last ~250 kyr. Altabet and Francois (1994) suggest diagenesis of low labile material giving a depleted $\delta^{15}N$ signal. Diagenesis, which leaves a lighter signal, does not reflect nitrate utilisation. However, Pedersen (pers.comm., 2000) disagrees and suggests a long-term or evolutionary signal, implying a different nitrate source or environment. The argument for a

different environment is supported by the concurrent change in mean $\delta^{15}N$ in core MD962084, as well as changes seen in the planktonic foraminiferal assemblages at about this time (Chapter 4).

6.6.2 Core MD962084 (Olifants River Slope)

Although the sediments in core MD962084 are organic-rich compared to core MD962080, they are considerably poorer in organic carbon than sediments in the Northern Benguela Region (e.g. Wefer *et al.*, 1998) indicating that upwelling in the SBR was not consistent (or sufficient) enough to create the elevated levels of productivity seen in the NBR. The difference in TOC is also likely to be a result of lower burial rates in the SBR which would allow for greater decomposition of organic carbon, whilst in the NBR, high burial rates can lead to increased carbon preservation (Gorgas and Wilkens, 2002). Because of the core location, offshore from Namaqualand, a coastal semi-desert, it is likely that the organic matter in this core is mostly marine-derived. However, the high C/N ratios and coincident low $\delta^{15}N$ values observed in MIS 14 and 6 and at the beginning of MIS 11, point to the possibility of terrigenous input from the Olifants River. Nevertheless, given that there is no sedimentological evidence of terrestrial input at these times, it is assumed that the majority of the organic matter is of marine origin. Most of the C/N ratios are intermediate between unaltered marine algal organic matter and fresh terrestrial material (10-35) (Meyers, 1994; Mueller and Voss, 1999). An alternative explanation to a terrigenous source for values higher than fresh marine algal values is that selective loss of nitrogen-rich proteinaceous matter and consequent elevation of the elemental ratios may have occurred during the sedimentation of marine organic matter. Evidence of early diagenetic alteration of C/N values is common under areas of high productivity, such as upwelling areas (Meyers, 1997) and can indicate the presence of a strongly developed oxygen minimum zone near the seafloor. The coincidence of high C/N ratios and high organic matter content could point to diagenetic elevation of C/N ratios as a consequence of enhanced organ matter preservation. The relative enrichment in $\delta^{13}C_{org}$ in this core, relative to core MD962080, may reflect differences in phytoplankton carbon metabolism (Bentaleb *et al.*, 1996), different dominant plankton species and higher primary productivity offshore of the upwelling system than on the Agulhas Bank.

The carbon isotope records for the planktonic foraminifer *Gr. inflata* do not follow a G-IG cyclicity, but show abrupt oscillations associated with longer-term trends. The larger range in the $\delta^{13}C$ record for this core compared to the Agulhas Bank core can be explained by stronger fractionation from the ambient seawater equilibrium, which varies between upwelling and non-upwelling periods

(Reynolds-Sautter and Thunell, 1991). Very high pelagic carbonate production during MIS 11, 9 and 7 (Hodell, 1993) characterises the "Mid-Brunhes climatic event". This period is recorded, to some extent, in both cores, but not as an outstanding event, especially in the light of the $\delta^{13}C$ enrichment from MIS 15-12 in core MD962084. This may be as a result of the "Mid-Brunhes dissolution cycle" (Bassinot *et al.*, 1994a), which is clearly recorded in the low calcium carbonate content and muddier sediment texture (Fig. 5.2, pg. 5-9), and may have affected the $^{13}C/^{12}C$ ratios.

The concentration of nitrate in the surface water and the degree to which it is utilised are the dominant controls on the $\delta^{15}N$ signals. "Lazy feeding" could explain the very depleted $\delta^{15}N$ values observed in this core. This occurs when there is sufficient (or excess) nutrient and food available, so one or two trophic levels are skipped. The presence of oxygen-depleted subsurface waters, a regular occurrence in the SBR in recent times (Bailey, 1991), would lead to denitrification in the water column and at the sediment-water interface, rendering the isotopic composition of the source nitrate heavy. Heavy $\delta^{15}N$ values, coincident with the high organic carbon concentrations, reflect delivery of $\delta^{15}N$-enriched nitrate to the surface water from the underlying zone of denitricfication. Similar conditions exist today and are interpreted to have existed in the past in the eastern tropical North Pacific Ocean (Ganeshram *et al.*, 1995). The decreases in organic carbon content in the glacial sediments argue for a reduced supply of organic detritus to the seafloor as a result of decreased productivity. Depleted $\delta^{15}N$ values indicate less depletion of the available nitrate pool, supporting the idea of lower productivity. The lower half of the record shows the opposite trend, with depleted $\delta^{15}N$ values coinciding with high TOC and $\delta^{13}C_{org}$ enrichment, particularly in MIS 11, and *vice versa* in MIS 12. This may suggest a period of high productivity and high nutrient availability and, consequently, less depletion of the nitrate pool leading to low $\delta^{15}N$ values.

These finding are in contrast with those of Holmes (1996) and Holmes *et al.* (1997; 1999), which showed increased productivity during glacial periods in the Angola Basin. Decreases in $\delta^{15}N$ during glacial periods are interpreted as decreased relative nitrate utilisation, as a result of increased nitrate supply to surface water due to more vigorous circulation. Larger excess nitrate concentrations (thus lower relative use) are consistent with cooler SST and stronger upwelling and, offshore, the seaward extension of upwelling filaments brings nutrient-rich water to the euphotic zone and leads to elevated productivity and relatively lower $\delta^{15}N$ values.

The data presented here indicate that the SBR and NBR operate differently in glacial periods and fluctuate on different time scales. During the cold stages, the greater share of organic carbon

accumulation shifted to the NBR upwelling system (Rühlemann *et al.*, 1999). The northward compression of the South Atlantic Anticyclone (SAA) during glacial periods would have caused an intensification of the trade-wind system, increasing the upwelling of nutrient-rich subsurface waters off Namibia and Angola. In contrast, in the SBR, the equatorward migration of the SAA would have resulted in decreased southeasterly wind stress and subsequent decrease in upwelling (much like the modern winter conditions). Palaeoproductivity in the open ocean decreased concurrently, probably as a result of lower nutrient concentration of glacial intermediate waters (Rühlemann *et al.*, 1999) and this is reflected in the SBR. Thus, the SBR experienced different forcings and responded differently from the NBR to global climatic fluctuations.

The variations in the planktonic $\delta^{13}C$ records of both cores for the last ~300 kyr are also seen in the planktonic $\delta^{13}C$ signal for nutrient-depleted surface waters in the western equatorial Atlantic (Curry and Crowley, 1987) and has been described elsewhere in the global oceans (e.g. Labeyrie and Duplessy, 1985; Schneider *et al.*, 1994). Thus, because these are global signals, the $\delta^{13}C$ variations cannot reflect changes in upwelling and productivity alone, but are also likely to be a result of changes in surface-water $\delta^{13}C_{\Sigma CO2}$ (Schneider *et al.*, 1994). The coherence between the records of organic carbon, $\delta^{13}C_{org}$, $\delta^{15}N$ and $\delta^{13}C_{inflata}$ imply that variations in the flux of organic carbon in the SBR are a result of productivity variations, most likely driven by changes in upwelling, as a result of latitudinal changes in the position of the southern hydrological fronts and their associated water masses. The timing of the changes observed in these data and possible forcing mechamisms are discussed in the following chapter.

CHAPTER 7: DRIVING FORCES and TIMING OF CHANGES:- WAVELET ANALYSIS.

This chapter deals with the timing of the changes in the proxies investigated in the previous chapters and the possible forcing and feedback mechanisms behind those changes. The use of continuous wavelet analysis as an alternative to spectral analysis is introduced. The major proxies in both cores are subjected to wavelet analysis. The results are compared in an effort to discern changes in dominant forcing and feedbacks within each core and between the two cores. The use of wavelet transform is an emergent technique in palaeoclimatic research. Owing to the complex nature of the data, a general, rather than detailed, interpretation of the results is presented.

7.1 INTRODUCTION

Over the past million years, the Earth's climate has been dominated by glaciation cycles with periods of about 100, 41 and 23 kyr (Imbrie *et al.*, 1993). These Milankovitch cycles of eccentricity, obliquity and precession are related to changes in the earth's orbital parameters, which lead to changes in the distance of the earth from the sun and consequent variability in the receipt of solar radiation (Milankovitch, 1930). The Milankovitch theory (Milankovitch, 1930) identifies three different cycles:

(1) The eccentricity of the earth's orbit, whereby the earth's orbit undergoes a change from almost circular to highly elliptical over a quasi-cyclic period of about 100 kyr. At, present, the variation in distance between the earth and the sun is possibly at its smallest, with the distance being approximately 147 x 10^6 km at perihelion and 152 x 10^6 km at aphelion (Preston-Whyte and Tyson, 1988).

(2) The obliquity of the ecliptic, whereby the tilt of the earth's axis varies from 21.8° to 24.4° over a 41 kyr period, affecting the range of seasonality. At present, the earth's axis is tilted at about 23.5° (Preston-Whyte and Tyson, 1988).

(3) The precession of the equinoxes, where the times of perihelion (when the earth is nearest the sun) and aphelion (when the earth is furthest away from the sun) change regularly. At present the perihelion is around January 2nd, i.e. in the austral summer (Preston-Whyte and Tyson, 1988). The complete cycle produces two periodicites of about 23 000 years and 19 000 years.

Researchers are interested in the nature of the cyclicity of climate change, because one of the continuing problems in climatology is the link between fluctuations in solar radiation and weather and climate. While changes in solar radiation intensity and variations in the earth's orbit are the cause of the earth receiving more or less solar radiation, fluctuations that are not on the Milankovitch time-scales need to be explained. It is the totality of both the small-scale (local) and large-scale (global) variability that constitute climate change. The climate signal represents the culmination of interactions and feedbacks between various physical processes operating over a wide range of spatial and temporal scales (Bolton *et al.*, 1995). This signal is not stationary, but comprises a variety of frequency regimes that may have localised time-intervals or span large periods of time (Lau and Weng, 1995). Traditionally, spectral analysis is the tool most frequently applied to time series in order to determine dominant frequencies of change within the data set. However, one of the major drawbacks of this technique is that it assumes that the changes are linear and constant in time. Wavelet transform is an analytical technique well-suited to the study of multiscale, non-stationary processes occurring over finite spatial and temporal domains (Torrence and Compo, 1998). Spectral analysis does not contain any time dependence of the signal, with the result that it cannot detect how the signal is changing with time. Wavelet transform, on the other hand, provides a continuous spectrum which adapts to the entire time-frequency domain (Lau and Weng, 1995), revealing the non-stationary nature and time-varying characteristics of the frequency components (Gupta *et al.*, 2001).

7.2 PREVIOUS WORK

7.2.1 The Nature of Climatic Shifts

The cause of the fluctuations in the Pleistocene ice sheets has long posed an intriguing scientific puzzle. Over the last ~750 kyr, the global shifts have been of the order of 100 kyr. However, the differences in solar radiation as a result of orbital eccentricity are not sufficient to induce such dramatic climate change and consequently some feedback mechanisms must be involved. Theories include both external factors, such as variations in the amount of solar energy reaching the earth, and internal elements such as variations in albedo, the growth and decay of ice sheets, deep ocean circulation and the distribution of carbon dioxide between the atmosphere and the ocean (Hays *et al.*, 1976). Changes in the Southern Hemisphere over the past 450 kyr were assessed using three indices of global climate in marine sediments; $\delta^{18}O$ of *Gg. bulloides*, summer sea surface temperature, and relative abundance of the radiolarian *Cycladophora davisiana* (Hays *et al.*, 1976). The frequency-domain and time-domain tests of the records

revealed that climate variability was concentrated in three peaks at ~ 23, 42 and 100 kyr. As these peaks correspond to the dominant periodicities associated with the earth's solar orbit, the authors concluded that changes in the earth's orbital geometry are the fundamental cause of the succession of Quaternary glacial cycles (Hays *et al.*, 1976). It is now widely believed that these astronomical influences either drive the major climatic cycles externally or set the phase of oscillations that are driven internally (Imbrie *et al.*, 1992).

The Pleistocene glacial cycles can be used to test ideas about the mechanisms of the climate system's response to known external forcing and feedback. Imbrie *et al.* (1992) provide an array of observations from numerous open-ocean sites showing how key parts of the system varied at Milankovitch frequencies (Milankovitch, 1930) over the past 400 kyr. Using standard spectral analysis techniques to focus on the three main cycles, they developed a conceptual model of the governing processes based on the four end-member states needed to describe the system's evolution (interglacial, preglacial, glacial and deglacial). The authors argue that the 23- and 41-kyr cycles of glaciation are continuous, linear responses to orbitally-driven changes in the Arctic radiation budget. The results show that as the system varies continuously, but at different rates, between the four extreme states, there is a shift between two modes of ocean circulation: Early in deglaciation, the Nordic and boreal mechanisms reinforce each other and drive the global thermohaline overturning at its maximum rate; conversely, early in preglaciation, the boreal mechanism operates alone with overturning at its minimum.

The eccentricity of the earth's orbit is believed to be generated by amplitude and frequency modulations of the obliquity. The deviation of the obliquity signal from the main 41-kyr component was investigated by Mélice *et al.* (2001). The spectra of both the amplitude and frequency modulations of the 41-kyr component display significant power at 171 and 97 kyr, which suggests that this deviation is the origin of the 100-kyr cycle that dominates Late Pleistocene records. However, the origin of the 97-kyr cycle is totally distinct from the origin of the 100-kyr periods in the eccentricity, implying that the variability of the Earth's obliquity alone cannot be at the origin of the 100-kyr climatic cycles. The authors concluded that frequency modulation of the the obilquity signal is unresolved and is only meaningful if the components at 41 kyr, 54 kyr and 29 kyr are investigated separately.

The Mid-Pleistocene transition, from a dominant 41-kyr cycle to a dominant 100-kyr cycle at about 750 kyr B.P., has been the focus of numerous studies and is central to theories on the onset

of glaciation (Bolton *et al.*, 1995). The application of wavelet transform analysis to the $\delta^{18}O$ records of two deep-sea sediment cores (ODP sites 677 and 806) and the SPECMAP stack (Imbrie *et al.*, 1984) reveals differences and similarities in the patterns of change in time-frequency space for the Mid-Pleistocene transition (Bolton *et al.*, 1995). A ~75-kyr cycle is seen in the sediment cores in the region of 800-900 kyr B.P.. The transition is recorded slightly later (~743 kyr B.P.) in the SPECMAP stack and shows a shorter initial period of ~54 kyr. The authors attribute the differences in timing to timescale errors in the SPECMAP stack.

Lau and Weng (1995) applied wavelet transforms to two widely used Northern Hemisphere climate series. By comparing wavelet transform to a musical score, the authors illustrate the importance of local versus global information within the climate signals. A 2.5-myr deep-sea sediment record of $\delta^{18}O$ shows an abrupt upcore change in the oscillation regime at 0.7 myr B.P. from a 40-kyr dominated frequency to a 100-kyr dominated frequency. Subharmonics near the 40-kyr cycle are also detected. A shorter, contemporary 140-year climate signal of Northern Hemisphere sea-surface temperature reveals numerous oscillatory modes. The results from both analyses suggest that variations in the earth's climate are consistent with those exhibited by a non-linear dynamic system under external forcings.

Torrence and Compo (1998) used the time series of the El Nino-Southern Oscillation (ENSO) to provide a practical guide to wavelet transform analysis. They showed that variance of ENSO changed on interdecadal timescales. Variation in the Southern Oscillation Index (SOI) was significantly high during two periods within the data set (1880-1920 and 1960-1990) and significantly lower for the period 1920-1960. The analysis revealed a 15-yr modulation of the SOI with a 2-8 yr frequency in sea surface temperature (SST) variability.

7.2.2 Periodicity of Climate Change in the Southeast Atlantic and Southwest Indian Oceans

Latitudinal movements of the Subtropical Convergence (STC) and the Antarctic Polar Front (APF) in the southern Indian Ocean during the Late Quaternary are inferred from spectral analysis of four SST records that show significant and coherent variance in all three primary orbital forcings (Howard and Prell, 1992). The shifts in the two oceanic fronts are attributed to variations in westerly wind strength in subtropical to subpolar latitudes or north-south migrations

of the entire westerly wind belt. The wind stress is particularly enhanced by zonal asymmetries in sea-ice fields in the Southern Ocean (Howard and Prell, 1992).

The Benguela Current system performs a combination of two types of precessional movements (Jansen *et al.*, 1996). North-south shifts in the Angola-Benguela Front (ABF) precede swings between more zonal and more meridional directions of the Benguela Oceanic Current by 6.6 kyr. Schneider *et al.* (1995) used spectral analysis to show that the zonality of the Benguela Current varies in phase with minimum boreal summer insolation, resulting in SST variations on the Walvis Ridge that are in phase with SST variations in the equatorial Atlantic. Variance in SST at the Walvis Ridge is significant at all three of the Earth's orbital frequencies, but SST records from the Angola Basin vary significantly only in precessional and eccentricity cycles (Schneider *et al.*, 1995). In addition, SST variations in the Angola Basin lag those at the Walvis Ridge and the equatorial Atlantic by about 3 kyr.

Jansen *et al.* (1996) used planktonic foraminiferal data from three cores on the Angola-Zaire margin to reconstruct the palaeopositions of the ABF for the last 180 kyr. Spectral analysis of the records show that shifts in the position of the ABF contain significant variance in the 23-kyr orbital frequency band, together with a strong 100-kyr frequency component. Additionally, there is a large amount of variance at 15 kyr, which is the sum frequency of the 23-kyr and very weak 41-kyr cycles (Jansen *et al.*, 1996). The 100-kyr component is well-documented in the *N. dutertrei* record from the Walvis Ridge and the northern Cape Basin (Oberhänsli, 1991).

Spectral analysis indicates that Pleistocene variations in "upwelling' and "eastern boundary" foraminiferal assemblages in the central equatorial Atlantic are centred on the 23-kyr and 100-kyr frequency bands (Mix and Morey, 1996). Most of the variance suggests that advection of cool waters from the Benguela Current system is a key factor in large-scale climatic change at the equator. Results point to a succession of events in a coupled atmosphere-ocean system. Mix and Morey (1996) suggest that early changes in the zonal component of the trade-winds began the glacial cycle. A later effect of a cool ocean adjacent to a relatively warmer African continent intensified meridional winds that drew cool Benguela water toward the equator in the central Atlantic.

Spectral analysis of sedimentary records of alkenone and organic carbon concentrations in cores recovered from the Guinea and Angola Basins and at the Walvis Ridge shows that surface

circulation and productivity changes in the east-equatorial South Atlantic Ocean responded to 23-kyr and 100-kyr cyclical forcings for at least the last 350 kyr (Schneider *et al.*, 1996). Changes in SST and productivity in the eastern Angola Basin were found to lag those observed in the equatorial Atlantic and on the Walvis Ridge by ~3500 years, at the 23-kyr cycle. Covarying SST and palaeoproductivity changes at the equator and the Walvis Ridge are thought to be driven by changes in zonal trade-wind intensity which, in turn, forces variations in coastal and equatorial upwelling intensity as well as advection of cold Benguela waters from the south. SST and palaeoproductivity changes at the equator and the Walvis Ridge lead changes in ice volume. Schneider *et al.* (1996) found that, north of 20°S, changes in SST and productivity were not significantly affected by the 41-kyr cycle, suggesting that the obliquity cycle, so characteristic of Northern Hemisphere climate change, did not substantially influence surface circulation in the tropical and subtropical South Atlantic Ocean.

The presence of a 41-kyr cyclicity in the nitrogen isotope ratio of sediments from the Zaire Fan and Angola Basin, as indicated by spectral analysis, provides evidence of glacial-interglacial (G-IG) fluctuations in nitrate concentrations in this region (Holmes *et al.*, 1997). More pronounced fluctuations in $\delta^{15}N$ at the 23-kyr period indicate that changes in the trade-wind driven upwelling intensity drive nutrient availability and productivity off the south-west African coast (Holmes *et al.*, 1997; 1999).

7.3 METHODS

The data used in this research are complex; the data sets comprise two cores of different lengths and with differing sedimentation rates. A depth-constant sampling interval resulted in two time series with differing sampling intervals in time. Large changes over time are observed in both records. Standard spectral analysis techniques may prove less helpful, as these cannot detect the progression of a signal over time. In spectral analysis, the dominant cyclicity is dependent on the length (time) of the record and the place in time investigated, so that a successful interpretation is often related to choosing the correct "length" of time. Therefore use has been made of a new technique, continuous wavelet transform. Wavelet transform is a useful technique for analysing time series with different timescales and is particularly useful when the amplitudes and frequencies of the dominant cycles are time-dependent (Torrence and Compo, 1998).

Wavelet Transform is a generalised form of Fourier transform and windowed Fourier transform (Lau and Weng, 1995). The Fourier transform does not contain any time dependence of the signal and therefore cannot provide any local information regarding the time evolution of its spectral characteristics (Lau and Weng, 1995). In a windowed Fourier transform, a time series is examined under a fixed time-frequency window with constant intervals in the time and frequency domains (Lau and Weng, 1995). A wavelet transform uses generalised local base functions (wavelets) that can be narrowed to focus on the high-frequency signals (such as abrupt changes), or stretched to resolve the low-frequency background and translated with a flexible resolution in both frequency and time (Lau and Weng, 1995). Wavelet analysis involves a transform from a one-dimensional time series (frequency spectrum) to a diffuse two-dimensional time-frequency image (Torrence and Compo, 1998). By decomposing a time series into time-frequency space, one is able to determine both the dominant modes of variability and how those modes vary in time. The resultant image gives information about both frequency and amplitude modulation within the time series. However, one of the drawbacks of this technique is that one is unable, at present, to ascertain the significance level of the detected frequencies of change.

All the proxy data from both cores were subjected to wavelet transform analysis. The data were analysed using a programme written by J.-L. Mélice (Mélice *et al.*, 2001). The program computes the continuous wavelet transform (CWT) of any time series, using a complex Morlet wavelet (Morlet, 1983). The theory of the CWT used in the program to generate the following results is described in Appendix B of Mélice *et al.*, (2001). The data for core MD962080 (Agulhas Bank Slope) were interpolated at 1 kyr, whereas the data for core MD962084 (Olifants River Slope) were interpolated at 0. 5 kyr. The difference is due to higher sedimentation rates, and therefore higher resolution, on the Olifants River Slope.

The continuous cross-wavelet technique was used to compare proxies from each core to the planktonic oxygen isotope data (as a representation of SST and global ice-volume) from the relevant core. This was done in order to detect variations in the timing of changes in different proxies within the same core relative to global changes. Time-lags between the two cores were investigated by cross-spectrum analysis of the same proxy in both cores. For these analyses data from both cores were interpolated at 1 kyr in order to produce equally-sized matrices. The theory describing cross-wavelet spectrum analysis and the estimation of instantaneous phase difference and time lag between two time series is given in Mélice and Servain (2002).

7.4 RESULTS

The moduli (amplitudes) of the CWT for the different proxies are presented in Figures 7.1 and 7.2. The colour scale indicates the re-scaled value of the modulus. Each scale has zero as the minimum (dark blue). High amplitudes are indicated in dark red. The intensity of the signal is shown by the closeness of the contours. In conventional spectral analysis this is equivalent to the height of the peak. The vertical period or frequency axis has a logarithmic scale Tick marks and labels correspond to periods of 5, 10, 21 (accounting for the 19–23 kyr precessional cycle), 41, 100, 200 and 400 kyr. The horizontal axis represents age in kyr B.P.. The $\delta^{13}C_{org}$ record from core MD962080 was analysed twice in order to remove the overriding influence of the strongly depleted values in MIS 7. Two wavelet transforms are presented; the first with the original data and the second without stage 7 data. This effect of the detection of one major shift in the data set as the dominant frequency is possibly a shortcoming in this technique. Two wavelet transforms are presented for $\delta^{15}N$ in core MD 962084; one to reflect the influence of low-frequency changes (>100 kyr) and one focussing on high frequencies. There was no difference in the resultant image for the other proxies when analysed for high and low frequency changes.

7.4.1 Core MD962080 (Agulhas Bank Slope)

The $\delta^{18}O$ record of *Gr. inflata* reflects the salinity and temperature of the surface waters and can be considered to reflect global ice volume (Bolton *et al.*, 1995). The CWT for core MD962080 (Fig. 7.1a) shows that the global ice volume has two dominant regimes of quasi-periodic oscillations: the first fluctuates around the 100-kyr cycle and is strongest at 400 kyr B.P. (with a frequency of ~90 kyr), 200 kyr B.P. (with a frequency just greater than 100 kyr) and 700 kyr B.P. Superimposed on this is the 41-kyr cycle that is strongest at 650-600 kyr B.P., 450-350 kyr B.P. and 120-180 kyr B.P. The obliquity (41-kyr) signal undergoes a rapid frequency modulation near 600 kyr B.P. when it is influenced by the precession (19-23 kyr) signal. A weak precession signal is seen, with its highest amplitude around 400 kyr B.P. The frequency of the eccentricity (100-kyr) signal is modulated by an additional 200-kyr periodicity over the last 400 kyr.

The CWT for the $\delta^{13}C$ record of *Gr. inflata* shows a strong 400-kyr component for the length of the record (Fig 7.1b). A dominant 80-kyr frequency regime is detected in the transform between 500 and 200 kyr B.P. as well as between 800 and 600kyr B.P. A 200-kyr periodicity is seen

between 750 and 500 kyr B.P., whilst a higher frequency band centred at about 170 kyr is present between 300 and 100 kyr B.P. The 21-kyr period exhibits a repeating pattern with a period of ~100 kyr with the added influence of ~10- and 5-kyr periods in the last 300 kyr.

7.4.1.1 Periodicities in Foraminiferal Assemblages

The contribution of the Transitional Assemblage to the planktonic foraminiferal population is affected most strongly by variations in the earth's obliquity (Fig. 7.1c). The 41-kyr cycle is strongest around 800, 550 and 100 kyr B.P. and it is enhanced by the precession signal at ~800, 480 and 70 kyr B.P. There is a transition to the eccentricity frequency regime between 780 and 550 kyr B.P. A weaker, long-term frequency (~200 kyr) is observed for the last 500 kyr of the record.

Long-term variability in the Cosmopolitan Assemblage for the last 600 kyr corresponds to the 200-kyr period observed in the Transitional Assemblage (Fig. 7.1d). The strongest periodicity in this record is the obliquity signal between 600 and 500 kyr B.P. and coincident influence of the precession signal. The abrupt change in the amplitude of variation within the record at this time is reflected in the CWT.

Two main frequency bands corresponding to the obliquity and precession cycles are detected in the CWT for the Subantarctic Assemblage (Fig. 7.1e). A high-frequency, noisy pulsing centred at 10 kyr is seen, whilst a weaker, long-term signal with a period of ~300 kyr occurs between 700 and 400 kyr B.P.

The CWT for the Mixed-Temperate Assemblage exhibits the influence of all three orbital parameters (Fig. 7.1f). This is not surprising as this assemblage reflects the tropics and low-latitudes which closely record variations in the orbital parameters. The long-term 200-kyr-frequency regime dominates the entire record. The eccentricity signal is most dominant over the last 350 kyr of the record and for the period 700 – 500 kyr B.P., which also experiences the influence of the 41-kyr cycle. Variations in the earth's obliquity have a significant effect on the foraminiferal record over the last 300 kyr. The 21-kyr periodicity exhibits a beating pattern caused by the interaction of the 19 and 23 kyr periods, which is at times overprinted by higher (7-5 kyr) frequency variations.

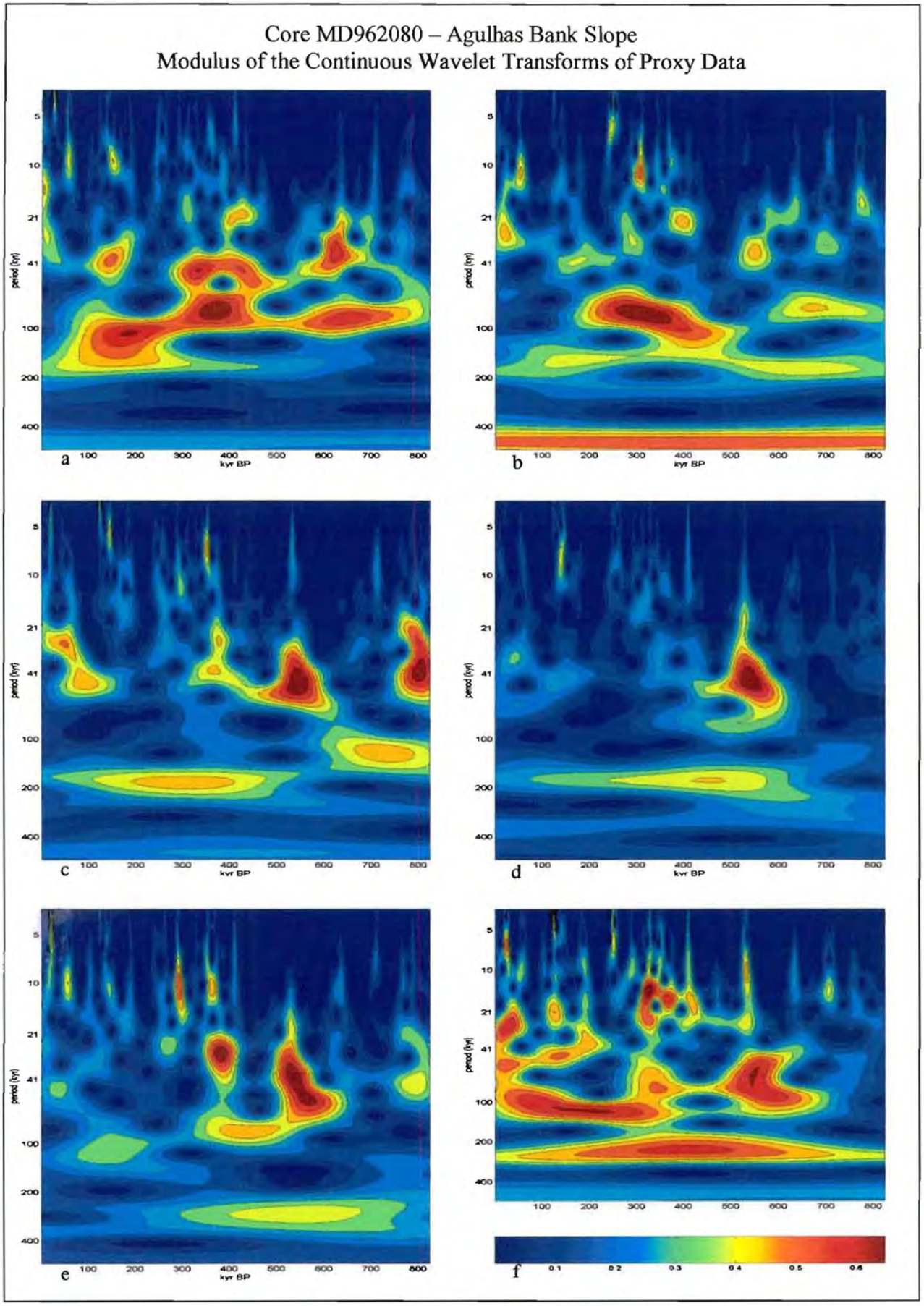

Figure 7.1: Modulus of the continuous wavelet transform of (a) $\delta^{18}O$ *Gr. inflata*, (b) $\delta^{18}O$ *Gr. inflata* (c) Transitional Assemblage, (d) Cosmopolitan Assemblage, (e) Subantarctic Assemblage and (f) Mixed-Temperate Assemblage for core MD962080. The colour scale indicates the re-scaled value of the modulus. Each scale has zero as the minimum. The vertical frequency axis, in kyr, has a logarithmic scale. Age, in kyr B.P., is shown on the horizontal scale.

Variability within the younger half of the Tropical planktonic foraminiferal Assemblage record is aperiodic. The CWT shows two frequency regimes for the period 600–300 kyr B.P. (Fig 7.1g). The dominant obliquity signal shows a frequency modulation of the 41-kyr cycle with slightly higher frequencies for the older part of the record (near 800 kyr B.P. and 600 kyr B.P.), moderating to lower frequencies near 400 kyr B.P. A low-frequency component with a period centred at 200 kyr is present in the record prior to 350 kyr.

The rapid change in the *Gr. menardii* record to peak absolute abundance at ~620 kyr (Fig. 4.6a, pg. 4-39) is reflected in the CWT as a period of high-amplitude variability between 700 and 500 kyr B.P. (Fig. 7.1h). This period shows a 100-kyr cyclicity, whilst the rest of the record has random variability.

7.4.1.2 Periodicities in Calcium Carbonate Preservation Indicators

The CWT for the calcium carbonate content shows an upcore change in periodicity of variability within the record (Fig. 7.1i). The older portion of the record shows variability corresponding to a period of 10 kyr (at ~700 kyr B.P.), which switches to periods of 21 and 41 kyr between 700 and 600 kyr B.P. There is a step-like transition to the eccentricity frequency regime around 500 kyr B.P., although this frequency is modulated by the influence of the other two orbital parameters (obliquity and precession) at ~300 kyr B.P. A subharmonic with a 300-kyr period affects the entire record.

The coarse fraction record is dominated by low-frequency variability (Fig. 7.1j). The CWT shows a strong eccentricity component for the prominent cycles of 400 and 125-100 kyr throughout the record. A frequency band centred at 200 kyr is detected prior to 600 kyr B.P. The obliquity signal is strongest around 700 kyr B.P., where the 100-kyr signal weakens slightly. The influence of this 41-kyr cyclicity is seen until 500 kyr B.P. and also in the very recent part of the record. A high-frequency (13-15 kyr) is seen at 40 and 250 kyr B.P.

The eccentricity cycle is the dominant frequency regime behind the variability in the carbonate preservation index (Fig. 7.1k). The CWT shows a step-like transition at 500 kyr B.P. from a frequency regime centred at 80 kyr, which is strongest between 700 and 520 kyr B.P, to a 100-kyr period between 480 and 250 kyr B.P. The 41-kyr cycle is strongly superimposed on the eccentricity signal around 400 kyr B.P. A weak precession signal, alternating with a 10-kyr

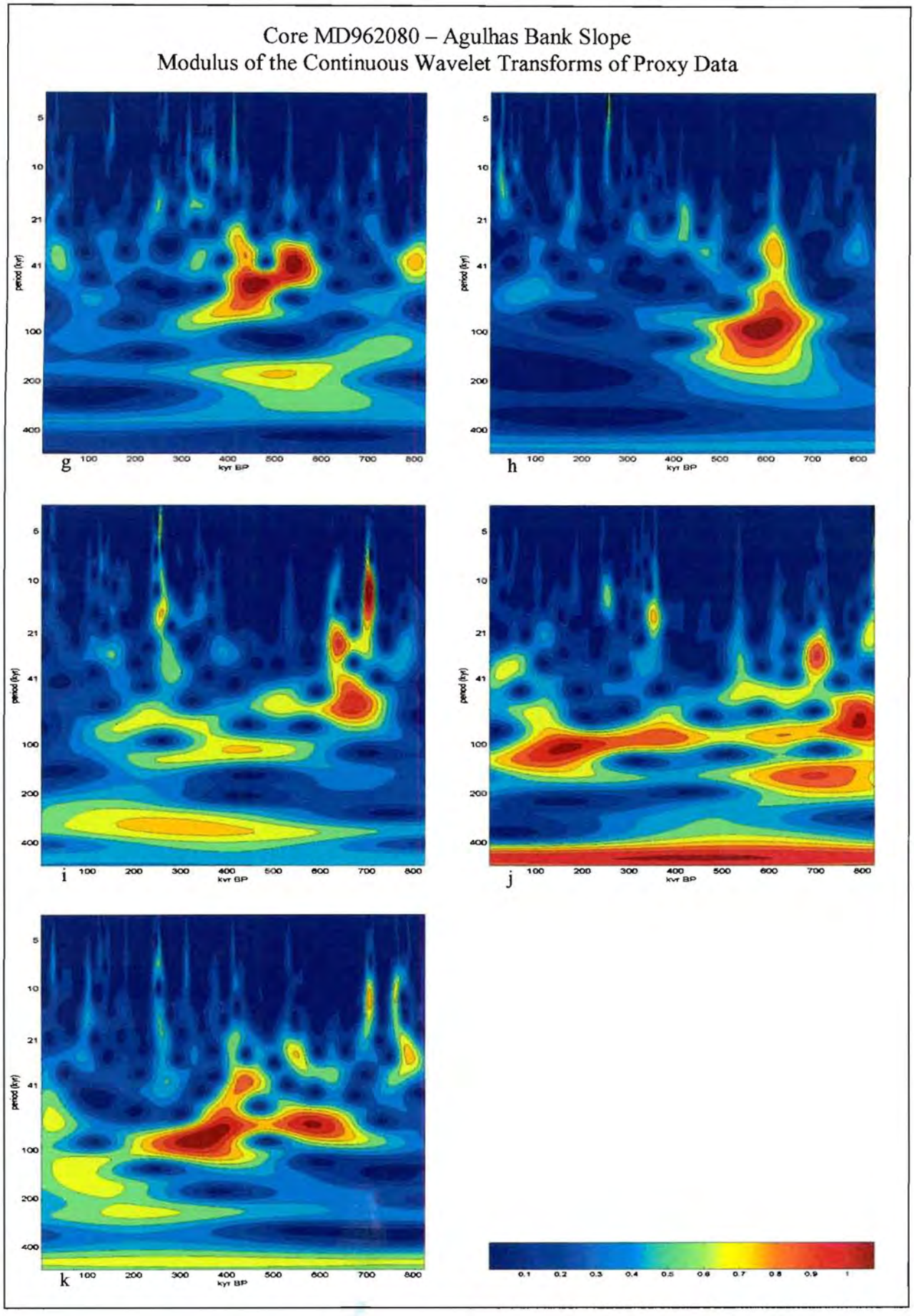

Figure 7.1: Modulus of the continuous wavelet transform of (g) Tropical Assemblage, (h) Absolute abundance of *Gr. menardii*, (i) % Calcium carbonate, (j) Coarse fraction and (k) Preservation index for core MD962080. The colour scale indicates the re-scaled value of the modulus. Each scale has zero as the minimum. The vertical frequency axis, in kyr, has a logarithmic scale. Age, in kyr B.P., is shown on the horizontal scale.

period, is seen prior to 550 kyr B.P.

7.4.1.3 Periodicities in Palaeoproductivity and Nutrient Proxies

Varibility with depth in the total organic carbon (TOC) content of the core is dominated by two frequency regimes. There is a change between the two frequency regimes at 400kyr B.P. The 41-kyr cycle, which is dominant between 600 and 450 kyr B.P., changes to a 100-kyr cycle, which is shown to be the dominant periodicity until ~150 kyr B.P. (Fig. 7.1l). A frequency band centred at 80 kyr is detected towards the end of the record near 800 kyr B.P. The 21-kyr cycle is only initiated at 300 kyr B.P. A low-frequency modulation of the obliquity cycle with a period in frequency band centred at ~170 kyr is seen in the record between 500 and 250 kyr B.P.

A change in nitrate source or nitrogen cycle reflected by the mean change in the $\delta^{15}N$ record at ~250 kyr B.P. (Chapter 6, pg. 6-16) is coincident with the peak amplitude of the dominant frequency regimes as shown in the CWT (Fig. 7.1m). Two dominant frequency bands are detected; one, centred at 200 kyr, is present over the last 400 kyr of the record and a second band, centred at 80 kyr, dominates between 750 and 650 kyr B.P. and around 300 kyr B.P. A weak obliquity signal is seen at intervals throughout the record. High-frequency variability with a period of ~7-kyr is seen at 350 and 250 kyr B.P.

The strongly depleted $\delta^{13}C_{org}$ values in MIS 7 (Fig. 6.1b, pg. 6-17) are reflected in the CWT by the strong 100-kyr period signal between 300 and 150 kyr B.P. (Fig. 7.1n). If this sudden depletion is removed from the record, four main frequency bands centred at ~125, ~80, ~30 and ~15 kyr are detected (Fig. 7.1o). Over the last 300 kyr, the low-frequency signals dominate over the high-frequency signals. The 125-kyr period dominates the record between 600 and 300 kyr B.P., after which there is a transition to the 80-kyr period which is initiated at ~250 kyr B.P. and continues to the top of the core. There is a weak 30-kyr periodicity around 700 and 550 kyr B.P. and a stronger signal for the between 200 and 100 kyr B.P. The data fluctuate with a period of 15-kyr at 300 kyr B.P. and at 100 kyr B.P. These periods have high-frequency variability superimposed on them.

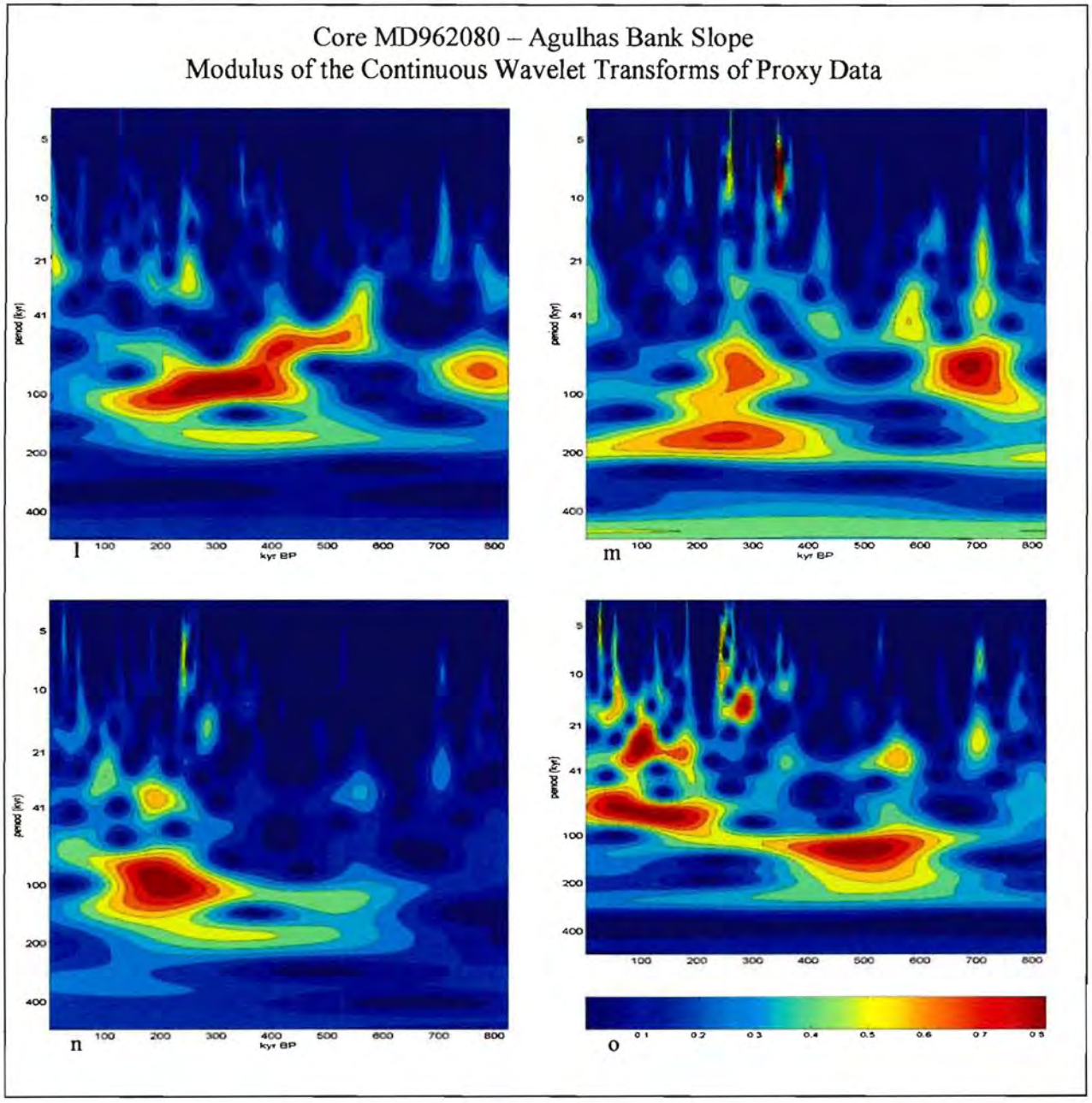

Figure 7.1: Modulus of the continuous wavelet transform of (l) % TOC, (m) $\delta^{15}N_{bulk}$, (n) $\delta^{13}C_{org}$ and (o) $\delta^{13}C_{org}$ minus MIS 7 data for core MD962080. The colour scale indicates the re-scaled value of the modulus. Each scale has zero as the minimum. The vertical frequency axis, in kyr, has a logarithmic scale. Age, in kyr B.P., is shown on the horizontal scale.

7.4.2 Core MD962084 (Olifants River Slope)

The CWT for the $\delta^{18}O$ record of *Gr. inflata* for core MD962084 (Fig. 7.2a) shows that fluctuations in the global ice volume over the last 500 kyr are dominated by the eccentricity (100-kyr) signal. The 41-kyr cycle dominates around 800 and 600 kyr B.P. and in the very recent part of the record. The weaker influence of the precession (19-23 kyr) signal is seen in the $\delta^{18}O$ record particularly at ~350 kyr B.P. and between 250 and 130 kyr B.P.

Similarly, the CWT for the $\delta^{13}C$ record of *Gr. inflata* exhibits the influence of all the orbital parameters (Fig. 7.2b). The eccentricity signal dominates this record. A 400-kyr component is reflected across the entire record; the 200-kyr frequency is recorded for the period 600 – 200 kyr B.P., and the dominant 100-kyr cycle is seen strongly between 800 and 700 kyr B.P. and over the last 500 kyr B.P. Where the eccentricity cycle weakens at ~650 kyr B.P., the precession cycle dominates. This orbital periodicity is also strong around 200 kyr B.P. The obliquity signal is strongly superimposed on the eccentricity signal around 350 kyr B.P. Pulsing high-frequency fluctuations (~7-kyr) are seen at 150 kyr intervals (at 400 kyr B.P., 250 kyr B.P., ~70 kyr B.P.) over the last 400 kyr of the record.

7.4.2.1 Periodicities in Foraminiferal Assemblages

A persistent, though variable high-frequency cycle is present in throughout the Subantarctic planktonic foraminiferal Assemblage record (Fig. 7.2c). The precession cycle and a periodicity centred at 15 kyr are most dominant. A very high frequency (~5-7 kyr) cycle is present, having highest amplitude variations between ~450 and 350 kyr B.P. At lower frequencies, the record shows a ~300 kyr frequency modulation.

The CWT for the Mixed-Intermediate planktonic foraminiferal Assemblage displays a strong power at 400 kyr (Fig. 7.2d). This reflects a long-term change in dominant surface waters from oligotrophic to more nutrient-rich intermediate waters. At Milankovitch frequencies, the influence of the eccentricity cycle is seen most strongly between 500 and 300 kyr B.P. However, combination tones of the precession signal, fluctuating between 19 and 23 kyr, are more consistent throughout the record.

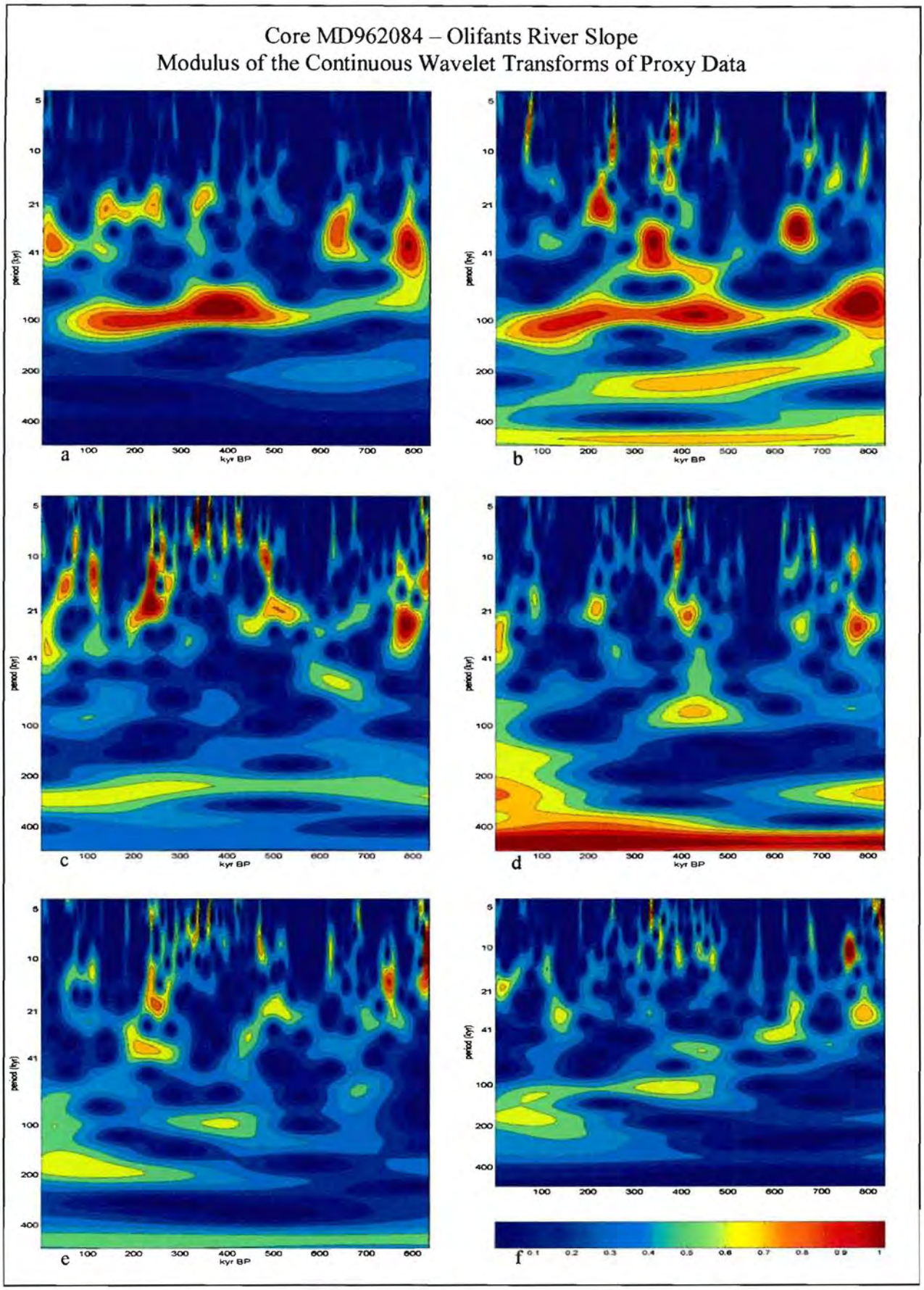

Figure 7.1: Modulus of the continuous wavelet transform of (a) $\delta^{18}O$ *Gr. inflata*, (b) $\delta^{18}O$ *Gr. inflata* (c) Subantarctic Assemblage, (d) Mixed-Intermediate Assemblage, (e) Transitional Assemblage and (f) Warm-Cosmopolitan Assemblage for core MD962084. The colour scale indicates the re-scaled value of the modulus. Each scale has zero as the minimum. The vertical frequency axis, in kyr, has a logarithmic scale. Age, in kyr B.P., is shown on the horizontal scale.

The Transitional Assemblage shows predominantly high-frequency variability (Fig. 7.2e), with frequency bands centred at ~ 7, 10 and 15 kyr. The precession signal is strongest near 250 kyr B.P. and at 500 kyr B.P. The CWT shows a 30-kyr cycle at 450 kyr B.P. and between 300 and 200 kyr B.P. A weak 100-kyr cycle is present between 450 and 350 kyr B.P. The general decrease in this assemblage over the last ~250 kyr is reflected in the ~180-kyr period which is initiated around 250 kyr B.P.

Cyclical variability within the Warm-Cosmopolitan Assemblage is weak (Fig. 7.2f). However, as this assemblage contributes only 3% to the overall variance within the planktonic foraminiferal population, it's significance in terms of interpreting the dynamics of the surface water masses in the SBR is considerably less than the other Assemblages. Weak periodicities with frequency bands centred at 7, ~12, 21, 30, ~56, 100, 125 and 170 are detected in the CWT.

Fluctuations within the Tropical Assemblage are dominated by high-frequency variability throughout the record (Fig. 7.2g). The 7-kyr cycle exhibits a beating pattern with a period of ~200 kyr, which is not associated with any significant power at the 200-kyr period band, whilst a 10-15-kyr cycle occurs at intervals throughout the record. Combination tones of the precession cycle are seen. A long-term frequency (>400 kyr) is also present throughout the record. A weak 125 kyr cycle is present for the last 200 kyr of the record, whilst the obliquity (41-kyr) signal is strongest for the period 600 –500 kyr B.P.

The record of absolute abundance of *Gr. menardii* produces a random or aperiodic signal. The only signal detected is a time of high-frequency variability between 500 and 400 kyr B.P. (Fig. 7.2h).

7.4.2.2 Periodicities in Calcium Carbonate Preservation Indicators

The CWT for the calcium carbonate content shows the influence of both the eccentricity and the obliquity signals (Fig. 7.2i). The 41-kyr cycle is weaker and appears more sporadically than the 100-kyr cycle, which is particularly prevalent over the last 300 kyr.

The coarse fraction record is also influenced by two of the orbital parameters: obliquity and eccentricity (Fig. 7.2j). The CWT shows an abrupt, step-like transition at ~350 kyr B.P. from the obliquity signal to the dominant eccentricity signal. As with the carbonate content, the

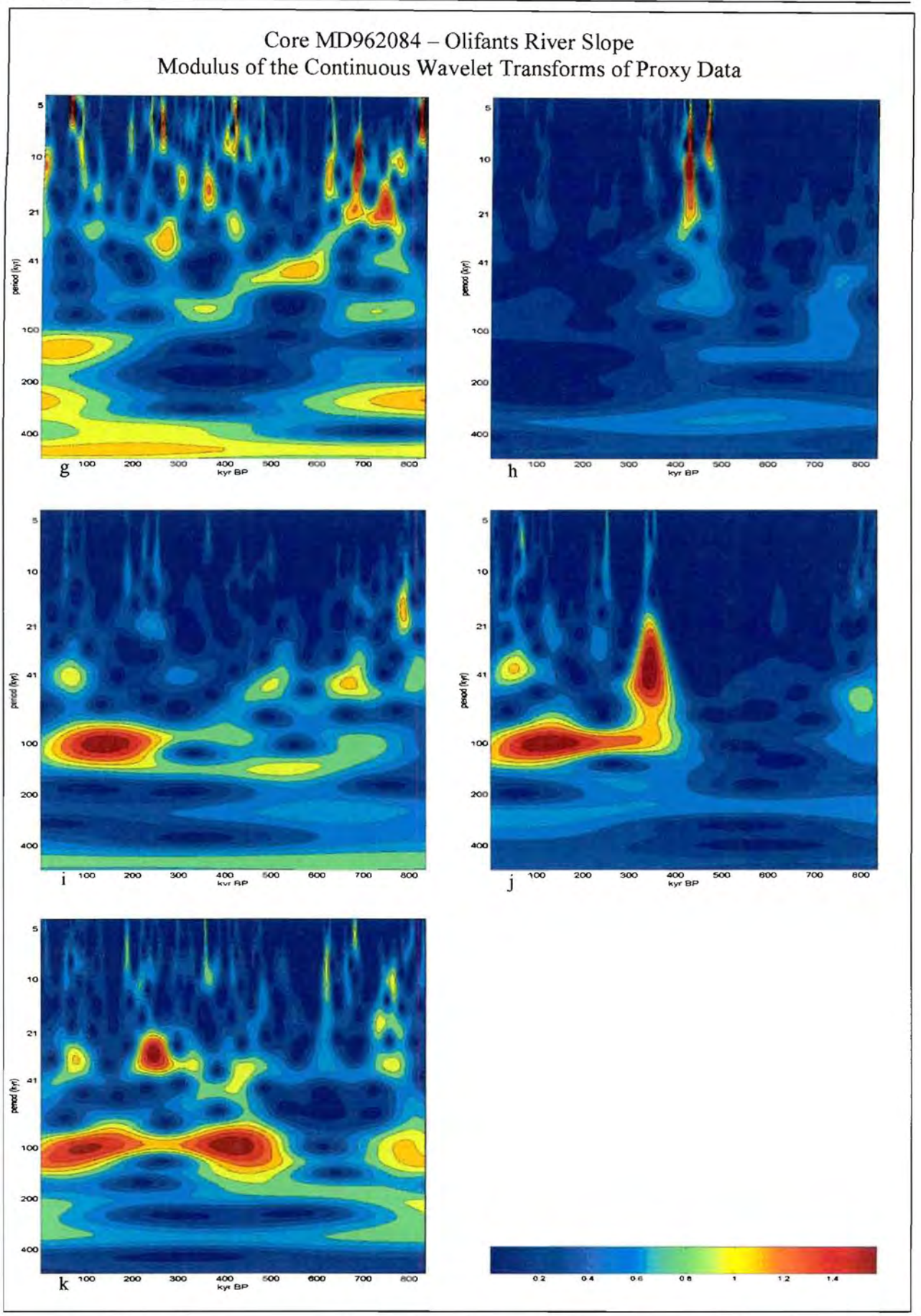

Figure 7.1: Modulus of the continuous wavelet transform of (g) Tropical Assemblage, (h) Absolute abundance of *Gr. menardii*, (i) % Calcium carbonate, (j) Coarse fraction and (k) Preservation index for core MD962084. The colour scale indicates the re-scaled value of the modulus. Each scale has zero as the minimum. The vertical frequency axis, in kyr, has a logarithmic scale. Age, in kyr B.P., is shown on the horizontal scale.

eccentricity forcing dominates over the last 300 kyr of the record, with obliquity showing a lesser influence.

The dominant forcing mechanism behind carbonate preservation in core MD962084 for the last 500 kyr is the 100-kyr cycle (Fig. 7.2k). The preservation index is also influenced by changes in the earth's obliquity, particularly around 300 kyr B.P. This proxy shows no high-frequency periods.

7.4.2.3 Periodicities in Palaeoproductivity and Nutrient Proxies

The obliquity signal most strongly influences the depth variation in the TOC content for the last 600 kyr (Fig. 7.2l). There is modulation of this signal to slightly lower frequencies of around 43 kyr. Frequency bands centred at 15 kyr and ~220 kyr are also detected. The 15-kyr cycle is strongest around 250 kyr B.P., but is also detected near the bottom end of the record. The low-frequency (~220 kyr) signal is present prior to 300 kyr B.P.

Cyclical variability is only observed in the younger half of the $\delta^{13}C_{org}$ record (Fig. 7.2m). Four frequency bands, centred at 5, ~10, ~23, ~50 and ~80 kyr, are detected in the CWT. The long-term variability with a period of ~80 kyr is overridden by the strong 5-kyr cycle at 400 kyr B.P. This is also the time period when the 50-kyr cycle is strongest. The combined influence of the eccentricity and obliquity signals and the obliquity and precession signals is seen at 450-350 kyr B.P. and around 200 kyr B.P. respectively.

A frequency band centred at ~220 kyr dominates the low-frequency component of the variability within the $\delta^{15}N$ record (Fig. 7.2n). The maximum amplitude of variation within this band occurs at ~250 kyr B.P., which is coincident with the timing of the change in mean the $\delta^{15}N$ value as discussed in Chapter 6 (pg. 6-19). If this overriding signal is removed and higher frequencies are focussed on (Fig. 7.2o), the eccentricity signal emerges strongly for the period 500-100 kyr B.P. A combination of precessional and obliquity forcing is seen near 800 kyr B.P. and over the last ~300 kyr. A high-frequency variability (~10 kyr) occurs at 200 kyr B.P., just after the change in mean $\delta^{15}N$.

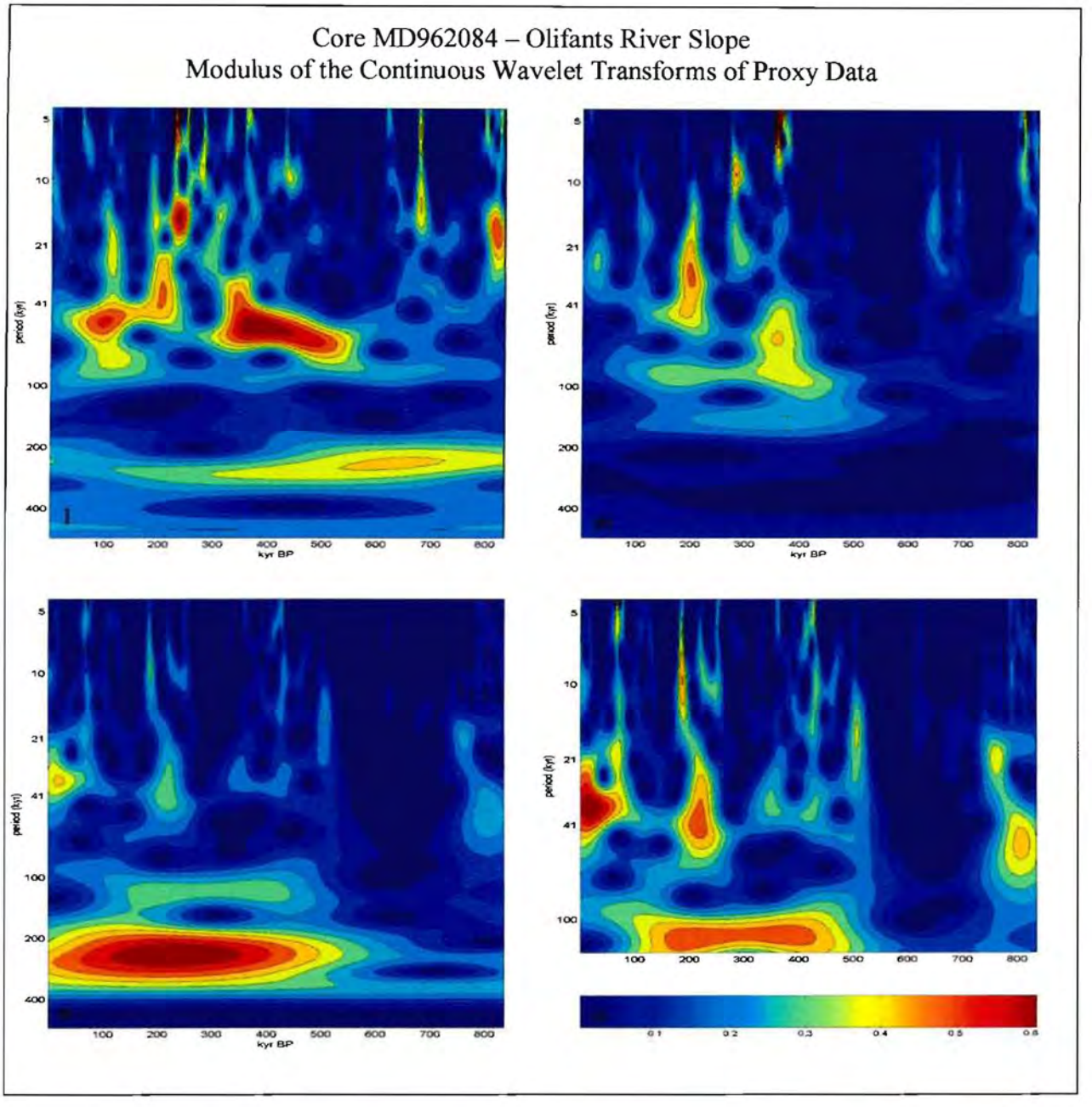

Figure 7.1: Modulus of the continuous wavelet transform of (l) % TOC, (m) $\delta^{13}C_{org}$, (n) $\delta^{15}N_{bulk}$ and (o) $\delta^{15}N_{bulk}$ restricted to periods < 150 kyr for core MD962084. The colour scale indicates the re-scaled value of the modulus. Each scale has zero as the minimum. The vertical frequency axis, in kyr, has a logarithmic scale. Age, in kyr B.P., is shown on the horizontal scale.

7.5 DISCUSSION

It must be borne in mind that the time series used here are complex and most of the wavelet transforms are fairly noisy. Thus, interpretations are made with caution and the significance of the results is not over-emphasised.

7.5.1 Core MD962080 (Agulhas Bank Slope)

Although all of the major orbital cycles are seen in the CWT for the $\delta^{18}O$ record of core MD962080, the time series is dominated by the eccentricity cycle, suggesting that the frequency structure may be a reflection of non-linear dynamical processes involving quasi-periodicity under the influence of external forcings. It is not surprising that the *Gr. inflata* records most strongly reflect global orbital variations, as these data have been tuned to the global signal in the development of the age model.

The foraminiferal assemblages exhibit different frequency patterns, indicating a greater response to changes in local conditions than to global changes. Nonetheless, all five assemblages are influenced by the obliquity signal. Changes in surface-water masses over the core site are due to varying influences of warm water from Agulhas rings and filaments and cold water intrusions across the STC. The STC is a wind-forced phenomenon and its position is controlled by the position of the zone of zero wind-stress-curl (Howard and Prell, 1992; Jansen *et al.*, 1996). This zone can be moved in two ways; latitudinal migration of the belt of westerlies or variations in the wind strength. Migrations are attributed to the 100 and 23-kyr cycles, and variations in wind strength to the 41-kyr cyclicity, being strongest in the high-latitudes (Jansen and van Haren, 2001). The precessional and eccentricity signals are felt to a lesser extent. Both signal are not always present in the records, suggesting that obliquity-driven changes in surface-water conditions force the responses seen in the planktonic foraminiferal population.

The proxy defined as being indicative of Agulhas water transfer, abundance of *Gr. menardii*, shows only one period of high cyclic variability. The apparent randomness of the signal is probably due to the fact that sampling resolution was too low to detect cyclic or pulsed variations in the transfer of thermohaline water into the Southeast Atlantic.

Carbonate dissolution imparts distinctive obliquity and eccentricity (both 100- and 400-kyr) signals in the carbonate preservation indices (sand contents and the foraminiferal preservation index). The similarity between the sand contents and $\delta^{18}O$ signal indicates that these cycles are a consequence of primary production, modulated by orbitally-forced variation in wind strength at high latitudes, and of dissolution at the sea floor resulting from variations in the chemical character of the intermediate and deep waters advected over the core sites from high latitudes. Cahnges in the advection of southern waters equatorward are modulated by the extent of the Antarctic sea-ice fields. During periods of minimal orbital eccentricity and maximum ice volume, increased sea-ice fields in the Southern Ocean pushed the westerly wind and trade-wind belts northwards (Imbrie *et al.*, 1993). As a consequence, the eccentricity-driven waxing and waning of the southern ice sheets probably also controls cyclical variations in carbonate production. According to Howard and Prell (1992), shifts in the hydrological fronts in the southern Indian Ocean also show a strong 41-kyr-obliquity signal. Our data suggest that the increased delivery of southern water masses to higher latitudes, as a result of equatorward migration of the hydrological fronts, drives the carbonate preservation/dissolution cycle. The weak 21-kyr signal indicates a degree insolation forcing on the primary carbonate producers, probably resulting in varying dominance of sand-size foraminifera and silt-size coccolithophorids.

Primary productivity indicators TOC, $\delta^{13}C_{org}$ and $\delta^{13}C_{inflata}$ register a strong 100-kyr component, particularly in the younger portion of the record. The strong variability in the 80-kyr frequency domain seen in the CWT of the $\delta^{15}N$ record may be a cross-product between the 100 and 41-kyr cycles. The results suggest that variations in nutrient availability and productivity on the Agulhas Bank Slope were driven by the local changes in circulation patterns, as well as by the influx of nutrient-depleted southern waters resulting from latitudinal migrations in the southern hydrological fronts, driven by variations in strength of the westerly wind belt and in response to the waxing and waning of the Antarctic sea-ice fields.

7.5.2 Core MD962084 (Olifants River Slope)

The dominant eccentricity cycle, seen in the $\delta^{18}O$ records of both cores, suggests that the Southeast Atlantic Ocean is sensitive to whatever mechanism drives the 100-kyr climatic response. While it may be correct to deduce that the two $\delta^{18}O$ records respond in similar ways to the same forcing, it must be borne in mind that these records have been tuned to the global signal in the creation of the age models.

The Angola-Benguela Front (ABF) performs meridional shifts over about 10 degrees of latitude during the Late Quaternary (Jansen *et al.*, 1996). The 23-kyr shifts of the ABF are approximately in phase with the global ice volume and are thought to be induced by precessional growth and decay of the ice fields in the Southern Ocean (Jansen *et al.*, 1996). Besides shifts in the precessional and eccentricity frequency bands, there is also significant variance at 15 kyr B.P. (Jansen *et al.*, 1996, Jansen and van Haren, 2001). Jansen *et al.* (1996) argue that the 15-kyr period is the sum frequency of the 23-kyr and the suppressed 41-kyr cycles. The Subantarctic and Tropical faunal Assemblages in core MD962084 show variability at both the precessional and eccentricity cycles, suggesting that the influx of Subantarctic waters over the core site is directly related to equatorward migration of the southern ice sheets. In addition, all of the foraminiferal assemblages exhibit high-frequency variation of 10 to 15 kyr, with little or no variation at the 41-kyr cycle. This orbital component is nearly absent at the ABF (Jansen *et al.*, 1996). The 15-kyr cycle is also evident in latitudinal movements of the Antarctic Polar Front (APF) (Jansen and van Haren, 2001) and sea-ice advances with a frequency of about 15 kyr, in phase with shifts in the APF (Armand, 2000).

As with core MD962080, the CWT for *Gr. menardii* indicates a random pattern of variation. Again, I suggest low sampling resolution as a reason for undetected cyclicity.

The CWT for carbonate content, sand content and carbonate preservation index strongly register the 41- and 100-kyr components at various times in the records. The same dominant components are recorded in the Agulhas Bank core. The waxing and waning of the southern ice sheets would cause changes in the chemical character and strength of the bottom waters over the core site, resulting in varying degrees of dissolution and winnowing. In addition, orbitally-forced variation in wind strength would affect upwelling and consequently primary productivity.

All three orbital (100, 41 and 23-kyr) frequencies are seen in the CWT of the productivity and nutrient proxies $\delta^{13}C_{org}$, $\delta^{13}C_{inflata}$ and $\delta^{15}N$. In the tropical Atlantic, organic carbon, used as an indicator of primary production, indicates a 23-kyr pattern of tropical insolation-forced changes in equatorial divergence (Verardo and McIntyre, 1994). However, the precessional signal is not seen in the TOC record of core MD962084. Co-varying SST and productivity changes at 23 and 100-kyr cycles on the Walvis Ridge and in the equatorial Atlantic suggest productivity changes are driven by variations in trade-wind intensity, which drives upwelling (Schneider *et al.*, 1995, 1996). The precession cycle is seen in the $\delta^{13}C_{org}$, $\delta^{13}C_{inflata}$ and $\delta^{15}N$ records, as well as in the Subantarctic foraminiferal Assemblage, indicating that changes in the trade wind-driven upwelling intensity and the advection of cold, nutrient-rich water from the south drive nutrient availability and productivity off the west coast of South Africa. Both Mix and Morey (1996) and Schneider *et al.*, (1996) found that variations in TOC lead SSTchanges. The data presented here indicate that changes in TOC lead changes in $\delta^{18}O$ for the period 400 – 100 kyr B.P. This may indicate that wind-driven upwelling responds faster to orbital forcing than advection of cold Subantarctic waters in the SBR. As the previous records cover only the last 300 kyr (Mix and Morely, 1996) and 350 kyr (Schneider *et al.*, 1996), this assumption may be valid for the period younger than 400 kyr B. P.. The longer record of core MD962084 indicates that prior to this time, variations in TOC lagged surface water temperature and salinity changes. The eccentricity and obliquity signals are more strongly reflected in the CWT than is the precession signal, pointing to variations in the strength or position of the westerly wind belt as a forcing mechanism for productivity changes. The presence of a strong 41- and 23-kyr signal in the $\delta^{15}N$ record over the last 100 years demonstrates that insolation changes affect nitrate availability and relative utilisation in the SBR. This finding correlates with research by Holmes *et al.* (1997, 1999), who found strong 23 and 41-kyr signals in the $\delta^{15}N$ records of cores collected in the NBR and Angola Basin. However, the dominant eccentricity signal seen in the Olifants River Slope sediments is not present in the northern records. This is may be because the NBR and Angola cores only spanned the last 300 kyr. The 200-kyr signal is strongest at 250 kyr and the 100-kyr signal is present between 500 and 100 kyrs B.P., whilst the 41-kyr signal appears only in the recent record (Fig. 7.2o). This discrepancy in results highlights a limitation of spectral analysis, the result is linked not only to the length of the record but also the place in time investigated. In contrast, wavelet transform detects dominant frequencies at different periods in time.

Whilst the 15 kyr signal is likely the result of interference between the 21- and 41-kyr cycles, climatic response at periods apparently unforced by orbital variations, such as the 200-kyr

signals observed in the foraminiferal assemblage, coarse fraction and $\delta^{15}N$ records and the 300-kyr periodicities in carbonate content from core MD962080 and the 200-300-kyr cycles observed in the TOC and $\delta^{15}N$ records from core MD962084, as well as the high-frequency pulsing fluctuations seen predominantly in foraminiferal abundance records of the SBR, suggests the importance of mechanisms internal to the climate system, e.g. atmosphere and ocean circulation, ocean-atmosphere interactions, ice-sheet growth and carbon cycles (Bolton *et al.*, 1995). These involve slow-response, non-linear feedback mechanisms and could account for the changing amplitudes of the low-frequency responses observed in the proxy data. Although the areas represented by the two cores do not respond identically to global climatic fluctuations, there are underlying similarities. The data from both cores indicate the primary importance of ice-sheet dynamics on the local and regional oceanography of the areas investigated. Changes result from latitudinal migrations in the southern hydrological fronts, driven by variations in strength of the westerly wind belt and in response to the waxing and waning of the Antarctic sea-ice fields. Carbonate preservation is controlled by changes in the bottom waters overlying the core sites, which vary as a result of latitudinal migrations in the westerly wind belts. The dominant signals in all proxies indicate that the Southeast Atlantic Ocean is highly sensitive to the mechanism that drives the 100-kyr climatic response. The data from cores MD962080 and MD962084 highlight the fact that previous interpretations of the functioning of the Benguela and equatorial Atlantic upwelling systems have been based only on the last 300-350 kyr (e.g. Holmes *et al.*, 1999; Mix and Morey, 1996; Schneider *et al.*, 1996). The longer records of the cores studied in this research show that the systems probably functioned differently prior to 400 kyr B.P.. The cores are compared and discussed in the following chapter.

Another application, which is not used or discussed in this thesis, but which may render additional useful information and will be explored for future publication, is that of cross-wavelet analysis. Phase relationships between different proxies within pre-defined periodicites can be explored, which may give insight into leads and lags between the two systems as well as between the proxy records and global climate change.

CHAPTER 8: SUMMARY and CONCLUSIONS

This chapter provides a synthesis and discussion of the main findings of this research. A synopsis of the results obtained from each core is given. The two cores are compared and similarities and differences are discussed. A palaeoceanographic history for the area represented by each core is proposed and broader regional comparisons are made. The main conclusions drawn from this research are presented, including inferences about the activity of Agulhas-water exchange and the functioning of the "Cape Valve". Some comments on this research are made at the end of this chapter.

8.1 SYNOPSIS OF RESULTS

8.1.1 Core MD 962080 (Agulhas Bank Slope)

- The average sedimentation rate at the site of core MD962080 is 2.35 cm/kyr. Pleistocene sedimentation rates on the Agulhas Bank Slope were generally within or below the average marine sedimentation rate range of 2-3 cm/kyr.
- Core MD962080 does not display the typical "Agulhas" foraminiferal composition, as defined by previous work on planktonic foraminifera in sediments from the Agulhas Bank and below the Agulhas Current (e.g. Lowry, 1987). Although all the typical "Agulhas" species are present in the core, they do not dominate the faunal population. The planktonic foraminiferal population is dominated by the transitional species *Gr. inflata* and the Subantarctic species *N. pachyderma* (d), reflecting the mixed nature of the water masses that pass over the core site.
- With the exception of the Subantarctic species *N. pachyderma* (d), the upcore distribution of the planktonic foraminiferal species in core MD962080 shows little correlation to glacial-interglacial (G-IG) cycles. Instead, the foraminiferal abundances fluctuate on shorter time-scales in response to local and regional changes in surface-water conditions. However, 'warm' species are generally more abundant in interglacial periods.
- Variable input of Indian Ocean waters into the southeast Atlantic, via the Agulhas Current, is indicated by the presence of Tropical/Subtropical planktonic foraminiferal species *N. dutertrei*,

Gs. trilobus, *Gs. sacculifer*, *Gs. ruber* (alba) and *Gr. menardii*, with maximum leakage occurring at glacial terminations.

- The faunal assemblages indicate rapid changes to intensely cold surface-water conditions during glacial stages MIS 14 (~560-530 kyr B.P.) and 12 (~470-430 kyr B.P.), with MIS 14 denoted as the coldest period investigated.
- A local response to the "Mid-Brunhes Climatic Event" at 400 – 300 kyr B.P. (Jansen *et al.*, 1986) is recorded in the faunal data, with an increase in the dominant Transitional Assemblage and concurrent decrease in the Cosmopolitan and Subtropical Assemblages. The planktonic foraminiferal assemblages indicate an upcore change to overall warmer surface-water conditions at ~250 kyr B.P.. and the development of a G-IG cyclicity from MIS 7 (~240-200 kyr B.P.) onwards.
- The count of absolute abundance of the tropical Indian Ocean foraminifer, *Gr. menardii*, reveals that this species is present throughout the length of core studied. Although MIS 11 (~420-360 kyr B.P.) does record some increase in *Gr. menardii* abundance, it is not a noticeable maximum as one might expect, given that this has been identified as one of the warmest stages in the Pleistocene with extreme poleward shifts in the Subtropical Convergence (STC) and Antarctic Polar Front (APF) (e.g. Howard and Prell, 1992; Niebler, 1995; Hodell *et al.*, 2000). Peak accumulation rates of *Gr. menardii* occur during the final stages of glaciation.
- Weight percent calcium carbonate data point to MIS 11 as being the period of highest carbonate production over the last 850 kyr.
- Coarse-fraction variations follow G-IG cycles with coarser textures defining glacial stages. Reduction in grain size is mainly the result of increased carbonate dissolution in warm periods through the breakdown of sand-size foraminifera, resulting in an increase in the fine-fraction. The carbonate preservation index indicates the $CaCO_3$ preservation is enhanced during glacial periods.
- Peak carbonate accumulation rates are centred on the final stages of glacial cycles or at G-IG transitions, with minimum values often occurring at the onset of glaciation.
- The coincidence of high mud contents and high organic carbon contents indicates that carbonate cycles on the Agulhas Banks Slope are driven by changes in productivity and preservation.
- Organic carbon content of the sediments is relatively low (mean = 1.41%). There is a general tendency towards increased organic carbon content during warm stages.

- Relatively low $\delta^{13}C_{org}$ values recorded in MIS 7 reflect enhanced phytoplankton production at this time.
- Palaeoproductivity proxies indicate low productivity in glacial periods over the core site.
- In general, glacial sediments record lower $\delta^{15}N$ values than interglacial sediments.
- There is a change in mean $\delta^{15}N$ to higher average values at about 250 kyr B.P. An upcore trend towards higher $\delta^{15}N$ values is initiated at this time.
- The presence of ammonium at the sediment-water interface is the most plausible explanation for the low $\delta^{15}N$ values. Regenerated nitrogen (ammonium) coupled with nutrient-deficient glacial waters facilitates nitrogen fixation by cyanobacteria, and accounts for the very low the $\delta^{15}N$ values during glacial stages 20, 18 and 8.
- Continuous wavelet transform (CWT) analysis indicates that obliquity-driven (41-kyr) changes in surface-water conditions force the responses seen in the planktonic foraminiferal population. Changes in the end-member faunal assemblages lead ice-volume changes (as recorded by $\delta^{18}O$) by up to 30 kyr for the majority of the time period investigated.
- Carbonate dissolution imparts distinctive obliquity and eccentricity (both 100- and 400-kyr) signals in the carbonate preservation indices (sand contents and foraminiferal preservation index). The weak 21-kyr signal indicates a degree of insolation forcing on the primary carbonate producers, probably resulting in varying dominance of sand-size foraminifera and silt-size coccolithophorids.
- Primary productivity indicators TOC, $\delta^{13}C_{org}$ and $\delta^{13}C_{inflata}$ register a strong 100-kyr component, particularly in the younger portion of the record. The $\delta^{15}N$ record shows strong frequency bands at 200 kyr and 80 kyr. The results suggest that variations in nutrient availability and productivity on the Agulhas Bank Slope were driven by the local changes in circulation patterns as well as the influx of nutrient-depleted southern waters, in response to latitudinal migrations of the southern hydrological fronts.

8.1.2 Core MD 962084 (Olifants River Slope)

- The average sedimentation rate of 5.4 cm/kyr on the Olifants River Slope is considerably higher than on the Agulhas Bank Slope (mean = 2.35 cm/kyr), but it is much lower than in the Northern Benguela Region (Lüderitz mean = 16 cm/kyr) and in the Angola Basin where sedimentation rates of up to 60 cm/kyr have been measured (Berger *et al.*, 2001).
- The faunal assemblage bears a clear transitional to Subantarctic character with *Gr. inflata* and *N. pachyderma* (d) being the dominant species.
- Changes in dominant water masses from offshore to mixed-intermediate are indicated by the inverse relationship between *Gr. inflata* and *Gg. bulloides*.
- An unusually strong upwelling episode is recorded in MIS 9 (~340 – 300 kyr B.P.) by peak abundance of the polar foraminifer *N. pachyderma* (s). This event is also recorded in comparable records from the SBR; ODP Site 1087 just northeast of this core (Giraudeau *et al.*, 2001) and MD962085 offshore of the Orange River (Chang *et al.*, 1999), as well as from the Walvis Ridge in the NBR (Ufkes *et al.*, 2000), indicating that it is a regional episode, consitent across the SBR and NBR.
- The faunal population indicates that MIS 11 (~420-360 kyr B.P.) was the warmest stage in the SBR in the last 850 kyr.
- The absolute abundance of *Gr. menardii* indicates a near-continuous presence of this species for the time period investigated, with only a few samples in the older portion of the core where no *Gr. menardii* were found.
- Sediment textures show a general coarsening-upward trend over the last 400 kyr. A G-IG cyclicity develops over the last 450 kyr, with higher carbonate content and coarser textures occurring in glacial periods.
- Carbonate contents and preservation peaks are centred on periods of rapid deglaciation in the final glacial stages or at transitions from glacial to interglacial conditions.
- Winnowing most likely accounts for the low carbonate accumulation rates in MIS 6 (~240-130 kyr B.P.).
- The change in carbonate content and texture between MIS 16 (~630 kyr B.P.) and MIS 10 (~360 kyr B.P.) points to a change in dominant carbonate producer from sand-size foraminifera to silt-size coccolithophorids.

- There is an indication of reduced Benguela circulation over the last 250 kyr, resulting in a change in dominant primary producers from calcareous plankton to siliceous diatoms as a result of the upwelling of silicate-enriched waters from the Angolan undercurrent.
- Organic carbon content (mean = 6%) in this core is considerably higher than for most deep-sea sediments from the South Atlantic (mean = 0.5%) (Keswani *et al.*, 1984), but it is still lower than Northern Benguela sediments.
- The predominantly marine source for organic carbon is indicated by average C/N ratios of 9.45. The coincidence of high C/N ratios and high organic matter content could point to diagenetic elevation of C/N ratios as a consequence of enhanced preservation of organic matter.
- There is a general pattern of higher $\delta^{15}N$ values (~4 - 7‰) during warm intervals and lower $\delta^{15}N$ values (~4 - 0.5‰) in glacial periods over the last 350 kyr. Glacial $\delta^{15}N$ values are generally lower than the $\delta^{15}N$ of interglacial sediments, suggesting less intense depletion of the surface nitrate pool during glacial periods.
- A strong upcore trend towards higher $\delta^{15}N$ values is observed for the last ~200 kyr.
- High $\delta^{15}N$ values, coincident with high organic carbon concentrations, reflect delivery of $\delta^{15}N$-enriched nitrate to the surface water from the underlying zone of denitrification, formed due to the presence of oxygen-deficient subsurface waters.
- The Subantarctic and Tropical faunal Assemblages in core MD962084 show variability at both the precessional (19-23kyr) and eccentricity (100-kyr) cycles. In addition, all of the foraminiferal assemblages exhibit high-frequency variation of 10 to 15 kyr, with little or no variation in the 41-kyr frequency band, suggesting that the influx of Subantarctic waters over the core site is directly related to equatorward migration of the southern ice sheets. Such expansion would result in a more northerly position of the polar fronts and consequent equatorward displacement of Subantarctic water masses.
- The CWT for carbonate content, sand content and carbonate preservation index strongly register the 41- and 100-kyr components at various times in the records.
- The precession cycle is seen in the $\delta^{13}C_{org}$, $\delta^{13}C_{inflata}$ and $\delta^{15}N$ records, but not in the TOC record. This is possibly related to burial rates and preservation of organic carbon.
- Changes in TOC lead changes in $\delta^{18}O$ (reflecting ice volume and SST) for the period 400 – 100 kyr B.P. However, prior to 400 kyr B.P. changes in TOC lagged $\delta^{18}O$ changes.

COMPARISON OF THE RESULTS FORM THE TWO CORES

Sedimentation rates on the Olifants River Slope (mean = 5.4 cm/kyr) are considerable higher than on the Agulhas Bank Slope (mean = 2.35 cm/kyr) for the period under investigation. In addition, the Olifants River Slope core is much muddier (i.e. lower sand contents, mean = 12%) than core MD962080 (mean sand content = 42%). Core MD962084 is more carbonate-rich than core MD962080 (mean 86% vs 74%), with an approximate three-fold increase in organic carbon content in core MD962084 (3-10%) compared to core MD962080 (0.5-2.7%). The mean $\delta^{13}C_{org}$ value for core MD962084 (-20.06‰) is higher than that of core MD962080 (-21.14‰) and the $\delta^{13}C_{org}$ values for bulk organic carbon in core MD962084 are more constrained than those for core MD962080. All these factors point to higher productivity in the Southern Benguela Region (SBR) than in the Agulhas Bank Region (ABR).

Local responses to the "Mid-Brunhes climatic event" are recorded in the foraminiferal assemblage data from both cores. A shift in mean contribution of the various factors is seen between MIS 11 and 7 and again at ~ 250-200 kyr B.P. The records in both cores show a change from high-frequency variability in MIS 11 - 7 to the development of a G-IG cyclicity after 250 kyr B.P. The faunal data indicate a change to overall warmer conditions in the ABR after ~250 kyr B.P. An increased contribution of the Mixed-Intermediate Assemblage in core MD962084 after 250 kyr B.P. implies a greater influence of intermediate and old-upwelled waters over the Olifants River Slope. The very high pelagic production, characteristic of the "Mid-Brunhes climatic event" in the Southern Ocean, as described by Hodell (1993), is recorded to some extent in the palaeoproductivity indicators in both cores. However, the significant increases in carbonate content in Southern Ocean sediments during MIS 11, 9 and 7 (Hodell, 1993) are not seen in either core. In fact, minimum carbonate values are recorded in MIS 7 in both cores. There is, however, a relative increase in carbonate content in stages 11 and 9 in core MD962080. The lack of major peaks in carbonate content in these intervals is likely as a result of the "Mid-Brunhes dissolution cycle" (Bassinot *et al.*, 1994a).

Similar responses to large-scale regional and global climate changes are recorded at both sites. The frequency of variation at both sites is driven, to a large extent, by the waxing and waning of the Antarctic sea-ice sheets and variations in the position and intensity of the westerly wind belt.

However, the data indicate that local changes in oceanography strongly affect the two areas represented by the two cores.

The two regions reflected by these sediment records are distinct in oceanographic character; the SBR being at the southern end of a highly productive upwelling system and the ABR lying just west of the warm, nutrient-deficient, scouring Agulhas Current. The data presented in this thesis reflect these differences in the past. Oxygen isotope ratios indicate that MIS 14 was the coldest period on the Agulhas Bank Slope, whereas MIS 12 is identified as the coldest period recorded in the SBR. This difference may be due to the influence of upwelled waters in the SBR, which may have been greater during MIS 12 than MIS14. Whilst the dominant foraminiferal species in both cores indicate the overall dominance of water masses that are transitional to Subantarctic in character, the planktonic foraminiferal assemblages accentuate the differences in surface-water conditions above the two core sites. The principal factor in core MD962080, the Transitional Assemblage, reflects the mixture of water masses that affect the region west of the Agulhas Bank, whilst the principal factor in core MD962084 is defined by the Subantarctic species *N. pachyderma* (d), reflecting the preeminence of cold upwelled waters in the SBR. The influence of the warm Agulhas Current waters over the site of core MD962080 is indicated by the high degree of variance accounted for by the second factor, the warm Cosmopolitan Assemblage. In contrast, in core MD962084, the high degree of variability accounted for by the second factor (the Mixed-intermediate Assemblage) reflects the variations in upwelling strength and the offshore extent of upwelled waters over the core site, whilst the warm Cosmopolitan Assemblage accounts for only a negligible fraction of the total variance in the Olifants River Slope core.

The differences in hydrological conditions are also discernible in the palaeoproductivity data. The larger range in the $\delta^{13}C_{inflata}$ record for core MD962084 compared to the Agulhas Bank core can be explained by stronger fractionation from the ambient seawater equilibrium, which varies between upwelling and non-upwelling periods (Reynolds-Sautter and Thunell, 1991). The generally higher $\delta^{13}C_{org}$ values in core MD962084, compared to core MD962080, reflect not only the disparity in productivity, but also differences in dominant plankton species in the two regions; the SBR has a higher standing stock of omnivorous euphausiids and dinoflagellates, whilst herbivorous copepods dominate the plankton in the ABR at present (Hutchings *et al.*, 1991). The nitrogen isotope ratios most strongly expose the differences in nutrient availability, nutrient type and productivity

functioning in the two regions. This proxy suggests that whilst there is a general excess of nutrients in glacial waters in the SBR, nutrient deficiency in the ABR leads to recycled production and nitrogen fixation. High productivity in the SBR during certain warm periods, combined with oxygen-depleted subsurface-waters leads to denitrification. There is no evidence of denitrification in the ABR. Despite differences in local productivity and nutrient activity, both cores show decreased productivity during glacial periods compared to interglacial periods. This contrast with finding in the NBR and equatorial Atlantic, where data indicate increased upwelling and productivity in glacial periods (e.g. Holmes *et al.*, 1997; 1999, Schneider *et al.*, 1994; 1995; 1996). Moreover, the $\delta^{15}N$ signal in both cores shows a general trend towards higher values over the last 250 kyr, suggesting a different nitrate source or a modified environment (as also indicated in the change in foraminiferal assemblage data). This finding is difficult to corroborate, as the only other nitrogen isotope work in the southeastern Atlantic region was carried out on sediment records from the NBR and equatorial Atlantic, which are generally less than 200 kyr old (300 kyr in one case), so no comparable data set exists for the nitrogen records presented in this thesis.

On average, *Gr. menardii* is seven times more abundant in core MD962080 compared to core MD962084 (Fig. 8.1). The consistently higher values in core MD962080 reflect the greater influence of tropical waters over the Agulhas Bank Slope for the time period investigated. These differences are related to the passage of Agulhas Rings into the Southeast Atlantic. Whilst the rings are likely to pass over the site of core MD962080, the most common pathways of rings shed into the South Atlantic are seaward of the site of core MD962084 (Fig. 4.8, pg.4-43).

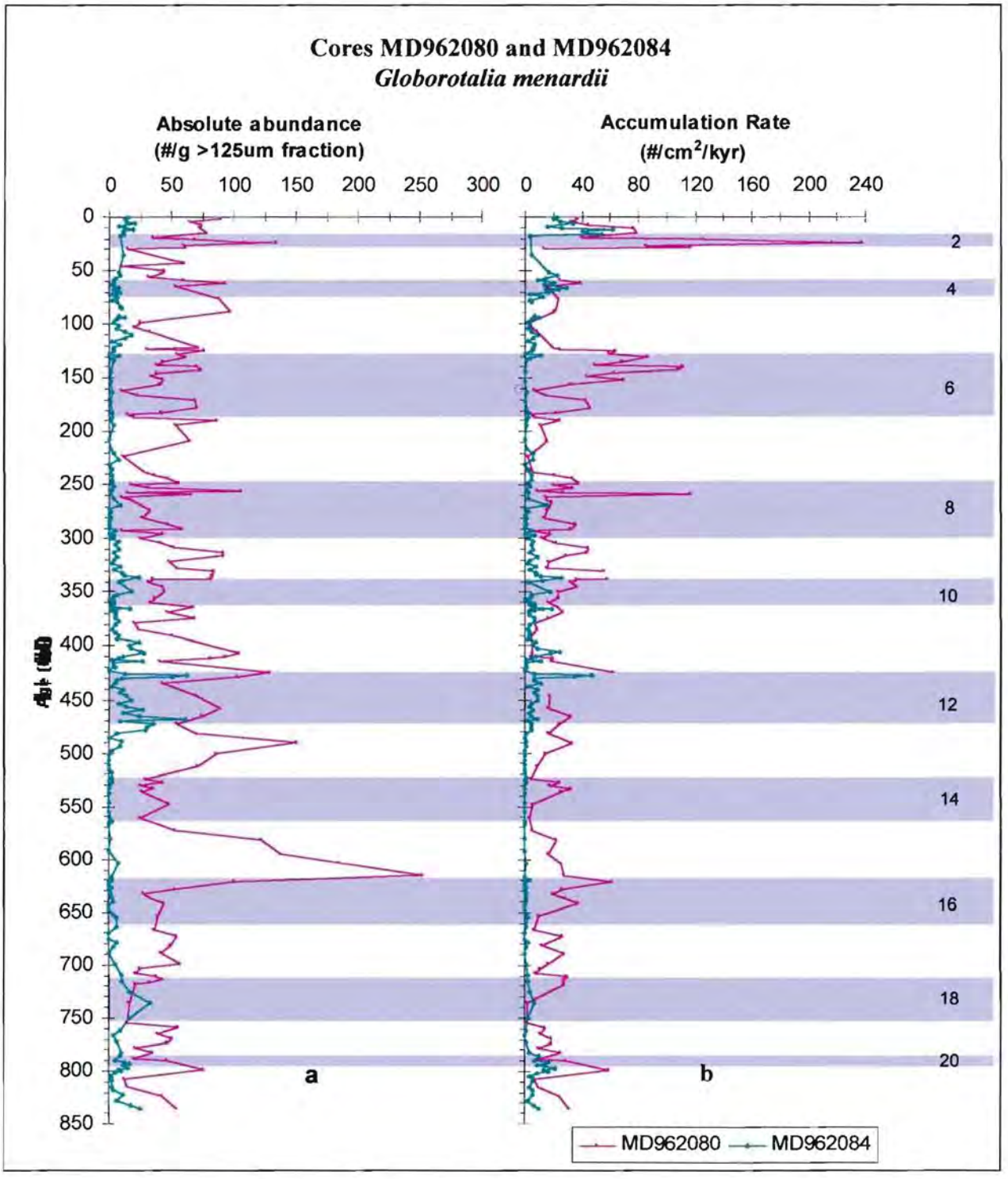

Figure 8.1: *Globorotalia menardii* absolute abundance (a) and accumulation rate (b) for cores MD962080 (red) and MD962084 (green). Grey-shaded bars represent inferred glacial marine isotope stages (MIS).

8.3 PALAEOCEANOGRAPHIC HISTORY

8.3.1 The Agulhas Bank Slope Region (Core MD 962080)

Core MD962080 (36°16'S, 19°28'E) lies in a zone influenced by waters from the Agulhas Current and the Agulhas Retroflection, as well as by waters from south of the southeast Atlantic Ocean (Fig. 2.4, pg. 2-10) The dominance of Transitional and Subantarctic planktonic foraminifera suggest that for the last 850 kyr the core site has been under the influence of cool-temperate, mixed water masses, with impacts from the warm waters of the Agulhas Current.

Low-frequency variations in surface-water conditions are observed from MIS 20 to MIS 14. The waters above the core site were particularly nutrient-depleted during glacial periods MIS 20 and 18, as indicated by the $\delta^{15}N$ values approaching zero at these times, which have been interpreted to indicate nitrogen fixation by cyanobacteria. Maximum abundance of *Gr. menardii* during deglaciation at the MIS 16/15 transition suggests a significant presence of Agulhas waters at this time. There was a rapid change to intensely cold conditions in MIS 14 and 12, with MIS 14 being identified as one of the coldest periods of the Pleistocene. The increase in cold-eutrophic foraminifera during these stages is probably related to an enhanced impact of Subantarctic waters as a consequence of equatorward migrations in the APF and STC, as documented by Hodell (1993) for these periods. The "mid-Brunhes dissolution cycle" (Bassinot *et al.*, 1994a), is clearly recorded in the low calcium carbonate content (MIS 15-14) and muddier sediment (decreased sand content in MIS 15-12).

The period MIS 13 – 9 is characterized by a general increasing trend in carbonate contents and organic carbon content, reflecting the high pelagic production characteristic of the "mid-Brunhes climatic event" (Hodell, 1993). This period is recorded to some extent, by other productivity indicators, but not as an outstanding event. Indeed, carbonate $\delta^{13}C$ values show a trend towards lower values for the period MIS 11-7. MIS 11 was the period of highest production, as indicated by peak values in carbonate content, TOC and $\delta^{13}C_{inflata}$. However, minimum carbonate content is observed in MIS 7. The planktonic foraminiferal record shows a change in surface-water conditions for the interval MIS 11 – 7. This period is characterized by an overall increase in the contribution of the Transitional Assemblage and a concurrent decrease in the warm Cosmopolitan and

Tropical/Subtropical Assemblages. Hodell (1993) used very low $\delta^{18}O$ values in MIS 11 and 9 to infer a southerly position of the APF in the Southern Ocean. $\delta^{18}O$ values in core MD962080 also indicate these as particularly warm stages. Nevertheless, the southward displacement of the APF was accompanied by a northward displacement of the STC (Howard and Prell, 1992; Hodell, 1993). Increased abundance of the Subantarctic species, *N. pachyderma* (d) in glacial stages supports the supposition that there were substantial equatorward migrations of the STC during glacial periods in this time-interval. However, any equatorward migration of the STC was not substantial enough to cut off the influence of warm Agulhas waters over the core site. This period shows increasing trends in carbonate preservation indices (sand contents, coarse fraction contents and % planktonic foraminifera). The data infer some oceanographic change linked to the "Mid-Bruhnes climatic event", a period in which Jansen *et al.* (1986) report intensified atmospheric and oceanic circulation in the Southern Hemisphere. This link is supported by the strong eccentricity signal seen in the CWT of $\delta^{18}O$, the Transitional foraminiferal Assemblage, the calcium carbonate, coarse fraction and TOC contents and the $\delta^{15}N$ record for the time-period 500 – 250 kyr B.P.

A profound change in surface-water conditions occurs during MIS 7 (250 – 200 kyr B.P.), when warmer surface waters replace the dominant mixed-Subantarctic-transitional water mass. A G-IG cyclicity develops in the faunal records from 250 kyr B.P. upcore. In addition, there is a change in mean $\delta^{15}N$, suggesting a change in nitrate source or environment. Sediment textural data reflect a change in bottom-water masses over the core location from NADW to USCW in glacial periods. The last 250 kyr record the highest productivity as indicated by, on average, higher carbonate content, increased carbonate preservation, relatively high TOC and a general increase in $\delta^{15}N$ values, perhaps reflecting more intense depletion of the available nitrate pool. Low surface productivity is indicated by depleted $\delta^{13}C_{inflata}$ values, during MIS 8, 6 and 2. Low glacial productivity is also indicated by the other proxies, but all data point to a strong increase in productivity in the Holocene.

The continuous presence of *Globorotalia menardii* throughout the length of core studied implies that the exchange of water from the South Indian Ocean to the South Atlantic Ocean was never entirely obstructed during the last 850 kyr.

8.3.2 Palaeoceanography of the Southern Benguela Region (Core MD 962084)

This core is situated in the SBR seaward of the seasonal Namaqua upwelling cell, in an area influenced by nutrient-rich upwelled waters, the filamentous region of mesotrophic old upwelled waters, the oligotrophic waters of the South Atlantic gyre, as well as the sporadic incursions of warm saline Indian Ocean waters carried by Agulhas rings. The dominance of transitional and Subantarctic planktonic foraminifera suggests that the core site has been under the influence of cool-temperate, mesotrophic mixed water masses for the last 850 kyr.

The influence of Agulhas waters over the core site is traced by relatively high accumulation rates of *Gr. menardii* in MIS 20. An increasing trend in the Subantarctic Assemblage, exclusively defined by *N. pachyderma* (d), is observed from the bottom of the record to MIS 17. There is a change in mean contribution of this factor to the total foraminiferal population to relatively low values in the period MIS 16 – 11. Both the Transitional and Mixed-intermediate Assemblages show relatively lower contributions prior to 650 kyr B.P., followed by a period of consistently average contributions from MIS 16 – 12. A replacement in the primary carbonate contributor from larger sand-size foraminifera to silt-size nannoplankton is indicated by the decreased sand contents, but contemporaneous high carbonate content for the period MIS 16 to 10. These changes may indicate a period of reduced or modified upwelling in the SBR between ~600 and 350 kyr B.P. The "Mid-Brunhes dissolution cycle" (Bassinot *et al.*, 1994a), is reflected in lower coarse fraction content and a reduced carbonate preservation index from MIS 15 – 13.

High pelagic carbonate production, characteristic of the "Mid-Brunhes climatic event" (Hodell, 1993), is seen in a relative increase in carbonate content for the period MIS 14-8 as well as in the elevated $\delta^{13}C_{inflata}$ values for the periods MIS 15-12 and also MIS 11 - 8. Coarse fraction contents and the carbonate preservation index indicate enhanced carbonate preservation during glacial stages MIS 12, 10 and in late stage 8. An overall increase in productivity during this period is denoted by a relative increase in TOC between MIS 15 and MIS 8.

Oxygen isotope ratios and foraminiferal data indicate that MIS 12 was one of the coldest periods in the Pleistocene record and there is an indication of increased upwelling in the SBR during this glacial stage. In contrast, stages 13, 11 and 7 are characterised by reduced upwelling and the

presence of warm stratified surface-waters over the core site. The lower organic carbon contents of glacial sediments after MIS 12 argues for a reduced supply of organic detritus to the seafloor as a result of decreased productivity. Low glacial $\delta^{15}N$ values indicate less depletion of the available nitrate pool, supporting the idea of lower glacial productivity. The foraminiferal record shows high-frequency variability for the period MIS 12 – 8. The faunal record shows a change in contribution of the Mixed-intermediate Assemblage from relatively higher values prior to MIS 12 to relatively lower values for the period MIS 12 – 8. There is an increase in relative contribution of the Transitional Assemblage from MIS 11 – 8. These observations suggest a substitution of mixed-intermediate and old upwelled water masses by offshore mesotrophic - oligotrphic waters over the core site in response to longitudinal migration of the frontal zones of the Benguela Upwelling System (BUS). The faunal population indicates that MIS 11 was the warmest stage in the period under investigation. MIS 11 is also identified as a period of high productivity and high nutrient availability by coincidentally high TOC and $\delta^{13}C_{org}$ values and low $\delta^{15}N$ values. A slight increase in the contribution of the Subantarctic Assemblage from MIS 10 to MIS 7 reflects greater influx of southern component waters into the SBR. These shifts in distributional trends may, in part, be viewed as a local response to the global oscillation of the "Mid-Brunhes climatic event" (Jansen *et al.*, 1986).

A unique episode of peak abundance of *N. pachyderma* (s) is recorded in MIS 9. This species is closely associated with strong coastal upwelling in the SBR (Giraudeau, 1993; Giraudeau and Rogers, 1994) and is the dominant species south of the Antarctic Polar Front (Niebler and Gersonde, 1998). Similar anomalous occurrences recorded in at least three other cores (Chang *et al.*, 1999; Giraudeau *et al.*, 2001; Ufkes *et al.*, 2000) indicate that this is a regional event. Thus, the data provide evidence of a period of particularly strong coastal upwelling or an equatorward migration of the polar fronts during this time. As no other data support a significant equatorward migration of the polar fronts, the most-likely explanation is enhanced upwelling of unknown forcing.

The above-mentioned change in dominant water mass over the core site between MIS 12 and 8 is reversed at the end of MIS 8 with intermediate old-upwelled waters (as indicated by the Mixed-Intermediate Assemblage) dominating over offshore waters (as indicated by the Transitional Assemblage) for the last 250 kyr. There is an indication of reduced Benguela circulation over the last 250 kyr resulting in a change in dominant primary producers from calcareous plankton to

siliceous diatoms, as a result of the upwelling of silicate-enriched waters from the Angolan undercurrent. A strong upcore trend towards higher $\delta^{15}N$ values over the last ~200 kyr denotes a change in environment or nitrate source. Eutrophic species (*N. pachyderma, N. dutertrei*, and *T. quinqueloba*) exhibit a general G-IG correlation, with increased abundances in glacial periods in this youngest portion of the core. This, together with low glacial $\delta^{15}N$ values implies generally higher nutrient levels in the glacial SBR for the last 200 kyr. However, this does not necessarily imply increased productivity during glacial periods. MIS 6 is identified as a period of high carbonate production and preservation, but low $CaCO_3$ accumulation rates signify a period of winnowing by strong bottom currents. A lower contribution of the Subantarctic Assemblage to the foraminiferal population, indicating relatively warmer surface waters, is observed after 200 kyr B.P,. Foraminiferal data from a number of cores collected in the Cape Basin (e.g. Little *et al.*, 1997a; Chen *et al.*, 2002) point to warmer surface water conditions in the Benguela System over the last 200 kyr.

The near-continuous presence of *Globorotalia menardii* throughout the core signifies uninterrupted transfer of Indian Ocean into the South Atlantic Ocean, at least over the last 850 kyr. This is a significant result in light of the ongoing discussion about the functioning of the "Cape Valve" during glacial periods.

8.4 CONCLUSIONS

8.4.1 The Agulhas Bank Slope Region

The present oceanography of the Agulhas Bank Slope region is complex, due to the interaction of numerous water masses, hydrological features and currents. The data presented in this thesis indicate that conditions were no less complex in the past. Previous inferences on the palaeomovements of the Agulhas System and the STC have generally been drawn from micropalaeontological studies carried out on sediment material from the Subantarctic Southern Ocean or from the southern border of subtropical gyres (e.g. Flores *et al.*, 1999; Howard and Prell, 1992; Prell *et al.*, 1979). These studies concluded that the palaeoceanographic history of this ocean realm is characterised by a series of uniform equatorward and poleward shifts of the belt of

hydrological fronts (STC and Antarctic Polar Front) and associated water masses, following a straightforward G-IG cyclicity. The planktonic foraminiferal and palaeoproductivity data sets obtained from core MD962080 suggest that the biotic response to surface hydrological changes near the southern tip of Africa is much more complex than supposed from these earlier studies and involves high- and low-frequency pulses outside of the well-recognised G-IG cycle timescales. Changes in surface-water masses over the Agulhas Bank Slope are due to varying influences of warm water from Agulhas rings and filaments and coldwater intrusions across the STC.

The dominance of Transitional and Subantarctic fauna indicates that the core site has lain predominantly under the influence of cool-temperate, mixed water masses. Incursions of cold subpolar waters over the core site are mostly expressed by the Subantarctic Assemblage that exhibits G-IG cyclicity over the last 250kyr. Warm water above the core site is mainly due to Agulhas rings and filaments, as well as westward movement of water across the Agulhas Bank.

Palaeoproductivity proxies reflect reduced glacial productivity, but enhanced carbonate preservation on the Agulhas Bank Slope during glacial periods. Carbonate preservation indices record strong obliquity and eccentricity signals. The data indicate that carbonate cycles are a consequence of primary production, modulated by orbitally-forced variation in wind strength at high latitudes and dissolution at the sea floor, as a consequence of variations in the chemical character of the intermediate and deep waters advected over the core sites from high latitudes, modulated by the extent of the Antarctic ice fields. Recycled production is prevalent on the Agulhas Bank. Variations in nutrient availability and productivity are driven by local circulation changes and the influx of nutrient-depleted southern waters, as a result of equatorward migrations of the southern hydrological fronts. These migrations are a response to variations in the westerly wind strength and the extent of the Antarctic ice sheets. Cross-wavelet analysis of oxygen isotope and planktonic foraminiferal assemblages suggests an early response of surface-water masses over the Agulhas Bank Slope to global climatic change.

8.4.2 The Southern Benguela Region and the Northern Benguela Region

Relationships between the upwelling intensity and spatial occurrence of the Benguela Coastal Current and G-IG cycles are complex (Oberhänsli, 1991). Faunal changes do not reflect G-IG periodicity over the last 850 kyr, implying that variations in surface-water conditions in the SBR were not strictly driven by latitudinal migrations of the southern hydrological fronts.

Although the sediments from the Olifants River Slope are organic-rich, compared to those from the Agulhas Bank Slope, they are considerably poorer in organic carbon than sediments in the NBR, indicating that upwelling in the SBR was not consistent enough to create the elevated levels of productivity seen in the NBR. Palaeoproductivity proxies indicate that changes in the trade wind-driven upwelling intensity and the advection of cold, nutrient-rich water from the south drive nutrient availability and productivity off the west coast of South Africa.

Based on previous studies on the Walvis Ridge and in the equatorial Atlantic the general expectation is that upwelling, and thus productivity, was strongest during glacial periods, particularly at the onset of glaciation (Wefer *et al.*, 1996). However, while this may be true for the NBR and the equatorial Atlantic, the SBR responded differently to global climatic change. Presently, strong upwelling episodes in this southernmost extremity of the Benguela system are the exception rather than the rule, whilst in the NBR periods of weak or no upwelling are anomalous. During cold stages, the greater share of organic carbon accumulation shifted to the NBR (Rühlemann *et al.*, 1999), in response to the latitudinal compression of the South Atlantic Anticyclone and consequent intensification of the trade wind system, resulting in increased upwelling of nutrient-rich subsurface waters off Namibia and Angola. In contrast, in the SBR, the equatorward migration of the SAA would have resulted in decreased southeasterly wind stress and a subsequent decrease in upwelling. Thus, whilst experiencing similar forcing mechanisms, the responses of the SBR to global climatic fluctuations were noticeably different from those of the NBR. The disparity observed between palaeoproductivity data from this study and previous studies undertaken in the NBR and the eastern equatorial Atlantic (Holmes, 1996; Holmes *et al.*, 1996; Kirst *et al.*, 1999; Little *et al.*, 1987a,b; Schneider *et al.*, 1994; 1995; 1996) suggest that wind-forced productivity and nutrient supply do not show similar responses along the entire coast of southwest Africa and that the BUS is not one continuous uniform system. Instead, wind forcing, production and sedimentation are much more

localized. The data presented in this thesis highlight differences between the SBR and NBR with respect to palaeoproductivity and responses to glacial-interglacial climate variability.

8.4.3 Changes related to the "Mid-Brunhes climatic event"

A shift in surface water mass dynamics between MIS 12 and 8 and again at about 250 kyr B.P. is recorded in foraminiferal, textural and nitrogen isotope data from both cores. This shift coincides with other changes observed in Southeast Atlantic sediments close to the MIS 8/7 boundary. For example, Flores *et al.* (1999) identify a warm episode (MIS 11 – 7) in the nannofossil assemblages which they interpret as reflecting the "Mid-Brunhes climatic event". Giraudeau *et al.* (2001) report a change in planktonic foraminiferal distributional trend at 250 kyr BP, with the initiation of a G-IG cyclicity in abundance variations, in ODP Site 1087 located in the southern Benguela upwelling region. In core MD962080, the abundance variations of the dominant foraminiferal species change from an ill-defined G-IG relationship prior to MIS 7, to a clear G-IG pattern thereafter, with a move to overall warmer surface-water conditions. In the SBR, there is a change in dominant surface-water masses at about 250 kyr B.P. Offshore waters dominate for the period MIS 12-8 after which intermediate and old-upwelled waters dominate over the Olifants River Slope. Both sites record a change in nitrate source or environment at about 250 kyr B.P.

8.4.4 Agulhas-Benguela interactions and the "Cape Valve"

The central problem of Late Quaternary circulation in the South Atlantic is its role in transferring heat and salt to the North Atlantic, as this affects global climate by modifying the intensity and, possibly timing, of glacial-interglacial fluctuations (Wefer *et al.*, 1999). The contribution of warm Agulhas water (as rings or filaments) to the Benguela Coastal Current is fundamental to the history of productivity off southwestern Africa. If one accepts that reseeding of *Gr. menardii* into the Atlantic Ocean is related to the functioning of the "Cape Valve", then the maximum accumulation rate of this species reflects maximum transfer of Agulhas waters around the tip of Africa. The coincident timing of the presence in the SBR of "Algoa Province" bivalve species from the south coast of South Africa (Pether, 1994) and increased counts of *Gr. menardii* reinforces the argument that this proxy is indicative of Agulhas water intrusions. As has been shown, variations in *Gr.*

menardii abundance and accumulation do appear to be affected by carbonate dissolution cycles. If, as indicated by the almost continuous record of *Gr. menardii* in both cores, Agulhas waters continued to pass into the southeast Atlantic throughout the last 850 kyr, then the argument for an earlier easterly retroflection of the Agulhas Current and the closing of the "Cape Valve" during glacial periods is obviated. This is particularly significant, since it implies that the exchange of water from the South Indian Ocean to the South Atlantic Ocean was never entirely obstructed by the STC, at least for the last 850 kyr. It is, nevertheless, conceivable that a more equatorward location of the STC could force the Agulhas Current Retroflection eastward and limit the throughflow of warmer subtropical water. Nonetheless, the data indicate that inter-ocean exchange was most effective at glacial terminations.

The dramatic difference in the number of *Gr. menardii* between the two cores and the differences in timing of maximum accumulation may imply that the source waters varied. Whilst Agulhas rings could have directly transported *Gr. menardii* to the Agulhas Bank Slope, leakage of Indian Ocean water into the SBR in glacial periods may have been of a different nature. It would have consisted of surface waters only and would not have included deep-reaching Agulhas rings. Both cores record maximum accumulation in recent times, supporting the idea of a Holocene resurgence of the Agulhas Current as suggested by Berger and Vincent (1986). The inconsistency between distributional trends of the dominant foraminiferal species and the *Gr. menardii* record suggests that this specific dynamic of Indian Ocean water inflow acted independently of changes in the nature of surface-water masses in the vicinity of the western Agulhas Bank Slope and in the SBR. However, it must be borne in mind that sampling resolution was probably too low to determine trends in the Agulhas water dispersal.

8.5 FINAL COMMENTS

Despite numerous studies showing very promising results on nutrient cycling from nitrogen isotope ratios, many uncertainties remain in deciphering the signals of this proxy. Changes in available nitrogen have been linked to changes in CO_2 partitioning between ocean and atmosphere, in that an increase in nitrate availability due to less water-column denitrification during glacials, would decrease the CO_2 in the ocean and atmosphere (Ganeshram *et al*, 1995). If nitrate concentration

changed in this manner, the $\delta^{15}N$ of the glacial ocean should have been lowered (Wefer *et al.*, 1999). Whilst the data presented in Chapter 6 show that glacial $\delta^{15}N$ values are indeed lower, the causes of the isotopic fluctuations are not obviously linked to CO_2 fluctuations. An important aspect regarding the use of $\delta^{15}N$ in palaeoceanography is the assumption that the $\delta^{15}N$ of the oceans has remained constant over time. Perhaps the predominantly low $\delta^{15}N$ values and the shift in mean $\delta^{15}N$ observed in both cores are related to an evolutionary signal.

Peak abundances of *Gr. menardii* occurring at glacial terminations are observed in both cores, indicating increased transfer of Indian Ocean water, via the Agulhas Current, into the SBR at these times. This hypothesis is supported by the occurrence of peak abundances of *N. dutertrei*, a species thriving in the Agulhas Current (Lowry, 1987), at glacial terminations in core MD 962080, as well as increased abundance of *Gs. ruber* at G-IG transitions in core MD962084. This exercise may have been useful in that it determined that transfer of warm saline water into the South Atlantic was not entirely cut-off during glacial periods, although the amount may have been substantially decreased. However, sampling resolution was too low to identify any periodicity in this transfer.

A number of the conclusions reached in this study contrast with results and trends seen in previous palaeoceanographic studies of the NBR, the equatorial Atlantic, and the Southern Ocean (e.g. Holmes *et al.*, 1997, 1999; Howard and Prell, 1994; Schneider *et al.*, 1994, 1996), where data point to increased glacial productivity and depletion of the nitrate pool and enhanced carbonate dissolution during glacial periods. The data presented here show that the Agulhas Bank Slope and Southern Benguela are discrete regions with unique characteristics and individual responses to global climatic forcing. Dominant periodicities recorded in the sediments off northern Namibia and Angola are only initiated in the last 300-400 kyr. The longer data sets presented in this thesis highlight the dependence of spectral analysis on the length of the record and the particular period of time investigated. Continuous wavelet transforms provide an alternative method of frequency detection and appear to be particularly well suited to analysis of palaeoclimate records. However, my nascent understanding of this promising technique prevented full exploitation of the data.

The data presented in this thesis reflect the complexity of the hydrographic conditions in the vicinity of the Agulhas Bank and in the SBR. The varying nature of the surface-water conditions are presumably associated with delivery of different water masses into the Southeast Atlantic via the

Agulhas Current and the functioning of the "Cape Valve". There is a lot more to be learned about the oceanographic processes occurring at the southern tip of Africa, both at present and in the past. Hopefully, this work provides a starting point for future detailed research in this multifaceted ocean realm.

REFERENCES

Altabet, M.A., 1988. Variations in nitrogen isotopic composition between sinking and suspended particles: Implications for nitrogen cycling and particle transformation in the open ocean. *Deep Sea Research,* 35: 535-554.

Altabet, M.A. and Francois, R., 1994. Sedimentary nitrogen isotopic ratios as a recorder for surface ocean nitrate utilization. *Global Biogeochemical Cycles,* 8: 103-116.

Altabet, M.A. and McCarthy, J.J., 1985. Temporal and spatial variations in the natural abundance of ^{15}N in POM from a warm-core ring. *Deep Sea Research,* 32: 755-772.

Altabet, M.A., Deusser, W.G., Honjo, S. and Stienen, C., 1991. Seasonal and depth-related changes in the source of sinking particles in the North Atlantic detected by $^{15}N/^{14}N$ ratios. *Nature,* 354: 136-139.

Altabet, M.A., Murray, D.W. and Prell, W.L., 1999. Climatically linked oscillations in Arabian Sea denitrification over the past 1 m.y.: Implications for the marine N cycle. *Paleoceanography,* 14(6): 732-743.

Armand, L.K., 2000. An ocean of ice - advances in the estimation of past sea ice in the Southern Ocean. *GSA Today,* 10(3): 1-7.

Arrhenius, G.O.S., 1952. Sediment cores from the East Pacific. *Reports of the Swedish Deep Sea Expedition, 1947-1948,* 5: 1-202.

Bailey, G.W., 1991. Organic carbon flux and the development of oxygen deficiency on the modern Benguela continental shelf south of 22°S: Spatial and temporal variability. In: Tyson, R.V and Pearson, T.H. (Eds). *Modern and Ancient Continental Shelf Anoxia,Geological Society of London, Special Publication,* 58:171-183.

Bailey, G.W. and Chapman, P., 1991. Chemical and physical oceanography. In: Short-term variability during an anchor station study in the Southern Benguela Upwelling System. *Progress in Oceanography,* 28: 9-37.

Bandy, O.L., 1972. Origin and development of *Globorotalia (Turborotalia) pachyderma* (Ehrenberg). *Micropaleontology,* 18(3): 294-318.

Bassinot, F.C., Beaufort, L., Vincent, E., Labeyrie, L.D, Rostek, F., Müller, P.J., Quidelleur X. and Lancelot, Y., 1994a. Coarse fraction fluctuations in pelagic carbonate sediments from the tropical Indian Ocean: A 1500-kyr record of carbonate dissolution. *Paleoceanography,* 9(4): 579-600.

Bassinot, F.C., Labeyrie, L.D., Vincent, E., Quideleur, X., Shackleton, N.J. and Lancelot, Y., 1994b. The astronomical theory of climate and the age of the Brunhes-Matuyama magnetic reversal. *Earth and Planetary Science Letters,* 126: 91-108.

Bé, A.W.H., 1967. Foraminiferal families: *Globigerinidea* and *Globorotalidae*. In: Fraser, J.H. (Ed.). *Fiches d'Identification du Zooplankton. Cons. Permanent Int. Explor. Mar. Charlottenlund, Denmark,* Sheet 108, pp. 1-8.

Bé, A.W. H. and Duplessy, J.C., 1976. Subtropical Convergence fluctuations and Quaternary climates in the middle latitudes of the Indian Ocean. *Science* 194: 419-422.

Bé, A.W.H. and Hamlin, O.G., 1967. Ecology of Recent planktonic foraminifera; - Part 3- distribution in the north Atlantic during the summer of 1962. *Micropalaeontology,* 13(1): 87-106.

Bé, A.W.H. and Hutson, W.H., 1977. Ecology of planktonic foraminifera and biogeographic patterns of life and fossil assemblages in the Indian Ocean. *Micropaleontology,* 23(4): 369-414.

Bé, A.W.H. and Tolderlund, D.S., 1971. Distribution and ecology of living planktonic foraminifera in surface waters if the Atlantic and Indian Oceans. In: Funnel, B.M. and Riedel, W.R. (Eds). *The Micropalaeontology of the Oceans.* Cambridge University Press, pp. 105-149.

Bentaleb, I., Fontugne, M., Descolas-Gros, C., Girardin, C., Mariotti, A., Pierre, C., Brunet, C. and Poisson, A., 1996. Organic carbon isotopic composition of phytoplankton and sea-surface pCO_2 reconstructions in the Southern Indian Ocean during the last 50, 000 yr. *Organic Geochemistry,* 24(4): 399-411.

Berger, W.H., 1967. Foraminiferal ooze: Solution at depths. *Science,* 156: 383-385.

Berger, W.H., 1973. Deep-sea carbonates: Pleistocene dissolution cycles. *Journal of Foraminiferal Research,* 3: 187-195.

Berger, W.H., 1977. Deep-sea carbonate and the late deglaciation preservation spike in pteropods and foraminifera. *Nature,* 269: 301-304.

Berger, W.H. and Vincent, E. 1986. Sporadic shutdown of North Atlantic deep water production during the Glacial-Holocene transition? *Nature,* 324: 53-55.

Berger, W.H. and Wefer, G., 1990. Export production: Seasonality and intermittency and paleoceanographic implications. *Palaeogeography, Palaeoclimatology, Palaeoecology,* 89: 245-254.

Berger, W.H.and Wefer, G.,1996. Expeditions into the past: Paleoceanographic studies in the South Atlantic. In: Wefer, G., Berger, W.H., Siedler, G. and Webb, D.J. (Eds). *The South Atlantic: Past and Present Circulation.* Springer-Verlag, Berlin, pp. 363-410.

Berger, W.H., Bonneau, M.C. and Parker, F.L., 1982. Foraminifera on the deep-sea floor: lysocline and dissolution rate. *Oceanologica Acta,* 5: 249-258.

Berger, W.H., Burke, S. and Vincent, E., 1987. Glacial-Holocene transition: Climate pulsations and sporadic shutdown of NADW production. In: Berger, W.H. and Labeyrie, L.D. (Eds). *Abrupt Climatic Change.* D Reidl, Dordrecht, pp 279-297.

Berger, W.H., Lange, C.B. and Wefer, G., 2001. Upwelling history of the Benguela-Namibia system: A sysnthesis of Leg 175 results. In: Wefer, G., berger, and Richter, C. (Eds). *Proceedings of the Ocean Drilling Program, Scientific Results*, 175: 1-103.

Bertrand, P., Balut, Y., Schneider, R., Chen, M-.T., Rogers, J. and shipboard participants., 1997. Scientific report of the NAUSICAA-IMAGES coring cruise: La Réunion October 20, 1996 - La Réunion November 25, 1996 aboard the S./V. *Marion Dufresne. Report l'Institut Francais pour la Recherche et la Technologie Polaires*, 97-1, pp. 1-381.

Bickert, T. and Wefer, G., 1996. Late Quaternary deep water circulation in the South Atlantic: Reconstruction from carbonate dissolution and benthic stable isotopes. In: Wefer, G., Berger, W.H., Siedler, G. and Webb, D.J. (Eds), *The South Atlantic: Past and Present Circulation.* Springer-Verlag, Berlin, pp. 599-620.

Biggs, D.C., Berkowitz, S.P., Altabet, M.A., Bidigare, R.R., DeMaster, D.J., Macko, S.A., Ondrusek, M.E. and Noh, I.L., 1989. A cooperative study of the upper ocean particulate fluxes. In: Barron, J., Anderson, J. Baldauf, J.G. and Larsen, B. (Eds). *Proceedings of the Ocean Drilling Program. Initial Reports,* 119: 109-120.

Birch, G.F. and Rogers, J., 1973. Nature of the sea floor between Lüderitz and Port Elizabeth. *South African Shipping News, Fishing Industry Review,* 28: 56-65.

Birch, G.F., Rogers, J., Bremner, J.M. and Moir, G.J., 1976. *Proceedings of the First Interdisciplinary Conference, Marine and Freshwater Research, South Africa,* Fische 20A, C1-D12.

Birch, G.F., Rogers, J. and Bremner, J.M., 1986. Texture and composition of surficial sediments on the continental margin of the Republics of South Africa, Transkei and Ciskei. Map *Geological Survey of South Africa, Marine Geoscience Unit, Series 3*, Sheets 1-4.

Blunier, T., Stocker, T.F., Chappellaz, J. and Raynaud, D., 1998. Phase lag of Antarctic and Greenland temperature in the last glacial and links between CO2 variations and Heinrich Events. *Abstracts, 6th International Conference on Paleoceanography*, Lisbon, Portugal. pp 22.

Bolton, E.W., Maasch, K.A. and Lilly, J.M., 1995. A wavelet analysis of Plio-Pleistocene climate indicators: A new view of periodicity evolution. *Geophysical Research Letters,* 22(20): 2753-2756.

Boyle, E.A. and Keigwin, L.D., 1982. Deep circulation of the North Atlantic over the last 200,000 years: Geochemical evidence. *Science,* 218: 784-787.

Bradshaw, J.S., 1959. Ecology of living planktonic foraminifera in the North and Equatorial Pacific Ocean. *Cushman Foundation Foraminiferal Research Contributions,* 10(2) : 25-64.

Bremner, J.M., 1981a. Shelf morphology and surficial sediment off central and northern South West Africa (Namibia). *Geo-Marine Letters*, 1: 91-96.

Bremner, J.M., 1981b. Sediments on the continental margin off South West Africa between latitudes 17° and 25°S. *Bulletin of the Joint Geological Survey/University of Cape Town Marine Geoscience Unit*, 10:1-233.

Bremner, J.M., Rogers, J. and Birch, G.F., 1986. Surficial sediments of the continental margin of South West Africa/Namibia. *Map Geological Survey of South West Africa (Namibia), Marine Geoscience Series*, 16 maps on 4 sheets.

Broecker, W.S., 1987. The Biggest Chill. In: White, J.C. (Ed). *Global Climate Change Linkages; Acid Rain, Air Quality, and Stratospheric Ozone*. Elsevier, New York, pp.13-22.

Broecker, W.S., 1991. The great ocean conveyor, *Oceanus*, 4: 79-89.

Broecker, W.S. and Denton,G.H., 1990. What drives glacial cycles? *Scientific American*, January 1990: 43-50.

Broecker, W.S., Peteet, D.M. and Rind, D., 1985. Does the ocean-atmosphere system have more than one stable mode of operation? *Nature*, 315: 21-25.

Burckle, L.H. and Clarke, D., 1976. Oceanographic conditions around Antarctica during the last glacial maximum. *EOS Transactions of the American Geophysical Union*, 57(4):258.

Burckle, L.H., Gayley-Robert, I., Ram, M. and Petet, J-R., 1988. Diatoms in Antarctic ice cores: some implications for the glacial history of Antarctica. *Geology* 16: 326-329.

Chang, Y.-P., Chang, C.-C., Wang, L.-W., Chen, M.-T., Wang, C-H. and Yu, E.-F., 1999. Planktonic foraminiferal sea surface temperature variations in the southeast Atlantic Ocean : A high-resolution record of MD962085 of thepast 400,000 years from IMAGES II-NAUSICAA Cruise. *Terrestrial-Atmosphere-Ocean Sciences*, 10 : 185-200.

Chapman, P. and Shannon, L.V., 1985. The Benguela Ecosystem. Part II. Chemistry and related processes. In: Barnes, M. (Ed.). *Oceanography and Marine Biology Annual Review*, 23:183-251.

Chappell, J. and Shackleton, N.J., 1986. Oxygen isotopes and sea level. *Nature*, 324: 137-140

Charles, C.D. and Fairbanks, R.G., 1990. Glacial to interglacial changes in isotopic gradients of Southern Ocean surface water. In: Bliel, U. and Thiede, J. (Eds.) *Geological History of the Polar Oceans: Arctic versus Antarctic*. Kluwer Academic, Dordrecht, pp. 519-538.

Charles, C.D. and Morely, J.J., 1988. The paleoceanographic significance of the radiolarian *Didyocyrtis tetrathalamus* in the eastern Cape Basin sediments. *Palaeogeography, Palaeoclimatology, Palaeoecology*, 66: 113-126.

Chen, M-.T, Bertrand, P., Balut, Y., Schneider, R, Rogers, J. and Taiwan IMAGES participants, 1998. IMAGES II Cruise (NAUSICAA) explores Quaternary climatic variability and linkage of Benguela and Agulhas Current Systems in the Southern Indian-Atlantic Ocean: Participation by consortium of Taiwan institutions (coordinated by National Taiwan University). *Journal of the Geological Society of China*, 41: 73-79.

Chen, M.-T., Chang, Y.-P., Chang, C.-C., Wang, L.-W., Wang, C.-H. and Yu, E.-F., 2002. Late Quaternary sea-surface temperature variations in the southeast Atlantic: a planktonic foraminifer faunal record of the past 600 000 yr (IMAGES II MD962085). *Marine Geology*, 180:163-182.

Christensen, B.A. and Giraudeau, J., 2002. Neogene and Quaternary evolution of the Benguela upwelling system. *Marine Geology* 180: 1-2.

Christensen, B.A., Kalbas, J.L., Maslin, M. and Murray, R.W., 2002. Paleoclimatic changes in southern Africa during the intensification of Northern Hemisphere glaciation: evidence from ODP Leg 175 Site 1085. *Marine Geology,* 180: 117-131.

Christison, I.D., 1985. *Foraminifera from the Continental Shelf of S.W. Africa.* MSc. Thesis, University College of Wales, Aberystwyth, 174pp.

Coplen, T.B., 1988. Normalisation of oxygen and hydrogen isotope data. *Chemical Geology,* 72: 293-297.

Crowley, T.J., 1983. Depth –dependent carbonate dissolution changes in the eastern North Atlantic during the last 170,000 years. *Marine Geology,* 54: 25-31.

Curry, W.B. and Crowley, T.J., 1987. The $\delta^{13}C$ of Equatorial Atlantic surface waters: Implications for Ice Age pCO_2 levels. *Paleoceanography,* 2: 489-517.

Dean, W.E., Arthur, M.A. and Claypool, G.E., 1986. Depletion of ^{13}C in Cretaceous marine organic matter: source, diagenetic or environmental signal. *Marine Geology,* 70: 119-157.

De Decker, A.H.B., 1970. Notes on an oxygen-depleted subsurface current off the west coast of South Africa. *Investl. Report Division of Sea Fisheries South Africa,* 84: 1-24.

De Decker, R.H., 1988. The wave regime on the inner shelf south of the Orange River and its implications for sediment transport. *South African Journal of Geology,* 91: 358-371.

De Ruijter, W., 1982. Asymptotic analysis of the Agulhas and Brazil Current systems. *Journal of Physical Oceanography,* 12: 361-373.

De Ruijter, W. P. M., Biastoch, A., Drijfhout, S. S., Lutjeharms, J. R. E., Matano, R. P., Pichevin,T., van Leeuwen, P. J. and Weijer, W., 1999. Indian-Atlantic inter-ocean exchange: dynamics, estimation and impact. *Journal of Geophysical Research* 104: 885-911.

Descolas-Gros, C. and Fontugne, M.R., 1985. Carbon fixationin marine phytoplankton: carboxylase activities and stable carbon isotope ratios: physiological and paleoclimatological aspects. *Marine Biology,* 87: 1-6.

Descolos-Gros, C. and Fontugne, M.R., 1990. Stable carbon isotope fractionation by marine phytoplankton during photosynthesis. *Plant, Cell and Environment,* 13: 207-218.

Diester-Haass, L., 1985. Late Quaternary sedimentation on the eastern Walvis Ridge, SE Atlantic (HPC 532 and 4 piston cores). *Marine Geology,* 65: 145-189.

Diester-Haass, L., Meyers, P.A. and Rothe, P., 1990. Miocene history of the Benguela Current and Antarctic ice volumes: Evidence from rhythmic sedimentation and current growth across the Wavis Ridge (Deep Sea Drilling Project Sites 362 and 532). *Paleoceanography,* 5(5): 685-707.

Dingle, R.V., 1973a. The geology of the continental shelf between Lüderitz and Cape Town (southwest Africa), with special reference to Tertiary strata. *Journal of the Geological Society of London*, 129: 337-363.

Dingle, R.V., 1973b. Regional distribution and thickness of post-Palaeozoic sediments on the continental margin of southern Africa. *Geoogical Magazine*, 110 (2): 97-102.

Dingle, R.V. and Hendey, Q.B., 1984. Late Mesozoic and Tertiary sediment supply to the eastern Cape Basin (SE Atlantic) and palaeo-drainage systems in southwestern Africa. *Marine Geology*, 56: 13-26.

Dingle, R.V. and Rogers, J. 1972. Pleistocene palaeogeography of the Agulhas Bank. *Transactions Royal Society of South Africa*, 40: 155-165.

Dingle, R.V., Siesser, W.G. and Newton, A.R., 1983. *Mesozoic and Tertiary Geology of Southern Africa*. Balkema, Rotterdam, 375pp.

Dingle, R.V., Birch, G.F., Bremner, J.M., De Decker, R.H., Du Plessis, A., Engelbrecht, J.C., Fincham, M.J., Fitton, T., Flemming, B.W., Gentle, R.I., Goodlad, S.W., Martin, A.K., Mills, E.G., Moir, G.J., Parker, R.J., Robson, S.H., Rogers, J., Salmon, D.A., Siesser, W.G., Simpson, E.S.W., Summerhayes, C.P., Westall, F., Winter, A. and Woodborne, M.W., 1987. Deep-sea sedimentary environments around southern Africa (south-east Atlantic and south-west Indian Oceans). *Annals of the South African Museum*, 98: 1-27 (+ 2 separate maps).

Döös, K., Artale, V., Blanke, B., Coward, A.C, Drijfhout, S., Killworth, P., Marsh, R., Marullo, S., Rupolo, V., Santoleri, R., Lee, M.-M. and Speich, S., 2002. http://www.misu.su.se/~doos/poster_tracmass.pdf

Droxler, A.W., Schlager, W., Whallon, C.C., 1983. Quaternary aragonite cycles and oxygen isotope records in Bahamian carbonate ooze. *Geology*, 11: 235-239.

Emiliani C., 1955. Pleistocene temperatures. *Journal of Geology*, 63: 538-578.

Eppley, R.W. and Peterson, B.J., 1979. Particulate matter flux and planktonic new production. *Nature*, 282: 677-680.

Ericson, D.B. and Wollin, G., 1968. Pleistocene climates and chronology in deep-sea sediments. *Science*, 162(3859): 1227-1234.

Esper, O., Zonneveld, K.A.F., Höll, C., Karwath, B., Kuhlmann, H., Schneider, R.R., Vink, A., Weise-Ihlo, I. and Willems, H., 2000. Reconstruction of palaeoceanographic conditions in the South Atlantic Ocean at the last two Terminations based on calcareous dinoflagellate cysts. *International Journal of Earth Sciences*, 88: 68-693.

Farrell, J.W. and Prell, W.L., 1989. Climate change and $CaCO_3$ preservation: an 800,000 year bathymetric reconstruction from the central equatorial Pacific Ocean. *Paleoceanography*, 4: 447-466.

Fischer, G., 1991. Stable carbon isotope ratios of plankton carbon and sinking organic matter from the Atlantic sector of the Southern Ocean. *Marine Chemistry*, 35: 581-596.

Flores, J.A., Gersonde, R. and Sierro, F.J., 1999. Pleistocene fluctuations in the Agulhas Current Retroflection based on the calcareous plankton record. *Marine Micropaleontology*, 37: 1-22.

Fontugne, M.R. and Duplessy, J.C, 1978. Carbon isotope ratio of marine plankton related to water masses. *Earth Planetary Science Letters*, 41: 365-371.

Fontugne, M.R. and Duplessy, J.C., 1981. Organic carbon fractionation by marine plankton in the temperature range –1 to 31°C. *Oceanologica Acta*, 4: 85-90.

Fontugne, M.R. and Duplessy, J.C, 1986. Variations of the monsoon regime during the Upper Quaternary: Evidence from the carbon isotopic record of organic matter in North Indian Ocean sediment cores. *Palaeogeography, Palaeoclimatology, Palaeoecology*, 56: 69-88.

Francois, R., Altabet, M.A. and Burckle, L.D., 1992. Glacial to interglacial changes in surface nitrate utilization in the Indian sector of the Southern Ocean as recorded by sediment $\delta^{15}N$. *Paleoceanography*, 7: 589-606.

Francois, R., Altabet, M.A., Goericke, R., McCorkle, D.C, Brunet, C. and Poisson, A., 1993a. Changes in the $\delta^{13}C$ surface water particulate organic matter across the Subtropical Convergence in the S.W. Indian Ocean. *Global Biogeochemical Cycle*, 7: 627-644.

Francois, R., Bacon, M., Altabet, M.A and Labeyrie, L.D., 1993b. Glacial/interglacial changes in sediment rain rate in the SW Indian sector of Subantarctic waters as recorded by ^{230}Th, ^{231}Pa, U, and $\delta^{15}N$. *Paleoceanography*, 8(5): 611-629.

Francois, R., Altabet, M.A., Yu, E.F., Sigman, D.M. Bacon, M.P., Frank, M., Bohrmann, G., Bareille, G. and Labeyrie, L., 1997. Contribution of Southern Ocean surface-water stratification to low atmospheric CO_2 concentrations during the last glacial period. *Nature*, 389: 929-935.

Freeman, K.H., 2001. Isotopic biogeochemistry of marine organic carbon. In: Valley, J.W. and Cole, D.R. (Eds). *Stable Isotope Geochemistry. Reviews in Mineralogy and Geochemistry*, 43: 579-607

Fry, B., 1988. Food web structure on Georges Bank from stable C, N and S isotopic compositions. *Limnology and Oceanography*, 33: 1182-1190. (Cited in Holmes *et al.*, 1999).

Ganeshram, R.S., Pedersen, T.F., Calvert, S.E. and Murray, J.W., 1995. Large changes in oceanic nutrient inventories from glacial to interglacial periods. *Nature*, 376: 755-757

Ganeshram, R.S., Pedersen, T.F., Calvert, S.E., McNiell, W. and Fontugne, M.R., 2000. Glacial-interglacial variability in denitrification in the world's oceans: Causes and consequences. *Paleoceanography*, 15(4): 361-376.

Gasse, F., 2000. Hydrological changes in the African tropics since the Last Glacial Maximum. *Quaternary Science Reviews*, 19: 189 – 211.

Gilchrist, A.R. and Summerfield, M.A., 1990. Differential denudation and flexural isostasy in formation of rifted-margin upwarps. *Nature*, 346: 739-742.

Giraudeau, J., 1993. Planktonic foraminiferal assemblages in surface sediments from the southwest African continental margin. *Marine Geology,* 110: 47-62.

Giraudeau, J. and Rogers, J., 1994. Phytoplankton biomass and sea-surface temperature estimates from sea-bed distribution of nannofossils and planktonic foraminifera in the Benguela Upwelling System. *Micropaleontology,* 40 (3): 275-285.

Giraudeau, J., Pierre, C. and Herve, L., 2001. A late Quaternary, high-resolution record of planktonic foraminiferal species distribution in the southern Benguela region: Site 1087. In: Wefer, G., Berger, W.H., and Richter, C. (Eds.), *Proceedings of the Ocean Drilling Program, Scientific Results,* 175: 1-16.

Goericke, R., 1994. Variations of marine plankton $\delta^{13}C$ with latitude, temperature and dissolved CO_2 in the world ocean. *Global Biogeochemistry Cycle,* 8: 85-90.

Gordon, A.L., 1985. Indian-Atlantic transfer of thermocline water at the Agulhas retroflection. *Science,* 227: 1030-1033.

Gordon, A. L., 1986. Inter-ocean exchange of thermocline water. *Journal of Geophysical Research,* 91: 5037-5046.

Gordon, A.L. and Haxby, W.F., 1990. Agulhas eddies invade the South Atlantic: Evidence from Geosat altimeter and shipboard conductivity-temperature-depth survey. *Journal of Geophysical Research,* 95(C3): 3117-3125.

Gordon, A.L., Weiss, R.F., Smethie, W.M. Jr, and Warner, M.J., 1992. Thermocline and intermediate water communication between the South Atlantic and Indian Oceans. *Journal of Geophysical Research,* 97(C5): 7223-7240.

Gorgas, T.J. and Wilkens, R.H., 2002. Sedimentation rates off SW Africa since the late Miocene deciphered from spectral analyses of borehole and GRA bulk density profiles : ODP Sites 1081-1084. *Marine Geology,* 180 : 29-48.

Gupta, A.K., Dhingra, H., Mélice, J.-L. and Anderson, D.M., 2001. Earth's eccentricity cycles and Indian summer monsoon variability over the past 2 million years: Evidence from deep-sea foraminifera. *Geophysical Research Letters,* 28(21): 4131-4134.

Hagelberg, T.K., Bond, M. and de Menocal, P., 1994. Milankovitch band forcing of sub Milankovitch climate variability during the Pleistocene. *Paleoceanography,* 9: 545-558.

Hansson, S., Hobbie, J.E., Elmgren, R., Larsson, U., Fry, B. and Johansson, S., 1997. The stable nitrogen isotope ratio as amarker of food-web interactions and fish migration. *Ecology,* 78: 2249-2257.

Hays, J.D, Imbrie, J. and Shackleton N.J., 1976. Variations in the Earth's orbit: pacemaker of the ice ages. *Science,* 194: 1121-1132.

Herbert, R.S., 1986. Late Holocene Climate Change: The Little Ice Age and El Niño from Planktonic Foraminifera in Sediments off Walvis Bay, South West Africa. *Bulletin of the Joint Geological Survey/University of Cape Town Marine Geoscience Unit,* 18: 1-45.

Hilbrecht, H., 1996. Extant planktic foraminifera and the physical environment in the Atlantic and Indian Oceans. *Mitteilungen aus dem Geologischen Institut der Eidgenössische Technischen Hochschule und der Universität Zürich, Neue Folge,* 300:1- 99

Hodell, D.A., 1993. Late Pleistocene paleoceanography of the South Atlantic Sector of the Southern Ocean: Ocean Drilling Programme Hole 704A. *Paleoceanography,* 8(1): 47-67.

Hodell, D.A., Charles, C.D., Ninnemann, U.S., 2000. Comparison of interglacial stages in the South Atlantic sector of the southern ocean for the past 450 kyr: Implications for Marine Isotope Stage (MIS) 11. *Global and Planetary Change,* 24: 7-26.

Holmes, M.E., 1996. Reconstruction of surface ocean nitrate utilization in the southeast Atlantic Ocean based on stable nitrogen isotopes. *Berichte, Fachbereich Geowissenschaften, Universität Bremen,* 83: 1-113.

Holmes, M.E., Eichner, C., Struck and Wefer, G., 1999. Reconstruction of surface ocean nitrate utilization using stable nitrogen isotopes in sinking particles and sediments. In: Fischer, G. and Wefer, G. (Eds). *Use of Proxies in Paleoceanography: Examples from the South Atlantic*. Springer-Verlag, Berlin, pp. 447-468.

Holmes, M.E., Müller, P.J., Schneider, R.R., Segl, M., Pätzold, J. and Wefer, G., 1996. Stable nitrogen isotopes in Angola Basin surface sediments. *Marine Geology,* 134: 1-12.

Holmes, M.E., Müller, P.J., Schneider, R.R., Segl, M. and Wefer, G., 1997. Reconstruction of past nutrient utilization in the eastern Angola Basin based on sedimentary $^{15}N/^{14}N$ ratios. *Paleoceanography,* 12: 604-614.

Holmes, M.E., Müller, P.J., Schneider, R.R., Segl, M. and Wefer,, 1998. Spatial variations in euphotic zone nitrate utilization based on $\delta^{15}N$ in surface sediments. *Geo-Marine Letters,* 18: 58-65.

Howard, W.R. and Prell, W.L., 1992. Late quaternary surface circulation of the Southern Indian Ocean and its relationship to orbital variations. *Paleoceanography,* 7 (1): 79-117.

Howard, W.R. and Prell, W.L., 1994. Late Quaternary $CaCO_3$ production and preservation in the Southern Ocean: Implications for oceanic and atmospheric carbon recycling. *Paleoceanography,* 9 (3): 453-482.

Hut, G., 1987. Stable isotope reference samples for geochemical and hydrological investigations. Report to the Director General. International Atomic Energy Agency, Vienna.

Hutchings, L., Pillar, S.C. and Verheye, H.M., 1991. Estimate of standing stock, production and consumption of meso- and macrozooplankton in the Benguela ecosystem. *South African Journal of Marine Science,* 11: 499-512.

Hutson, W.H., 1980. The Agulhas Current during the Late Pleistocene: Analysis of modern faunal analogs. *Science,* 207: 64-66.

IMAGES Homepage. http://www.images.pclab.ifg.uni-kiel.de

Imbrie, J. and Kipp, N., 1971. A new micropaleontological method for quantitative paleoclimatology: application to a Late Pleistocene Carribean core. In: Turekian, K.K. (Ed.), *Late Cenozoic Glacial Ages.* Yale University Press, New Haven, pp. 71-181.

Imbrie, J., Boyle, E. A., Clemens, S.C., Duffy, A., Howard, W.R., Kukla, G., Kutzbach, J., Martinson, D.G., McIntyre, A., Mix, A.C., Molfino, B., Morley, J.J., Peterson, L.C., Pisias, N.G., Prell, W.L., Raymo, M.E., Shackleton, N.J. and Toggweiler, J.R., 1992. On the structure and origin of major glaciation cycles. 1. Linear responses to Milankovitch forcing. *Paleoceanography,* 7(6): 701-738.

Imbrie, J., Berger, A., Boyle, E. A., Clemens, S.C., Duffy, A., Howard, W.R., Kukla, G., Kutzbach, J., Martinson, D.G., McIntyre, A., Mix, A.C., Molfino, B., Morley, J.J., Peterson, L.C., Pisias, N.G., Prell, W.L., Raymo, M.E., Shackleton, N.J. and Toggweiler, J.R., 1993. On the Structure and Origin of major Glaciation Cycles. 2. The 100,000-year cycle. *Paleoceanography,* 8(6): 699-735.

Imbrie, J., Hays, J.D., Martinson, D.G., McIntyre, A., Mix, A.C., Morely, J.J., Pisias, N.G., Prell, W.L. and Shackleton N.J., 1984. The orbital theory of Pleistocene climate: support for a revised chronology of the marine $\delta^{18}O$ record. In: Berger, A., Imbrie, J., Hays, J., Kukla, G. and Saltzman, B. (Eds), *Milankovitch and Climate, Part I,* Reidel, Dordrecht, pp. 269-305.

Jansen, J.H.F., Kuijpers, A. and Troelstra, S.R., 1986. A Mid-Brunhes climatic event: Long term changes in global atmosphere and ocean circulation. *Science,* 232: 619-622.

Jansen, J.H.F., Ufkes, E. and Schneider, R.R., 1996. Late Quaternary movements of the Angola Benguela Front, SE Atlantic, and Implications for advection in the Equatorial Ocean. In: Wefer, G., Berger, W.H., Siedler, G. and Webb, D.J. (Eds). *The South Atlantic: Past and Present Circulation.* Springer-Verlag Berlin, pp. 363-410.

Jansen, J.H.F. and van Haren, J.J.M., 2001. Milankovitch and 15-Ka shifts of the oceanic circumpolar front systems. *Abstracts 7th International Conference on Paleoceanography,* Sapporo, Japan. pp 126.

Jones, J.I., 1964. Significance of distribution of planktonic foraminifera in the equatorial undercurrent. *Micropaleontology,* 13: 489-501.

Jury, M.R., 1992. A review of the meteorology of the eastern Agulhas Bank. *South African Journal of Science,* 90: 109-113.

Jury, M.R., Kamstra, F. and Taunton-Clark, J., 1985. Diurnal wind cycles and upwelling off the southern portion of the Cape Peninsula in summer. *South African Journal of Marine Science,* 3: 1-10.

Kennett, J.P. and Srinivasan, M.S., 1983. *Neogene Planktonic Foraminifera. A Phylogenetic Atlas.* Hutchinson Ross Publishing, Stroudsburg, Pennsylvania, USA, 265pp.

Keswani, S.R., Dunham, K.W. and Meyers, P.A., 1984. Organic geochemistry of late Cenozoic sediments from the subtropical South Atlantic Ocean. *Marine Geology,* 61: 25-42.

Kirst, G.J., Schneider, R.R., Müller, P.J., von Storch, I. and Wefer, G., 1999. Late Quaternary Temperature Variability in the Benguela Current System Derived from Alkenones. *Quaternary Research,* 52: 92-103.

Labeyrie, L and Duplessy, J.C., 1985. Changes in oceanic $^{13}C/^{12}C$ ratio during the last 140,000 years: High latitude surface water records. *Palaeogeography, Palaeoclimatology, Palaeoecology*, 50: 217-240.

Lange, C., Berger, W.H., Lin, H.-L., and Shipboard Scientific Party, 1999. The Early Matuyama diatom maximum off SW Africa, Benguela Current System (ODP Leg 175). *Marine Geology* 161: 93-114.

Lau, K.-M. and Weng, H., 1995. Climate signal detection using Wavelet Transform: How to make a time series sing. *Bulletin of the American Meterological Society,* 76(12): 2391-2402.

Le, J. and Shackleton, N.J., 1992. Carbonate dissolution fluctuations in the western equatorial Pacific during the Late Quaternary. *Paleoceanography,* 7: 21-42.

Little, M.G., Schneider, R.R., Kroon, D., Price, B., Bickert, T. and Wefer, G., 1997a. Rapid palaeoceanographical changes in the Benguela Upwelling System for the last 160 000 years as indicated by abundances of planktonic foraminifera. *Palaeogeography, Palaeoclimatology, Palaeoecology*, 130: 135-161.

Little, M.G., Schneider, R.R., Kroon, D., Price, B., Summerhayes, C.P. and Segl, M., 1997b. Trade wind forcing of upwelling as a response to sub-Milankovitch climate variability. *Paleoceanography,* 12(4): 568-576.

Liu, K.-K. and Kaplan, I.R., 1989. The eastern tropical pacific as a source of ^{15}N-enriched nitrate in seawater off southern California. *Limnology Oceanography,* 34: 820-830.

Lowry, F.M.D., 1987. *Foraminiferal Thanatocoenoses from the Continental Shelf of Southern Africa.* Unpublished Ph.D. Thesis, Department of Geological Sciences, University College, London, 443pp.

Lutjeharms, J. R. E., 1985. Location of frontal systems between Africa and Antarctica: some preliminary results. *Deep-Sea Research,* 32: 1499-1509.

Lutjeharms, J.R.E., 1996. The exchange of water between the South Indian and South Atlantic Oceans. In: Wefer, G., Berger, W.H., Siedler, G. and Webb, D.J. (Eds). *The South Atlantic: Past and Present Circulation.* Springer-Verlag Berlin, pp. 363-410.

Lutjeharms, J. R. E. and Cooper, J., 1996. Interbasin leakage through Agulhas Current filaments. *Deep-Sea Research,* 43: 213-238.

Lutjeharms, J. R. E. and de Ruijter, W. P. M., 1996. The influence of the Agulhas Current on the adjacent coastal ocean: possible impacts of climate change. *Journal of Marine Systems,* 7: 321-336.

Lutjeharms, J.R.E. and Meeuwis, J.M., 1987. The extent and variability of South –East Atlantic upwelling. In: Payne, A.I.L., Gulland, J.A. and Brink, K.H. (Eds). *The Benguela and Comparable Ecosystems. South African Journal of Marine Science,* 5: 51-62.

Lutjeharms, J. R. E. and Meyer, A. A., 2000. The origin and circulation of bottom water on the Agulhas Bank, South Africa. Continental Shelf Research, submitted.

Lutjeharms, J. R. E., Monteiro, P. M. S., Tyson, P. D. and D. Obura, 2001. The oceans around southern Africa and regional effect of global change. *South African Journal of Science,* 97: 119-130.

Lutjeharms, J.R.E. and Stockton, P.L., 1987. Kinematics of the upwelling front off southern Africa. In: Payne, A.I.L., Gulland, J.A. and Brink, K.H. (Eds). *The Benguela and Comparable Ecosystems. South African Journal of Marine Science,* 5: 35-49.

Lutjeharms, J.R.E. and Valentine, H.R., 1987. Water types and volumetric considerations of the South-East Atlantic upwelling regime. In: Payne, A.I.L., Gulland, J.A. and Brink, K.H. (Eds). *The Benguela and Comparable Ecosystems. South African Journal of Marine Science,* 5: 63-71.

Lutjeharms, J. R. E. and Valentine, H. R., 1988a. Eddies at the Sub-Tropical Convergence south of Africa. *Journal of Physical Oceanography,* 18: 761-774.

Lutjeharms, J. R. E. and Valentine, H. R., 1988b. Evidence for persistent Agulhas rings south west of Cape Town. *South African Journal of Science,* 84: 781-783.

Lutjeharms, J. R. E. and van Ballegooyen, R. C., 1988a. The retroflection of the Agulhas Current. *Journal of Physical Oceanography,* 18: 1570-1583.

Lutjeharms, J. R. E. and van Ballegooyen, R. C., 1988b. Anomalous upstream retroflection in the Agulhas Current. *Science,* 240: 1770-1772.

Mackensen, A. and Bickert, T., 1999 Stable carbon isotopes in benthic foraminifera. In: Fischer, G. and Wefer, G. (Eds). *Use of Proxies in Paleoceanography: Examples from the South Atlantic.* Springer-Verlag, Berlin, pp 229-254.

Malmgren, B.A. and Kennett, J.P., 1977. Biometric differentiation between Recent *Globigerina bulloides* and *Globigerina falconensis* in the Southern Indian Ocean. *Journal of Foraminiferal Research,* 7(2): 130-148.

Martin, A.K. and Flemming, B.W., 1988. Physiography, structure and geological evolution of the Natal continental shelf. In: Schumann, E.H. (Ed). *Coastal Ocean Studies off Natal, South Africa,* Springer-Verlag, New York, pp 11-14.

Martin, A.K., Goodlad, S.W. and Salmon, D.A., 1982. Sedimentary basin in-fill in the northernmost Natal Valley; hiatus development and Agulhas Current paleoceanography. *Journal of the Geological Society of London,* 139: 183-201.

Matano, R.P., Simionato, C.G., de Ruijter, W.P., van Leeuween, P.J., Strub, P.T., Chelton, D.B. and Schlax, M.G., 1998. Seasonal variability in the Agulhas retroflection region. *Geophysical Research Letters,* 25: 4361-4364.

McIntyre, A., Ruddiman, W.F., Karlin, K. and Mix, A.C., 1989. Surface water response of the equatorial Atlantic Ocean to orbital forcing. *Paleoceanography,* 4: 19-55.

Meadows, M.E., 2001. The role of Quaternary environmental change in the evolution of landscapes: case studies from southern Africa. *Catena,* 42: 39-57.

Mélice, J.L and Servain, J., 2002. The tropical Atlantic meridional SST gradient index and its relationships with the SOI, NAO and Southern Ocean. *Climate Dynamics,* (in press).

Mélice, J.L., Coron, A. and Berger, A., 2001. Amplitude and frequency modulations of the Earth's obliquity for the last million years. *Journal of Climate,* 14: 1043-1054.

Meyers, P.A., 1994. Preservation of elemental and isotopic source identification of sedimentary organic matter. *Chemical Geology,* 144: 289-302.

Meyers, P. A., 1997. Organic geochemical proxies of paleoceanographic, paleolimnologic and paleoclimatic processes. *Organic Geochemistry,* 27: 213-250.

Milankovitch, M., 1930. Mathematische Klimalehre und Astronomische Theorie der Klimaschwankungen. In: Köppen, W.and Geiger, R. (Eds). *Handbuch der Klimatologie, Bd 1. Gerbrüder Borntraeger,* Berlin. 176pp. (Cited in Imbrie *et al.*, 1992; Preston-Whyte and Tyson, 1988.)

Minagawa, M. and Wada, E., 1984. Stepwise enrichment of ^{15}N along food chains: further evidence and the relation between $\delta^{15}N$ and animal age. *Geochimica Cosmochimica Acta,* 48: 1135-1140.

Mix, A.C. and Morey, A.E., 1996. Climate feedback and Pleistocene variations in the Atlantic South Equatorial Current. In: Wefer, G., Berger, W.H., Siedler, G. and Webb, D.J. (Eds), *The South Atlantic: Past and Present Circulation.* Springer-Verlag Berlin, pp 503-525.

Moore, T.C. Jr., Pisias, N.G. and Dunn, D.A., 1982. Carbonate time series of the Quaternary and late Miocene sediments in the Pacific Ocean: A spectral comparison. *Marine Geology,* 46: 217-233.

Morely, J.J. and Hays, J.D., 1979. Comparison of glacial and interglacial oceanographic conditions in the South Atlantic from variations in calcium carbonate and radiolarian distributions. *Quaternary Research,* 12: 396-408.

Morlet, J., 1983. Sampling theory and wave propagation. *NATO ASI Series,* Fl, Springer, Berlin, pp 233-261. (Cited in Lau and Weng, 1995; Mélice *et al.*, 2001.)

Mortlock, R.A., Charles, C.D., Froelich, P.N., Zibello, M.A., Saltzman, J., Hays, J.D. and Burckle, L.H., 1991. Evidence for lower productivity in the Antarctic Ocean during the last glaciation. *Nature,* 351: 220-223.

Mueller, A. and Voss, M., 1999. The palaeoenvironments of coastal lagoons in the southern Baltic Sea, II. $\delta^{13}C$ and $\delta^{15}N$ ratios of organic matter-sources and sediments. *Palaeogeography, Palaeoclimatology, Palaeoecology,* 145: 17-32.

Mulitza, S. Arz, H., Kemle-von Mücke, S., Moos, C., Niebler, H.-S., Pätzold, J. and Segl, M., 1999. The South Atlanitc Carbon Isotope Record of Planktonic Foraminifera. In: Fischer, G. and Wefer, G. (Eds). *Use of Proxies in Paleoceanography: Examples from the South Atlantic*. Springer-Verlag, Berlin, pp 427-445.

Müller, P.J., Cepek, M., Ruhland, G. and Schneider, R.R., 1997. Alkenone and coccolithophorid species changes in late Quaternary sediments from the Walvis Ridge: Implications for the alkenone paleotemperature method. *Palaeogeography, Palaeoclimatology, Palaeoecology,* 135: 71-96.

Müller, P.J., Schneider, R.R. and Ruhland, G., 1994. Late Quaternary PCO_2 variations in the Angola Current: evidence from organic carbon $\delta^{13}C$ and alkenone temperatures. In Zahn, R. Pedersen, T.F., Kaminski, M.A., Labeyrie, L. (eds). *Carbon Cycling in the Glacial Ocean: Constraints on the Oceans Role in Global Change*. NATO ASI Series, Vol 17, Springer, Berlin, pp 343-366.

Mullin, M.M., Rau, G. and Eppley, R.W., 1984. Stable nitrogen isotopes in zooplankton: some geographic and temporal variations in the North Pacific. *Limnology and Oceanography,* 29: 1267-1273.

Natakusa, T., Handa, N., Wada, E. and Wong, C.S., 1992. The dynamic changes of stable isotopic ratios of carbon and nitrogen in suspended and sedimented particulate organic matter during a phytoplankton bloom. *Journal of Marine Research,* 50: 267-296.

Nelson, G. and Hutchings, L., 1983. The Benguela upwelling area. *Progress in Oceanography,* 12(3): 333-356.

Nelson, G., 1985. Notes on the physical oceanography of the Cape Peninsula upwelling system. In: Shannon, L.V. (Ed.). *South African Colour and Upwelling Experiment*. Sea Fisheries Research Institute, Cape Town, pp. 63-95.

Nelson, G., 1989. Poleward motion in the Benguela area. In: Neshyba, S.J., Mooers, C.N.K., Smith R.L. and Barber, R.T. (Eds). *Poleward Flows along Eastern Ocean Boundaries*. Springer, New York, pp. 110-130.

Niebler, H-S, 1995. Reconstruction of paleo-environmental parameters using stable isotopes and faunal assemblages of planktonic foraminifera in the South Atlantic Ocean. *Berichte Polarforschung*, 167: 1-198.

Niebler, H-S. and Gersonde, R., 1998. A planktonic foraminiferal transfer function for the southern South Atlantic Ocean. *Marine Micropaleontology*, 34: 213-234.

Oberhänsli, H., 1991. Upwelling signals at the northeastern Walvis Ridge during the past 500,000 years. *Paleoceanography,* 6(1):53-71.

Oberhänsli, H., Blünier, C., Meinecke, G., Schmidt, H., Schneider, R. and Wefer, G., 1992. Planktonic foraminifers as tracers of ocean currents in the Eastern South Atlantic. *Paleoceanography,* 7(5): 607-632.

Ohkouchi, N. and Wada, E., 1997. Secular variations in sedimentary organic $\delta^{13}C$ during the last 35 M.Y. in the tropical Atlantic, Site 925. In: Shackleton, N.J., Curry, W.B., Richter, C. and Brawlower, T.J. (Eds). *Proceedings of the Ocean Drilling Program, Scientific Results* 154: 501-505.

Pancost, R., Freeman, K, H. and Patzkowsky, M.E., 1999. Organic matter source variation and the expression of a late Middle Ordovician carbon isotope excursion. *Geology,* 27: 1015-1018.

Parker, F.L., 1962. Planktonic foraminiferal species in Pacific sediments. *Micropaleontology,* 8 (2): 219-254.

Parkins, C.A., 1993. *Stable Carbon and Nitrogen Isotope Ratios in the Shallow-Water Cape Hake, Merluccius capensis (Castelnau) as Indicators of Trophic Position and Diet on the West and South Coasts of South Africa.* Unpublished MSc. Thesis, Department of Zoology, University of Cape Town, 60pp.

Partridge, T.C., 1997. Cainozoic environmental change in southern Africa, with special emphasis on the last 200,000 years. *Progress in Physical Geography,* 21: 3-22.

Partridge, T.C. and Maud, R.R., 1987. Geomorphic evolution of southern Africa since the Meozoic. *South African Journal of Geology,* 90(2): 179-208.

Penven, P., Lutjeharms, J. R. E., Marchesiello, P., Weeks, S. J. and Roy, C., 2001. Generation of cyclonic eddies by the Agulhas Current in the lee of the Agulhas Bank. *Geophysical Research Letters,* 28(6): 1055-1058.

Petersen, R.G. and Stramma, L., 1991. Upper-level circulation in the South Atlantic Ocean. *Progress in Oceanography,* 26: 1-173.

Peterson, L.C. and Prell, W.L., 1985. Carbonate dissolution in recent sediments of the eastern equatorial Indian Ocean: Preservation patterns and carbonate loss above the lysocline. *Marine Geology,* 64: 259-2990.

Pether, J. 1994. Molluscan evidence for enhanced deglacial advection of Agulhas water in the Benguela Current, off Southwestern Africa. *Palaeogeography, Palaeoclimatology, Palaeoecology,* 111: 99-117.

Pierre, C., Saliege, J.F., Urrutiaguer, M.J. and Giraudeau, J., 2001. Stable isotope record of the last 500 kyr at Site 1087 (Southern Cape Basin). In: Wefer, G., Berger, W.H. and Richter, C. (Eds). *Proceedings of the Ocean Drilling Program, Scientific Results,* 175: 1-22.

Pisias, N.G., Martinson, D.G., Moore, T.C. Jr. and Shackleton, N.J., 1984. High resolution stratigraphic correlation of benthic oxygen isotope records spanning the last 300,000 years. *Marine Geology,* 56: 119-136.

Popp, B.N., Trull, T., Kenig, F., Wakeham, S.G., Rust, T.M., Tilbrook, B., Griffiths, F.B., Wright, S.W., Marchant, H.J., Bidigare, R.R. and Laws, E.A., 1999. Controls on the carbon isotopic composition of Southern Ocean plankton. *Global Biogeochemical Cycles,* 13: 827-843.

Prell, W.L., Fox, C. Hutson, W.H., Matthews, R.K., Sommer, M., Williams, D., Bé, A.W.H. and Geitzenauer, K., 1976. A paleoceanographic reconstrruction of the Indian Ocean at 18,000 yr BP. Abstract. *Annals of the Geological Society of America,* pp1052-1053.

Prell, W.L., Hutson, W.H. and Williams, D.F., 1979. The Subtropical Convergence and Late Quaternary circulation in the southern Indian Ocean. *Marine Micropaleontology,* 4: 225-234.

Prell, W.L., Hutson, W.H., Williams, D.F, Bé, A.W.H., Geitzenauer, K and Molfino, B., 1980. Surface circulation of the Indian Ocean during the last glacial maximum, approximately 18,000 yr B.P. *Quaternary Research,* 14: 309-336.

Preston-Whyte, R.A. and Tyson, P.D., 1998. *The Atmosphere and Weather of Southern Africa.* Oxford University Press, Cape Town, 375pp.

Probyn, T.A., 1985. Nitrogen uptake by size-fractionated phytoplankton populations in the southern Benguela Upwelling System. *Marine Ecology Progress Series,* 22: 249-258.

Probyn, T.A., Mitchell-Innes, B.A. and Searson, S., 1995. Primary productivity and nitrogen uptake in the subsurface chlorophyll maximum on the Eastern Agulhas Bank. *Continental Shelf Research,* 15(15): 1903-1920.

Ravelo, A.C. and Fairbanks, R.G., 1992. Oxygen isotopic composition of multiple species of planktonic foraminifera. – Recorders of the modern photic zone temperature gradient. *Paleoceanography,* 7: 815-831.

Ravelo, A.C. and Fairbanks, R.G., 1995. Carbon isotopic fractionation in multiple species planktonic foraminifera from core-tops in the tropical Atlantic. *Journal of Foraminiferal Research,* 25: 53-74.

Rau, A.J., Rogers, J., Lutjeharms, J.R.E., Giraudeau, J., Lee-Thorp, J.A., Chen, M.-T. and Waelbroeck, C., 2002. A 450-kyr record of hydrological conditions on the western Agulhas Bank Slope, south of Africa. *Marine Geology,* 180: 183-201.

Rau, G.H., Takahashi, T. and Des Marais, D.J., 1989. Latitudinal variations in phytoplankton $\delta^{13}C$: implications for CO2 and productivity in past oceans. *Nature,* 341: 516-518.

Redfield, A.C., 1934. On the proportions of organic derivatives in seawater and their relation to the composition of plankton. *James Johnson Memorial Volume,* pp 176-192. (Cited in Freeman, 2001).

Reid, J.L., 1989. On the total geostrophic circulation of the South Atlantic Ocean: Flow patterns, tracers and transports. *Proceedings in Oceanography,* 23(3): 149-244.

Reid, J.R., 1996. On the circulation of the South Atlantic Ocean. . In: Wefer, G., Berger, W.H., Siedler, G. and Webb, D.J. (Eds). *The South Atlantic: Past and Present Circulation.* Springer-Verlag Berlin, pp. 13-44.

Reynolds-Sautter, L. and Thunell, R.C., 1991. Seasonal variability in the $\delta^{18}O$ and $\delta^{13}C$ of planktonic foraminifera from an upwelling environment: sediment trap results from the San Pedro Basin, Southern California Bight. *Paleoceanography,* 6: 307-334.

Rogers, J., 1971. Sedimentology of Quaternary deposits on the Agulhas Bank. *Bulletin of the Joint Geological Survey/University of Cape Town Marine Geoscience Unit,* 1: 1-117.

Rogers, J., 1999. Preliminary findings of the IMAGES-II Programme (International Marine Global changE Study) using giant piston cores from the continental slope and rise off southern Africa. *South African Journal of Geology,* 102: 384-390.

Rogers, J. and Bremner, J.M., 1991. The Benguela Ecosystem. Part VII. Marine Geological aspects. In: Barnes, M. (Ed.). *Oceanography Marine Biology Annual Review,* 29, 1-85. Aberdeen University Press, Aberdeen.

Romanek, C.S., Grossman, E.L. and Morse, J.W., 1992. Carbon isotopic fractionation in synthetic aragonite and calcite: effects of temperature and precipitation rate. *Geochimica Cosmochimica Acta,* 56: 419-430.

Rühlemann, C., Müller, P.J. and Schneider, R.R., 1999. Organic carbon and carbonate as paleoproductivity proxies: Examples from high and low productivity areas of the Tropical Atlantic. In: Fischer, G. and Wefer, G. (Eds). *Use of Proxies in Paleoceanography: Examples from the South Atlantic.* Springer-Verlag, Berlin, pp315-344.

Sackett, W.M., 1964. The depositional history and isotopic carbon composition of marine sediments. *Marine Geology,* 2: 173-185.

Sackett, W.M., Eckelmann, W.R., Bender, M.L. and Bé, A.W.H., 1965. Temperature dependence of carbon isotope composition in marine phytoplankton and sediments. *Science,* 148: 235-237.

Saito, T., Thompson, P.R. and Breger, D., 1981. *Systematic Index of Recent and Pleistocene Planktonic Foraminifera.* University of Tokyo Press, Tokyo, Japan, 190pp.

Sarnthein, M., Winn, K., Duplessy, J-C. and Fontugne, M.R., 1988. Global variations in surface ocean productivity in low and middle latitudes: influence on the CO_2 reservoirs of the deep ocean and the atmosphere during the last 21 000 years. *Paleoceanography,* 3: 361-399.

Schneider, R.R., Müller, P.J. and Ruhland, G., 1995. Late Quaternary surface circulation in the east equatorial South Atlantic: Evidence from alkenone sea surface temperatures. *Paleoceanography,* 10: 197-219.

Schneider, R.R., Müller, P.J. and Wefer, G., 1994. Late Quaternary paleoceanographic changes off the Congo deduced from stable carbon isotopes of planktonic foraminifera. *Palaeogeography, Palaeoclimatology, Palaeoecology,* 110: 255-274.

Schneider, R.R., Müller, P.J., Ruhland, G., Meinecke, G., Schmidt, H. and Wefer, G., 1996. Late Quaternary surface temperatures and productivity in the East-Equatorial South Atlantic: Response to changes in trade/monsoon wind forcing and surface water advection. In: Wefer, G., Berger, W.H., Siedler, G. and Webb, D.J. (Eds), *The South Atlantic: Past and Present Circulation.* Springer-Verlag Berlin, pp 527-551.

Schumann, E.H., 1989. The propagation of air pressure and wind systems along the South African coast. *South African Journal of Science,* 85: 382-285.

Schouten, M.W., 2001. *Indian-Atlantic Interocean Exchange : Variability and Controls.* Unpublished PhD Thesis, Fakulteit Natuur en Sterrenkunde, Universiteit Utrecht, 125pp.

Schumann, E.H., Perrins, L.-A. and Hunter, I.T., 1982. Upwelling along the south coast of the Cape Province, South Africa. *South African Journal of Science*, 78(6): 238-242.

Servain, J. and Legler, D.M., 1986. Empirical orthogonal function analysis of tropical Atlantic sea surface temperature and wind stress. *Journal of Geophysical Research,* 91: 181-191.

Siesser, 1972. Limestone lithofacies from the South African continental margin. *Sedimentary Geology*, 8: 83-112

Shackleton, N.J., 1967. Oxygen isotope analyses and Pleistocene temperatures re-assessed. *Nature, London,* 215: 15-17.

Shackleton, N.J., 1977. Carbon 13 in *Uvigerina*: tropical rainforest history and the equatorial Pacific carbonate dissolution cycles. In: Anderson, N.R. and Malahoff, A. (Eds). *The Fate of Fossil Fuel CO_2 in Oceans.* Plenum Press, New York, pp 401-427 (Cited in Mulitza *et al.*, 1999).

Shackleton, N.J., Hall, M.A., Line, J. and Shuxi, C., 1983. Carbon isotope data in core V 19-30 confirm reduced carbon dioxide concentration of the ice age atmosphere. *Nature,* 306: 319-322.

Shannon, L.V., 1985. The Benguela Ecosystem. Part I. Evolution of the Benguela, physical features and processes. In: Barnes, M. (Ed.). *Oceanography Marine Biology Annual Review,* 23: 105-182.

Shannon, L.V. and Anderson, F.P, 1982. Applications of satellite ocean colour imagery in the study of the Benguela Current System. *South African Journal of Photogrammetry, Remote Sensing and Cartography,* 13(3): 153-169.

Shannon, L.V. and Nelson, G., 1996. The Benguela: Large scale features and processes and system variability. In: Wefer, G., Berger, W.H., Siedler, G. and Webb, D.J. (Eds). *The South Atlantic: Past and Present Circulation.* Springer-Verlag Berlin, pp211-217.

Shannon, L.V. and O'Toole, M.J., 1998. Integrated overview of the oceanography and environmental variability of the Benguela Current region. *Synthesis and assessment of information on BCLME- Thematic Report 2 (UNDP/GEF RAF/96/G43),* 58pp.

Shannon, L.V. and van Rijswijck, M., 1969. Physical oceanography of the Walvis Ridge region. *Investigative Report, Division of Sea Fisheries South Africa* 58: 1-22.

Shannon, L.V., Agenbag, J.J., Walker, N.D. and Lutjeharms, J.R.E., 1990. A major perturbation in the Agulhas Retroflection area in 1986. *Deep-Sea Research,* 37 : 493-512.

Shannon, L.V., Lutjharms, J.R.E. and Agenbag, J.J., 1989. Episodic input of subantarctic water into the Benguela region. *South African Journal of Science,* 85: 317-322.

Shannon, L.V., Nelson. G and Jury, M.R., 1981. Hydrological and meteorological aspects of upwelling in the southern Benguela Current. In: Richards, F.A. (Ed.). *Coastal Upwelling, Coastal and Estuarine Sciences 1.* American Geophysical Union Washington, D.C., pp. 146-159.

Shemesh, A., Macko, S.A., Charles, C.D. and Rau, G.H., 1993. Isotopic evidence for reduced productivity in the glacial Southern Ocean. *Science,* 262: 407-410.

Sholto-Douglas, A.D., 1992. *Use of stable isotope ratios of carbon and nitrogen to elucidate pelagic marine food webs of the Benguela and Agulhas Bank regions of South Africa.* Unpublished MSc. Thesis, Department of Zoology, University of Cape Town, 84pp.

Simpson, E.S.W. and Forder, E., 1968. The Cape Submarine Canyon. Part I. Bathymetry. *Fisheries Bulletin of South Africa,* 5: 35-38.

Smith, W.H.F. and Sandwell, D.T., 1996. Global Seafloor topography. Measured and estimated from gravity data derived from satellite altimetry and shipboard depth soundings. http://www.ngdc.noaa.gov/mgg/image/global_topo_large.gif.

Stainforth, R.M. and Lamb, J.L., 1981. An evolution of planktonic foraminiferal zonation of the Oligocene. *University of Kansas Palaeontology Contributions,* Vol. 104.

Stramma, L. and Petersen, R.G., 1989. Geostrophic transport in the Benguela Current region. *Journal of Physical Oceanography,* 19: 1440-1448.

Stuut, J.-B. W., Prins, M.A., Schneider, R.R., Weltje, G.J., Jansen, J.H.F. and Postma, G., 2002. A 300-kyr record of aridity and wind strength in southwestern Africa: inferences from grain-size distributions of sediments on the Walvis ridge, S.E. Atlantic. *Marine Geology,* 180: 221-234.

Summerhayes, C.P., Kroon, D., Rosell-Melé, A., Jordan, R.W., Schrader, H.-J., Hearn, R., Villaneuva, J., Grimalt, J.O. and Eglinton, G., 1995. Variability in the Benguela Current upwelling system over the past 70,000 years. *Progress in Oceanography,* 35: 207-251.

Swart, V.P. and Largier, J.L., 1987. Thermal structure of the Agulhas Bank water. In: Payne, A.I.L., Gulland, J.A., and Brink, K.H. (Eds). *The Benguela and Comparable Ecosystems. South African Journal of Marine Science,* 5: 243-253.

Thomalla, S.J., 2001. *Phytoplankton Distribution and Nitrogen Dynamics in the Southwest Indian Subtropical gyre and Southern Ocean Waters.* Unpublished MSc. Thesis, Department of Oceanography, University of Cape Town. 156pp.

Thunell, R.C., 1976. Optimum indices of carbonate dissolution in deep-sea sediments. *Geology,* 4: 525-527.

Thunell, R.C. and Reynolds, L.A., 1984. Sedimentation of planktonic foraminifera; seasonal changes in species flux in the Panama Basin. *Micropaleontology,* 30(3): 243-262.

Torrence, C and Compo, G.P., 1998. A practical guide to wavelet analysis. *Bulletin of the American Meteorological Society,* 79(1): 61-78.

Ufkes, E., Jansen, J.H.F. and Brummer, G.-J.A., 1998. Living planktonic foraminifera in the eastern South Atlantic during spring: indicators of water masses, upwelling and the Congo (Zaire) River plume. *Marine Micropaleontology,* 33: 27-53.

Ufkes, E., Jansen, J.H.F. and Schneider, R.R., 2000. Anomalous occurrences of *Neogloboquadrina pachyderma* (left) in a 420-kyr upwelling record from the Walvis Ridge (SE Atlantic). *Marine Micropaleontology,* 40: 23-42.

Valentine, H.R., Lutjeharms, J.R.E. and Brundrit, G.B., 1993. The water masses and volumetry of the southern Agulhas Current region. *Deep-Sea Research,* 40(6): 1285-1305.

Van Andel, T.H., 1989. Late Pleistocene sea levels and the human exploitation of the shore and shelf of southern South Africa. *Journal of Field Archaeology,* 16: 133-155.

Van Ballegooyen, C., Gründlingh, M.L. and Lutjeharms, J.R.E., 1994. Eddy fluxes of heat and salt from the southwest Indian Ocean into the southeast Atlantic Ocean: a case study. *Journal of Geophysical Research,* 99(C7): 14053-14070.

Verardo, D.J. and McIntyre, A., 1994. Production and destruction: Control of biogenous sedimentation in the tropical Atlantic 0-300,000 years B.P.. *Paleoceanography,* 9: 63-86.

Vogel, J.C. and Fuls, A., 1978. The geographical distribution of Kranz grasses in South Africa. *South African Journal of Science,* 74: 209-215.

Volat, J.L., Pastouret, L. and Vergnaud-Grazzini, C., 1980. Dissolution and carbonate fluctuations in Pleistocene deep-sea cores: A review. *Marine Geology,* 34: 1-28.

Volbers, A.N.A and Henrich, R., 2002. Late Quaternary variations in calcium carbonate preservation of deep-sea sediments in the northern Cape Basin: Results from a multiproxy approach. *Marine Geology,* 180: 203-220.

Wada, E., Kadonaga, T. and Matsuo, S., 1975. ^{15}N abundance in naturally occurring substances and global assessment of denitrification from an isotopic viewpoint. *Geochimica Cosmochimica Acta,* 9: 139-148.

Wefer, G., Berger, W.H., Bickert, T., Donner, B., Fischer, G., Keemle-von Mücke, S., Meinecke, G., Müller, P.J., Mulitza, S., Niebler, H.-S., Pätzold, J., Schmidt, H., Schneider, R.R. and Segl, M., 1996. Late Quaternary surface circulation of the South Atlantic: The stable isotope record and implications for heat transport and productivity. In: Wefer, G., Berger, W.H., Siedler, G. and Webb, D.J. (Eds). *The South Atlantic: Past and Present Circulation.* Springer-Verlag Berlin, pp. 461-502.

Wefer, G., Berger, W.H., Richter, C and shipboard scientific party, 1998. *Proceedings of the Ocean Drilling Program, Initial Reports, Part I, Leg 175,* College Station, Texas. pp577.

Wefer, G., Berger, W.H., Bijma, J. and Fischer, G., 1999. Clues to Ocean History: a Brief Overview of Proxies. In: Fischer, G. and Wefer, G., (Eds). *Use of Proxies in paleoceanography: Examples from the South Atlantic.* Springer-Verlag, Berlin, pp 1-68.

Weijer, W., de Ruijter, W. P. M., Dijkstra, H. A. and van Leeuwen, P. J., 1999. Impact of interbasin exchange on the Atlantic overturning circulation. *Journal of Physical Oceanography,* 29: 2266-2284.

Williams, D.F., 1976. Southern Ocean fluctuations of the Polar Front and Subtropical Convergence in the southeast Indian Ocean. *Marine Micropaleontology*, 1: 363-375.

Winter, A. and Martin, K., 1990. Late Quaternary history of the Agulhas Current. *Paleoceanography*, 5(4): 479-486.

Wu, G. and Berger, W. 1991. Pleistocene $\delta^{18}O$ record from Ontong Java Plateau: effects of winnowing and dissolution. *Marine Geology*, 96: 193-209.

Wu, J.P., Calvert, S.E. and Wong, C.S., 1997. Nitrogen isotope variations in the subarctic northeast Pacific – relationship to nitrate utilization and trophic structure. *Deep-Sea Research*, 44: 287-314.

APPENDIX 1

OXYGEN ISOTOPE STRATIGRAPHY

CORE MD962080 (AGULHAS BANK SLOPE)

Depth (cm)	$\delta^{18}O$ *C. wuellerstorfi* (‰)	$\delta^{18}O$ G. inflata (‰)	Isotope Event	Age (kyr)
0				0
2.5	2.624	1.002		1
10.5	2.711	1.170		
20.5	2.810	1.540		
30.5	2.831	2.130		
40.5	3.605	1.790		
50.5	3.630	1.820	2.2	19
60.5	3.623	1.740		
70.5	3.549	1.620		
80.5	3.505	2.010		
90.5	3.477	1.300		
100.5	3.413	1.690		
110.5	3.354	1.160	3.1	30
120.5	3.419	1.390		
130.5	3.239	1.290		
140.5	3.178	1.480		
150.5	2.969	1.810	3.3	53
160.5	3.380	1.000		
170.5	3.331	1.500		
180.5	3.180	1.810		
190.5	3.443	1.380	4.2	65
200.5	2.992	1.140		
210.5	2.995	1.050		
220.5	2.481	1.080	5.3	99
230.5	2.582	1.000		
240.5	2.770	1.320		
250.5	2.239	0.980	5.5	122
260.5	2.322	0.830		
270.5	3.086	1.080		
280.5	3.912	1.440		
290.5	4.206	1.650		
300.5	4.261	2.050	6.2	135
310.5	4.136	1.800		
320.5	3.957	2.400		
330.5	4.231	2.320		
340.5	4.060	2.000		
350.5	3.920	2.300		
360.5	4.250	2.630	6.4	151
370.5	3.918	1.740		
380.5	3.785	1.830		
390.5	3.800	1.290		
400.5	3.981	1.810		
410.5	3.743	1.740		
420.5	3.902	1.880	6.6	182
430.5	3.805	1.930		
440.5	3.708	1.720		
450.5	3.352	1.090		
460.5	3.293	1.210		
470.5	3.420	1.250		
480.5	3.077	1.030		
490.5	2.798	1.490	7.5	238
500.5	3.322	1.340		

CORE MD962080 (AGULHAS BANK SLOPE)

Depth (cm)	$\delta^{18}O$ *C. wuellerstorfi* (‰)	$\delta^{18}O$ G. inflata (‰)	Isotope Event	Age (kyr)
510.5	3.826	1.170		
520.5	3.982	1.950	8.2	248
530.5	3.734	1.650		
540.5	3.429	1.850		
550.5	3.482	1.870		
560.5	3.702	1.980		
570.5	4.051	1.780		
580.5	3.922	1.870		
590.5	3.700	2.250		
600.5	4.054	1.950	8.4	266
610.5	3.962			
620.5	3.884	1.820		
630.5	3.519			
640.5	3.687	1.940		
650.5	3.555	2.380		
660.5	3.819	2.120		
670.5	3.608	2.030		
680.5	3.382	1.710		
690.5	3.359	2.320	9.1	309
700.5	3.440	1.920		
710.5	3.448	1.870		
720.5	2.766	1.020		
730.5	2.420	1.510	9.3	328
740.5	3.180	1.340		
750.5				
760.5				
770.5	4.220	2.270	10.2	340
780.5	4.090	2.220		
790.5	4.110	2.390		
800.5	3.905	2.880		
810.5	3.884	2.510		
820.5	3.976	2.630		
830.5	3.984	2.030		
840.5	3.785	2.530		
850.5	3.734	2.120		
860.5	3.550	2.120	11.1	369
870.5	3.688	1.830		
880.5	3.638	1.990		
890.5	3.113	1.530		
900.5	2.849	2.330		
910.5	2.431	1.090	11.3	406
920.5	2.649	1.550		
930.5	2.740	1.220		
940.5	3.280	2.010		
950.5				
960.5	3.310	2.010		
970.5		2.510		
980.5		3.140	12.2	434
990.5		2.290		
1000.5		2.360	12.3	458
1030.5	3.730		13.1	481
1040.5	3.670			

CORE MD962080 (AGULHAS BANK SLOPE)

Depth (cm)	$\delta^{18}O$ *C. wuellerstorfi* (‰)	$\delta^{18}O$ G. inflata (‰)	Isotope Event	Age (kyr)
1050.5	3.119		13.13	500
1060.5	3.083			
1070.5	3.003		13.3	524
1080.5	3.560	2.150		
1090.5	3.333			
1100.5	3.659	2.441		
1110.5	3.730	2.505	14.2	536
1120.5	3.157	2.765		
1130.5		1.835		
1140.5	2.845	2.067	15.1	573
1150.5	3.528	1.668	15.2	582
1160.5	3.375	2.139	15.3	594
1170.5	3.656	1.600	15.4	604
1180.5	3.100	1.599	15.5	615
1190.5	3.569	2.167		
1200.5	4.381	2.967	16.2	628
1210.5	4.321	3.151		
1220.5	4.167	2.370		
1230.5	4.001	2.214	16.3	642
1240.5	4.011	2.430		
1250.5	3.825	2.055	17.1	666
1260.5	3.659	2.153		
1270.5	3.291	1.597		
1280.5	3.203	1.471	17.3	688
1290.5	3.838	2.368	17.4	699
1300.5	3.803	2.431		
1310.5	2.760	1.806	17.5	708
1320.5	3.198	2.244		
1330.5	3.905	2.164		
1340.5	4.107			
1350.5	4.212		18.2	718
1360.5	4.043			
1370.5	4.062	2.241	18.4	754
1380.5	3.571	2.064		
1390.5	3.201	1.362	19.1	765
1400.5	3.544	1.566		
1410.5	4.381	1.779		
1420.5		1.629		
1430.5		2.154	19.3	782
1440.5		2.198		
1450.5		1.985		
1460.5		2.385	20.2	799
1470.5		2.333		807
1480.5		2.369		815
1490.5		2.028	21.1	824
1500.5		2.488	21.2	835

ODP SITE 1087

Depth (cm)	$\delta^{18}O$ *C. wuellerstorfi* (‰)	$\delta^{18}O$ G. inflata (‰)	Isotope Event	Age (kyr)
0	2.51	1.11		
5	2.51	1.07		
10	2.44	0.91		
15	2.91	0.99		
20		0.63		
25	2.55	0.84		
30	2.77	1.27		
35		1.27		
40	2.75	1.23		
45	2.69	1.23		
50	3.23	1.87	2	11
55	3.63	1.63		
60	3.75	2.34		
65	3.87	2.38		
70	3.57	1.83		
75	4.03	2.07	2.2	19
80	3.9	1.77		
85	3.58	1.59		
90	3.83	1.86		
95	3.66	2.28		
100	3.45	1.35		
105	3.19	1.88	3.3	52
110	3.84	2.26		
115	3.4	2.08		
120	3.51	1.74		
125	3.85	2.11		
130	3.6	1.95		
135	3.24	1.97		
140				
145				
150	3.75	2.07		
155	3.51	1.73		
160	3.25	1.53		
165	3.38	1.71		
170	3.53	2.21		
175	3.06	1.49	5.1	80
180	3.28	1.36		
185	3.14	1.1		
190	3.25	1.15		
195	3.52	1.13		
200	3.73	1.42		
205	3.46	1.32		
210	3.22	1.69		
215	3.56	1.17		
220	3.28	1.33		
225	3.06	1.59		
230	2.94	1.57		
235	3.23	1.93		
240	3.11	1.89		
245	2.89	1.19	5.3	99
250	3.4	1.16		

ODP SITE 1087

Depth (cm)	$\delta^{18}O$ *C. wuellerstorfi* (‰)	$\delta^{18}O$ G. inflata (‰)	Isotope Event	Age (kyr)
255				
260				
265	3.16	1.4		
275	2.88	1.62		
280	2.7	0.91		
285	2.64	0.87		
290	2.31	1.41		
295	2.32	1.21		
300	2.69	1.06		
305	2.19	1.39	5.5	122
310	2.56	1.61		
315	2.42	1.54	6	127
320	3.7	2.38		
325	3.58	2.07		
330	3.44	2.1		
335	3.89	2.16		
340	3.59	1.71		
345	3.73	2.2		
350	3.68	2.12	6.2	135
355	3.81	2.13		
360	2.99	2.22		
365	3.75	1.72		
370	3.57	1.34		
375	3.1	1.84	6.4	151
380	4.06	1.82		
385		1.79		
390		2.05		
395		1.86		
400		1.53		
405	3.37	1.36		
410	3.34	1.89		
415	2.66	1.86	6.5	171
420	3.4	1.4		
425		1.34	6.6	183
430	3.38	1.64		
435	3.37	1.65		
440				
445				
450	2.77	1.11	7.1	194
455	3.21	1.99		
460	3.25	1.72		
465	2.65	1.7	7.3	216
470	2.82	2.21		
475	2.97	1.72		
480	3.29	1.59		
485	3.44	1.6		
490		1.53		
497	3.24	1		
500	3.14	1.02		
505	2.64	1.4	8	242
510	2.97	1.46		
515	2.9	1.41		

ODP SITE 1087

Depth (cm)	$\delta^{18}O$ *C. wuellerstorfi* (‰)	$\delta^{18}O$ G. inflata (‰)	Isotope Event	Age (kyr)
520	2.92	1.63		
525	3.49	2.17		
530	3.21	2.29		
535	3.67	1.79		
540	3.59	1.71		
545		2.17		
555		2.08		
560		1.61		
565	3.39	1.96		
570	3.81	2.15		
575	3.66	2.14		
580	3.44	1.83		
585		2.12		
590	3.25	1.69		
595	3.03	1.48		
600	3.78	1.65		
605	3.14	1.57		
610	2.99	1.99		
615	3.57	1.67		
620	2.91	1.82		
625	3.86	1.96		
630	3.37	2.2		
635		1.47		
640	3.2	2.05		
645	3.35	1.89		
651	3.27	2.16		
656	3.48	2.23		
661	3.74	1.81		
666	3.63	1.74		
671	3.47	1.72		
676	3.53	2.04		
681	3.37	1.55		
686	3.42	1.62		
691	3.46	1.6		
696	3.37	0.98		
701	3.01	1.48		
706	2.63	1.48	8.5	287
711	3.42	1.73		
716	3.42	1.84		
721	3.56	2.17		
726	3.47	1.85		
731	3.02	1.62		
736	3.17	2.04		
741	2.9	1.52	9.1	309
746	3.28	1.8		
751	3.15	1.86		
756	3.09	1.37		
761	2.92	0.9		
766	2.75	1.26		
771	2.7	1.45		
776	2.82	2.02	9.3	331
781	2.7	1.39		

ODP SITE 1087

Depth (cm)	$\delta^{18}O$ *C. wuellerstorfi* (‰)	$\delta^{18}O$ G. inflata (‰)	Isotope Event	Age (kyr)
786	3.54	1.6		
791		1.93		
796	3.11	1.34		
801	3.58	1.75		
806				
811				
816				
821				
826				
831				
836				
840	3.52	1.82		
843	3.6	1.56		
846	3.51	1.55		
851				
856	3.33	2.32		
861	3.45	1.66		
866	3.56	2		
871	3.02	1.79		
876	3.53	1.61		
881	3.3	1.41		
886	2.86	1.45		
891	3.4	1.5		
896	3.28	1.47		
901	3.08	1.42		
906	3.75	1.47	10.4	357
911	3.62	1.37		
916		1.62		
921	3.4	1.47	11	632
926	3.06	1.52		
931	3.5	1.54		
936	3.05	1.61		
941	3.09	1.66		
946	3.02	1.4		
951	2.94	1.31		
956	3.15	1.92		
961	3.17	1.78		
966	2.88	1.43		
971	3.02	1.32		
976	2.99	1.35		
981	2.81	1.24		
986	2.73	1.2		
991		1.1		
996	3.16	1.05		
1001	2.63	1.16		
1006	2.8	1.14		
1011	2.5	1.95		
1016	2.6	0.9		
1021	2.69	0.96		
1026	2.37	1.08		
1031		0.97		
1036	2.76	1.11		

ODP SITE 1087

Depth (cm)	$\delta^{18}O$ *C. wuellerstorfi* (‰)	$\delta^{18}O$ G. inflata (‰)	Isotope Event	Age (kyr)
1041	2.43	1.34		
1046	2.66	0.9		
1051	2.19	1.1		
1056	2.59	1.14		
1061	2.7	1.16		
1066	2.45	1.12		
1071	2.67	1.15		
1076	2.49	1.23		
1081	2.6	1.14		
1086	2.89	1.91		
1091	2.46	1.58		
1096	2.51			
1101	2.83	1.63		
1106	2.81	1.64		
1111	3.3	1.57		
1116	2.4	1.35		
1121				
1126	3.01	2.07		
1131	3.12	1.81		
1136	3.35	1.52		
1141		1.65		
1146	2.98	1.65		
1151	3.3	1.5	12	423
1156	3.26	2.3		
1161	3.9	2.01		
1166	3.71	2.23		
1171	3.59	1.96		
1176	3.67	2.11		
1181	3.53	2.27		
1186	3.66	2.55		
1191	3.95	2.96		
1196	3.73	3.17		
1201	3.94	2.72	12.2	434/453
1206	4.09	2.62		
1211		3.05		
1216	4.13	3.04		
1221	4.01	2.92		
1226	4.02	2.53	12.4	471/468
1231	4.27	2.4		
1236	4.21	2.21		
1241		2.34	13	478
1246	3.97	2.51		
1251	3.43	1.86		
1256	3.98	2.02		
1270	3.74	1.56		
1276	3.69	1.44		
1281	3.68	1.51		
1286		2.15		
1290	3.73	1.76		
1295	3.67	1.7		
1300	3.7	1.65		

CORE MD962084 (OLIFANTS RIVER SLOPE)

Depth (cm)	δ^{18}O G. inflata (‰)	Isotope Event	Age (kyr)
2.5		0	0
10.5	1.328		
20.5	1.300		
30.5	1.377		
40.5	1.406		
50.5	1.294		
60.5	1.415		
70.5	1.326		
80.5	1.510		
90.5	1.012		
100.5	1.259		
110.5	1.759	2	11.5
120.5	1.753		
130.5	1.602		
140.5	1.529		
150.5	1.654		
160.5	1.677		
170.5	1.376		
180.5	1.996		
190.5	2.046		
200.5	2.132		
210.5	2.419	2.2	18
220.5	2.407		
230.5	1.812		
240.5	1.758		
250.5	1.653	3.3	52
260.5	1.756		
270.5	2.146		
280.5	2.177		
290.5	2.029		
300.5			
310.5	2.026		
320.5	2.466	4.2	62
330.5	2.241		
340.5	2.007		
350.5	1.888		
360.5	1.957		
370.5	1.916		
380.5	2.031		
390.5	2.014		
400.5	1.900		
410.5	1.961		
420.5	2.124		
430.5	1.733		
440.5	1.868		
450.5	1.932		
460.5	1.618		
470.5	1.947		
480.5	1.633		
490.5	1.708		
500.5	1.814		

CORE MD962084 (OLIFANTS RIVER SLOPE)

Depth (cm)	δ^{18}O G. inflata (‰)	Isotope Event	Age (kyr)
510.5	1.787		
520.5	1.743		
530.5	1.486	5.1	79.5
540.5			
550.5	1.500		
560.5	1.584		
570.5			
580.5			
590.5	1.569		
600.5	1.494		
610.5	1.557		
620.5	1.355	5.3	98
630.5	1.566		
640.5	1.470		
650.5	1.417		
660.5	1.476		
670.5	1.242		
680.5	1.062		
690.5	1.139		
700.5	1.038	5.5	122
710.5	1.100		
720.5	1.639		
730.5	1.895	6/5	127
740.5	2.154		
750.5	2.371		
760.5	2.617	6.2	134
770.5	1.981		
780.5	2.641		
790.5	1.840		
800.5	2.167		
810.5	2.413	6.6	182
820.5	2.201		
830.5	1.643		
840.5	1.458		
850.5	1.555		
860.5	1.434		
870.5	1.357	7.1	194
880.5	1.738		
890.5	1.512		
900.5	1.281	7.3	214
910.5	1.332		
920.5	1.436		
930.5	1.546		
940.5	1.801		
950.5	1.922		
960.5	1.882		
970.5	1.933		
980.5	1.558		
990.5	1.630		
1000.5	1.407	7.5	237
1010.5	1.440		
1020.5	1.883		

CORE MD962084 (OLIFANTS RIVER SLOPE)

Depth (cm)	$\delta^{18}O$ G. inflata (‰)	Isotope Event	Age (kyr)
1030.5	2.080		
1040.5	2.419		
1050.5	2.511		
1060.5	2.575	8.2	248.5
1070.5	2.087		
1080.5	2.131	8.3	257
1090.5	2.303		
1100.5	2.212		
1110.5	1.894		
1120.5	2.220		
1130.5	1.874		
1140.5	1.630		
1150.5	1.609	8.5	287
1160.5	1.861		
1170.5	1.962		
1180.5	2.218		
1190.5	1.955		
1200.5	2.095		
1210.5	2.164		
1220.5	2.414	8.6	297
1230.5	2.016		
1240.5	2.396		
1250.5	1.693	9.1	309
1260.5	1.746		
1270.5	1.889		
1280.5	1.882	9.2	315
1290.5	1.773		
1300.5	1.849		
1310.5	1.695		
1320.5	1.603		
1330.5	1.568		
1340.5	1.697		
1350.5	1.729		
1360.5	1.597		
1370.5	1.368		
1380.5	1.240		
1390.5	1.152	9.3	329.5
1400.5	1.267		
1410.5	1.289		
1420.5	1.794		
1430.5	2.111		
1440.5	2.360		
1450.5	2.723	10.2	340.5
1460.5	2.257	10.3	349
1470.5	2.306		
1480.5	2.525		
1490.5	2.664	10.4	357
1500.5	2.391		
1510.5	2.725		
1520.5	2.655		
1530.5	2.709		
1540.5	2.371		

CORE MD962084 (OLIFANTS RIVER SLOPE)

Depth (cm)	$\delta^{18}O$ G. inflata (‰)	Isotope Event	Age (kyr)
1550.5	2.531		
1560.5	2.492		
1570.5	2.849		
1580.5	1.839		
1590.5	2.017		
1600.5	1.953		
1610.5	2.013		
1620.5	1.766	11.1	368.5
1630.5	1.963		
1640.5	2.627		
1650.5	1.954		
1660.5	2.234		
1670.5	1.841		
1680.5	1.871		
1690.5	1.499		
1700.5	1.746		
1710.5	1.635		
1720.5			
1730.5	1.680		
1740.5	1.564	11.3	405.5
1750.5	1.726		
1760.5	1.454		
1770.5	1.558		
1780.5	1.543		
1790.5	1.816		
1800.5	1.790		
1810.5	1.784		
1820.5	2.073		
1830.5	1.911		
1840.5	1.897		
1850.5	2.055		
1860.5	2.146		
1870.5	2.326		
1880.5	2.235		
1890.5	2.648		
1900.5	3.046	12.2	434
1910.5	2.855		
1920.5	2.505		
1930.5	2.398		
1940.5			
1950.5			
1960.5	2.260		
1970.5	2.349		
1980.5	2.449	12.33	460
1990.5	1.717		
2000.5	2.016		
2010.5	1.912		
2020.5	2.207		
2030.5	1.723		
2040.5	1.724		
2050.5	1.700		
2060.5	1.398	13.11	481

CORE MD962084 (OLIFANTS RIVER SLOPE)

Depth (cm)	$\delta^{18}O$ G. inflata (‰)	Isotope Event	Age (kyr)
2070.5	1.760		
2080.5	1.959		
2090.5	1.797		
2100.5	1.542		
2110.5	1.557		
2120.5	2.215		
2130.5	1.951		
2140.5	2.045		
2150.5	2.095		
2160.5	1.677	13.3	523
2170.5	1.902		
2180.5	2.151	14/13	527
2190.5	2.175		
2200.5	2.504	14.2	538
2210.5	2.306		
2220.5	2.428		
2230.5	2.592	14.4	563
2240.5	2.448		
2250.5	2.401	15/14	567
2260.5	2.359		
2270.5	2.328		
2280.5	2.187		
2290.5	2.024	15.5	616
2300.5	2.187		
2310.5	2.470		
2320.5	2.404		
2330.5	2.969		
2340.5	2.803		
2350.5	2.971		
2360.5	3.286	16.2	628
2370.5	3.040		
2380.5	2.491		
2390.5	2.636		
2400.5	1.895		
2410.5	1.812		
2420.5	2.663		
2430.5	2.602		
2440.5	2.756		
2450.5	2.511		
2460.5	1.915	17.1	667
2470.5	2.092		
2480.5	2.062		
2490.5	2.328		
2500.5	2.002		
2510.5	1.841		
2520.5	1.828		
2530.5	1.562		
2540.5	1.416	17.3	688.5
2550.5	1.870		
2560.5	1.813		
2570.5	2.133		
2580.5	2.290		

CORE MD962084 (OLIFANTS RIVER SLOPE)

Depth (cm)	$\delta^{18}O$ G. inflata (‰)	Isotope Event	Age (kyr)
2590.5	2.059		
2600.5	1.780		
2610.5	2.285		
2620.5	1.867		
2630.5	2.112		
2640.5			
2650.5	1.766		
2660.5	2.041		
2670.5			
2680.5	2.036		
2690.5	2.117		
2700.5	1.574		
2710.5	1.617		
2720.5	1.449	19.3	782
2730.5			
2740.5	1.743		
2750.5			
2760.5	2.958		
2770.5	2.816		
2780.5	3.477	20.2	793
2790.5	3.191		
2800.5	3.028		
2810.5	2.897		
2820.5	2.807		
2830.5	2.891		
2840.5	2.775		
2850.5	2.521		
2860.5	2.301		
2870.5	2.538		
2880.5	2.352		
2890.5	2.370		
2900.5	2.377		
2910.5	1.908		
2920.5	2.128		
2930.5	1.717	21.1	820
2940.5	2.066		
2950.5	1.952		
2960.5	2.258		
2970.5	2.427		
2980.5	1.994		
2990.5	1.784		
3000.5	1.577	21.3	838

APPENDIX 2

SEDIMENTATION RATES
and
BULK MASS ACCUMULATION RATES

CORE MD962080 (AGULHAS BANK SLOPE)

Depth (cm)	Age (kyr)	Sedimentation Rate (cm/kyr)	Dry Bulk Density (g/cc)	BMAR (g/cm^2/kyr)
2.5	1	2.658	0.993	2.640
10.5	4	2.658	1.022	2.717
20.5	8	2.658	1.158	3.078
30.5	11	2.658	1.157	3.075
40.5	15	2.658	1.173	3.117
50.5	19	2.658	1.072	2.848
60.5	21	5.455	1.062	5.795
70.5	23	5.455	1.099	5.997
80.5	24	5.455	1.080	5.894
90.5	26	5.455	1.081	5.898
100.5	28	5.455	1.069	5.832
110.5	30	5.455	1.075	5.865
120.5	43	1.739		
130.5	46	1.739		
140.5	50	1.739		
150.5	53	1.739		
160.5	56	1.143		
170.5	59	1.143	1.125	1.286
180.5	62	1.143	1.150	1.314
190.5	65	1.143	1.170	1.337
200.5	76	0.882	1.119	0.987
210.5	88	0.882	1.102	0.972
220.5	99	0.882	1.090	0.962
230.5	103	1.304	1.087	1.418
240.5	107	1.304	1.082	1.411
250.5	122	1.304	1.056	1.377
260.5	124	3.846	1.033	3.973
270.5	125	3.846	1.011	3.888
280.5	127	3.846	1.170	4.502
290.5	131	3.846	1.157	4.449
300.5	135	3.846	1.100	4.230
310.5	138	3.750	1.074	4.029
320.5	140	3.750	1.149	4.310
330.5	143	3.750	1.098	4.119
340.5	146	3.750	1.085	4.068
350.5	148	3.750	1.036	3.885
360.5	151	3.750	1.056	3.962
370.5	155	1.935	1.146	2.219
380.5	161	1.935	1.090	2.111
390.5	166	1.935	1.045	2.023
400.5	171	1.935	1.084	2.097
410.5	177	1.935	1.095	2.119
420.5	182	1.935	1.152	2.230
430.5	183	1.250	1.170	1.463
440.5	187	1.250	1.149	1.436
450.5	190	1.250	1.131	1.413
460.5	194	1.250	1.133	1.416
470.5	209	1.250	1.119	1.399
480.5	223	1.250	1.118	1.398
490.5	238	1.250	1.156	1.445

CORE MD962080 (AGULHAS BANK SLOPE)

Depth (cm)	Age (kyr)	Sedimentation Rate (cm/kyr)	Dry Bulk Density (g/cc)	BMAR (g/cm^2/kyr)
500.5	241	3.000	1.158	3.473
510.5	244	3.000	1.285	3.856
520.5	248	3.000	1.229	3.688
530.5	250	4.444	1.208	5.367
540.5	252	4.444	1.209	5.374
550.5	255	4.444	1.207	5.364
560.5	257	4.444	1.128	5.011
570.5	259	4.444	1.118	4.967
580.5	261	4.444	1.183	5.259
590.5	264	4.444	1.265	5.622
600.5	266	4.444	1.275	5.666
610.5	273	2.093	1.290	2.699
620.5	280	2.093	1.271	2.660
630.5	287	2.093	1.231	2.576
640.5	290	2.093	1.245	2.606
650.5	292	2.093	1.211	2.535
660.5	295	2.093	1.214	2.541
670.5	300	2.093	1.244	2.603
680.5	304	2.093	1.224	2.561
690.5	309	2.093	1.185	2.480
700.5	312	2.105	1.233	2.597
710.5	315	2.105	1.114	2.346
720.5	321	2.105	1.156	2.434
730.5	328	2.105	1.172	2.467
740.5	331	3.333	1.198	3.995
750.5	334	3.333	1.244	4.146
760.5	337	3.333		
770.5	340	3.333		
780.5	343	3.103	1.154	3.581
790.5	346	3.103	1.176	3.648
800.5	350	3.103	1.198	3.717
810.5	353	3.103	1.253	3.887
820.5	356	3.103	1.144	3.550
830.5	359	3.103	1.269	3.938
840.5	363	3.103	1.242	3.856
850.5	366	3.103	1.282	3.980
860.5	369	3.103	1.246	3.868
870.5	374	1.351	1.228	1.659
880.5	379	1.351	1.255	1.696
890.5	384	1.351	1.259	1.701
900.5	390	1.351	1.234	1.668
910.5	406	1.351	1.225	1.655
920.5	409	2.500	1.190	2.975
930.5	411	2.500	1.205	3.012
940.5	414	2.500	1.162	2.906
950.5	419	2.500	1.272	3.180
960.5	424	2.500	1.273	3.183
970.5	429	2.500		
980.5	434	2.500		
990.5	446	0.833	1.153	0.961
1000.5	458	0.833	1.212	1.010

CORE MD962080 (AGULHAS BANK SLOPE)

Depth (cm)	Age (kyr)	Sedimentation Rate (cm/kyr)	Dry Bulk Density (g/cc)	BMAR (g/cm^2/kyr)
1010.5	466	1.304	1.266	1.651
1020.5	473	1.304	1.303	1.699
1030.5	481	1.304	1.304	1.701
1040.5	491	1.053	1.302	1.370
1050.5	500	1.053	1.231	1.296
1060.5	512	0.833	1.251	1.042
1070.5	524	0.833	1.246	1.038
1080.5	527	3.333	1.322	4.407
1090.5	530	3.333	1.332	4.440
1100.5	533	3.333	1.285	4.283
1110.5	536	3.333	1.306	4.353
1120.5	548	0.811	1.307	1.060
1130.5	561	0.811	1.225	0.994
1140.5	573	0.811	1.272	1.031
1150.5	582	1.111	1.213	1.348
1160.5	594	0.833	1.277	1.064
1170.5	604	1.000	1.312	1.312
1180.5	615	0.909	1.273	1.157
1190.5	621	1.538	1.235	1.900
1200.5	628	1.538	1.249	1.922
1210.5	633	2.143	1.225	2.625
1220.5	637	2.143	1.248	2.675
1230.5	642	2.143	1.234	2.644
1240.5	654	0.833	1.244	1.036
1250.5	666	0.833	1.279	1.066
1260.5	673	1.364	1.261	1.720
1270.5	681	1.364	1.229	1.676
1280.5	688	1.364	1.214	1.655
1290.5	699	0.909	1.193	1.084
1300.5	703	2.222	1.283	2.851
1310.5	708	2.222	1.228	2.730
1320.5	711	4.000	1.223	4.892
1330.5	713	4.000	1.240	4.962
1340.5	716	4.000	1.271	5.085
1350.5	718	4.000	1.237	4.947
1360.5	736	0.556	1.277	0.709
1370.5	754	0.556	1.200	0.667
1380.5	759	1.818	1.263	2.296
1390.5	765	1.818	1.237	2.248
1400.5	769	2.353	1.287	3.029
1410.5	774	2.353	1.278	3.006
1420.5	778	2.353	1.216	2.860
1430.5	782	2.353	1.174	2.763
1440.5	788	1.205	1.142	1.376
1450.5	790	1.205	1.260	1.518
1460.5	799	1.205	1.184	1.427
1470.5	807	1.205	1.161	1.399
1480.5	815	1.205	1.175	1.416
1490.5	824	1.205	1.200	1.446
1500.5	835	1.205	1.102	1.327

CORE MD962084 (OLIFANTS RIVER SLOPE)

Depth (cm)	Age (kyr)	Sedimentation Rate (cm/kyr)	Dry Bulk Density (g/cc)	BMAR (g/cm^2/kyr)
2	0.50	9.565	1.534	14.670
10.5	1.05	9.565	1.589	15.200
20.5	2.09	9.565	1.532	14.655
30.5	3.14	9.565	1.592	15.228
40.5	4.18	9.565	1.569	15.012
50.5	5.23	9.565	1.559	14.914
60.5	6.27	9.565	1.652	15.798
70.5	7.32	9.565	1.670	15.970
80.5	8.36	9.565	1.704	16.304
90.5	9.41	9.565	1.669	15.960
100.5	10.45	9.565	1.652	15.800
110.5	11.50	15.385	1.644	25.298
120.5	12.15	15.385	1.648	25.352
130.5	12.80	15.385	1.602	24.652
140.5	13.45	15.385	1.592	24.493
150.5	14.10	15.385	1.634	25.136
160.5	14.75	15.385	1.669	25.680
170.5	15.40	15.385	1.685	25.930
180.5	16.05	15.385	1.673	25.740
190.5	16.70	15.385	1.707	26.258
200.5	17.35	15.385	1.678	25.821
210.5	18.00	1.176	1.709	2.010
220.5	26.50	1.176	1.634	1.923
230.5	35.00	1.176	1.605	1.888
240.5	43.50	1.176	1.641	1.931
250.5	52.00	7.000	1.618	11.327
260.5	53.43	7.000	1.615	11.307
270.5	54.86	7.000	1.657	11.602
280.5	56.29	7.000	1.644	11.507
290.5	57.71	7.000	1.649	11.542
300.5	59.14	7.000	1.668	11.673
310.5	60.57	7.000	1.650	11.547
320.5	62.00	12.000	1.673	20.071
330.5	62.83	12.000	1.660	19.924
340.5	63.67	12.000	1.665	19.976
350.5	64.50	12.000	1.673	20.074
360.5	65.33	12.000	1.685	20.214
370.5	66.17	12.000	1.685	20.222
380.5	67.00	12.000	1.716	20.597
390.5	67.83	12.000	1.699	20.389
400.5	68.67	12.000	1.693	20.319
410.5	69.50	12.000	1.685	20.217
420.5	70.33	12.000	1.716	20.596
430.5	71.17	12.000	1.674	20.094
440.5	72.00	12.000	1.679	20.148
450.5	72.83	12.000	1.698	20.377
460.5	73.67	12.000	1.698	20.373
470.5	74.50	12.000	1.706	20.478
480.5	75.33	12.000	1.755	21.057
490.5	76.17	12.000	1.773	21.282

CORE MD962084 (OLIFANTS RIVER SLOPE)

Depth (cm)	Age (kyr)	Sedimentation Rate (cm/kyr)	Dry Bulk Density (g/cc)	BMAR (g/cm^2/kyr)
500.5	77.00	12.000	1.750	21.002
510.5	77.83	12.000	1.741	20.895
520.5	78.67	12.000	1.729	20.749
530.5	79.50	4.865	1.728	8.406
540.5	81.56	4.865	1.719	8.362
550.5	83.61	4.865		
560.5	85.67	4.865		
570.5	87.72	4.865		
580.5	89.78	4.865	1.688	8.212
590.5	91.83	4.865	1.708	8.310
600.5	93.89	4.865	1.764	8.583
610.5	95.94	4.865	1.710	8.319
620.5	98.00	3.333	1.710	5.701
630.5	101.00	3.333	1.699	5.665
640.5	104.00	3.333	1.697	5.657
650.5	107.00	3.333	1.696	5.655
660.5	110.00	3.333	1.708	5.695
670.5	113.00	3.333	1.739	5.798
680.5	116.00	3.333	1.701	5.671
690.5	119.00	3.333	1.679	5.597
700.5	122.00	6.000	1.681	10.086
710.5	123.67	6.000	1.745	10.470
720.5	125.33	6.000	1.716	10.295
730.5	127.00	4.286	1.742	7.468
740.5	129.33	4.286	1.727	7.401
750.5	131.67	4.286	1.714	7.347
760.5	134.00	1.042	1.714	1.786
770.5	143.60	1.042	1.722	1.794
780.5	153.20	1.042	1.715	1.787
790.5	162.80	1.042	1.740	1.813
800.5	172.40	1.042	1.751	1.824
810.5	182.00	5.000	1.755	8.773
820.5	184.00	5.000	1.760	8.801
830.5	186.00	5.000	1.768	8.840
840.5	188.00	5.000	1.767	8.833
850.5	190.00	5.000	1.743	8.717
860.5	192.00	5.000	1.747	8.736
870.5	194.00	1.500	1.696	2.544
880.5	200.67	1.500	1.713	2.570
890.5	207.33	1.500	1.691	2.537
900.5	214.00	4.348	1.709	7.432
910.5	216.30	4.348	1.748	7.601
920.5	218.60	4.348	1.779	7.733
930.5	220.90	4.348	1.770	7.697
940.5	223.20	4.348	1.743	7.580
950.5	225.50	4.348	1.761	7.655
960.5	227.80	4.348	1.701	7.398
970.5	230.10	4.348	1.710	7.435
980.5	232.40	4.348	1.703	7.404
990.5	234.70	4.348	1.723	7.491
1000.5	237.00	5.217	1.730	9.028

CORE MD962084 (OLIFANTS RIVER SLOPE)

Depth (cm)	Age (kyr)	Sedimentation Rate (cm/kyr)	Dry Bulk Density (g/cc)	BMAR (g/cm^2/kyr)
1010.5	238.92	5.217	1.731	9.029
1020.5	240.83	5.217	1.719	8.967
1030.5	242.75	5.217	1.718	8.963
1040.5	244.67	5.217	1.705	8.895
1050.5	246.58	5.217	1.723	8.987
1060.5	248.50	2.353	1.737	4.087
1070.5	252.78	2.353	1.771	4.167
1080.5	257.00	2.333	1.727	4.030
1090.5	261.29	2.333	1.770	4.130
1100.5	265.57	2.333	1.767	4.123
1110.5	269.86	2.333	1.764	4.117
1120.5	274.14	2.333	1.751	4.086
1130.5	278.43	2.333	1.750	4.084
1140.5	282.71	2.333	1.764	4.115
1150.5	287.00	7.000	1.766	12.359
1160.5	288.43	7.000	1.831	12.818
1170.5	289.86	7.000	1.781	12.469
1180.5	291.29	7.000	1.771	12.400
1190.5	292.71	7.000	1.775	12.424
1200.5	294.14	7.000	1.747	12.231
1210.5	295.57	7.000	1.759	12.316
1220.5	297.00	2.500	1.727	4.318
1230.5	301.00	2.500	1.712	4.280
1240.5	305.00	2.500	1.725	4.311
1250.5	309.00	5.000	1.741	8.703
1260.5	311.00	5.000	1.720	8.601
1270.5	313.00	5.000	1.711	8.554
1280.5	315.00	7.586	1.713	12.997
1290.5	316.32	7.586	1.720	13.047
1300.5	317.64	7.586	1.733	13.149
1310.5	318.95	7.586	1.679	12.741
1320.5	320.27	7.586	1.750	13.279
1330.5	321.59	7.586	1.716	13.020
1340.5	322.91	7.586	1.658	12.579
1350.5	324.23	7.586	1.729	13.118
1360.5	325.55	7.586	1.741	13.207
1370.5	326.86	7.586	1.751	13.286
1380.5	328.18	7.586	1.738	13.188
1390.5	329.50	5.455	1.717	9.366
1400.5	331.33	5.455	1.723	9.397
1410.5	333.17	5.455	1.764	9.624
1420.5	335.00	5.455	1.803	9.832
1430.5	336.83	5.455	1.780	9.711
1440.5	338.67	5.455	1.760	9.600
1450.5	340.50	1.176	1.809	2.129
1460.5	349.00	3.750	1.828	6.857
1470.5	351.67	3.750	1.800	6.751
1480.5	354.33	3.750	1.728	6.481
1490.5	357.00	11.304	1.730	19.552
1500.5	357.88	11.304	1.760	19.899
1510.5	358.77	11.304	1.748	19.756

CORE MD962084 (OLIFANTS RIVER SLOPE)

Depth (cm)	Age (kyr)	Sedimentation Rate (cm/kyr)	Dry Bulk Density (g/cc)	BMAR (g/cm^2/kyr)
1520.5	359.65	11.304	1.729	19.542
1530.5	360.54	11.304	1.701	19.233
1540.5	361.42	11.304	1.705	19.274
1550.5	362.31	11.304	1.706	19.280
1560.5	363.19	11.304	1.714	19.374
1570.5	364.08	11.304	1.718	19.423
1580.5	364.96	11.304	1.701	19.229
1590.5	365.85	11.304	1.717	19.408
1600.5	366.73	11.304	1.743	19.701
1610.5	367.62	11.304	1.726	19.509
1620.5	368.50	3.243	1.737	5.633
1630.5	371.58	3.243	1.722	5.586
1640.5	374.67	3.243	1.728	5.603
1650.5	377.75	3.243	1.724	5.590
1660.5	380.83	3.243	1.718	5.573
1670.5	383.92	3.243	1.709	5.542
1680.5	387.00	3.243	1.702	5.520
1690.5	390.08	3.243	1.707	5.538
1700.5	393.17	3.243	1.719	5.575
1710.5	396.25	3.243	1.708	5.540
1720.5	399.33	3.243	1.732	5.616
1730.5	402.42	3.243	1.736	5.630
1740.5	405.50	5.614	1.742	9.781
1750.5	407.28	5.614	1.743	9.784
1760.5	409.06	5.614	1.713	9.615
1770.5	410.84	5.614	1.706	9.576
1780.5	412.63	5.614	1.709	9.595
1790.5	414.41	5.614	1.709	9.592
1800.5	416.19	5.614	1.707	9.585
1810.5	417.97	5.614	1.721	9.663
1820.5	419.75	5.614	1.716	9.636
1830.5	421.53	5.614	1.735	9.739
1840.5	423.31	5.614	1.745	9.799
1850.5	425.09	5.614	1.744	9.790
1860.5	426.88	5.614	1.734	9.737
1870.5	428.66	5.614	1.751	9.830
1880.5	430.44	5.614	1.741	9.775
1890.5	432.00	5.614	1.786	10.026
1900.5	434.00	5.614	1.787	10.032
1910.5	437.25	3.077	1.789	5.505
1920.5	440.50	3.077	1.808	5.564
1930.5	443.75	3.077	1.834	5.642
1940.5	447.00	3.077	1.821	5.602
1950.5	450.25	3.077	1.862	5.731
1960.5	453.50	3.077	1.854	5.705
1970.5	456.75	3.077	1.814	5.581
1980.5	460.00	3.077	1.778	5.471
1990.5	462.63	3.810	1.782	6.788
2000.5	465.25	3.810	1.793	6.829
2010.5	467.88	3.810	1.752	6.675
2020.5	470.50	3.810	1.782	6.789

CORE MD962084 (OLIFANTS RIVER SLOPE)

Depth (cm)	Age (kyr)	Sedimentation Rate (cm/kyr)	Dry Bulk Density (g/cc)	BMAR (g/cm^2/kyr)
2030.5	473.13	3.810	1.767	6.731
2040.5	475.75	3.810	1.772	6.752
2050.5	478.38	3.810	1.761	6.710
2060.5	481.00	3.810	1.760	6.706
2070.5	485.20	2.381	1.782	4.242
2080.5	489.40	2.381	1.770	4.214
2090.5	493.60	2.381	1.776	4.229
2100.5	497.80	2.381	1.782	4.242
2110.5	502.00	2.381	1.784	4.249
2120.5	506.20	2.381	1.795	4.274
2130.5	510.40	2.381	1.794	4.271
2140.5	514.60	2.381	1.778	4.233
2150.5	518.80	2.381	1.790	4.261
2160.5	523.00	2.381	1.793	4.269
2170.5	525.00	5.000	1.796	8.979
2180.5	527.00	5.000	1.796	8.981
2190.5	532.50	1.818	1.801	3.275
2200.5	538.00	1.818	1.776	3.229
2210.5	546.33	1.200	1.782	2.138
2220.5	554.67	1.200	1.780	2.135
2230.5	563.00	1.200	1.759	2.111
2240.5	565.00	5.000	1.768	8.841
2250.5	567.00	5.000	1.780	8.899
2260.5	579.25	0.816	1.784	1.457
2270.5	591.50	0.816	1.777	1.450
2280.5	603.75	0.816	1.795	1.465
2290.5	616.00	0.816	1.779	1.452
2300.5	617.71	5.833	1.783	10.399
2310.5	619.43	5.833	1.840	10.732
2320.5	621.14	5.833	1.838	10.723
2330.5	622.86	5.833	1.827	10.658
2340.5	624.57	5.833	1.808	10.545
2350.5	626.29	5.833	1.824	10.640
2360.5	628.00	5.833	1.799	10.496
2370.5	631.90	2.564	1.815	4.654
2380.5	635.80	2.564	1.793	4.597
2390.5	639.70	2.564	1.754	4.498
2400.5	643.60	2.564	1.783	4.571
2410.5	647.50	2.564	1.774	4.549
2420.5	651.40	2.564	1.800	4.615
2430.5	655.30	2.564	1.774	4.549
2440.5	659.20	2.564	1.774	4.548
2450.5	663.10	2.564	1.788	4.585
2460.5	667.00	2.564	1.777	4.556
2470.5	669.69	3.721	1.811	6.738
2480.5	672.38	3.721	1.803	6.710
2490.5	675.06	3.721	1.796	6.683
2500.5	677.75	3.721	1.788	6.652
2510.5	680.44	3.721	1.774	6.599
2520.5	683.13	3.721	1.777	6.610
2530.5	685.81	3.721	1.782	6.631

CORE MD962084 (OLIFANTS RIVER SLOPE)

Depth (cm)	Age (kyr)	Sedimentation Rate (cm/kyr)	Dry Bulk Density (g/cc)	BMAR (g/cm^2/kyr)
2540.5	688.50	3.721	1.787	6.650
2550.5	693.69	1.925	1.838	3.538
2560.5	698.89	1.925	1.816	3.496
2570.5	704.08	1.925	1.810	3.484
2580.5	709.28	1.925	1.790	3.447
2590.5	714.47	1.925	1.781	3.428
2600.5	719.67	1.925	1.804	3.474
2610.5	724.86	1.925	1.816	3.496
2620.5	730.06	1.925	1.780	3.427
2630.5	735.25	1.925	1.830	3.523
2640.5	740.44	1.925	1.840	3.542
2650.5	745.64	1.925	1.794	3.453
2660.5	750.83	1.925	1.797	3.460
2670.5	756.03	1.925	1.785	3.437
2680.5	761.22	1.925	1.793	3.452
2690.5	766.42	1.925	1.748	3.365
2700.5	771.61	1.925	1.777	3.421
2710.5	776.81	1.925	1.774	3.415
2720.5	782.00	1.925	1.747	3.362
2730.5	783.83	5.455	1.750	9.547
2740.5	785.67	5.455	1.771	9.659
2750.5	787.50	5.455	1.758	9.587
2760.5	789.33	5.455	1.762	9.609
2770.5	791.17	5.455	1.728	9.425
2780.5	793.00	5.455	1.750	9.544
2790.5	794.80	5.556	1.719	9.550
2800.5	796.60	5.556	1.717	9.537
2810.5	798.40	5.556	1.750	9.724
2820.5	800.20	5.556	1.747	9.705
2830.5	802.00	5.556	1.757	9.759
2840.5	803.80	5.556	1.738	9.654
2850.5	805.60	5.556	1.759	9.772
2860.5	807.40	5.556	1.757	9.762
2870.5	809.20	5.556	1.767	9.816
2880.5	811.00	5.556	1.772	9.845
2890.5	812.80	5.556	1.752	9.733
2900.5	814.60	5.556	1.783	9.908
2910.5	816.40	5.556	1.775	9.860
2920.5	818.20	5.556	1.759	9.774
2930.5	820.00	5.556	1.784	9.913
2940.5	822.57	3.889	1.804	7.017
2950.5	825.14	3.889	1.776	6.907
2960.5	827.71	3.889	1.789	6.959
2970.5	830.29	3.889	1.810	7.040
2980.5	832.86	3.889	1.766	6.869
2990.5	835.43	3.889	1.763	6.857

APPENDIX 3

SCANNING ELECTRON MICROGRAPHS OF PLANKTONIC FORAMINIFERA
and
DESCRIPTIONS OF ENVIRONMENTAL CHARACTERISTICS

The scanning electron micrographs shown in the following pages were taken at the South African Museum and the Electron Microscope Unit of the University of Cape Town.

ENVIRONMENTAL CHARACTERISTICS OF INDIVIDUAL FORAMINIFERAL SPECIES

Neogloboquadrina pachyderma (Ehrenberg, 1861)

Neogloboquadrina pachyderma is the best indicator of polar waters (Bé and Tolderlund, 1971) and is the dominant species south of the STC (Hutson, 1980). Also, this species best shows environment-related coiling ratios, with a dominance of four-chambered, sinistrally-coiled morphotypes at high latitudes being replaced by dominantly dextrally-coiled four-chambered forms in Subantarctic latitudes, which in turn are replaced by four-and-a-half-chambered forms in temperate waters (Kennett and Srinivasan, 1983). *N. pachyderma* (sinistrally coiled), whilst low in average abundance, is the cold-water end-member of the faunal assemblage, occurring predominantly in surface waters with temperatures below 9°C in the Pacific Ocean (Bandy, 1972) or below 7.5°C in the North Atlantic (Bé and Hamlin, 1967) or below 5°C (Bé and Hutson, 1977). *N. pachyderma* (dextrally coiled) is indicative of cool (10-18°C) Subantarctic waters with surface-water densities greater than 25.5 kg/m^3 (Hilbrecht, 1996). Juveniles are more common in surface waters (Bé and Hamlin, 1967), whilst adults, with a thicker shell and a reduced final chamber descend deeper (Bé and Tolderlund, 1971). In the Benguela system, *N. pachyderma* (d) prefers the mesotrophic, higher nutrient levels of upwelled filaments (Little *et al.*, 1997). In this study, each morphotype was counted separately and each is expressed relative to the total foraminiferal population.

Turborotalia quinqueloba (Natland, 1938)

The cold-temperate water Subantarctic species, *Turborotalia quinqueloba,* is relatively rare in living plankton, but it is widespread in the sediments (Bé and Hutson, 1977). Kennett and Srinivasan (1983) report it to be abundant in temperate and subtropical sediments from the Indo-Pacific region, whilst Parker (1962) reports its occurrence in the Pacific Ocean between 20°S and 60°S. The optimal occurrence in the plankton is in surface waters at 9 - 10°C and 34.5 psu (practical salinity units) salinity (Bé and Hutson, 1977). This species thrives in water masses with little seasonal variation in salinity, low vertical temperature gradients and no or limited water stratification. Relative abundances in the sediment of > 10% may be indicative of intermediate or deepwater formation (Hilbrecht, 1996).

Neogloboquadrina pachyderma (sinistral)

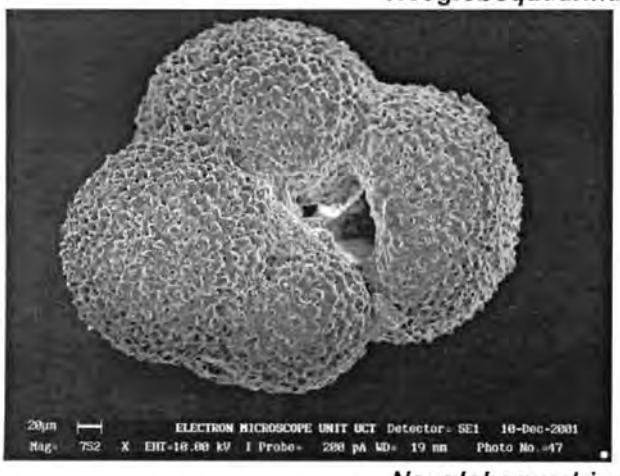

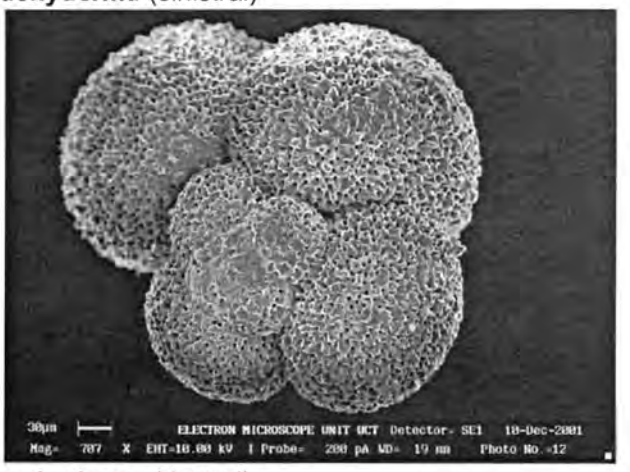

Neogloboquadrina pachyderma (dextral)

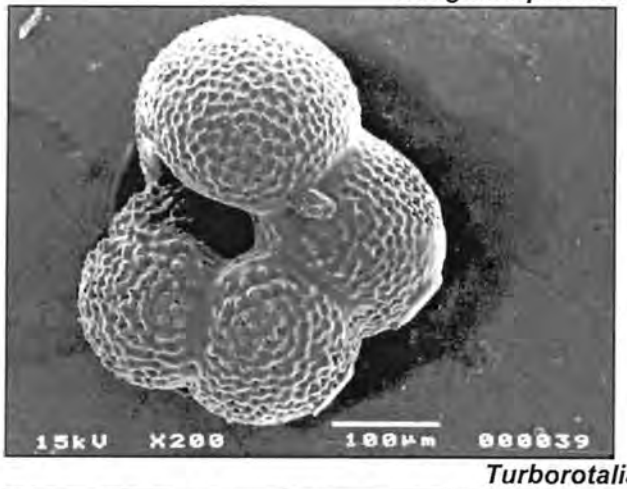

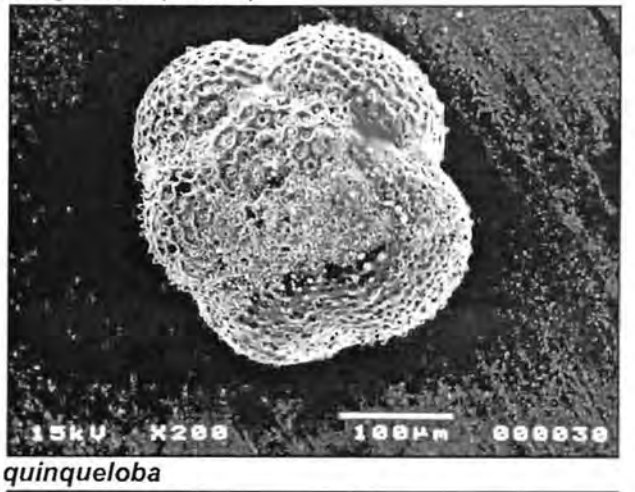

Turborotalia quinqueloba

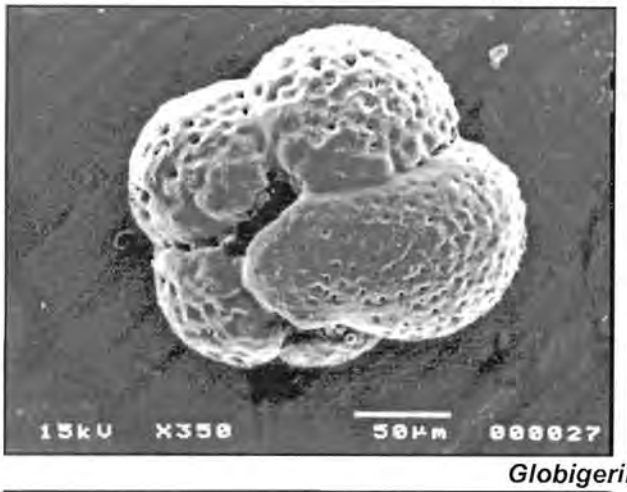

Globigerina bulloides

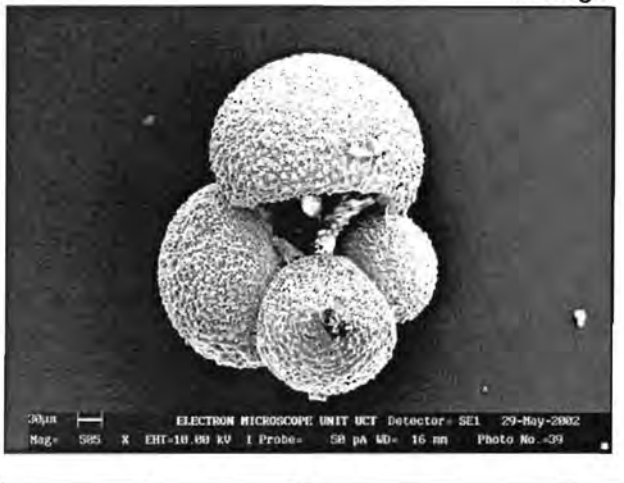

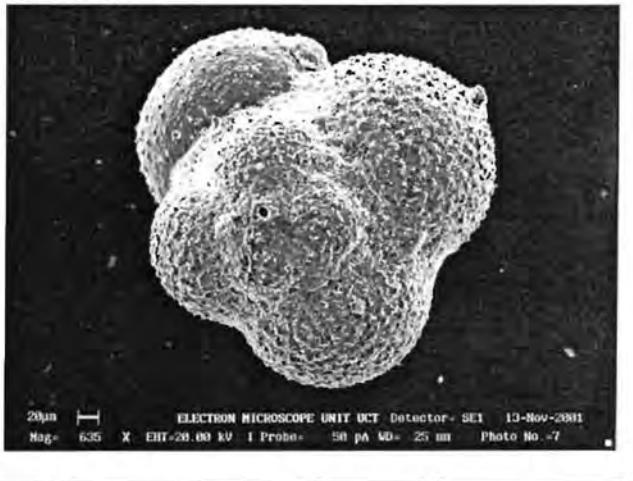

Globigerina bulloides (d'Orbigny, 1826)

Globigerina bulloides is a cold-water species with an optimum temperature and salinity range of 2 - 10°C and 34 – 35 psu respectively (Bé, 1969), although it does tolerate a range of sea-surface temperatures, salinity, temperature gradients and density stratification (Hilbrecht, 1996). It is dominant in Subantarctic to cool subtropical waters (Bé and Tolderlund, 1971), living between 0 and 100 m water depth in the north and equatorial Pacific (Bradshaw, 1959). Bé and Tolderlund (1971) and Bé and Hutson (1977) combined *Gg. falconensis* and *Gg. bulloides* counts in their study of the biogeographic patterns of foraminifera, because the two species show morphological intergradation. They found the species to be a common constituent of the southern transitional zone of the southern Atlantic and Indian Oceans (40°S to 55°S), where mixing of subpolar and subtropical waters occurs, with water temperatures ranging from 0 to 27°C. However, later work (Giraudeau, 1993; Niebler and Gersonde, 1998) indicated that *Gg. falconensis* occurs more frequently in sediments underlying subtropical waters. Therefore, the occurrence of each species is cited individually in this study. Research suggests that *Gg. bulloides* has a preference for productive environments and may be related to the phytoplankton bloom succession (Hilbrecht, 1996). *Gg. bulloides* is common in sediments below the Benguela Current System, preferring waters slightly offshore of the upwelling cells and filaments (Giraudeau, 1993).

Globigerinita glutinata (Egger, 1893)

Globigerinita glutinata is one of the most widespread living species, occurring over a wide range of temperatures and salinity (Bé and Hutson, 1977). There is a distinct bimodal distribution in relative abundance versus most physical parameters (Hilbrecht, 1996). *Ga. glutinata* is equally abundant under warm and cool conditions with peak abundances at sea surface temperatures (SST)of 10°C and 28°C and within a sea surface salinity range of 34 – 37 psu (Hilbrecht, 1996). *Ga. glutinata* is abundant in the sediments of the Arabian Sea and in the Indian Ocean north of 55°S, and is also found along the continental margins of Australia, Tanzania and Madagascar in relatively high abundances (Bé and Hutson, 1977). This species is often abundant adjacent to upwelling zones and may occur in the late stage of the bloom succession and at the margins of productive areas (Hilbrecht, 1996). Thunell and Reynolds (1984) suggest that *Ga. glutinata* is most productive in the surface water when the surface mixed layer is deep and upwelling is increasing. However, the generally cosmopolitan nature of this species does not easily lend itself to reflecting distinctive water masses and climatic variations.

Globorotalia inflata (d'Orbigny, 1839)

Globorotalia inflata is indigenous to and the most abundant species of the Southern Transitional Zone (45 - 35°S) between Subantarctic and Subtropical waters (Bé and Hutson, 1977; Hutson, 1980). *Gr. inflata* has relatively broad tolerances in SST (13 - 20°C), salinity (35 – 36 psu) and temperature at 200m depth (10 - 17°C). It shows a preference for water masses with little seasonal variation in salinity and is abundant under a wider range of physical parameters during summer compared to winter conditions (Hilbrecht, 1996). The present-day foraminiferal assemblage dominated by *Gr. inflata* occurs north of the STC (Hutson, 1980) in surface-water temperatures of , whilst in the Benguela Current peak abundances occur between 15 and 19°C (Bé and Hutson, 1977; Hutson, 1980). An abundance of *Gr. inflata* is indicative of Transitional waters between warm and cool temperate regions, low nutrient content and reduced primary productivity. *Gr. inflata* inhabits offshore regions in the Southern Benguela Region (SBR) as well as the nutrient-poor incursions of Angola Current waters into the northern Benguela region (Little *et al.*, 1997).

Globorotalia truncatulinoides (d'Orbigny, 1839)

Globorotalia truncatulinoides is distinctive of oligotrophic waters with high surface salinity (35.6 psu) and low nutrient content (Bé and Hutson, 1977). Together with *Gr. inflata,* this species defines the transitional faunal zone in the South Atlantic (Bé and Tolderlund, 1971). It occurs over a very broad SST range of 4 - 27°C (Bé and Tolderlund, 1971, Kennett and Srinivasan, 1985) with peak abundance between 17 and 22°C. *Gr. truncatulinoides* is a deep-dwelling species which ascends to shallower depths during its winter reproductive period (Hibrecht, 1996). Hutson (1980) separates the two forms (sinistrally- and dextrally coiled) into Subantarctic and Transitional/Subtropical assemblages, respectively. However, the scarcity of this species in the sediments off southern Africa necessitated a combined presentation of counts in this study. The sinistral variety is most common in Transitional and Subantarctic waters in the South Atlantic (Christison, 1985), and it is the more common variety in both cores examined in this study. The change in relative abundances of the two forms is gradational along environmental gradients (Hilbrecht, 1996).

Globigerinita glutinata

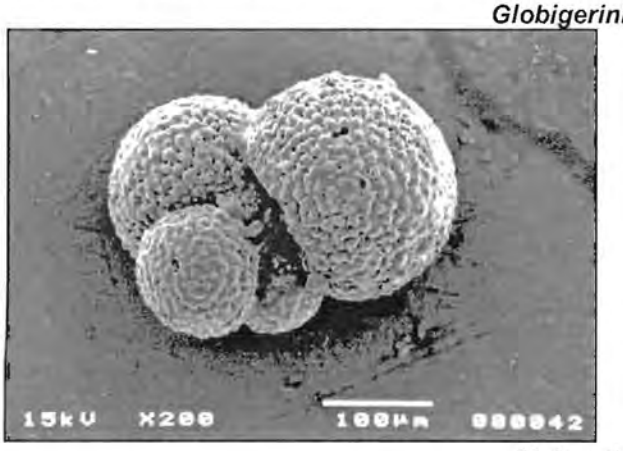

Globorotalia inflata

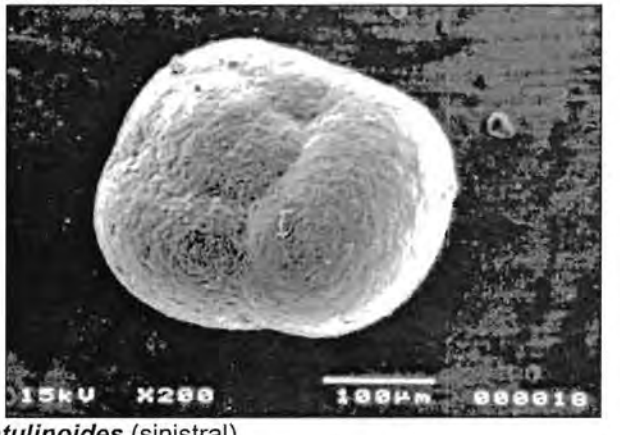

Globorotalia truncatulinoides (sinistral)

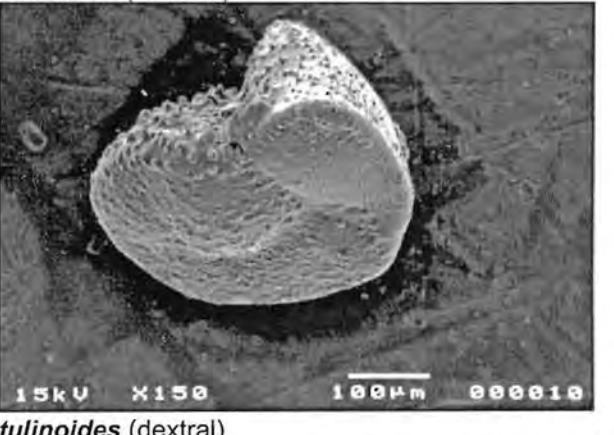

Globorotalia truncatulinoides (dextral)

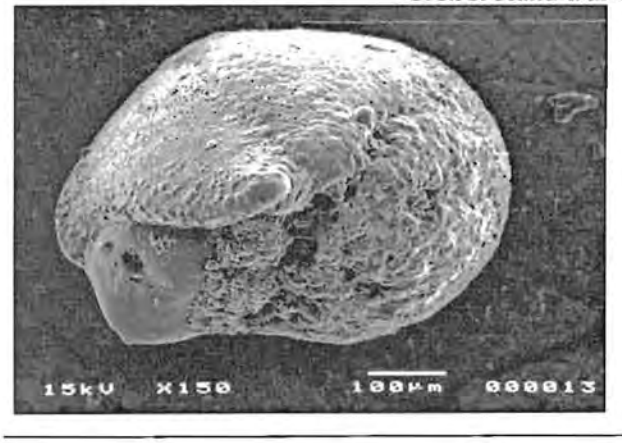

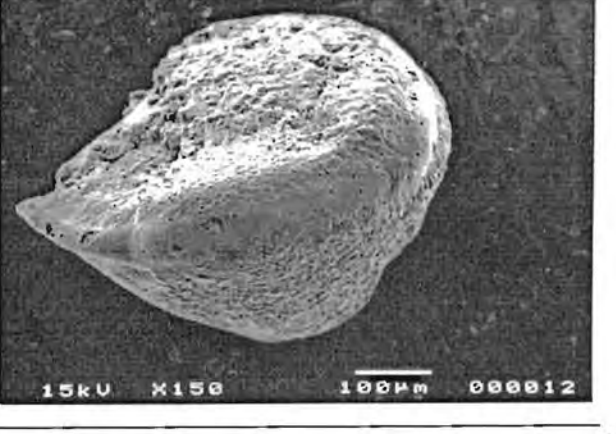

Globorotalia scitula (Brady, 1882)

Globorotalia scitula is a widespread, but sparsely distributed species, associated with cool, deeper waters, >100 m (Bé, 1969). Although *Gr. scitula* occurs in waters with a wide range of SSTs (13 - 25°C) and salinity (34.5 – 36.5 psu), this species shows a preference for areas with low seasonal salinity variation, low vertical temperature and density gradients (Hilbrecht, 1996), and peaks in cooler deeper waters (200 m temperature mean 15°C). This temperate species is found occasionally in plankton tows north of 40°S, but some abnormally high frequencies have been found near the Agulhas Current (Bé and Hutson, 1977).

Globorotalia hirsuta (d'Orbigny, 1839)

The warm-temperate species, *Globorotalia hirsuta*, occurs sparsely in the Southern Transitional Zone between 20 and 43°S (Bé and Hutson, 1977). It has similar ecological requirements to *Gr. truncatulinoides*, living in waters with surface temperatures ranging from 14 - 26°C (Bé and Tolderlund, 1971) and a salinity range of 35.5 – 36.5 psu (Hilbrecht, 1996). Peak abundances in the South Atlantic occur in surface-water temperatures of 17°C (Christison, 1985). The deep-dwelling *Gr. hirsuta* is a good indicator of minimal vertical temperature gradient and stratification, being intolerant of areas where the temperature gradient exceeds 5°C and the density difference between the surface and 200m exceeds 1kg/m^3 in winter (Hilbrecht, 1996). The optimal deep-water temperature range for this species is 10 - 20°C. *Gr. hirsuta* rarely constitutes more than 5% of the planktonic foraminiferal assemblage (Bé and Hutson, 1977).

Globorotalia crassaformis (Galloway and Wissler, 1927)

Gr. crassaformis is associated with cool (200m temperature 15 -18°C), high salinity (35.5 - 36.8 psu) deeper waters (Bé and Hutson, 1977; Hilbrecht, 1996). In adult stages, it lives below the euphotic zone (Bé and Hamlin, 1967), thriving below the seasonal thermocline and deep chlorophyll maximum (Ravelo and Fairbanks, 1992). In the equatorial undercurrent this species occurs as a distinct water mass below the seasonal thermocline (Jones, 1964). The species is widespread, but

Globorotalia scitula

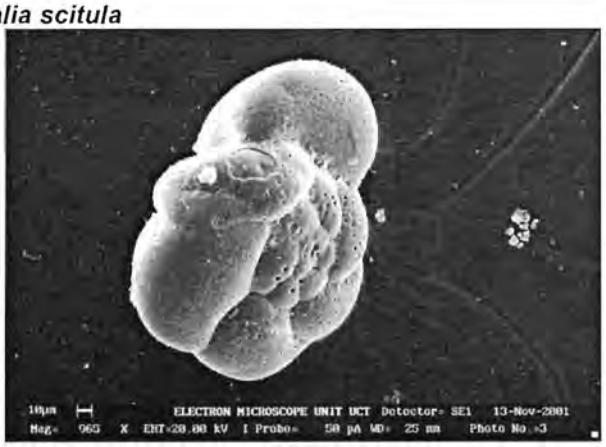

Globorotalia hirsuta

Globorotalia crassaformis

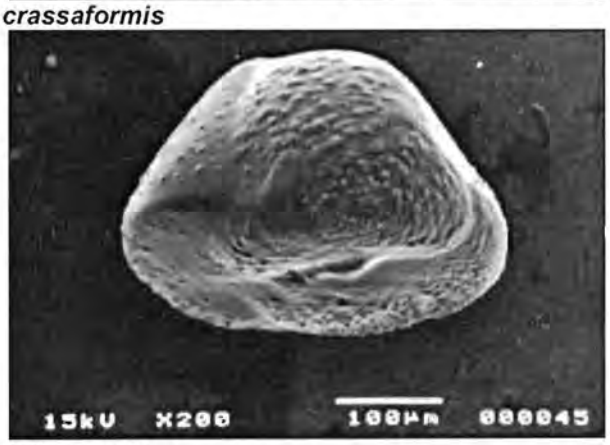

Globigerina falconensis

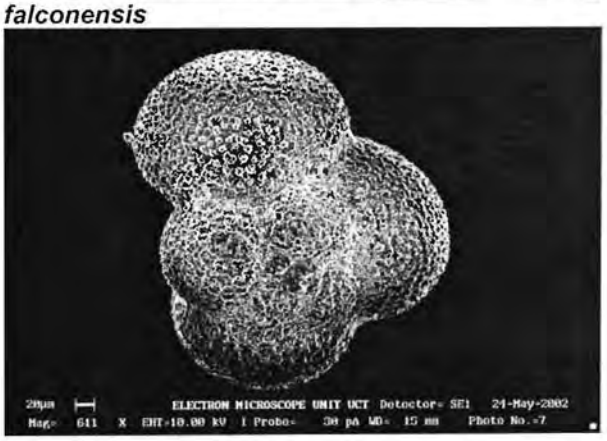

sparse in subtropical and warm-temperate areas. The broad tolerance for warmer surface-water temperatures (mean 20 - 25°C), surface water density, vertical temperature gradients and stratification are similar to the bimodal distributions of *Gg. bulloides* and *Ga. glutinata* and may suggest some relation to seasonal productivity at low latitudes (Hilbrecht, 1996).

Globigerina falconensis (Blow, 1959)

The warm-temperate species, *Gg. falconensis*, is the warmer variation of *Gg. bulloides* and the two species have previously been grouped together on the basis of morphological similarity (e.g. Bé and Tolderlund, 1971; Bé and Hutson, 1977). However, despite the similarity in morphology, the relative abundances of the two species in relation to physical parameters is distinctly different (Hilbrecht, 1996). Distributions of *Gg. falconensis* are skewed towards water masses with increased summer SST (mean 18°C) and salinity (mean 36 psu) (Hilbrecht, 1996), occurring more frequently in sediments underlying subtropical waters (Bé and Hutson, 1977), as compared to the preferred cool water environment of *Gg. bulloides*. In this study, the taxonomic concept described by Malmgren and Kennett (1977) has been used to distinguish *Gg. falconensis* from *Gg. bulloides*. Forms exhibiting a small last chamber with an apertural lip and a small aperture were classified as Gg. falconensis. This species so identified is also smaller overall than *Gg. bulloides*.

Globigerinella calida (Parker, 1962)

Ge. calida occurs over a wide geographical range, but is more common in mid-low latitudes (Saito, Thompson and Breger, 1981), preferring tropical to warm subtropical (Kennett and Srinivasan, 1983) and subtropical to temperate waters of the Pacific Ocean (Saito, Thompson and Breger, 1981). A warm, deeper-water habitat is suggested by the common occurrence of this species in the mixed layer in the Caribbean (Hilbrecht, 1996) and also by the fact that distributions are skewed towards areas with high temperatures at 200 m (15 - 21°C). Optimum surface water conditions are 23 - 28°C and 35 – 36.2 psu salinity (Hilbrecht, 1996).

Neogloboquadrina dutertrei (d'Orbigny, 1839)

The common warm-water species *Neogloboquadrina dutertrei* exhibits a wide biogeographic range of tropical and subtropical environments (Hilbrecht, 1996). It is common in tropical productive environments and is associated with western boundary currents (such as the Agulhas Current) with highest percentages occurring in the sediments of equatorial regions and along continental margins (Bé and Hutson, 1977). Opitmal occurrence is at 23 - 25°C SST and 33 - 35 psu salinity. In contrast to other species with a wide biogeographic range (e.g. *G. truncatulinoides* and *G. bulloides*), *N. dutertrei* is restricted to areas with relatively warm (14 - 18°C) waters at 200m depth (Hilbrecht, 1996). Data from sediment traps from the Panama Basin indicate that there is a pronounced abundance peak in *N. dutertrei* between 25 and 50 m water depth, corresponding to the steep thermocline, area of highest productivity and associated chlorophyll maximum (Thunell and Reynolds, 1984). Some researchers (e.g. Chang *et al.*, 1999) combine this species with the subpolar species *N. pachyderma* (d), citing morphological intergradation. However, in this study, the species are counted separately, based on their environmental preferences. The species name *N. dutertrei* was given to specimens which showed a wide and deep umbilicus and five or more chambers with a charcteristic rosette pattern, as defined by Kennett and Srinivasan (1983). All intergrades (transitional forms with more than four chambers and compact tests without umbilical teeth) were lumped with *N. pachyderma* (d).

Globigerinoides trilobus (Reuss, 1850)

Globigerinoides trilobus is a tropical to temperate species. Stainforth *et al.* (1981) considered *Gs. trilobus* to be an ecological variant of *G. sacculifer*, being less tolerant of cooler waters than the latter. However, Christison (1985) suggests that it is *Gs. trilobus* that favours cooler water and the greater abundance of *Gs. trilobus* relative to *Gs. sacculifer* in this research tends to support this view, as the samples used in this study were taken in Temperate-Transitional waters.

Globigerinella calida

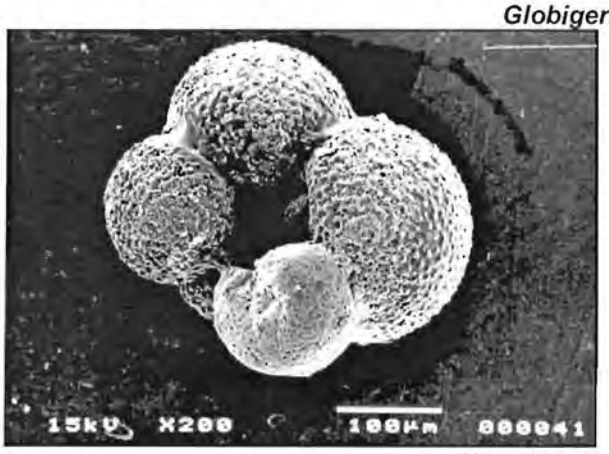

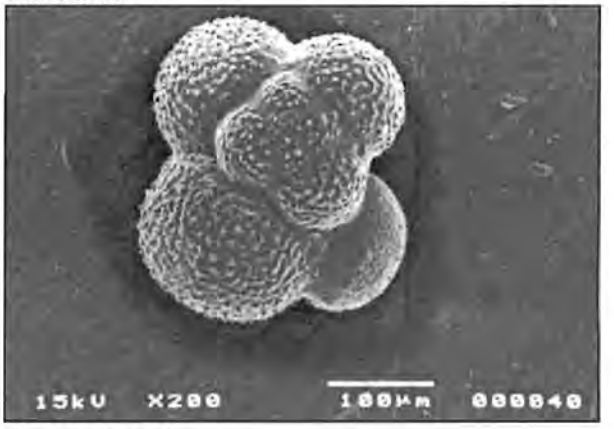

Neogloboquadrina dutertrei

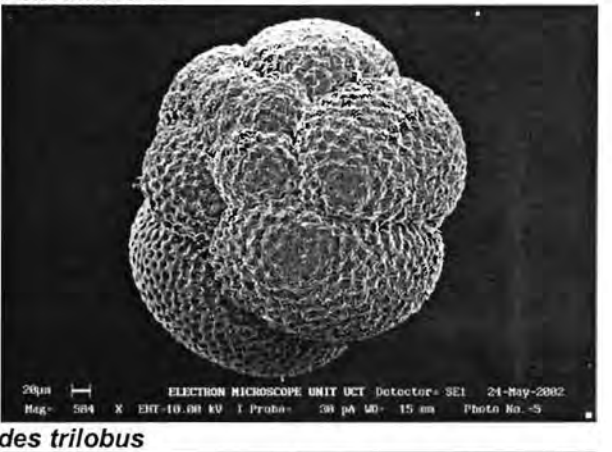

Globigerinoides trilobus

Globigerinoides sacculifer

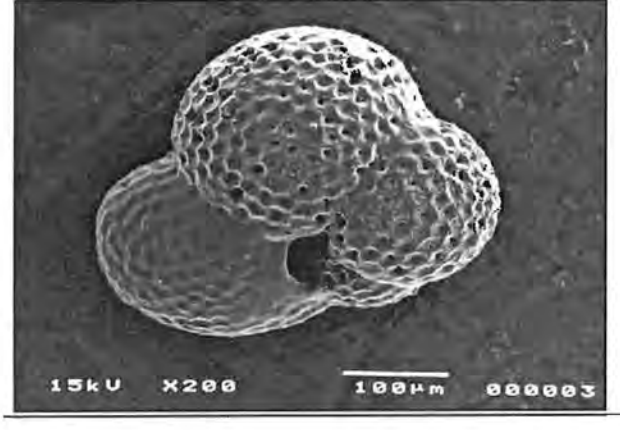

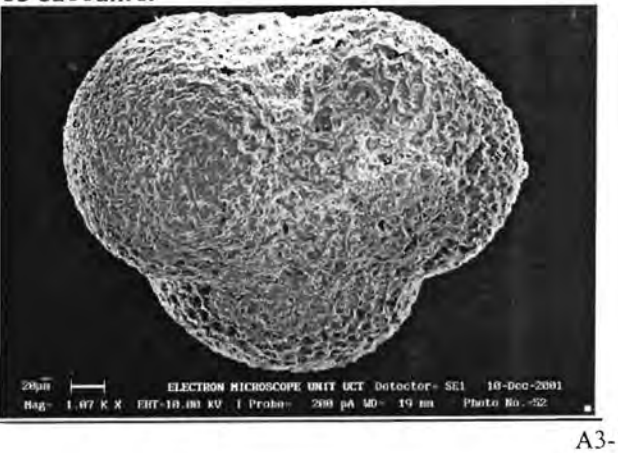

Globierinoides sacculifer (Brady, 1877)

Next to *Globigerinoides ruber, Globigerinoides sacculifer* is the most abundant species in Subtropical waters (Bé and Hutson, 1977) and the most abundant in Tropical waters (Bé and Tolderlund, 1971). Each species occupies a discrete niche, where one is dominant over the other (Bé and Tolderlund, 1971). *Gs. sacculifer* is dominant in Tropical oceanic waters with a surface temperature range of 24 - 30°C and surface salinity ~34.9 psu (Bé and Hutson, 1977). Although this species shows a maximum abundance in water masses with near-average marine salinity, it's tolerance for a broad range of salinities (34.5 – 37 psu) makes it an unreliable salinity indicator.

Globigerinoides ruber (alba) (d'Orbigny, 1839)

Globigerinoides ruber occurs in a range of environments from equatorial to warm-temperate. This widespread species dominates in subtropical waters with surface temperatures ranging from 14 to 30°C (peak 24.2 - 26°C) and salinity ranging from 34.5 to 36 psu and is second in abundance only to *Gs. sacculifer* in tropical waters (Bé and Hutson, 1977). When relative abundances are less than 10%, the species has a narrow tolerance for salinity deviation from the marine average of 35.5 psu (Hilbrecht, 1996). Its dominance appears to increase in the oligotrophic Indian Central Waters (Bé and Hutson, 1977). The pink-shelled variety (forma rosea), favouring warmer waters, is absent from the Indian Ocean today, but is reported to have been present during MIS 7 (Bé and Hutson, 1977). The counts reported here refer to the white-shelled variety *Gs. ruber* (forma alba). Herbert (1986) reported forma rosea in sediments collected off northern Namibia.

Globorotalia menardii (Parker, Jones and Brady, 1865)

Globorotalia menardii is a Subtropical/Tropical species thriving in equatorial regions with surface water temperatures of 17 – 27.5°C and surface salinities of 34 – 37.2 psu (Hilbrecht, 1996). Optimal occurrence occurs at 22.6°C and 35 psu (Bé and Hutson, 1977).

Globigerinoides ruber (alba)

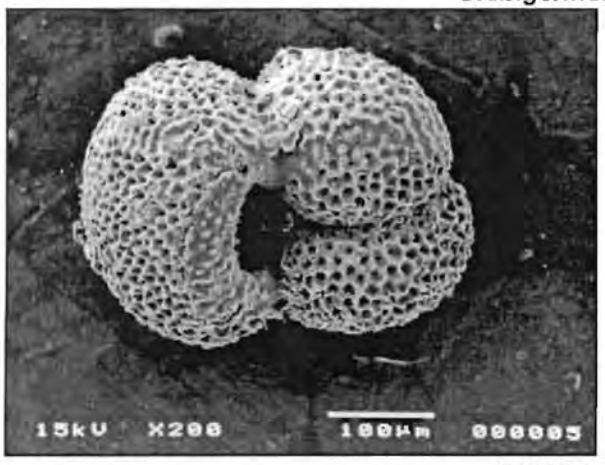

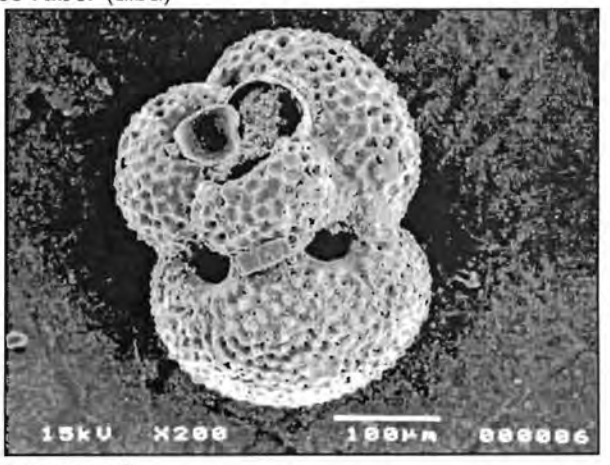

Globorotalia menardii

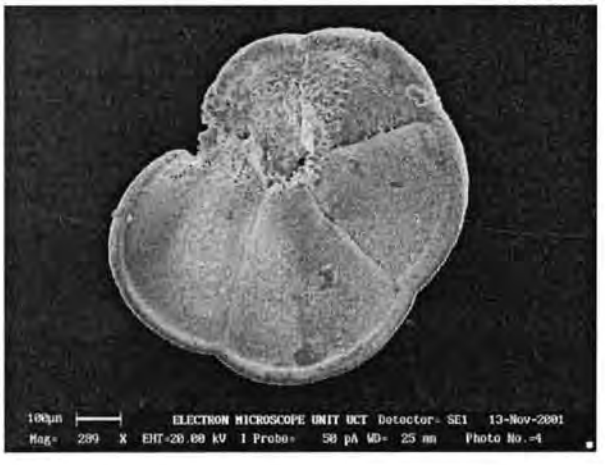

APPENDIX 4

PLANKTONIC FORMAINIFERAL CENSUS COUNTS
and
RELATIVE ABUNDANCES

CORE MD962080 (AGULHAS BANK SLOPE)

SAMPLE DEPTH (cm)	2	%	10	%	20	%	30	%	40	%	50	%	60	%	70	%	80	%	90	%
SPECIES COUNTED																				
G. pachyderma (sinistral)	4	1.34	4	1.33	2	0.63	2	0.80	2	0.74	1	0.30	2	0.74	1	0.35	2	0.75	1	0.36
G. pachyderma (dextral)	48	16.11	51	17.00	48	15.09	51	20.48	55	20.37	60	17.86	81	29.89	64	22.22	56	20.97	61	21.79
G. bulloides	24	8.05	29	9.67	33	10.38	32	12.85	23	8.52	50	14.88	34	12.55	40	13.89	35	13.11	31	11.07
G. scitula	7	2.35	9	3.00	13	4.09	12	4.82	15	5.56	20	5.95	6	2.21	6	2.08	11	4.12	7	2.50
G. glutinata	31	10.40	26	8.67	34	10.69	22	8.84	22	8.15	30	8.93	20	7.38	25	8.68	18	6.74	18	6.43
G. inflata	84	28.19	89	29.67	76	23.90	45	18.07	49	18.15	83	24.70	50	18.45	75	26.04	67	25.09	72	25.71
G. falconensis	21	7.05	17	5.67	27	8.49	21	8.43	30	11.11	22	6.55	20	7.38	18	6.25	21	7.87	15	5.36
G. hirsuta	0	0.00	0	0.00	0	0.00	0	0.00	1	0.37	0	0.00	0	0.00	0	0.00	0	0.00	2	0.71
G. truncatulinoides (d)	0	0.00	0	0.00	0	0.00	1	0.40	1	0.37	2	0.60	0	0.00	0	0.00	0	0.00	0	0.00
G. truncatulinoides (s)	9	3.02	3	1.00	2	0.63	4	1.61	4	1.48	6	1.79	4	1.48	4	1.39	3	1.12	3	1.07
G. ruber (alba)	15	5.03	10	3.33	15	4.72	8	3.21	4	1.48	6	1.79	5	1.85	6	2.08	8	3.00	10	3.57
G. trilobus	10	3.36	10	3.33	15	4.72	10	4.02	8	2.96	3	0.89	5	1.85	4	1.39	7	2.62	7	2.50
G. sacculifer	9	3.02	10	3.33	9	2.83	8	3.21	10	3.70	9	2.68	9	3.32	7	2.43	4	1.50	9	3.21
G. dutertrei	11	3.69	16	5.33	12	3.77	6	2.41	8	2.96	7	2.08	3	1.11	12	4.17	4	1.50	12	4.29
G. menardii	0	0.00	0	0.00	2	0.63	0	0.00	4	1.48	0	0.00	0	0.00	3	1.04	0	0.00	0	0.00
G. crassaformis	3	1.01	0	0.00	2	0.63	2	0.80	5	1.85	3	0.89	1	0.37	0	0.00	1	0.37	2	0.71
G. calida	3	1.01	8	2.67	4	1.26	6	2.41	5	1.85	4	1.19	9	3.32	7	2.43	9	3.37	7	2.50
T. quinqeloba	3	1.01	0	0.00	6	1.89	5	2.01	11	4.07	12	3.57	4	1.48	3	1.04	3	1.12	3	1.07
Other	16	5.37	18	6.00	18	5.66	14	5.62	13	4.81	18	5.36	18	6.64	13	4.51	18	6.74	20	7.14
TOTAL	298	100.00	300	100.00	318	100.00	249	100.00	270	100.00	336	100.00	271	100.00	288	100.00	267	100.00	280	100.00
Complete Forams	298		300		318		249		270		336		271		288		267		280	
Fragments	160		137		102		76		79		105		107		118		91		97	
Split	8		10		6		7		9		10		10		10		10.5		10	

SAMPLE DEPTH (cm)	100	%	110	%	120	%	130	%	140	%	150	%	160	%	170	%	180	%	190	%
SPECIES COUNTED																				
G. pachyderma (sinistral)	1	0.38	3	1.00	2	0.61	2	0.79	4	1.17	3	1.02	4	1.33	6	1.89	6	1.83	4	1.65
G. pachyderma (dextral)	69	25.94	69	22.92	63	19.21	39	15.48	76	22.29	69	23.47	42	14.00	60	18.87	70	21.41	45	18.60
G. bulloides	10	3.76	16	5.32	24	7.32	18	7.14	9	2.64	21	7.14	24	8.00	36	11.32	20	6.12	19	7.85
G. scitula	10	3.76	12	3.99	10	3.05	16	6.35	21	6.16	7	2.38	13	4.33	7	2.20	24	7.34	11	4.55
G. glutinata	18	6.77	25	8.31	43	13.11	23	9.13	33	9.68	18	6.12	28	9.33	31	9.75	29	8.87	44	18.18
G. inflata	83	31.20	90	29.90	78	23.78	70	27.78	102	29.91	85	28.91	90	30.00	94	29.56	66	20.18	48	19.83
G. falconensis	9	3.38	15	4.98	16	4.88	14	5.56	22	6.45	12	4.08	15	5.00	9	2.83	22	6.73	16	6.61
G. hirsuta	1	0.38	2	0.66	3	0.91	2	0.79	2	0.59	4	1.36	2	0.67	2	0.63	2	0.61	1	0.41
G. truncatulinoides (d)	0	0.00	0	0.00	0	0.00	1	0.40	0	0.00	0	0.00	0	0.00	0	0.00	0	0.00	0	0.00
G. truncatulinoides (s)	2	0.75	2	0.66	7	2.13	2	0.79	2	0.59	6	2.04	6	2.00	7	2.20	6	1.83	5	2.07
G. ruber (alba)	3	1.13	7	2.33	7	2.13	5	1.98	2	0.59	2	0.68	0	0.00	2	0.63	0	0.00	0	0.00
G. trilobus	6	2.26	7	2.33	16	4.88	12	4.76	16	4.69	16	5.44	21	7.00	10	3.14	15	4.59	16	6.61
G. sacculifer	18	6.77	15	4.98	18	5.49	13	5.16	6	1.76	7	2.38	10	3.33	9	2.83	12	3.67	5	2.07
G. dutertrei	8	3.01	9	2.99	7	2.13	6	2.38	6	1.76	4	1.36	0	0.00	6	1.89	6	1.83	3	1.24
G. menardii	0	0.00	0	0.00	2	0.61	0	0.00	0	0.00	0	0.00	0	0.00	0	0.00	0	0.00	0	0.00
G. crassaformis	1	0.38	0	0.00	3	0.91	1	0.40	3	0.88	6	2.04	4	1.33	4	1.26	3	0.92	2	0.83
G. calida	5	1.88	3	1.00	4	1.22	6	2.38	7	2.05	6	2.04	4	1.33	6	1.89	12	3.67	7	2.89
T. quinqeloba	4	1.50	4	1.33	4	1.22	3	1.19	10	2.93	3	1.02	10	3.33	4	1.26	7	2.14	2	0.83
Other	18	6.77	22	7.31	21	6.40	19	7.54	20	5.87	25	8.50	27	9.00	25	7.86	27	8.26	14	5.79
TOTAL	266	100.00	301	100.00	328	100.00	252	100.00	341	100.00	294	100.00	300	100.00	318	100.00	327	100.00	242	100.00
Complete Forams	266		301		328		252		341		294		300		318		327		242	
Fragments	188		203		278		189		315		295		269		296		297		170	
Split	10		9		8		9		9		9		9		9		9		10.5	

CORE MD962080 (AGULHAS BANK SLOPE)

SAMPLE DEPTH (cm)	200	%	210	%	220	%	230	%	240	%	250	%	260	%	270	%	280	%	290	%
SPECIES COUNTED																				
G. pachyderma (sinistral)	2	0.65	0	0.00	2	0.65	0	0.00	4	1.20	2	0.60	3	0.81	3	0.95	1	0.30	1	0.30
G. pachyderma (dextral)	58	18.83	42	12.92	48	15.53	33	11.07	50	15.02	34	10.21	48	12.94	27	8.54	58	17.47	63	18.98
G. bulloides	29	9.42	28	8.62	33	10.68	28	9.40	25	7.51	24	7.21	42	11.32	30	9.49	30	9.04	16	4.82
G. scitula	13	4.22	21	6.46	3	0.97	10	3.36	16	4.80	18	5.41	20	5.39	16	5.06	12	3.61	6	1.81
G. glutinata	36	11.69	21	6.46	35	11.33	42	14.09	42	12.61	48	14.41	30	8.09	50	15.82	37	11.14	36	10.84
G. inflata	67	21.75	82	25.23	76	24.60	73	24.50	70	21.02	72	21.62	81	21.83	58	18.35	85	25.60	82	24.70
G. falconensis	25	8.12	28	8.62	27	8.74	34	11.41	36	10.81	45	13.51	32	8.63	35	11.08	18	5.42	28	8.43
G. hirsuta	2	0.65	0	0.00	0	0.00	3	1.01	2	0.60	3	0.90	9	2.43	0	0.00	0	0.00	3	0.90
G. truncatulinoides (d)	0	0.00	2	0.62	0	0.00	3	1.01	3	0.90	0	0.00	0	0.00	2	0.63	3	0.90	0	0.00
G. truncatulinoides (s)	2	0.65	13	4.00	2	0.65	7	2.35	3	0.90	4	1.20	2	0.54	3	0.95	2	0.60	3	0.90
G. ruber (alba)	10	3.25	12	3.69	15	4.85	9	3.02	0	0.00	7	2.10	2	0.54	9	2.85	12	3.61	4	1.20
G. trilobus	16	5.19	24	7.38	15	4.85	24	8.05	20	6.01	21	6.31	33	8.89	16	5.06	24	7.23	18	5.42
G. sacculifer	7	2.27	9	2.77	9	2.91	9	3.02	12	3.60	15	4.50	12	3.23	9	2.85	4	1.20	3	0.90
G. dutertrei	6	1.95	2	0.62	12	3.88	4	1.34	16	4.80	7	2.10	9	2.43	10	3.16	7	2.11	10	3.01
G. menardii	0	0.00	0	0.00	2	0.65	2	0.67	0	0.00	2	0.60	0	0.00	0	0.00	2	0.60	2	0.60
G. crassaformis	3	0.97	4	1.23	2	0.65	0	0.00	3	0.90	2	0.60	2	0.54	0	0.00	0	0.00	2	0.60
G. calida	2	0.65	4	1.23	4	1.29	6	2.01	7	2.10	6	1.80	9	2.43	12	3.80	13	3.92	18	5.42
T. quinqeloba	3	0.97	0	0.00	6	1.94	2	0.67	3	0.90	3	0.90	10	2.70	9	2.85	3	0.90	13	3.92
Other	27	8.77	33	10.15	18	5.83	9	3.02	21	6.31	20	6.01	27	7.28	27	8.54	21	6.33	24	7.23
TOTAL	308	100.00	325	100.00	309	100.00	298	100.00	333	100.00	333	100.00	371	100.00	316	100.00	332	100.00	332	100.00
Complete Forams	308		325		309		298		333		333		371		316		332		332	
Fragments	194		245		97		198		160		160		133		85		124		85	
Split	10		9		9		9		9		9		9		9		10		10	

SAMPLE DEPTH (cm)	300	%	310	%	320	%	330	%	340	%	350	%	360	%	370	%	380	%	390	%
SPECIES COUNTED																				
G. pachyderma (sinistral)	0	0.00	16	5.05	0	0.00	1	0.33	4	1.24	4	1.16	0	0.00	0	0.00	0	0.00	1	0.38
G. pachyderma (dextral)	47	19.58	73	23.03	72	23.23	57	18.75	70	21.74	73	21.22	63	22.50	67	19.31	75	21.19	57	21.59
G. bulloides	15	6.25	51	16.09	18	5.81	20	6.58	36	11.18	28	8.14	19	6.79	21	6.05	37	10.45	21	7.95
G. scitula	13	5.42	7	2.21	13	4.19	15	4.93	6	1.86	12	3.49	8	2.86	18	5.19	12	3.39	7	2.65
G. glutinata	26	10.83	24	7.57	27	8.71	42	13.82	21	6.52	34	9.88	25	8.93	43	12.39	33	9.32	33	12.50
G. inflata	58	24.17	66	20.82	90	29.03	75	24.67	106	32.92	73	21.22	70	25.00	91	26.22	84	23.73	57	21.59
G. falconensis	14	5.83	10	3.15	27	8.71	22	7.24	28	8.70	27	7.85	17	6.07	24	6.92	21	5.93	27	10.23
G. hirsuta	0	0.00	0	0.00	0	0.00	0	0.00	2	0.62	0	0.00	0	0.00	0	0.00	2	0.56	3	1.14
G. truncatulinoides (d)	0	0.00	0	0.00	2	0.65	0	0.00	0	0.00	3	0.87	0	0.00	2	0.58	2	0.56	0	0.00
G. truncatulinoides (s)	6	2.50	4	1.26	4	1.29	0	0.00	0	0.00	3	0.87	3	1.07	4	1.15	2	0.56	1	0.38
G. ruber (alba)	2	0.83	10	3.15	7	2.26	6	1.97	10	3.11	12	3.49	12	4.29	12	3.46	6	1.69	3	1.14
G. trilobus	20	8.33	7	2.21	7	2.26	15	4.93	7	2.17	13	3.78	14	5.00	18	5.19	24	6.78	16	6.06
G. sacculifer	1	0.42	4	1.26	2	0.65	10	3.29	6	1.86	9	2.62	3	1.07	6	1.73	4	1.13	0	0.00
G. dutertrei	4	1.67	6	1.89	4	1.29	4	1.32	3	0.93	10	2.91	5	1.79	7	2.02	9	2.54	7	2.65
G. menardii	0	0.00	2	0.63	0	0.00	0	0.00	0	0.00	0	0.00	0	0.00	2	0.58	0	0.00	1	0.42
G. crassaformis	0	0.00	3	0.95	3	0.97	0	0.00	0	0.00	0	0.00	1	0.36	0	0.00	2	0.56	0	0.00
G. calida	8	3.33	9	2.84	15	4.84	13	4.28	4	1.24	13	3.78	9	3.21	7	2.02	15	4.24	12	4.55
T. quinqeloba	11	4.58	0	0.00	6	1.94	9	2.96	4	1.24	10	2.91	15	5.36	10	2.88	13	3.67	10	3.79
Other	15	6.25	25	7.89	13	4.19	15	4.93	15	4.66	20	5.81	16	5.71	15	4.32	13	3.67	8	3.03
TOTAL	240	100.00	317	100.00	310	100.00	304	100.00	322	100.00	344	100.00	280	100.00	347	100.00	354	100.00	264	100.04
Complete Forams	240		317		310		304		322		344		280		347		354		260	
Fragments	87		102		100		71		103		89		79		106		105		59	
Split	10		10		11		11		10		9		11		10		11		11	

CORE MD962080 (AGULHAS BANK SLOPE)

SAMPLE DEPTH (cm)	400	%	410	%	420	%	430	%	440	%	450	%	460	%	470	%	480	%	490	%
SPECIES COUNTED																				
G. pachyderma (sinistral)	0	0.00	6	1.78	1	0.38	4	1.29	3	0.94	1	0.39	3	1.08	1	0.32	0	0.00	0	0.00
G. pachyderma (dextral)	51	19.92	60	17.75	61	23.02	67	21.68	75	23.44	44	17.25	43	15.52	48	15.43	69	19.77	58	18.65
G. bulloides	32	12.50	37	10.95	26	9.81	31	10.03	31	9.69	18	7.06	36	13.00	36	11.58	42	12.03	28	9.00
G. scitula	8	3.13	15	4.44	15	5.66	27	8.74	10	3.13	9	3.53	4	1.44	10	3.22	18	5.16	13	4.18
G. glutinata	14	5.47	22	6.51	11	4.15	21	6.80	16	5.00	9	3.53	24	8.66	22	7.07	19	5.44	25	8.04
G. inflata	74	28.91	90	26.63	78	29.43	73	23.62	97	30.31	89	34.90	81	29.24	88	28.30	102	29.23	87	27.97
G. falconensis	18	7.03	30	8.88	15	5.66	16	5.18	18	5.63	13	5.10	22	7.94	20	6.43	13	3.72	21	6.75
G. hirsuta	0	0.00	0	0.00	0	0.00	0	0.00	0	0.00	2	0.78	2	0.72	0	0.00	6	1.72	0	0.00
G. truncatulinoides (d)	0	0.00	0	0.00	0	0.00	0	0.00	2	0.63	2	0.78	0	0.00	0	0.00	1	0.29	0	0.00
G. truncatulinoides (s)	2	0.78	0	0.00	2	0.75	6	1.94	2	0.63	1	0.39	2	0.72	3	0.96	6	1.72	4	1.29
G. ruber (alba)	5	1.95	2	0.59	3	1.13	0	0.00	4	1.25	7	2.75	7	2.53	12	3.86	1	0.29	13	4.18
G. trilobus	9	3.52	10	2.96	2	0.75	7	2.27	7	2.19	4	1.57	3	1.08	6	1.93	4	1.15	9	2.89
G. sacculifer	6	2.34	9	2.66	7	2.64	13	4.21	10	3.13	6	2.35	7	2.53	9	2.89	13	3.72	13	4.18
G. dutertrei	7	2.73	16	4.73	11	4.15	4	1.29	7	2.19	4	1.57	6	2.17	9	2.89	7	2.01	6	1.93
G. menardii	1	0.39	0	0.00	0	0.00	0	0.00	0	0.00	1	0.39	0	0.00	0	0.00	0	0.00	2	0.64
G. crassaformis	2	0.78	3	0.89	0	0.00	2	0.65	2	0.63	5	1.96	0	0.00	4	1.29	3	0.86	3	0.96
G. calida	8	3.13	16	4.73	13	4.91	7	2.27	3	0.94	7	2.75	5	1.81	6	1.93	6	1.72	4	1.29
T. quinqeloba	4	1.56	4	1.18	4	1.51	7	2.27	6	1.88	0	0.00	5	1.81	6	1.93	2	0.57	0	0.00
Other	15	5.86	18	5.33	16	6.04	24	7.77	27	8.44	33	12.94	27	9.75	31	9.97	37	10.60	25	8.04
TOTAL	256	100.00	338	100.00	265	100.00	309	100.00	320	100.00	255	100.00	277	100.00	311	100.00	349	100.00	311	100.00
Complete Forams	256		338		265		309		320		255		277		311		349		311	
Fragments	81		124		104		181		188		160		155		205		229		217	
Split	11.5		10		12.5		10		11		11.5		9		10		10		11	

SAMPLE DEPTH (cm)	500	%	510	%	520	%	530	%	540	%	550	%	560	%	570	%	580	%	590	%
SPECIES COUNTED																				
G. pachyderma (sinistral)	9	2.69	4	1.27	12	3.52	16	5.37	12	4.04	9	2.99	13	4.36	9	3.02	6	2.01	7	2.21
G. pachyderma (dextral)	73	21.86	64	20.25	69	20.23	61	20.47	66	22.22	58	19.27	64	21.48	61	20.47	64	21.40	82	25.87
G. bulloides	27	8.08	34	10.76	43	12.61	21	7.05	21	7.07	25	8.31	19	6.38	22	7.38	24	8.03	31	9.78
G. scitula	7	2.10	18	5.70	10	2.93	7	2.35	7	2.36	9	2.99	9	3.02	4	1.34	7	2.34	13	4.10
G. glutinata	37	11.08	25	7.91	22	6.45	21	7.05	27	9.09	15	4.98	13	4.36	31	10.40	20	6.69	18	5.68
G. inflata	84	25.15	91	28.80	94	27.57	78	26.17	76	25.59	90	29.90	111	37.25	102	34.23	109	36.45	87	27.44
G. falconensis	18	5.39	16	5.06	24	7.04	7	2.35	27	9.09	16	5.32	12	4.03	13	4.36	12	4.01	18	5.68
G. hirsuta	0	0.00	0	0.00	0	0.00	0	0.00	0	0.00	0	0.00	0	0.00	0	0.00	0	0.00	0	0.00
G. truncatulinoides (d)	0	0.00	0	0.00	0	0.00	0	0.00	0	0.00	2	0.66	2	0.67	0	0.00	0	0.00	0	0.00
G. truncatulinoides (s)	7	2.10	2	0.63	2	0.59	6	2.01	3	1.01	4	1.33	2	0.67	9	3.02	2	0.67	0	0.00
G. ruber (alba)	4	1.20	4	1.27	12	3.52	6	2.01	10	3.37	6	1.99	4	1.34	3	1.01	9	3.01	3	0.95
G. trilobus	10	2.99	9	2.85	6	1.76	15	5.03	3	1.01	7	2.33	7	2.35	6	2.01	3	1.00	7	2.21
G. sacculifer	13	3.89	4	1.27	6	1.76	15	5.03	13	4.38	7	2.33	9	3.02	2	0.67	7	2.34	2	0.63
G. dutertrei	6	1.80	7	2.22	3	0.88	2	0.67	4	1.35	10	3.32	9	3.02	7	2.35	4	1.34	4	1.26
G. menardii	0	0.00	0	0.00	2	0.59	0	0.00	2	0.67	3	1.00	0	0.00	0	0.00	0	0.00	0	0.00
G. crassaformis	3	0.90	4	1.27	3	0.88	7	2.35	3	1.01	6	1.99	0	0.00	2	0.67	2	0.67	0	0.00
G. calida	4	1.20	2	0.63	3	0.88	10	3.36	6	2.02	4	1.33	3	1.01	9	3.02	6	2.01	9	2.84
T. quinqeloba	3	0.90	12	3.80	9	2.64	6	2.01	4	1.35	10	3.32	3	1.01	6	2.01	7	2.34	12	3.79
Other	29	8.68	20	6.33	21	6.16	20	6.71	13	4.38	20	6.64	18	6.04	12	4.03	17	5.69	24	7.57
TOTAL	334	100.00	316	100.00	341	100.00	298	100.00	297	100.00	301	100.00	298	100.00	298	100.00	299	100.00	317	100.00
Complete Forams	334		316		341		298		297		301		298		298		299		317	
Fragments	245		148		277		247		151		205		119		96		141		233	
Split	9		9		10		9		8		7		10		10		9		8	

CORE MD962080 (AGULHAS BANK SLOPE)

SAMPLE DEPTH (cm)	600	%	610	%	620	%	630	%	640	%	650	%	660	%	670	%	680	%	690	%
SPECIES COUNTED																				
G. pachyderma (sinistral)	6	1.77	7	1.92	0	0.00	4	1.22	0	0.00	3	0.90	17	5.63	3	0.99	0	0.00	6	1.88
G. pachyderma (dextral)	90	26.55	108	29.59	73	24.01	88	26.83	54	18.06	85	25.60	101	33.44	70	23.03	73	22.53	75	23.51
G. bulloides	18	5.31	25	6.85	21	6.91	12	3.66	21	7.02	15	4.52	23	7.62	15	4.93	12	3.70	25	7.84
G. scitula	12	3.54	13	3.56	10	3.29	4	1.22	13	4.35	10	3.01	7	2.32	7	2.30	15	4.63	9	2.82
G. glutinata	37	10.91	30	8.22	33	10.86	37	11.28	37	12.37	36	10.84	20	6.62	31	10.20	30	9.26	40	12.54
G. inflata	91	26.84	99	27.12	87	28.62	91	27.74	105	35.12	93	28.01	67	22.19	90	29.61	99	30.56	84	26.33
G. falconensis	31	9.14	16	4.38	21	6.91	16	4.88	13	4.35	18	5.42	7	2.32	15	4.93	16	4.94	9	2.82
G. hirsuta	0	0.00	0	0.00	0	0.00	3	0.91	2	0.67	2	0.60	0	0.00	2	0.66	0	0.00	2	0.63
G. truncatulinoides (d)	0	0.00	0	0.00	0	0.00	0	0.00	0	0.00	0	0.00	0	0.00	0	0.00	0	0.00	0	0.00
G. truncatulinoides (s)	0	0.00	0	0.00	0	0.00	2	0.61	2	0.67	2	0.60	4	1.32	2	0.66	3	0.93	2	0.63
G. ruber (alba)	0	0.00	3	0.82	2	0.66	7	2.13	6	2.01	0	0.00	13	4.30	2	0.66	2	0.62	3	0.94
G. trilobus	19	5.60	15	4.11	13	4.28	12	3.66	6	2.01	15	4.52	7	2.32	15	4.93	12	3.70	15	4.70
G. sacculifer	3	0.88	4	1.10	10	3.29	7	2.13	0	0.00	7	2.11	2	0.66	6	1.97	6	1.85	7	2.19
G. dutertrei	6	1.77	6	1.64	4	1.32	9	2.74	12	4.01	6	1.81	11	3.64	12	3.95	15	4.63	7	2.19
G. menardii	0	0.00	0	0.00	0	0.00	0	0.00	0	0.00	0	0.00	1	0.33	0	0.00	0	0.00	2	0.63
G. crassaformis	0	0.00	2	0.55	0	0.00	2	0.61	2	0.67	3	0.90	2	0.66	0	0.00	3	0.93	2	0.63
G. calida	2	0.59	12	3.29	3	0.99	7	2.13	0	0.00	3	0.90	8	2.65	3	0.99	4	1.23	4	1.25
T. quinqeloba	3	0.88	4	1.10	7	2.30	6	1.83	4	1.34	4	1.20	3	0.99	3	0.99	9	2.78	3	0.94
Other	21	6.19	21	5.75	20	6.58	21	6.40	22	7.36	30	9.04	9	2.98	28	9.21	25	7.72	24	7.52
TOTAL	339	100.00	365	100.00	304	100.00	328	100.00	299	100.00	332	100.00	302	100.00	304	100.00	324	100.00	319	100.00
Complete Forams	339		365		304		328		299		332		302		304		324		319	
Fragments	279		432		362		384		402		413		342		312		367		397	
Split	7		8		9		9		9		9		9		9		9		8	

SAMPLE DEPTH (cm)	700	%	710	%	720	%	730	%	740	%	750	%	760	%	770	%	780	%	790	%
SPECIES COUNTED																				
G. pachyderma (sinistral)	7	2.27	2	0.67	2	0.63	0	0.00	2	0.65					0	0.00	3	1.01	1	0.40
G. pachyderma (dextral)	75	24.27	67	22.48	61	19.37	51	18.09	50	16.18					63	18.58	52	17.51	60	24.10
G. bulloides	40	12.94	15	5.03	10	3.17	48	17.02	30	9.71	NO	SAMPLE			31	9.14	34	11.45	15	6.02
G. scitula	10	3.24	10	3.36	9	2.86	9	3.19	6	1.94					7	2.06	9	3.03	6	2.41
G. glutinata	31	10.03	18	6.04	27	8.57	30	10.64	37	11.97					46	13.57	33	11.11	32	12.85
G. inflata	97	31.39	81	27.18	85	26.98	50	17.73	67	21.68					75	22.12	70	23.57	57	22.89
G. falconensis	6	1.94	18	6.04	15	4.76	22	7.80	24	7.77					30	8.85	27	9.09	23	9.24
G. hirsuta	0	0.00	0	0.00	4	1.27	3	1.06	0	0.00					2	0.59	0	0.00	1	0.40
G. truncatulinoides (d)	0	0.00	2	0.67	2	0.63	4	1.42	0	0.00					0	0.00	0	0.00	0	0.00
G. truncatulinoides (s)	2	0.65	3	1.01	3	0.95	7	2.48	2	0.65					2	0.59	4	1.35	1	0.40
G. ruber (alba)	4	1.29	6	2.01	6	1.90	6	2.13	10	3.24		NO	SAMPLE		9	2.65	3	1.01	0	0.00
G. trilobus	3	0.97	7	2.35	13	4.13	13	4.61	13	4.21					16	4.72	6	2.02	9	3.61
G. sacculifer	2	0.65	13	4.36	10	3.17	13	4.61	4	1.29					7	2.06	7	2.36	5	2.01
G. dutertrei	7	2.27	10	3.36	18	5.71	3	1.06	21	6.80					16	4.72	4	1.35	3	1.20
G. menardii	0	0.00	0	0.00	4	1.27	2	0.71	0	0.00					0	0.00	0	0.00	0	0.00
G. crassaformis	3	0.97	0	0.00	2	0.63	2	0.71	0	0.00					0	0.00	2	0.67	1	0.40
G. calida	0	0.00	9	3.02	10	3.17	9	3.19	21	6.80					10	2.95	3	1.01	7	2.81
T. quinqeloba	2	0.65	6	2.01	4	1.27	0	0.00	6	1.94					3	0.88	10	3.37	8	3.21
Other	20	6.47	31	10.40	30	9.52	10	3.55	16	5.18					22	6.49	30	10.10	20	8.03
TOTAL	309	100.00	298	100.00	315	100.00	282	100.00	309	100.00					339	100.00	297	100.00	249	100.00
Complete Forams	309		298		315		282		309						339		297		251	
Fragments	253		401		330		187		187			NO	SAMPLE		213		190		142	
Split	9		10		9		9		7						9		8		10	

CORE MD962080 (AGULHAS BANK SLOPE)

SAMPLE DEPTH (cm)	800	%	810	%	820	%	830	%	840	%	850	%	860	%	870	%	880	%	890	%
SPECIES COUNTED																				
G. pachyderma (sinistral)	3	0.90	2	0.68	2	0.57	0	0.00	4	1.16	7	2.21	9	2.96	0	0.00	2	0.74	0	0.00
G. pachyderma (dextral)	78	23.28	72	24.32	64	18.34	40	15.38	79	22.97	69	21.77	50	16.45	78	26.17	67	24.81	54	18.49
G. bulloides	45	13.43	42	14.19	54	15.47	36	13.85	42	12.21	33	10.41	25	8.22	39	13.09	27	10.00	20	6.85
G. scitula	7	2.09	4	1.35	7	2.01	2	0.77	7	2.03	7	2.21	10	3.29	10	3.36	15	5.56	16	5.48
G. glutinata	19	5.67	25	8.45	24	6.88	22	8.46	28	8.14	22	6.94	28	9.21	34	11.41	21	7.78	28	9.59
G. inflata	99	29.55	52	17.57	102	29.23	79	30.38	99	28.78	84	26.50	79	25.99	58	19.46	76	28.15	114	39.04
G. falconensis	13	3.88	27	9.12	15	4.30	15	5.77	15	4.36	9	2.84	10	3.29	20	6.71	10	3.70	7	2.40
G. hirsuta	2	0.60	2	0.68	9	2.58	0	0.00	2	0.58	3	0.95	2	0.66	2	0.67	0	0.00	2	0.68
G. truncatulinoides (d)	0	0.00	0	0.00	0	0.00	0	0.00	0	0.00	0	0.00	0	0.00	0	0.00	0	0.00	0	0.00
G. truncatulinoides (s)	0	0.00	0	0.00	2	0.57	4	1.54	0	0.00	2	0.63	9	2.96	0	0.00	3	1.11	2	0.68
G. ruber (alba)	3	0.90	4	1.35	6	1.72	2	0.77	2	0.58	0	0.00	3	0.99	4	1.34	3	1.11	0	0.00
G. trilobus	3	0.90	4	1.35	10	2.87	9	3.46	3	0.87	10	3.15	6	1.97	12	4.03	7	2.59	9	3.08
G. sacculifer	7	2.09	7	2.36	12	3.44	7	2.69	7	2.03	7	2.21	6	1.97	4	1.34	7	2.59	7	2.40
G. dutertrei	12	3.58	4	1.35	10	2.87	7	2.69	4	1.16	18	5.68	13	4.28	4	1.34	3	1.11	0	0.00
G. menardii	2	0.60	0	0.00	2	0.57	0	0.00	0	0.00	0	0.00	0	0.00	0	0.00	0	0.00	0	0.00
G. crassaformis	0	0.00	2	0.68	0	0.00	2	0.77	0	0.00	2	0.63	6	1.97	0	0.00	2	0.74	2	0.68
G. calida	13	3.88	9	3.04	6	1.72	10	3.85	12	3.49	12	3.79	4	1.32	7	2.35	3	1.11	4	1.37
T. quinqeloba	9	2.69	4	1.35	9	2.58	3	1.15	3	0.87	2	0.63	4	1.32	4	1.34	0	0.00	2	0.68
Other	20	5.97	36	12.16	15	4.30	22	8.46	37	10.76	30	9.46	40	13.16	22	7.38	24	8.89	25	8.56
TOTAL	335	100.00	296	100.00	349	100.00	260	100.00	344	100.00	317	100.00	304	100.00	298	100.00	270	100.00	292	100.00
Complete Forams	335		296		349		260		344		317		304		298		270		292	
Fragments	192		168		175		142		222		238		297		236		383		433	
Split	9		8		8		9		8		9		10		10		8		8.5	

SAMPLE DEPTH (cm)	900	%	910	%	920	%	930	%	940	%	950	%	960	%	970	%	980	%	990	%
SPECIES COUNTED																				
G. pachyderma (sinistral)	0	0.00	0	0.00	2	0.62	0	0.00	1	0.39			0	0.00	2	0.69	7	2.22	3	0.98
G. pachyderma (dextral)	33	11.11	57	18.10	69	21.36	41	16.60	45	17.58			50	18.05	60	20.83	78	24.68	70	22.80
G. bulloides	28	9.43	30	9.52	45	13.93	13	5.26	11	4.30			20	7.22	25	8.68	18	5.70	22	7.17
G. scitula	4	1.35	9	2.86	4	1.24	17	6.88	23	8.98			10	3.61	10	3.47	7	2.22	4	1.30
G. glutinata	28	9.43	27	8.57	21	6.50	23	9.31	23	8.98			27	9.75	33	11.46	22	6.96	39	12.70
G. inflata	121	40.74	85	26.98	84	26.01	75	30.36	73	28.52			65	23.47	75	26.04	102	32.28	88	28.66
G. falconensis	12	4.04	18	5.71	30	9.29	7	2.83	4	1.56			18	6.50	12	4.17	25	7.91	15	4.89
G. hirsuta	0	0.00	2	0.63	2	0.62	3	1.21	1	0.39			2	0.72	0	0.00	2	0.63	4	1.30
G. truncatulinoides (d)	0	0.00	2	0.63	0	0.00	0	0.00	2	0.78	NO	SAMPLE	0	0.00	0	0.00	0	0.00	2	0.65
G. truncatulinoides (s)	6	2.02	7	2.22	7	2.17	3	1.21	2	0.78			0	0.00	0	0.00	2	0.63	2	0.65
G. ruber (alba)	16	5.39	15	4.76	7	2.17	10	4.05	2	0.78			13	4.69	11	3.82	4	1.27	6	1.95
G. trilobus	3	1.01	7	2.22	4	1.24	12	4.86	17	6.64			11	3.97	9	3.13	4	1.27	3	0.98
G. sacculifer	4	1.35	7	2.22	9	2.79	10	4.05	7	2.73			16	5.78	13	4.51	16	5.06	12	3.91
G. dutertrei	7	2.36	15	4.76	4	1.24	6	2.43	15	5.86			17	6.14	13	4.51	2	0.63	6	1.95
G. menardii	2	0.67	0	0.00	0	0.00	0	0.00	1	0.39			1	0.36	0	0.00	0	0.00	3	0.98
G. crassaformis	2	0.67	0	0.00	2	0.62	0	0.00	1	0.39			1	0.36	0	0.00	2	0.63	0	0.00
G. calida	3	1.01	12	3.81	3	0.93	7	2.83	8	3.13			10	3.61	7	2.43	10	3.16	9	2.93
T. quinqeloba	6	2.02	2	0.63	10	3.10	3	1.21	4	1.56			0	0.00	6	2.08	3	0.95	6	1.95
Other	22	7.41	20	6.35	20	6.19	17	6.88	16	6.25			16	5.78	12	4.17	12	3.80	13	4.23
TOTAL	297	100.00	315	100.00	323	100.00	247	100.00	256	100.00			277	100.00	288	100.00	316	100.00	307	100.00
Complete Forams	297		315		323		247		256		NO	SAMPLE	277		288		316		307	
Fragments	422		385		307		223		92				104		203		190		259	
Split	9		7		5		8		8				9		9		9		9	

CORE MD962080 (AGULHAS BANK SLOPE)

SAMPLE DEPTH (cm)	1000	%	1010	%	1020	%	1030	%	1040	%	1050	%	1060	%	1070	%	1080	%	1090	%
SPECIES COUNTED																				
G. pachyderma (sinistral)	10	3.51	11	2.87	7	2.57	5	1.95	16	4.73	4	1.47	2	0.57	5	1.49	6	1.56	9	2.99
G. pachyderma (dextral)	58	20.35	72	18.80	41	15.07	39	15.18	47	13.91	55	20.22	67	19.20	48	14.29	70	18.18	79	26.25
G. bulloides	13	4.56	12	3.13	12	4.41	8	3.11	12	3.55	14	5.15	19	5.44	10	2.98	12	3.12	31	10.30
G. scitula	7	2.46	2	0.52	7	2.57	7	2.72	6	1.78	3	1.10	6	1.72	3	0.89	6	1.56	3	1.00
G. glutinata	27	9.47	40	10.44	30	11.03	23	8.95	31	9.17	35	12.87	43	12.32	41	12.20	45	11.69	28	9.30
G. inflata	60	21.05	87	22.72	50	18.38	47	18.29	74	21.89	55	20.22	79	22.64	53	15.77	55	14.29	40	13.29
G. falconensis	11	3.86	11	2.87	13	4.78	8	3.11	15	4.44	14	5.15	7	2.01	16	4.76	12	3.12	19	6.31
G. hirsuta	3	1.05	2	0.52	3	1.10	4	1.56	4	1.18	0	0.00	3	0.86	7	2.08	6	1.56	0	0.00
G. truncatulinoides (d)	0	0.00	0	0.00	0	0.00	0	0.00	0	0.00	1	0.37	2	0.57	0	0.00	0	0.00	0	0.00
G. truncatulinoides (s)	3	1.05	4	1.04	5	1.84	11	4.28	4	1.18	2	0.74	6	1.72	17	5.06	17	4.42	3	1.00
G. ruber (alba)	4	1.40	6	1.57	5	1.84	3	1.17	4	1.18	4	1.47	10	2.87	5	1.49	11	2.86	7	2.33
G. trilobus	23	8.07	45	11.75	26	9.56	21	8.17	24	7.10	17	6.25	15	4.30	32	9.52	26	6.75	13	4.32
G. sacculifer	11	3.86	13	3.39	9	3.31	13	5.06	15	4.44	4	1.47	10	2.87	16	4.76	11	2.86	9	2.99
G. dutertrei	14	4.91	24	6.27	19	6.99	14	5.45	24	7.10	10	3.68	19	5.44	19	5.65	35	9.09	12	3.99
G. menardii	1	0.35	0	0.00	0	0.00	2	0.78	2	0.59	1	0.37	0	0.00	1	0.30	3	0.78	2	0.66
G. crassaformis	0	0.00	0	0.00	0	0.00	3	1.17	1	0.30	1	0.37	3	0.86	2	0.60	1	0.26	6	1.99
G. calida	6	2.11	7	1.83	5	1.84	7	2.72	11	3.25	7	2.57	6	1.72	6	1.79	11	2.86	7	2.33
T. quinqeloba	3	1.05	8	2.09	9	3.31	6	2.33	21	6.21	8	2.94	6	1.72	8	2.38	12	3.12	6	1.99
Other	31	10.88	39	10.18	31	11.40	36	14.01	27	7.99	37	13.60	46	13.18	47	13.99	46	11.95	27	8.97
TOTAL	285	100.00	383	100.00	272	100.00	257	100.00	338	100.00	272	100.00	349	100.00	336	100.00	385	100.00	301	100.00
Complete Forams	285		383		272		257		338		272		349		336		385		301	
Fragments	124		224		248		187		178		158		225		444		403		298	
Split	9		9		10		9		8		9		7		8		8		8	

SAMPLE DEPTH (cm)	1100	%	1110	%	1120	%	1130	%	1140	%	1150	%	1160	%	1170	%	1180	%	1190	%
SPECIES COUNTED																				
G. pachyderma (sinistral)	18	7.38	21	7.05	3	0.89	8	2.13	8	3.25	7	2.19	2	0.63	0	0.00	2	0.58	7	2.19
G. pachyderma (dextral)	77	31.56	108	36.24	84	24.93	57	15.16	44	17.89	69	21.56	72	22.57	72	21.82	70	20.23	49	15.36
G. bulloides	20	8.20	12	4.03	22	6.53	12	3.19	22	8.94	33	10.31	24	7.52	24	7.27	21	6.07	16	5.02
G. scitula	6	2.46	0	0.00	10	2.97	18	4.79	6	2.44	10	3.13	7	2.19	2	0.61	6	1.73	10	3.13
G. glutinata	20	8.20	18	6.04	24	7.12	59	15.69	44	17.89	52	16.25	27	8.46	37	11.21	31	8.96	52	16.30
G. inflata	18	7.38	48	16.11	90	26.71	77	20.48	39	15.85	52	16.25	61	19.12	76	23.03	75	21.68	79	24.76
G. falconensis	14	5.74	10	3.36	16	4.75	19	5.05	14	5.69	22	6.88	28	8.78	22	6.67	27	7.80	18	5.64
G. hirsuta	0	0.00	0	0.00	9	2.67	0	0.00	1	0.41	2	0.63	4	1.25	0	0.00	0	0.00	3	0.94
G. truncatulinoides (d)	0	0.00	2	0.67	0	0.00	1	0.27	2	0.81	0	0.00	2	0.63	0	0.00	4	1.16	2	0.63
G. truncatulinoides (s)	0	0.00	3	1.01	0	0.00	5	1.33	0	0.00	2	0.63	2	0.63	2	0.61	2	0.58	3	0.94
G. ruber (alba)	5	2.05	6	2.01	0	0.00	24	6.38	8	3.25	6	1.88	7	2.19	0	0.00	13	3.76	6	1.88
G. trilobus	15	6.15	7	2.35	6	1.78	21	5.59	9	3.66	6	1.88	9	2.82	13	3.94	15	4.34	21	6.58
G. sacculifer	6	2.46	10	3.36	7	2.08	17	4.52	7	2.85	9	2.81	9	2.82	13	3.94	15	4.34	7	2.19
G. dutertrei	6	2.46	10	3.36	21	6.23	14	3.72	8	3.25	6	1.88	12	3.76	12	3.64	10	2.89	12	3.76
G. menardii	0	0.00	0	0.00	0	0.00	0	0.00	0	0.00	3	0.94	0	0.00	0	0.00	0	0.00	0	0.00
G. crassaformis	2	0.82	15	5.03	3	0.89	4	1.06	0	0.00	0	0.00	3	0.94	3	0.91	0	0.00	3	0.94
G. calida	5	2.05	7	2.35	3	0.89	8	2.13	7	2.85	7	2.19	10	3.13	6	1.82	16	4.62	6	1.88
T. quinqeloba	8	3.28	6	2.01	2	0.59	9	2.39	4	1.63	9	2.81	3	0.94	3	0.91	6	1.73	7	2.19
Other	24	9.84	15	5.03	37	10.98	23	6.12	23	9.35	25	7.81	37	11.60	45	13.64	33	9.54	18	5.64
TOTAL	244	100.00	298	100.00	337	100.00	376	100.00	246	100.00	320	100.00	319	100.00	330	100.00	346	100.00	319	100.00
Complete Forams	244		298		337		376		243		320		319		330		346		319	
Fragments	158		265		335		100		133		188		203		241		267		161	
Split	9		9		8		8		8		8		9		9		9		10	

CORE MD962080 (AGULHAS BANK SLOPE)

SAMPLE DEPTH (cm)	1200	%	1210	%	1220	%	1230	%	1240	%	1250	%	1260	%	1270	%	1280	%	1290	%
SPECIES COUNTED																				
G. pachyderma (sinistral)	10	2.96	10	2.39	11	3.53	12	3.59	12	3.76	11	3.65	14	3.90	4	1.78	3	1.23	7	2.11
G. pachyderma (dextral)	54	15.98	58	13.88	70	22.44	62	18.56	54	16.93	43	14.29	51	14.21	32	14.22	36	14.81	45	13.60
G. bulloides	22	6.51	28	6.70	13	4.17	14	4.19	13	4.08	17	5.65	19	5.29	11	4.89	10	4.12	15	4.53
G. scitula	14	4.14	19	4.55	11	3.53	13	3.89	15	4.70	12	3.99	3	0.84	2	0.89	7	2.88	5	1.51
G. glutinata	38	11.24	53	12.68	35	11.22	35	10.48	41	12.85	39	12.96	41	11.42	28	12.44	26	10.70	43	12.99
G. inflata	75	22.19	88	21.05	62	19.87	66	19.76	49	15.36	55	18.27	70	19.50	36	16.00	44	18.11	73	22.05
G. falconensis	11	3.25	18	4.31	14	4.49	13	3.89	12	3.76	14	4.65	17	4.74	9	4.00	11	4.53	19	5.74
G. hirsuta	2	0.59	4	0.96	1	0.32	1	0.30	4	1.25	2	0.66	6	1.67	2	0.89	3	1.23	3	0.91
G. truncatulinoides (d)	0	0.00	0	0.00	0	0.00	0	0.00	0	0.00	0	0.00	0	0.00	0	0.00	0	0.00	0	0.00
G. truncatulinoides (s)	8	2.37	5	1.20	5	1.60	9	2.69	11	3.45	5	1.66	10	2.79	12	5.33	2	0.82	5	1.51
G. ruber (alba)	6	1.78	11	2.63	2	0.64	8	2.40	8	2.51	5	1.66	8	2.23	4	1.78	8	3.29	11	3.32
G. trilobus	22	6.51	20	4.78	10	3.21	27	8.08	15	4.70	29	9.63	29	8.08	20	8.89	22	9.05	27	8.16
G. sacculifer	14	4.14	18	4.31	13	4.17	16	4.79	16	5.02	13	4.32	15	4.18	13	5.78	12	4.94	22	6.65
G. dutertrei	11	3.25	20	4.78	20	6.41	19	5.69	19	5.96	9	2.99	15	4.18	8	3.56	14	5.76	4	1.21
G. menardii	2	0.59	0	0.00	0	0.00	0	0.00	1	0.31	0	0.00	1	0.28	0	0.00	1	0.41	0	0.00
G. crassaformis	3	0.89	2	0.48	1	0.32	4	1.20	4	1.25	3	1.00	10	2.79	4	1.78	1	0.41	2	0.60
G. calida	8	2.37	9	2.15	9	2.88	11	3.29	8	2.51	0	0.00	2	0.56	5	2.22	4	1.65	12	3.63
T. quinqeloba	23	6.80	21	5.02	12	3.85	9	2.69	14	4.39	11	3.65	12	3.34	3	1.33	7	2.88	11	3.32
Other	15	4.44	34	8.13	23	7.37	15	4.49	23	7.21	33	10.96	36	10.03	32	14.22	32	13.17	27	8.16
TOTAL	338	100.00	418	100.00	312	100.00	334	100.00	319	100.00	301	100.00	359	100.00	225	100.00	243	100.00	331	100.00
Complete Forams	338		418		312		334		319		301		359		225		243		331	
Fragments	79		82		85		100		123		131		171		159		144		122	
Split	10		10		11		10.5		10.5		9		9		9		9		9	

SAMPLE DEPTH (cm)	1300	%	1310	%	1320	%	1330	%	1340	%	1350	%	1360	%	1370	%	1380	%	1390	%
SPECIES COUNTED																				
G. pachyderma (sinistral)	5	1.20	4	1.08	8	2.13	10	2.81	10	3.66	17	4.40	12	5.19	20	5.75	12	3.79	10	2.81
G. pachyderma (dextral)	60	14.42	46	12.47	57	15.16	38	10.67	37	13.55	60	15.54	30	12.99	43	12.36	43	13.56	72	20.22
G. bulloides	12	2.88	12	3.25	12	3.19	12	3.37	11	4.03	15	3.89	6	2.60	16	4.60	15	4.73	16	4.49
G. scitula	10	2.40	11	2.98	18	4.79	17	4.78	8	2.93	12	3.11	9	3.90	7	2.01	14	4.42	11	3.09
G. glutinata	44	10.58	48	13.01	59	15.69	41	11.52	23	8.42	49	12.69	23	9.96	28	8.05	36	11.36	43	12.08
G. inflata	84	20.19	93	25.20	77	20.48	69	19.38	68	24.91	99	25.65	54	23.38	80	22.99	58	18.30	55	15.45
G. falconensis	13	3.13	15	4.07	19	5.05	19	5.34	9	3.30	9	2.33	9	3.90	16	4.60	16	5.05	13	3.65
G. hirsuta	7	1.68	1	0.27	0	0.00	4	1.12	5	1.83	8	2.07	5	2.16	4	1.15	4	1.26	7	1.97
G. truncatulinoides (d)	0	0.00	0	0.00	1	0.27	0	0.00	0	0.00	0	0.00	0	0.00	0	0.00	0	0.00	0	0.00
G. truncatulinoides (s)	22	5.29	6	1.63	5	1.33	6	1.69	9	3.30	3	0.78	3	1.30	9	2.59	9	2.84	7	1.97
G. ruber (alba)	15	3.61	11	2.98	24	6.38	18	5.06	7	2.56	3	0.78	2	0.87	6	1.72	13	4.10	9	2.53
G. trilobus	27	6.49	33	8.94	21	5.59	25	7.02	19	6.96	21	5.44	19	8.23	24	6.90	21	6.62	24	6.74
G. sacculifer	25	6.01	17	4.61	17	4.52	18	5.06	13	4.76	10	2.59	8	3.46	14	4.02	7	2.21	17	4.78
G. dutertrei	23	5.53	13	3.52	14	3.72	18	5.06	9	3.30	19	4.92	8	3.46	13	3.74	13	4.10	22	6.18
G. menardii	2	0.48	1	0.27	0	0.00	0	0.00	2	0.73	2	0.52	1	0.43	1	0.29	0	0.00	2	0.56
G. crassaformis	4	0.96	6	1.63	4	1.06	3	0.84	7	2.56	8	2.07	6	2.60	6	1.72	5	1.58	5	1.40
G. calida	9	2.16	19	5.15	8	2.13	8	2.25	3	1.10	14	3.63	9	3.90	9	2.59	10	3.15	15	4.21
T. quinqeloba	11	2.64	6	1.63	9	2.39	5	1.40	8	2.93	7	1.81	6	2.60	8	2.30	7	2.21	13	3.65
Other	43	10.34	27	7.32	23	6.12	45	12.64	25	9.16	30	7.77	21	9.09	44	12.64	34	10.73	15	4.21
TOTAL	416	100.00	369	100.00	376	100.00	356	100.00	273	100.00	386	100.00	231	100.00	348	100.00	317	100.00	356	100.00
Complete Forams	416		369		376		356		273		386		231		348		317		356	
Fragments	399		157		100		178		135		164		146		129		247		121	
Split	9		9		8		9		10		10		10		10		9		11	

CORE MD962080 (AGULHAS BANK SLOPE)

SAMPLE DEPTH (cm)	1400	%	1410	%	1420	%	1430	%	1440	%	1450	%	1460	%	1470	%	1480	%	1490	%
SPECIES COUNTED																				
G. pachyderma (sinistral)	16	4.145	11	3.560	5	1.779	9	2.632	7	1.944	10	3.040	12	5.150	12	3.550	6	1.802	13	4.643
G. pachyderma (dextral)	65	16.839	50	16.181	40	14.235	53	15.497	67	18.611	50	15.198	37	15.880	65	19.231	68	20.420	44	15.714
G. bulloides	12	3.109	16	5.178	12	4.270	11	3.216	10	2.778	11	3.343	8	3.433	17	5.030	23	6.907	9	3.214
G. scitula	12	3.109	7	2.265	9	3.203	5	1.462	17	4.722	10	3.040	4	1.717	19	5.621	6	1.802	7	2.500
G. glutinata	44	11.399	33	10.680	39	13.879	53	15.497	34	9.444	36	10.942	29	12.446	46	13.609	44	13.213	31	11.071
G. inflata	77	19.948	60	19.417	55	19.573	59	17.251	71	19.722	86	26.140	55	23.605	35	10.355	47	14.114	54	19.286
G. falconensis	20	5.181	13	4.207	7	2.491	9	2.632	18	5.000	17	5.167	15	6.438	18	5.325	9	2.703	19	6.786
G. hirsuta	9	2.332	1	0.324	6	2.135	3	0.877	8	2.222	8	2.432	6	2.575	3	0.888	6	1.802	7	2.500
G. truncatulinoides (d)	0	0.000	0	0.000	0	0.000	1	0.292	1	0.278	0	0.000	0	0.000	0	0.000	0	0.000	0	0.000
G. truncatulinoides (s)	7	1.813	8	2.589	6	2.135	7	2.047	3	0.833	6	1.824	6	2.575	3	0.888	4	1.201	8	2.857
G. ruber (alba)	13	3.368	10	3.236	10	3.559	15	4.386	10	2.778	5	1.520	5	2.146	5	1.479	8	2.402	7	2.500
G. trilobus	34	8.808	22	7.120	19	6.762	23	6.725	23	6.389	23	6.991	8	3.433	24	7.101	14	4.204	20	7.143
G. sacculifer	11	2.850	13	4.207	12	4.270	17	4.971	11	3.056	9	2.736	11	4.721	19	5.621	22	6.607	11	3.929
G. dutertrei	19	4.922	26	8.414	21	7.473	23	6.725	26	7.222	19	5.775	11	4.721	18	5.325	28	8.408	17	6.071
G. menardii	2	0.518	1	0.324	1	0.356	0	0.000	0	0.000	0	0.000	1	0.429	1	0.296	2	0.601	0	0.000
G. crassaformis	1	0.259	6	1.942	3	1.068	3	0.877	3	0.833	3	0.912	3	1.288	3	0.888	5	1.502	4	1.429
G. calida	1	0.259	1	0.324	7	2.491	10	2.924	6	1.667	8	2.432	6	2.575	8	2.367	12	3.604	8	2.857
T. quinqeloba	5	1.295	5	1.618	4	1.423	4	1.170	17	4.722	7	2.128	3	1.288	15	4.438	7	2.102	5	1.786
Other	38	9.845	26	8.414	25	8.897	37	10.819	28	7.778	21	6.383	13	5.579	27	7.988	22	6.607	16	5.714
TOTAL	386	100	309	100	281	100	342	100	360	100	329	100	233	100	338	100	333	100	280	100
Complete Forams	386		309		281		342		360		329		233		338		333		280	
Fragments	324		285		351		243		219		135		200		235		163		119	
Split	8		9		9		10		10		10.5		11.5		10		10.5		9.5	

CORE MD962084 (OLIFANTS RIVER SLOPE)

SAMPLE DEPTH (cm)	2	%	10	%	20	%	30	%	40	%	50	%	60	%	70	%	80	%	90	%
SPECIES COUNTED																				
G. pachyderma (sinistral)	3	1.55	5	1.40	4	1.50	2	0.80	8	2.70	4	1.18	9	2.95	7	2.11	7	2.88	8	2.67
G. pachyderma (dextral)	38	19.59	66	18.44	55	20.60	35	13.94	53	17.91	60	17.75	59	19.34	59	17.77	45	18.52	50	16.67
G. bulloides	19	9.79	35	9.78	22	8.24	23	9.16	35	11.82	36	10.65	29	9.51	36	10.84	25	10.29	35	11.67
G. scitula	2	1.03	8	2.23	9	3.37	11	4.38	10	3.38	8	2.37	18	5.90	17	5.12	7	2.88	15	5.00
G. glutinata	8	4.12	20	5.59	6	2.25	16	6.37	18	6.08	18	5.33	17	5.57	19	5.72	15	6.17	15	5.00
G. inflata	50	25.77	91	25.42	61	22.85	73	29.08	60	20.27	78	23.08	63	20.66	75	22.59	57	23.46	63	21.00
G. falconensis	14	7.22	27	7.54	22	8.24	19	7.57	21	7.09	21	6.21	22	7.21	20	6.02	17	7.00	21	7.00
G. hirsuta	0	0.00	3	0.84	0	0.00	7	2.79	3	1.01	4	1.18	3	0.98	2	0.60	3	1.23	0	0.00
G. truncatulinoides (d)	1	0.52	0	0.00	1	0.37	0	0.00	0	0.00	2	0.59	2	0.66	1	0.30	1	0.41	0	0.00
G. truncatulinoides (s)	4	2.06	2	0.56	2	0.75	1	0.40	5	1.69	5	1.48	4	1.31	3	0.90	2	0.82	6	2.00
G. ruber (alba)	1	0.52	4	1.12	7	2.62	1	0.40	6	2.03	5	1.48	4	1.31	5	1.51	4	1.65	5	1.67
G. trilobus	3	1.55	8	2.23	8	3.00	6	2.39	5	1.69	7	2.07	5	1.64	5	1.51	4	1.65	8	2.67
G. sacculifer	2	1.03	3	0.84	4	1.50	1	0.40	6	2.03	12	3.55	5	1.64	10	3.01	6	2.47	7	2.33
G. dutertrei	10	5.15	13	3.63	12	4.49	9	3.59	6	2.03	5	1.48	7	2.30	13	3.92	7	2.88	13	4.33
G. menardii	0	0.00	1	0.28	0	0.00	0	0.00	1	0.34	0	0.00	2	0.66	0	0.00	0	0.00	1	0.33
G. crassaformis	1	0.52	1	0.28	2	0.75	1	0.40	1	0.34	0	0.00	2	0.66	2	0.60	3	1.23	4	1.33
G. calida	11	5.67	7	1.96	11	4.12	11	4.38	12	4.05	16	4.73	5	1.64	10	3.01	3	1.23	10	3.33
T. quinqeloba	4	2.06	9	2.51	4	1.50	2	0.80	6	2.03	13	3.85	8	2.62	11	3.31	4	1.65	6	2.00
G. uvula	4	2.06	10	2.79	4	1.50	7	2.79	10	3.38	11	3.25	9	2.95	7	2.11	7	2.88	5	1.67
Other	19	9.79	45	12.57	33	12.36	26	10.36	30	10.14	33	9.76	32	10.49	30	9.04	26	10.70	28	9.33
TOTAL	194	100.00	358	100.00	267	100.00	251	100.00	296	100.00	338	100.00	305	100.00	332	100.00	243	100.00	300	100.00
Complete Forams	88		360		266		250		294		326		308		340		239		295	
Fragments	100		326		207		243		243		229		250		213		146		198	
Split	7		7		8		8		7		8		8		9		8		8	

SAMPLE DEPTH (cm)	100	%	110	%	120	%	130	%	140	%	150	%	160	%	170	%	180	%	190	%
SPECIES COUNTED																				
G. pachyderma (sinistral)	5	1.95	2	0.54	9	3.25	3	0.98	7	2.68	10	3.69	8	2.05	5	2.34	6	2.01	7	3.02
G. pachyderma (dextral)	31	12.06	57	15.28	44	15.88	47	15.36	41	15.71	49	18.08	65	16.67	41	19.16	56	18.73	52	22.41
G. bulloides	36	14.01	52	13.94	37	13.36	37	12.09	24	9.20	38	14.02	43	11.03	27	12.62	33	11.04	31	13.36
G. scitula	18	7.00	12	3.22	21	7.58	15	4.90	29	11.11	29	10.70	32	8.21	9	4.21	27	9.03	20	8.62
G. glutinata	21	8.17	29	7.77	25	9.03	25	8.17	19	7.28	21	7.75	38	9.74	21	9.81	28	9.36	19	8.19
G. inflata	43	16.73	94	25.20	43	15.52	74	24.18	57	21.84	48	17.71	71	18.21	43	20.09	51	17.06	43	18.53
G. falconensis	15	5.84	28	7.51	20	7.22	22	7.19	20	7.66	20	7.38	34	8.72	17	7.94	18	6.02	15	6.47
G. hirsuta	2	0.78	2	0.54	2	0.72	0	0.00	0	0.00	4	1.48	3	0.77	1	0.47	1	0.33	0	0.00
G. truncatulinoides (d)	0	0.00	0	0.00	0	0.00	0	0.00	2	0.77	0	0.00	0	0.00	0	0.00	0	0.00	0	0.00
G. truncatulinoides (s)	3	1.17	7	1.88	3	1.08	2	0.65	4	1.53	2	0.74	4	1.03	3	1.40	4	1.34	0	0.00
G. ruber (alba)	8	3.11	7	1.88	7	2.53	8	2.61	2	0.77	2	0.74	4	1.03	4	1.87	1	0.33	2	0.86
G. trilobus	7	2.72	9	2.41	6	2.17	12	3.92	4	1.53	5	1.85	16	4.10	5	2.34	7	2.34	5	2.16
G. sacculifer	11	4.28	10	2.68	5	1.81	16	5.23	5	1.92	6	2.21	15	3.85	7	3.27	9	3.01	4	1.72
G. dutertrei	11	4.28	10	2.68	3	1.08	8	2.61	4	1.53	3	1.11	10	2.56	4	1.87	10	3.34	8	3.45
G. menardii	1	0.39	0	0.00	0	0.00	2	0.65	2	0.77	1	0.37	1	0.26	1	0.47	0	0.00	1	0.43
G. crassaformis	0	0.00	0	0.00	1	0.36	0	0.00	0	0.00	0	0.00	0	0.00	1	0.47	1	0.33	0	0.00
G. calida	9	3.50	10	2.68	12	4.33	8	2.61	9	3.45	4	1.48	9	2.31	8	3.74	13	4.35	7	3.02
T. quinqeloba	6	2.33	9	2.41	6	2.17	4	1.31	6	2.30	6	2.21	9	2.31	4	1.87	12	4.01	4	1.72
G. uvula	8	3.11	7	1.88	5	1.81	7	2.29	4	1.53	2	0.74	3	0.77	3	1.40	7	2.34	3	1.29
Other	22	8.56	28	7.51	28	10.11	16	5.23	22	8.43	21	7.75	25	6.41	10	4.67	15	5.02	11	4.74
TOTAL	257	100.00	373	100.00	277	100.00	306	100.00	261	100.00	271	100.00	390	100.00	214	100.00	299	100.00	232	100.00
Complete Forams	259		388		284		310		268		284		400		216		263		233	
Fragments	123		117		112		123		176		129		156		91		125		88	
Split	10		8		9		9		10		10		9		10		11		11	

CORE MD962084 (OLIFANTS RIVER SLOPE)

SAMPLE DEPTH (cm)	200	%	210	%	220	%	230	%	240	%	250	%	260	%	270	%	280	%	290	%
SPECIES COUNTED																				
G. pachyderma (sinistral)	8	3.03	8	2.66	13	4.89	10	3.62	8	2.66	5	1.91	9	3.03	7	2.67	12	2.45	4	1.77
G. pachyderma (dextral)	53	20.08	65	21.59	76	28.57	53	19.20	80	26.58	41	15.65	58	19.53	62	23.66	123	25.10	53	23.45
G. bulloides	30	11.36	34	11.30	29	10.90	34	12.32	38	12.62	35	13.36	30	10.10	34	12.98	73	14.90	28	12.39
G. scitula	21	7.95	16	5.32	9	3.38	23	8.33	21	6.98	16	6.11	21	7.07	7	2.67	24	4.90	7	3.10
G. glutinata	18	6.82	20	6.64	15	5.64	16	5.80	19	6.31	19	7.25	25	8.42	19	7.25	40	8.16	14	6.19
G. inflata	54	20.45	59	19.60	48	18.05	45	16.30	53	17.61	54	20.61	42	14.14	66	25.19	77	15.71	34	15.04
G. falconensis	21	7.95	18	5.98	17	6.39	22	7.97	15	4.98	21	8.02	22	7.41	13	4.96	31	6.33	13	5.75
G. hirsuta	3	1.14	2	0.66	1	0.38	1	0.36	1	0.33	2	0.76	11	3.70	0	0.00	2	0.41	1	0.44
G. truncatulinoides (d)	0	0.00	0	0.00	1	0.38	0	0.00	1	0.33	0	0.00	0	0.00	0	0.00	1	0.20	1	0.44
G. truncatulinoides (s)	4	1.52	5	1.66	2	0.75	1	0.36	5	1.66	0	0.00	3	1.01	1	0.38	5	1.02	1	0.44
G. ruber (alba)	4	1.52	3	1.00	1	0.38	4	1.45	3	1.00	2	0.76	5	1.68	2	0.76	4	0.82	4	1.77
G. trilobus	4	1.52	9	2.99	4	1.50	6	2.17	7	2.33	6	2.29	6	2.02	3	1.15	9	1.84	6	2.65
G. sacculifer	3	1.14	11	3.65	9	3.38	8	2.90	6	1.99	8	3.05	7	2.36	3	1.15	11	2.24	7	3.10
G. dutertrei	7	2.65	13	4.32	8	3.01	6	2.17	10	3.32	9	3.44	4	1.35	8	3.05	13	2.65	13	5.75
G. menardii	0	0.00	0	0.00	0	0.00	0	0.00	0	0.00	1	0.38	1	0.34	0	0.00	1	0.20	1	0.44
G. crassaformis	0	0.00	0	0.00	1	0.38	0	0.00	1	0.33	1	0.38	0	0.00	1	0.38	0	0.00	0	0.00
G. calida	8	3.03	10	3.32	11	4.14	14	5.07	6	1.99	8	3.05	13	4.38	6	2.29	13	2.65	5	2.21
T. quinqeloba	7	2.65	10	3.32	3	1.13	10	3.62	9	2.99	5	1.91	10	3.37	7	2.67	8	1.63	9	3.98
G. uvula	4	1.52	7	2.33	4	1.50	3	1.09	6	1.99	4	1.53	10	3.37	8	3.05	14	2.86	5	2.21
Other	15	5.68	11	3.65	14	5.26	20	7.25	12	3.99	25	9.54	20	6.73	15	5.73	29	5.92	20	8.85
TOTAL	264	100.00	301	100.00	266	100.00	276	100.00	301	100.00	262	100.00	297	100.00	262	100.00	490	100.00	226	100.00
Complete Forams	264		305		272		284		303		268		297		262		490		226	
Fragments	89		94		105		94		133		183		126		100		134		85	
Split	11		10		11		10		10		9		10		9		10		10	

SAMPLE DEPTH (cm)	300	%	310	%	320	%	330	%	340	%	350	%	360	%	370	%	380	%	390	%
SPECIES COUNTED																				
G. pachyderma (sinistral)	6	2.30	5	1.82	4	1.19	4	1.61	8	2.13	6	1.44	5	1.93	4	2.01	5	1.50	5	1.73
G. pachyderma (dextral)	57	21.84	66	24.09	81	24.11	49	19.76	67	17.82	85	20.33	51	19.69	42	21.11	62	18.56	43	14.88
G. bulloides	20	7.66	41	14.96	40	11.90	23	9.27	45	11.97	53	12.68	29	11.20	25	12.56	36	10.78	29	10.03
G. scitula	18	6.90	9	3.28	16	4.76	7	2.82	14	3.72	6	1.44	13	5.02	9	4.52	19	5.69	17	5.88
G. glutinata	10	3.83	20	7.30	22	6.55	20	8.06	31	8.24	38	9.09	20	7.72	13	6.53	23	6.89	20	6.92
G. inflata	49	18.77	51	18.61	64	19.05	50	20.16	83	22.07	96	22.97	58	22.39	45	22.61	74	22.16	69	23.88
G. falconensis	34	13.03	19	6.93	17	5.06	11	4.44	20	5.32	25	5.98	16	6.18	12	6.03	14	4.19	12	4.15
G. hirsuta	0	0.00	0	0.00	0	0.00	1	0.40	1	0.27	1	0.24	0	0.00	1	0.50	4	1.20	1	0.35
G. truncatulinoides (d)	1	0.38	1	0.36	0	0.00	0	0.00	0	0.00	0	0.00	0	0.00	0	0.00	0	0.00	0	0.00
G. truncatulinoides (s)	2	0.77	3	1.09	3	0.89	4	1.61	2	0.53	4	0.96	3	1.16	7	3.52	3	0.90	1	0.35
G. ruber (alba)	2	0.77	1	0.36	4	1.19	3	1.21	3	0.80	2	0.48	3	1.16	0	0.00	2	0.60	7	2.42
G. trilobus	2	0.77	2	0.73	8	2.38	4	1.61	9	2.39	9	2.15	3	1.16	2	1.01	8	2.40	6	2.08
G. sacculifer	3	1.15	6	2.19	7	2.08	8	3.23	9	2.39	13	3.11	5	1.93	5	2.51	18	5.39	9	3.11
G. dutertrei	8	3.07	9	3.28	18	5.36	17	6.85	16	4.26	11	2.63	13	5.02	6	3.02	10	2.99	12	4.15
G. menardii	0	0.00	0	0.00	0	0.00	2	0.81	3	0.80	2	0.48	0	0.00	0	0.00	0	0.00	0	0.00
G. crassaformis	0	0.00	1	0.36	0	0.00	1	0.40	2	0.53	2	0.48	1	0.39	2	1.01	2	0.60	0	0.00
G. calida	9	3.45	11	4.01	7	2.08	6	2.42	8	2.13	9	2.15	4	1.54	6	3.02	8	2.40	7	2.42
T. quinqeloba	7	2.68	5	1.82	13	3.87	4	1.61	9	2.39	11	2.63	4	1.54	3	1.51	5	1.50	9	3.11
G. uvula	7	2.68	4	1.46	9	2.68	3	1.21	7	1.86	3	0.72	0	0.00	0	0.00	2	0.60	4	1.38
Other	26	9.96	20	7.30	23	6.85	31	12.50	39	10.37	42	10.05	31	11.97	17	8.54	39	11.68	38	13.15
TOTAL	261	100.00	274	100.00	336	100.00	248	100.00	376	100.00	418	100.00	259	100.00	199	100.00	334	100.00	289	100.00
Complete Forams	261		274		336		240		367		408		250		189		324		279	
Fragments	120		104		125		96		105		138		138		87		128		134	
Split	11		9		8		10		9		9		9.5		10		9		10	

CORE MD962084 (OLIFANTS RIVER SLOPE)

SAMPLE DEPTH (cm)	400	%	410	%	420	%	430	%	440	%	450	%	460	%	470	%	480	%	490	%
SPECIES COUNTED																				
G. pachyderma (sinistral)	4	1.56	3	1.34	4	1.38	4	1.25	1	0.61	4	1.64	4	2.14	3	1.28	6	1.86	4	2.06
G. pachyderma (dextral)	50	19.53	47	20.98	52	17.93	74	23.20	43	26.22	43	17.62	36	19.25	50	21.37	63	19.50	26	13.40
G. bulloides	34	13.28	24	10.71	34	11.72	21	6.58	10	6.10	24	9.84	13	6.95	20	8.55	31	9.60	19	9.79
G. scitula	8	3.13	12	5.36	12	4.14	12	3.76	4	2.44	11	4.51	14	7.49	14	5.98	18	5.57	11	5.67
G. glutinata	22	8.59	14	6.25	18	6.21	20	6.27	13	7.93	14	5.74	11	5.88	21	8.97	19	5.88	16	8.25
G. inflata	55	21.48	49	21.88	49	16.90	62	19.44	28	17.07	43	17.62	41	21.93	49	20.94	66	20.43	38	19.59
G. falconensis	10	3.91	6	2.68	14	4.83	8	2.51	4	2.44	6	2.46	6	3.21	8	3.42	15	4.64	10	5.15
G. hirsuta	3	1.17	4	1.79	0	0.00	1	0.31	1	0.61	1	0.41	2	1.07	3	1.28	2	0.62	3	1.55
G. truncatulinoides (d)	1	0.39	0	0.00	1	0.34	0	0.00	0	0.00	0	0.00	0	0.00	0	0.00	1	0.31	0	0.00
G. truncatulinoides (s)	3	1.17	1	0.45	5	1.72	6	1.88	1	0.61	3	1.23	1	0.53	2	0.85	2	0.62	2	1.03
G. ruber (alba)	5	1.95	3	1.34	3	1.03	5	1.57	1	0.61	4	1.64	3	1.60	1	0.43	4	1.24	5	2.58
G. trilobus	6	2.34	3	1.34	9	3.10	7	2.19	3	1.83	2	0.82	3	1.60	3	1.28	11	3.41	7	3.61
G. sacculifer	7	2.73	6	2.68	8	2.76	8	2.51	3	1.83	6	2.46	2	1.07	6	2.56	8	2.48	7	3.61
G. dutertrei	12	4.69	9	4.02	16	5.52	18	5.64	14	8.54	10	4.10	9	4.81	8	3.42	11	3.41	8	4.12
G. menardii	1	0.39	0	0.00	0	0.00	2	0.63	0	0.00	0	0.00	1	0.53	1	0.43	0	0.00	0	0.00
G. crassaformis	0	0.00	1	0.45	0	0.00	1	0.31	0	0.00	2	0.82	0	0.00	0	0.00	0	0.00	0	0.00
G. calida	3	1.17	4	1.79	8	2.76	9	2.82	2	1.22	8	3.28	7	3.74	5	2.14	11	3.41	2	1.03
T. quinqeloba	6	2.34	5	2.23	7	2.41	10	3.13	4	2.44	4	1.64	4	2.14	4	1.71	5	1.55	3	1.55
G. uvula	4	1.56	4	1.79	5	1.72	4	1.25	3	1.83	5	2.05	5	2.67	6	2.56	3	0.93	4	2.06
Other	22	8.59	29	12.95	45	15.52	47	14.73	29	17.68	54	22.13	25	13.37	30	12.82	47	14.55	29	14.95
TOTAL	256	100.00	224	100.00	290	100.00	319	100.00	164	100.00	244	100.00	187	100.00	234	100.00	323	100.00	194	100.00
Complete Forams	246		216		284		309		164		244		177		220		310		184	
Fragments	113		126		186		276		124		195		190		139		255		128	
Split	10		9		9		10		9		9		9		9		9		9	

SAMPLE DEPTH (cm)	500	%	510	%	520	%	530	%	540	%	550	%	560	%	570	%	580	%	590	%
SPECIES COUNTED																				
G. pachyderma (sinistral)	9	2.99	2	1.08	6	1.61	3	1.29	6	2.33	6	2.13	8	2.04					4	1.89
G. pachyderma (dextral)	45	14.95	30	16.22	62	16.62	39	16.81	42	16.34	46	16.31	57	14.54					27	12.74
G. bulloides	23	7.64	19	10.27	30	8.04	24	10.34	29	11.28	29	10.28	43	10.97					14	6.60
G. scitula	26	8.64	8	4.32	22	5.90	8	3.45	14	5.45	17	6.03	20	5.10					9	4.25
G. glutinata	18	5.98	10	5.41	36	9.65	15	6.47	18	7.00	19	6.74	30	7.65					16	7.55
G. inflata	69	22.92	42	22.70	61	16.35	42	18.10	45	17.51	63	22.34	72	18.37					46	21.70
G. falconensis	17	5.65	8	4.32	21	5.63	13	5.60	14	5.45	30	10.64	22	5.61	NO	SAMPLE			8	3.77
G. hirsuta	8	2.66	2	1.08	9	2.41	3	1.29	2	0.78	1	0.35	7	1.79					2	0.94
G. truncatulinoides (d)	2	0.66	1	0.54	1	0.27	0	0.00	0	0.00	0	0.00	1	0.26					0	0.00
G. truncatulinoides (s)	6	1.99	6	3.24	6	1.61	6	2.59	3	1.17	2	0.71	10	2.55			NO	SAMPLE	4	1.89
G. ruber (alba)	5	1.66	2	1.08	6	1.61	2	0.86	4	1.56	0	0.00	7	1.79					4	1.89
G. trilobus	6	1.99	5	2.70	7	1.88	6	2.59	5	1.95	0	0.00	8	2.04					4	1.89
G. sacculifer	11	3.65	3	1.62	16	4.29	10	4.31	8	3.11	6	2.13	18	4.59					7	3.30
G. dutertrei	7	2.33	8	4.32	14	3.75	12	5.17	9	3.50	9	3.19	15	3.83					17	8.02
G. menardii	2	0.66	1	0.54	0	0.00	1	0.43	0	0.00	0	0.00	0	0.00					0	0.00
G. crassaformis	4	1.33	2	1.08	2	0.54	3	1.29	4	1.56	0	0.00	3	0.77					2	0.94
G. calida	7	2.33	3	1.62	7	1.88	4	1.72	5	1.95	6	2.13	10	2.55					9	4.25
T. quinqeloba	6	1.99	3	1.62	8	2.14	5	2.16	7	2.72	6	2.13	15	3.83					8	3.77
G. uvula	5	1.66	3	1.62	12	3.22	6	2.59	9	3.50	5	1.77	3	0.77					6	2.83
Other	25	8.31	27	14.59	47	12.60	30	12.93	33	12.84	37	13.12	43	10.97					25	11.79
TOTAL	301	100.00	185	100.00	373	100.00	232	100.00	257	100.00	282	100.00	392	100.00					212	100.00
Complete Forams	295		180		365		322		250		275		385		NO	SAMPLE			200	
Fragments	322		200		411		392		359		256		431						137	
Split			7		7		8		8		10		7						8	

CORE MD962084 (OLIFANTS RIVER SLOPE)

SAMPLE DEPTH (cm)	600	%	610	%	620	%	630	%	640	%	650	%	660	%	670	%	680	%	690	%
SPECIES COUNTED																				
G. pachyderma (sinistral)	5	2.50	8	2.56	5	1.74	6	1.59	5	2.02	5	2.62	7	3.52	7	2.03	5	2.17	7	1.90
G. pachyderma (dextral)	25	12.50	45	14.42	41	14.29	59	15.65	31	12.55	22	11.52	34	17.09	46	13.33	21	9.13	26	7.07
G. bulloides	17	8.50	18	5.77	27	9.41	31	8.22	25	10.12	20	10.47	17	8.54	31	8.99	19	8.26	38	10.33
G. scitula	10	5.00	19	6.09	19	6.62	21	5.57	16	6.48	13	6.81	8	4.02	17	4.93	11	4.78	27	7.34
G. glutinata	16	8.00	24	7.69	25	8.71	33	8.75	26	10.53	23	12.04	26	13.07	29	8.41	21	9.13	44	11.96
G. inflata	34	17.00	59	18.91	48	16.72	66	17.51	49	19.84	33	17.28	30	15.08	62	17.97	51	22.17	77	20.92
G. falconensis	13	6.50	22	7.05	14	4.88	18	4.77	13	5.26	10	5.24	14	7.04	20	5.80	17	7.39	23	6.25
G. hirsuta	5	2.50	4	1.28	4	1.39	8	2.12	1	0.40	3	1.57	4	2.01	4	1.16	4	1.74	6	1.63
G. truncatulinoides (d)	0	0.00	0	0.00	0	0.00	1	0.27	0	0.00	0	0.00	1	0.50	2	0.58	4	1.74	0	0.00
G. truncatulinoides (s)	2	1.00	9	2.88	3	1.05	6	1.59	4	1.62	2	1.05	9	4.52	10	2.90	7	3.04	8	2.17
G. ruber (alba)	5	2.50	5	1.60	8	2.79	6	1.59	4	1.62	1	0.52	2	1.01	5	1.45	5	2.17	12	3.26
G. trilobus	7	3.50	8	2.56	7	2.44	14	3.71	8	3.24	10	5.24	7	3.52	9	2.61	9	3.91	14	3.80
G. sacculifer	7	3.50	6	1.92	12	4.18	18	4.77	12	4.86	9	4.71	7	3.52	12	3.48	9	3.91	16	4.35
G. dutertrei	8	4.00	17	5.45	11	3.83	8	2.12	8	3.24	4	2.09	6	3.02	16	4.64	7	3.04	11	2.99
G. menardii	0	0.00	2	0.64	0	0.00	1	0.27	1	0.40	1	0.52	0	0.00	1	0.29	0	0.00	1	0.27
G. crassaformis	0	0.00	0	0.00	4	1.39	4	1.06	3	1.21	0	0.00	1	0.50	4	1.16	3	1.30	2	0.54
G. calida	8	4.00	12	3.85	7	2.44	9	2.39	6	2.43	6	3.14	3	1.51	10	2.90	1	0.43	8	2.17
T. quinqeloba	6	3.00	7	2.24	8	2.79	10	2.65	1	0.40	3	1.57	2	1.01	7	2.03	3	1.30	8	2.17
G. uvula	5	2.50	10	3.21	7	2.44	9	2.39	4	1.62	6	3.14	5	2.51	10	2.90	5	2.17	6	1.63
Other	27	13.50	37	11.86	37	12.89	49	13.00	30	12.15	20	10.47	16	8.04	43	12.46	28	12.17	34	9.24
TOTAL	200	100.00	312	100.00	287	100.00	377	100.00	247	100.00	191	100.00	199	100.00	345	100.00	230	100.00	368	100.00
Complete Forams	190		300		280		370		240		187		199		345		230		358	
Fragments	135		342		274		400		281		234		221		424		253		295	
Split	9		8		8		7		8		9		8		7		8		8	

SAMPLE DEPTH (cm)	700	%	710	%	720	%	730	%	740	%	750	%	760	%	770	%	780	%	790	%
SPECIES COUNTED																				
G. pachyderma (sinistral)	7	3.20	7	3.15	8	2.09	6	2.18	5	2.10	12	2.79	5	2.02	7	2.67	7	1.60	6	2.42
G. pachyderma (dextral)	22	10.05	22	9.91	52	13.61	40	14.55	29	12.18	75	17.44	46	18.62	48	18.32	69	15.75	44	17.74
G. bulloides	15	6.85	17	7.66	24	6.28	15	5.45	19	7.98	18	4.19	5	2.02	8	3.05	18	4.11	11	4.44
G. scitula	16	7.31	12	5.41	17	4.45	14	5.09	11	4.62	27	6.28	21	8.50	17	6.49	39	8.90	13	5.24
G. glutinata	21	9.59	25	11.26	41	10.73	30	10.91	23	9.66	42	9.77	16	6.48	21	8.02	42	9.59	24	9.68
G. inflata	37	16.89	40	18.02	69	18.06	52	18.91	51	21.43	77	17.91	54	21.86	57	21.76	74	16.89	48	19.35
G. falconensis	14	6.39	9	4.05	28	7.33	13	4.73	12	5.04	19	4.42	10	4.05	11	4.20	19	4.34	9	3.63
G. hirsuta	3	1.37	7	3.15	6	1.57	5	1.82	5	2.10	5	1.16	6	2.43	8	3.05	8	1.83	7	2.82
G. truncatulinoides (d)	1	0.46	1	0.45	1	0.26	0	0.00	0	0.00	2	0.47	0	0.00	1	0.38	0	0.00	1	0.40
G. truncatulinoides (s)	4	1.83	4	1.80	6	1.57	6	2.18	4	1.68	5	1.16	3	1.21	4	1.53	5	1.14	2	0.81
G. ruber (alba)	7	3.20	5	2.25	16	4.19	4	1.45	3	1.26	11	2.56	6	2.43	2	0.76	4	0.91	2	0.81
G. trilobus	13	5.94	8	3.60	12	3.14	11	4.00	10	4.20	17	3.95	5	2.02	8	3.05	15	3.42	9	3.63
G. sacculifer	12	5.48	11	4.95	18	4.71	7	2.55	10	4.20	14	3.26	10	4.05	8	3.05	12	2.74	3	1.21
G. dutertrei	12	5.48	11	4.95	21	5.50	17	6.18	10	4.20	17	3.95	11	4.45	14	5.34	25	5.71	11	4.44
G. menardii	0	0.00	1	0.45	2	0.52	0	0.00	0	0.00	1	0.23	3	1.21	2	0.76	0	0.00	0	0.00
G. crassaformis	0	0.00	0	0.00	2	0.52	3	1.09	0	0.00	3	0.70	1	0.40	3	1.15	3	0.68	1	0.40
G. calida	4	1.83	2	0.90	4	1.05	3	1.09	5	2.10	12	2.79	5	2.02	6	2.29	18	4.11	10	4.03
T. quinqeloba	5	2.28	6	2.70	11	2.88	6	2.18	4	1.68	10	2.33	6	2.43	7	2.67	10	2.28	6	2.42
G. uvula	6	2.74	7	3.15	8	2.09	9	3.27	6	2.52	9	2.09	5	2.02	4	1.53	15	3.42	7	2.82
Other	20	9.13	27	12.16	36	9.42	34	12.36	31	13.03	54	12.56	29	11.74	26	9.92	55	12.56	34	13.71
TOTAL	219	100.00	222	100.00	382	100.00	275	100.00	238	100.00	430	100.00	247	100.00	262	100.00	438	100.00	248	100.00
Complete Forams	215		216		378		268		230		420		247		255		435		240	
Fragments	159		167		213		180		133		190		155		120		250		184	
Split	9		9		8		9		9		9		10		10		9		9	

CORE MD962084 (OLIFANTS RIVER SLOPE)

SAMPLE DEPTH (cm)	800	%	810	%	820	%	830	%	840	%	850	%	860	%	870	%	880	%	890	%
SPECIES COUNTED																				
G. pachyderma (sinistral)	8	2.67	6	2.71	9	2.49	7	3.78	9	2.47	4	1.86	7	3.33	6	2.05	7	2.24	6	2.97
G. pachyderma (dextral)	51	17.00	39	17.65	60	16.57	26	14.05	56	15.34	36	16.74	31	14.76	42	14.38	62	19.81	44	21.78
G. bulloides	22	7.33	13	5.88	16	4.42	11	5.95	17	4.66	9	4.19	7	3.33	16	5.48	21	6.71	4	1.98
G. scitula	19	6.33	6	2.71	17	4.70	6	3.24	7	1.92	6	2.79	7	3.33	5	1.71	7	2.24	7	3.47
G. glutinata	19	6.33	12	5.43	39	10.77	12	6.49	30	8.22	18	8.37	19	9.05	22	7.53	22	7.03	26	12.87
G. inflata	53	17.67	39	17.65	54	14.92	43	23.24	79	21.64	49	22.79	51	24.29	60	20.55	62	19.81	31	15.35
G. falconensis	19	6.33	9	4.07	10	2.76	5	2.70	16	4.38	11	5.12	16	7.62	12	4.11	11	3.51	5	2.48
G. hirsuta	7	2.33	7	3.17	8	2.21	5	2.70	6	1.64	3	1.40	4	1.90	7	2.40	8	2.56	5	2.48
G. truncatulinoides (d)	2	0.67	1	0.45	1	0.28	1	0.54	2	0.55	0	0.00	1	0.48	2	0.68	1	0.32	1	0.50
G. truncatulinoides (s)	11	3.67	7	3.17	11	3.04	2	1.08	5	1.37	4	1.86	6	2.86	6	2.05	8	2.56	4	1.98
G. ruber (alba)	8	2.67	3	1.36	5	1.38	3	1.62	9	2.47	2	0.93	5	2.38	16	5.48	14	4.47	5	2.48
G. trilobus	7	2.33	7	3.17	8	2.21	4	2.16	11	3.01	8	3.72	5	2.38	7	2.40	8	2.56	10	4.95
G. sacculifer	11	3.67	5	2.26	8	2.21	4	2.16	14	3.84	6	2.79	7	3.33	11	3.77	15	4.79	7	3.47
G. dutertrei	20	6.67	16	7.24	23	6.35	17	9.19	28	7.67	16	7.44	8	3.81	15	5.14	15	4.79	12	5.94
G. menardii	0	0.00	1	0.45	3	0.83	1	0.54	2	0.55	0	0.00	0	0.00	1	0.34	1	0.32	2	0.99
G. crassaformis	4	1.33	4	1.81	3	0.83	2	1.08	1	0.27	1	0.47	0	0.00	1	0.34	1	0.32	0	0.00
G. calida	7	2.33	4	1.81	11	3.04	4	2.16	12	3.29	6	2.79	6	2.86	7	2.40	8	2.56	4	1.98
T. quinqeloba	9	3.00	8	3.62	14	3.87	6	3.24	8	2.19	3	1.40	4	1.90	4	1.37	7	2.24	7	3.47
G. uvula	6	2.00	8	3.62	8	2.21	4	2.16	8	2.19	5	2.33	4	1.90	8	2.74	4	1.28	5	2.48
Other	17	5.67	26	11.76	54	14.92	22	11.89	45	12.33	28	13.02	22	10.48	44	15.07	31	9.90	17	8.42
TOTAL	300	100.00	221	100.00	362	100.00	185	100.00	365	100.00	215	100.00	210	100.00	292	100.00	313	100.00	202	100.00
Complete Forams	300		216		360		185		360		210		210		292		313		202	
Fragments	264		196		344		377		516		183		311		428		363		270	
Split	7		8		8		8		7		8		7		7		7		7	

SAMPLE DEPTH (cm)	900	%	910	%	920	%	930	%	940	%	950	%	960	%	970	%	980	%	990	%
SPECIES COUNTED																				
G. pachyderma (sinistral)	8	1.92	3	0.82	5	1.98	4	1.24	5	1.98	7	2.66	2	0.76	2	1.01	6	1.77	5	2.05
G. pachyderma (dextral)	85	20.43	68	18.63	55	21.83	66	20.50	49	19.37	57	21.67	58	22.05	55	27.64	83	24.48	50	20.49
G. bulloides	24	5.77	22	6.03	5	1.98	11	3.42	8	3.16	9	3.42	9	3.42	4	2.01	12	3.54	11	4.51
G. scitula	11	2.64	17	4.66	7	2.78	11	3.42	10	3.95	8	3.04	6	2.28	3	1.51	9	2.65	10	4.10
G. glutinata	34	8.17	28	7.67	32	12.70	28	8.70	18	7.11	20	7.60	19	7.22	20	10.05	23	6.78	26	10.66
G. inflata	64	15.38	73	20.00	50	19.84	67	20.81	45	17.79	51	19.39	49	18.63	30	15.08	64	18.88	35	14.34
G. falconensis	23	5.53	25	6.85	16	6.35	13	4.04	11	4.35	12	4.56	8	3.04	5	2.51	17	5.01	6	2.46
G. hirsuta	8	1.92	5	1.37	4	1.59	6	1.86	4	1.58	4	1.52	6	2.28	7	3.52	5	1.47	6	2.46
G. truncatulinoides (d)	1	0.24	0	0.00	1	0.40	0	0.00	0	0.00	0	0.00	0	0.00	0	0.00	0	0.00	2	0.82
G. truncatulinoides (s)	13	3.13	8	2.19	4	1.59	7	2.17	5	1.98	8	3.04	3	1.14	4	2.01	7	2.06	3	1.23
G. ruber (alba)	6	1.44	7	1.92	7	2.78	12	3.73	5	1.98	9	3.42	13	4.94	5	2.51	10	2.95	8	3.28
G. trilobus	10	2.40	11	3.01	7	2.78	9	2.80	14	5.53	15	5.70	14	5.32	14	7.04	20	5.90	7	2.87
G. sacculifer	12	2.88	15	4.11	16	6.35	12	3.73	11	4.35	8	3.04	6	2.28	5	2.51	14	4.13	9	3.69
G. dutertrei	40	9.62	16	4.38	11	4.37	16	4.97	11	4.35	19	7.22	14	5.32	15	7.54	17	5.01	9	3.69
G. menardii	1	0.24	0	0.00	0	0.00	0	0.00	2	0.79	1	0.38	0	0.00	0	0.00	1	0.29	0	0.00
G. crassaformis	3	0.72	4	1.10	1	0.40	2	0.62	0	0.00	1	0.38	0	0.00	1	0.50	1	0.29	1	0.41
G. calida	20	4.81	13	3.56	7	2.78	17	5.28	11	4.35	8	3.04	9	3.42	4	2.01	8	2.36	9	3.69
T. quinqeloba	8	1.92	9	2.47	4	1.59	7	2.17	5	1.98	4	1.52	8	3.04	2	1.01	5	1.47	5	2.05
G. uvula	9	2.16	9	2.47	4	1.59	8	2.48	8	3.16	1	0.38	6	2.28	1	0.50	5	1.47	12	4.92
Other	36	8.65	32	8.77	16	6.35	26	8.07	31	12.25	21	7.98	33	12.55	22	11.06	32	9.44	30	12.30
TOTAL	416	100.00	365	100.00	252	100.00	322	100.00	253	100.00	263	100.00	263	100.00	199	100.00	339	100.00	244	100.00
Complete Forams	416		365		252		322		253		263		263		199		339		244	
Fragments	223		207		253		210		189		186		308		260		365		246	
Split	7		8		8		8		9		10		9						8	

CORE MD962084 (OLIFANTS RIVER SLOPE)

SAMPLE DEPTH (cm)	1000	%	1010	%	1020	%	1030	%	1040	%	1050	%	1060	%	1070	%	1080	%	1090	%
SPECIES COUNTED																				
G. pachyderma (sinistral)	2	0.97	5	2.65	4	1.27	6	2.24	8	3.08	8	4.37	7	3.26	5	2.16	5	2.42	9	3.03
G. pachyderma (dextral)	29	14.01	26	13.76	68	21.66	64	23.88	58	22.31	43	23.50	49	22.79	59	25.43	43	20.77	70	23.57
G. bulloides	11	5.31	12	6.35	21	6.69	14	5.22	14	5.38	13	7.10	6	2.79	8	3.45	12	5.80	7	2.36
G. scitula	7	3.38	10	5.29	6	1.91	5	1.87	5	1.92	3	1.64	5	2.33	8	3.45	4	1.93	17	5.72
G. glutinata	18	8.70	17	8.99	29	9.24	27	10.07	26	10.00	15	8.20	13	6.05	15	6.47	20	9.66	27	9.09
G. inflata	44	21.26	46	24.34	52	16.56	46	17.16	40	15.38	22	12.02	39	18.14	42	18.10	33	15.94	57	19.19
G. falconensis	10	4.83	11	5.82	12	3.82	8	2.99	6	2.31	9	4.92	8	3.72	2	0.86	11	5.31	3	1.01
G. hirsuta	6	2.90	0	0.00	2	0.64	1	0.37	1	0.38	4	2.19	5	2.33	4	1.72	6	2.90	2	0.67
G. truncatulinoides (d)	2	0.97	0	0.00	1	0.32	0	0.00	0	0.00	0	0.00	0	0.00	0	0.00	1	0.48	1	0.34
G. truncatulinoides (s)	5	2.42	3	1.59	2	0.64	12	4.48	7	2.69	6	3.28	1	0.47	3	1.29	4	1.93	4	1.35
G. ruber (alba)	9	4.35	10	5.29	14	4.46	5	1.87	4	1.54	2	1.09	5	2.33	13	5.60	3	1.45	11	3.70
G. trilobus	12	5.80	3	1.59	9	2.87	11	4.10	11	4.23	6	3.28	11	5.12	7	3.02	12	5.80	10	3.37
G. sacculifer	11	5.31	9	4.76	9	2.87	4	1.49	10	3.85	7	3.83	9	4.19	6	2.59	7	3.38	15	5.05
G. dutertrei	11	5.31	12	6.35	25	7.96	25	9.33	18	6.92	20	10.93	9	4.19	14	6.03	12	5.80	10	3.37
G. menardii	0	0.00	0	0.00	0	0.00	0	0.00	0	0.00	0	0.00	0	0.00	0	0.00	0	0.00	0	0.00
G. crassaformis	0	0.00	0	0.00	0	0.00	2	0.75	1	0.38	0	0.00	0	0.00	2	0.86	1	0.48	1	0.34
G. calida	2	0.97	4	2.12	15	4.78	9	3.36	11	4.23	4	2.19	4	1.86	9	3.88	3	1.45	4	1.35
T. quinqeloba	4	1.93	5	2.65	9	2.87	8	2.99	8	3.08	6	3.28	9	4.19	11	4.74	6	2.90	13	4.38
G. uvula	4	1.93	5	2.65	10	3.18	2	0.75	5	1.92	2	1.09	7	3.26	2	0.86	5	2.42	8	2.69
Other	20	9.66	11	5.82	26	8.28	19	7.09	27	10.38	13	7.10	28	13.02	22	9.48	19	9.18	28	9.43
TOTAL	207	100.00	189	100.00	314	100.00	268	100.00	260	100.00	183	100.00	215	100.00	232	100.00	207	100.00	297	100.00
Complete Forams	207		189		314		268		260		183		215		232		207		297	
Fragments	216		147		141		112		143		99		166		158		144		248	
Split	8		9		8		8		8		9		9		9		9		9	

SAMPLE DEPTH (cm)	1100	%	1110	%	1120	%	1130	%	1140	%	1150	%	1160	%	1170	%	1180	%	1190	%
SPECIES COUNTED																				
G. pachyderma (sinistral)	5	2.19	4	1.23	4	1.45	6	2.49	1	0.40	9	2.77	5	1.44	1	0.41	9	4.09	9	3.19
G. pachyderma (dextral)	50	21.93	70	21.54	54	19.64	51	21.16	54	21.34	64	19.69	55	15.85	38	15.57	52	23.64	57	20.21
G. bulloides	0	0.00	16	4.92	10	3.64	5	2.07	4	1.58	12	3.69	8	2.31	8	3.28	0	0.00	7	2.48
G. scitula	13	5.70	14	4.31	7	2.55	9	3.73	7	2.77	11	3.38	12	3.46	1	0.41	6	2.73	5	1.77
G. glutinata	26	11.40	21	6.46	15	5.45	10	4.15	20	7.91	13	4.00	16	4.61	13	5.33	10	4.55	10	3.55
G. inflata	43	18.86	72	22.15	68	24.73	41	17.01	47	18.58	60	18.46	87	25.07	54	22.13	37	16.82	56	19.86
G. falconensis	7	3.07	8	2.46	14	5.09	11	4.56	6	2.37	7	2.15	18	5.19	11	4.51	5	2.27	6	2.13
G. hirsuta	4	1.75	6	1.85	7	2.55	2	0.83	3	1.19	4	1.23	9	2.59	1	0.41	5	2.27	9	3.19
G. truncatulinoides (d)	1	0.44	1	0.31	0	0.00	0	0.00	1	0.40	2	0.62	3	0.86	0	0.00	0	0.00	2	0.71
G. truncatulinoides (s)	6	2.63	7	2.15	6	2.18	8	3.32	16	6.32	17	5.23	19	5.48	11	4.51	9	4.09	11	3.90
G. ruber (alba)	6	2.63	12	3.69	7	2.55	6	2.49	9	3.56	10	3.08	19	5.48	13	5.33	1	0.45	11	3.90
G. trilobus	11	4.82	12	3.69	11	4.00	18	7.47	24	9.49	22	6.77	21	6.05	18	7.38	23	10.45	21	7.45
G. sacculifer	10	4.39	11	3.38	7	2.55	10	4.15	6	2.37	16	4.92	5	1.44	10	4.10	8	3.64	8	2.84
G. dutertrei	12	5.26	23	7.08	12	4.36	15	6.22	16	6.32	20	6.15	12	3.46	18	7.38	11	5.00	14	4.96
G. menardii	0	0.00	1	0.31	0	0.00	0	0.00	2	0.79	1	0.31	1	0.29	2	0.82	1	0.45	0	0.00
G. crassaformis	0	0.00	0	0.00	1	0.36	2	0.83	0	0.00	2	0.62	4	1.15	1	0.41	0	0.00	3	1.06
G. calida	4	1.75	4	1.23	9	3.27	10	4.15	5	1.98	10	3.08	7	2.02	10	4.10	9	4.09	5	1.77
T. quinqeloba	4	1.75	3	0.92	5	1.82	2	0.83	5	1.98	3	0.92	6	1.73	7	2.87	6	2.73	7	2.48
G. uvula	3	1.32	5	1.54	3	1.09	4	1.66	5	1.98	5	1.54	2	0.58	2	0.82	2	0.91	3	1.06
Other	23	10.09	35	10.77	35	12.73	31	12.86	22	8.70	37	11.38	38	10.95	25	10.25	26	11.82	38	13.48
TOTAL	228	100.00	325	100.00	275	100.00	241	100.00	253	100.00	325	100.00	347	100.00	244	100.00	220	100.00	282	100.00
Complete Forams	228		325		275		241		253		325		347		244		220		282	
Fragments	210		359		240		450		420		503		511		389		236		250	
Split	8		5		6		6		6		6		6		5.5		7		6	

CORE MD962084 (OLIFANTS RIVER SLOPE)

SAMPLE DEPTH (cm)	1200	%	1210	%	1220	%	1230	%	1240	%	1250	%	1260	%	1270	%	1280	%	1290	%
SPECIES COUNTED																				
G. pachyderma (sinistral)	8	3.09	6	2.68	3	1.43	5	2.21	4	1.22	7	2.48	7	2.93	9	2.84	9	2.59	6	2.41
G. pachyderma (dextral)	49	18.92	42	18.75	41	19.52	50	22.12	77	23.40	61	21.63	45	18.83	76	23.97	74	21.26	41	16.47
G. bulloides	8	3.09	6	2.68	5	2.38	10	4.42	14	4.26	5	1.77	4	1.67	11	3.47	12	3.45	3	1.20
G. scitula	7	2.70	5	2.23	3	1.43	4	1.77	2	0.61	13	4.61	8	3.35	10	3.15	4	1.15	4	1.61
G. glutinata	21	8.11	11	4.91	12	5.71	12	5.31	27	8.21	19	6.74	12	5.02	18	5.68	21	6.03	9	3.61
G. inflata	51	19.69	48	21.43	51	24.29	50	22.12	59	17.93	51	18.09	64	26.78	67	21.14	75	21.55	50	20.08
G. falconensis	8	3.09	4	1.79	4	1.90	5	2.21	6	1.82	3	1.06	5	2.09	7	2.21	8	2.30	3	1.20
G. hirsuta	0	0.00	6	2.68	4	1.90	4	1.77	4	1.22	10	3.55	8	3.35	5	1.58	5	1.44	3	1.20
G. truncatulinoides (d)	0	0.00	1	0.45	0	0.00	0	0.00	0	0.00	2	0.71	0	0.00	1	0.32	1	0.29	0	0.00
G. truncatulinoides (s)	7	2.70	13	5.80	9	4.29	8	3.54	14	4.26	20	7.09	7	2.93	4	1.26	11	3.16	11	4.42
G. ruber (alba)	5	1.93	4	1.79	9	4.29	4	1.77	3	0.91	4	1.42	5	2.09	9	2.84	10	2.87	7	2.81
G. trilobus	20	7.72	16	7.14	8	3.81	13	5.75	21	6.38	15	5.32	17	7.11	19	5.99	15	4.31	28	11.24
G. sacculifer	6	2.32	9	4.02	6	2.86	1	0.44	9	2.74	12	4.26	10	4.18	9	2.84	16	4.60	4	1.61
G. dutertrei	15	5.79	7	3.13	6	2.86	14	6.19	23	6.99	10	3.55	9	3.77	20	6.31	31	8.91	12	4.82
G. menardii	0	0.00	0	0.00	0	0.00	0	0.00	0	0.00	0	0.00	0	0.00	0	0.00	1	0.29	0	0.00
G. crassaformis	0	0.00	3	1.34	1	0.48	1	0.44	0	0.00	1	0.35	1	0.42	1	0.32	2	0.57	3	1.20
G. calida	10	3.86	5	2.23	5	2.38	7	3.10	8	2.43	3	1.06	7	2.93	8	2.52	9	2.59	2	0.80
T. quinqeloba	5	1.93	10	4.46	7	3.33	3	1.33	6	1.82	5	1.77	4	1.67	3	0.95	2	0.57	5	2.01
G. uvula	1	0.39	3	1.34	3	1.43	1	0.44	7	2.13	5	1.77	2	0.84	3	0.95	2	0.57	1	0.40
Other	38	14.67	25	11.16	33	15.71	34	15.04	45	13.68	36	12.77	24	10.04	37	11.67	40	11.49	57	22.89
TOTAL	259	100.00	224	100.00	210	100.00	226	100.00	329	100.00	282	100.00	239	100.00	317	100.00	348	100.00	249	100.00
Complete Forams	259		224		210		226		329		282		239		317		348		249	
Fragments	198		183		196		242		367		439		330		363		387		433	
Split	6		6		6		6		6.5		6.5		6		6		5		5	

SAMPLE DEPTH (cm)	1300	%	1310	%	1320	%	1330	%	1340	%	1350	%	1360	%	1370	%	1380	%	1390	%
SPECIES COUNTED																				
G. pachyderma (sinistral)	5	1.66	9	4.50	13	5.02	31	10.26	29	10.55	7	2.23	4	1.52	7	2.78	7	2.62	14	4.27
G. pachyderma (dextral)	72	23.84	35	17.50	41	15.83	42	13.91	44	16.00	62	19.75	39	14.83	49	19.44	41	15.36	45	13.72
G. bulloides	9	2.98	1	0.50	5	1.93	7	2.32	5	1.82	8	2.55	2	0.76	7	2.78	6	2.25	9	2.74
G. scitula	6	1.99	2	1.00	8	3.09	5	1.66	1	0.36	5	1.59	3	1.14	6	2.38	6	2.25	9	2.74
G. glutinata	16	5.30	8	4.00	11	4.25	23	7.62	13	4.73	25	7.96	24	9.13	18	7.14	18	6.74	18	5.49
G. inflata	78	25.83	47	23.50	65	25.10	50	16.56	66	24.00	57	18.15	48	18.25	38	15.08	56	20.97	64	19.51
G. falconensis	4	1.32	5	2.50	4	1.54	7	2.32	7	2.55	7	2.23	7	2.66	9	3.57	8	3.00	6	1.83
G. hirsuta	2	0.66	4	2.00	2	0.77	3	0.99	3	1.09	1	0.32	3	1.14	5	1.98	10	3.75	4	1.22
G. truncatulinoides (d)	0	0.00	0	0.00	2	0.77	2	0.66	0	0.00	2	0.64	2	0.76	0	0.00	0	0.00	3	0.91
G. truncatulinoides (s)	6	1.99	8	4.00	9	3.47	8	2.65	7	2.55	8	2.55	14	5.32	3	1.19	6	2.25	13	3.96
G. ruber (alba)	8	2.65	6	3.00	7	2.70	7	2.32	9	3.27	9	2.87	11	4.18	13	5.16	11	4.12	14	4.27
G. trilobus	23	7.62	16	8.00	20	7.72	18	5.96	14	5.09	20	6.37	15	5.70	21	8.33	14	5.24	18	5.49
G. sacculifer	9	2.98	7	3.50	8	3.09	14	4.64	7	2.55	11	3.50	7	2.66	9	3.57	10	3.75	10	3.05
G. dutertrei	9	2.98	4	2.00	12	4.63	28	9.27	18	6.55	23	7.32	17	6.46	14	5.56	19	7.12	27	8.23
G. menardii	0	0.00	0	0.00	0	0.00	1	0.33	1	0.36	0	0.00	0	0.00	1	0.40	0	0.00	0	0.00
G. crassaformis	3	0.99	3	1.50	1	0.39	1	0.33	0	0.00	2	0.64	1	0.38	1	0.40	1	0.37	4	1.22
G. calida	10	3.31	5	2.50	11	4.25	12	3.97	12	4.36	16	5.10	8	3.04	9	3.57	10	3.75	13	3.96
T. quinqeloba	6	1.99	1	0.50	7	2.70	8	2.65	5	1.82	5	1.59	2	0.76	2	0.79	3	1.12	7	2.13
G. uvula	4	1.32	4	2.00	3	1.16	2	0.66	2	0.73	4	1.27	6	2.28	4	1.59	3	1.12	7	2.13
Other	32	10.60	35	17.50	30	11.58	33	10.93	32	11.64	42	13.38	50	19.01	36	14.29	38	14.23	43	13.11
TOTAL	302	100.00	200	100.00	259	100.00	302	100.00	275	100.00	314	100.00	263	100.00	252	100.00	267	100.00	328	100.00
Complete Forams	302		200		259		302		275		314		263		252		267		328	
Fragments	362		302		335		275		322		354		314		432		329		441	
Split	6		6		5		6		5		6		6		5		5		6	

CORE MD962084 (OLIFANTS RIVER SLOPE)

SAMPLE DEPTH (cm)	1400	%	1410	%	1420	%	1430	%	1440	%	1450	%	1460	%	1470	%	1480	%	1490	%
SPECIES COUNTED																				
G. pachyderma (sinistral)	23	7.52	16	5.41	16	5.90	19	6.79	7	2.43	6	2.27	5	1.96	6	2.83	6	1.51	10	3.65
G. pachyderma (dextral)	57	18.63	70	23.65	27	9.96	32	11.43	56	19.44	28	10.61	47	18.43	44	20.75	54	13.60	42	15.33
G. bulloides	3	0.98	10	3.38	12	4.43	16	5.71	16	5.56	9	3.41	9	3.53	11	5.19	12	3.02	0	0.00
G. scitula	9	2.94	3	1.01	6	2.21	3	1.07	10	3.47	5	1.89	7	2.75	2	0.94	6	1.51	7	2.55
G. glutinata	18	5.88	19	6.42	23	8.49	21	7.50	20	6.94	25	9.47	20	7.84	14	6.60	23	5.79	22	8.03
G. inflata	57	18.63	56	18.92	53	19.56	59	21.07	44	15.28	54	20.45	54	21.18	52	24.53	88	22.17	54	19.71
G. falconensis	9	2.94	9	3.04	11	4.06	8	2.86	12	4.17	10	3.79	9	3.53	3	1.42	9	2.27	5	1.82
G. hirsuta	2	0.65	4	1.35	2	0.74	2	0.71	0	0.00	2	0.76	0	0.00	2	0.94	3	0.76	5	1.82
G. truncatulinoides (d)	0	0.00	4	1.35	3	1.11	2	0.71	0	0.00	1	0.38	0	0.00	0	0.00	1	0.25	0	0.00
G. truncatulinoides (s)	3	0.98	7	2.36	6	2.21	6	2.14	10	3.47	6	2.27	7	2.75	5	2.36	13	3.27	5	1.82
G. ruber (alba)	10	3.27	10	3.38	7	2.58	9	3.21	10	3.47	9	3.41	8	3.14	14	6.60	20	5.04	21	7.66
G. trilobus	18	5.88	16	5.41	20	7.38	19	6.79	21	7.29	16	6.06	9	3.53	7	3.30	31	7.81	22	8.03
G. sacculifer	12	3.92	9	3.04	12	4.43	11	3.93	3	1.04	10	3.79	11	4.31	1	0.47	16	4.03	10	3.65
G. dutertrei	32	10.46	20	6.76	20	7.38	20	7.14	23	7.99	19	7.20	16	6.27	13	6.13	20	5.04	8	2.92
G. menardii	0	0.00	1	0.34	0	0.00	1	0.36	0	0.00	0	0.00	0	0.00	0	0.00	0	0.00	0	0.00
G. crassaformis	3	0.98	3	1.01	0	0.00	3	1.07	0	0.00	1	0.38	1	0.39	1	0.47	4	1.01	2	0.73
G. calida	14	4.58	9	3.04	9	3.32	12	4.29	13	4.51	11	4.17	13	5.10	7	3.30	9	2.27	8	2.92
T. quinqeloba	3	0.98	5	1.69	12	4.43	9	3.21	9	3.13	9	3.41	9	3.53	1	0.47	9	2.27	14	5.11
G. uvula	6	1.96	8	2.70	4	1.48	4	1.43	1	0.35	6	2.27	5	1.96	3	1.42	8	2.02	8	2.92
Other	27	8.82	17	5.74	28	10.33	24	8.57	33	11.46	37	14.02	25	9.80	26	12.26	65	16.37	31	11.31
TOTAL	306	100.00	296	100.00	271	100.00	280	100.00	288	100.00	264	100.00	255	100.00	212	100.00	397	100.00	274	100.00
Complete Forams	306		296		271		280		288		264		255		212		397		274	
Fragments	364		253		188		190		201		184		199		242		556		482	
Split	6		6		7		7		8		7		8		7		5		1	

SAMPLE DEPTH (cm)	1500	%	1510	%	1520	%	1530	%	1540	%	1550	%	1560	%	1570	%	1580	%	1590	%
SPECIES COUNTED																				
G. pachyderma (sinistral)	5	1.83	6	3.26	6	2.33	3	1.64	3	1.33	3	1.30	6	1.90	5	2.25	6	2.11	3	1.42
G. pachyderma (dextral)	69	25.27	30	16.30	45	17.51	17	9.29	33	14.67	30	13.04	62	19.68	57	25.68	37	13.03	36	17.06
G. bulloides	13	4.76	3	1.63	6	2.33	6	3.28	3	1.33	2	0.87	12	3.81	3	1.35	5	1.76	2	0.95
G. scitula	5	1.83	4	2.17	6	2.33	0	0.00	2	0.89	5	2.17	8	2.54	3	1.35	1	0.35	1	0.47
G. glutinata	13	4.76	13	7.07	10	3.89	8	4.37	14	6.22	11	4.78	19	6.03	17	7.66	21	7.39	18	8.53
G. inflata	67	24.54	55	29.89	61	23.74	48	26.23	52	23.11	62	26.96	61	19.37	50	22.52	67	23.59	72	34.12
G. falconensis	3	1.10	3	1.63	3	1.17	9	4.92	6	2.67	2	0.87	23	7.30	10	4.50	9	3.17	4	1.90
G. hirsuta	0	0.00	2	1.09	5	1.95	5	2.73	4	1.78	7	3.04	2	0.63	3	1.35	13	4.58	1	0.47
G. truncatulinoides (d)	0	0.00	1	0.54	1	0.39	1	0.55	1	0.44	0	0.00	1	0.32	0	0.00	0	0.00	0	0.00
G. truncatulinoides (s)	3	1.10	2	1.09	5	1.95	4	2.19	9	4.00	6	2.61	16	5.08	7	3.15	11	3.87	4	1.90
G. ruber (alba)	15	5.49	14	7.61	22	8.56	14	7.65	14	6.22	23	10.00	10	3.17	7	3.15	7	2.46	8	3.79
G. trilobus	13	4.76	11	5.98	8	3.11	4	2.19	10	4.44	7	3.04	16	5.08	8	3.60	15	5.28	13	6.16
G. sacculifer	7	2.56	4	2.17	5	1.95	2	1.09	3	1.33	1	0.43	7	2.22	4	1.80	6	2.11	2	0.95
G. dutertrei	16	5.86	13	7.07	21	8.17	5	2.73	9	4.00	8	3.48	21	6.67	11	4.95	18	6.34	12	5.69
G. menardii	0	0.00	0	0.00	0	0.00	2	1.09	1	0.44	2	0.87	1	0.32	0	0.00	2	0.70	0	0.00
G. crassaformis	1	0.37	3	1.63	0	0.00	4	2.19	4	1.78	0	0.00	2	0.63	3	1.35	0	0.00	0	0.00
G. calida	8	2.93	8	4.35	5	1.95	3	1.64	4	1.78	2	0.87	4	1.27	4	1.80	9	3.17	6	2.84
T. quinqeloba	5	1.83	0	0.00	6	2.33	1	0.55	3	1.33	1	0.43	6	1.90	0	0.00	2	0.70	0	0.00
G. uvula	1	0.37	2	1.09	5	1.95	5	2.73	3	1.33	5	2.17	3	0.95	3	1.35	5	1.76	0	0.00
Other	29	10.62	10	5.43	37	14.40	42	22.95	47	20.89	53	23.04	35	11.11	27	12.16	50	17.61	29	13.74
TOTAL	273	100.00	184	100.00	257	100.00	183	100.00	225	100.00	230	100.00	315	100.00	222	100.00	284	100.00	211	100.00
Complete Forams	273		184		257		183		225		230		315		222		284		211	
Fragments	182		175		479		355		405		616		675		319		752		317	
Split	7		5		4		4		4		3		4		4		4		4	

CORE MD962084 (OLIFANTS RIVER SLOPE)

SAMPLE DEPTH (cm)	1600	%	1610	%	1620	%	1630	%	1640	%	1650	%	1660	%	1670	%	1680	%	1690	%
SPECIES COUNTED																				
G. pachyderma (sinistral)	8	2.33	5	1.54	6	2.12	2	0.99	3	1.35	5	1.58	10	2.99	6	2.06	5	1.62	5	1.89
G. pachyderma (dextral)	66	19.24	55	16.98	49	17.31	28	13.79	31	13.90	53	16.77	47	14.07	48	16.49	50	16.23	28	10.57
G. bulloides	5	1.46	11	3.40	12	4.24	6	2.96	2	0.90	9	2.85	8	2.40	11	3.78	21	6.82	3	1.13
G. scitula	5	1.46	7	2.16	7	2.47	4	1.97	3	1.35	9	2.85	6	1.80	12	4.12	4	1.30	3	1.13
G. glutinata	19	5.54	14	4.32	11	3.89	15	7.39	10	4.48	25	7.91	14	4.19	14	4.81	13	4.22	16	6.04
G. inflata	71	20.70	78	24.07	86	30.39	50	24.63	57	25.56	67	21.20	75	22.46	66	22.68	74	24.03	50	18.87
G. falconensis	8	2.33	13	4.01	9	3.18	3	1.48	5	2.24	3	0.95	5	1.50	10	3.44	6	1.95	4	1.51
G. hirsuta	13	3.79	8	2.47	0	0.00	0	0.00	3	1.35	5	1.58	2	0.60	2	0.69	5	1.62	4	1.51
G. truncatulinoides (d)	1	0.29	0	0.00	3	1.06	0	0.00	1	0.45	1	0.32	7	2.10	0	0.00	0	0.00	0	0.00
G. truncatulinoides (s)	5	1.46	17	5.25	7	2.47	7	3.45	11	4.93	17	5.38	19	5.69	17	5.84	20	6.49	21	7.92
G. ruber (alba)	14	4.08	9	2.78	9	3.18	12	5.91	15	6.73	5	1.58	11	3.29	3	1.03	9	2.92	7	2.64
G. trilobus	24	7.00	17	5.25	16	5.65	17	8.37	16	7.17	25	7.91	25	7.49	26	8.93	18	5.84	23	8.68
G. sacculifer	11	3.21	8	2.47	8	2.83	6	2.96	3	1.35	6	1.90	10	2.99	8	2.75	8	2.60	11	4.15
G. dutertrei	16	4.66	16	4.94	12	4.24	8	3.94	8	3.59	16	5.06	13	3.89	18	6.19	20	6.49	17	6.42
G. menardii	1	0.29	3	0.93	0	0.00	0	0.00	0	0.00	1	0.32	0	0.00	0	0.00	0	0.00	0	0.00
G. crassaformis	2	0.58	4	1.23	1	0.35	3	1.48	1	0.45	3	0.95	2	0.60	1	0.34	1	0.32	3	1.13
G. calida	13	3.79	8	2.47	8	2.83	3	1.48	5	2.24	13	4.11	9	2.69	3	1.03	9	2.92	8	3.02
T. quinqeloba	7	2.04	2	0.62	1	0.35	3	1.48	3	1.35	2	0.63	6	1.80	2	0.69	6	1.95	10	3.77
G. uvula	5	1.46	6	1.85	6	2.12	0	0.00	2	0.90	3	0.95	3	0.90	3	1.03	7	2.27	3	1.13
Other	49	14.29	43	13.27	32	11.31	36	17.73	44	19.73	48	15.19	62	18.56	41	14.09	32	10.39	49	18.49
TOTAL	343	100.00	324	100.00	283	100.00	203	100.00	223	100.00	316	100.00	334	100.00	291	100.00	308	100.00	265	100.00
Complete Forams	343		324		283		203		223		316		334		291		308		265	
Fragments	382		658		363		405		488		429		569		587		432		546	
Split	6		4		4		6		5		5		4		4		5		4	

SAMPLE DEPTH (cm)	1700	%	1710	%	1720	%	1730	%	1740	%	1750	%	1760	%	1770	%	1780	%	1790	%
SPECIES COUNTED																				
G. pachyderma (sinistral)	5	1.57	7	2.36	6	2.70	7	3.10	6	1.93	5	1.74	5	1.85	5	2.17	3	1.28	7	2.81
G. pachyderma (dextral)	57	17.92	49	16.55	35	15.77	31	13.72	52	16.72	54	18.82	48	17.71	47	20.43	39	16.67	48	19.28
G. bulloides	1	0.31	8	2.70	2	0.90	6	2.65	9	2.89	6	2.09	6	2.21	5	2.17	4	1.71	8	3.21
G. scitula	7	2.20	9	3.04	4	1.80	4	1.77	7	2.25	2	0.70	5	1.85	2	0.87	5	2.14	6	2.41
G. glutinata	15	4.72	15	5.07	7	3.15	17	7.52	23	7.40	16	5.57	19	7.01	12	5.22	12	5.13	15	6.02
G. inflata	50	15.72	74	25.00	44	19.82	34	15.04	69	22.19	61	21.25	55	20.30	49	21.30	44	18.80	47	18.88
G. falconensis	4	1.26	3	1.01	4	1.80	8	3.54	5	1.61	10	3.48	10	3.69	5	2.17	3	1.28	5	2.01
G. hirsuta	4	1.26	4	1.35	2	0.90	4	1.77	6	1.93	4	1.39	2	0.74	2	0.87	1	0.43	2	0.80
G. truncatulinoides (d)	5	1.57	1	0.34	0	0.00	2	0.88	1	0.32	0	0.00	1	0.37	2	0.87	0	0.00	3	1.20
G. truncatulinoides (s)	29	9.12	12	4.05	9	4.05	15	6.64	22	7.07	13	4.53	16	5.90	15	6.52	23	9.83	15	6.02
G. ruber (alba)	12	3.77	14	4.73	4	1.80	7	3.10	14	4.50	13	4.53	7	2.58	6	2.61	7	2.99	11	4.42
G. trilobus	26	8.18	11	3.72	24	10.81	17	7.52	16	5.14	16	5.57	18	6.64	13	5.65	18	7.69	12	4.82
G. sacculifer	6	1.89	10	3.38	4	1.80	2	0.88	10	3.22	13	4.53	9	3.32	10	4.35	5	2.14	9	3.61
G. dutertrei	22	6.92	20	6.76	20	9.01	14	6.19	16	5.14	25	8.71	19	7.01	16	6.96	22	9.40	16	6.43
G. menardii	2	0.63	0	0.00	1	0.45	3	1.33	1	0.32	0	0.00	0	0.00	0	0.00	0	0.00	0	0.00
G. crassaformis	1	0.31	3	1.01	2	0.90	2	0.88	3	0.96	2	0.70	1	0.37	1	0.43	1	0.43	2	0.80
G. calida	4	1.26	13	4.39	7	3.15	8	3.54	11	3.54	6	2.09	5	1.85	10	4.35	5	2.14	7	2.81
T. quinqeloba	8	2.52	1	0.34	6	2.70	4	1.77	3	0.96	7	2.44	6	2.21	2	0.87	2	0.85	4	1.61
G. uvula	3	0.94	4	1.35	4	1.80	5	2.21	4	1.29	3	1.05	2	0.74	2	0.87	4	1.71	6	2.41
Other	57	17.92	38	12.84	37	16.67	36	15.93	33	10.61	31	10.80	37	13.65	26	11.30	36	15.38	26	10.44
TOTAL	318	100.00	296	100.00	222	100.00	226	100.00	311	100.00	287	100.00	271	100.00	230	100.00	234	100.00	249	100.00
Complete Forams	318		296		222		226		311		287		271		230		234		249	
Fragments	543		416		296		275		384		389		305		418		380		368	
Split	3		4		5		5		5		4		4		5		5		5	

CORE MD962084 (OLIFANTS RIVER SLOPE)

SAMPLE DEPTH (cm)	1800	%	1810	%	1820	%	1830	%	1840	%	1850	%	1860	%	1870	%	1880	%	1890	%
SPECIES COUNTED																				
G. pachyderma (sinistral)	2	0.70	4	1.05	3	1.30	7	2.60	9	2.24	8	2.22	3	0.91	4	1.07	8	2.45	3	1.10
G. pachyderma (dextral)	51	17.83	77	20.26	43	18.61	39	14.50	81	20.20	66	18.33	55	16.77	52	13.90	56	17.13	52	19.05
G. bulloides	0	0.00	2	0.53	4	1.73	4	1.49	7	1.75	8	2.22	19	5.79	20	5.35	12	3.67	14	5.13
G. scitula	3	1.05	6	1.58	6	2.60	5	1.86	8	2.00	7	1.94	13	3.96	6	1.60	14	4.28	6	2.20
G. glutinata	19	6.64	21	5.53	13	5.63	21	7.81	24	5.99	26	7.22	44	13.41	44	11.76	26	7.95	23	8.42
G. inflata	65	22.73	65	17.11	54	23.38	64	23.79	73	18.20	79	21.94	64	19.51	101	27.01	49	14.98	55	20.15
G. falconensis	4	1.40	6	1.58	2	0.87	6	2.23	7	1.75	9	2.50	14	4.27	22	5.88	8	2.45	12	4.40
G. hirsuta	2	0.70	2	0.53	4	1.73	3	1.12	5	1.25	6	1.67	5	1.52	3	0.80	3	0.92	1	0.37
G. truncatulinoides (d)	1	0.35	1	0.26	1	0.43	1	0.37	2	0.50	3	0.83	2	0.61	2	0.53	2	0.61	0	0.00
G. truncatulinoides (s)	20	6.99	19	5.00	10	4.33	15	5.58	19	4.74	15	4.17	5	1.52	7	1.87	6	1.83	5	1.83
G. ruber (alba)	7	2.45	17	4.47	4	1.73	7	2.60	15	3.74	11	3.06	5	1.52	9	2.41	5	1.53	8	2.93
G. trilobus	27	9.44	32	8.42	14	6.06	22	8.18	28	6.98	25	6.94	18	5.49	18	4.81	16	4.89	12	4.40
G. sacculifer	5	1.75	13	3.42	4	1.73	4	1.49	17	4.24	12	3.33	16	4.88	16	4.28	15	4.59	9	3.30
G. dutertrei	32	11.19	44	11.58	27	11.69	19	7.06	29	7.23	22	6.11	25	7.62	15	4.01	22	6.73	19	6.96
G. menardii	0	0.00	2	0.53	0	0.00	0	0.00	0	0.00	0	0.00	1	0.30	1	0.27	0	0.00	0	0.00
G. crassaformis	4	1.40	2	0.53	3	1.30	1	0.37	4	1.00	2	0.56	0	0.00	0	0.00	1	0.31	0	0.00
G. calida	9	3.15	19	5.00	10	4.33	7	2.60	17	4.24	14	3.89	10	3.05	12	3.21	22	6.73	7	2.56
T. quinqeloba	6	2.10	3	0.79	1	0.43	3	1.12	8	2.00	3	0.83	3	0.91	12	3.21	8	2.45	10	3.66
G. uvula	1	0.35	3	0.79	2	0.87	2	0.74	4	1.00	2	0.56	3	0.91	4	1.07	6	1.83	7	2.56
Other	28	9.79	42	11.05	26	11.26	39	14.50	44	10.97	42	11.67	23	7.01	26	6.95	48	14.68	30	10.99
TOTAL	286	100.00	380	100.00	231	100.00	269	100.00	401	100.00	360	100.00	328	100.00	374	100.00	327	100.00	273	100.00
Complete Forams	286		380		231		269		401		360		328		374		327		273	
Fragments	318		422		298		340		321		303		170		177		159		134	
Split	5		5		5		5		5		6		7		6		7		8	

SAMPLE DEPTH (cm)	1900	%	1910	%	1920	%	1930	%	1940	%	1950	%	1960	%	1970	%	1980	%	1990	%
SPECIES COUNTED																				
G. pachyderma (sinistral)	9	2.53	12	3.85	10	3.75	13	3.05	2	0.62	6	1.73	4	2.27	5	2.09	4	1.69	3	1.39
G. pachyderma (dextral)	64	17.98	57	18.27	50	18.73	93	21.83	50	15.43	61	17.58	23	13.07	40	16.74	34	14.35	34	15.74
G. bulloides	13	3.65	11	3.53	10	3.75	11	2.58	11	3.40	8	2.31	5	2.84	2	0.84	2	0.84	2	0.93
G. scitula	17	4.78	15	4.81	14	5.24	10	2.35	16	4.94	8	2.31	8	4.55	5	2.09	2	0.84	3	1.39
G. glutinata	35	9.83	37	11.86	25	9.36	36	8.45	32	9.88	35	10.09	15	8.52	25	10.46	18	7.59	22	10.19
G. inflata	61	17.13	50	16.03	37	13.86	90	21.13	53	16.36	65	18.73	32	18.18	56	23.43	46	19.41	39	18.06
G. falconensis	6	1.69	6	1.92	5	1.87	14	3.29	8	2.47	2	0.58	7	3.98	3	1.26	6	2.53	4	1.85
G. hirsuta	1	0.28	6	1.92	4	1.50	2	0.47	11	3.40	7	2.02	7	3.98	1	0.42	9	3.80	3	1.39
G. truncatulinoides (d)	0	0.00	0	0.00	0	0.00	0	0.00	0	0.00	0	0.00	0	0.00	2	0.84	1	0.42	0	0.00
G. truncatulinoides (s)	5	1.40	7	2.24	3	1.12	4	0.94	6	1.85	9	2.59	4	2.27	4	1.67	11	4.64	4	1.85
G. ruber (alba)	3	0.84	4	1.28	8	3.00	4	0.94	4	1.23	5	1.44	5	2.84	1	0.42	4	1.69	2	0.93
G. trilobus	23	6.46	26	8.33	20	7.49	20	4.69	23	7.10	25	7.20	11	6.25	23	9.62	22	9.28	18	8.33
G. sacculifer	14	3.93	14	4.49	14	5.24	18	4.23	19	5.86	20	5.76	3	1.70	7	2.93	8	3.38	6	2.78
G. dutertrei	16	4.49	6	1.92	12	4.49	24	5.63	13	4.01	18	5.19	10	5.68	12	5.02	10	4.22	17	7.87
G. menardii	0	0.00	0	0.00	0	0.00	0	0.00	1	0.31	1	0.29	0	0.00	1	0.42	1	0.42	1	0.46
G. crassaformis	0	0.00	1	0.32	1	0.37	1	0.23	0	0.00	1	0.29	0	0.00	2	0.84	1	0.42	0	0.00
G. calida	12	3.37	11	3.53	8	3.00	23	5.40	10	3.09	11	3.17	4	2.27	6	2.51	5	2.11	8	3.70
T. quinqeloba	23	6.46	9	2.88	12	4.49	14	3.29	19	5.86	15	4.32	8	4.55	11	4.60	10	4.22	9	4.17
G. uvula	16	4.49	10	3.21	7	2.62	14	3.29	11	3.40	11	3.17	3	1.70	5	2.09	7	2.95	3	1.39
Other	38	10.67	30	9.62	27	10.11	35	8.22	35	10.80	39	11.24	27	15.34	28	11.72	36	15.19	38	17.59
TOTAL	356	100.00	312	100.00	267	100.00	426	100.00	324	100.00	347	100.00	176	100.00	239	100.00	237	100.00	216	100.00
Complete Forams	356		312		267		426		324		347		176		239		237		216	
Fragments	146		147		138		186		192		293		195		290		346		253	
Split	9		9		8		8		8		8		8		7		6.5		7	

CORE MD962084 (OLIFANTS RIVER SLOPE)

SAMPLE DEPTH (cm)	2000	%	2010	%	2020	%	2030	%	2040	%	2050	%	2060	%	2070	%	2080	%	2090	%
SPECIES COUNTED																				
G. pachyderma (sinistral)	3	1.39	3	1.42	5	1.97	7	2.76	3	1.13	2	0.62	3	1.18	5	2.02	7	2.37	3	1.22
G. pachyderma (dextral)	47	21.76	50	23.58	65	25.59	41	16.14	48	18.11	56	17.23	51	20.08	36	14.57	73	24.75	49	20.00
G. bulloides	2	0.93	2	0.94	6	2.36	7	2.76	5	1.89	10	3.08	8	3.15	6	2.43	4	1.36	3	1.22
G. scitula	2	0.93	1	0.47	8	3.15	2	0.79	3	1.13	7	2.15	4	1.57	10	4.05	1	0.34	4	1.63
G. glutinata	16	7.41	15	7.08	18	7.09	20	7.87	21	7.92	20	6.15	15	5.91	18	7.29	24	8.14	25	10.20
G. inflata	54	25.00	53	25.00	43	16.93	57	22.44	68	25.66	69	21.23	64	25.20	72	29.15	64	21.69	52	21.22
G. falconensis	3	1.39	2	0.94	7	2.76	4	1.57	8	3.02	8	2.46	3	1.18	6	2.43	3	1.02	6	2.45
G. hirsuta	2	0.93	3	1.42	2	0.79	4	1.57	5	1.89	5	1.54	1	0.39	1	0.40	8	2.71	4	1.63
G. truncatulinoides (d)	2	0.93	1	0.47	1	0.39	0	0.00	2	0.75	0	0.00	1	0.39	0	0.00	1	0.34	0	0.00
G. truncatulinoides (s)	6	2.78	4	1.89	3	1.18	7	2.76	10	3.77	11	3.38	11	4.33	9	3.64	12	4.07	7	2.86
G. ruber (alba)	6	2.78	4	1.89	4	1.57	5	1.97	1	0.38	8	2.46	5	1.97	3	1.21	2	0.68	4	1.63
G. trilobus	17	7.87	16	7.55	19	7.48	18	7.09	22	8.30	26	8.00	18	7.09	14	5.67	23	7.80	17	6.94
G. sacculifer	7	3.24	4	1.89	9	3.54	14	5.51	9	3.40	7	2.15	5	1.97	3	1.21	6	2.03	6	2.45
G. dutertrei	7	3.24	17	8.02	19	7.48	17	6.69	9	3.40	27	8.31	15	5.91	15	6.07	23	7.80	16	6.53
G. menardii	0	0.00	0	0.00	0	0.00	1	0.39	3	1.13	0	0.00	0	0.00	2	0.81	0	0.00	0	0.00
G. crassaformis	2	0.93	1	0.47	0	0.00	0	0.00	4	1.51	2	0.62	2	0.79	1	0.40	5	1.69	2	0.82
G. calida	5	2.31	1	0.47	10	3.94	10	3.94	8	3.02	5	1.54	5	1.97	9	3.64	7	2.37	6	2.45
T. quinqeloba	3	1.39	2	0.94	5	1.97	6	2.36	3	1.13	10	3.08	3	1.18	7	2.83	3	1.02	11	4.49
G. uvula	2	0.93	5	2.36	5	1.97	2	0.79	5	1.89	4	1.23	7	2.76	5	2.02	3	1.02	3	1.22
Other	30	13.89	28	13.21	25	9.84	32	12.60	28	10.57	48	14.77	33	12.99	25	10.12	26	8.81	27	11.02
TOTAL	216	100.00	212	100.00	254	100.00	254	100.00	265	100.00	325	100.00	254	100.00	247	100.00	295	100.00	245	100.00
Complete Forams	216		212		254		254		265		325		254		247		295		245	
Fragments	249		245		268		369		433		934		498		473		930		614	
Split	6		5		6		5		6		5		5		5		3		4	

SAMPLE DEPTH (cm)	2100	%	2110	%	2120	%	2130	%	2140	%	2150	%	2160	%	2170	%	2180	%	2190	%
SPECIES COUNTED																				
G. pachyderma (sinistral)	7	2.69	8	2.23	7	2.46	5	1.82	7	2.13	12	4.18	7	2.38	9	3.02	11	2.77	10	2.69
G. pachyderma (dextral)	46	17.69	65	18.11	54	18.95	47	17.15	55	16.77	50	17.42	38	12.93	44	14.77	72	18.14	78	20.97
G. bulloides	10	3.85	11	3.06	15	5.26	11	4.01	17	5.18	18	6.27	16	5.44	18	6.04	30	7.56	19	5.11
G. scitula	6	2.31	5	1.39	3	1.05	14	5.11	8	2.44	5	1.74	5	1.70	5	1.68	7	1.76	9	2.42
G. glutinata	21	8.08	27	7.52	22	7.72	14	5.11	28	8.54	20	6.97	22	7.48	20	6.71	28	7.05	29	7.80
G. inflata	66	25.38	80	22.28	73	25.61	39	14.23	71	21.65	64	22.30	77	26.19	63	21.14	79	19.90	81	21.77
G. falconensis	11	4.23	15	4.18	4	1.40	9	3.28	6	1.83	6	2.09	5	1.70	5	1.68	9	2.27	7	1.88
G. hirsuta	4	1.54	1	0.28	6	2.11	9	3.28	7	2.13	0	0.00	1	0.34	4	1.34	5	1.26	2	0.54
G. truncatulinoides (d)	0	0.00	1	0.28	1	0.35	0	0.00	1	0.30	0	0.00	1	0.34	0	0.00	0	0.00	3	0.81
G. truncatulinoides (s)	6	2.31	8	2.23	10	3.51	13	4.74	11	3.35	2	0.70	6	2.04	6	2.01	7	1.76	5	1.34
G. ruber (alba)	4	1.54	10	2.79	4	1.40	5	1.82	8	2.44	9	3.14	8	2.72	7	2.35	10	2.52	5	1.34
G. trilobus	12	4.62	24	6.69	17	5.96	20	7.30	29	8.84	21	7.32	26	8.84	17	5.70	17	4.28	25	6.72
G. sacculifer	10	3.85	9	2.51	13	4.56	10	3.65	10	3.05	9	3.14	10	3.40	9	3.02	18	4.53	11	2.96
G. dutertrei	13	5.00	20	5.57	12	4.21	16	5.84	12	3.66	21	7.32	16	5.44	14	4.70	25	6.30	23	6.18
G. menardii	0	0.00	3	0.84	2	0.70	1	0.36	1	0.30	0	0.00	0	0.00	0	0.00	1	0.25	0	0.00
G. crassaformis	6	2.31	3	0.84	2	0.70	3	1.09	2	0.61	0	0.00	3	1.02	3	1.01	3	0.76	2	0.54
G. calida	6	2.31	14	3.90	4	1.40	6	2.19	9	2.74	11	3.83	5	1.70	11	3.69	16	4.03	19	5.11
T. quinqeloba	7	2.69	11	3.06	4	1.40	9	3.28	10	3.05	9	3.14	7	2.38	16	5.37	9	2.27	6	1.61
G. uvula	1	0.38	5	1.39	2	0.70	3	1.09	6	1.83	7	2.44	5	1.70	8	2.68	7	1.76	9	2.42
Other	24	9.23	39	10.86	30	10.53	40	14.60	30	9.15	23	8.01	36	12.24	39	13.09	43	10.83	29	7.80
TOTAL	260	100.00	359	100.00	285	100.00	274	100.00	328	100.00	287	100.00	294	100.00	298	100.00	397	100.00	372	100.00
Complete Forams	260		359		285		274		328		287		271		298		397		372	
Fragments	487		594		513		444		707		506		616		689		628		668	
Split	4		4		3		4		4		6		5		5		6		5	

CORE MD962084 (OLIFANTS RIVER SLOPE)

SAMPLE DEPTH (cm)	2200	%	2210	%	2220	%	2230	%	2240	%	2250	%	2260	%	2270	%	2280	%	2290	%
SPECIES COUNTED																				
G. pachyderma (sinistral)	4	1.34	6	2.74	7	1.88	3	1.09	7	2.50	3	1.11	6	2.06	7	2.16	5	2.04	9	2.55
G. pachyderma (dextral)	57	19.13	33	15.07	70	18.82	45	16.36	37	13.21	55	20.30	62	21.31	49	15.12	37	15.10	62	17.56
G. bulloides	14	4.70	11	5.02	21	5.65	12	4.36	11	3.93	11	4.06	12	4.12	20	6.17	16	6.53	11	3.12
G. scitula	10	3.36	4	1.83	7	1.88	5	1.82	4	1.43	3	1.11	4	1.37	2	0.62	8	3.27	7	1.98
G. glutinata	25	8.39	17	7.76	31	8.33	31	11.27	30	10.71	18	6.64	22	7.56	32	9.88	23	9.39	24	6.80
G. inflata	62	20.81	52	23.74	72	19.35	51	18.55	55	19.64	61	22.51	56	19.24	80	24.69	44	17.96	67	18.98
G. falconensis	6	2.01	7	3.20	6	1.61	5	1.82	6	2.14	8	2.95	6	2.06	7	2.16	8	3.27	14	3.97
G. hirsuta	2	0.67	5	2.28	8	2.15	5	1.82	6	2.14	2	0.74	4	1.37	5	1.54	2	0.82	1	0.28
G. truncatulinoides (d)	2	0.67	0	0.00	1	0.27	0	0.00	0	0.00	0	0.00	1	0.34	0	0.00	0	0.00	0	0.00
G. truncatulinoides (s)	5	1.68	2	0.91	11	2.96	7	2.55	5	1.79	7	2.58	6	2.06	9	2.78	9	3.67	2	0.57
G. ruber (alba)	6	2.01	6	2.74	8	2.15	4	1.45	5	1.79	4	1.48	4	1.37	4	1.23	0	0.00	3	0.85
G. trilobus	17	5.70	13	5.94	32	8.60	24	8.73	24	8.57	24	8.86	16	5.50	15	4.63	18	7.35	34	9.63
G. sacculifer	9	3.02	6	2.74	12	3.23	7	2.55	8	2.86	15	5.54	7	2.41	9	2.78	9	3.67	6	1.70
G. dutertrei	11	3.69	11	5.02	16	4.30	15	5.45	13	4.64	14	5.17	20	6.87	22	6.79	19	7.76	34	9.63
G. menardii	0	0.00	0	0.00	1	0.27	0	0.00	0	0.00	0	0.00	0	0.00	0	0.00	0	0.00	0	0.00
G. crassaformis	3	1.01	1	0.46	3	0.81	3	1.09	3	1.07	0	0.00	2	0.69	0	0.00	0	0.00	6	1.70
G. calida	8	2.68	5	2.28	12	3.23	11	4.00	7	2.50	7	2.58	16	5.50	13	4.01	10	4.08	12	3.40
T. quinqeloba	11	3.69	7	3.20	7	1.88	5	1.82	3	1.07	4	1.48	11	3.78	11	3.40	6	2.45	16	4.53
G. uvula	6	2.01	8	3.65	7	1.88	3	1.09	4	1.43	2	0.74	4	1.37	5	1.54	7	2.86	9	2.55
Other	40	13.42	25	11.42	40	10.75	39	14.18	52	18.57	33	12.18	32	11.00	34	10.49	24	9.80	36	10.20
TOTAL	298	100.00	219	100.00	372	100.00	275	100.00	280	100.00	271	100.00	291	100.00	324	100.00	245	100.00	353	100.00
Complete Forams	298		219		372		275		280		271		291		324		245		353	
Fragments	352		345		524		502		561		465		412		416		428		438	
Split	7		8		6		7		6.5		7.5		8		7		7		7	

SAMPLE DEPTH (cm)	2300	%	2310	%	2320	%	2330	%	2340	%	2350	%	2360	%	2370	%	2380	%	2390	%
SPECIES COUNTED																				
G. pachyderma (sinistral)	10	2.00	7	2.10	8	3.04	5	2.11	10	3.41	8	2.65	9	4.17	5	2.07	15	3.97	7	2.99
G. pachyderma (dextral)	103	20.56	64	19.16	47	17.87	50	21.10	48	16.38	52	17.22	50	23.15	54	22.41	78	20.63	39	16.67
G. bulloides	33	6.59	27	8.08	10	3.80	10	4.22	10	3.41	16	5.30	5	2.31	14	5.81	14	3.70	7	2.99
G. scitula	7	1.40	9	2.69	6	2.28	1	0.42	5	1.71	12	3.97	4	1.85	1	0.41	4	1.06	7	2.99
G. glutinata	49	9.78	38	11.38	22	8.37	21	8.86	17	5.80	22	7.28	15	6.94	19	7.88	20	5.29	20	8.55
G. inflata	100	19.96	58	17.37	57	21.67	63	26.58	79	26.96	65	21.52	43	19.91	63	26.14	82	21.69	47	20.09
G. falconensis	11	2.20	7	2.10	7	2.66	4	1.69	9	3.07	3	0.99	5	2.31	6	2.49	13	3.44	3	1.28
G. hirsuta	2	0.40	3	0.90	2	0.76	2	0.84	10	3.41	2	0.66	4	1.85	4	1.66	8	2.12	6	2.56
G. truncatulinoides (d)	0	0.00	0	0.00	0	0.00	0	0.00	0	0.00	0	0.00	0	0.00	0	0.00	0	0.00	0	0.00
G. truncatulinoides (s)	13	2.59	5	1.50	6	2.28	13	5.49	8	2.73	7	2.32	7	3.24	10	4.15	6	1.59	6	2.56
G. ruber (alba)	4	0.80	4	1.20	3	1.14	2	0.84	0	0.00	2	0.66	5	2.31	2	0.83	8	2.12	4	1.71
G. trilobus	34	6.79	20	5.99	17	6.46	18	7.59	25	8.53	17	5.63	13	6.02	12	4.98	27	7.14	16	6.84
G. sacculifer	11	2.20	8	2.40	8	3.04	5	2.11	11	3.75	8	2.65	14	6.48	9	3.73	8	2.12	5	2.14
G. dutertrei	38	7.58	17	5.09	11	4.18	5	2.11	18	6.14	18	5.96	14	6.48	8	3.32	25	6.61	15	6.41
G. menardii	0	0.00	0	0.00	0	0.00	1	0.42	0	0.00	0	0.00	0	0.00	1	0.41	0	0.00	0	0.00
G. crassaformis	5	1.00	3	0.90	2	0.76	2	0.84	5	1.71	3	0.99	5	2.31	7	2.90	9	2.38	3	1.28
G. calida	12	2.40	12	3.59	9	3.42	4	1.69	6	2.05	10	3.31	7	3.24	4	1.66	6	1.59	5	2.14
T. quinqeloba	24	4.79	15	4.49	13	4.94	7	2.95	6	2.05	12	3.97	3	1.39	5	2.07	18	4.76	10	4.27
G. uvula	1	0.20	4	1.20	6	2.28	5	2.11	5	1.71	6	1.99	3	1.39	3	1.24	10	2.65	7	2.99
Other	44	8.78	33	9.88	29	11.03	19	8.02	21	7.17	39	12.91	10	4.63	14	5.81	27	7.14	27	11.54
TOTAL	501	100.00	334	100.00	263	100.00	237	100.00	293	100.00	302	100.00	216	100.00	241	100.00	378	100.00	234	100.00
Complete Forams	501		334		263		237		293		302		216		241		378		234	
Fragments	332		243		317		482		661		376		397		354		636		333	
Split	7		8		8		6		5		6.5		5		5		5		6	

CORE MD962084 (OLIFANTS RIVER SLOPE)

SAMPLE DEPTH (cm)	2400	%	2410	%	2420	%	2430	%	2440	%	2450	%	2460	%	2470	%	2480	%	2490	%
SPECIES COUNTED																				
G. pachyderma (sinistral)	4	2.35	3	3.41	5	2.23	4	1.75	5	2.05	7	2.93	5	1.52	2	0.77	10	2.94	6	2.97
G. pachyderma (dextral)	22	12.94	12	13.64	36	16.07	40	17.54	52	21.31	52	21.76	74	22.49	56	21.46	52	15.29	50	24.75
G. bulloides	10	5.88	7	7.95	12	5.36	12	5.26	7	2.87	5	2.09	10	3.04	11	4.21	18	5.29	6	2.97
G. scitula	12	7.06	2	2.27	3	1.34	3	1.32	4	1.64	2	0.84	1	0.30	1	0.38	9	2.65	2	0.99
G. glutinata	11	6.47	4	4.55	22	9.82	19	8.33	16	6.56	18	7.53	29	8.81	16	6.13	22	6.47	15	7.43
G. inflata	30	17.65	15	17.05	53	23.66	56	24.56	61	25.00	55	23.01	70	21.28	41	15.71	67	19.71	41	20.30
G. falconensis	7	4.12	6	6.82	1	0.45	11	4.82	3	1.23	1	0.42	9	2.74	11	4.21	9	2.65	3	1.49
G. hirsuta	4	2.35	2	2.27	4	1.79	1	0.44	6	2.46	3	1.26	6	1.82	7	2.68	6	1.76	1	0.50
G. truncatulinoides (d)	0	0.00	0	0.00	0	0.00	0	0.00	0	0.00	0	0.00	0	0.00	0	0.00	0	0.00	0	0.00
G. truncatulinoides (s)	1	0.59	3	3.41	14	6.25	3	1.32	12	4.92	14	5.86	6	1.82	14	5.36	9	2.65	9	4.46
G. ruber (alba)	3	1.76	0	0.00	4	1.79	3	1.32	3	1.23	7	2.93	7	2.13	2	0.77	3	0.88	7	3.47
G. trilobus	14	8.24	6	6.82	8	3.57	8	3.51	18	7.38	17	7.11	29	8.81	25	9.58	26	7.65	13	6.44
G. sacculifer	9	5.29	5	5.68	8	3.57	9	3.95	4	1.64	10	4.18	12	3.65	13	4.98	15	4.41	7	3.47
G. dutertrei	7	4.12	6	6.82	15	6.70	18	7.89	23	9.43	14	5.86	24	7.29	21	8.05	24	7.06	15	7.43
G. menardii	0	0.00	0	0.00	0	0.00	0	0.00	0	0.00	0	0.00	0	0.00	0	0.00	0	0.00	0	0.00
G. crassaformis	3	1.76	0	0.00	5	2.23	4	1.75	5	2.05	4	1.67	6	1.82	2	0.77	6	1.76	1	0.50
G. calida	9	5.29	1	1.14	8	3.57	6	2.63	6	2.46	6	2.51	7	2.13	6	2.30	8	2.35	3	1.49
T. quinqeloba	5	2.94	3	3.41	4	1.79	6	2.63	1	0.41	4	1.67	6	1.82	6	2.30	8	2.35	3	1.49
G. uvula	5	2.94	1	1.14	4	1.79	6	2.63	3	1.23	2	0.84	4	1.22	4	1.53	10	2.94	6	2.97
Other	14	8.24	12	13.64	18	8.04	19	8.33	15	6.15	18	7.53	24	7.29	23	8.81	38	11.18	14	6.93
TOTAL	170	100.00	88	100.00	224	100.00	228	100.00	244	100.00	239	100.00	329	100.00	261	100.00	340	100.00	202	100.00
Complete Forams	170		88		224		228		244		239		329		261		340		202	
Fragments	273		114		274		315		297		569		448		356		544		294	
Split	0		0		5		6		5		4		4		5		5		5	

SAMPLE DEPTH (cm)	2500	%	2510	%	2520	%	2530	%	2540	%	2550	%	2560	%	2570	%	2580	%	2590	%
SPECIES COUNTED																				
G. pachyderma (sinistral)	9	3.53	7	2.80	7	1.96	1	0.45	5	1.79	5	1.37	9	2.73			6	1.66	7	3.00
G. pachyderma (dextral)	49	19.22	51	20.40	81	22.69	58	26.01	60	21.43	65	17.76	60	18.18			81	22.44	38	16.31
G. bulloides	11	4.31	11	4.40	7	1.96	10	4.48	15	5.36	19	5.19	8	2.42			18	4.99	16	6.87
G. scitula	8	3.14	4	1.60	1	0.28	1	0.45	1	0.36	6	1.64	8	2.42	NO	SAMPLE	2	0.55	4	1.72
G. glutinata	27	10.59	27	10.80	19	5.32	19	8.52	30	10.71	31	8.47	29	8.79			26	7.20	14	6.01
G. inflata	45	17.65	30	12.00	57	15.97	26	11.66	45	16.07	48	13.11	60	18.18			54	14.96	38	16.31
G. falconensis	2	0.78	13	5.20	8	2.24	5	2.24	7	2.50	8	2.19	9	2.73			10	2.77	2	0.86
G. hirsuta	1	0.39	3	1.20	6	1.68	0	0.00	2	0.71	2	0.55	0	0.00			3	0.83	4	1.72
G. truncatulinoides (d)	0	0.00	0	0.00	0	0.00	0	0.00	0	0.00	0	0.00	0	0.00			0	0.00	0	0.00
G. truncatulinoides (s)	12	4.71	7	2.80	22	6.16	6	2.69	16	5.71	16	4.37	13	3.94			9	2.49	11	4.72
G. ruber (alba)	6	2.35	3	1.20	4	1.12	5	2.24	3	1.07	7	1.91	11	3.33			8	2.22	7	3.00
G. trilobus	21	8.24	17	6.80	31	8.68	19	8.52	21	7.50	43	11.75	18	5.45			25	6.93	12	5.15
G. sacculifer	6	2.35	11	4.40	13	3.64	8	3.59	9	3.21	12	3.28	11	3.33			14	3.88	10	4.29
G. dutertrei	12	4.71	13	5.20	42	11.76	33	14.80	22	7.86	23	6.28	30	9.09			36	9.97	9	3.86
G. menardii	0	0.00	0	0.00	0	0.00	0	0.00	0	0.00	0	0.00	1	0.30			0	0.00	0	0.00
G. crassaformis	3	1.18	1	0.40	3	0.84	0	0.00	2	0.71	3	0.82	4	1.21			2	0.55	2	0.86
G. calida	4	1.57	8	3.20	9	2.52	4	1.79	9	3.21	9	2.46	9	2.73			12	3.32	8	3.43
T. quinqeloba	5	1.96	7	2.80	4	1.12	4	1.79	5	1.79	7	1.91	12	3.64			11	3.05	8	3.43
G. uvula	8	3.14	8	3.20	4	1.12	3	1.35	2	0.71	7	1.91	4	1.21			8	2.22	7	3.00
Other	26	10.20	29	11.60	39	10.92	21	9.42	26	9.29	55	15.03	34	10.30			36	9.97	36	15.45
TOTAL	255	100.00	250	100.00	357	100.00	223	100.00	280	100.00	366	100.00	330	100.00			361	100.00	233	100.00
Complete Forams	255		250		357		223		280		366		330				361		233	
Fragments	517		237		651		192		375		346		391		NO	SAMPLE	463		295	
Split	5		8		6		7		8		7		8				7		7	

CORE MD962084 (OLIFANTS RIVER SLOPE)

SAMPLE DEPTH (cm)	2600	%	2610	%	2620	%	2630	%	2640	%	2650	%	2660	%	2670	%	2680	%	2690	%
SPECIES COUNTED																				
G. pachyderma (sinistral)	4	1.61	8	2.67	7	1.67	4	1.11	4	4.82	2	0.90	2	0.64	16	4.48	2	0.87	14	3.62
G. pachyderma (dextral)	48	19.28	69	23.00	74	17.70	57	15.83	19	22.89	40	18.10	58	18.47	62	17.37	49	21.30	49	12.66
G. bulloides	13	5.22	8	2.67	25	5.98	12	3.33	1	1.20	8	3.62	6	1.91	3	0.84	7	3.04	24	6.20
G. scitula	1	0.40	0	0.00	12	2.87	4	1.11	7	8.43	3	1.36	5	1.59	29	8.12	2	0.87	19	4.91
G. glutinata	20	8.03	23	7.67	25	5.98	29	8.06	6	7.23	19	8.60	21	6.69	39	10.92	21	9.13	36	9.30
G. inflata	49	19.68	67	22.33	64	15.31	66	18.33	12	14.46	40	18.10	69	21.97	48	13.45	49	21.30	83	21.45
G. falconensis	4	1.61	1	0.33	9	2.15	10	2.78	2	2.41	10	4.52	1	0.32	13	3.64	7	3.04	17	4.39
G. hirsuta	6	2.41	5	1.67	3	0.72	5	1.39	0	0.00	0	0.00	8	2.55	2	0.56	2	0.87	4	1.03
G. truncatulinoides (d)	0	0.00	0	0.00	0	0.00	0	0.00	0	0.00	1	0.45	0	0.00	0	0.00	0	0.00	0	0.00
G. truncatulinoides (s)	12	4.82	16	5.33	14	3.35	14	3.89	8	9.64	8	3.62	14	4.46	5	1.40	10	4.35	7	1.81
G. ruber (alba)	7	2.81	8	2.67	23	5.50	17	4.72	2	2.41	7	3.17	14	4.46	2	0.56	12	5.22	10	2.58
G. trilobus	19	7.63	17	5.67	23	5.50	26	7.22	6	7.23	16	7.24	24	7.64	25	7.00	9	3.91	16	4.13
G. sacculifer	4	1.61	8	2.67	11	2.63	15	4.17	1	1.20	8	3.62	12	3.82	12	3.36	6	2.61	17	4.39
G. dutertrei	14	5.62	15	5.00	34	8.13	15	4.17	4	4.82	9	4.07	21	6.69	13	3.64	11	4.78	18	4.65
G. menardii	0	0.00	0	0.00	0	0.00	0	0.00	0	0.00	0	0.00	1	0.32	0	0.00	0	0.00	1	0.26
G. crassaformis	2	0.80	6	2.00	3	0.72	2	0.56	1	1.20	4	1.81	2	0.64	1	0.28	3	1.30	3	0.78
G. calida	4	1.61	8	2.67	13	3.11	7	1.94	2	2.41	7	3.17	8	2.55	18	5.04	3	1.30	13	3.36
T. quinqeloba	4	1.61	5	1.67	8	1.91	8	2.22	2	2.41	5	2.26	8	2.55	26	7.28	2	0.87	27	6.98
G. uvula	3	1.20	5	1.67	11	2.63	15	4.17	0	0.00	5	2.26	6	1.91	14	3.92	3	1.30	10	2.58
Other	35	14.06	31	10.33	59	14.11	54	15.00	6	7.23	29	13.12	34	10.83	29	8.12	32	13.91	19	4.91
TOTAL	249	100.00	300	100.00	418	100.00	360	100.00	83	100.00	221	100.00	314	100.00	357	100.00	230	100.00	387	100.00
Complete Forams	249		300		418		360		83		221		314		357		230		387	
Fragments	396		369		350		431		228		262		427		323		308		190	
Split	6		5.5		6		5		0		7		5		0		7		7	

SAMPLE DEPTH (cm)	2700	%	2710	%	2720	%	2730	%	2740	%	2750	%	2760	%	2770	%	2780	%	2790	%
SPECIES COUNTED																				
G. pachyderma (sinistral)	4	1.41	7	1.54	3	1.21	2	0.85	7	2.48			15	3.60	10	3.01	15	5.40	12	3.73
G. pachyderma (dextral)	55	19.37	83	18.28	50	20.16	50	21.19	59	20.92			53	12.71	39	11.75	32	11.51	46	14.29
G. bulloides	5	1.76	10	2.20	7	2.82	9	3.81	9	3.19			35	8.39	24	7.23	16	5.76	23	7.14
G. scitula	2	0.70	3	0.66	5	2.02	5	2.12	6	2.13			21	5.04	14	4.22	8	2.88	10	3.11
G. glutinata	11	3.87	41	9.03	15	6.05	23	9.75	24	8.51	NO	SAMPLE	55	13.19	33	9.94	29	10.43	29	9.01
G. inflata	58	20.42	92	20.26	43	17.34	41	17.37	64	22.70			88	21.10	70	21.08	69	24.82	65	20.19
G. falconensis	7	2.46	13	2.86	9	3.63	5	2.12	13	4.61			10	2.40	8	2.41	7	2.52	8	2.48
G. hirsuta	4	1.41	4	0.88	3	1.21	3	1.27	1	0.35			1	0.24	0	0.00	0	0.00	1	0.31
G. truncatulinoides (d)	0	0.00	0	0.00	1	0.40	0	0.00	0	0.00			0	0.00	0	0.00	0	0.00	0	0.00
G. truncatulinoides (s)	20	7.04	22	4.85	7	2.82	7	2.97	3	1.06			3	0.72	8	2.41	7	2.52	12	3.73
G. ruber (alba)	8	2.82	8	1.76	6	2.42	2	0.85	4	1.42			5	1.20	7	2.11	3	1.08	7	2.17
G. trilobus	30	10.56	22	4.85	21	8.47	18	7.63	8	2.84			20	4.80	13	3.92	11	3.96	18	5.59
G. sacculifer	10	3.52	10	2.20	6	2.42	11	4.66	6	2.13			13	3.12	13	3.92	15	5.40	11	3.42
G. dutertrei	16	5.63	36	7.93	16	6.45	12	5.08	23	8.16			17	4.08	12	3.61	10	3.60	14	4.35
G. menardii	0	0.00	2	0.44	1	0.40	0	0.00	0	0.00			0	0.00	1	0.30	0	0.00	0	0.00
G. crassaformis	4	1.41	1	0.22	5	2.02	3	1.27	1	0.35			2	0.48	3	0.90	2	0.72	5	1.55
G. calida	7	2.46	12	2.64	8	3.23	9	3.81	12	4.26			18	4.32	8	2.41	11	3.96	14	4.35
T. quinqeloba	4	1.41	5	1.10	5	2.02	5	2.12	13	4.61			24	5.76	32	9.64	15	5.40	25	7.76
G. uvula	5	1.76	8	1.76	3	1.21	9	3.81	7	2.48			16	3.84	17	5.12	10	3.60	8	2.48
Other	34	11.97	75	16.52	34	13.71	22	9.32	22	7.80			21	5.04	20	6.02	18	6.47	14	4.35
TOTAL	284	100.00	454	100.00	248	100.00	236	100.00	282	100.00			417	100.00	332	100.00	278	100.00	322	100.00
Complete Forams	284		454		248		236		282				417		332		278		322	
Fragments	371		510		228		139		196		NO	SAMPLE	153		94		108		144	
Split	8		6		8		9		8				8		7		8		7	

CORE MD962084 (OLIFANTS RIVER SLOPE)

SAMPLE DEPTH (cm)	2800	%	2810	%	2820	%	2830	%	2840	%	2850	%	2860	%	2870	%	2880	%	2890	%
SPECIES COUNTED																				
G. pachyderma (sinistral)	20	4.17	16	4.57	12	4.29	15	5.51	14	3.72	12	4.17	11	3.54	13	4.28	12	4.08	16	4.85
G. pachyderma (dextral)	83	17.29	55	15.71	58	20.71	56	20.59	69	18.35	49	17.01	52	16.72	62	20.39	56	19.05	61	18.48
G. bulloides	34	7.08	11	3.14	16	5.71	14	5.15	11	2.93	13	4.51	17	5.47	12	3.95	18	6.12	17	5.15
G. scitula	22	4.58	14	4.00	10	3.57	6	2.21	11	2.93	7	2.43	12	3.86	12	3.95	12	4.08	21	6.36
G. glutinata	38	7.92	35	10.00	27	9.64	21	7.72	34	9.04	20	6.94	27	8.68	16	5.26	31	10.54	40	12.12
G. inflata	106	22.08	87	24.86	66	23.57	57	20.96	85	22.61	74	25.69	70	22.51	66	21.71	62	21.09	53	16.06
G. falconensis	19	3.96	9	2.57	7	2.50	8	2.94	12	3.19	13	4.51	11	3.54	12	3.95	14	4.76	12	3.64
G. hirsuta	5	1.04	2	0.57	0	0.00	1	0.37	1	0.27	4	1.39	1	0.32	4	1.32	1	0.34	3	0.91
G. truncatulinoides (d)	0	0.00	0	0.00	0	0.00	0	0.00	1	0.27	1	0.35	0	0.00	0	0.00	0	0.00	0	0.00
G. truncatulinoides (s)	3	0.63	5	1.43	5	1.79	5	1.84	8	2.13	8	2.78	4	1.29	9	2.96	9	3.06	6	1.82
G. ruber (alba)	7	1.46	4	1.14	6	2.14	1	0.37	2	0.53	6	2.08	4	1.29	5	1.64	1	0.34	2	0.61
G. trilobus	20	4.17	15	4.29	7	2.50	7	2.57	15	3.99	5	1.74	15	4.82	6	1.97	12	4.08	17	5.15
G. sacculifer	18	3.75	13	3.71	15	5.36	10	3.68	17	4.52	9	3.13	12	3.86	10	3.29	9	3.06	11	3.33
G. dutertrei	15	3.13	18	5.14	7	2.50	15	5.51	23	6.12	20	6.94	16	5.14	15	4.93	11	3.74	18	5.45
G. menardii	0	0.00	0	0.00	1	0.36	0	0.00	1	0.27	1	0.35	0	0.00	0	0.00	0	0.00	0	0.00
G. crassaformis	5	1.04	4	1.14	2	0.71	1	0.37	3	0.80	4	1.39	4	1.29	2	0.66	0	0.00	1	0.30
G. calida	17	3.54	10	2.86	7	2.50	15	5.51	10	2.66	11	3.82	9	2.89	8	2.63	7	2.38	12	3.64
T. quinqeloba	28	5.83	20	5.71	14	5.00	8	2.94	26	6.91	7	2.43	17	5.47	18	5.92	12	4.08	14	4.24
G. uvula	14	2.92	11	3.14	9	3.21	8	2.94	11	2.93	4	1.39	5	1.61	11	3.62	9	3.06	7	2.12
Other	26	5.42	21	6.00	11	3.93	24	8.82	22	5.85	20	6.94	24	7.72	23	7.57	18	6.12	19	5.76
TOTAL	480	100.00	350	100.00	280	100.00	272	100.00	376	100.00	288	100.00	311	100.00	304	100.00	294	100.00	330	100.00
Complete Forams	480		350		280		272		376		288		311		304		294		330	
Fragments	200		124		113		133		117		83		139		100		119		191	
Split	8		8		10		9		8		9		9		9		9		9	

SAMPLE DEPTH (cm)	2900	%	2910	%	2920	%	2930	%	2940	%	2950	%	2960	%	2970	%	2980	%	2990	%
SPECIES COUNTED																				
G. pachyderma (sinistral)	9	3.59	10	3.75	8	3.17	8	3.07	10	3.77	11	4.60	9	3.46	6	1.88	5	1.83	13	3.83
G. pachyderma (dextral)	46	18.33	35	13.11	47	18.65	31	11.88	38	14.34	44	18.41	40	15.38	65	20.38	35	12.82	46	13.57
G. bulloides	8	3.19	15	5.62	13	5.16	20	7.66	11	4.15	6	2.51	12	4.62	17	5.33	9	3.30	13	3.83
G. scitula	11	4.38	16	5.99	11	4.37	10	3.83	9	3.40	4	1.67	1	0.38	10	3.13	5	1.83	9	2.65
G. glutinata	17	6.77	22	8.24	20	7.94	18	6.90	27	10.19	18	7.53	38	14.62	28	8.78	21	7.69	23	6.78
G. inflata	65	25.90	52	19.48	51	20.24	67	25.67	50	18.87	60	25.10	31	11.92	54	16.93	76	27.84	76	22.42
G. falconensis	13	5.18	11	4.12	14	5.56	13	4.98	7	2.64	8	3.35	9	3.46	13	4.08	17	6.23	9	2.65
G. hirsuta	3	1.20	2	0.75	1	0.40	1	0.38	3	1.13	0	0.00	0	0.00	3	0.94	2	0.73	4	1.18
G. truncatulinoides (d)	0	0.00	0	0.00	0	0.00	0	0.00	1	0.38	1	0.42	0	0.00	0	0.00	1	0.37	0	0.00
G. truncatulinoides (s)	5	1.99	3	1.12	3	1.19	1	0.38	4	1.51	9	3.77	7	2.69	4	1.25	15	5.49	14	4.13
G. ruber (alba)	3	1.20	6	2.25	3	1.19	8	3.07	5	1.89	2	0.84	4	1.54	3	0.94	7	2.56	11	3.24
G. trilobus	8	3.19	9	3.37	10	3.97	12	4.60	15	5.66	8	3.35	22	8.46	16	5.02	15	5.49	20	5.90
G. sacculifer	9	3.59	17	6.37	9	3.57	6	2.30	8	3.02	4	1.67	9	3.46	5	1.57	5	1.83	10	2.95
G. dutertrei	11	4.38	14	5.24	8	3.17	12	4.60	26	9.81	13	5.44	18	6.92	29	9.09	15	5.49	10	2.95
G. menardii	0	0.00	0	0.00	0	0.00	0	0.00	0	0.00	0	0.00	0	0.00	0	0.00	2	0.73	1	0.29
G. crassaformis	2	0.80	1	0.37	4	1.59	4	1.53	2	0.75	5	2.09	0	0.00	3	0.94	2	0.73	5	1.47
G. calida	6	2.39	10	3.75	8	3.17	10	3.83	12	4.53	13	5.44	7	2.69	10	3.13	3	1.10	8	2.36
T. quinqeloba	10	3.98	15	5.62	17	6.75	17	6.51	9	3.40	11	4.60	10	3.85	11	3.45	0	0.00	8	2.36
G. uvula	6	2.39	14	5.24	4	1.59	5	1.92	7	2.64	3	1.26	10	3.85	7	2.19	3	1.10	5	1.47
Other	19	7.57	15	5.62	21	8.33	18	6.90	21	7.92	19	7.95	33	12.69	35	10.97	35	12.82	54	15.93
TOTAL	251	100.00	267	100.00	252	100.00	261	100.00	265	100.00	239	100.00	260	100.00	319	100.00	273	100.00	339	100.00
Complete Forams	251		267		252		261		265		239		260		319		273		339	
Fragments	137		150		130		133		153		165		194		168		300		404	
Split	9.5		10		9		9		8		8		7		7		6		6	

APPENDIX 5

PLANKTONIC FORAMINIFERAL ASSEMBLAGES FACTOR SCORES

Varimax factor components matrixes derived from Q-mode factor analysis of the foraminiferal census data.

Core MD962080 (Agulhas Bank Slope)

Depth (cm)	Age (kyr)	Comm.	Factor 1	Factor 2	Factor 3	Factor 4
2.5	1	0.992	0.693	0.560	0.347	0.270
10.5	4	0.997	0.727	0.521	0.362	0.245
20.5	8	0.994	0.626	0.562	0.378	0.377
30.5	11	0.997	0.528	0.470	0.581	0.394
40.5	15	0.987	0.525	0.494	0.571	0.347
50.5	19	0.987	0.670	0.424	0.451	0.387
60.5	21	0.996	0.515	0.360	0.729	0.263
70.5	23	0.998	0.667	0.426	0.521	0.302
80.5	24	0.998	0.678	0.406	0.509	0.336
90.5	26	0.998	0.686	0.447	0.514	0.236
100.5	28	0.988	0.715	0.483	0.486	0.054
110.5	30	0.994	0.712	0.505	0.458	0.132
120.5	43	0.991	0.593	0.606	0.453	0.247
130.5	46	0.991	0.706	0.566	0.331	0.246
140.5	50	0.998	0.687	0.546	0.429	0.132
150.5	53	0.994	0.716	0.474	0.486	0.130
160.5	56	0.998	0.730	0.558	0.274	0.249
170.5	59	0.998	0.727	0.488	0.407	0.231
180.5	62	0.987	0.563	0.541	0.556	0.228
190.5	65	0.994	0.455	0.649	0.466	0.340
200.5	76	0.994	0.577	0.552	0.482	0.347
210.5	88	0.980	0.688	0.532	0.288	0.346
220.5	99	0.990	0.622	0.561	0.382	0.369
230.5	103	0.991	0.569	0.630	0.246	0.453
240.5	107	0.987	0.531	0.634	0.393	0.374
250.5	122	0.991	0.513	0.648	0.248	0.476
260.5	124	0.991	0.600	0.564	0.346	0.406
270.5	125	0.993	0.448	0.658	0.254	0.538
280.5	127	0.987	0.640	0.576	0.399	0.290
290.5	131	0.984	0.612	0.584	0.441	0.236
300.5	135	0.986	0.598	0.595	0.446	0.236
310.5	138	0.990	0.595	0.380	0.611	0.292
320.5	140	0.994	0.692	0.474	0.475	0.212
330.5	143	0.994	0.593	0.598	0.430	0.291
340.5	146	0.994	0.761	0.406	0.424	0.260
350.5	148	0.997	0.572	0.534	0.548	0.284
360.5	151	0.982	0.632	0.522	0.511	0.208
370.5	155	0.995	0.630	0.587	0.419	0.256
380.5	161	0.988	0.611	0.522	0.511	0.280
390.5	166	0.986	0.527	0.557	0.529	0.322
400.5	171	0.998	0.737	0.419	0.441	0.284
410.5	177	0.989	0.699	0.464	0.426	0.308
420.5	182	0.991	0.744	0.396	0.489	0.189
430.5	183	0.976	0.657	0.441	0.528	0.250
440.5	187	0.998	0.749	0.411	0.484	0.182
450.5	190	0.997	0.842	0.411	0.305	0.154
460.5	194	0.995	0.741	0.438	0.353	0.353
470.5	209	0.998	0.750	0.455	0.354	0.313
480.5	223	0.991	0.767	0.398	0.432	0.232
490.5	238	0.992	0.718	0.486	0.409	0.266

Core MD962080 (Agulhas Bank Slope)

Depth (cm)	Age (kyr)	Comm.	Factor 1	Factor 2	Factor 3	Factor 4
500.5	241	0.994	0.636	0.526	0.510	0.217
510.5	244	0.992	0.724	0.457	0.442	0.246
520.5	248	0.990	0.719	0.407	0.470	0.291
530.5	250	0.985	0.680	0.527	0.470	0.122
540.5	252	0.982	0.647	0.486	0.514	0.234
550.5	255	0.993	0.762	0.459	0.413	0.170
560.5	257	0.994	0.812	0.442	0.363	0.083
570.5	259	0.991	0.752	0.500	0.377	0.162
580.5	261	0.997	0.804	0.433	0.375	0.143
590.5	264	0.995	0.695	0.396	0.563	0.187
600.5	266	0.992	0.611	0.512	0.544	0.189
610.5	273	0.997	0.640	0.450	0.603	0.117
620.5	280	0.996	0.663	0.510	0.490	0.206
630.5	287	0.997	0.630	0.532	0.540	0.100
640.5	290	0.992	0.756	0.522	0.309	0.192
650.5	292	0.997	0.649	0.523	0.518	0.130
660.5	295	0.988	0.551	0.410	0.716	0.053
670.5	300	0.995	0.683	0.544	0.458	0.128
680.5	304	0.994	0.704	0.536	0.434	0.110
690.5	309	0.998	0.628	0.543	0.512	0.175
700.5	312	0.997	0.724	0.419	0.486	0.202
710.5	315	0.997	0.701	0.486	0.492	0.134
720.5	321	0.997	0.679	0.584	0.418	0.108
730.5	328	0.987	0.503	0.454	0.524	0.486
740.5	330	0.979	0.557	0.587	0.434	0.346
750.5	331					
760.5	333					
770.5	335	0.995	0.550	0.585	0.469	0.348
780.5	337	0.993	0.630	0.486	0.453	0.389
790.5	338	0.996	0.556	0.530	0.560	0.255
800.5	340	0.994	0.736	0.380	0.504	0.218
810.5	345	0.997	0.522	0.362	0.671	0.376
820.5	350	0.993	0.735	0.419	0.411	0.300
830.5	355	0.991	0.747	0.454	0.335	0.326
840.5	359	0.997	0.722	0.399	0.504	0.239
850.5	364	0.991	0.691	0.469	0.508	0.168
860.5	369	0.991	0.706	0.535	0.398	0.201
870.5	374	0.995	0.517	0.438	0.652	0.326
880.5	379	0.993	0.703	0.429	0.525	0.191
890.5	384	0.998	0.812	0.474	0.278	0.148
900.5	390	0.994	0.835	0.465	0.136	0.223
910.5	406	0.994	0.698	0.506	0.414	0.260
920.5	409	0.991	0.685	0.381	0.508	0.342
930.5	411	0.984	0.730	0.571	0.311	0.165
940.5	414	0.969	0.686	0.605	0.343	0.109
950.5	419					
960.5	424	0.989	0.612	0.585	0.440	0.248
970.5	429	0.994	0.639	0.553	0.472	0.223
980.5	434	0.990	0.733	0.447	0.469	0.150
990.5	446	0.995	0.665	0.520	0.476	0.194

Core MD962080 (Agulhas Bank Slope)

Depth (cm)	Age (kyr)	Comm.	Factor 1	Factor 2	Factor 3	Factor 4
1000.5	458	0.993	0.551	0.640	0.513	0.120
1010.5	466	0.977	0.535	0.706	0.428	0.078
1020.5	473	0.990	0.473	0.746	0.414	0.187
1030.5	481	0.992	0.516	0.726	0.422	0.118
1040.5	491	0.974	0.565	0.710	0.356	0.127
1050.5	500	0.992	0.520	0.631	0.524	0.202
1060.5	512	0.996	0.587	0.628	0.470	0.149
1070.5	524	0.980	0.394	0.789	0.408	0.183
1080.5	527	0.983	0.366	0.733	0.537	0.112
1090.5	530	0.996	0.392	0.469	0.750	0.244
1100.5	533	0.988	0.226	0.420	0.855	0.140
1110.5	536	0.982	0.417	0.402	0.803	-0.028
1120.5	548	0.987	0.675	0.467	0.545	0.111
1130.5	561	0.983	0.485	0.735	0.369	0.236
1140.5	573	0.996	0.386	0.642	0.523	0.357
1150.5	582	0.996	0.420	0.545	0.605	0.362
1160.5	594	0.997	0.549	0.493	0.611	0.262
1170.5	604	0.988	0.595	0.541	0.532	0.228
1180.5	615	0.991	0.588	0.556	0.516	0.242
1190.5	621	0.998	0.562	0.698	0.340	0.250
1200.5	628	0.982	0.574	0.661	0.406	0.210
1210.5	633	0.985	0.556	0.681	0.373	0.267
1220.5	637	0.989	0.513	0.612	0.578	0.122
1230.5	642	0.998	0.506	0.698	0.481	0.140
1240.5	654	0.981	0.403	0.726	0.508	0.182
1250.5	666	0.994	0.464	0.738	0.392	0.254
1260.5	673	0.985	0.514	0.722	0.390	0.209
1270.5	681	0.974	0.418	0.754	0.417	0.227
1280.5	688	0.990	0.484	0.740	0.409	0.196
1290.5	699	0.977	0.541	0.714	0.327	0.254
1300.5	703	0.984	0.538	0.735	0.366	0.136
1310.5	708	0.986	0.593	0.728	0.253	0.196
1320.5	711	0.983	0.485	0.735	0.369	0.236
1330.5	713	0.988	0.518	0.763	0.276	0.241
1340.5	716	0.993	0.661	0.664	0.304	0.133
1350.5	718	0.988	0.624	0.674	0.348	0.127
1360.5	736	0.985	0.603	0.711	0.302	0.131
1370.5	754	0.984	0.638	0.667	0.312	0.166
1380.5	759	0.986	0.508	0.718	0.390	0.246
1390.5	765	0.995	0.395	0.696	0.576	0.152
1400.5	769	0.985	0.506	0.720	0.428	0.157
1410.5	774	0.989	0.507	0.710	0.437	0.162
1420.5	778	0.995	0.487	0.762	0.369	0.178
1430.5	782	0.997	0.406	0.782	0.420	0.165
1440.5	778	0.986	0.522	0.676	0.483	0.123
1450.5	790	0.995	0.633	0.681	0.326	0.150
1460.5	799	0.978	0.586	0.671	0.383	0.179
1470.5	807	0.985	0.245	0.704	0.610	0.234
1480.5	815	0.988	0.364	0.659	0.604	0.181
1490.5	824	0.990	0.493	0.728	0.422	0.183

Core MD962084 (Olifants River Slope)

Depth (cm)	Age (kyr)	Comm.	Factor 1	Factor 2	Factor 3	Factor 4
2.5	0.0	0.984	0.446	0.674	0.568	-0.013
10.5	1.0	0.990	0.412	0.705	0.564	0.031
20.5	2.1	0.985	0.494	0.675	0.531	-0.043
30.5	3.1	0.980	0.288	0.689	0.643	0.084
40.5	4.2	0.989	0.432	0.768	0.457	0.066
50.5	5.2	0.983	0.415	0.723	0.529	0.068
60.5	6.3	0.995	0.463	0.747	0.462	0.054
70.5	7.3	0.997	0.423	0.746	0.505	0.079
80.5	8.4	0.993	0.426	0.727	0.529	0.049
90.5	9.4	0.996	0.421	0.753	0.491	0.069
100.5	10.5	0.987	0.337	0.807	0.388	0.238
110.5	11.5	0.997	0.323	0.764	0.538	0.102
120.5	12.2	0.986	0.400	0.830	0.314	0.183
130.5	12.8	0.990	0.351	0.745	0.534	0.152
140.5	13.5	0.986	0.351	0.772	0.471	0.145
150.5	14.1	0.988	0.392	0.841	0.315	0.127
160.5	14.8	0.991	0.429	0.779	0.384	0.212
170.5	15.4	0.991	0.449	0.776	0.409	0.134
180.5	16.1	0.993	0.484	0.776	0.335	0.202
190.5	16.7	0.991	0.501	0.792	0.322	0.088
200.5	17.4	0.995	0.452	0.782	0.409	0.076
210.5	18.0	0.997	0.535	0.733	0.406	0.092
220.5	26.5	0.988	0.626	0.700	0.315	-0.026
230.5	35.0	0.985	0.464	0.809	0.311	0.105
240.5	43.5	0.994	0.595	0.737	0.303	0.020
250.5	52.0	0.996	0.364	0.810	0.435	0.128
260.5	53.4	0.986	0.520	0.772	0.281	0.167
270.5	54.9	0.997	0.475	0.732	0.468	0.019
280.5	56.3	0.996	0.566	0.780	0.247	0.045
290.5	57.7	0.992	0.614	0.722	0.292	0.052
300.5	59.1	0.963	0.492	0.747	0.372	-0.005
310.5	60.6	0.996	0.526	0.782	0.320	0.011
320.5	62.0	0.994	0.575	0.724	0.366	0.046
330.5	62.8	0.996	0.543	0.679	0.470	0.092
340.5	63.7	0.999	0.436	0.744	0.483	0.116
350.5	64.5	0.996	0.457	0.737	0.467	0.082
360.5	65.3	0.993	0.462	0.742	0.472	0.060
370.5	66.2	0.992	0.468	0.750	0.458	0.018
380.5	67.0	0.987	0.449	0.732	0.488	0.097
390.5	67.8	0.992	0.365	0.719	0.567	0.136
400.5	68.7	0.993	0.476	0.733	0.457	0.096
410.5	69.5	0.989	0.498	0.717	0.468	0.044
420.5	70.3	0.997	0.525	0.737	0.400	0.098
430.5	71.2	0.995	0.629	0.618	0.456	0.043
440.5	72.0	0.991	0.707	0.578	0.365	0.038
450.5	72.8	0.989	0.507	0.727	0.441	0.064
460.5	73.7	0.985	0.494	0.676	0.513	0.079
470.5	74.5	0.991	0.526	0.703	0.445	0.103
480.5	75.3	0.994	0.507	0.713	0.473	0.067
490.5	76.2	0.991	0.396	0.726	0.514	0.206

Core MD962084 (Olifants River Slope)

Depth (cm)	Age (kyr)	Comm.	Factor 1	Factor 2	Factor 3	Factor 4
500.5	77.0	0.993	0.369	0.710	0.563	0.133
510.5	77.8	0.994	0.426	0.697	0.566	0.057
520.5	78.7	0.990	0.504	0.722	0.404	0.219
530.5	79.5	0.993	0.496	0.722	0.454	0.118
540.5	81.6	0.994	0.450	0.776	0.412	0.143
550.5	83.6	0.984	0.352	0.792	0.471	0.081
560.5	85.7	0.990	0.418	0.753	0.459	0.185
570.5	87.7					
580.5	89.8					
590.5	91.8	92	0.993	0.416	0.625	0.598
600.5	93.9	94	0.992	0.415	0.722	0.477
610.5	95.9	96	0.990	0.461	0.671	0.521
620.5	98.0	98	0.992	0.440	0.745	0.430
630.5	101.0	101	0.996	0.478	0.709	0.458
640.5	104.0	104	0.984	0.360	0.735	0.495
650.5	107.0	107	0.991	0.359	0.734	0.424
660.5	110.0	110	0.962	0.533	0.681	0.366
670.5	113.0	113	0.995	0.430	0.716	0.492
680.5	116.0	116	0.986	0.275	0.668	0.621
690.5	119.0	119	0.989	0.206	0.713	0.544
700.5	122.0	122	0.990	0.391	0.644	0.504
710.5	123.7	124	0.982	0.364	0.655	0.523
720.5	125.3	125	0.976	0.452	0.655	0.503
730.5	127.0	127	0.984	0.495	0.618	0.524
740.5	129.3	129	0.994	0.377	0.670	0.577
750.5	131.7	132	0.996	0.556	0.617	0.485
760.5	134.0	134	0.988	0.512	0.592	0.556
770.5	143.6	144	0.988	0.531	0.589	0.559
780.5	153.2	153	0.980	0.527	0.632	0.448
790.5	162.8	163	0.987	0.548	0.611	0.508
800.5	172.4	172	0.994	0.529	0.670	0.469
810.5	182.0	182	0.979	0.591	0.591	0.509
820.5	184.0	184	0.982	0.606	0.587	0.428
830.5	186.0	186	0.987	0.443	0.579	0.634
840.5	188.0	188	0.996	0.501	0.569	0.608
850.5	190.0	190	0.990	0.512	0.573	0.604
860.5	192.0	192	0.980	0.414	0.596	0.641
870.5	194.0	194	0.979	0.468	0.590	0.619
880.5	200.7	201	0.984	0.573	0.611	0.522
890.5	207.3	207	0.987	0.704	0.492	0.404
900.5	214.0	214	0.992	0.668	0.585	0.399
910.5	216.3	216	0.991	0.529	0.660	0.501
920.5	218.6	219	0.963	0.607	0.555	0.475
930.5	220.9	221	0.989	0.588	0.568	0.534
940.5	223.2	223	0.990	0.628	0.556	0.500
950.5	225.5	226	0.995	0.661	0.522	0.519
960.5	227.8	228	0.986	0.663	0.522	0.504
970.5	230.1	230	0.984	0.799	0.438	0.371
980.5	232.4	232	0.992	0.686	0.538	0.471
990.5	234.7	235	0.977	0.657	0.585	0.374

Core MD962084 (Olifants River Slope)

Depth (cm)	Age (kyr)	Comm.	Factor 1	Factor 2	Factor 3	Factor 4
1000.5	237.0	237	0.983	0.470	0.566	0.620
1010.5	238.9	239	0.988	0.377	0.640	0.615
1020.5	240.8	241	0.986	0.654	0.594	0.408
1030.5	242.8	243	0.989	0.715	0.524	0.421
1040.5	244.7	245	0.995	0.709	0.548	0.390
1050.5	246.6	247	0.988	0.746	0.556	0.282
1060.5	248.5	249	0.986	0.668	0.533	0.473
1070.5	249.5	250	0.982	0.699	0.515	0.446
1080.5	250.5	251	0.988	0.665	0.579	0.416
1090.5	251.5	252	0.988	0.644	0.539	0.463
1100.5	252.5	253	0.983	0.661	0.486	0.489
1110.5	253.5	254	0.989	0.597	0.562	0.555
1120.5	254.5	255	0.994	0.522	0.562	0.630
1130.5	255.5	256	0.987	0.698	0.480	0.501
1140.5	256.5	257	0.992	0.704	0.409	0.545
1150.5	257.5	258	0.991	0.658	0.480	0.557
1160.5	260.5	260	0.993	0.464	0.489	0.719
1170.5	263.4	263	0.982	0.540	0.456	0.675
1180.5	266.4	266	0.980	0.756	0.382	0.486
1190.5	269.3	269	0.990	0.649	0.446	0.601
1200.5	272.3	272	0.990	0.629	0.495	0.563
1210.5	275.2	275	0.985	0.591	0.465	0.626
1220.5	278.2	278	0.993	0.541	0.497	0.660
1230.5	281.1	281	0.994	0.631	0.513	0.576
1240.5	284.1	284	0.997	0.722	0.486	0.473
1250.5	287.0	287	0.977	0.677	0.464	0.515
1260.5	289.5	290	0.991	0.516	0.472	0.693
1270.5	292.0	292	0.994	0.666	0.511	0.531
1280.5	294.5	295	0.993	0.641	0.486	0.578
1290.5	297.0	297	0.984	0.611	0.359	0.673
1300.5	299.5	300	0.996	0.597	0.488	0.616
1310.5	302.0	302	0.986	0.541	0.418	0.704
1320.5	306.0	306	0.983	0.498	0.445	0.718
1330.5	310.0	310	0.936	0.585	0.416	0.552
1340.5	313.3	313	0.940	0.499	0.439	0.684
1350.5	316.5	317	0.993	0.679	0.464	0.536
1360.5	319.8	320	0.979	0.601	0.408	0.632
1370.5	323.0	323	0.972	0.699	0.470	0.479
1380.5	326.3	326	0.988	0.545	0.478	0.652
1390.5	329.5	330	0.991	0.548	0.449	0.659
1400.5	331.3	331	0.972	0.646	0.431	0.549
1410.5	333.2	333	0.989	0.697	0.489	0.503
1420.5	335.0	335	0.983	0.439	0.489	0.639
1430.5	336.8	337	0.974	0.446	0.505	0.656
1440.5	338.7	339	0.983	0.683	0.532	0.446
1450.5	340.5	341	0.996	0.446	0.491	0.662
1460.5	349.0	349	0.992	0.570	0.547	0.575
1470.5	351.7	352	0.981	0.551	0.527	0.624
1480.5	354.3	354	0.990	0.494	0.453	0.712
1490.5	357.0	357	0.967	0.547	0.405	0.640

Core MD962084 (Olifants River Slope)

Depth (cm)	Age (kyr)	Comm.	Factor 1	Factor 2	Factor 3	Factor 4
1500.5	357.9	358	0.989	0.619	0.519	0.571
1510.5	358.8	359	0.982	0.444	0.438	0.756
1520.5	359.7	360	0.973	0.524	0.458	0.681
1530.5	360.5	361	0.966	0.254	0.499	0.804
1540.5	361.4	361	0.983	0.483	0.448	0.733
1550.5	362.3	362	0.955	0.363	0.425	0.791
1560.5	363.2	363	0.984	0.613	0.545	0.544
1570.5	364.1	364	0.986	0.656	0.499	0.541
1580.5	365.0	365	0.980	0.466	0.445	0.731
1590.5	365.8	366	0.986	0.413	0.432	0.780
1600.5	366.7	367	0.987	0.619	0.452	0.616
1610.5	367.6	368	0.996	0.510	0.509	0.686
1620.5	368.5	369	0.995	0.423	0.518	0.738
1630.5	371.6	372	0.982	0.457	0.444	0.737
1640.5	374.7	375	0.991	0.448	0.399	0.786
1650.5	377.8	378	0.987	0.584	0.452	0.638
1660.5	380.8	381	0.990	0.504	0.418	0.731
1670.5	383.9	384	0.987	0.544	0.483	0.656
1680.5	387.0	387	0.991	0.501	0.523	0.672
1690.5	390.1	390	0.987	0.520	0.333	0.715
1700.5	393.2	393	0.978	0.710	0.315	0.572
1710.5	396.3	396	0.989	0.502	0.478	0.704
1720.5	399.3	399	0.973	0.624	0.345	0.660
1730.5	402.4	402	0.977	0.622	0.423	0.572
1740.5	405.5	406	0.984	0.552	0.464	0.665
1750.5	407.3	407	0.992	0.620	0.445	0.626
1760.5	409.1	409	0.993	0.616	0.455	0.617
1770.5	410.8	411	0.988	0.647	0.435	0.612
1780.5	412.6	413	0.983	0.648	0.356	0.627
1790.5	414.4	414	0.986	0.645	0.474	0.573
1800.5	416.2	416	0.989	0.633	0.323	0.672
1810.5	418.0	418	0.991	0.739	0.337	0.545
1820.5	419.8	420	0.983	0.608	0.409	0.648
1830.5	421.5	422	0.992	0.522	0.406	0.719
1840.5	423.3	423	0.995	0.696	0.422	0.560
1850.5	425.1	425	0.996	0.601	0.455	0.639
1860.5	426.9	427	0.976	0.551	0.576	0.499
1870.5	428.7	429	0.985	0.383	0.576	0.665
1880.5	430.4	430	0.980	0.650	0.534	0.454
1890.5	432.2	432	0.994	0.587	0.575	0.533
1900.5	434.0	434	0.987	0.608	0.539	0.464
1910.5	437.3	437	0.995	0.622	0.521	0.444
1920.5	440.5	441	0.989	0.672	0.522	0.401
1930.5	443.8	444	0.992	0.626	0.529	0.523
1940.5	447.0	447	0.981	0.573	0.528	0.484
1950.5	450.3	450	0.993	0.621	0.461	0.547
1960.5	453.5	454	0.980	0.514	0.522	0.591
1970.5	456.8	457	0.992	0.554	0.419	0.646
1980.5	460.0	460	0.985	0.571	0.390	0.654
1990.5	462.6	463	0.990	0.631	0.404	0.571

Core MD962084 (Olifants River Slope)

Depth (cm)	Age (kyr)	Comm.	Factor 1	Factor 2	Factor 3	Factor 4
2000.5	465.3	465	0.998	0.602	0.434	0.649
2010.5	467.9	468	0.989	0.647	0.415	0.620
2020.5	470.5	471	0.993	0.757	0.472	0.425
2030.5	473.1	473	0.991	0.556	0.454	0.654
2040.5	475.8	476	0.990	0.531	0.459	0.681
2050.5	478.4	478	0.989	0.598	0.456	0.631
2060.5	481.0	481	0.994	0.576	0.466	0.661
2070.5	485.2	485	0.986	0.412	0.490	0.739
2080.5	489.4	489	0.992	0.712	0.409	0.554
2090.5	493.6	494	0.992	0.635	0.452	0.577
2100.5	497.8	498	0.992	0.493	0.550	0.648
2110.5	502.0	502	0.993	0.569	0.506	0.622
2120.5	506.2	506	0.992	0.523	0.524	0.649
2130.5	510.4	510	0.987	0.669	0.514	0.471
2140.5	514.6	515	0.998	0.546	0.514	0.614
2150.5	518.8	519	0.984	0.546	0.537	0.598
2160.5	523.0	523	0.993	0.417	0.493	0.724
2170.5	525.0	525	0.985	0.493	0.558	0.618
2180.5	527.0	527	0.992	0.565	0.600	0.534
2190.5	532.5	533	0.992	0.616	0.533	0.552
2200.5	538.0	538	0.998	0.578	0.561	0.556
2210.5	546.3	546	0.993	0.464	0.552	0.654
2220.5	554.7	555	0.996	0.617	0.519	0.548
2230.5	563.0	563	0.989	0.599	0.488	0.549
2240.5	565.0	565	0.987	0.516	0.483	0.621
2250.5	567.0	567	0.987	0.607	0.491	0.596
2260.5	579.3	579	0.993	0.664	0.512	0.513
2270.5	591.5	592	0.995	0.466	0.547	0.645
2280.5	603.8	604	0.993	0.567	0.557	0.516
2290.5	616.0	616	0.965	0.629	0.458	0.549
2300.5	617.7	618	0.991	0.631	0.541	0.503
2310.5	619.4	619	0.994	0.603	0.607	0.432
2320.5	621.1	621	0.995	0.558	0.531	0.590
2330.5	622.9	623	0.994	0.547	0.495	0.640
2340.5	624.6	625	0.981	0.485	0.475	0.704
2350.5	626.3	626	0.988	0.547	0.555	0.585
2360.5	628.0	628	0.984	0.685	0.470	0.525
2370.5	631.9	632	0.992	0.552	0.549	0.605
2380.5	635.8	636	0.978	0.614	0.498	0.581
2390.5	639.7	640	0.991	0.585	0.484	0.594
2400.5	643.6	644	0.959	0.472	0.599	0.524
2410.5	647.5	648	0.959	0.506	0.611	0.514
2420.5	651.4	651	0.974	0.508	0.513	0.642
2430.5	655.3	655	0.993	0.499	0.574	0.612
2440.5	659.2	659	0.989	0.618	0.438	0.638
2450.5	663.1	663	0.994	0.644	0.426	0.619
2460.5	667.0	667	0.992	0.671	0.457	0.553
2470.5	669.7	670	0.987	0.738	0.444	0.461
2480.5	672.4	672	0.987	0.556	0.524	0.593
2490.5	675.1	675	0.993	0.709	0.456	0.522

Core MD962084 (Olifants River Slope)

Depth (cm)	Age (kyr)	Comm.	Factor 1	Factor 2	Factor 3	Factor 4
2500.5	677.8	678	0.986	0.652	0.487	0.506
2510.5	680.4	680	0.986	0.724	0.530	0.331
2520.5	683.1	683	0.995	0.783	0.360	0.479
2530.5	685.8	686	0.988	0.834	0.391	0.300
2540.5	688.5	689	0.992	0.720	0.479	0.442
2550.5	693.7	694	0.994	0.718	0.436	0.433
2560.5	698.9	699	0.994	0.652	0.466	0.545
2570.5	704.1					
2580.5	709.3	709	0.996	0.752	0.479	0.412
2590.5	714.5	714	0.970	0.593	0.562	0.519
2600.5	719.7	720	0.994	0.635	0.487	0.572
2610.5	724.9	725	0.992	0.656	0.450	0.588
2620.5	730.1	730	0.979	0.655	0.531	0.485
2630.5	735.3	735	0.980	0.584	0.480	0.597
2640.5	740.4	740	0.965	0.727	0.437	0.409
2650.5	745.6	746	0.986	0.621	0.512	0.545
2660.5	750.8	751	0.992	0.613	0.413	0.650
2670.5	756.0	756	0.981	0.621	0.505	0.365
2680.5	761.2	761	0.976	0.617	0.504	0.574
2690.5	766.4	766	0.989	0.402	0.622	0.580
2700.5	771.6	772	0.996	0.656	0.378	0.631
2710.5	776.8	777	0.987	0.625	0.463	0.594
2720.5	782.0	782	0.991	0.695	0.465	0.525
2730.5	783.8	784	0.992	0.686	0.500	0.468
2740.5	785.7	786	0.994	0.585	0.550	0.549
2750.5	787.5					
2760.5	789.3	789	0.992	0.392	0.643	0.519
2770.5	791.2	791	0.958	0.369	0.613	0.559
2780.5	793.0	793	0.985	0.349	0.575	0.649
2790.5	794.8	795	0.970	0.474	0.586	0.559
2800.5	796.6	797	0.991	0.471	0.651	0.539
2810.5	798.4	798	0.994	0.458	0.543	0.631
2820.5	800.2	800	0.989	0.518	0.613	0.538
2830.5	802.0	802	0.983	0.582	0.586	0.514
2840.5	803.8	804	0.985	0.545	0.535	0.575
2850.5	805.6	806	0.994	0.466	0.571	0.650
2860.5	807.4	807	0.993	0.496	0.595	0.579
2870.5	809.2	809	0.981	0.557	0.586	0.544
2880.5	811.0	811	0.991	0.534	0.629	0.506
2890.5	812.8	813	0.993	0.603	0.599	0.399
2900.5	814.6	815	0.993	0.473	0.580	0.631
2910.5	816.4	816	0.980	0.430	0.629	0.531
2920.5	818.2	818	0.983	0.528	0.631	0.504
2930.5	820.0	820	0.981	0.323	0.628	0.657
2940.5	822.6	823	0.996	0.552	0.510	0.554
2950.5	825.1	825	0.977	0.519	0.513	0.643
2960.5	827.7	828	0.982	0.651	0.462	0.364
2970.5	830.3	830	0.993	0.662	0.565	0.437
2980.5	832.9	833	0.981	0.379	0.503	0.750
2990.5	835.4	835	0.995	0.455	0.521	0.692

APPENDIX 6

COUNTS OF *Globorotalia menardii*
in the >125 um FRACTION
for
ABSOLUTE ABUNDANCE and ACCUMULATION RATES

CORE MD962080 (AGULHAS BANK SLOPE)

Depth (cm)	Age (kyr)	Wt>125 um (g)	# menardii in >125µm fraction	# menardii /g >125µm	Sample wt (g)	# menardii /g bulk sed	BMAR (g/cm2/kyr)	*Gr. menardii* AR (#/cm2/kyr)
2.5	1	1.113	100	89.847	7	14.286	2.640	37.713
10.5	4	1.975	128	64.810	10.7	11.963	2.717	32.507
20.5	8	2.383	176	73.856	12.1	14.545	3.078	44.773
30.5	11	2.400	176	73.333	7.1	24.789	3.075	76.232
40.5	15	2.871	224	78.022	8.8	25.455	3.117	79.349
50.5	19	2.647	96	36.267	6.7	14.328	2.848	40.813
60.5	21	2.781	192	69.040	8.8	21.818	5.795	126.444
70.5	23	3.534	384	108.659	10.6	36.226	5.997	217.254
80.5	24	2.843	384	135.069	9.5	40.421	5.894	238.224
90.5	26	2.112	128	60.606	8.8	14.545	5.898	85.787
100.5	28	3.091	192	62.116	9.6	20.000	5.832	116.635
110.5	30	1.031	16	15.519	7.1	2.254	5.865	13.216
120.5	43	1.608	96	59.701	7.2	13.333		
130.5	46	1.482	16	10.796	6	2.667		
140.5	50	2.166	96	44.321	6.2	15.484		
150.5	53	2.271	96	42.272	6.7	14.328		
160.5	56	1.969	64	32.504	6.6	9.697		
170.5	59	3.159	192	60.779	10.1	19.010	1.286	24.450
180.5	62	3.422	320	93.513	10.6	30.189	1.314	39.675
190.5	65	1.788	96	53.691	8.4	11.429	1.337	15.283
200.5	76	2.514	224	89.101	9.2	24.348	0.987	24.037
210.5	88	1.983	192	96.823	8.9	21.573	0.972	20.968
220.5	99	1.250	32	25.600	9.5	3.368	0.962	3.239
230.5	103	1.572	32	20.356	9.7	3.299	1.418	4.677
240.5	107	1.941	64	32.973	10.1	6.337	1.411	8.940
250.5	122	2.214	160	72.267	10.8	14.815	1.377	20.399
260.5	124	1.563	48	30.710	7.8	6.154	3.973	24.449
270.5	125	2.509	192	76.525	11.6	16.552	3.888	64.355
280.5	127	2.303	128	55.580	9.7	13.196	4.502	59.404
290.5	131	3.129	192	61.361	9.9	19.394	4.449	86.291
300.5	135	4.444	192	43.204	11.8	16.271	4.230	68.819
310.5	138	3.382	128	37.847	10.3	12.427	4.029	50.065
320.5	140	2.251	160	71.080	6.2	25.806	4.310	111.234
330.5	143	2.595	192	73.988	7.3	26.301	4.119	108.335
340.5	146	2.945	112	38.031	7.2	15.556	4.068	63.284
350.5	148	2.297	80	34.828	7	11.429	3.885	44.405
360.5	151	3.680	160	43.478	9.1	17.582	3.962	69.656
370.5	155	3.848	160	41.580	10.9	14.679	2.219	32.571
380.5	161	3.150	32	10.159	9.3	3.441	2.111	7.262
390.5	166	2.763	64	23.163	8.7	7.356	2.023	14.882
400.5	171	3.262	224	68.670	10.9	20.550	2.097	43.098
410.5	177	2.743	192	69.996	8.9	21.573	2.119	45.707
420.5	182	3.000	128	42.667	12.7	10.079	2.230	22.475
430.5	183	2.012	32	15.905	9.5	3.368	1.463	4.927
440.5	187	3.112	64	20.566	12.7	5.039	1.436	7.237
450.5	190	1.825	160	87.671	9.2	17.391	1.413	24.582
460.5	194	1.797	96	53.422	11.9	8.067	1.416	11.422
470.5	209	1.942	128	65.911	11	11.636	1.399	16.280
480.5	223	1.404	16	11.396	8.6	1.860	1.398	2.600
490.5	238	1.138	32	28.120	8.5	3.765	1.445	5.440
500.5	241	1.747	64	36.634	10.3	6.214	3.473	21.583
510.5	244	1.697	80	47.142	9.1	8.791	3.856	33.895
520.5	248	1.405	80	56.940	7.8	10.256	3.688	37.823
530.5	250	1.838	32	17.410	8.5	3.765	5.367	20.204
540.5	252	2.026	64	31.589	10.2	6.275	5.374	33.721
550.5	255	0.170	18	105.882	10.2	1.765	5.364	9.467

CORE MD962080 (AGULHAS BANK SLOPE)

Depth (cm)	Age (kyr)	Wt>125 um (g)	# menardii in >125μm fraction	# menardii /g >125μm	Sample wt (g)	# menardii /g bulk sed	BMAR (g/cm2/kyr)	*Gr. menardii* AR (#/cm2/kyr)
560.5	257	4.092	64	15.640	11.7	5.470	5.011	27.413
570.5	259	3.375	224	66.370	9.5	23.579	4.967	117.122
580.5	261	3.121	32	10.253	11.1	2.883	5.259	15.161
590.5	264	1.745	32	18.338	11.6	2.759	5.622	15.509
600.5	266	1.541	32	20.766	9.4	3.404	5.666	19.289
610.5	273	1.425	48	33.684	8.3	5.783	2.699	15.611
620.5	280	1.812	48	26.490	9.7	4.948	2.660	13.163
630.5	287	2.671	128	47.922	9.2	13.913	2.576	35.845
640.5	290	2.156	128	59.369	10.3	12.427	2.606	32.382
650.5	292	1.635	16	9.786	8.2	1.951	2.535	4.946
660.5	295	1.480	64	43.243	8.8	7.273	2.541	18.478
670.5	300	1.261	32	25.377	6.8	4.706	2.603	12.251
680.5	304	1.307	56	42.846	6.4	8.750	2.561	22.410
690.5	309	2.412	128	53.068	7.1	18.028	2.480	44.710
700.5	312	1.387	128	92.286	7.5	17.067	2.597	44.317
710.5	315	1.214	112	92.257	8.9	12.584	2.346	29.517
720.5	321	1.317	64	48.595	9.5	6.737	2.434	16.398
730.5	328	0.863	48	55.620	7.4	6.486	2.467	16.004
740.5	331	0.947	80	84.477	5.7	14.035	3.995	56.063
750.5	334						4.146	
760.5	337							
770.5	340	1.339	112	83.645	9.3	12.043		
780.5	343	1.569	128	81.581	7.9	16.203	3.581	58.029
790.5	346	2.239	80	35.730	7.8	10.256	3.648	37.419
800.5	350	3.016	96	31.830	11	8.727	3.717	32.443
810.5	353	1.818	80	44.004	8.4	9.524	3.887	37.021
820.5	356	1.240	56	45.161	8.4	6.667	3.550	23.664
830.5	359	1.714	64	37.340	10.8	5.926	3.938	23.337
840.5	363	1.204	40	33.223	9.3	4.301	3.856	16.584
850.5	366	0.948	64	67.511	10.8	5.926	3.980	23.583
860.5	369	1.523	72	47.275	10.4	6.923	3.868	26.778
870.5	374	1.377	96	69.717	9.3	10.323	1.659	17.123
880.5	379	1.523	32	21.011	8.4	3.810	1.696	6.460
890.5	384	1.631	40	24.525	7.8	5.128	1.701	8.725
900.5	390	0.772	40	51.813	13.9	2.878	1.668	4.799
910.5	406	0.266	28	105.263	7.8	3.590	1.655	5.942
920.5	409	0.128	12	93.750	8.1	1.481	2.975	4.407
930.5	411	0.685	56	81.752	8.3	6.747	3.012	20.319
940.5	414	1.169	48	41.061	7.1	6.761	2.906	19.644
950.5	419						3.180	
960.5	424	1.235	160	129.555	8.1	19.753	3.183	62.873
970.5	429	1.687	176	104.327	11.1	15.856		
980.5	434	1.861	80	42.988	8.8	9.091		
990.5	446	2.704	192	71.006	10.5	18.286	0.961	17.566
1000.5	458	1.128	101	89.539	6.2	16.290	1.010	16.459
1010.5	466	2.010	153	76.119	7.7	19.870	1.651	32.799
1020.5	473	2.285	127	55.580	8.9	14.270	1.699	24.246
1030.5	481	1.015	72	70.936	7.4	9.730	1.701	16.554
1040.5	491	1.751	264	150.771	10.8	24.444	1.370	33.489
1050.5	500	1.380	120	86.957	10.9	11.009	1.296	14.267
1060.5	512	1.043	75	71.908	8.6	8.721	1.042	9.088
1070.5	524	1.271	38	29.898	9.8	3.878	1.038	4.026
1080.5	527	1.136	49	43.134	8.9	5.506	4.407	24.263
1090.5	530	1.582	40	25.284	10	4.000	4.440	17.762
1100.5	533	2.420	88	36.364	11.5	7.652	4.283	32.773
1110.5	536	2.212	59	26.673	10	5.900	4.353	25.681

CORE MD962080 (AGULHAS BANK SLOPE)

Depth (cm)	Age (kyr)	Wt>125 um (g)	# menardii in >125μm fraction	# menardii /g >125μm	Sample wt (g)	# menardii /g bulk sed	BMAR (g/cm2/kyr)	*Gr. menardii* AR (#/cm2/kyr)
1120.5	548	0.984	48	48.780	8.3	5.783	1.060	6.130
1130.5	561	1.112	29	26.079	8.9	3.258	0.994	3.237
1140.5	573	1.022	55	53.816	9.6	5.729	1.031	5.908
1150.5	582	1.129	139	123.118	8.4	16.548	1.348	22.309
1160.5	594	1.046	145	138.623	9.2	15.761	1.064	16.767
1170.5	604	1.048	195	186.069	9.7	20.103	1.312	26.367
1180.5	615	1.042	263	252.399	10.8	24.352	1.157	28.174
1190.5	621	3.801	383	100.763	11.8	32.458	1.900	61.662
1200.5	628	2.087	112	53.666	8.1	13.827	1.922	26.579
1210.5	633	2.523	70	27.745	8.9	7.865	2.625	20.647
1220.5	637	3.418	118	34.523	10.9	10.826	2.675	28.958
1230.5	642	2.864	128	44.693	8.8	14.545	2.644	38.453
1240.5	654	2.193	87	39.672	9.3	9.355	1.036	9.696
1250.5	666	1.855	70	37.736	10.9	6.422	1.066	6.846
1260.5	673	2.891	159	54.998	10.2	15.588	1.720	26.804
1270.5	681	1.563	79	50.544	10.4	7.596	1.676	12.730
1280.5	688	4.063	172	42.333	10.1	17.030	1.655	28.184
1290.5	699	3.087	179	57.985	11.6	15.431	1.084	16.729
1300.5	703	1.549	39	25.178	9.8	3.980	2.851	11.348
1310.5	708	1.386	31	22.367	10.3	3.010	2.730	8.216
1320.5	711	1.802	70	38.846	11.1	6.306	4.892	30.852
1330.5	713	1.284	56	43.614	9.8	5.714	4.962	28.352
1340.5	716	1.712	58	33.879	10.6	5.472	5.085	27.823
1350.5	718	2.824	61	21.601	10.9	5.596	4.947	27.685
1360.5	736	1.860	31	16.667	12.1	2.562	0.709	1.817
1370.5	754	2.702	41	15.174	12.2	3.361	0.667	2.240
1380.5	759	1.106	62	56.058	9.7	6.392	2.296	14.678
1390.5	765	1.056	42	39.773	8.5	4.941	2.248	11.109
1400.5	769	1.337	69	51.608	10.9	6.330	3.029	19.176
1410.5	774	1.172	55	46.928	8.700	6.322	3.006	19.007
1420.5	778	1.543	33	21.387	8.900	3.708	2.860	10.605
1430.5	782	2.427	87	35.847	9.200	9.457	2.763	26.133
1440.5	788	3.076	65	21.131	8.700	7.471	1.376	10.283
1450.5	790	4.157	198	47.631	10.300	19.223	1.518	29.186
1460.5	799	5.440	417	76.654	9.900	42.121	1.427	60.091
1470.5	807	3.025	38	12.562	8.500	4.471	1.399	6.254
1480.5	815	3.430	51	14.869	7.100	7.183	1.416	10.169
1490.5	824	3.881	169	43.545	9.800	17.245	1.446	24.928
1500.5	835	5.517			9.600	0.000	1.327	

CORE MD962084 (OLIFANTS RIVER SLOPE)

Depth (cm)	Age (kyr)	Wt>125 um (g)	# menardii in >125μm fraction	# menardii /g >125μm	Sample wt (g)	# menardii /g bulk sed	BMAR (g/cm2/kyr)	*Gr. menardii* AR (#/cm2/kyr)
2	0	0.326	5	15.337	3.259	1.534	14.670	22.507
20	2.1	0.548	7	12.774	5.137	1.363	14.655	19.970
40	4.2	0.488	7	14.344	4.196	1.668	15.012	25.045
60	6.3	0.503	10	19.881	4.652	2.150	15.798	33.959
80	8.4	0.786	6	7.634	6.394	0.938	16.304	15.299
100	10.5	0.818	10	12.225	6.031	1.658	15.800	26.198
120	12.2	0.713	14	19.635	5.774	2.425	25.352	61.471
140	13.5	0.884	10	11.312	6.052	1.652	24.493	40.470
160	14.8	0.789	9	11.407	5.440	1.654	25.680	42.486
180	16.1	0.914	11	12.035	5.242	2.098	25.740	54.013
210	18.0	1.067	10	9.372	5.340	1.873	2.010	3.765
230	35.0	0.783	9	11.494	3.900	2.308	1.888	4.357
250	52.0	0.888	7	7.883	4.845	1.445	11.327	16.366
270	54.9	1.069	9	8.419	4.641	1.939	11.602	22.499
290	57.7	1.314	7	5.327	5.651	1.239	11.542	14.298
300	59.1	2.094	7	3.343	8.996	0.778	11.673	9.083
320	62.0	1.318	5	3.794	4.898	1.021	20.071	20.489
340	63.7	1.373	4	2.913	5.913	0.676	19.976	13.513
360	65.3	0.746	6	8.043	4.086	1.468	20.214	29.683
380	67.0	0.894	3	3.356	4.109	0.730	20.597	15.038
390	67.8	1.19	6	5.042	5.105	1.175	20.389	23.964
410	69.5	0.721	5	6.935	5.393	0.927	20.217	18.744
430	71.2	0.521	5	9.597	6.411	0.780	20.094	15.671
440	72.0	0.403	1	2.481	5.510	0.181	20.148	3.657
460	73.7	0.562	3	5.338	5.735	0.523	20.373	10.657
480	75.3	0.479	3	6.263	5.290	0.567	21.057	11.942
510	77.8	0.408	1	2.451	5.584	0.179	20.895	3.742
530	79.5	0.598	4	6.689	7.026	0.569	8.406	4.786
550	83.6	0.571	5	8.757	5.594	0.894		
560	85.7	0.381	4	10.499	3.885	1.030		
570								
580								
590	91.8	0.395	3	7.595	3.722	0.806	8.310	6.698
600	93.9	0.737	9	12.212	7.383	1.219	8.583	10.463
610	95.9	0.601	4	6.656	6.657	0.601	8.319	4.998
620	98.0	0.519	2	3.854	6.331	0.316	5.701	1.801
630	101.0	0.377	3	7.958	5.685	0.528	5.665	2.989
640	104.0	0.487	3	6.160	6.882	0.436	5.657	2.466
650	107.0	0.303	4	13.201	5.479	0.730	5.655	4.128
660	110.0	0.379	7	18.470	4.696	1.491	5.695	8.489
670	113.0	0.316	4	12.658	4.357	0.918	5.798	5.323
680	116.0	0.884	2	2.262	6.423	0.311	5.671	1.766
690	119.0	0.68	6	8.824	5.400	1.111	5.597	6.218
700	122.0	0.902	3	3.326	5.828	0.515	10.086	5.192
710	123.7	0.719	3	4.172	5.380	0.558	10.470	5.838
720	125.3	0.81	3	3.704	6.123	0.490	10.295	5.044
730	127.0	0.774	0	0.000	4.929	0.000	7.468	0.000
740	129.3	1.413	11	7.785	7.390	1.488	7.401	11.017

CORE MD962084 (OLIFANTS RIVER SLOPE)

Depth (cm)	Age (kyr)	Wt>125 um (g)	# menardii in >125μm fraction	# menardii /g >125μm	Sample wt (g)	# menardii /g bulk sed	BMAR (g/cm2/kyr)	*Gr. menardii* AR (#/cm2/kyr)
750	131.7	1.538	3	1.951	7.229	0.415	7.347	3.049
760	134.0	1.478	6	4.060	6.360	0.943	1.786	1.684
770	143.6	1.351	1	0.740	6.268	0.160	1.794	0.286
780	153.2	1.357	1	0.737	5.653	0.177	1.787	0.316
790	162.8	1.129	3	2.657	5.891	0.509	1.813	0.923
800	172.4	0.627	1	1.595	5.327	0.188	1.824	0.342
810	182.0	0.668	2	2.994	7.131	0.280	8.773	2.460
830	186.0	0.66	2	3.030	6.980	0.287	8.840	2.533
850	190.0	0.643	1	1.555	6.032	0.166	8.717	1.445
870	194.0	0.535	2	3.738	5.836	0.343	2.544	0.872
890	207.3	0.685	0	0.000	5.946	0.000	2.537	0.000
910	216.3	1.036	1	0.965	6.771	0.148	7.601	1.123
930	220.9	1.12	5	4.464	6.970	0.717	7.697	5.522
950	225.5	0.646	5	7.740	6.428	0.778	7.655	5.954
970	230.1	0.361	0	0.000	5.622	0.000	7.435	0.000
990	234.7	0.822	2	2.433	5.699	0.351	7.491	2.629
1000	237.0	0.576	1	1.736	5.190	0.193	9.028	1.740
1020	240.8	1.091	3	2.750	5.750	0.522	8.967	4.678
1040	244.7	1.178	3	2.547	5.370	0.559	8.895	4.969
1060	248.5	1.336	4	2.994	5.907	0.677	4.087	2.768
1080	250.5	1.445	6	4.152	7.005	0.857	4.030	3.452
1110	253.5	0.369	1	2.710	5.345	0.187	4.117	0.770
1130	255.5	0.859	1	1.164	5.809	0.172	4.084	0.703
1150	257.5	0.949	1	1.054	6.680	0.150	12.359	1.850
1170	263.4	0.292	1	3.425	6.062	0.165	12.469	2.057
1190	269.3	0.784	7	8.929	5.649	1.239	12.424	15.396
1200	272.3	0.923		0.000	8.730	0.000	12.231	0.000
1210	275.2	0.694	1	1.441	5.844	0.171	12.316	2.107
1220	278.2	0.929		0.000	6.921	0.000	4.318	0.000
1230	281.1	0.972	1	1.029	6.626	0.151	4.280	0.646
1240	284.1	1.471		0.000	6.928	0.000	4.311	0.000
1250	287.0	1.736	1	0.576	6.710	0.149	8.703	1.297
1260	289.5	0.589		0.000	6.810	0.000	8.601	0.000
1270	292.0	0.808	4	4.950	7.025	0.569	8.554	4.871
1280	294.5	0.445		0.000	5.728	0.000	12.997	0.000
1290	297.0	0.693	3	4.329	6.238	0.481	13.047	6.274
1300	299.5	0.581	1	1.721	6.993	0.143	13.149	1.880
1310	302.0	0.38	3	7.895	6.286	0.477	12.741	6.081
1320	306.0	0.433	2	4.619	6.691	0.299	13.279	3.969
1330	310.0	0.409	3	7.335	6.303	0.476	13.020	6.197
1340	313.3	0.268	1	3.731	4.229	0.236	12.579	2.974
1350	316.5	0.945	6	6.349	9.020	0.665	13.118	8.726
1360	319.8	0.25	1	4.000	4.125	0.242	13.207	3.202
1370	323.0	0.422	1	2.370	4.762	0.210	13.286	2.790
1380	326.3	0.326	3	9.202	4.932	0.608	13.188	8.022
1390	329.5	0.609	2	3.284	5.670	0.353	9.366	3.304
1400	331.3	0.414	4	9.662	5.092	0.786	9.397	7.381
1410	333.2	0.423	5	11.820	5.768	0.867	9.624	8.343
1420	335.0	0.378	5	13.228	4.501	1.111	9.832	10.922

CORE MD962084 (OLIFANTS RIVER SLOPE)

Depth (cm)	Age (kyr)	Wt>125 um (g)	# menardii in >125μm fraction	# menardii /g >125μm	Sample wt (g)	# menardii /g bulk sed	BMAR (g/cm2/kyr)	*Gr. menardii* AR (#/cm2/kyr)
1430	336.8	0.661	16	24.206	5.988	2.672	9.711	25.948
1440	338.7	0.866	9	10.393	6.750	1.333	9.600	12.800
1450	340.5	0.812	6	7.389	5.080	1.181	2.129	2.514
1460	349.0	0.839	15	17.878	5.645	2.657	6.857	18.219
1470	351.7	0.725	5	6.897	6.750	0.741	6.751	5.001
1480	354.3	0.969	4	4.128	6.168	0.649	6.481	4.203
1490	357.0	0.691	0	0.000	6.049	0.000	19.552	0.000
1500	357.9	0.588	1	1.701	8.493	0.118	19.899	2.343
1510	358.8	0.279	1	3.584	5.734	0.174	19.756	3.445
1520	359.7	0.272	1	3.676	5.993	0.167	19.542	3.261
1530	360.5	0.461	2	4.338	5.592	0.358	19.233	6.879
1540	361.4	0.314	1	3.185	5.510	0.181	19.274	3.498
1550	362.3	0.384	1	2.604	4.649	0.215	19.280	4.147
1560	363.2	0.885	2	2.260	5.652	0.354	19.374	6.855
1570	364.1	0.538	2	3.717	6.279	0.319	19.423	6.187
1580	365.0	0.297	5	16.835	4.948	1.011	19.229	19.431
1590	365.8	0.462	3	6.494	4.669	0.643	19.408	12.470
1600	366.7	0.782	2	2.558	5.826	0.343	19.701	6.763
1610	367.6	0.613	1	1.631	5.850	0.171	19.509	3.335
1620	368.5	0.578	3	5.190	5.730	0.524	5.633	2.949
1630	371.6	0.696	4	5.747	5.976	0.669	5.586	3.739
1640	374.7	1.487	7	4.707	5.842	1.198	5.603	6.714
1650	377.8	1.253	9	7.183	8.036	1.120	5.590	6.261
1660	380.8	0.727	4	5.502	5.839	0.685	5.573	3.817
1670	383.9	0.672	2	2.976	5.728	0.349	5.542	1.935
1680	387.0	0.698	4	5.731	5.789	0.691	5.520	3.814
1690	390.1	0.383	3	7.833	5.748	0.522	5.538	2.890
1700	393.2	0.291	2	6.873	4.692	0.426	5.575	2.377
1710	396.3	0.374	9	24.064	6.467	1.392	5.540	7.710
1720	399.3	0.363	6	16.529	5.830	1.029	5.616	5.779
1730	402.4	0.743	13	17.497	7.729	1.682	5.630	9.469
1740	405.5	0.546	14	25.641	5.446	2.571	9.781	25.145
1750	407.3	0.349	10	28.653	5.481	1.824	9.784	17.851
1760	409.1	0.421	5	11.876	5.962	0.839	9.615	8.063
1770	410.8	0.367	3	8.174	6.381	0.470	9.576	4.502
1780	412.6	0.362	1	2.762	6.032	0.166	9.595	1.591
1790	414.4	0.258	7	27.132	6.081	1.151	9.592	11.042
1800	416.2	0.244	1	4.098	6.530	0.153	9.585	1.468
1810	418.0	0.264	1	3.788	6.604	0.151	9.663	1.463
1820	419.8	0.206	1	4.854	6.202	0.161	9.636	1.554
1830	421.5	0.216	0	0.000	5.699	0.000	9.739	0.000
1840	423.3	0.224	0	0.000	4.967	0.000	9.799	0.000
1850	425.1	0.323	4	12.384	5.659	0.707	9.790	6.920
1860	426.9	0.51	32	62.745	6.620	4.834	9.737	47.067
1870	428.7	0.273	14	51.282	3.901	3.589	9.830	35.277
1880	430.4	0.404	4	9.901	5.752	0.695	9.775	6.798
1890	432.2	0.641	4	6.240	6.160	0.649	10.026	6.510
1900	434.0	1.107	6	5.420	5.532	1.085	10.032	10.880
1910	437.3	1.126	3	2.664	7.690	0.390	5.505	2.148

CORE MD962084 (OLIFANTS RIVER SLOPE)

Depth (cm)	Age (kyr)	Wt>125 um (g)	# menardii in >125μm fraction	# menardii /g >125μm	Sample wt (g)	# menardii /g bulk sed	BMAR (g/cm2/kyr)	*Gr. menardii* AR (#/cm2/kyr)
1920	440.5	0.86	10	11.628	6.490	1.541	5.564	8.573
1930	443.8	0.809	7	8.653	5.540	1.264	5.642	7.129
1940	447.0	0.629	9	14.308	5.760	1.563	5.602	8.753
1950	450.3	0.777	14	18.018	9.180	1.525	5.731	8.740
1960	453.5	0.853	7	8.206	8.405	0.833	5.705	4.751
1970	456.8	0.297	4	13.468	7.219	0.554	5.581	3.092
1980	460.0	0.337	9	26.706	8.170	1.102	5.471	6.027
1990	462.6	0.349	4	11.461	7.288	0.549	6.788	3.725
2000	465.3	0.205	5	24.390	7.336	0.682	6.829	4.654
2010	467.9	0.161	10	62.112	7.208	1.387	6.675	9.261
2020	470.5	0.211	2	9.479	7.308	0.274	6.789	1.858
2030	473.1	0.138	5	36.232	6.751	0.741	6.731	4.985
2040	475.8	0.163	5	30.675	7.037	0.711	6.752	4.797
2050	478.4	0.203	6	29.557	8.389	0.715	6.710	4.799
2060	481.0	0.172	1	5.814	7.285	0.137	6.706	0.921
2070	485.2	0.237	0	0.000	8.074	0.000	4.242	0.000
2080	489.4	0.193	2	10.363	9.143	0.219	4.214	0.922
2090	493.6	0.111	1	9.009	6.947	0.144	4.229	0.609
2100	497.8	0.396	1	2.525	9.570	0.104	4.242	0.443
2110	502.0	0.2	0	0.000	6.922	0.000	4.249	0.000
2120	506.2	0.16	0	0.000	7.540	0.000	4.274	0.000
2130	510.4	0.263	0	0.000	7.260	0.000	4.271	0.000
2140	514.6	0.233	0	0.000	6.768	0.000	4.233	0.000
2150	518.8	0.328	1	3.049	7.638	0.131	4.261	0.558
2160	523.0	0.355	1	2.817	6.770	0.148	4.269	0.631
2170	525.0	0.325	0	0.000	6.638	0.000	8.979	0.000
2180	527.0	0.468	1	2.137	8.218	0.122	8.981	1.093
2190	532.5	0.305	0	0.000	7.478	0.000	3.275	0.000
2200	538.0	0.363	0	0.000	6.920	0.000	3.229	0.000
2210	546.3	0.433	0	0.000	7.926	0.000	2.138	0.000
2220	554.7	0.73	0	0.000	6.470	0.000	2.135	0.000
2230	563.0	0.445	1	2.247	6.660	0.150	2.111	0.317
2240	565.0	0.467	0	0.000	7.968	0.000	8.841	0.000
2250	567.0	0.652	0	0.000	9.036	0.000	8.899	0.000
2260	579.3	0.532	1	1.880	8.400	0.119	1.457	0.173
2270	591.5	0.512	0	0.000	6.790	0.000	1.450	0.000
2280	603.8	0.532	4	7.519	6.756	0.592	1.465	0.867
2290	616.0	0.752	2	2.660	6.907	0.290	1.452	0.420
2300	617.7	0.63	1	1.587	7.636	0.131	10.399	1.362
2310	619.4	0.71	2	2.817	7.343	0.272	10.732	2.923
2320	621.1	0.55	0	0.000	8.270	0.000	10.723	0.000
2330	622.9	0.539	0	0.000	9.241	0.000	10.658	0.000
2340	624.6	0.529	0	0.000	8.509	0.000	10.545	0.000
2350	626.3	0.482	1	2.075	8.118	0.123	10.640	1.311
2360	628.0	0.451	0	0.000	7.468	0.000	10.496	0.000
2370	631.9	0.598	1	1.672	7.418	0.135	4.654	0.627
2380	635.8	0.375	1	2.667	7.830	0.128	4.597	0.587
2390	639.7	0.567	2	3.527	7.796	0.257	4.498	1.154
2400	643.6	0.203	0	0.000	7.197	0.000	4.571	0.000

CORE MD962084 (OLIFANTS RIVER SLOPE)

Depth (cm)	Age (kyr)	Wt>125 um (g)	# menardii in >125µm fraction	# menardii /g >125µm	Sample wt (g)	# menardii /g bulk sed	BMAR (g/cm2/kyr)	*Gr. menardii* AR (#/cm2/kyr)
2410	647.5	0.236	0	0.000	8.393	0.000	4.549	0.000
2420	651.4	0.263	1	3.802	6.695	0.149	4.615	0.689
2430	655.3	0.431	3	6.961	7.527	0.399	4.549	1.813
2450	663.1	0.342	2	5.848	7.441	0.269	4.585	1.232
2470	669.7	0.327	0	0.000	7.477	0.000	6.738	0.000
2490	675.1	0.366	0	0.000	7.980	0.000	6.683	0.000
2500	677.8	0.296	2	6.757	7.797	0.257	6.652	1.706
2520	683.1	0.272	1	3.676	7.229	0.138	6.610	0.914
2540	688.5	0.45	0	0.000	7.420	0.000	6.650	0.000
2560	698.9	0.631	3	4.754	7.765	0.386	3.496	1.351
2580	709.3	0.411	4	9.732	7.096	0.564	3.447	1.943
2590	714.5	0.412	4	9.709	7.325	0.546	3.428	1.872
2610	724.9	0.361	6	16.620	7.152	0.839	3.496	2.933
2630	735.3	0.455	15	32.967	7.421	2.021	3.523	7.121
2660	750.8	0.249	4	16.064	5.972	0.670	3.460	2.317
2680	761.2	0.349	3	8.596	6.357	0.472	3.452	1.629
2690	766.4	0.309	1	3.236	7.213	0.139	3.365	0.466
2700	771.6	0.52	3	5.769	9.300	0.323	3.421	1.103
2720	782.0	0.573	6	10.471	7.104	0.845	3.362	2.840
2740	785.7	0.838	7	8.353	6.326	1.107	9.659	10.689
2760	789.3	1.082	5	4.621	7.337	0.681	9.609	6.548
2770	791.2	0.782	10	12.788	5.760	1.736	9.425	16.363
2780	793.0	0.672	11	16.369	6.924	1.589	9.544	15.162
2790	794.8	0.509	6	11.788	6.190	0.969	9.550	9.257
2800	796.6	1.232	19	15.422	8.390	2.265	9.537	21.598
2810	798.4	1.107	9	8.130	6.282	1.433	9.724	13.932
2820	800.2	1.106	11	9.946	6.511	1.689	9.705	16.396
2830	802.0	0.925	5	5.405	5.390	0.928	9.759	9.053
2840	803.8	1.101	2	1.817	6.667	0.300	9.654	2.896
2850	805.6	1.348	4	2.967	7.443	0.537	9.772	5.251
2870	809.2	1.437	4	2.784	7.185	0.557	9.816	5.465
2900	814.6	1.286	3	2.333	7.745	0.387	9.908	3.838
2920	818.2	1.027	4	3.895	6.582	0.608	9.774	5.940
2940	822.6	0.523	6	11.472	7.190	0.834	7.017	5.856
2960	827.7	0.457	3	6.565	8.830	0.340	6.959	2.364
2980	832.9	0.388	7	18.041	7.603	0.921	6.869	6.324
2990	835.4	0.39	10	25.641	6.868	1.456	6.857	9.984

APPENDIX 7

RAW DATA FOR CALCIUM CARBONATECONTENTS
SEDIMENT TEXTURE
and
CARBONATE PRESERVATION INDEX

CORE MD962080 (AGULHAS BANK SLOPE)

Depth (cm)	Age (kyr)	$CaCO_3$ %	Wt sample (g)	Wt >63um (g)	Sand content % > 63um	Wt sample (g)	Wt >125um (g)	Coarse frn % >125um	# forams	# fragments	Preservation Index (foram/foram+frag)%	$CaCO_3$ MAR ($g/cm^2/kyr$)
2.5	1	70.07	6.114	2.423	39.63	7.000	1.113	15.90	298	160	65.07	1.85
10.5	4	74.33	7.911	3.893	49.21	10.700	1.975	18.46	300	137	68.65	2.02
20.5	8	75.00	11.922	6.284	52.71	12.100	2.383	19.69	318	102	75.71	2.31
30.5	11	75.67	5.158	2.904	56.30	7.100	2.400	33.80	249	76	76.62	2.33
40.5	15	75.44	6.795	4.088	60.16	8.800	2.871	32.63	270	79	77.36	2.35
50.5	19	76.18	6.939	4.600	66.29	6.700	2.647	39.51	336	105	76.19	2.17
60.5	21	72.11	8.922	5.501	61.66	8.800	2.781	31.60	271	107	71.69	4.18
70.5	23	78.08	6.167	3.218	52.18	10.600	3.534	33.34	288	118	70.94	4.68
80.5	24	78.67	8.715	4.668	53.56	9.500	2.843	29.93	267	91	74.58	4.64
90.5	26	79.11	7.714	4.224	54.76	8.800	2.112	24.00	280	97	74.27	4.67
100.5	28	80.43	9.289	4.774	51.39	9.600	3.091	32.20	266	188	58.59	4.69
110.5	30	74.86	6.613	2.971	44.93	7.100	1.031	14.52	301	203	59.72	4.39
120.5	43	75.87	6.208	2.627	42.32	7.200	1.608	22.33	328	278	54.13	
130.5	46	77.35	6.117	3.074	50.25	6.000	1.482	24.70	252	189	57.14	
140.5	50	79.64	5.954	3.498	58.75	6.200	2.166	34.94	341	315	51.98	
150.5	53	78.30	6.170	3.446	55.85	6.700	2.271	33.90	294	295	49.92	
160.5	56	78.29	5.861	3.625	61.85	6.600	1.969	29.83	300	269	52.72	
170.5	59	77.65	10.128	5.312	52.45	10.100	3.159	31.28	318	296	51.79	1.00
180.5	62	78.86	10.198	5.077	49.78	10.600	3.422	32.28	327	297	52.40	1.04
190.5	65	77.75	7.663	3.333	43.49	8.400	1.788	21.29	242	170	58.74	1.04
200.5	76	81.37	9.441	4.452	47.16	9.200	2.514	27.33	308	194	61.35	0.80
210.5	88	81.95	6.907	3.443	49.85	8.900	1.983	22.28	325	245	57.02	0.80
220.5	99	77.42	8.077	2.506	31.03	9.500	1.250	13.16	309	97	76.11	0.74
230.5	103	71.66	10.014	2.172	21.69	9.700	1.572	16.21	298	198	60.08	1.02
240.5	107	77.33	9.343	3.003	32.14	10.100	1.941	19.22	333	160	67.55	1.09
250.5	122	75.64	9.302	3.101	33.34	10.800	2.214	20.50	333	160	67.55	1.04
260.5	124	76.52	7.676	2.788	36.32	7.800	1.563	20.04	371	133	73.61	3.04
270.5	125	73.24	8.788	3.511	39.95	11.600	2.509	21.63	316	85	78.80	2.85
280.5	127	69.79	8.236	3.668	44.54	9.700	2.303	23.74	332	124	72.81	3.14
290.5	131	77.43	7.370	4.288	58.18	9.900	3.129	31.61	332	85	79.62	3.45
300.5	135	77.06	11.041	7.345	66.52	11.800	4.444	37.66	240	87	73.39	3.26
310.5	138	78.95	9.815	6.465	65.87	10.300	3.382	32.83	317	102	75.66	3.18

CORE MD962080 (AGULHAS BANK SLOPE)

Depth (cm)	Age (kyr)	$CaCO_3$ %	Wt sample (g)	Wt >63um (g)	Sand content % > 63um	Wt sample (g)	Wt >125um (g)	Coarse frn % >125um	# forams	# fragments	Preservation Index (foram/foram+frag)%	$CaCO_3$ MAR ($g/cm^2/kyr$)
320.5	140	79.38	5.557	3.500	62.98	6.200	2.251	36.31	310	100	75.61	3.42
330.5	143	76.76	6.387	4.091	64.05	7.300	2.595	35.55	304	71	81.07	3.16
340.5	146	81.02	7.642	5.115	66.93	7.200	2.945	40.90	322	103	75.76	3.30
350.5	148	80.30	6.666	4.568	68.53	7.000	2.297	32.81	344	89	79.45	3.12
360.5	151	76.51	8.412	5.578	66.31	9.100	3.680	40.44	280	79	77.99	3.03
370.5	155	72.93	9.695	6.435	66.37	10.900	3.848	35.30	347	106	76.60	1.62
380.5	161	74.58	7.100	4.758	67.01	9.300	3.150	33.87	354	105	77.12	1.57
390.5	166	80.75	9.931	6.050	60.92	8.700	2.763	31.76	260	59	81.50	1.63
400.5	171	77.97	7.611	4.704	61.81	10.900	3.262	29.93	256	81	75.96	1.64
410.5	177	78.94	7.883	5.181	65.72	8.900	2.743	30.82	338	124	73.16	1.67
420.5	182	72.87	13.275	7.256	54.66	12.700	3.000	23.62	265	104	71.82	1.62
430.5	183	70.58	10.051	5.345	53.18	9.500	2.012	21.18	309	181	63.06	1.03
440.5	187	71.67	6.897	4.117	59.69	12.700	3.112	24.50	320	188	62.99	1.03
450.5	190	69.78	8.379	4.012	47.88	9.200	1.825	19.84	255	160	61.45	0.99
460.5	194	67.65	7.739	3.378	43.65	11.900	1.797	15.10	277	155	64.12	0.96
470.5	209	62.45	10.141	4.462	44.00	11.000	1.942	17.65	311	205	60.27	0.87
480.5	223	67.61	6.454	2.379	36.86	8.600	1.404	16.33	349	229	60.38	0.94
490.5	238	68.71	8.228	3.197	38.86	8.500	1.138	13.39	311	217	58.90	0.99
500.5	241	76.97	8.912	3.025	33.94	10.300	1.747	16.96	334	245	57.69	2.67
510.5	244	70.99	8.175	4.127	50.48	9.100	1.697	18.65	316	148	68.10	2.74
520.5	248	69.86	6.208	3.362	54.16	7.800	1.405	18.01	341	277	55.18	2.58
530.5	250	68.75	10.330	4.978	48.19	8.500	1.838	21.62	298	247	54.68	3.69
540.5	252	74.49	7.489	3.226	43.08	10.200	2.026	19.86	297	151	66.29	4.00
550.5	255	67.29	8.451	4.447	52.62	10.200	0.170		301	205	59.49	3.61
560.5	257	81.22	11.146	7.015	62.94	11.700	4.092	34.97	298	119	71.46	4.07
570.5	259	78.49	7.745	5.032	64.97	9.500	3.375	35.53	298	96	75.63	3.90
580.5	261	78.62	9.347	5.821	62.28	11.100	3.121	28.12	299	141	67.95	4.13
590.5	264	66.95	8.307	4.127	49.68	11.600	1.745	15.04	317	233	57.64	3.76
600.5	266	65.19	8.088	4.030	49.83	9.400	1.541	16.39	339	279	54.85	3.69
610.5	273	68.44	8.070	4.105	50.87	8.300	1.425	17.17	365	432	45.80	1.85
620.5	280	69.33	9.776	4.781	48.91	9.700	1.812	18.68	304	362	45.65	1.84
630.5	287	79.39	9.534	4.744	49.76	9.200	2.671	29.03	328	384	46.07	2.05

CORE MD962080 (AGULHAS BANK SLOPE)

Depth (cm)	Age (kyr)	$CaCO_3$ %	Wt sample (g)	Wt >63um (g)	Sand content % > 63um	Wt sample (g)	Wt >125um (g)	Coarse frn % >125um	# forams	# fragments	Preservation Index (foram/foram+frag)%	$CaCO_3$ MAR ($g/cm^2/kyr$)
640.5	290	81.96	10.134	4.332	42.75	10.300	2.156	20.93	299	402	42.65	2.14
650.5	292	79.16	8.788	4.003	45.55	8.200	1.635	19.94	332	413	44.56	2.01
660.5	295	78.82	8.560	3.744	43.74	8.800	1.480	16.82	302	342	46.89	2.00
670.5	300	76.78	6.858	2.693	39.27	6.800	1.261	18.54	304	312	49.35	2.00
680.5	304	79.96	7.807	3.266	41.83	6.400	1.307	20.42	324	367	46.89	2.05
690.5	309	79.16	6.266	3.189	50.89	7.100	2.412	33.97	319	397	44.55	1.96
700.5	312	78.31	7.478	3.011	40.26	7.500	1.387	18.49	309	253	54.98	2.03
710.5	315	77.30	8.579	3.617	42.16	8.900	1.214	13.64	298	401	42.63	1.81
720.5	321	78.48	10.120	3.603	35.60	9.500	1.317	13.86	315	330	48.84	1.91
730.5	328	81.63	9.468	2.488	26.28	7.400	0.863	11.66	282	187	60.13	2.01
740.5	330	78.23	5.643	2.196	38.92	5.700	0.947	16.61	309	187	62.30	3.12
750.5	331											
760.5	333											
770.5	335	76.06	8.677	3.011	34.70	9.300	1.339	14.40	339	213	61.41	
780.5	337	72.89	7.257	3.716	51.21	7.900	1.569	19.86	297	190	60.99	2.61
790.5	338	75.83	8.225	4.655	56.60	7.800	2.239	28.71	251	142	63.87	2.77
800.5	340	78.35	9.459	5.807	61.39	11.000	3.016	27.42	335	192	63.57	2.91
810.5	345	74.05	7.161	3.690	51.53	8.400	1.818	21.64	296	168	63.79	2.88
820.5	350	69.33	10.362	2.890	27.89	8.400	1.240	14.76	349	175	66.60	2.46
830.5	355	74.48	9.935	4.231	42.59	10.800	1.714	15.87	260	142	64.68	2.93
840.5	359	73.51	8.167	4.096	50.15	9.300	1.204	12.95	344	222	60.78	2.83
850.5	364	74.22	9.456	4.582	48.46	10.800	0.948	8.78	317	238	57.12	2.95
860.5	369	74.73	8.468	3.902	46.08	10.400	1.523	14.64	304	297	50.58	2.89
870.5	374	76.42	8.305	3.174	38.22	9.300	1.377	14.81	298	236	55.81	1.27
880.5	379	74.14	8.264	2.926	35.41	8.400	1.523	18.13	270	383	41.35	1.26
890.5	384	83.94	8.302	2.565	30.90	7.800	1.631	20.91	292	433	40.28	1.43
900.5	390	85.34	13.045	2.186	16.76	13.900	0.772	5.55	297	422	41.31	1.42
910.5	406	80.59	7.673	0.466	6.07	7.800	0.266	3.41	315	385	45.00	1.33
920.5	409	81.49	8.178	0.341	4.17	8.100	0.128	1.58	323	307	51.27	2.42
930.5	411	82.00	7.325	0.367	5.01	8.300	0.685	8.25	247	223	52.55	2.47
940.5	414	82.64	6.944	0.815	11.74	7.100	1.169	16.46	256	92	73.56	2.40
950.5	419											

CORE MD962080 (AGULHAS BANK SLOPE)

Depth (cm)	Age (kyr)	$CaCO_3$ %	Wt sample (g)	Wt >63um (g)	Sand content % > 63um	Wt sample (g)	Wt >125um (g)	Coarse frn % >125um	# forams	# fragments	Preservation Index (foram/foram+frag)%	$CaCO_3$ MAR ($g/cm^2/kyr$)
960.5	424	80.22	8.079	1.352	16.73	8.100	1.235	15.25	277	104	72.70	2.55
970.5	429	76.88	9.381	1.850	19.72	11.100	1.687	15.20	288	203	58.66	
980.5	434	75.67	7.075	1.457	20.59	8.800	1.861	21.15	316	190	62.45	
990.5	446	77.83	8.611	1.795	20.85	10.500	2.704	25.75	307	259	54.24	0.75
1000.5	458	75.44	6.582	0.910	13.83	6.200	1.546	24.94	285	124	69.68	0.76
1010.5	466	74.60	7.562	1.516	20.05	7.700	2.428	31.53	383	224	63.10	1.23
1020.5	473	72.63	8.855	1.452	16.40	8.900	2.703	30.37	272	248	52.31	1.23
1030.5	481	69.08	7.528	1.405	18.66	7.400	1.433	19.36	257	187	57.88	1.18
1040.5	491	70.06	10.614	1.510	14.23	10.800	2.169	20.08	338	178	65.50	0.96
1050.5	500	75.03	11.382	0.755	6.63	10.900	1.798	16.50	272	158	63.26	0.97
1060.5	512	78.87	8.633	0.578	6.70	8.600	1.461	16.99	349	225	60.80	0.82
1070.5	524	76.27	8.950	0.515	5.75	9.800	1.416	14.45	336	444	43.08	0.79
1080.5	527	75.64	7.862	0.622	7.91	8.900	1.554	17.46	385	403	48.86	3.33
1090.5	530	76.01	10.002	1.344	13.44	10.000	2.000	20.00	301	298	50.25	3.38
1100.5	533	72.42	9.916	2.004	20.21	11.500	2.838	24.68	244	158	60.70	3.10
1110.5	536	66.27	9.619	3.682	38.28	10.000	2.630	26.30	298	265	52.93	2.88
1120.5	548	66.38	7.890	1.485	18.82	8.300	1.218	14.67	337	335	50.15	0.70
1130.5	561	67.56	8.733	0.723	8.28	8.900	1.530	17.19	376	100	78.99	0.67
1140.5	573	68.00	8.564	1.362	15.90	9.600	1.152	12.00	243	133	64.63	0.70
1150.5	582	64.76	8.706	1.608	18.47	8.400	1.460	17.38	320	188	62.99	0.87
1160.5	594	64.20	7.667	1.852	24.16	9.200	1.552	16.87	319	203	61.11	0.68
1170.5	604	64.88	9.939	2.590	26.06	9.700	1.048	10.80	330	241	57.79	0.85
1180.5	615	66.92	10.650	2.250	21.13	10.800	1.042	9.65	346	267	56.44	0.77
1190.5	621	72.99	10.269	5.082	49.49	11.800	3.801	32.21	319	161	66.46	1.39
1200.5	628	61.00	7.750	4.291	55.37	8.100	2.087	25.77	338	79	81.06	1.17
1210.5	633	71.78	8.186	4.774	58.32	8.900	2.523	28.35	418	82	83.60	1.88
1220.5	637	74.23	9.642	5.662	58.72	10.900	3.418	31.36	312	85	78.59	1.99
1230.5	642	85.00	9.284	6.032	64.97	8.800	2.864	32.55	334	100	76.96	2.25
1240.5	654	67.03	8.587	4.399	51.23	9.300	2.193	23.58	319	123	72.17	0.69
1250.5	666	65.74	11.599	5.138	44.30	10.900	1.855	17.02	301	131	69.68	0.70
1260.5	673	63.71	9.116	3.276	35.94	10.200	2.891	28.34	359	171	67.74	1.10
1270.5	681	65.62	9.906	2.846	28.73	10.400	1.563	15.03	225	159	58.59	1.10

CORE MD962080 (AGULHAS BANK SLOPE)

Depth (cm)	Age (kyr)	$CaCO_3$ %	Wt sample (g)	Wt >63um (g)	Sand content % > 63um	Wt sample (g)	Wt >125um (g)	Coarse frn % >125um	# forams	# fragments	Preservation Index (foram/foram+frag)%	$CaCO_3$ MAR ($g/cm^2/kyr$)
1280.5	688	72.57	8.298	4.088	49.26	10.100	4.063	40.23	243	144	62.79	1.20
1290.5	699	85.02	10.866	5.236	48.19	11.600	3.087	26.61	331	122	73.07	0.92
1300.5	703	60.85	9.665	2.756	28.52	9.800	1.549	15.81	416	399	51.04	1.73
1310.5	708	74.47	10.687	1.691	15.82	10.300	1.386	13.46	369	157	70.15	2.03
1320.5	711	78.12	9.023	2.156	23.89	11.100	1.802	16.23	376	100	78.99	3.82
1330.5	713	71.62	9.465	2.057	21.73	9.800	1.284	13.10	356	178	66.67	3.55
1340.5	716	68.58	9.716	3.507	36.10	10.600	1.712	16.15	273	135	66.91	3.49
1350.5	718	71.37	11.715	5.395	46.05	10.900	2.824	25.91	386	164	70.18	3.53
1360.5	736	64.72	11.113	4.320	38.87	12.100	1.860	15.37	231	146	61.27	0.46
1370.5	754	70.96	10.592	3.820	36.06	12.200	2.702	22.15	348	129	72.96	0.47
1380.5	759	71.90	9.220	3.016	32.71	9.700	1.106	11.40	317	247	56.21	1.65
1390.5	765	71.55	7.464	1.858	24.89	8.500	1.056	12.42	356	121	74.63	1.61
1400.5	769	67.37	11.332	3.195	28.19	10.900	1.337	12.27	386	324	54.37	2.04
1410.5	774	66.48	8.715	2.559	29.36	8.700	1.172	13.47	309	285	52.02	2.00
1420.5	778	69.02	8.889	2.730	30.71	8.900	1.543	17.34	281	351	44.46	1.97
1430.5	782	72.34	8.405	3.094	36.81	9.200	2.427	26.38	342	243	58.46	2.00
1440.5	788	74.41	8.463	4.419	52.22	8.700	3.076	35.36	360	219	62.18	1.02
1450.5	790	76.65	10.543	5.925	56.20	10.300	4.157	40.36	329	135	70.91	1.16
1460.5	799	69.60	10.053	7.921	78.79	9.900	5.440	54.95	233	200	53.81	0.99
1470.5	807	75.44	8.057	4.975	61.75	8.500	3.025	35.59	338	235	58.99	1.06
1480.5	815	73.68	6.558	4.223	64.39	7.100	3.430	48.31	333	163	67.14	1.04
1490.5	824	74.85	9.058	6.678	73.72	9.800	3.881	39.60	280	119	70.18	1.08

CORE MD962084 (OLIFANTS RIVER SLOPE)

Depth (cm)	Age (kyr)	$CaCO_3$ %	Wt sample (g)	Wt >63um (g)	Sand content % > 63um	Wt sample (g)	Wt >125um (g)	Coarse frn % >125um	# forams	# fragments	Preservation Index (foram/foram+frag)%	$CaCO_3$ MAR ($g/cm^2/kyr$)
2.5	0.00	87.567	3.182	1.020	32.055	3.259	0.326	10.003	88	100	46.81	12.846
10.5	1.05	85.406	3.696	0.177	4.789	3.756	0.339	9.026	360	326	52.48	12.981
20.5	2.09	84.432	5.092	0.828	16.261	5.137	0.548	10.668	266	207	56.24	12.373
30.5	3.14	85.220	5.088	0.780	15.330	5.135	0.504	9.815	250	243	50.71	12.977
40.5	4.18	86.145	4.118	0.537	13.040	4.196	0.488	11.630	294	243	54.75	12.933
50.5	5.23	84.840	5.477	0.879	16.049	5.52	0.625	11.322	326	229	58.74	12.653
60.5	6.27	85.169	4.600	0.608	13.217	4.652	0.503	10.813	308	250	55.20	13.455
70.5	7.32	86.040	5.638	1.012	17.950	5.698	0.664	11.653	340	213	61.48	13.741
80.5	8.36	85.881	6.543	1.660	25.371	6.394	0.786	12.293	239	146	62.08	14.002
90.5	9.41	86.617	5.997	1.181	19.693	5.995	0.765	12.761	295	198	59.84	13.824
100.5	10.45	89.112	5.995	1.074	17.915	6.031	0.818	13.563	259	123	67.80	14.079
110.5	11.50	87.072	5.337	0.674	12.629	5.373	0.625	11.632	388	117	76.83	22.027
120.5	12.15	87.293	5.758	0.949	16.481	5.774	0.713	12.348	284	112	71.72	22.131
130.5	12.80	88.002	4.043	0.805	19.911	4.071	0.57	14.001	310	123	71.59	21.694
140.5	13.45	90.689	6.017	1.143	18.996	6.052	0.884	14.607	268	176	60.36	22.212
150.5	14.10	87.922	6.406	1.195	18.654	6.397	0.867	13.553	284	129	68.77	22.100
160.5	14.75	88.351	5.434	1.061	19.525	5.44	0.789	14.504	400	156	71.94	22.689
170.5	15.40	89.696	5.133	1.164	22.677	5.17	0.811	15.687	216	91	70.36	23.258
180.5	16.05	90.246	5.192	1.350	26.002	5.242	0.914	17.436	263	125	67.78	23.229
190.5	16.70	89.972	6.162	1.781	28.903	5.881	1.203	20.456	233	88	72.59	23.625
200.5	17.35	92.022	5.309	2.009	37.841	5.346	1.3	24.317	264	89	74.79	23.761
210.5	18.00	89.536	5.316	2.022	38.036	5.34	1.067	19.981	305	94	76.44	1.800
220.5	26.50	90.324	5.276	1.984	37.604	5.297	1.183	22.333	272	105	72.15	1.737
230.5	35.00	88.115	3.891	1.042	26.780	3.9	0.783	20.077	284	94	75.13	1.664
240.5	43.50	88.392	5.736	1.580	27.545	5.742	1.18	20.550	303	133	69.50	1.707
250.5	52.00	87.211	4.799	0.925	19.275	4.845	0.888	18.328	268	183	59.42	9.879
260.5	53.43	87.713	6.050	2.221	36.711	6.05	1.167	19.289	297	126	70.21	9.918
270.5	54.86	91.429	4.634	1.685	36.362	4.641	1.069	23.034	262	100	72.38	10.608
280.5	56.29	94.735	4.235	1.557	36.765	4.255	1.048	24.630	490	134	78.53	10.901

CORE MD962084 (OLIFANTS RIVER SLOPE)

Depth (cm)	Age (kyr)	$CaCO_3$ %	Wt sample (g)	Wt >63um (g)	Sand content % > 63um	Wt sample (g)	Wt >125um (g)	Coarse frn % >125um	# forams	# fragments	Preservation Index (foram/foram+frag)%	$CaCO_3$ MAR ($g/cm^2/kyr$)
290.5	57.71	90.793	5.600	2.662	47.536	5.651	1.314	23.253	226	85	72.67	10.480
300.5	59.14	90.658	8.942	2.727	30.497	8.996	2.094	23.277	261	120	68.50	10.583
310.5	60.57	90.433	7.172	2.844	39.654	7.178	1.805	25.146	274	104	72.49	10.442
320.5	62.00	90.911	4.886	1.963	40.176	4.898	1.318	26.909	336	125	72.89	18.247
330.5	62.83	90.480	6.068	2.219	36.569	6.08	1.568	25.789	240	96	71.43	18.027
340.5	63.67	90.485	5.890	1.886	32.020	5.913	1.373	23.220	367	105	77.75	18.075
350.5	64.50	89.711	5.004	1.472	29.416	5.022	1.138	22.660	408	138	74.73	18.009
360.5	65.33	89.452	4.034	1.091	27.045	4.086	0.746	18.257	250	138	64.43	18.082
370.5	66.17	90.243	5.686	1.834	32.255	5.737	1.231	21.457	189	87	68.48	18.249
380.5	67.00	89.732	4.047	1.204	29.750	4.109	0.894	21.757	324	128	71.68	18.482
390.5	67.83	90.167	5.079	1.698	33.432	5.105	1.19	23.310	279	134	67.55	18.384
400.5	68.67	89.205	5.081	2.082	40.976	5.118	1.279	24.990	246	113	68.52	18.125
410.5	69.50	87.311	5.404	0.921	17.043	5.393	0.721	13.369	216	126	63.16	17.651
420.5	70.33	85.446	5.473	0.698	12.754	5.483	0.52	9.484	284	186	60.43	17.599
430.5	71.17	85.566	6.382	0.605	9.480	6.411	0.521	8.127	309	276	52.82	17.194
440.5	72.00	86.190	5.492	0.559	10.178	5.51	0.403	7.314	164	124	56.94	17.366
450.5	72.83	84.467	9.374	0.875	9.334	9.388	0.799	8.511	244	195	55.58	17.211
460.5	73.67	84.154	5.729	0.575	10.037	5.735	0.562	9.799	177	190	48.23	17.144
470.5	74.50	83.958	5.578	1.194	21.406	5.588	0.68	12.169	220	139	61.28	17.193
480.5	75.33	82.618	5.290	0.519	9.811	5.29	0.479	9.055	310	255	54.87	17.397
490.5	76.17	85.528	7.046	1.487	21.104	7.065	0.712	10.078	184	128	58.97	18.202
500.5	77.00	80.542	6.204	0.503	8.108	6.221	0.403	6.478	295	322	47.81	16.916
510.5	77.83	81.163	5.598	0.450	8.039	5.584	0.408	7.307	180	200	47.37	16.959
520.5	78.67	80.920	5.968	0.548	9.182	5.991	0.41	6.844	365	411	47.04	16.790
530.5	79.50	79.733	7.016	0.591	8.424	7.026	0.598	8.511	322	392	45.10	6.702
540.5	81.56	78.908	6.498	0.430	6.617	6.521	0.596	9.140	250	359	41.05	6.598
550.5	83.61	78.701	5.572	0.378	6.784	5.594	0.571	10.207	275	256	51.79	
560.5	85.67	80.138	3.854	0.394	10.223	3.885	0.381	9.807	385	431	47.18	
570.5	87.72											
580.5	89.78											

CORE MD962084 (OLIFANTS RIVER SLOPE)

Depth (cm)	Age (kyr) (kyr)	$CaCO_3$ %	Wt sample (g)	Wt >63um (g)	Sand content % > 63um	Wt sample (g)	Wt >125um (g)	Coarse frn % >125um	# forams	# fragments	Preservation Index (foram/foram+frag)%	$CaCO_3$ MAR ($g/cm^2/kyr$)
590.5	91.83	80.311	3.697	0.295	7.979	3.722	0.395	10.613	200	137	59.35	6.674
600.5	93.89	84.090	7.353	1.282	17.435	7.383	0.737	9.982	190	135	58.46	7.218
610.5	95.94	82.574	6.623	0.917	13.846	6.657	0.601	9.028	300	342	46.73	6.869
620.5	98.00	81.802	6.302	0.748	11.869	6.331	0.519	8.198	280	274	50.54	4.663
630.5	101.00	81.772	5.661	0.653	11.535	5.685	0.377	6.631	370	400	48.05	4.632
640.5	104.00	82.566	6.840	0.874	12.778	6.882	0.487	7.076	240	281	46.07	4.671
650.5	107.00	85.076	5.438	0.534	9.820	5.479	0.303	5.530	187	234	44.42	4.811
660.5	110.00	85.956	4.669	0.749	16.042	4.696	0.379	8.071	199	221	47.38	4.895
670.5	113.00	85.981	4.326	0.656	15.164	4.357	0.316	7.253	345	424	44.86	4.985
680.5	116.00	85.743	6.390	1.321	20.673	6.423	0.884	13.763	230	253	47.62	4.862
690.5	119.00	84.873	5.362	1.095	20.421	5.4	0.68	12.593	358	295	54.82	4.750
700.5	122.00	85.788	5.760	0.892	15.486	5.828	0.902	15.477	215	159	57.49	8.652
710.5	123.67	86.278	5.347	0.913	17.075	5.38	0.719	13.364	216	167	56.40	9.033
720.5	125.33	85.940	6.101	1.171	19.194	6.123	0.81	13.229	378	213	63.96	8.848
730.5	127.00	86.890	4.923	1.186	24.091	4.929	0.774	15.703	268	180	59.82	6.489
740.5	129.33	86.968	7.360	2.563	34.823	7.39	1.413	19.120	230	133	63.36	6.437
750.5	131.67	87.917	7.213	2.574	35.686	7.229	1.538	21.275	420	190	68.85	6.459
760.5	134.00	90.266	6.332	2.919	46.099	6.36	1.478	23.239	247	155	61.44	1.612
770.5	143.60	91.367	6.265	2.268	36.201	6.268	1.351	21.554	255	120	68.00	1.639
780.5	153.20	89.183	5.634	1.785	31.683	5.653	1.357	24.005	435	250	63.50	1.593
790.5	162.80	89.110	5.877	1.519	25.847	5.891	1.129	19.165	240	184	56.60	1.615
800.5	172.40	84.360	5.315	0.478	8.993	5.327	0.627	11.770	300	264	53.19	1.539
810.5	182.00	82.046	7.100	0.568	8.000	7.131	0.668	9.368	216	196	52.43	7.198
820.5	184.00	84.279	5.507	0.509	9.243	5.528	0.86	15.557	360	344	51.14	7.417
830.5	186.00	80.931	6.946	0.420	6.047	6.98	0.66	9.456	185	377	32.92	7.155
840.5	188.00	79.807	7.233	0.266	3.678	7.288	0.871	11.951	360	516	41.10	7.049
850.5	190.00	75.490	5.998	0.266	4.435	6.032	0.643	10.660	210	183	53.44	6.580
860.5	192.00	78.490	6.031	0.252	4.178	6.048	1.222	20.205	210	311	40.31	6.857
870.5	194.00	80.627	5.824	0.200	3.434	5.836	0.535	9.167	292	428	40.56	2.051
880.5	200.67	80.004	5.660	0.146	2.580	5.689	0.946	16.629	313	363	46.30	2.056

CORE MD962084 (OLIFANTS RIVER SLOPE)

Depth (cm)	Age (kyr)	$CaCO_3$ %	Wt sample (g)	Wt >63um (g)	Sand content % > 63um	Wt sample (g)	Wt >125um (g)	Coarse frn % >125um	# forams	# fragments	Preservation Index (foram/foram+frag)%	$CaCO_3$ MAR ($g/cm^2/kyr$)
890.5	207.33	81.208	5.912	0.193	3.265	5.946	0.685	11.520	202	270	42.80	2.060
900.5	214.00	81.232	7.012	0.290	4.136	7.046	0.945	13.412	416	223	65.10	6.037
910.5	216.30	82.650	6.929	0.423	6.105	6.771	1.036	15.301	365	207	63.81	6.283
920.5	218.60	83.333	7.342	0.464	6.320	7.354	1.242	16.889	252	253	49.90	6.444
930.5	220.90	86.377	6.964	0.948	13.613	6.97	1.12	16.069	322	210	60.53	6.649
940.5	223.20	88.031	9.287	1.624	17.487	9.314	1.4	15.031	253	189	57.24	6.673
950.5	225.50	83.755	6.317	0.497	7.868	6.428	0.646	10.050	263	186	58.57	6.411
960.5	227.80	83.355	6.689	0.213	3.184	7.291	0.426	5.843	263	308	46.06	6.166
970.5	230.10	86.450	6.012	0.182	3.027	5.622	0.361	6.421	199	260	43.36	6.427
980.5	232.40	82.728	6.070	0.214	3.526	6.075	0.412	6.782	339	365	48.15	6.125
990.5	234.70	85.154	5.979	0.229	3.830	5.699	0.822	14.424	244	246	49.80	6.379
1000.5	237.00	86.028	5.181	0.221	4.266	5.19	0.576	11.098	207	216	48.94	7.767
1010.5	238.92	87.872	6.392	0.774	12.109	6.389	1.08	16.904	189	147	56.25	7.934
1020.5	240.83	89.683	5.870	0.714	12.164	5.75	1.091	18.974	314	141	69.01	8.042
1030.5	242.75	89.313	6.558	1.061	16.179	6.373	1.413	22.172	268	112	70.53	8.005
1040.5	244.67	88.258	5.388	0.709	13.159	5.37	1.178	21.937	260	143	64.52	7.850
1050.5	246.58	88.260	7.894	0.982	12.440	7.912	2.403	30.372	183	99	64.89	7.932
1060.5	248.50	88.717	5.893	0.735	12.472	5.907	1.336	22.617	215	166	56.43	3.626
1070.5	249.50	89.535	6.373	1.168	18.327	6.392	1.502	23.498	232	158	59.49	3.731
1080.5	250.50	89.530	6.986	1.267	18.136	7.005	1.445	20.628	207	144	58.97	3.608
1090.5	251.50	89.567	5.723	1.656	28.936	5.743	0.807	14.052	297	248	54.50	3.699
1100.5	252.50	88.466	5.228	1.824	34.889	5.26	0.614	11.673	228	210	52.05	3.647
1110.5	253.50	85.336	5.326	0.421	7.905	5.345	0.369	6.904	325	359	47.51	3.513
1120.5	254.50	84.360	5.642	0.392	6.948	5.66	0.93	16.431	275	240	53.40	3.447
1130.5	255.50	85.212	5.793	0.408	7.043	5.809	0.859	14.787	241	450	34.88	3.480
1140.5	256.50	90.014	5.526	0.377	6.822	5.547	0.625	11.267	253	420	37.59	3.704
1150.5	257.50	89.360	6.675	0.482	7.221	6.68	0.949	14.207	325	503	39.25	11.044
1160.5	260.45	91.354	6.252	0.358	5.726	6.281	0.566	9.011	347	511	40.44	11.709
1170.5	263.40	90.288	6.050	0.447	7.388	6.062	0.292	4.817	244	389	38.55	11.258
1180.5	266.35	89.091	6.988	0.619	8.858	7.016	1.152	16.420	220	236	48.25	11.047

CORE MD962084 (OLIFANTS RIVER SLOPE)

Depth (cm)	Age (kyr)	$CaCO_3$ %	Wt sample (g)	Wt >63um (g)	Sand content % > 63um	Wt sample (g)	Wt >125um (g)	Coarse frn % >125um	# forams	# fragments	Preservation Index (foram/foram+frag)%	$CaCO_3$ MAR ($g/cm^2/kyr$)
1190.5	269.30	87.567	5.616	0.359	6.392	5.649	0.784	13.879	282	250	53.01	10.879
1200.5	272.25	87.718	8.608	0.320	3.717	8.73	0.923	10.573	259	198	56.67	10.729
1210.5	275.20	86.030	5.734	0.146	2.546	5.844	0.694	11.875	224	183	55.04	10.595
1220.5	278.15	84.740	6.888	0.222	3.223	6.921	0.929	13.423	210	196	51.72	3.659
1230.5	281.10	85.480	6.591	0.110	1.669	6.626	0.972	14.669	226	242	48.29	3.658
1240.5	284.05	86.555	6.900	0.224	3.246	6.928	1.471	21.233	329	367	47.27	3.732
1250.5	287.00	87.036	6.664	0.223	3.346	6.71	1.736	25.872	282	439	39.11	7.575
1260.5	289.50	87.436	6.786	0.220	3.242	6.81	0.589	8.649	239	330	42.00	7.520
1270.5	292.00	87.542	7.002	0.156	2.228	7.025	0.808	11.502	317	363	46.62	7.489
1280.5	294.50	87.466	5.710	0.164	2.872	5.728	0.445	7.769	348	387	47.35	11.368
1290.5	297.00	88.121	6.211	0.130	2.093	6.238	0.693	11.109	249	433	36.51	11.497
1300.5	299.50	88.133	6.983	0.357	5.112	6.993	0.581	8.308	302	362	45.48	11.588
1310.5	302.00	87.993	6.256	0.328	5.243	6.286	0.38	6.045	200	302	39.84	11.211
1320.5	306.00	88.189	6.664	0.350	5.252	6.691	0.433	6.471	259	335	43.60	11.711
1330.5	310.00	87.890	6.255	0.310	4.956	6.303	0.409	6.489	302	275	52.34	11.443
1340.5	313.25	86.413	4.204	0.136	3.235	4.229	0.268	6.337	275	322	46.06	10.870
1350.5	316.50	86.203	8.982	0.306	3.407	9.02	0.945	10.477	314	354	47.01	11.308
1360.5	319.75	86.559	4.109	0.110	2.677	4.125	0.25	6.061	263	314	45.58	11.432
1370.5	323.00	87.453	4.740	0.179	3.776	4.762	0.422	8.862	252	432	36.84	11.619
1380.5	326.25	87.253	4.912	0.210	4.275	4.932	0.326	6.610	267	329	44.80	11.507
1390.5	329.50	86.847	5.645	0.294	5.208	5.67	0.609	10.741	328	441	42.65	8.134
1400.5	331.33	88.747	5.068	0.357	7.044	5.092	0.414	8.130	306	364	45.67	8.339
1410.5	333.17	88.462	5.748	0.383	6.663	5.768	0.423	7.334	296	253	53.92	8.514
1420.5	335.00	90.075	4.478	0.574	12.818	4.501	0.378	8.398	271	188	59.04	8.856
1430.5	336.83	90.731	5.963	0.432	7.245	5.988	0.661	11.039	280	190	59.57	8.811
1440.5	338.67	89.929	6.728	1.439	21.388	6.75	0.866	12.830	288	201	58.90	8.633
1450.5	340.50	89.096	5.071	2.368	46.697	5.08	0.812	15.984	264	184	58.93	1.896
1460.5	349.00	90.167	5.638	2.731	48.439	5.645	0.839	14.863	255	199	56.17	6.182
1470.5	351.67	89.376	6.737	2.551	37.866	6.75	0.725	10.741	212	242	46.70	6.034
1480.5	354.33	88.321	6.159	0.936	15.197	6.168	0.969	15.710	397	556	41.66	5.724

CORE MD962084 (OLIFANTS RIVER SLOPE)

Depth (cm)	Age (kyr)	$CaCO_3$ %	Wt sample (g)	Wt >63um (g)	Sand content % > 63um	Wt sample (g)	Wt >125um (g)	Coarse frn % >125um	# forams	# fragments	Preservation Index (foram/foram+frag)%	$CaCO_3$ MAR ($g/cm^2/kyr$)
1490.5	357.00	87.044	6.045	1.249	20.662	6.049	0.691	11.423	274	482	36.24	17.019
1500.5	357.88	87.092	8.454	0.119	1.408	8.493	0.588	6.923	273	182	60.00	17.330
1510.5	358.77	87.520	5.708	0.060	1.051	5.734	0.279	4.866	184	175	51.25	17.290
1520.5	359.65	87.292	5.974	0.101	1.691	5.993	0.272	4.539	257	479	34.92	17.059
1530.5	360.54	88.664	5.575	0.064	1.148	5.592	0.461	8.244	183	355	34.01	17.053
1540.5	361.42	86.638	5.485	0.075	1.367	5.51	0.314	5.699	225	405	35.71	16.699
1550.5	362.31	84.134	4.619	0.068	1.472	4.649	0.384	8.260	230	616	27.19	16.221
1560.5	363.19	84.116	5.626	0.073	1.298	5.652	0.885	15.658	315	675	31.82	16.296
1570.5	364.08	85.965	6.260	0.066	1.054	6.279	0.538	8.568	222	319	41.04	16.697
1580.5	364.96	86.898	4.930	0.048	0.974	4.948	0.297	6.002	284	752	27.41	16.710
1590.5	365.85	85.756	4.646	0.038	0.818	4.669	0.462	9.895	211	317	39.96	16.644
1600.5	366.73	88.690	5.790	0.056	0.967	5.826	0.782	13.423	343	382	47.31	17.473
1610.5	367.62	86.728	6.832	0.080	1.171	5.85	0.613	10.479	324	658	32.99	16.920
1620.5	368.50	84.723	5.713	0.059	1.033	5.73	0.578	10.087	283	363	43.81	4.773
1630.5	371.58	87.005	5.973	0.052	0.871	5.976	0.696	11.647	203	405	33.39	4.860
1640.5	374.67	87.310	5.830	0.069	1.184	5.842	1.487	25.454	223	488	31.36	4.892
1650.5	377.75	86.474	8.027	0.117	1.458	8.036	1.253	15.592	316	429	42.42	4.834
1660.5	380.83	86.892	5.827	0.069	1.184	5.839	0.727	12.451	334	569	36.99	4.842
1670.5	383.92	86.430	5.713	0.062	1.085	5.728	0.672	11.732	291	587	33.14	4.790
1680.5	387.00	86.311	5.778	0.078	1.350	5.789	0.698	12.057	308	432	41.62	4.764
1690.5	390.08	86.317	5.732	0.069	1.204	5.748	0.383	6.663	265	546	32.68	4.780
1700.5	393.17	85.294	4.674	0.016	0.342	4.692	0.291	6.202	318	543	36.93	4.755
1710.5	396.25	86.900	6.443	0.042	0.652	6.467	0.374	5.783	296	416	41.57	4.815
1720.5	399.33	86.193	5.800	0.058	1.000	5.83	0.363	6.226	222	296	42.86	4.840
1730.5	402.42	86.705	7.722	0.066	0.855	7.729	0.743	9.613	226	275	45.11	4.881
1740.5	405.50	87.288	5.414	0.034	0.628	5.446	0.546	10.026	311	384	44.75	8.538
1750.5	407.28	89.190	5.441	0.039	0.717	5.481	0.349	6.367	287	389	42.46	8.726
1760.5	409.06	89.573	5.932	0.040	0.674	5.962	0.421	7.061	271	305	47.05	8.612
1770.5	410.84	90.135	6.388	0.019	0.297	6.381	0.367	5.751	230	418	35.49	8.631
1780.5	412.63	90.834	6.015	0.053	0.881	6.032	0.362	6.001	234	380	38.11	8.715

CORE MD962084 (OLIFANTS RIVER SLOPE)

Depth (cm)	Age (kyr)	$CaCO_3$ %	Wt sample (g)	Wt >63um (g)	Sand content % > 63um	Wt sample (g)	Wt >125um (g)	Coarse frn % >125um	# forams	# fragments	Preservation Index (foram/foram+frag)%	$CaCO_3$ MAR ($g/cm^2/kyr$)
1790.5	414.41	90.246	6.066	0.035	0.577	6.081	0.258	4.243	249	368	40.36	8.656
1800.5	416.19	90.193				6.53	0.244	3.737	286	318	47.35	8.645
1810.5	417.97	91.157				6.604	0.264	3.998	380	422	47.38	8.809
1820.5	419.75	91.542				6.202	0.206	3.322	231	298	43.67	8.821
1830.5	421.53	92.084				5.699	0.216	3.790	269	340	44.17	8.968
1840.5	423.31	92.309	NO			4.967	0.224	4.510	401	321	55.54	9.045
1850.5	425.09	91.757	DATA			5.659	0.323	5.708	360	303	54.30	8.983
1860.5	426.88	92.169				6.62	0.51	7.704	328	170	65.86	8.975
1870.5	428.66	93.149				3.901	0.273	6.998	374	177	67.88	9.156
1880.5	430.44	93.494				5.752	0.404	7.024	327	159	67.28	9.139
1890.5	432.22	92.947		NO		6.16	0.641	10.406	273	134	67.08	9.319
1900.5	434.00	91.088		DATA		5.532	1.107	20.011	356	146	70.92	9.138
1910.5	437.25	91.486				7.69	1.126	14.642	312	147	67.97	5.037
1920.5	440.50	91.801				6.49	0.86	13.251	267	138	65.93	5.108
1930.5	443.75	91.079				5.54	0.809	14.603	426	186	69.61	5.138
1940.5	447.00	89.857				5.76	0.629	10.920	324	192	62.79	5.034
1950.5	450.25	88.508			NO	9.18	0.777	8.464	347	293	54.22	5.072
1960.5	453.50	87.547			DATA	8.405	0.853	10.149	176	195	47.44	4.994
1970.5	456.75	84.897				7.219	0.297	4.114	239	290	45.18	4.738
1980.5	460.00	83.765				8.17	0.337	4.125	237	346	40.65	4.583
1990.5	462.63	83.399				7.288	0.349	4.789	216	253	46.06	5.661
2000.5	465.25	84.841	7.408	0.201	2.713	7.336	0.205	2.794	216	249	46.45	5.794
2010.5	467.88	84.951	7.271	0.186	2.558	7.208	0.161	2.234	212	245	46.39	5.671
2020.5	470.50	84.649	7.391	0.225	3.044	7.308	0.211	2.887	254	268	48.66	5.747
2030.5	473.13	86.106	6.819	0.170	2.493	6.751	0.138	2.044	254	369	40.77	5.796
2040.5	475.75	86.597	7.110	0.159	2.236	7.037	0.163	2.316	265	433	37.97	5.847
2050.5	478.38	86.364	8.546	0.166	1.942	8.389	0.203	2.420	325	934	25.81	5.795
2060.5	481.00	86.546	7.364	0.102	1.385	7.285	0.172	2.361	254	498	33.78	5.804
2070.5	485.20	87.047	8.137	0.135	1.659	8.074	0.237	2.935	247	473	34.31	3.693
2080.5	489.40	85.607	9.218	0.131	1.421	9.143	0.193	2.111	295	930	24.08	3.608

CORE MD962084 (OLIFANTS RIVER SLOPE)

Depth (cm)	Age (kyr)	$CaCO_3$ %	Wt sample (g)	Wt >63um (g)	Sand content % > 63um	Wt sample (g)	Wt >125um (g)	Coarse frn % >125um	# forams	# fragments	Preservation Index (foram/foram+frag)%	$CaCO_3$ MAR ($g/cm^2/kyr$)
2090.5	493.60	87.138	7.015	0.083	1.183	6.947	0.111	1.598	245	614	28.52	3.685
2100.5	497.80	84.419	9.539	0.148	1.552	9.57	0.396	4.138	260	487	34.81	3.581
2110.5	502.00	86.154	6.925	0.254	3.668	6.922	0.2	2.889	359	594	37.67	3.660
2120.5	506.20	82.046	7.524	0.174	2.313	7.54	0.16	2.122	285	513	35.71	3.507
2130.5	510.40	82.607	7.245	0.206	2.843	7.26	0.263	3.623	274	444	38.16	3.528
2140.5	514.60	82.904	6.743	0.249	3.693	6.768	0.233	3.443	328	707	31.69	3.509
2150.5	518.80	86.001	7.614	0.333	4.374	7.638	0.328	4.294	287	506	36.19	3.664
2160.5	523.00	88.189	6.745	0.401	5.945	6.77	0.355	5.244	271	616	30.55	3.765
2170.5	525.00	89.270	6.623	0.510	7.700	6.638	0.325	4.896	298	689	30.19	8.015
2180.5	527.00	89.535				8.218	0.468	5.695	397	628	38.73	8.041
2190.5	532.50	92.498	7.463	0.370	4.958	7.478	0.305	4.079	372	668	35.77	3.029
2200.5	538.00	90.789	6.906	0.219	3.171	6.92	0.363	5.246	298	352	45.85	2.932
2210.5	546.33	86.892	7.886	0.150	1.902	7.926	0.433	5.463	219	345	38.83	1.858
2220.5	554.67	89.411	6.445	0.156	2.420	6.47	0.73	11.283	372	524	41.52	1.909
2230.5	563.00	88.884	8.628	0.229	2.654	6.66	0.445	6.682	275	502	35.39	1.876
2240.5	565.00	89.073	7.916	0.170	2.148	7.968	0.467	5.861	280	561	33.29	7.875
2250.5	567.00	88.802	8.980	0.454	5.056	9.036	0.652	7.216	271	465	36.82	7.903
2260.5	579.25	90.037	8.358	0.598	7.155	8.4	0.532	6.333	291	412	41.39	1.311
2270.5	591.50	89.526	6.756	0.254	3.760	6.79	0.512	7.541	324	416	43.78	1.298
2280.5	603.75	90.790	6.728	0.403	5.990	6.756	0.532	7.874	245	428	36.40	1.330
2290.5	616.00	89.994	6.885	0.540	7.843	6.907	0.752	10.888	353	438	44.63	1.307
2300.5	617.71	89.454	7.624	0.943	12.369	7.636	0.63	8.250	501	332	60.14	9.302
2310.5	619.43	89.459	7.316	0.749	10.238	7.343	0.71	9.669	334	243	57.89	9.600
2320.5	621.14	88.403	8.340	1.089	13.058	8.27	0.55	6.651	263	317	45.34	9.479
2330.5	622.86	85.952	9.195	1.084	11.789	9.241	0.539	5.833	237	482	32.96	9.161
2340.5	624.57	84.959	8.478	0.663	7.820	8.509	0.529	6.217	293	661	30.71	8.959
2350.5	626.29	83.579	8.085	0.574	7.100	8.118	0.482	5.937	302	376	44.54	8.892
2360.5	628.00	82.797	7.433	0.292	3.928	7.468	0.451	6.039	216	397	35.24	8.691
2370.5	631.90	81.514	7.396	0.298	4.029	7.418	0.598	8.061	241	354	40.50	3.793
2380.5	635.80	81.039	7.814	0.326	4.172	7.83	0.375	4.789	378	636	37.28	3.725

CORE MD962084 (OLIFANTS RIVER SLOPE)

Depth (cm)	Age (kyr) (kyr)	$CaCO_3$ %	Wt sample (g)	Wt >63um (g)	Sand content % > 63um	Wt sample (g)	Wt >125um (g)	Coarse frn % >125um	# forams	# fragments	Preservation Index (foram/foram+frag)%	$CaCO_3$ MAR ($g/cm^2/kyr$)
2390.5	639.70	80.950	7.764	0.324	4.173	7.796	0.567	7.273	234	333	41.27	3.641
2400.5	643.60	79.984	7.187	0.078	1.085	7.197	0.203	2.821	170	273	38.37	3.656
2410.5	647.50	82.759	8.362	0.131	1.567	8.393	0.236	2.812	88	114	43.56	3.765
2420.5	651.40	81.891	6.660	0.087	1.306	6.695	0.263	3.928	224	274	44.98	3.779
2430.5	655.30	82.640	7.512	0.163	2.170	7.527	0.431	5.726	228	315	41.99	3.759
2440.5	659.20	83.132	6.835	0.241	3.526	6.813	0.412	6.047	244	297	45.10	3.781
2450.5	663.10	84.682	7.413	0.206	2.779	7.441	0.342	4.596	239	569	29.58	3.883
2460.5	667.00	82.705	7.839	0.150	1.914	7.861	0.396	5.038	329	448	42.34	3.768
2470.5	669.69	83.192	7.462	0.112	1.501	7.477	0.327	4.373	261	356	42.30	5.605
2480.5	672.38	82.608	8.129	0.297	3.654	8.15	0.337	4.135	340	544	38.46	5.543
2490.5	675.06	81.981	7.957	0.142	1.785	7.98	0.366	4.586	202	294	40.73	5.478
2500.5	677.75	79.518	7.777	0.062	0.797	7.797	0.296	3.796	255	517	33.03	5.289
2510.5	680.44	77.396	7.761	0.087	1.121	7.783	0.306	3.932	250	237	51.33	5.108
2520.5	683.13	76.599	7.193	0.118	1.640	7.229	0.272	3.763	357	651	35.42	5.063
2530.5	685.81	78.736	6.787	0.265	3.905	6.808	0.31	4.553	223	192	53.73	5.221
2540.5	688.50	82.440	7.363	0.240	3.260	7.42	0.45	6.065	280	375	42.75	5.482
2550.5	693.69	82.281	9.148	0.378	4.132	9.131	0.597	6.538	366	346	51.40	2.911
2560.5	698.89	86.727	7.713	0.426	5.523	7.765	0.631	8.126	330	391	45.77	3.032
2570.5	704.08	88.856	7.703	0.438	5.686	7.729	0.639	8.268				3.096
2580.5	709.28	84.845	7.033	0.259	3.683	7.096	0.411	5.792	361	463	43.81	2.924
2590.5	714.47	82.063	7.270	0.189	2.600	7.325	0.412	5.625	233	295	44.13	2.813
2600.5	719.67	83.795	6.836	0.043	0.629	6.835	0.275	4.023	249	396	38.60	2.911
2610.5	724.86	81.412	7.151	0.079	1.105	7.152	0.361	5.048	300	369	44.84	2.846
2620.5	730.06	80.033	8.196	0.119	1.452	8.18	0.428	5.232	418	350	54.43	2.743
2630.5	735.25	79.389	7.432	0.253	3.404	7.421	0.455	6.131	360	431	45.51	2.797
2640.5	740.44	81.042	7.420	0.233	3.140	7.243	0.261	3.603	83	228	26.69	2.871
2650.5	745.64	76.137	8.188	0.123	1.502	8.269	0.339	4.100	221	262	45.76	2.629
2660.5	750.83	79.543	6.011	0.503	8.368	5.972	0.249	4.169	314	427	42.38	2.752
2670.5	756.03	79.423	5.925	0.464	7.831	5.965	0.117	1.961	357	323	52.50	2.730
2680.5	761.22	80.570	6.350	0.246	3.874	6.357	0.349	5.490	230	308	42.75	2.782

CORE MD962084 (OLIFANTS RIVER SLOPE)

Depth (cm)	Age (kyr)	$CaCO_3$ %	Wt sample (g)	Wt >63um (g)	Sand content % > 63um	Wt sample (g)	Wt >125um (g)	Coarse frn % >125um	# forams	# fragments	Preservation Index (foram/foram+frag)%	$CaCO_3$ MAR ($g/cm^2/kyr$)
2690.5	766.42	80.987	7.275	0.175	2.405	7.213	0.309	4.284	387	190	67.07	2.725
2700.5	771.61	81.036	9.299	0.092	0.989	9.3	0.52	5.591	284	371	43.36	2.772
2710.5	776.81	76.080	7.276	0.183	2.515	7.267	0.439	6.041	454	510	47.10	2.598
2720.5	782.00	82.250	7.098	0.194	2.733	7.104	0.573	8.066	248	228	52.10	2.766
2730.5	783.83	82.337	7.688	0.269	3.499	7.681	0.809	10.532	236	139	62.93	7.860
2740.5	785.67	84.452	6.343	0.854	13.464	6.326	0.838	13.247	282	196	59.00	8.158
2750.5	787.50	83.503	7.530	1.065	14.143	7.542						8.006
2760.5	789.33	83.103	7.316	1.425	19.478	7.337	1.082	14.747	417	153	73.16	7.985
2770.5	791.17	75.629	5.713	0.744	13.023	5.76	0.782	13.576	332	94	77.93	7.128
2780.5	793.00	76.958	6.928	0.929	13.409	6.924	0.672	9.705	278	108	72.02	7.345
2790.5	794.80	75.618	6.184	0.716	11.578	6.19	0.509	8.223	322	144	69.10	7.222
2800.5	796.60	80.672	8.336	1.339	16.063	8.39	1.232	14.684	480	200	70.59	7.694
2810.5	798.40	84.850	6.247	1.726	27.629	6.282	1.107	17.622	350	124	73.84	8.251
2820.5	800.20	83.189	6.476	1.395	21.541	6.511	1.106	16.987	280	113	71.25	8.074
2830.5	802.00	85.162	5.347	1.189	22.237	5.39	0.925	17.161	272	133	67.16	8.311
2840.5	803.80	85.948	6.628	2.236	33.736	6.667	1.101	16.514	376	117	76.27	8.298
2850.5	805.60	86.134	7.421	1.758	23.690	7.443	1.348	18.111	288	83	77.63	8.417
2860.5	807.40	87.269	7.329	1.873	25.556	7.355	1.269	17.254	311	139	69.11	8.519
2870.5	809.20	87.303	7.167	1.646	22.966	7.185	1.437	20.000	304	100	75.25	8.570
2880.5	811.00	87.846	7.575	1.744	23.023	7.628	1.173	15.378	294	119	71.19	8.649
2890.5	812.80	87.783	7.116	1.913	26.883	7.141	1.438	20.137	330	191	63.34	8.544
2900.5	814.60	85.979	7.759	2.165	27.903	7.745	1.286	16.604	251	137	64.69	8.519
2910.5	816.40	82.831	7.011	1.886	26.901	7.037	1.036	14.722	267	150	64.03	8.167
2920.5	818.20	87.050	6.561	1.493	22.756	6.582	1.027	15.603	252	130	65.97	8.508
2930.5	820.00	86.075	6.840	0.866	12.661	6.896	0.7	10.151	261	133	66.24	8.533
2940.5	822.57	85.930	7.161	0.914	12.764	7.19	0.523	7.274	265	153	63.40	6.030
2950.5	825.14	82.747	8.105	1.106	13.646	8.125	0.555	6.831	239	165	59.16	5.716
2960.5	827.71	82.818	8.805	0.416	4.725	8.83	0.457	5.176	260	194	57.27	5.763
2970.5	830.29	80.813	7.600	0.445	5.855	7.628	0.494	6.476	319	168	65.50	5.689
2980.5	832.86	80.945	7.555	0.198	2.621	7.603	0.388	5.103	273	300	47.64	5.560
2990.5	835.43	79.517	6.835	0.147	2.151	6.868	0.39	5.679	339	404	45.63	5.453

APPENDIX 8

RAW DATA FOR PALAEOPRODUCTIVITY PROXIES:
TOTAL ORGANIC CARBON
and
STABLE ISOTOPE RATIOS

CORE MD962080 (AGULHAS BANK SLOPE)

Depth (cm)	Age (kyr)	TOC (%)	$\delta^{13}C_{org}$ (‰)	$\delta^{15}N$ (‰)	C/N	$\delta^{13}C_{inflata}$ (‰)
2.5	1	2.303	-20.150	7.744	7.010	0.795
10.5	4	2.394	-19.806	8.034	6.664	0.800
20.5	8	1.730	-19.878	7.734	6.645	0.470
30.5	11	1.507	-20.068	7.634	6.719	0.510
40.5	15	1.277	-20.177	7.134	6.625	0.240
50.5	19	1.301	-20.095	6.184	7.064	0.400
60.5	21	1.320	-20.041	5.554	7.116	0.700
70.5	23	1.494	-20.656	6.474	6.814	1.000
80.5	24	1.612	-20.258	6.334	7.256	1.030
90.5	26	1.572	-20.104	6.414	7.333	0.890
100.5	28	1.578	-22.018	6.091	6.387	0.780
110.5	30	1.464	-21.537	6.581	5.515	0.590
120.5	43	1.250	-21.010	7.061	4.810	0.720
130.5	46	1.329	-21.445	6.721	5.354	0.620
140.5	50	1.503	-21.526	6.691	5.957	0.920
150.5	53	1.792	-22.796	7.111	6.558	1.130
160.5	56	1.359	-21.182	6.061	5.575	0.620
170.5	59	1.125	-21.079	6.671	4.540	0.790
180.5	62	1.405	-21.365	6.811	5.401	1.040
190.5	65	1.215	-22.018	5.656	4.980	0.800
200.5	76	1.504	-20.245	5.156	6.007	0.560
210.5	88	1.807	-20.570	5.026	7.157	0.680
220.5	99	2.205	-22.922	5.786	7.575	0.680
230.5	103	1.865	-22.262	6.286	5.701	0.430
240.5	107	1.450	-21.114	5.266	4.765	0.530
250.5	122	1.507	-22.146	5.606	4.907	0.570
260.5	124	1.355	-21.844	6.606	4.757	0.480
270.5	125	1.633	-22.505	5.986	6.085	0.080
280.5	127	0.991	-22.412	5.516	4.334	0.300
290.5	131	1.122	-20.960	4.106	5.829	0.060
300.5	135	1.226	-20.987	5.006	5.914	0.040
310.5	138	1.363	-21.292	4.626	7.525	0.320
320.5	140	1.451	-21.035	3.646	7.593	0.230
330.5	143	1.200	-20.844	3.966	6.918	0.210
340.5	146	1.429	-20.444	3.596		0.120
350.5	148	1.605	-20.768	5.286	8.527	0.440
360.5	151	1.461	-20.530	3.486	9.072	0.410
370.5	155	1.579	-21.340	3.936	9.593	0.330
380.5	161	1.158	-20.730	2.876	7.564	0.210
390.5	166	1.712	-20.758	3.226	7.647	0.280
400.5	171	1.711	-20.096	4.815	7.343	0.260
410.5	177	1.544	-20.532	6.196	5.682	0.150
420.5	182	1.487	-20.700	3.866	6.839	0.013
430.5	183	1.178	-21.984	6.026	5.180	0.300
440.5	187	1.180	-22.354	4.656	5.052	0.320
450.5	190	1.626	-23.896	3.826	1.534	0.420
460.5	194	2.133	-24.603	5.036	10.385	0.520
470.5	209	2.421	-23.850	5.546	3.297	0.660
480.5	223	2.382	-23.629	5.846	3.414	0.560
490.5	238	2.224	-23.525	6.726	1.767	0.820
500.5	241	1.241	-20.375	7.896	6.472	0.740

CORE MD962080 (AGULHAS BANK SLOPE)

Depth (cm)	Age (kyr)	TOC (%)	$\delta^{13}C_{org}$ (‰)	$\delta^{15}N$ (‰)	C/N	$\delta^{13}C_{inflata}$ (‰)
510.5	244	0.984	-22.296	5.096	4.009	0.220
520.5	248	1.187	-20.421	5.326	6.944	0.600
530.5	250	1.305	-21.006	5.420	5.178	0.220
540.5	252	1.215	-20.254	6.820	9.203	0.600
550.5	255	1.252	-21.216	4.540	10.486	0.220
560.5	257	1.689	-20.616	4.520	17.939	0.350
570.5	259	1.540	-20.644	7.920	7.219	0.410
580.5	261	1.487	-20.635	4.510	13.386	0.190
590.5	264	1.253	-21.893	2.700	8.776	0.440
600.5	266	0.821	-20.700	1.950	7.570	0.310
610.5	273	1.056	-20.904	0.200	10.237	
620.5	280	1.159	-22.293	0.080	10.904	0.920
630.5	287	1.662	-20.532	0.500	15.305	
640.5	290	1.623	-20.486	2.390	13.676	0.540
650.5	292	1.755	-21.550	1.334	12.983	0.940
660.5	295	1.775	-21.531	1.884	1.103	1.000
670.5	300	1.924	-21.273	1.914	13.356	0.870
680.5	304	1.795	-20.690	1.944	13.290	0.930
690.5	309	1.884	-21.674	1.374	14.796	1.200
700.5	312	1.834	-21.340	4.766	7.937	0.300
710.5	315	2.006	-21.330	4.336	7.765	0.740
720.5	321	1.952	-21.616	2.596	8.874	0.610
730.5	328	2.029	-21.483	2.966	10.379	0.210
740.5	330	1.739	-22.131	2.586	9.490	0.420
750.5	334					
760.5	337					
770.5	340	1.887	-21.693	3.816	7.869	0.620
780.5	343	1.492	-21.521	1.256	6.796	0.400
790.5	346	2.006	-21.979	6.846	3.638	0.410
800.5	350	1.361	-20.486	0.756	6.497	0.830
810.5	353	1.252	-20.857	2.824	7.735	0.687
820.5	356	1.245	-20.848	2.364	8.818	0.670
830.5	359	1.441	-20.932	2.304	10.483	0.790
840.5	363	1.371	-20.440	4.134	10.458	0.980
850.5	366	1.408	-20.882	2.414	11.076	1.010
860.5	369	1.676	-21.721	5.124	5.203	1.050
870.5	374	1.602	-21.206	5.024	5.292	0.640
880.5	379	2.044	-21.330	4.684	6.600	1.190
890.5	384	1.822	-20.940	4.274	5.878	1.190
900.5	390	2.444	-21.235	4.154	8.191	1.460
910.5	406	2.747	-21.697	6.275	9.353	0.980
920.5	409	2.687	-21.995	5.495	9.661	1.160
930.5	411	2.361	-22.213	6.075	10.311	0.870
940.5	414	1.683	-21.851	5.455	10.022	0.600
950.5	419					
960.5	424	1.343	-22.014	6.814	9.486	0.570
970.5	429	1.098	-21.615	3.294	9.003	0.720
980.5	434	1.116	-21.778	2.894	9.292	0.900
990.5	446	1.311	-21.724	3.454	8.303	0.730
1000.5	458	1.435	-21.164	4.364	4.601	0.890

CORE MD962080 (AGULHAS BANK SLOPE)

Depth (cm)	Age (kyr)	TOC (%)	$\delta^{13}C_{org}$ (‰)	$\delta^{15}N$ (‰)	C/N	$\delta^{13}C_{inflata}$ (‰)
1010.5	466	1.255	-20.542	4.214	4.600	0.900
1020.5	473	1.047	-20.596	3.604	3.860	1.050
1030.5	481	1.051	-20.282	3.444	3.780	
1040.5	491	0.955	-20.749	3.524	3.660	
1050.5	500	1.496	-19.862	4.194	4.993	
1060.5	512	1.764	-19.643	4.144	6.005	
1070.5	524	1.625	-20.148	5.604	5.544	
1080.5	527	1.369	-20.882	4.244	4.820	1.450
1090.5	530	1.481	-20.349	4.614	5.206	
1100.5	533	1.173	-20.819	4.459	6.967	1.109
1110.5	536	0.884	-20.656	3.865	3.000	1.046
1120.5	548	0.997	-20.837	3.149	5.574	0.835
1130.5	561	2.051	-22.665	3.238	11.056	1.189
1140.5	573	1.095	-21.453	5.799	5.710	1.156
1150.5	582	0.968	-20.964	4.168	6.786	0.592
1160.5	594	1.106	-21.326	1.649	5.668	1.108
1170.5	604	0.714	-20.964	5.230	5.696	0.888
1180.5	615	1.085	-20.756	4.699	5.497	1.055
1190.5	621	0.908	-20.801	5.810	2.489	0.672
1200.5	628	0.857	-20.792	3.565	4.117	0.696
1210.5	633	1.031	-20.656	4.930	4.428	0.864
1220.5	637	1.129	-20.955	4.909	4.843	0.523
1230.5	642	0.714	-20.548	2.495	3.390	0.252
1240.5	654	0.860	-20.955	1.940	3.522	0.586
1250.5	666	0.915	-20.910	2.330	3.603	0.501
1260.5	673	0.948	-21.054	2.670	3.514	0.949
1270.5	681	1.200	-21.027	2.925	3.369	0.997
1280.5	688	1.417	-20.629	4.225	6.145	0.904
1290.5	699	1.130	-19.806	4.939	6.125	0.690
1300.5	703	0.946	-21.308	5.769	4.584	1.053
1310.5	708	1.810	-20.756	6.999	7.200	0.762
1320.5	711	1.387	-21.543	3.945	14.296	0.857
1330.5	713	1.110	-20.810	3.025	6.768	0.432
1340.5	716	0.920	-20.195	0.165	8.947	
1350.5	718	0.966	-20.195	0.735	9.664	
1360.5	736	0.862	-20.484	0.295	8.525	
1370.5	754	1.146	-20.457	0.835	9.842	0.848
1380.5	759	1.624	-20.901	1.475	11.169	0.647
1390.5	765	1.535	-21.045	1.605	11.163	0.693
1400.5	769	1.436	-20.484	3.305	9.218	0.848
1410.5	774	1.517	-21.154	2.665	9.638	0.440
1420.5	778	1.784	-21.715	3.640	9.524	0.321
1430.5	782	1.723	-21.254	3.510	12.252	0.638
1440.5	788	1.074	-21.498	0.810	10.148	0.475
1450.5	790	0.891	-20.910	3.477	4.118	0.219
1460.5	799	0.457	-21.000	3.357	2.702	0.187
1470.5	807	0.759	-20.249	4.045	3.835	0.454
1480.5	815	0.703	-20.439	5.475	3.176	0.260
1490.5	824	0.628	-20.946	5.775	3.329	0.286
1500.5	835	0.916	-21.136	3.545	5.253	0.684

CORE MD962084 (OLIFANTS RIVER SLOPE)

Depth (cm)	Age (kyr)	TOC (%)	$\delta^{13}C_{org}$ (‰)	$\delta^{15}N$ (‰)	C/N	$\delta^{13}C_{inflata}$ (‰)
2.5	0.00	7.645	-19.226	7.120	6.818	
10.5	1.05	8.189	-19.112	6.880	7.040	1.181
20.5	2.09	7.892	-19.465	6.050	6.295	1.186
30.5	3.14	7.404	-19.236	6.310	6.664	1.307
40.5	4.18	7.062	-19.379	6.760	6.590	0.899
50.5	5.23	6.236	-19.379	7.060	5.979	1.115
60.5	6.27	7.177	-18.950	6.620	6.478	1.163
70.5	7.32	6.407	-19.532	6.560	6.736	1.070
80.5	8.36	6.376	-19.541	6.440	6.544	0.908
90.5	9.41	6.917	-19.360	7.110	7.922	0.815
100.5	10.45	7.374	-19.370	6.630	8.902	0.637
110.5	11.50			6.730		0.875
120.5	12.15	7.767	-19.370	6.870	8.821	0.822
130.5	12.80	6.855	-16.549	6.770	7.938	0.777
140.5	13.45	8.179	-19.503	6.660	9.325	0.753
150.5	14.10	8.760	-19.341	6.560	10.288	0.904
160.5	14.75	7.842	-19.494	6.460	9.975	0.729
170.5	15.40	7.730	-19.809	6.560	10.044	0.429
180.5	16.05	9.421	-19.427	6.260	10.770	0.694
190.5	16.70	8.736	-19.417	5.950	10.342	0.778
200.5	17.35	5.600	-18.860	4.850	7.822	0.724
210.5	18.00	7.509	-20.919	4.630	12.047	0.775
220.5	26.50	6.116	-19.713	3.780	10.575	0.738
230.5	35.00	6.605	-17.457	5.380	9.326	0.823
240.5	43.50	6.296	-19.723	4.990	9.178	0.752
250.5	52.00	6.980	-19.694	5.500	9.249	0.840
260.5	53.43	7.046	-19.494	5.220	10.067	0.909
270.5	54.86	6.988	-19.580	4.500	11.415	0.791
280.5	56.29	5.742	-20.000	4.130	10.222	0.820
290.5	57.71	7.056	-19.923	4.060	12.272	0.864
300.5	59.14	7.345	-19.799	4.310	13.000	
310.5	60.57	5.902	-19.914	3.560	11.347	0.784
320.5	62.00	5.978	-19.790	3.130	11.378	1.057
330.5	62.83	6.759	-19.847	3.850	12.382	1.087
340.5	63.67	6.572	-19.723	3.690	11.219	0.947
350.5	64.50	7.262	-19.799	3.470	12.337	0.961
360.5	65.33	6.479	-19.675	4.240	11.458	0.899
370.5	66.17	6.215	-19.732	3.390	11.767	0.889
380.5	67.00	5.480	-20.152	2.810	12.086	0.615
390.5	67.83	5.468	-20.028	2.820	12.645	0.655
400.5	68.67	4.277	-19.933	2.330	10.926	0.603
410.5	69.50	4.938	-19.799	6.251	10.509	0.752
420.5	70.33	5.242	-19.713	5.068	12.340	1.131
430.5	71.17	5.474	-19.723	5.029	12.823	1.030
440.5	72.00	5.200	-19.646	5.483	11.334	1.219
450.5	72.83	4.807	-19.761	5.223	11.843	1.151
460.5	73.67	4.399	-19.923	5.898	10.198	1.202
470.5	74.50	4.052	-20.200	5.085	11.008	0.687
480.5	75.33	3.867	-19.942	5.622	9.478	1.001
490.5	76.17	3.874	-19.895	4.789	11.705	0.999
500.5	77.00	3.966	-19.363	6.792	7.996	1.182

CORE MD962084 (OLIFANTS RIVER SLOPE)

Depth (cm)	Age (kyr)	TOC (%)	$\delta^{13}C_{org}$ (‰)	$\delta^{15}N$ (‰)	C/N	$\delta^{13}C_{inflata}$ (‰)
510.5	77.83	4.068	-19.458	2.963	7.836	1.212
520.5	78.67	4.999	-19.278	3.890	7.740	1.122
530.5	79.50	4.430	-19.307	4.060	6.471	0.940
540.5	81.56	4.338	-19.534	4.230	6.308	
550.5	83.61	3.982	-19.970	3.770	6.254	1.067
560.5	85.67	3.946	-19.952	3.770	6.385	1.079
570.5	87.72					
580.5	89.78					
590.5	91.83	3.965	-19.856	3.430	6.386	1.025
600.5	93.89	4.831	-20.162	3.240	10.657	0.716
610.5	95.94	5.057	-19.952	3.780	8.370	0.822
620.5	98.00	4.669	-18.888	3.560	7.627	0.725
630.5	101.00	4.721	-19.847	3.280	8.306	0.767
640.5	104.00	4.867	-19.780	3.310	8.546	1.012
650.5	107.00	7.835	-17.959	4.460	10.026	0.872
660.5	110.00	7.802	-17.770	3.810	10.479	0.859
670.5	113.00	8.442	-17.835	3.920	11.683	0.845
680.5	116.00	6.225	-19.837	3.070	11.437	0.964
690.5	119.00	5.520	-20.276	3.280	9.862	0.868
700.5	122.00	4.856	-20.321	2.800	10.459	0.891
710.5	123.67	4.996	-20.463	3.010	10.408	0.580
720.5	125.33	3.315	-20.415	2.820	8.260	0.526
730.5	127.00	4.229	-20.510	2.100	10.153	0.422
740.5	129.33	4.495	-20.458	2.263	11.703	0.448
750.5	131.67	4.962	-20.735	2.133	14.460	0.541
760.5	134.00	3.848	-21.744	0.913	12.733	0.537
770.5	143.60	4.115	-20.744	0.763	12.715	0.361
780.5	153.20	4.353	-20.534	0.883	14.527	0.544
790.5	162.80	4.732	-20.553	0.213	15.762	0.380
800.5	172.40	4.212	-20.444	0.633	12.079	0.410
810.5	182.00	4.360	-20.321	1.583	11.626	0.752
820.5	184.00	5.886	-21.998	0.263	14.794	0.719
830.5	186.00	4.206	-20.510	1.273	11.274	0.861
840.5	188.00	3.779	-20.169	4.053	5.390	0.753
850.5	190.00	3.179	-20.245	3.143	5.442	1.061
860.5	192.00	4.487	-19.638	2.773	7.320	0.948
870.5	194.00	6.657	-18.325	1.983	10.490	0.851
880.5	200.67	7.891	-16.965	3.403	12.843	0.774
890.5	207.33	6.077	-19.914	3.433	10.885	1.120
900.5	214.00	5.029	-19.869	1.743	7.318	1.133
910.5	216.30	4.271	-20.338	2.443	8.017	1.138
920.5	218.60	3.843	-20.500	2.423	7.587	0.888
930.5	220.90	3.693	-20.759	1.983	8.542	0.604
940.5	223.20	3.464	-20.931	4.472	7.328	0.652
950.5	225.50	4.539	-20.385	5.216	7.077	0.740
960.5	227.80	5.354	-20.309	5.184	7.444	0.936
970.5	230.10	9.363	-20.318	5.157	11.093	1.112
980.5	232.40	4.096	-20.328	6.008	4.152	1.017
990.5	234.70	5.652	-20.529	6.380	6.086	0.841
1000.5	237.00	4.560	-20.143	6.167	5.646	0.923
1010.5	238.92	4.241	-20.467	5.216	5.872	0.490

CORE MD962084 (OLIFANTS RIVER SLOPE)

Depth (cm)	Age (kyr)	TOC (%)	$\delta^{13}C_{org}$ (‰)	$\delta^{15}N$ (‰)	C/N	$\delta^{13}C_{inflata}$ (‰)
1020.5	240.83	5.348	-21.050	5.147	8.101	0.477
1030.5	242.75	7.362	-20.964	5.369	9.968	0.550
1040.5	244.67	6.822	-20.372	5.638	7.009	0.723
1050.5	246.58	7.066	-20.238	5.354	7.661	0.669
1060.5	248.50	7.196	-20.630	5.625	7.854	0.684
1070.5	249.50	7.444	-20.897	5.088	8.678	0.534
1080.5	250.50	6.518	-20.906	4.704	7.587	0.416
1090.5	251.50	3.800	-20.687	4.056	5.053	0.540
1100.5	252.50	3.495	-20.949	3.700	5.704	0.590
1110.5	253.50	6.242	-19.525	5.196	9.155	1.014
1120.5	254.50	5.253	-20.294	5.617	8.155	1.254
1130.5	255.50	5.976	-19.813	5.353	9.495	1.146
1140.5	256.50	5.617	-20.535	5.108	10.685	1.131
1150.5	257.50	6.636	-20.315	5.753	12.032	0.989
1160.5	260.45	6.097	-20.554	4.680	13.347	0.983
1170.5	263.40	5.319	-20.391	4.708	12.171	1.059
1180.5	266.35	6.492	-20.208	4.508	11.704	1.052
1190.5	269.30	6.473	-20.140	4.697	10.483	0.987
1200.5	272.25	5.482	-20.393	4.569	10.643	1.119
1210.5	275.20	6.815	-19.013	4.940	10.582	1.119
1220.5	278.15	6.958	-23.161	4.804	10.524	1.230
1230.5	281.10	3.458	-22.181	5.097	4.486	0.977
1240.5	284.05	6.517	-18.803	4.556	9.191	1.087
1250.5	287.00	5.800	-20.054	4.895	10.103	1.103
1260.5	289.50	6.456	-19.712	4.991	11.003	1.116
1270.5	292.00	6.659	-18.726	4.675	9.847	1.096
1280.5	294.50	6.746	-18.762	5.007	9.247	1.221
1290.5	297.00	8.062	-21.300	4.755	11.764	1.138
1300.5	299.50	7.881	-20.683	4.764	12.309	1.089
1310.5	302.00	6.308	-20.201	4.955	10.957	1.086
1320.5	306.00	5.700	-20.268	4.410	10.485	0.936
1330.5	310.00	5.500	-20.316	4.563	10.093	1.093
1340.5	313.25	7.891	-18.694	4.832	11.391	1.093
1350.5	316.50	7.505	-19.318	4.934	10.681	1.259
1360.5	319.75	7.285	-19.855	4.857	10.629	1.164
1370.5	323.00	5.869	-20.710	5.164	9.867	1.295
1380.5	326.25	8.007	-20.420	5.312	13.857	1.162
1390.5	329.50	6.050	-20.710	5.278	10.364	1.117
1400.5	331.33	7.359	-20.219	5.735	12.601	1.156
1410.5	333.17	5.377	-20.467	5.461	10.143	0.828
1420.5	335.00	4.802	-20.849	4.792	12.344	0.534
1430.5	336.83	5.185	-21.164	4.598	13.565	0.471
1440.5	338.67	5.056	-20.887	4.750	11.482	0.538
1450.5	340.50	4.815	-20.601	4.280	11.154	0.796
1460.5	349.00	4.093	-20.486	3.930	3.325	0.709
1470.5	351.67	5.210	-21.088	4.130	4.193	1.080
1480.5	354.33	6.305	-20.649	4.410	5.000	1.222
1490.5	357.00	7.654	-16.841	5.330	5.565	1.251
1500.5	357.88	8.075	-17.538	4.720	5.928	1.213
1510.5	358.77	5.850	-20.467	4.580	4.469	1.161
1520.5	359.65	6.414	-20.261	4.340	4.981	1.356

CORE MD962084 (OLIFANTS RIVER SLOPE)

Depth (cm)	Age (kyr)	TOC (%)	$\delta^{13}C_{org}$ (‰)	$\delta^{15}N$ (‰)	C/N	$\delta^{13}C_{inflata}$ (‰)
1530.5	360.54	9.918	-18.673	4.960	7.402	1.488
1540.5	361.42	8.361	-15.991	5.150	5.873	1.300
1550.5	362.31	9.620	-15.823	5.230	6.513	1.408
1560.5	363.19	10.134	-16.458	4.740	10.894	1.458
1570.5	364.08	8.615	-16.340	4.030	11.018	1.295
1580.5	364.96	7.446	-18.438	3.530	11.318	0.917
1590.5	365.85	9.873	-16.015	3.750	11.734	1.029
1600.5	366.73	9.045	-15.801	3.830	11.640	1.261
1610.5	367.62	7.955	-17.612	3.580	10.816	0.853
1620.5	368.50	6.487	-18.909	2.940	9.455	0.982
1630.5	371.58	8.263	-16.674	2.720	12.221	1.014
1640.5	374.67	7.809	-18.680	2.940	11.640	1.548
1650.5	377.75	7.983	-16.544	2.160	13.587	0.818
1660.5	380.83	6.089	-19.530	2.540	10.197	1.066
1670.5	383.92	6.430	-19.159	2.780	10.754	1.113
1680.5	387.00	5.908	-20.467	1.800	11.028	0.930
1690.5	390.08	6.356	-20.534	1.790	12.100	1.540
1700.5	393.17	6.297	-20.420	1.560	13.969	1.136
1710.5	396.25	5.587	-20.715	2.570	12.012	1.067
1720.5	399.33	5.054	-20.929	1.860	11.660	
1730.5	402.42	6.067	-20.649	1.220	14.485	1.097
1740.5	405.50	5.308	-20.830	1.600	12.239	1.067
1750.5	407.28	5.038	-21.164	1.800	12.084	0.995
1760.5	409.06	5.383	-21.126	0.450	16.178	1.282
1770.5	410.84	6.259	-21.202	1.350	17.127	1.328
1780.5	412.63	7.331	-20.983	1.770	17.297	1.255
1790.5	414.41	7.177	-20.881	1.490	15.527	1.110
1800.5	416.19	6.798	-20.948	0.370	11.798	1.267
1810.5	417.97	6.721	-21.120	1.280	14.666	1.201
1820.5	419.75	7.694	-20.891	1.270	17.376	0.946
1830.5	421.53	7.491	-21.053	0.200	18.065	0.950
1840.5	423.31	7.582	-21.158	0.940	18.781	0.818
1850.5	425.09	6.808	-21.224	1.750	15.597	0.819
1860.5	426.88	5.915	-21.434	0.860	17.373	0.697
1870.5	428.66	5.997	-21.425	4.020	13.167	0.529
1880.5	430.44	6.267	-21.520	3.690	13.801	0.773
1890.5	432.22	6.876	-21.596	3.150	16.513	0.865
1900.5	434.00	3.898	-21.595	2.530	9.918	0.704
1910.5	437.25	4.249	-20.546	3.460	9.891	0.809
1920.5	440.50	5.447	-20.335	3.270	12.477	0.800
1930.5	443.75	4.405	-20.412	3.060	10.060	0.848
1940.5	447.00	3.483	-20.326	3.170	7.763	
1950.5	450.25	5.085	-20.374	3.530	10.215	
1960.5	453.50	3.732	-20.479	3.210	7.924	1.111
1970.5	456.75	3.452	-20.287	3.330	5.693	1.259
1980.5	460.00	5.228	-20.028	4.210	7.041	1.389
1990.5	462.63	4.964	-20.191	4.970	7.350	1.296
2000.5	465.25	5.646	-20.165	4.300	5.475	1.378
2010.5	467.88	5.914	-20.117	4.090	8.166	1.491
2020.5	470.50	6.956	-19.543	4.820	8.761	1.755
2030.5	473.13	6.101	-19.878	4.660	9.100	1.424

CORE MD962084 (OLIFANTS RIVER SLOPE)

Depth (cm)	Age (kyr)	TOC (%)	$\delta^{13}C_{org}$ (‰)	$\delta^{15}N$ (‰)	C/N	$\delta^{13}C_{inflata}$ (‰)
2040.5	475.75	6.505	-19.802	4.280	8.633	1.549
2050.5	478.38	6.218	-18.861	4.870	7.988	1.744
2060.5	481.00	7.199	-19.017	4.330	9.851	1.456
2070.5	485.20	7.278	-19.007	4.660	10.086	1.578
2080.5	489.40	6.620	-19.562	4.510	8.755	1.560
2090.5	493.60	5.509	-19.716	4.800	7.589	1.352
2100.5	497.80	5.275	-19.754	4.630	7.390	1.524
2110.5	502.00	5.612	-19.754	2.410	7.437	1.388
2120.5	506.20	5.248	-20.195	3.220	11.721	1.401
2130.5	510.40	5.126	-20.127	4.710	6.157	1.582
2140.5	514.60	4.678	-20.223	4.760	6.593	1.685
2150.5	518.80	5.288	-20.204	4.440	7.863	1.591
2160.5	523.00	5.793	-19.916	4.870	9.436	1.410
2170.5	525.00	5.946	-20.184	3.937	9.531	1.385
2180.5	527.00	6.073	-20.194	4.063	18.073	1.435
2190.5	532.50	6.474	-20.213	0.533	16.843	1.303
2200.5	538.00	7.740	-20.079	1.632	20.429	1.368
2210.5	546.33	7.612	-20.261	3.082	15.343	1.452
2220.5	554.67	7.864	-19.964	0.893	15.872	1.604
2230.5	563.00	8.031	-19.620	3.083	21.096	1.597
2240.5	565.00	7.095	-19.955	3.574	12.320	1.518
2250.5	567.00	6.670	-20.117	4.578		1.571
2260.5	579.25	6.363	-20.443	4.460	11.424	1.503
2270.5	591.50	6.875	-20.471	4.571	11.285	1.465
2280.5	603.75	6.715	-20.519	4.652	11.140	1.377
2290.5	616.00	7.059	-20.471	4.758	11.964	1.037
2300.5	617.71	4.495	-20.602	4.842	8.373	1.119
2310.5	619.43	6.446	-20.625	4.953	12.248	1.192
2320.5	621.14	6.080	-20.605	4.183	10.592	0.815
2330.5	622.86	5.661	-20.338	4.057	8.400	1.218
2340.5	624.57	6.882	-20.117	4.587	9.500	1.188
2350.5	626.29	5.943	-20.237	4.504	7.873	1.169
2360.5	628.00	5.473	-20.439	4.503	6.665	1.268
2370.5	631.90	6.833	-19.265	4.860	8.696	1.371
2380.5	635.80	5.816	-20.525	4.469	7.141	0.937
2390.5	639.70	5.791	-20.487	4.559	7.151	0.915
2400.5	643.60	7.260	-19.735	4.680	8.553	0.773
2410.5	647.50	7.481	-17.705	4.569	9.695	0.730
2420.5	651.40	6.507	-20.042	4.331	9.436	1.136
2430.5	655.30	6.216	-20.092	4.397	9.375	1.219
2440.5	659.20	5.792	-20.362	4.412	9.548	1.410
2450.5	663.10	5.408	-20.487	4.433	8.110	1.471
2460.5	667.00	4.991	-20.573	4.343	6.736	0.923
2470.5	669.69	4.132	-20.429	4.761	6.253	1.022
2480.5	672.38	4.827	-20.458	4.451	7.001	1.146
2490.5	675.06	4.500	-20.352	4.312	5.670	1.030
2500.5	677.75	8.084	-20.481	4.294	10.379	1.071
2510.5	680.44	3.658	-20.291	4.326	5.151	0.821
2520.5	683.13	3.533	-20.304	4.603	5.901	1.411
2530.5	685.81	3.056	-20.583	4.753	5.030	1.184
2540.5	688.50	4.099	-22.301	4.998	6.951	1.148

CORE MD962084 (OLIFANTS RIVER SLOPE)

Depth (cm)	Age (kyr)	TOC (%)	$\delta^{13}C_{org}$ (‰)	$\delta^{15}N$ (‰)	C/N	$\delta^{13}C_{inflata}$ (‰)
2550.5	693.69	3.929	-20.496	4.546	8.099	1.257
2560.5	698.89	3.567	-20.698	4.613	7.232	0.975
2570.5	704.08	3.998	-20.660	4.917	6.251	1.249
2580.5	709.28	5.118	-20.381	4.587	2.399	1.100
2590.5	714.47	5.585	-20.689	4.984	7.838	0.872
2600.5	719.67	5.218	-20.548	5.088	8.452	1.038
2610.5	724.86	4.147	-20.730	5.059	6.558	1.236
2620.5	730.06	4.123	-20.881	4.863	5.204	0.845
2630.5	735.25	5.149	-20.679	5.162	2.361	1.232
2640.5	740.44	4.361	-20.852	5.080	0.722	
2650.5	745.64	4.307	-20.823	4.068	2.152	0.949
2660.5	750.83	5.268	-20.198	5.202	6.324	1.299
2670.5	756.03	5.590	-20.131	5.722	3.444	
2680.5	761.22	4.736	-20.410	5.264	2.584	1.398
2690.5	766.42	5.063	-20.256	3.828	6.644	1.308
2700.5	771.61	5.081	-20.487	4.860	0.947	1.148
2710.5	776.81	4.695	-20.715	5.677	0.861	1.212
2720.5	782.00	5.215	-20.849	5.670	2.561	1.153
2730.5	783.83	5.275	-20.935	5.113	7.685	
2740.5	785.67	4.409	-20.725	5.416	2.346	0.788
2750.5	787.50	5.197	-21.183	4.224	2.935	
2760.5	789.33	5.563	-20.558	3.607	9.755	0.508
2770.5	791.17	5.552	-20.510	4.496	3.023	0.779
2780.5	793.00	6.063	-20.725	4.106	10.565	0.875
2790.5	794.80	6.548	-20.658	4.310		0.784
2800.5	796.60	7.756	-21.518	3.611	12.761	0.730
2810.5	798.40	5.510	-20.958	2.921		0.331
2820.5	800.20	6.668	-19.530	3.094	11.282	0.654
2830.5	802.00	7.472	-21.347	3.046	2.840	0.546
2840.5	803.80	5.694	-21.186	2.288	0.948	0.511
2850.5	805.60	6.774	-20.605	2.549	1.119	0.667
2860.5	807.40	8.613	-21.177	2.757	3.044	0.334
2870.5	809.20	7.888	-16.767	2.319	2.940	0.601
2880.5	811.00	8.163	-21.309	2.811	4.800	0.323
2890.5	812.80	6.319	-21.087	3.312	10.490	0.456
2900.5	814.60	7.423	-21.060	4.113	13.497	0.505
2910.5	816.40	5.471	-20.883	4.003	11.652	0.441
2920.5	818.20	4.233	-21.374	3.615	6.563	0.461
2930.5	820.00	4.654	-21.186	4.295	9.908	0.670
2940.5	822.57	5.282	-21.368	4.039	8.504	0.848
2950.5	825.14	8.660	-22.759	4.218	12.271	0.861
2960.5	827.71	6.469	-21.174	4.863	9.942	1.018
2970.5	830.29	8.433	-22.338	4.691	12.376	1.120
2980.5	832.86	6.669	-20.797	4.916	8.352	1.039
2990.5	835.43	7.056	-18.838	5.011		0.789
3000.5	838.00	7.418	-20.797	5.666		0.931